PB87-147625

Proceedings: Symposium on the Transfer and Utilization of Particulate Control Technology (6th). Volume 2

Radian Corp., Research Triangle Park, NC

Prepared for

Environmental Protection Agency
Research Triangle Park, NC

Dec 86

U.S. Department of Commerce
National Technical Information Service
NTIS

PB87-147625

EPA/600/9-86/031b
December 1986

Proceedings: Sixth Symposium on the Transfer and Utilization of Particulate Control Technology

Volume 2

Holly Rossi, Compiler

Radian Corporation
P.O. Box 13000
Research Triangle Park, North Carolina 27709

EPA Contract 68-02-3994, Task 46

EPA Project Officer:
Dale L. Harmon
Air and Energy Engineering Research Laboratory
Research Triangle Park, NC 27711

EPRI Project Manager:
R.F. Altman
Air Quality Control Program
Coal Combustion Systems Division
Palo Alto, California 94304

AIR AND ENERGY ENGINEERING RESEARCH LABORATORY
OFFICE OF RESEARCH AND DEVELOPMENT
U.S. ENVIRONMENTAL PROTECTION AGENCY
RESEARCH TRIANGLE PARK, NC 27711

REPRODUCED BY
U.S. DEPARTMENT OF COMMERCE
NATIONAL TECHNICAL
INFORMATION SERVICE
SPRINGFIELD, VA. 22161

TECHNICAL REPORT DATA
(Please read Instructions on the reverse before completing)

1. REPORT NO. EPA/600/9-86/031b	2.	3. RECIPIENT'S ACCESSION NO.
4. TITLE AND SUBTITLE Proceedings: Sixth Symposium on the Transfer and Utilization of Particulate Control Technology; Volume 2		5. REPORT DATE December 1986 6. PERFORMING ORGANIZATION CODE
7. AUTHOR(S) Holly Rossi, Compiler		8. PERFORMING ORGANIZATION REPORT NO. EPRI CS-4918
9. PERFORMING ORGANIZATION NAME AND ADDRESS Radian Corporation P.O. Box 13000 Research Triangle Park, North Carolina 27709		10. PROGRAM ELEMENT NO. 11. CONTRACT/GRANT NO. 68-02-3994, Task 46
12. SPONSORING AGENCY NAME AND ADDRESS EPA, Office of Research and Development Air and Energy Engineering Research Laboratory Research Triangle Park, NC 27711		13. TYPE OF REPORT AND PERIOD COVERED Proceedings; February 1986 14. SPONSORING AGENCY CODE EPA/600/13

15. SUPPLEMENTARY NOTES AEERL project officer is Dale L. Harmon, Mail Drop 61, 919/541-2429.

16. ABSTRACT These proceedings document the Sixth Symposium on the Transfer and Utilization of Particulate Control Technology, in New Orleans, LA, February 25-28, 1986. The symposium, the second of its kind to be sponsored jointly by EPA and EPRI, was devoted to discussions of particulate emissions control. Its objectives were to promote the transfer of results of particulate control research to potential users of technologies, and to provide a medium for exchange of ideas between researchers in the fields of particulate control development and application. The proceedings contain 84 papers presented by EPA and other federal and state agency representatives, EPRI staff members, representatives of utility companies, equipment and process suppliers, university representatives, and research and development companies. Additionally, individuals from Australia, Canada, Denmark, Great Britain, Italy, Japan, and South Africa presented information on worldwide technological developments. Electrostatic precipitators and fabric filters were the major topics discussed. Other topics of interest included system operation and maintenance, fugitive emission control, integrated control processes (e.g., SO2 and particulate control), and advanced energy applications (e.g., high temperature applications).

17. KEY WORDS AND DOCUMENT ANALYSIS

a. DESCRIPTORS		b. IDENTIFIERS/OPEN ENDED TERMS	c. COSATI Field/Group	
Pollution	Processing	Pollution Control	13B	13H
Particles	Leakage	Stationary Sources	14G	
Electrostatic Precipitators		Particulate	13I	
Filters	Sulfur Dioxide	Fabric Filters		07B
Fabrics	Nitrogen Oxides	Fugitive Emissions	11E	
Maintenance			15E	

18. DISTRIBUTION STATEMENT Release to Public	19. SECURITY CLASS *(This Report)* Unclassified	21. NO. OF PAGES 570
	20. SECURITY CLASS *(This page)* Unclassified	22. PRICE

EPA Form 2220-1 (9-73)

NOTICE

This document has been reviewed in accordance with U.S. Environmental Protection Agency policy and approved for publication. Mention of trade names or commercial products does not constitute endorsement or recommendation for use.

PREFACE

The Sixth Symposium on the Transfer and Utilization of Particulate Control Technology was held in New Orleans, Louisiana, February 25 through 28, 1986. This Symposium, the second of its kind to be jointly sponsored by EPA and EPRI, was devoted to the discussion of particulate emissions control. The Symposium's objectives were to promote the transfer of results of particulate control research to potential users of technologies, and to provide a medium for exchange of ideas among researchers in the fields of particulate control development and application.

The Symposium proceedings contain 84 papers presented by EPA and other Federal and State agency representatives, EPRI staff members, representatives of utility companies, equipment and process suppliers, university representatives, and research and development companies. Additionally, individuals from Australia, Canada, Denmark, Great Britain, Italy, Japan, and South Africa presented information on worldwide technological developments. Electrostatic precipitators and fabric filters were the major topics discussed during the Symposium. Other topics of interest included system operation and maintenance, fugitive emission control, integrated control processes (e.g., SO_2 and particulate control or NO_x and particulate control), and advanced energy applications (e.g., high temperature or pressure applications).

Symposium cochairmen were Ralph F. Altman, Project Manager in the Air Quality Control Program of the EPRI's Coal Combustion Systems Division; and Dale L. Harmon, Project Officer in the Particulate Technology Branch of the EPA's Air and Energy Engineering Research Laboratory. Participants in the introductory plenary session were John S. Maulbetsch, Program Manager in the Air Quality Control Program of the EPRI's Coal Combustion Systems Division; Norman Plaks, Chief of the Particulate Technology Branch of the EPA's Air and Energy Engineering Laboratory; and keynote speaker Grady B. Nichols, Southern Research Institute.

- Integrated Control Processes I
- ESP: Fundamentals I
- ESP: Controls and Energy Consumption
- Integrated Control Processes II

Friday, February 28

- ESP: Fundamentals II
- ESP: Design Considerations
- Fugitive Emissions

Volume 1 of the Proceedings contains 26 papers presented in the Scrubbers, Opacity/Measurements, Advanced Energy Applications I and II, and Integrated Control Processes I and II Sessions.

Volume 2 of the Proceedings contains 35 papers on electrostatic precipitator technology presented in the Hot-Side Precipitator, Performance Enhancement I and II, Performance Estimating (Modeling), Advanced Technology, Fundamentals I and II, Control and Energy Consumption, and Design Considerations Sessions.

Volume 3 of the Proceedings contains 23 papers presented in the FF: Advanced Concepts I and II, FF: Practical Considerations, FF: Pilot-Scale Studies, Operation and Maintenance, and Fugitive Emissions Sessions.

Seven papers presented at the Symposium (nos. 3, 37, 41, 50, 51, 55, and 76 in the Symposium program) were not submitted for publication in the Proceedings.

- Integrated Control Processes I
- ESP: Fundamentals I
- ESP: Controls and Energy Consumption
- Integrated Control Processes II

Friday, February 28

- ESP: Fundamentals II
- ESP: Design Considerations
- Fugitive Emissions

Volume 1 of the Proceedings contains 26 papers presented in the Scrubbers, Opacity/Measurements, Advanced Energy Applications I and II, and Integrated Control Processes I and II Sessions.

Volume 2 of the Proceedings contains 35 papers on electrostatic precipitator technology presented in the Hot-Side Precipitator, Performance Enhancement I and II, Performance Estimating (Modeling), Advanced Technology, Fundamentals I and II, Control and Energy Consumption, and Design Considerations Sessions.

Volume 3 of the Proceedings contains 23 papers presented in the FF: Advanced Concepts I and II, FF: Practical Considerations, FF: Pilot-Scale Studies, Operation and Maintenance, and Fugitive Emissions Sessions.

Seven papers presented at the Symposium (nos. 3, 37, 41, 50, 51, 55, and 76 in the Symposium program) were not submitted for publication in the Proceedings.

NOTICE

This document has been reviewed in accordance with U.S. Environmental Protection Agency policy and approved for publication. Mention of trade names or commercial products does not constitute endorsement or recommendation for use.

PREFACE

The Sixth Symposium on the Transfer and Utilization of Particulate Control Technology was held in New Orleans, Louisiana, February 25 through 28, 1986. This Symposium, the second of its kind to be jointly sponsored by EPA and EPRI, was devoted to the discussion of particulate emissions control. The Symposium's objectives were to promote the transfer of results of particulate control research to potential users of technologies, and to provide a medium for exchange of ideas among researchers in the fields of particulate control development and application.

The Symposium proceedings contain 84 papers presented by EPA and other Federal and State agency representatives, EPRI staff members, representatives of utility companies, equipment and process suppliers, university representatives, and research and development companies. Additionally, individuals from Australia, Canada, Denmark, Great Britain, Italy, Japan, and South Africa presented information on worldwide technological developments. Electrostatic precipitators and fabric filters were the major topics discussed during the Symposium. Other topics of interest included system operation and maintenance, fugitive emission control, integrated control processes (e.g., SO_2 and particulate control or NO_x and particulate control), and advanced energy applications (e.g., high temperature or pressure applications).

Symposium cochairmen were Ralph F. Altman, Project Manager in the Air Quality Control Program of the EPRI's Coal Combustion Systems Division; and Dale L. Harmon, Project Officer in the Particulate Technology Branch of the EPA's Air and Energy Engineering Research Laboratory. Participants in the introductory plenary session were John S. Maulbetsch, Program Manager in the Air Quality Control Program of the EPRI's Coal Combustion Systems Division; Norman Plaks, Chief of the Particulate Technology Branch of the EPA's Air and Energy Engineering Laboratory; and keynote speaker Grady B. Nichols, Southern Research Institute.

ABSTRACT

These Proceedings document the Sixth Symposium on the Transfer and Utilization of Particulate Control Technology, held February 25 through 28, 1986, in New Orleans, Louisiana. The Symposium was sponsored by the U. S. EPA's Air and Energy Engineering Research Laboratory in Research Triangle Park, North Carolina, and EPRI's Coal Combustion Systems Division, in Palo Alto, California.

The objectives of the Symposium were to provide an opportunity for the exchange of knowledge and to stimulate new ideas in the field of particulate control research with the goal of extending the technology and aiding its diffusion among designers, users, and educators. Fabric filters and electrostatic precipitators were the major topics, but novel concepts and advanced technologies were also explored. Topics discussed in each day's sessions are listed below:

Tuesday, February 25

- Plenary Session
- ESP: Hot-Side Precipitator
- FF: Advanced Concepts I
- Scrubbers
- ESP: Performance Enhancement I
- FF: Advanced Concepts II
- Opacity/Measurements

Wednesday, February 26

- ESP: Performance Enhancement II
- FF: Practical Considerations
- Advanced Energy Applications I
- ESP: Performance Estimating (Modeling)
- FF: Pilot-Scale Studies
- Advanced Energy Applications II

Thursday, February 27

- ESP: Advanced Technology
- Operation and Maintenance

ACKNOWLEDGEMENT

The assistance of Holly Rossi, Radian Corporation, in compiling these Proceedings is gratefully acknowledged.

TABLE OF CONTENTS

VOLUME 1, PLENARY, SCRUBBERS, OPACITY/MEASUREMENTS, ADVANCED ENERGY APPLICATIONS I, ADVANCED ENERGY APPLICATIONS II, INTEGRATED CONTROL PROCESSES I, AND INTEGRATED CONTROL PROCESSES II

VOLUME 2, ELECTROSTATIC PRECIPITATOR TECHNOLOGY: HOT-SIDE PRECIPITATOR STUDIES, PERFORMANCE ENHANCEMENT I, PERFORMANCE ENHANCEMENT II, PERFORMANCE ESTIMATING (MODELING), ADVANCED TECHNOLOGY, FUNDAMENTALS I, CONTROLS AND ENERGY CONSUMPTION, FUNDAMENTALS II, AND DESIGN CONSIDERATIONS,

VOLUME 3, FF: ADVANCED CONCEPTS I, FF: ADVANCED CONCEPTS II, FF: PRACTICAL CONSIDERATIONS, FF: PILOT SCALE STUDIES, OPERATION AND MAINTENANCE, FUGITIVE EMISSIONS

VOLUME 1

PLENARY, SCRUBBERS, OPACITY/MEASUREMENTS, ADVANCED ENERGY APPLICATIONS I, ADVANCED ENERGY APPLICATIONS II, INTEGRATED CONTROL PROCESSES I, AND INTEGRATED CONTROL PROCESSES II

Section Page

PLENARY SESSION
Ralph F. Altman, Chairman

Keynote Address: Particulate Matter Control - The Rapidly Advancing Technology P-1
Grady B. Nichols*

Session C-1: SCRUBBERS
Dale L. Harmon, Chairman

Development of Improved Single Drop Collection Efficiency Correlations for Microcomputer Modeling of Venturi Scrubber Performance 1-1
K. Ellwood, A. W. Gnyp, C. C. St. Pierre, and S. Viswanathan*

Fume Filtration Through a Dynamic Liquid Spray Curtain 2-1
H. H. Elliott*, H. L. Marschall, and D. G. Jones

Session C-2: OPACITY/MEASUREMENTS
Phil A. Lawless, Chairman

Options to Alleviate Plume Opacity Problems Caused by Condensation Aerosols 3-1
A. S. Damle*, D. S. Ensor, and L. E. Sparks

Relationship of Opacity to the Loss Mechanisms in ESP's 4-1
D. S. Ensor, P. A. Lawless*, and L. E. Sparks

---

*Denotes speaker.

ection Page

Stack Opacity Model 5-1
D. J. Mormile, G. C. Stegmann, and B. F. Piper*

The Collection of Fine Particulate in Power Plant Electrostatic Precipitators 6-1
L. T. McEvoy, K. R. Parker, and A. Russell-Jones*

Predicting the Particle Size Distribution of Fly Ash 7-1
R. S. Dahlin*, J. P. Gooch, and L. Y. Sadler, III

Quality Assurance Considerations for Particle Sizing Measurements 8-1
G. L. Johnson* and C. E. Tatsch

ession C-3: ADVANCED ENERGY APPLICATIONS I
John S. Maulbetsch, Chairman

Technical and Economic Evaluation of High Temperature and High Pressure Particulate Cleanup Systems 9-1
R. Zaharchuk* and L. N. Rubow

Particulate Control at High Temperature and Pressure for Emerging Electric Power Generation Technologies 10-1
R. C. Bedick and R. J. Dellefield*

The Testing and Evaluation of Ceramic Filter Fabrics 11-1
R. Chang*, J. Sawyer, H. Lips, R. C. Bedick, and R. J. Dellefield

Hot Gas Clean-Up by Means of Porous Ceramic Filter Elements 12-1
P. Eggerstedt* and J. F. Zievers

Test and Development of Woven Ceramic Bag and Porous Ceramic Candle Filters for HTHP Application .... **
T. E. Lippert*, D. F. Ciliberti, O. J. Tassicker, and S. G. Drenker

ession C-4: ADVANCED ENERGY APPLICATIONS II
George A. Rinard, Chairman

Results of Parametric Tests on an Electrostatic Precipitator Operating at High Temperature and High Pressure Conditions 13-1
G. A. Rinard, D. E. Rugg*, M. Durham, and J. Armstrong

Design of Baghouse and Electrostatic Precipitator for the Coal-Fired Flow Facility 14-1
J. P. Foote*

---

*Denotes speaker.

**This paper was presented, but a manuscript was not submitted.

Section Page

Granular Bed Filter Component Design for High Temperature and High Pressure 15-1
K. B. Wilson*

The Interaction of a Gas with Solid and Liquid Particles in a Rotating System 16-1
H. Heshmat* and O. Pinkus

The Development and Testing of a Compact Cross Flow Filter for High Temperature Applications in Advanced Energy Systems .. **
D. F. Ciliberti and T. E. Lippert

Session C-5: INTEGRATED CONTROL PROCESSES I
J. Edward Cichanowicz, Chairman

Particulate Control Integration with Wet Scrubber SO$_2$ Removal and Waste Generation 17-1
P. M. Maroney*, S. A. Davidson, S. M. Katzberger, and J. E. Cichanowicz

Kinetics of Reaction Between Hydrated Lime and Sulfur Dioxide 18-1
A. S. Damle*, K. Ramanathan, and D. L. Harmon

Mini Spray Dryers for Low-Cost SO$_2$ Control 19-1
C. B. Sedman and L. E. Sparks*

Electrostatic Precipitator Performance Characterization in Spray Dryer Flue Gas Desulfurization Systems 20-1
G. E. Bresowar*, R. F. Robards, and R. A. Runyan

Fabric Filter Operating Experience on a Dry FGD System at Austell Box Board Corporation 21-1
W. H. Bradley*

Session C-6: INTEGRATED CONTROL PROCESSES II
G. E. Bresowar, Chairman

Results of Pilot-Scale Tests of E-SO$_x$ 22-1
L. E. Sparks*, G. H. Ramsey, R. E. Valentine, and N. Plaks

Researches for Optimal Integrated Flue Gas Treatment 23-1
G. Dinelli and M. Rea*

Utility Case History on Firing Enhanced Emulsified Fuel Oil to Reduce Particulate and NO$_x$ Emissions 24-1
E. S. Behrens*

---

*Denotes speaker.

**This paper was presented, but a manuscript was not submitted.

Section .... Page

Particulate Control Devices for Municipal Refuse-to-Energy Plants 25-1
M. Kapner*

Integrated Control Device for Micronic and Submicronic Particulate and Acidic Gas Control 26-1
T. K. Ewan* and O. L. Holland

Appendix:Attendees A-1

VOLUME 2

ELECTROSTATIC PRECIPITATOR TECHNOLOGY: HOT-SIDE PRECIPITATOR STUDIES, PERFORMANCE ENHANCEMENT I, PERFORMANCE ENHANCEMENT II, PERFORMANCE ESTIMATING (MODELING), ADVANCED TECHNOLOGY, FUNDAMENTALS I, CONTROLS AND ENERGY CONSUMPTION, FUNDAMENTALS II, AND DESIGN CONSIDERATIONS,

Session A-1: HOT-SIDE PRECIPITATOR STUDIES
Wallis A. Harrison, Chairman

Hot Precipitators and Duct Design Considerations 1-1
J. A. Werhane*, W. G. Doran, and O. Zaben

Considerations for the Cyclic Operation of Hot-Side Electrostatic Precipitators 2-1
F. C. Southworth*, R. K. Miller, and C. A. Altin

Structural Investigation of Large Hot-Side Electrostatic Precipitators .... **
C. A. Altin*

Session A-2: PERFORMANCE ENHANCEMENT I
B. G. McKinney, Chairman

A Comparison of Electrostatic Precipitator Performance Enhancement Technologies 3-1
J. Dalmon, G. L. Dalton*, and R. S. Hansen

Baltimore Gas and Electric Experience with Combined SO_3/NH_3 Injection for Precipitator Performance Improvement 4-1
W. E. Cummings, Jr.* and W. H. Reamy

A Design Methodology for Optimized Water Conditioning of High Resistivity Fly Ash 5-1
N. W. Frisch* and W. T. Hartshorn

A New Chemical Conditioner Together with Good Operations and Maintenance Program Management Helps Meet Emissions Objectives 6-1
R. K. Sinha*

*Denotes speaker.

**This paper was presented, but a manuscript was not submitted.

Section Page

Session A-3: PERFORMANCE ENHANCEMENT II
Ralph F. Altman, Chairman

Evaluation of Broad and Narrow Pulse Energization of a Cold-Side Electrostatic Precipitator 7-1
H. R. Osmers* and D. J. Sugumele

Full Scale Demonstration Results of Electrostatic Precipitator Pulse Energization 8-1
T. W. Lugar* and J. M. Friday

Field Evaluation of Pulse Energization under Different Operating Conditions 9-1
S. Masuda* and S. Hosokawa

Long-Term Experience with Pulsed Energization of ESP's at a Danish Power Station 10-1
K. Porle*, R. Karlsson, and B. Kirkegaard

Session A-4: PERFORMANCE ESTIMATING (MODELING)
Ronald B. Mosley, Chairman

An Improved Model for Predicting Fly Ash Resistivity 11-1
R. E. Bickelhaupt* and L. E. Sparks

A Selected Review of Critical Parameters and Formulae for Design and Performance Evaluation of Electrostatic Precipitators 12-1
H. J. Hall*

Predicting Cold-Side Precipitator Performance Based Upon Coal and Ash Chemistry 13-1
F. A. Horney and V. H. Belba*

Evolution of an Interactive Model for Predicting Voltage-Current Curves in ESP's with Novel Electrodes .... **
P. A. Lawless* and L. E. Sparks

Approximate Method to Calculate Characteristics of Contaminated-Wire and Strip-Discharge Electrodes 14-1
K. J. McLean*, L. E. Sparks, and G. H. Ramsey

Session A-5: ADVANCED TECHNOLOGY
Leslie E. Sparks, Chairman

Pilot Plant Evaluation of the Cooled-Electrode Precharger as an ESP Retrofit Device .... **
M. Durham*, G. A. Rinard, and D. E. Rugg

*Denotes speaker.

**This paper was presented, but a manuscript was not submitted.

Section Page

Pilot-Scale Evaluation of ESP Wide Plate Spacing 15-1
R. F. Altman*, E. C. Landham, Jr., J. L. DuBard,
and H. L. Wheeler

Pilot-Scale Evaluation of ESP Intermittent Energization 16-1
E. C. Landham, Jr.*, J. L. DuBard, W. E. Piulle,
and L. F. Rettenmaier

Operating Results of Moving Electrode Type Electrostatic
Precipitators for Coal-Fired Boilers 17-1
H. Asano*, H. Yabuta, and M. Ohtsuka

Pilot-Scale Evaluation of Multi-Stage Electrostatic
Precipitator .... **
L. E. Sparks*, G. M. Ramsey, and N. Plaks

Session A-6: FUNDAMENTALS I
Sidney A. Self, Chairman

Medium-Sulfur Coal and Fly Ash Resistivity 18-1
W. A. Harrison*, J. K. Nicholson, J. L. DuBard,
and L. E. Sparks

The Effect of High Mass Loading on Fly Ash Precipitators 19-1
M. G. Faulkner*, J. L. DuBard, and L. E. Sparks

The Effective Dielectric Constant of Fly Ash 20-1
R. P. Young*, J. L. DuBard, and L. E. Sparks

Diagnostic Technology of Precipitator Operation 21-1
S. Masuda*, T. Itagaki, and S. Hosokawa

Session B-6: CONTROLS AND ENERGY CONSUMPTION
James L. DuBard, Chairman

Electrostatic Precipitator Power Measurements 22-1
P. Gelfand*, E. C. Landham, Jr., and L. F. Rettenmaier

ESP Energy Management and Optimization of Collection
Efficiency 23-1
B. Borowy*, M. McLauchlin, and W. F. Frazier

The Evaluation of Tests and the Economic Implications
of Power Reduction on Electrostatic Precipitators 24-1
D. L. Lueckenotte* and V. L. Kunzweiler

First Utility Application of a New Microprocessor-Based
Distributed Control System for Electrostatic Precipitators 25-1
G. R. Gawreluk*, M. Barav, and S. R. Coco

---

*Denotes speaker.

**This paper was presented, but a manuscript was not submitted.

Section Page

Power Consumption of Opacity Feedback Controlled Electrostatic Precipitator Transformer-Rectifiers 26-1
J. J. Roosma* and J. B. Howard

Interactive Electrostatic Precipitator Controls .... **
C. A. Altin*, R. E. Comer, P. T. Nielsen, and R. J. Burgess

Session A-7: FUNDAMENTALS II
Owen Tassiker, Chairman

Electric Field Measurements in an Operating Precipitator 27-1
J. L. DuBard*, E. C. Landham, Jr., and R. F. Altman

Finite-Diffusivity Effects in Single-Stage Precipitators - Theory and Experiment 28-1
S. A. Self*, M. Mitchner, D. H. Choi, K. D. Kihm, and R. Leach

Three-Dimensional Calculations of Negative Tuft Corona 29-1
M. K. Owen*, T. Yamamoto, P. A. Lawless, and L. E. Sparks

The Simulation of Corona Discharges under Practical Precipitator Conditions 30-1
I. Gallimberti*

Some Electrical Characteristics of Back Corona 31-1
K. J. McLean*, L. E. Sparks, and G. H. Ramsey

Session B-7: DESIGN CONSIDERATIONS
Sidney R. Orem, Chairman

Laboratory Measurements of Some Electrical Parameters in Conventional and Wide Duct Precipitators 32-1
A. A. Elmoursi and G. S. P. Castle*

Influence of Gas Distribution on Precipitator Performance 33-1
L. Lind*

Development and Testing of a Collecting Curtain for an Electrostatic Precipitator 34-1
H. L. Engelbrecht* and R. J. McMullan

Characterization of Discharge Electrode Performance: Results of Laboratory and Pilot Plant Experiments 35-1
L. A. Hawkins* and H. L. Wheeler

---

*Denotes speaker.

**This paper was presented, but a manuscript was not submitted.

Section Page

VOLUME 3

FF: ADVANCED CONCEPTS I, FF: ADVANCED CONCEPTS II, FF: PRACTICAL CONSIDERATIONS, FF: PILOT SCALE STUDIES, OPERATION AND MAINTENANCE, FUGITIVE EMISSIONS

Session B-1: FF: ADVANCED CONCEPTS I
Louis S. Hovis, Chairman

Distribution of Fly Ash in a Filter Bag Operating with a Charged Axial Electrode 1-1
G. E. R. Lamb* and K. T. Duffy

Study of Electrostatically Stimulated Filtration Fundamentals 2-1
D. W. VanOsdell, A. S. Viner*, K. D. Carter, and L. S. Hovis

Session B-2: FF: ADVANCED CONCEPTS II
Norman Plaks, Chairman

Mathematical Model for Advanced Electrically Stimulated Fabric Filtration 3-1
T. Yamamoto*, D. S. Ensor, R. B. Mosley, L. S. Hovis, and N. Plaks

Advanced ESFF Laboratory Test Results 4-1
R. B. Mosley*, L. S. Hovis, and B. E. Daniel

Advanced ESFF Applied to a Stoker Coal-Fired Boiler 5-1
G. P. Greiner*, A. S. Viner, L. S. Hovis, and R. Gibbs

Advanced Electrostatic Fabric Filtration Experience at Southwestern Public Service Company 6-1
R. Serrurier*

Economics of Advanced Electrostatic Stimulation of Fabric Filtration 7-1
L. S. Hovis* and A. S. Viner

Session B-3: FF: PRACTICAL CONSIDERATIONS
John D. McKenna, Chairman

Evaluation of Acid-Resistant Synthetic Needled Felt Filter Media in Coal-Fired Boiler Pulse-Jet Baghouses 8-1
W. T. Grubb*

Laboratory Studies of the Filtration Performance of Various Filter Media under Simulated Field Conditions 9-1
P. E. Frankenburg*

*Denotes speaker.

**This paper was presented, but a manuscript was not submitted.

Section | Page

Evaluation of a Specific Type of Filter Bag Supplied by Various Vendors 10-1
Y. J. Chen*, P. N. Roberts, and T. D. Tarnok

Catenary Analysis of a Fabric Filter Bag During Reverse-Gas Cleaning 11-1
E. A. Samuel* and J. G. Musgrove

Aerosol Deposition in Fabric Filters 12-1
D. S. Ensor*, T. Yamamoto, and A. S. Viner

Session B-4: FF: PILOT SCALE STUDIES
John Maulbetsch, Chairman

Performance of a High-Sulfur-Coal, Pilot-Scale Fabric Filter 13-1
R. F. Heaphy*, R. R. Wilson, and W. E. Piulle

Flue Gas Conditioning for Improved Baghouse Performance 14-1
D. L. Laudal* and S. J. Miller

Session B-5: OPERATION AND MAINTENANCE
Robert P. Gehri, Chairman

Operation and Maintenance Experience at Harrington Station 15-1
W. Hooks, O. Plunk*, and D. L. Harmon

Computer Monitoring of Pilot Plant Baghouse Performance 16-1
A. S. Viner*, L. M. Fickel, and L. S. Hovis

The Design of Repairs to Upgrade 10-Year-Old Industrial Precipitators 17-1
V. L. Kunzweiler* and J. B. Landwehr

Performance Improvement History of Inadequately Performing Precipitators 18-1
J. G. Musgrove*, W. R. Lane, and M. W. Wei

Performance Improvement and Fire Prevention in Fly Ash Collection System at a 50MW Wood-Fired Power Plant 19-1
E. Gal* and M. Murphy

Session C-7: FUGITIVE EMISSIONS
Dale L. Harmon, Chairman

Identification, Assessment, and Control of Fugitive Particulate Emissions 20-1
C. Cowherd, Jr.*, J. S. Kinsey, and D. L. Harmon

*Denotes speaker.

**This paper was presented, but a manuscript was not submitted.

Section Page

Process Fugitive Particulates - Design Methods for Enclosures 21-1
H. D. Goodfellow, T. Cesta, E. R. Kashdan, D. W. Coy, and J. J. Spivey[*]

Field Evaluation of Windscreens as a Fugitive Dust Control Measure for Materials Storage Piles 22-1
R. A. Zimmer[*], K. Axetell, Jr., and T. C. Ponder, Jr.

Measurement of Fugitive Emissions in a Coal-Fired Power Plant 23-1
G. E. Muleski[*], F. J. Pendleton, and W. A. Rugenstein

---

[*] Denotes speaker.

[**] This paper was presented, but a manuscript was not submitted.

Session B-1: FF: ADVANCED CONCEPTS I

Louis S. Hovis, Chairman
U. S. EPA/AEERL
Research Triangle Park, NC

DISTRIBUTION OF FLY ASH IN A FILTER BAG OPERATING WITH A CHARGED AXIAL ELECTRODE

by: George E. R. Lamb and Kathleen T. Duffy
Textile Research Institute
Princeton, New Jersey 08542

ABSTRACT

Further progress in the development of techniques for electric stimulation of fabric filtration (ESFF) will require participation of baghouse users in testing the concept and providing valuable feedback from full-scale operation experience. Participation is more likely to be assured if the ESFF system is simple, relatively inexpensive, and easy to maintain.

The original system developed at the Textile Research Institute consisted of a bag fitted with alternate live and ground wires spaced an inch apart. An approach to simpler systems has taken the form of a charged axial electrode (or "axode") with all bag electrodes grounded. The work described here centers on further simplification and optimization of this arrangement by studying the effect of axode diameter and number of grounded wires in the bag, including a system which requires no bag wires.

This paper has been reviewed in accordance with the U. S. Environmental Protection Agency's peer and administrative review policies and approved for presentation and publication.

INTRODUCTION

It has been established that baghouse filter performance may be greatly improved by magnifying the electrostatic component of the various mechanisms that cooperate in the capture of particles by the filter. A number of approaches have been successful in achieving such improvement. These include electrical precharging of the aerosol (1, 2), use of filters made of electret fibers (3), use of bags with electrodes raised to high potential (4, 5, 6), and combinations of aerosol precharging and bags fitted with electrodes (7).

Extended experimentation both in the laboratory and at the pilot plant stage indicates that, for the greatest performance improvement, the aerosol must carry a considerable charge. In practice this means that some precharging procedure will be necessary in most cases. With such an arrangement, reductions in pressure drop of two orders of magnitude have been observed in the laboratory with concurrent large reductions in penetration (7). The pressure drop reduction has been shown to be directly due to extensive redistribution of the dust over the area of the bag. There is usually a skewing of the dust deposition toward the bag entrance and toward the electrodes, and calculations of the reductions in pressure drop according to a parallel resistance model for observed dust mass redistribution patterns have agreed well with measured values. In addition, there is evidence that there is a smaller contribution from the fact that, with a field applied, dust deposits in the less dense surface regions of the filter fabric (7). The relative contributions of these two effects — redistribution in the fabric plane and normal to it — vary depending on how non-uniform the areal dust distribution is. When the aerosol has little charge, the second effect may play the major role.

The reason that electrostatic effects reduce penetration along with pressure drop seems at first fairly obvious. It has been shown (8) that the capture efficiency of a single fiber can increase by two orders of magnitude if an electric field is set up in its neighborhood. The efficiency of an entire filter would then likewise be expected to increase. However, the applicability of single fiber capture criteria to cases where the fiber mat or fabric is thickly covered with dust may reasonably be placed in doubt. In a number of instances it has been suggested that, when the theoretical efficiency of a fabric is very high, mechanisms of penetration assume control (9, 10). These mechanisms are pinhole formation and seepage, the latter being a form of dust cake instability, which is relevant in this context.

It has been shown that, if a fabric is coated with a metallic film so as to eliminate electrostatic effects, penetration increases rapidly with the number of cleaning cycles, indicating a decrease in cake stability (11). In unrelated studies, the efficiency of a bag filter was shown to vary depending on the nature of the fly ash filtered (12). The important variable was found to be the sodium salt content of the coal. Since the fly ash particles from high sodium coal were found to have rough surfaces, while those from low sodium coal were smooth, it was inferred that the rough surface particles formed a more stable dust cake, leading to lower penetration. It may be supposed that electrostatic effects likewise influence efficiency because of increased cake stability rather than through increases in single fiber efficiency, although it is not clear what experimental approach could be taken to determine the relative magnitudes of the two effects. This consideration may, however, have as an important application the possible use of electrostatics in cases where local coal usage creates problems of unusually high penetration in baghouses.

While the advantages of electric stimulation of fabric filters (ESFF) are no longer in doubt, adoption of the technique by users appears to await the development of a convenient practical system. The system developed at TRI, consisting of a bag with alternately grounded and high voltage electrodes and a "lightning-rod" precharger, has given excellent results, but has not worked as well in other locations. A second disadvantage is the necessity to make separate connections to the alternate electrodes, which would require the development of techniques to make them rapidly and dependably. Some resistance from users may also come over the price premium that would have to be charged for the specially woven bag fabrics.

The mechanisms that control pressure drop in a filter bag used with integral electrodes and with a lightning-rod precharger in the mode described above have been studied. It was found that there is a cylindrical space at the center of the bag, the space having a radius half the bag radius, within which the electric field generated by the electrodes in the bag is almost zero. This suggested that other electrode configurations, if they could avoid this "dead space," might be even more effective. A configuration involving a precharger wire hanging axially inside the bag appeared promising in this respect. Workers at the EPA Air and Energy Engineering Research Laboratory (AEERL) have already obtained encouraging results with such a configuration (13). They have named this system advanced ESFF to distinguish it from systems that use only electrodes in the bag wall with little or no particle precharging.

The work described here was intended to supplement the work done at the EPA AEERL by studying some of the variables that are likely to affect performance of a bag filter with a charged axial electrode. One such variable is the diameter of the axial electrode, and another is the number of electrodes in the bag. Both of these were examined, the objective being optimum performance consistent with simple design so as to reduce eventual bag costs and minimize user resistance.

EXPERIMENTAL RESULTS

STUDIES OF AXODE DIAMETER

A one-bag laboratory baghouse was used which had been constructed for work under a previous EPA cooperative agreement. The baghouse was provided with means for programming sequences of filtering and cleaning cycles. Cleaning was by reverse air with shaking. Pulverized coal fly ash was metered into the incoming air stream and dispersed by a compressed air jet.

Initial measurements were made with single-wire axial electrodes of 0.25 mm and 1.00 mm diameter and with a cable of eight 0.25 mm wires. For reasons of convenience, the abbreviation "axode" for "axial electrode" has been used throughout. All bag wires were grounded for these measurements.

Each data point in Figures 1-4 was obtained after at least ten 1-hour operating cycles, when the pressure drop had reached steady state. Values of pressure drop ratio (PDR), the ratio of pressure drop measured under the experimental conditions to that with no electric stimulation, were obtained with the three axodes at 1.5 cm/s face velocity, and efficiency was determined by sampling the downstream flow for an hour. When the two single-wire results for PDR are compared on the basis of the potential on the axode (Figure 1), the 0.25 mm axode appears to give better response, since it produces a given PDR value with a lower potential; the cable yields values that are close to those for the single 0.25 mm wire. This comparison, however, ignores the current drawn, which is different for the different axodes.

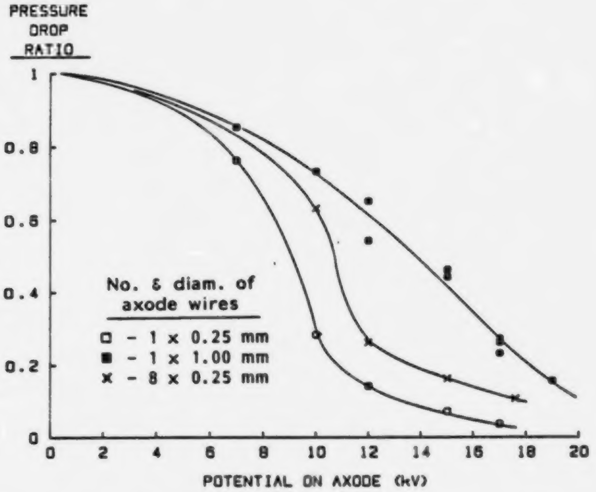

Figure 1 Dependence of pressure drop ratio on voltage applied to axode. Bag fitted with 0.15 mm diameter wires, 2.5 cm apart, parallel to bag axis. All bag electrodes grounded.

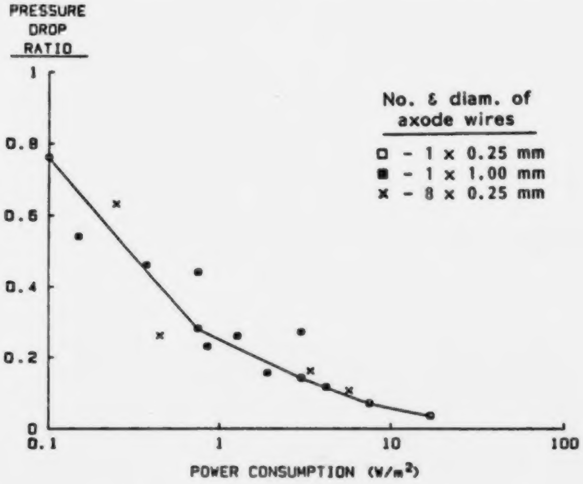

Figure 2 The same data as in Figure 1 plotted as a function of power consumption.

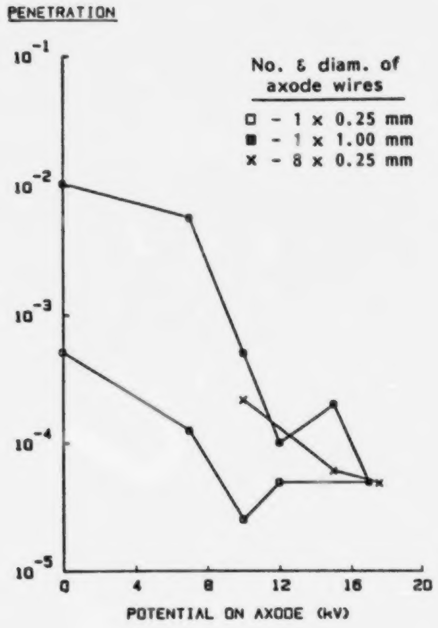

Figure 3 Penetration during experiments in Figures 1 and 2.

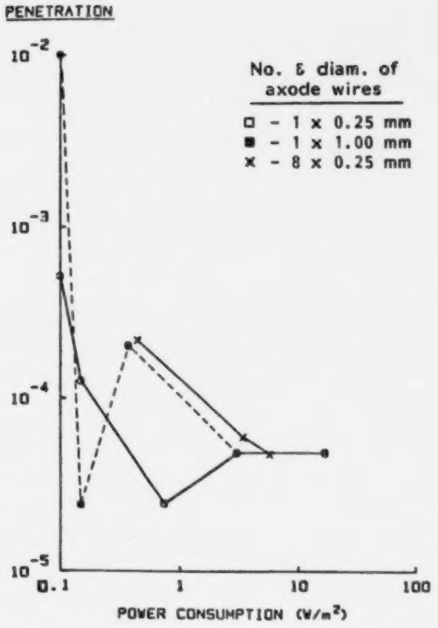

Figure 4 The same data as in Figure 3 plotted as a function of power consumption.

If now the PDR values are compared on the basis of the power consumed, as in Figure 2, the points for the three axodes are seen to coincide. Figures 3 and 4 show that this is also true for penetration. Although there is a great deal of scatter in the points in Figure 4, due mainly to the difficulty of measuring accurately penetrations of the order of 10^{-4}, it is clear that the values for the three axodes do not show the divergence seen in Figure 3. The interesting conclusion can therefore be drawn that the performance of a bag operating with an axode appears to be independent of axode diameter if comparison is on the basis of power consumption.

BAGS WITH DIFFERENT NUMBERS OF ELECTRODES

In order to study the dependence of pressure drop reduction on the number of bag electrodes, bags with 2, 7, and 14 wires were prepared and run for 24 one-hour cycles. The results, obtained with the eight-wire cable axode at 15 kV, are shown in Figure 5. A point is included in the figure for a bag with no wires, although the conditions were different for this point, as explained below.

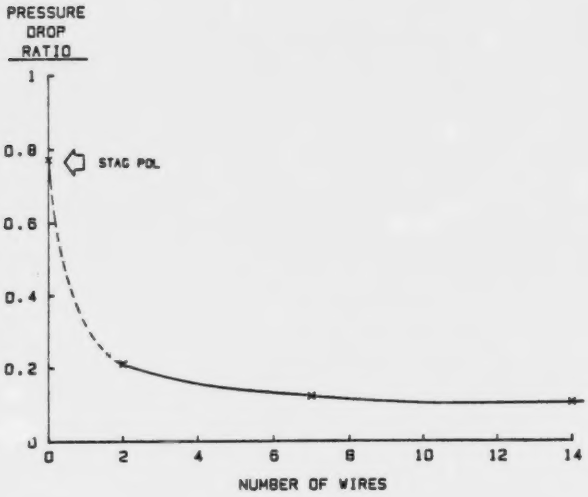

Figure 5 Dependence of PDR on number of electrode wires in the bag. All measurements at face velocity of 1.5 cm/s with an eight-wire axode at 15 kV.

Pressure drop in a bag operating with a charged axode is reduced from he level found in conventional filtration because of the Coulomb forces that rive the particles toward the bag and cause a dust distribution skewed toward he bag bottom. It might be assumed, therefore, that the effect of the lectric field depends on the potential difference between the axode and the ag. If the bag contains grounded electrodes, then the potential difference is simply equal to the potential applied to the axode. If the bag has no ires, but the axodes of neighboring bags are at opposite potentials, then he potential difference (ΔV) from axode to bag will be slightly smaller but f the same order of magnitude. For example, if the bag center-to-center istances are two bag diameters and neighboring axodes are at plus and minus 5 kV, the axode-to-bag ΔV will be 11.9 kV, rather than the 15 kV that it ould be with grounded bags. If the axode voltages are raised to about 19 kV, he axode-to-bag ΔV is raised back to 15 kV. Thus, with this simple device esignated "staggered polarity," or "stag pol," the ΔV can be duplicated with nly a modest increase in applied voltage. With "stag pol," a conventional aghouse could be converted to ESFF operation without the need to change bags. n addition, possible back corona effects would be eliminated, since the onditions giving rise to back corona would not exist.

With our one-bag baghouse, the principle clearly could be tested only by imulation. In the baghouse the bag occupied the center of a 30x40 cm space. lectrodes were suspended at the corners of the box, so that their distance rom the bag axis was 22 cm, or about twice the bag diameter. The corner lectrodes thus occupied the positions of the axodes in the four neighboring ags in a multibag baghouse.

The data point for "staggered polarity" in Figure 5, however, shows that this principle failed to give the pressure drop reductions obtained with bag electrodes. The figure also shows that within the range explored, the reduction in pressure drop increased with increasing numbers of bag wires. The work described in the following section was undertaken to explain this behavior.

AREAL DENSITY SCANNER

A device for scanning a bag and measuring the mass per unit area of deposited dust was constructed. The device uses a 100 microcurie strontium-90 source and a Geiger counter, both mounted so as to be kept in a constant relative position across a gap in the device into which the bag fits, as shown in Figure 6. Some degree of collimation was achieved by means of holes drilled in plastic pieces. The source was a small cylinder 2 mm in diameter and 10 mm long, and the actual radioactive material was a small pellet located at one end of the cylinder behind a 0.1 mm-thick window. The source was placed at the bottom of a 4-mm hole drilled in one of the plastic pieces. The counter was placed behind a second 13 mm thick plastic piece with a 4-mm hole drilled in it, the two holes aligned so that only a 4-mm beam could proceed unimpeded from source to counter. Because there was a tendency for the counter output to fluctuate rather severely, making accurate measurement difficult, the fluctuations were damped by placing a 1-mF capacitor across the recorder input.

For these measurements, the bag seam was not stitched, but was held by clamps. The bag was run for 2 hours, after which it was carefully removed from the baghouse and unclamped. The opened bag, now a rectangle of fabric, was placed in the scanner. The source and counter holder moved across the bag, and the output was fed to a recorder so that the dust mass distribution was displayed as a profile at a particular height in the bag. By repeating scans at different heights, a map of the distribution was obtained over the entire bag, providing an instant visual representation of the pattern of dust distribution obtained on the different bags. The scans showed that dust tends to be attracted to the wires, leaving comparatively cleaner areas in between.

Quantitative interpretation was made by taking numerous readings of the counter output from the recorder trace, and converting them to dust load densities using a calibration curve obtained separately. Such values are plotted in Figure 7. It was assumed that the resistance to flow, R_i, of an element of bag area was proportional to the areal density of dust deposited. By analogy with the rule for electrical resistors, the resistance R of the whole bag should then be given by

$$R = [\Sigma \frac{1}{R_i}]^{-1} \quad .$$

Since the flow was kept constant for all bags, the calculated resistance was proportional to the pressure drop, so that calculated resistances could be used to calculate in turn the pressure drop ratios shown in Table 1. It can be seen that these values are somewhat higher than those obtained directly from the measured pressure drops. The ranking is the same, however, indicating that the observed distribution is partly responsible for the

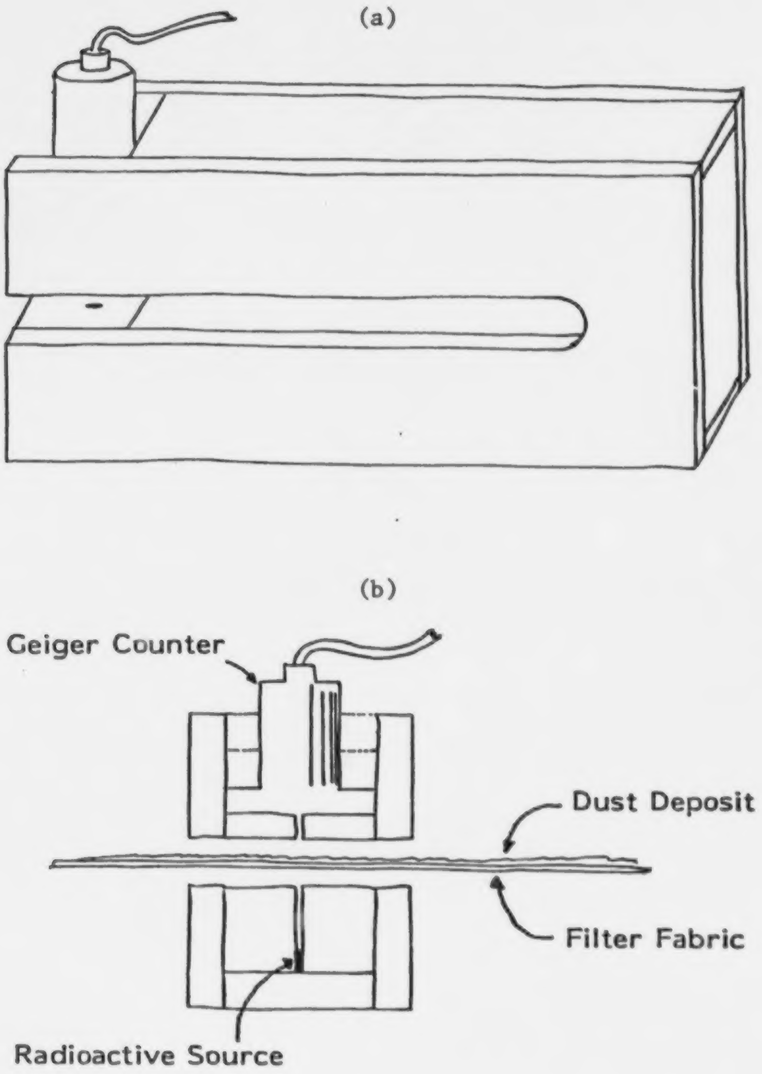
(a)
(b)
Geiger Counter
Dust Deposit
Filter Fabric
Radioactive Source

Figure 6 Device for measuring the areal density of the dust deposit on a filter fabric. a) Side view. b) End view.

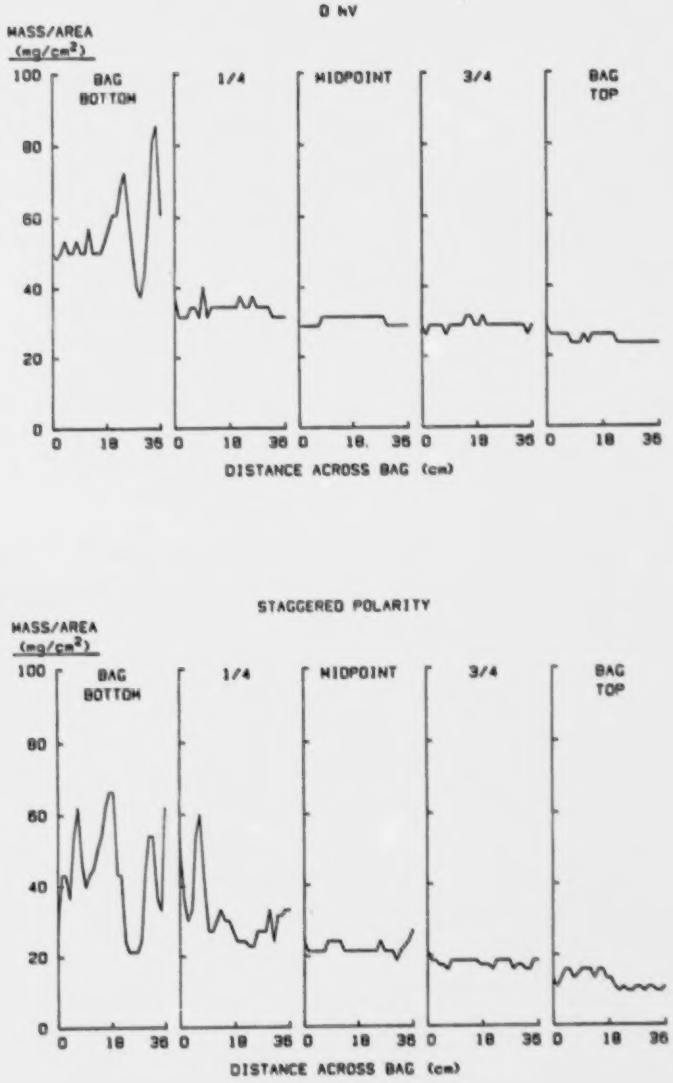

Figure 7 Areal density of dust measured by the scanner after filtration with no field applied to the eight-wire axode (0 kV), with staggered polarity, and with 15 kV on the cable axode and three different numbers of grounded bag electrodes. In the last three cases, the density peaks at the electrodes are clearly seen. Irregular formation at the bottom of the bag is probably due to turbulent flow. (Sheet 1 of 2.)

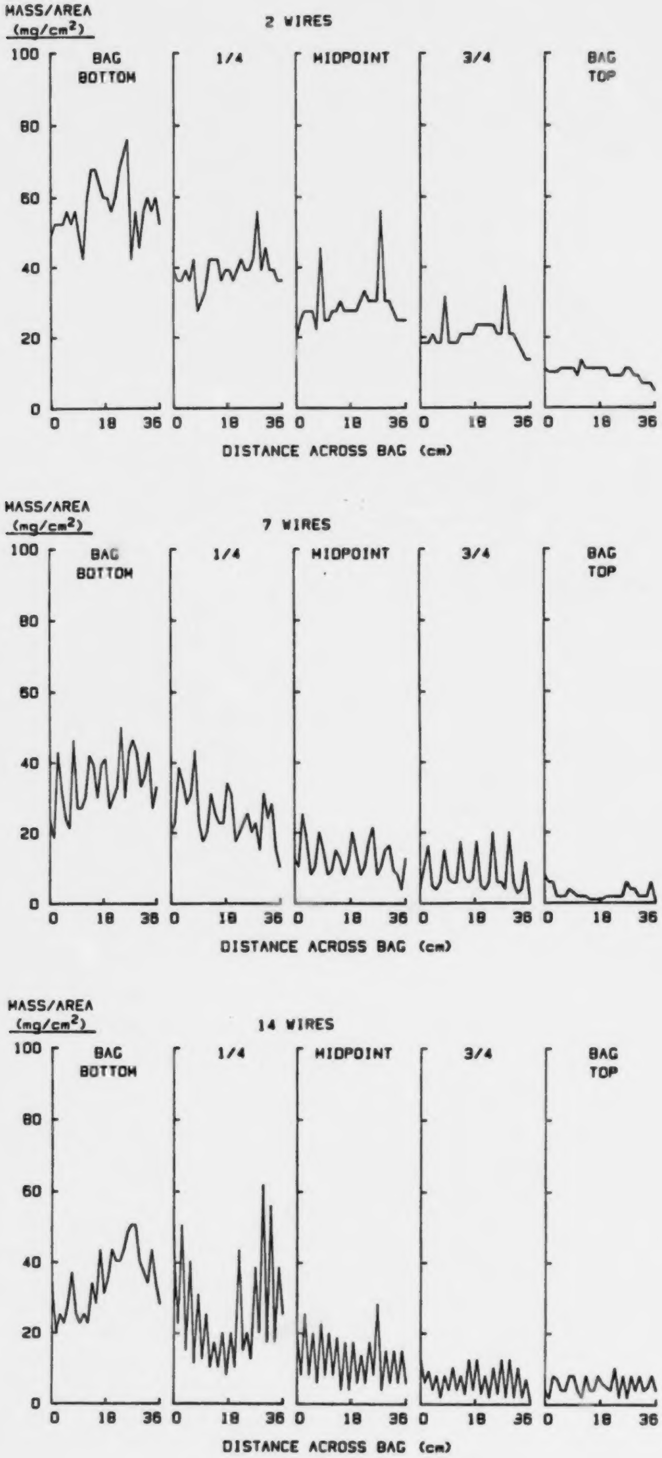

Figure 7 Sheet 2 of 2.

differences in performance. Another contributing factor may be that, with an electric field, the dust cake structure is more porous. This would yield pressure drops lower than might be predicted from areal density data and would account for the discrepancy between calculated and observed values. This possibility was not investigated.

TABLE 1. PRESSURE DROP RATIO AND MASS COLLECTED AFTER ONE TWO-HOUR FILTRATION CYCLE WITH VARIOUS ELECTRODE ARRANGEMENTS. $\Delta V = 15$ kV.

Number of wires in bag	Observed PDR	Calculated PDR	Total mass collected on bag (g)
No field	1.00	1.00	110
2	0.29	0.73	94
7	0.12	0.22	70
14	0.06	0.23	48
Stag pol, dead wt.	0.45	0.67	77
Stag pol, live wt.	0.35	0.53	52

Table 1 also lists the total mass of dust collected in the one-cycle measurements. It can be seen that, when a field is applied, the mass is consistently lower than without a field. It is not certain whether this is due to loss of dust on removing the bag or to some form of electrostatic repulsion which reduces the amount of dust that enters the bag during a run. Neither explanation appears plausible. The dust cake formed with an electric field is more fragile, and the heavy accumulations on the electrodes are more likely to fall off. Certainly some dust is seen to fall away no matter how carefully the bag is removed. However, a loss of about 50 percent seems hard to account for by this means. At the same time, it seems unlikely that electrostatic effects could be responsible, because the charged axode was shorter than the bag. The weight that kept the axode straight was connected to the axode by an insulator (dead weight). Charged dust particles would thus not be expected to come within the field generated by the axode until they were already inside the bag. However, some effect was detected when the insulator was replaced by a metal link. The weight, which protruded below the tube sheet, then became charged (live weight), and there was a noticeable drop in the mass collected (Figure 8) as well as in the PDR. The question has not been resolved, but the likelihood must be taken into account that pressure drop reduction is partly due to lower dust loading; i.e., to loss of dust from the air stream before it enters the bag. Even if this were shown to be a significant contribution, it would not necessarily alter the practical significance of the observed effects.

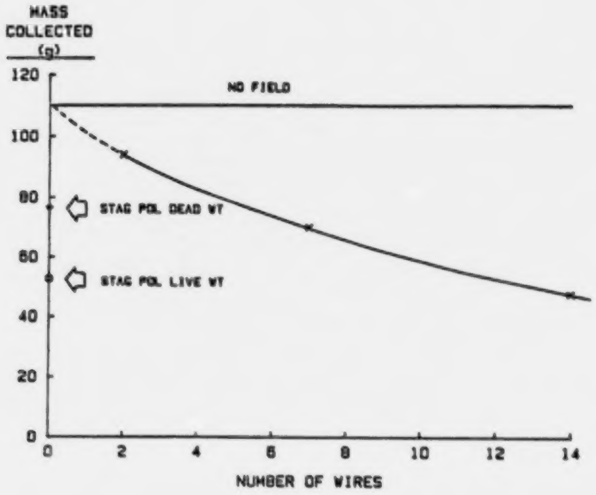

Figure 8 Dependence of total mass collected on number of grounded bag electrode wires. Eight-wire axode with $\Delta V = 15$ kV.

CONCLUSIONS

1) The performance of a bag operating with a charged axial electrode depends on the power consumed in the electrode circuit.

2) For acceptable ESFF performance, as few as two bag electrodes appear sufficient. Bag electrodes cannot be dispensed with altogether, as for instance by alternating polarities in adjacent bag axodes. With bag electrodes, dust distribution is altered in the tangential direction; that is to say, the dust accumulates on the electrodes, leaving comparatively clear spaces between. Measurements of areal dust density distributions confirm the importance of this effect.

3) Part of the pressure drop reduction produced by the axode may be due to reduced dust loading.

REFERENCES

1. Helfritch, D. J. Performance of Electrostatically Aided Fabric Filter. Chemical Engineering Progress. 73, August 1977.

2. Penney, G. W. Electrostatic Effects in Fabric Filtration, Volume I. EPA-600/7-78-142a (NTIS No. PB 288576). September 1978.

3. Van Turnhout, J., van Bochove, C., and van Veldhuizen, G. J. Electret Fibers for High Efficiency Filtration of Polluted Gases. Staub-Reinhaltung der Luft. 36: 36, 1976.

4. Van Osdell, D. W., Greiner, G. P., Lamb, G. E. R., and Hovis, L. S. Electrostatic Augmentation of Fabric Filtration. In: Third Symposium on the Transfer and Utilization of Particulate Control Technology, Volume I. EPA-600/9-82-005a (NTIS No. PB 83-149583). July 1982.

5. Rivers, R. D. Non-Ionizing Electrostatic Air Filters. ASHRAE Journal. 4: 37, February 1962.

6. Lamb, G. E. R. and Costanza, P. A. A Low-Energy Electrified Filter System. Filtration & Separation. 17: 319, 1980.

7. Lamb, G. E. R., Jones, R. I., and Lee, W. V. Electrical Stimulation of Fabric Filtration. Part IV: Enhancement by Particle Precharging. Textile Res. J. 54: 308, 1984.

8. Oak, M. J., Saville, D. A., and Lamb, G. E. R. Particle Capture on Fibers in Strong Electric Fields. J. Colloid Interface Sci. 106: 490, 1985.

9. Leith, D. and Ellenbecker, M. J. Overall and Particle-Size Dependent Mass Flux From a Pulse-Jet Filter. Paper presented at the Third World Filtration Congress, Downingtown, PA. September 1982.

10. Leith, D. S., Rudnick, S. N., and First, M. W. High Velocity, High Efficiency Aerosol Filtration. EPA-600/2-76-020 (NTIS No. PB 249457/AS), January 1976.

11. Lamb, G. E. R. and Costanza, P. A. Role of Filter Structure and Electrostatics in Dust-Cake Formation. Textile Res. J. 50: 661, 1980.

12. Miller, S. J. and Sears, D. R. The Influence of Coal-Specific Fly Ash Properties Upon Baghouse Performance: A Comparison of Two Extreme Examples. In: Proceedings: Fifth Symposium on the Transfer and Utilization of Particulate Control Technology, Volume 3. EPA-600/9-86-008c (NTIS No. PB 86-167178). February 1986.

13. Hovis, L. S., Daniel, B. E., and Donovan, R. P. Electrostatic Enhancement of Fabric Filtration of Fly Ash and Spray Dryer By-Products. Paper presented at EPRI Third Conference on Fabric Filter Technology for Coal-Fired Power Plants, Scottsdale, Arizona. November 1985.

STUDY OF ELECTROSTATICALLY STIMULATED FILTRATION FUNDAMENTALS

by: D. W. VanOsdell, A. S. Viner, and K. D. Carter
Center for Aerosol Technology
Research Triangle Institute
P. O. Box 12194
Research Triangle Park, North Carolina 27709

L. S. Hovis
Air and Energy Engineering Research Laboratory
U. S. Environmental Protection Agency
Research Triangle Park, North Carolina 27711

ABSTRACT

Electrostatically augmented (EA) filtration has been shown to perform better than conventional filtration. The fundamental causes of the improved performance remain unclear, however, and were the objects of this research. Preliminary results of bench-scale experiments conducted with an EA filter and of a mathematical modeling study of EA filtration are presented below. The performance of the experimental filter was evaluated by recording overall filter pressure drop at the operating face velocity and measuring filter permeability, dust cake mass, and dust cake porosity as functions of position on the filter. From these measurements, the specific resistance of the dust cake was calculated as a function of position on the filter. The mathematical model of the flow field and particle trajectories was used to predict the dust deposition pattern. Also, the dust cake resistance was estimated as a function of position and averaged over the filter surface.

The model showed that inertial forces were negligible under most conditions and that gravitational, fluid drag, and coulombic forces controlled the motion of the particles as they approached the filter surface. Coulombic forces dominated the particle trajectories under many conditions and, apparently, caused the visible particle accumulation near the electrodes. Though coulombic forces accounted for the gross distribution of dust on the filter, other forces appear to control the fine structure of the dust cake. Porosity and specific dust cake resistance were relatively constant over most of the filter surface. At high field strengths, a small increase in porosity (and consequent decrease in dust cake flow resistance) was observed near the electrodes.

This paper has been reviewed in accordance with the U. S. Environmental Protection Agency's peer review and administrative review policies and approved for presentation and publication.

INTRODUCTION

Electrostatic augmentation's potential for improving fabric filter performance has been demonstrated by a number of research groups. Many forms of EA filtration have been proposed and tested (1). It has been shown repeatedly that EA filters have a higher particle collection efficiency and a lower pressure drop than do conventional filters. This paper describes research on the form of EA filtration developed at Textile Research Institute (2) and known as electrostatically stimulated fabric filtration (ESFF). In ESFF, the electrostatic stimulation is created with parallel electrodes of alternating polarity which are located in the plane of the filter material. The gas flow is perpendicular to the plane of the electrodes. The particles are not artificially charged in the ESFF system.

Despite considerable effort, it has been difficult to determine exactly why an ESFF filter performs better than a conventional filter does, or how the electrical forces affect the filter and dust cake. While EA filters normally are both more efficient and have lower pressure drops than do conventional filters, the pressure drop reduction is most important. Conventional fabric filters already meet pollution control requirements, while high pressure drop increases the cost of the operation. For a fabric filter, pressure drop is commonly expressed as:

$$\Delta P = K_1V + K_2WV , \qquad (1)$$

where: ΔP = total filter pressure drop, Pa;
K_1 = cleaned filter drag, N s/m^3;
V = filter face velocity, m/s;
K_2 = dust cake specific flow resistance, 1/s; and
W = dust areal density, kg/m^2.

For an operating fabric filter, all of these parameters are averages obtained from the overall baghouse flows, pressure drop, and dust loads. K_1 is normally defined as the drag of a well broken-in fabric just after cleaning. For this research, however, the filters were not cleaned, and K_1 is the clean filter drag calculated from the initial pressure drop and the face velocity. Also, K_2 and W may describe either the entire filter cake or a smaller test region. Overall filter values of K_2 and W were determined from overall filter measurements, and local values of K_2 and W determined from the same measurements made on small portions of the dust cake.

The observed improvement in performance of the EA filter may result from at least three basic mechanisms (3).

1. Surface deposition of particles may be enhanced (2). This would occur because the electrical forces enhance collection of particles by fibers on the upstream side of the filter. In this mechanism, K_2 is reduced because more of the particles are collected in the low fiber density upstream region of the filter, and K_1 is reduced because the dust is more easily removed during cleaning.

2. It has also been shown that EA filtration changes the character of the dust deposit. The electric field may cause the dust to form a deposit that is more porous than that found without an electric field. Also postulated in the literature (3) is the possibility that the electric field strengthens the dust cake, making the porous structure less likely to collapse and increase flow resistance.

3. Performance improvements may be due to gross redistribution of dust on the filter. A nonuniform dust deposit results in improved pressure drop performance.

The primary purpose of the research described in this paper was to evaluate the relative importance to pressure drop reduction of the second and third mechanisms listed above. That is, are the improvements shown by EA filters caused by dust cake maldistribution due to coulombic forces, by porosity changes in the dust cake, or a combination of the two?

EXPERIMENTAL

OVERVIEW

The experimental portion of the work was conducted with a laboratory EA filter collecting fly ash redispersed in dry air. Once an adequate dust cake had been collected on a test filter, the filter and dust cake were removed from the apparatus and tested. These tests determined (as functions of position with respect to the electrodes) the permeability, dust areal density, and porosity. The specific dust cake flow resistance was calculated as a function of position, compared to the measured overall filter flow resistance and to predictions made based on dust deposit patterns from the model.

APPARATUS

Experimental Filter

Figure 1 is a schematic drawing of the experimental filtration equipment. Fly ash was fed from the screw feeder, dispersed by a jet of compressed air, then diluted further with compressed air to the proper flow rate. If desired, the particles could be neutralized (to Boltzman equilibrium) by exposing them to ions from a Kr-85 source. Between the neutralizer and the filter holder, the duct system was constructed of an acrylic sheet with a 10.2- by 10.2-cm cross section. The particle stream then passed through an electrical mobility control section. The electrical mobility control section was a parallel-plate electrostatic precipitator (ESP) which was operated at a potential difference sufficient to remove all particles above a target mobility. For this work the ESP voltage was less than 20 V. Flow through the ESP and the filter was upward to simplify mathematical modeling (gravity acting along the flow direction). The flow path was unobstructed to preserve a uniform flow stream near the filter. The filter dust cakes normally adhered well enough to the test filter so the filter could be removed without damaging the cake.

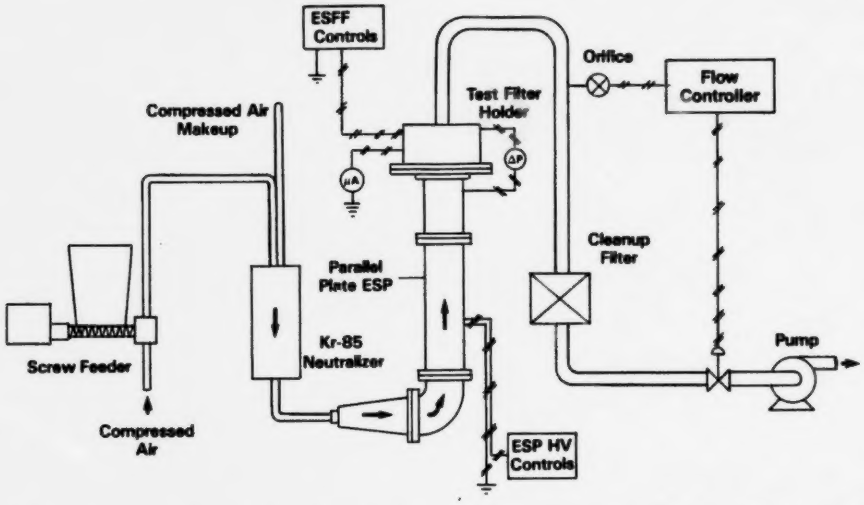
ESFF Controls
Compressed Air Makeup
Test Filter Holder
Orifice
Flow Controller
μA
ΔP
Parallel Plate ESP
Cleanup Filter
Kr-85 Neutralizer
Screw Feeder
Compressed Air
Pump
ESP HV Controls

Figure 1. Schematic drawing of laboratory ESFF test apparatus.

Figure 2 is a schematic drawing of the test filter holder. The test filter was supported by the EA electrodes (0.3175-cm-diameter steel rods). Alternate electrodes were connected to the positive and negative high voltage terminals of the power supply. For this research, the negative electrodes were grounded and the positive electrodes raised to the desired test voltage. Gelman A/E glass fiber filters were used. This filter medium is relatively smooth across the face and has a high enough efficiency to prevent most dust penetration into the filter. Thus, the study was focused primarily on the dust cake and was influenced only to a minor extent by interactions between the filter and the dust. Routine filter operating parameters such as flow rate (controlled by the flow controller) and filter pressure drop were recorded for each test run. The total dust mass which was collected on a filter also was determined.

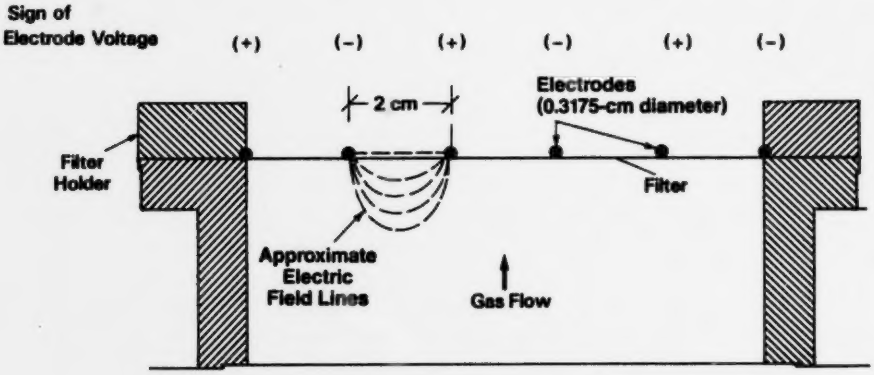
Sign of Electrode Voltage
(+)
(-)
(+)
(-)
(+)
(-)
2 cm
Electrodes (0.3175-cm diameter)
Filter Holder
Filter
Approximate Electric Field Lines
Gas Flow

Figure 2. Schematic drawing of test filter holder.

Redispersed Dust Properties

The particle size of the dust was determined at each test velocity with a cascade impactor. The net charge-to-mass ratio for the dust also was determined at each test velocity using a Faraday cup and internal filter. Electrical current from collected particles was measured with an electrometer. The dust mass was measured by weighing the filter.

Dust Cake Specific Flow Resistance

Evaluation of the mechanisms which cause EA filter enhancement required determining K_2 as a function of position on the filter. If K_2 were found to vary with position on the filter when the electric field was ON and not when it was OFF, then changes in the dust cake structure explain at least part of the EA effect. Determining the value of K_2 required measuring the flow rate at a known pressure drop (permeability) and the mass of dust per unit area (areal mass density) for the filter regions of interest. Wall effects were expected to have a significant impact on the dust cake in the vicinity of the filter holder wall. Therefore, measurements were made only between, and including, the four innermost electrodes. The test regions were narrow rectangles oriented parallel to the electrodes.

The overall filter permeability was determined for each filter cake from the final pressure drop and known flow rate. The flow resistance of the clean filter media was calculated from the initial pressure drop at a known flow rate. To measure permeability as a function of position, a filter holder incorporating 25 separate cells was constructed. Each cell was equipped for flow and pressure measurement. Figure 3 is a simplified drawing of the apparatus. The dimensions of the cells were 0.243 cm in width and 10 cm in length, and the test filter was placed in the apparatus with the electrode positions aligned along the cells' long axis. Thus, the measurement cells were parallel to the electrode positions.

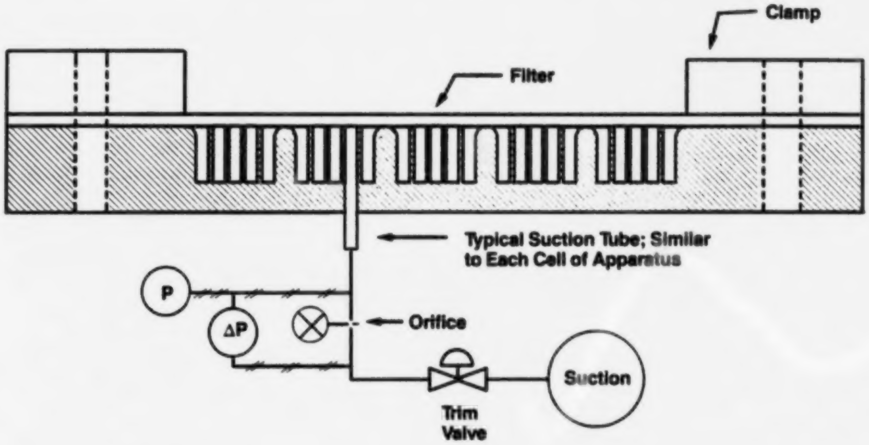

Figure 3. Schematic drawing of micropermeability tester.

A permeability measurement was made by adjusting each cell's valve to achieve the same target pressure downstream of the filter and then reading the flow rate for each cell. Flow leakage between cells was minimized because the downstream absolute pressures were the same in all the cells. Data were only collected from the middle 15 cells, but all cells were adjusted to have the same downstream pressure drop. The permeability of each test filter was measured at two or three fixed pressure drops which were each lower than the filter's maximum pressure drop during operation.

The overall areal mass density of the collected dust was measured for each test filter by weighing the filter before and after use. Division by the filtration area of 102.9 cm^2 gave the average. Areal density as a function of position was determined by Sr-90 beta particle attenuation (4). A schematic drawing of the beta source, Geiger tube, and movable carriage of the beta mass sensing instrument (beta gauge) is shown in Figure 4. The carriage was connected to the penholder of an upside-down digital plotter which moved the carriage to different locations on the filter. The beta particle beam was collimated in a slit and then passed through a rectangular region (approximately 0.107 cm deep by 1 cm wide) of the dust cake. The long axis of the beta beam was aligned parallel to the electrodes, and 33 areal density measurements were made on each pass across the filter. The measurement points corresponded to the center of each permeability apparatus cell and over the divider between each cell for the middle 15 positions. The beta attenuation instrument was calibrated against both glass fiber filters of known areal density and uniform dust cakes of known areal density. The results were essentially identical. The instrument was operated for a count period of about 17 s at 900 to 1200 counts/s, depending on the amount of attenuation. The pulses from the Geiger tube were accumulated in an event counter and transferred to a microcomputer at the end of each counting period. The same microcomputer controlled the movement of the carriage from one position to another.

Measurement of Porosity as a Function of Position

The appearance of the dust cakes collected on an EA filter suggests that the porosity of the dust collection may vary with position on the filter. Porosity of a dust cake may be calculated from:

$$\varepsilon = 1 - \frac{W}{\rho_p L}, \qquad (2)$$

where: ε = porosity, dimensionless;
ρ_p = density of individual particle, kg/m^3;
L = thickness of dust cake, m; and
W = dust areal density, kg/m^2.

W was determined by the beta gauge, while L was measured directly using a microscope to examine the cut edge of the deposit and a vernier scale (~ 3-μm divisions) to measure the thickness. All thickness measurements were performed on cuts made across the electrodes. Averaging several measurements made at the same position (relative to the electrodes)

rovided the thickness for that position. The porosity was determined
ithin the bounds of each cell of the permeability apparatus.

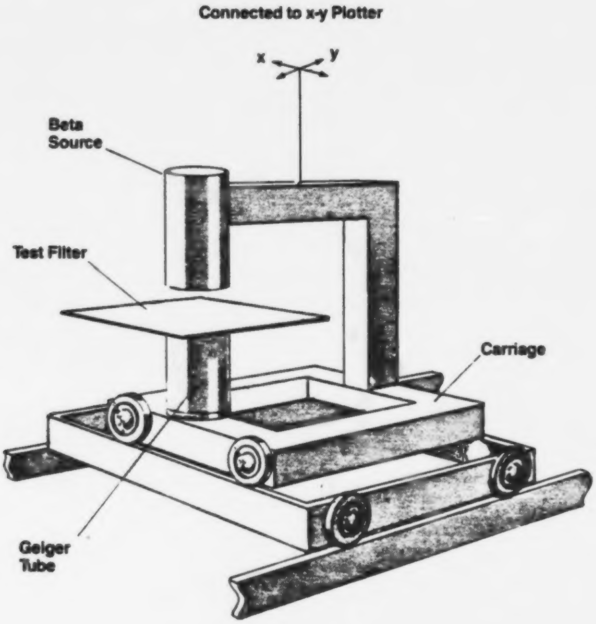

Figure 4. Drawing of beta gauge filter and carriage arrangement.

ESULTS

est Filter Appearance

Filters were tested at velocities of 0.01, 0.03, and 0.05 m/s and elec-
rode potentials of 0, 4, and 8 kV (with an electrode spacing of 0.02 m, and
or neutralized particles and particles having a maximum mobility of 1 ×
0^{-7} m^2/V s). In general, the dust deposits consisted of regions of rela-
ively uniform thickness between the electodes, with deposits of increased
hickness appearing directly over the electrodes. The deposits were uniform
ver the entire face of the filter when no potential was applied to the
lectrodes. Increasing the electric potential on the electrodes caused a
arger fraction of the deposition to occur at the electrodes, while increas-
ng the velocity tended to reduce the fraction of the deposition at the
lectrodes. The deposits at the positive (high voltage) electrode sometimes
ppeared to be less dense than those at the negative (grounded) electrode;
therwise, the deposits near the two electrodes were very similar.

Examples of filter deposits (for gas velocities of 0.01 m/s and 0-, 4-,
nd 8-kV electrode potential) appear in Figure 5. The 4- and 8-kV potential
ilters shown in Figure 5 display an extreme in the spectrum of dust cake
onuniformity. Even under microscopic examination no particles were found
n the clear regions. Dust cakes of this kind formed on the test filter
hen it was operated at a relative humidity (RH) near 30 percent. (At

(+)
Electrode Positions
(−)

a. 0 kV Potential and gas flow velocity of 0.01 m/s (Filter 2F4 photographed vertically downward)

(+)
Electrode Positions
(−)

b. 4 kV Potential and gas flow velocity of 0.01 m/s (Filter 711F1 photographed obliquely)

(+)
Electrode Positions
(−)

c. 8 kV Potential and gas flow velocity of 0.01 m/s (Filter 711F2 photographed obliquely)

Figure 5. Photographs of selected test filters.

10 percent or less RH, the dust cake appeared uniform except for increased deposits over the electrodes.) While the dust cakes shown in Figure 5 varied in depth between filters and on a single filter, the structure of the dust cakes was similar. The deposits over the electrodes were observed (while the filter was operating) to consist of dendritic particle aggregates aligned approximately perpendicular to the filter surface. The dendritic structure largely collapsed when the filter and dust cake were removed from the filter holder. The differences between dust cakes collected at high and low humidities are thought to be due to changes in the electric field caused by increased filter and dust conductivity at the higher humidity but have not yet been throughly investigated. The filters having very nonuniform deposits were chosen for presentation in this paper because they show the wide range of nonuniformity possible in an EA filter.

Filter Areal Density, Drag, and Specific Dust Cake Resistance

Figure 6 presents the areal density profiles for the three filters from Figure 5. The abscissa represents position along an edge of the dust cake, with the electrodes standing perpendicular to the plane of the page. If the filter identified in Figure 2 were removed from the filter holder and turned dust side up, the abscissa of Figure 6 would apply. The positive, high voltage electrodes were located at 0, 4, and 8 cm, while the negative, grounded electrodes were located at 2, 6, and 10 cm.

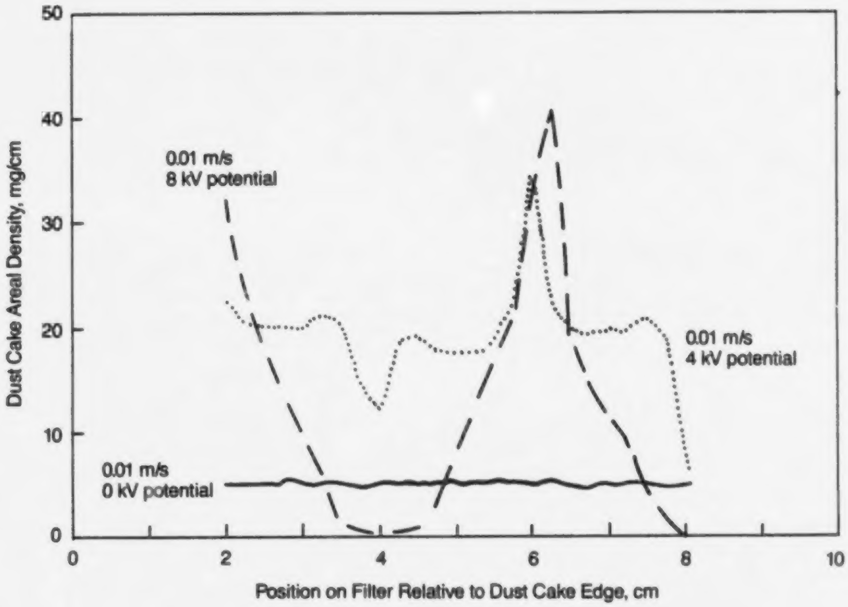

Figure 6. Measured dust cake areal density.

The areal density profiles agreed with the results expected based on visual inspection. Integrating the individual areal density measurements over the entire filter surface and comparing that to the density obtained by weighing the filter helped to verify the procedure. For these three filters, the beta gauging procedure indicated areal densities that were 101, 102, and 119 percent, respectively, of those values determined by weighing the dust deposit. The filter face velocities obtained from the permeability measurements are shown in Figure 7. The dust cake permeability measurements for each test cell maintained an inverse relationship to the dust cake areal density. This behavior would be expected if the dust cake specific flow resistance were relatively constant.

Figure 8 displays K_2 calculated as a function of position for the three filters. K_2 was calculated by applying Equation 1 to a single region of the filter and substituting the measured values of K_1, W, and V for that region. The K_2 calculations were sensitive to errors in W. These errors became relatively large at low areal densities, as in the 8-kV case. Some of the extremely large and small K_2 values were omitted from Figure 8. The integrated average of the individual K_2 values were 103, 105, and 240 percent, respectively, of the overall K_2 for the three filters. The very large difference for the 8-kV case arises from the extremely large values of K_2 that were calculated in the low areal density regions of the filter.

Filter Porosity and Calculated K_2

Figure 9 presents the results of dust cake thickness measurements for the three filters. Each data point is the average of five measurements made at the indicated position. From these thickness measurements, Equation 2 was used to calculate the porosity of the dust cake. The calculated porosities for the three filters appear in Figure 10. The extreme variations in porosity near the electrodes for the 8-kV potential case were suspect because the relative errors in the thickness and the areal density measurements became significant for thin dust deposits. Some points were omitted from Figure 10 because they were well off-scale. However, measurement error does not explain all of the K_2 variations near the electrodes. Apparently the porosity in the vicinity of the electrodes was reduced by the electric field. Additional measurements for dust cakes collected at high potential will be required to confirm this phenomenon, given the high variability of the data.

From these porosity measurements and the data on particle size, it was possible to calculate K_2 as a function of position on the filter. Rudnick's slip flow formula (5) was used to calculate the K_2 values shown in Figure 11. The calculated K_1 values depend strongly on the porosity. By comparing Figures 8 and 11, one can see that the K_2 values calculated from the porosity measurements using Rudnick's slip flow equation do not agree very well with those calculated from the permeability measurements. This is not very surprising, because Rudnick's procedure was not presumed to provide more than a first estimate of K_2 (6). In this case, the porosity of the test dust is greater than is common for fly ash, and larger-than-normal errors could be expected. The greatest differences between Rudnick's equation and the data occur for the 0 kV potential case.

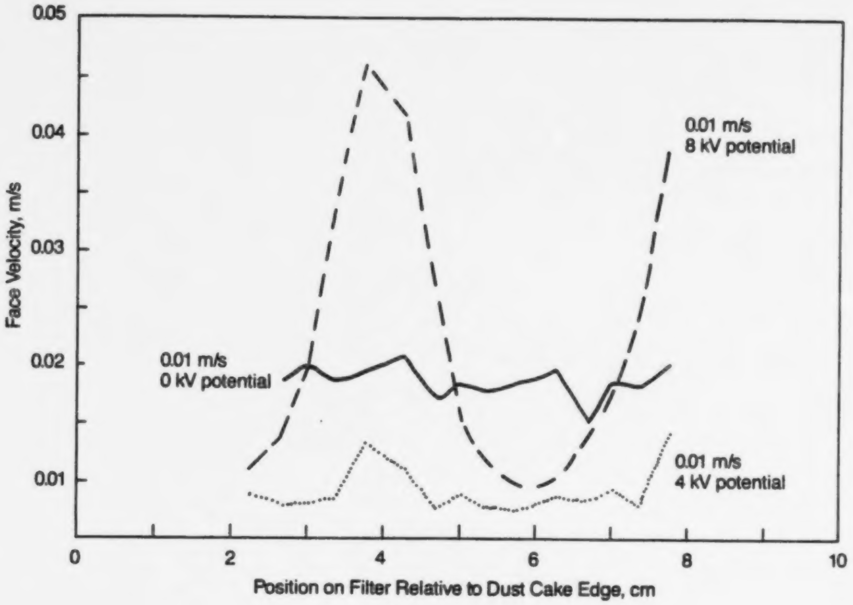

Figure 7. Measured face velocity through filter at 0.50 kPa pressure drop.

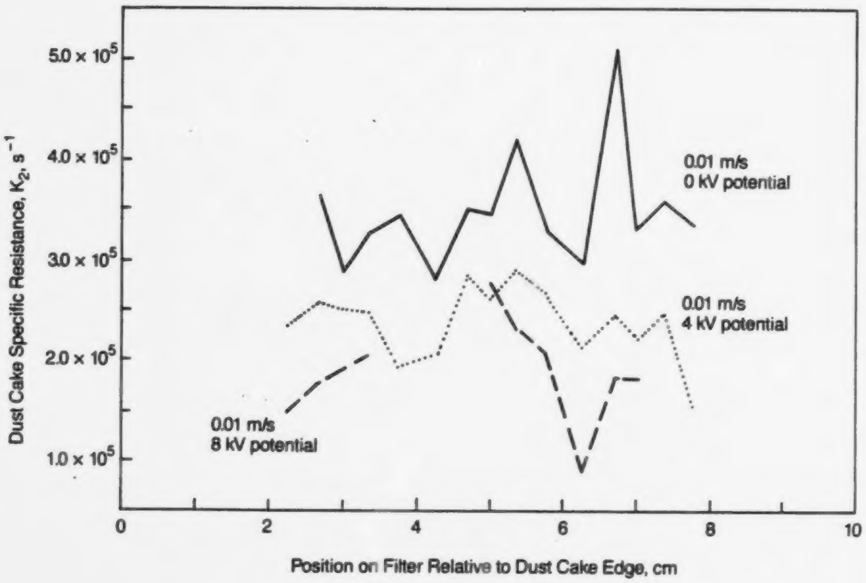

Figure 8. K_2 calculated from measured areal density and face velocity.

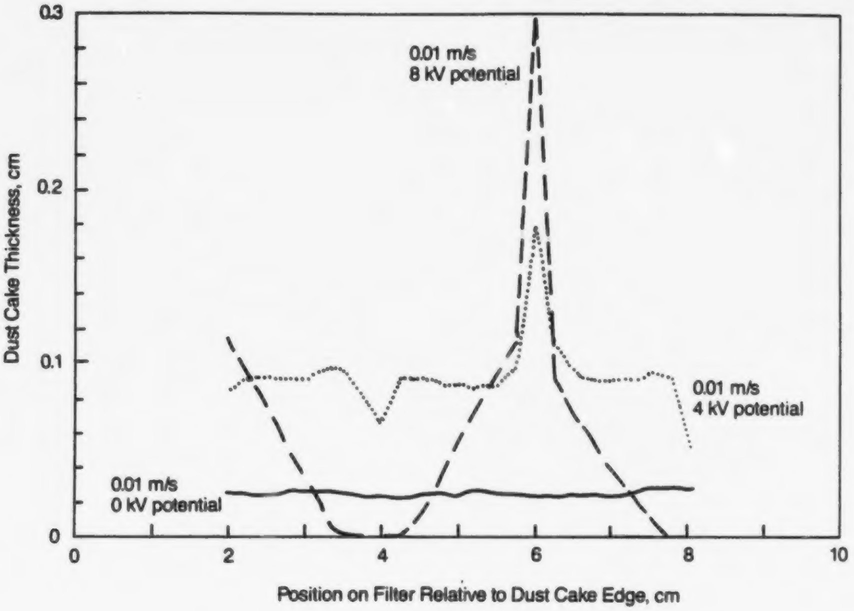

Figure 9. Measured dust cake thickness.

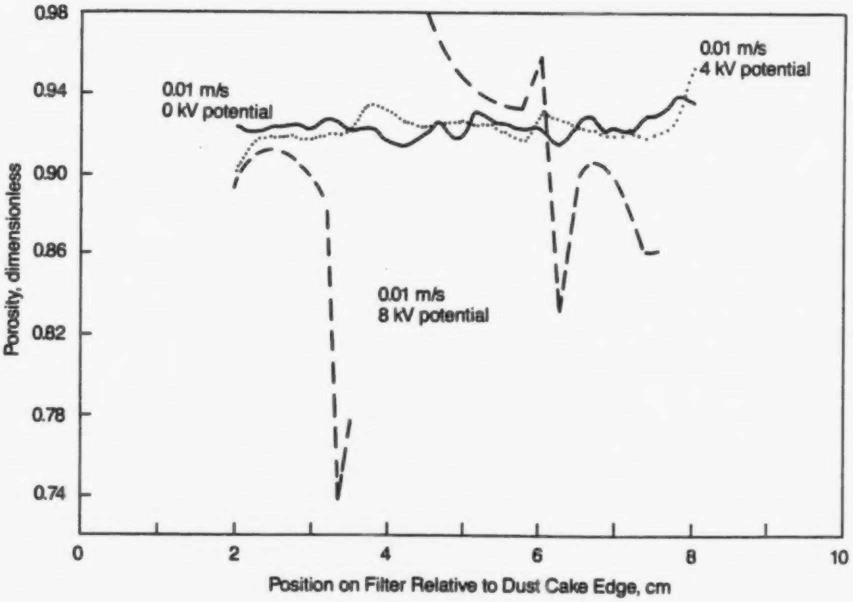

Figure 10. Porosity calculated from thickness measurement.

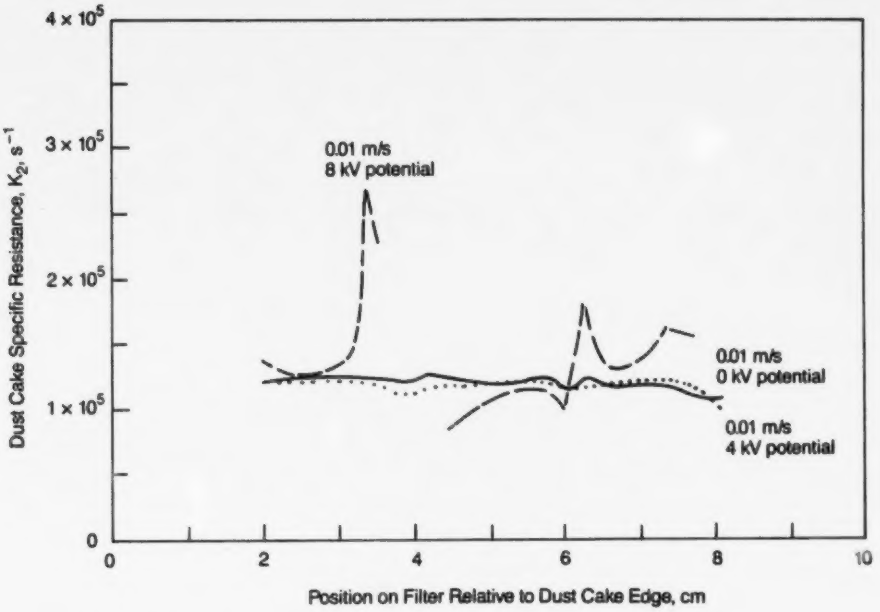

Figure 11. K_2 calculated from measured porosity and particle size using Rudnick's slip-flow formula (5).

MODELING

A mathematical model was developed to evaluate the significance of the experimental results. Only a brief description is possible in this paper. Using an upwind-differencing technique (7), the model first calculated the flow field for a rectangular region extending from a starting position 2 electrode spacings away from the filter to the filter surface. In width, the region extended from the centerline of one electrode to the centerline of an adjacent electrode (having opposite polarity).

The initial flow field was calculated by assuming a uniform velocity coming into the region, mirror-image boundaries at the sides (above the two electrodes), and a uniform velocity profile at the filter. Once the flow field was determined, particle trajectories were calculated numerically for particles having the desired diameter and a particular electrical mobility or range of mobilities. The particle trajectory calculations were started at 321 locations along the upstream boundary of the region. Both positive and negative particles are assumed to be present. The particle equation of motion included gravity, the coulombic force term, and the fluid drag. Inertial forces were shown to be negligible for the operating region of interest and were not included. The model noted the point at which the collected particles contacted the filter and accumulated records of the calculated mass distribution between the electrodes. From a calculated value of K_2 and the estimated areal distribution, the flow resistance of the dust deposit as a function of position was calculated. In addition, the overall average K_2 and pressure drop were computed. The results of the cycle were printed, along with a graph showing the dust mass distribution calculated for the cycle.

Following a given cycle, the calculated areal density was used to update the filter velocity profile. This new velocity profile was then used to recalculate the flow field, and new particle trajectories were computed. The cycle was repeated until a target final pressure drop was reached.

The model successfully predicted the appearance of the dust deposits from the relatively low humidity filter runs because the form of the electric field is relatively well understood for that case. In the high humidity case, the electric field is changed by the filter and dust cake conductivity, and the model has not been modified to accommodate that electric field distribution. The low humidity case is thought to be representative of most fabric filter applications. Prediction of K_2 for the model suffered from the same lack of a suitable predictive equation as did K_2 prediction from the porosity distribution.

CONCLUSIONS

1. Experimental procedures were developed that permitted the analysis of filter performance over small filter areas and, thus, small-scale phenomena.

2. While coulombic forces appear to account for the general appearance of the ESFF patch filter dust cakes, they did not account for the fine structure of the ESFF dust cake in the region near the electrodes.

3. For the dust under consideration, applying Rudnick's slip flow equation resulted in values of K_2 which were less than the experimental values by a factor of 2 to 3. The larger deviations occurred when no electric field was present.

REFERENCES

1. Donovan, R.P. and VanOsdell, D.W. Electrical Enhancement of Fabric Filtration. In: N.P. Cheremisinoff, (ed.), Encyclopedia of Fluid Mechanics, Volume IV, Solids and Gas-Solids Flows, Chap. 46. Gulf Publishing Company, 1986.

2. Lamb, G.E.R. and Costanza, P.A. A Low-Energy Electrified Filter System. Filtration and Separation. 17: 319, July/August 1980.

3. VanOsdell, D.W., Donovan, R.P., and Hovis, L.S. Flow Resistance Reduction Mechanisms for Electrostatically Augmented Filtration. In: Proceedings: Fifth Symposium on the Transfer and Utilization of Particulate Control Technology, Volume 3. EPA-600/9-86-008c (NTIS PB 86 167 178), U. S. Environmental Protection Agency, Research Triangle Park, North Carolina, February 1986. p. 18-1.

4. Viner, A.S., Gardner, R.P., and Hovis, L.S. Measurement of The Spatial Distribution of Mass on a Filter. In: Proceedings: Fifth Symposium on the Transfer and Utilization of Particulate Control Technology, Volume 3. EPA-600/9-86-008c (NTIS PB 86 167 178), U. S. Environmental Protection Agency, Research Triangle Park, North Carolina, February 1986. p. 14-1.

5. Rudnick, S. N. Fundamental Factors Governing Specific Resistance of Filter Dust Cakes. Sc. D. Dissertation, Environmental Health Sciences, Harvard University, 1978.

6. Dennis, R. and J.A. Dirgo. Comparison of Laboratory and Field Derived K2 Values for Dust Collected on Fabric Filters. Filtration and Separation. 18(5): 394, September/October, 1981.

7. Yeh, H-C. A Fundamental Study of Aerosol Filtration by Fibrous Filters. Ph. D. Dissertation, Mechanical Engineering, University of Minnesota, 1972.

Session B-2: FF: ADVANCED CONCEPTS II

Norman Plaks, Chairman
U. S. EPA/AEERL
Research Triangle Park, NC

MATHEMATICAL MODEL FOR ADVANCED ELECTRICALLY STIMULATED FABRIC FILTRATION

Toshiaki Yamamoto, David S. Ensor
Research Triangle Institute
Research Triangle Park, North Carolina 27709

and

Ronald B. Mosley, Louis S. Hovis, Norman Plaks
Air and Energy Engineering Research Laboratory
U.S. Environmental Protection Agency
Research Triangle Park, North Carolina 27711

ABSTRACT

Laboratory and pilot studies have demonstrated successfully that an advanced center-wire Electrically Stimulated Fabric Filter (ESFF) can be operated at a significantly lower pressure drop than a conventional reverse-air fabric filter.

A comprehensive mathematical model has been developed to predict behavior and detailed deposition processes of the ESFF. The model incorporates flow modification that results from variations in particle distributions on the bag filter. Time-dependent gas streamlines, particle streamlines, and mass distributions are evaluated, and the corresponding areal mass density, pressure drop ratio (PDR), and modified specific resistance coefficient (K_2^*) are demonstrated for typical ESFF operating conditions.

The results obtained from the model study illustrate a significant reduction in the pressure drop and provide an insight into the deposition process. Laboratory and pilot studies, performed for a range of operating parameters, support the model's conclusions.

This paper has been reviewed in accordance with the U.S. Environmental Protection Agency's peer and administrative review policies and approved for presentation and publication.

MATHEMATICAL MODEL FOR ADVANCED ELECTRICALLY STIMULATED FABRIC FILTRATION

INTRODUCTION

Advanced Electrically Stimulated Fabric Filtration (ESFF), in which the corona wire resides at the center and the bag filter surface is grounded, has been demonstrated successfully in laboratory and pilot plant studies using pulverized coal ashes (1,2). The results indicate a significant reduction in overall pressure drop during a typical filtration cycle when compared with conventional reverse-air fabric filtration.

A detailed knowledge of the particle deposition process is essential for a further understanding of fabric filtration. In conjunction with both laboratory and pilot studies, an existing mathematical model with an advanced ESFF configuration (3) was further extended to incorporate changes in the flow field that resulted from variations in particle distributions on the bag filter. Time-dependent gas streamlines, particle streamlines, and mass distributions were evaluated, and the corresponding areal mass density, pressure drop ratio (PDR), and modified specific resistance coefficient (K_2^*) values are demonstrated for typical ESFF operating conditions. This paper focuses on a detailed formulation of the mathematical model with detailed illustrations of the deposition process.

MATHEMATICAL MODELING

FORMULATION WITHOUT DUST CAKE

Figure 1 depicts the advanced ESFF reverse-air configuration where the flow comes from the bottom and leaves through the side of the filter. The corona wire resides at the center where the high voltage power supply is applied. The model first calculates flow field and particle trajectories for a single-size particle. At this point, the values for both the electric field strength and the velocity of an individual particle moving toward the filter surface are calculated. The model then determines the composite dust deposition profile for an assumed particle size distribution. During the time interval, the gas streamlines are assumed to be unchanged by the deposited particles. A detailed description of the methodologies follows.

Gas Streamlines

Solving the Navier-Stokes equation with appropriate boundary conditions is appropriate for determining the flow field. However, certain, suitably chosen, analytical functions that satisfy the boundary conditions would be similar to solutions of the Navier-Stokes equation. This is especially true with large aspect ratios (ratios of the filter length [L] to the filter radius [R]). Figure 2 presents a schematic diagram and coordinate system for the advanced ESFF configuration. By assuming uniform distributions of inlet and outlet flow velocity (U_0 and V_0, respectively), the intercepting points z_i for the gas streamline (Ψ_i, starting at the position r_i) can be determined by applying the mass conservation conditions:

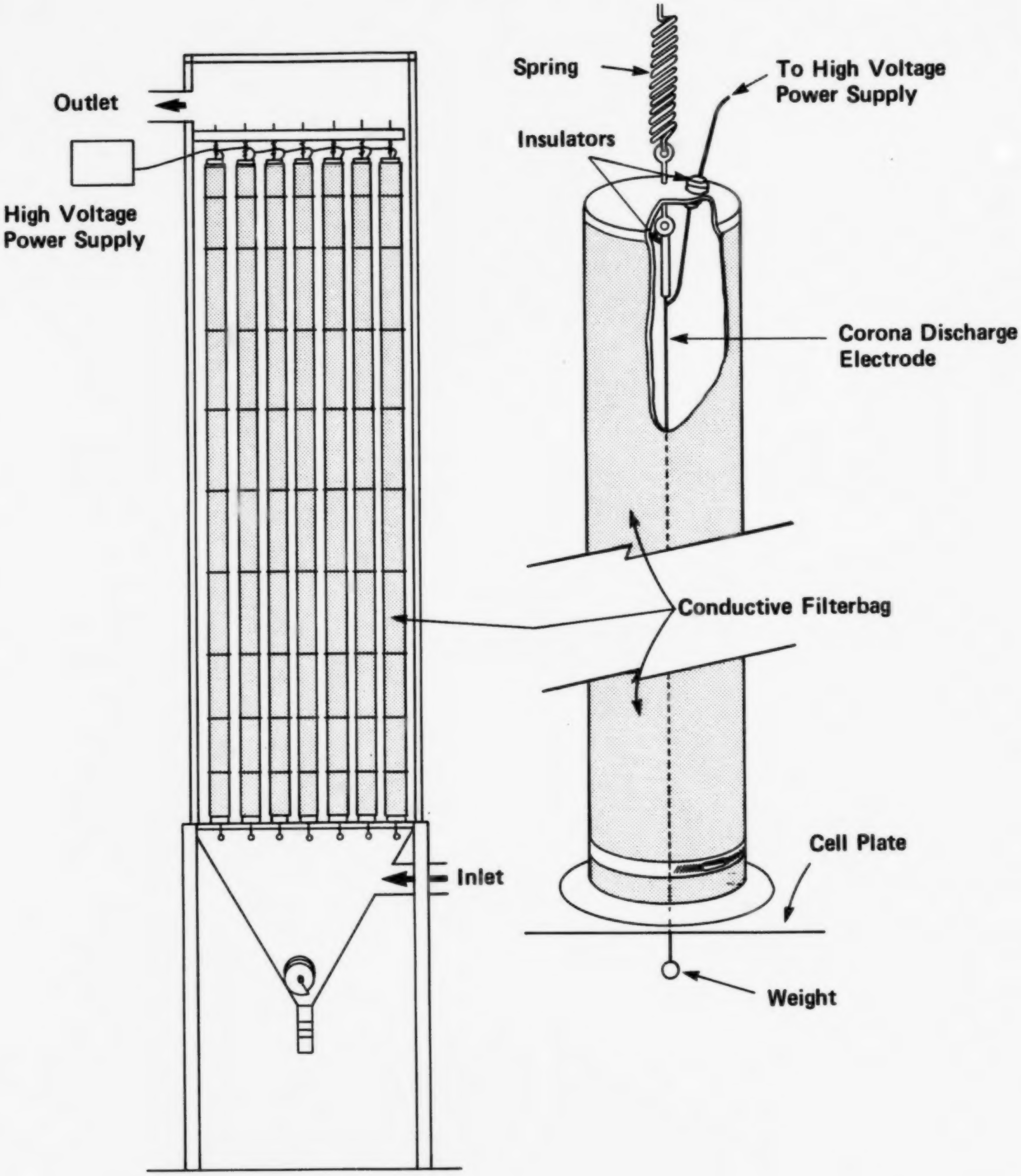
Spring
To High Voltage Power Supply
Outlet
Insulators
High Voltage Power Supply
Corona Discharge Electrode
Conductive Filterbag
Cell Plate
Inlet
Weight

Figure 1. Advanced ESFF reverse-air configuration.

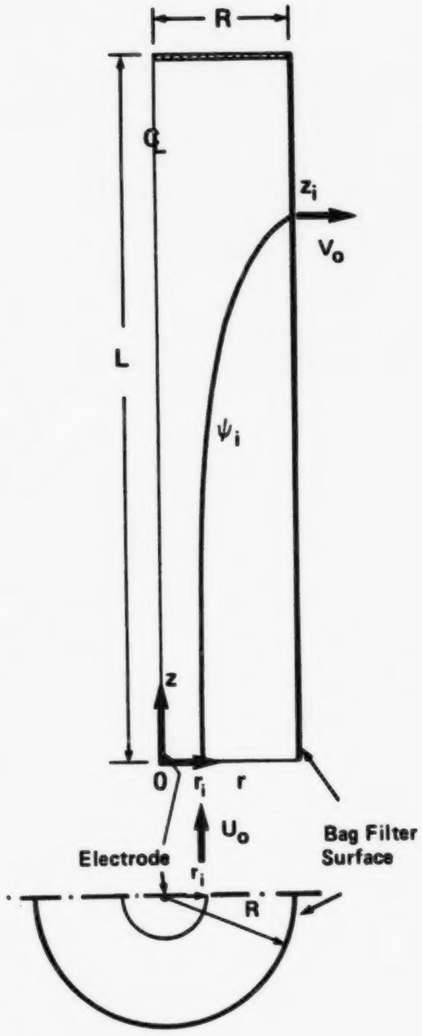
R
L
℄
z_i
V_o
ψ_i
z
0
r_i
r
U_o
Electrode
r_i
R
Bag Filter Surface

Figure 2. Schematic diagram and coordinate system for advanced ESFF.

$$z_i = L - \left(\frac{U_o}{V_o}\right) \frac{r_i^2}{2R} = L \left[1 - \left(\frac{r_i}{R}\right)^2 \right]. \tag{1}$$

A quasi-theoretical, super elliptic function is assumed for the spatial dependence (r,z) of a given gas streamline, Ψ_i, which is represented by:

$$r = R \left\{ 1 - \left[1 - \left(\frac{r_i}{R}\right)\right]\left[1 - \left(\frac{z}{z_i}\right)^n \right]^{1/n} \right\}_{\Psi_i} . \tag{2}$$

A value of n = 2 was used in this presentation. The radius (R) at the filter inlet is divided into 10 segments (i = 10), and the bag length (L) is divided into 40 segments (n = 40) in the z-direction.

Particle Charging

In field-charging theory, the charge on a nonconductive particle [q(t)] is given as a function of time by:

$$q(t) = q_s \frac{1}{(1 + \tau/t)} , \tag{3}$$

where

$$q_s = 12 \pi \frac{k}{(k+2)} \epsilon_o a^2 E_o \tag{4}$$

$$\tau = \frac{4\epsilon_o E_o}{J} , \tag{5}$$

where q_s = saturation charge; $E_o = V/R$ = average field; V = applied voltage; J = current density; k = relative dielectric constant; ϵ_o = permittivity of vacuum; and a = particle radius.

For typical ESFF operation with a dielectric particle ($E_o = 3.0\times10^5$ V/m, $J = 1\times10^{-4}$ A/m^2), the time constant (τ) becomes 0.1 second from Equation (5). Because the value of charging time (t) is several times greater than τ, it is reasonable to assume that the charge on the particles is close to that of the saturation charge (q_s).

Particle Mobility

If particle inertia is ignored, the migration velocity (V_p) of the charged particle under the influence of an electric field can be expressed as:

$$V_p = \frac{C_c \, q \, E}{6 \pi \eta a} = K_p E , \tag{6}$$

re C_c = 1.0 = Cunningham slip coefficient, and η = viscosity of the gas.

refore, the particle mobility (K_p) can be written as:

$$K_p = \frac{qC_c}{6\,\pi\,\eta\,a} = \frac{2\epsilon_0 ka\ C_c E_0}{(k+2)\,\eta} = f\,(E_0,a,\eta) \quad . \tag{7}$$

particle mobility becomes a function of both a and E_0 for known gas rmodynamic properties.

ctric Field

Due to axial symmetry, the electric field function for the wire-cylinder ctrodes reduces to a one-dimensional problem if end effects are ignored. the ionic space charges are ignored, the electric field at any radius r)] can be determined from the relationship:

$$E(r) = \frac{V}{r\ \ln\,(R/r_a)} \quad , \tag{8}$$

re r_a = the radius of the discharge wire. The local migration velocity of charged particle [$V_p(r,z)$] is obtained by substituting Equations (8) and in Equation (6).

ticle Trajectories

Figure 3 shows a schematic diagram of both gas (Ψ_i) and particle (Φ_i) eamlines, starting at the position r_i. The position (r',z') for Φ_i can be ressed by:

$$(r_n{}')_{\Phi_i} = \left[r'_{n-1} + \left(\frac{\Delta z}{w_{n-1}}\right) V_{p_{n-1}} + (r_n - r_{n-1})\right]_{\Psi_i} \quad . \tag{9}$$

The gas velocity in the z direction [w(r,z)] is determined by the gas eamlines. This velocity varies from w(r,0) = U_0 at the filter inlet to ,z) = 0 at the outlet; whereas, gas velocity in the r-direction varies from r,0) = 0 to $v_r(R,z)$ = V_0. Therefore, w(r,z) for a given Ψ_i at location n the z-direction is expressed as:

$$w_n = w_{n-1}\left[1 - \left(\frac{r_n - r_{n-1}}{R - r_n}\right)\right]_{\Psi_i} \quad . \tag{10}$$

The particle behavior can be described by introducing the dimensionless ES ber (3) and then defining it as:

$$N_{ES} = \frac{K_p\ E_o}{A/C} = g\left(\frac{a\ E_o{}^2 L}{U_o\ R\ \eta}\right) \quad , \tag{11}$$

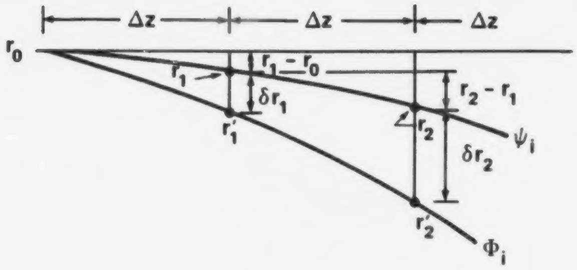

Figure 3. Schematic diagram of gas (Ψ_i) and particle (Φ_i) streamlines.

where A/C = air-to-cloth ratio and g = constant. The ES number is the ratio of the average particle migration velocity to the filter face velocity. The higher the ES number, the greater the effect of electrostatic enhancement becomes. One can see from Equation (7) or (11) that direct enhancement is attained by increasing a, E_0, and L and decreasing U_0, R, and η.

Composite Layer Distribution

The relative layer thickness (l_i) can be determined in terms of adjacent gas and particle streamlines for a single particle size:

$$l_i = \left(\frac{z_{\Psi_i} - z_{\Psi_{i-1}}}{z_{\Phi_i} - z_{\Phi_{i-1}}} \right)_{r = R} . \tag{12}$$

Note that the flow streamlines are assumed to be undisturbed during the time interval. When a particle size distribution is assumed, the mass fraction in each particle size band is calculated. The areal mass density distribution then is computed by summing the fraction of total mass contained in that particular size band. In this presentation, a log-normal particle size distribution was used.

FORMULATION WITH DUST CAKE

The flow field must be modified because of the deposited particles. Similar calculations are repeated after the gas streamlines have been changed. Time-dependent areal mass density, modified specific resistance coefficient (K_2^*), and PDR then are calculated. The specific resistance coefficient of the dust cake for the conventional bag filter (K_2), inlet flow velocity (U_0), and particle concentration (C) are assumed to be constant.

Flow Modification

As a result of the earlier calculations for the composite layer distribution, the local areal mass density and face velocity distributions are determined. In classical theory the local flow resistance (S_i) is expressed as:

$$S_i = S_r + K_2 W_i \tag{13}$$

$$W_i = \left(\frac{CU_o Dt}{4L}\right)\bar{T}_i \quad , \tag{14}$$

where $\sum_{i=1}^{n} \bar{T}_i = 1.0$, $\bar{T}_i$ = relative dust thickness, S_r = the residual stress when the bag is clean, W_i = local areal mass density, t = time, and D = bag diameter.

In the case of ESFF, the flow resistance at segment i (S_i) can be expressed:

$$S_i = S_r + K_2 W_i = S_r + K_2\left(\frac{CU_o Dt}{4L}\right)\bar{T}_i \quad . \tag{15}$$

Therefore, the overall drag (S) caused by the fabric and any accumulated dust becomes:

$$S(t) = \left(\sum_{i=1}^{n} A_i/S_i\right)^{-1} A = \frac{1}{\left(\frac{\Delta\bar{z}_1}{S_1} + \frac{\Delta\bar{z}_2}{S_2} + \ldots. + \frac{\Delta\bar{z}_n}{S_n}\right)}$$

$$= \left[\sum_{i=1}^{n}\left(\frac{\Delta\bar{z}_i}{S_r + K_2 W \bar{T}_i}\right)\right]^{-1} = S_r^* + K_2^* W \quad , \tag{16}$$

where A = filter face area; A_i = filter face area at the segment i; $\Delta\bar{z}_i$ = $\Delta z/L$; W = average areal mass density; S_r^* = residual stress for ESFF (= S_r though commonly less than that of the conventional bag filter); and K_2^* = modified K_2 value for the ESFF resulting from the nonuniform dust layer.

The pressure drop after the time interval, t_o , is written:

$$P(t_o) = S(t_o)V_o \quad . \tag{17}$$

Because the pressure drop is the same through all areas of the dust layer, the local velocity (v_i) can be calculated by:

$$v_i(t_o) = P(t_o)/S_i(t_o) \quad . \tag{18}$$

The points at which the gas streamlines intersect the fabric surface are modified in a manner that conserves the total mass of the gas. The new points of intersection (z_i^*) can be determined by:

$$z_i^* = \frac{1}{U_o} \sum_{i=1}^{n} v_i \, z_i \quad . \tag{19}$$

The flow streamlines are recalculated by substituting z_i^* into z_i in Equation (2). The particle trajectories and composite layer distribution are calculated according to the modified flow field. Then the areal mass density distribution is computed by summing the mass fractions contained in the particle size bands. The relative thickness ($\bar{T}_i^*$), with respect to initial uniform layer thickness, now is expressed in terms of initial z_i, modified particle trajectories, and face velocity:

$$\bar{T}_i^*(t_o) = \left(\frac{z_{\psi_i} - z_{\psi_{i-1}}}{z_{\phi'_i} - z_{\phi'_{i-1}}} \right) \left(\frac{v_i}{V_o} \right) \quad . \tag{20}$$

The values of time-dependent modified K_2^* and PDR can be calculated by:

$$K_2^*(t_o) = \frac{1}{W} \left\{ \left[\sum_{i=1}^{n} \left(\frac{\Delta z_{\phi_i}}{S_r + K_2 W \, T_i} \right) \right]^{-1} - S_r^* \right\} \tag{21}$$

$$\text{PDR}\ (t_o) = \frac{K_2^*\ (t_o)}{K_2} \quad . \tag{22}$$

These simulations are repeated in a similar manner for each time increment. Time-dependent areal mass density and PDR, resulting from the variations in dust thickness, are obtained.

RESULTS AND DISCUSSION

The simulations were performed by using a spreadsheet (Lotus 1-2-3) under the following conditions: D = 0.204 m (8 in.); L = 7.32 m (24 ft); A/C = 1.22 m/min (4 ft/min); T = 150 °C (300 °F); V = 23 kV; $2r_a$ = 3.2 mm (1/8 in.); bulk density of the particles = 1.5 g/cm^3, K_2 = 3.0 N-min/g-m; S_r = 350 N-min/m^3, with uniform inlet gas velocity and uniform particle concentration, C = 4.59 g/m^3 (2.0 gr/ft^3). The log-normal particle distribution with a mass mean diameter (MMD) of 10.0 µm and a standard deviation of 1.65 were assumed. Particle trajectory calculations were performed for 1-, 4-, 6-, 8-, 10-, 12-, 14-, 16-, 18-, 20-, 26-, and 38-µm diameter particles using the time-dependent flow field. Note that the gas streamlines are assumed to be unchanged during the time interval of the calculations.

Figure 4 plots the relative dust thickness as a function of position for a number of particle sizes (2a = 1, 4, 8, 10, 16, and 26 μm), assuming the filter is clean. In the absence of an electric field, the relative thickness becomes uniform (1). The deposition pattern moves toward the bag filter inlet as the particle size increases, but the maximum thickness occurs in the area immediately adjacent to the minimum dust layer region.

Figure 5 shows both gas and particle streamlines for an MMD of 2 μm and 10 μm, respectively, with the filter being clean. In the absence of an electric field, the particle trajectories are the same as the gas streamlines. Note that the relative radius is chosen as 0 at the filter surface and 1.0 at the center of the filter. As seen in the figure, the charged particles' trajectories are enhanced considerably by the electric field. The behavior of the charged particles is well-characterized by the dimensionless ES number (3).

Figure 6 shows the gas and particle trajectories after 240 min of operation. The gas streamlines were computed also for t = 1, 30, 60, 120, 180, and 240 min. Although the gas streamlines are modified considerably because of the deposited particles, the trajectory of particles greater than 10 μm is not affected significantly by the gas streamlines. On the other hand, 2-μm particles are shifted downstream in the bag as time elapses. Because the coulomb force dominates for large particles, large-particle trajectories are less sensitive to the flow field than are small-particle trajectories.

Figures 7 and 8 illustrate the variations in the face velocity and the normalized mass distributions, respectively, for t = 1, 30, 60, 120, 180, and 240 min. When the bag is clean, the face velocity is uniform initially [1.22 m/min (4 ft/min)]. A large fraction of the mass tends to deposit near the bag inlet. As the particles accumulate on the bag surface, the flow resistance increases, resulting in local decreases in face velocities. Consequently, a greater fraction of the total flow shifts toward the top of the bag where the dust cake is thinner. However, the velocity profile and mass distribution do not continue to change beyond t = 120 min. This implies that the flow streamlines, as well as particle trajectories, approach a steady state.

The cumulative areal mass density distributions are also shown in Figure 9. Although a quantitative comparison cannot be made, the shape of the profile agrees well with laboratory observations (1). It is interesting to note that the mass fraction beyond the normalized bag length ($\overline{z}_i$) of 0.7 is comprised of particles that are 1 μm or smaller after 240 min of ESFF operation. In other words, no particle larger than 4 μm exists beyond $\overline{z}_i$ = 0.7. Similarly, 6-, 8-, and 10-μm particles do not exist beyond $\overline{z}_i$ = 0.6, 0.5, and 0.4, respectively.

Figure 10 shows the normalized mass fraction distribution for 1-, 4-, and 10-μm particles. As shown in the figure, the smaller particles are carried farther downstream as time elapses while larger particles are relatively unchanged in distribution. This type of information may prove to be extremely

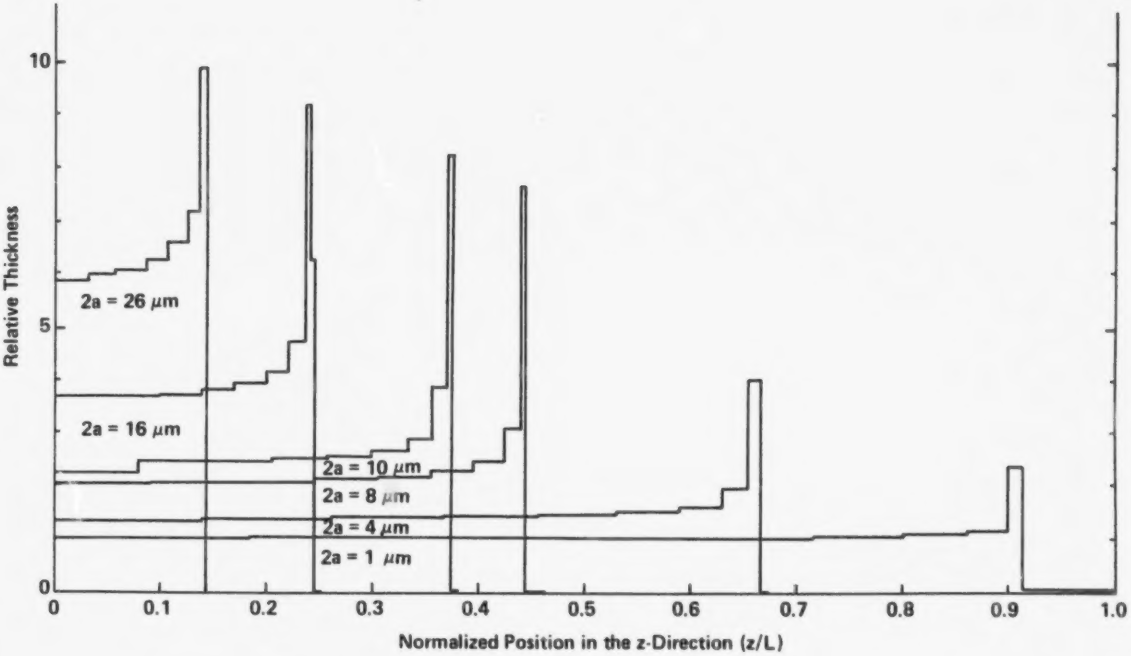

Figure 4. Dust layer distribution as a function of particle size.

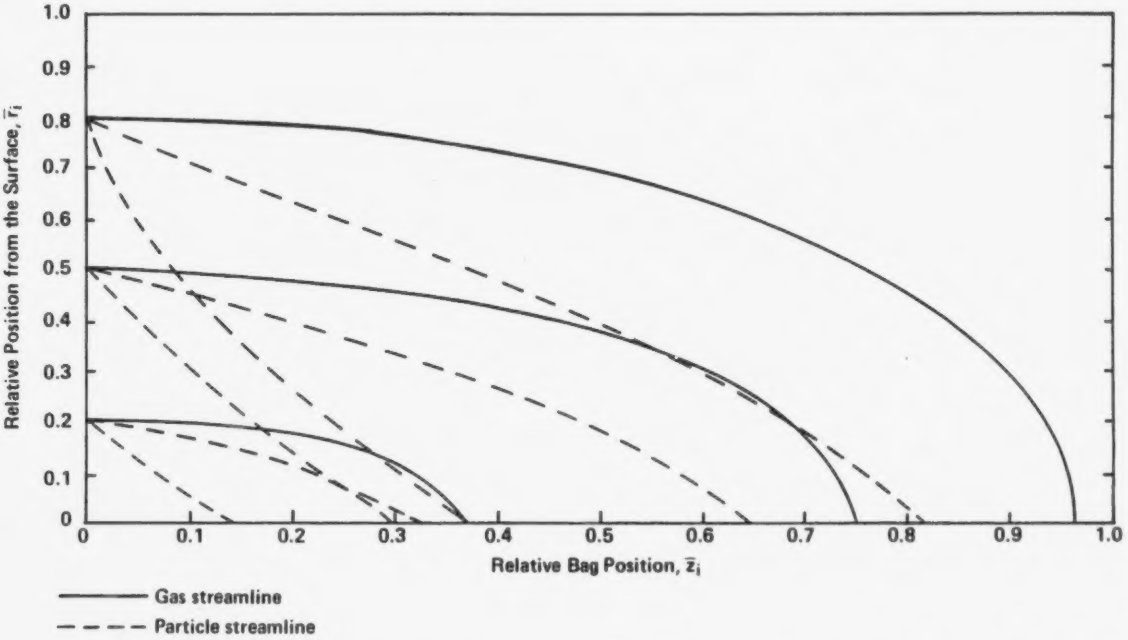

Figure 5. Gas and particle streamlines for clean surface.

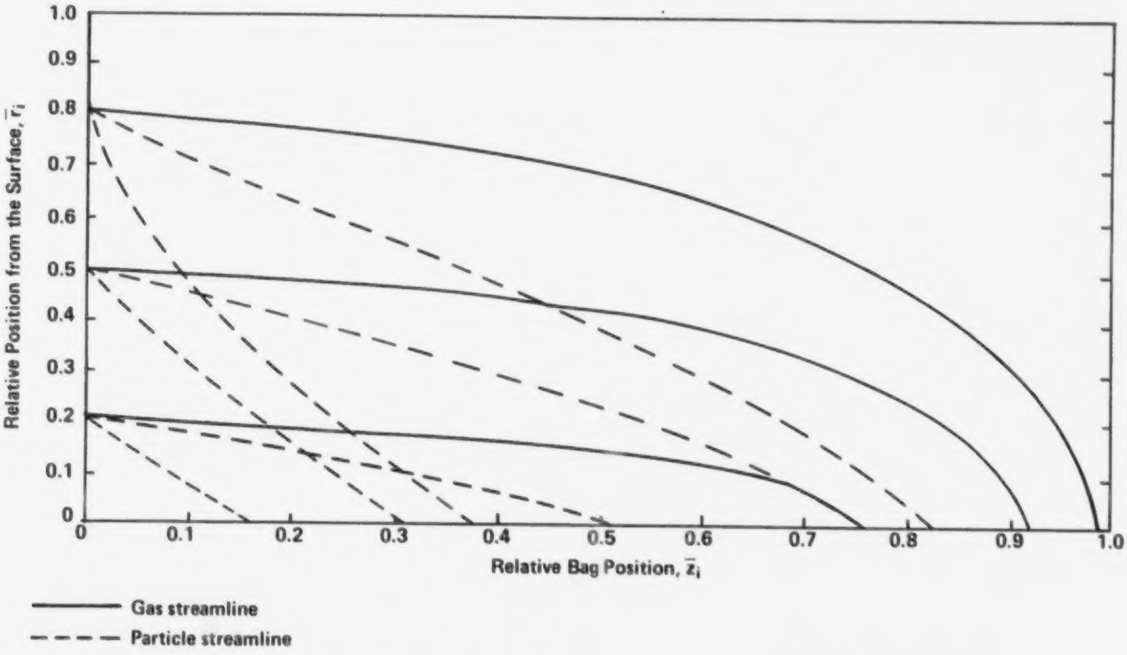

Figure 6. Gas and particle streamlines with deposited particles (t = 240 min).

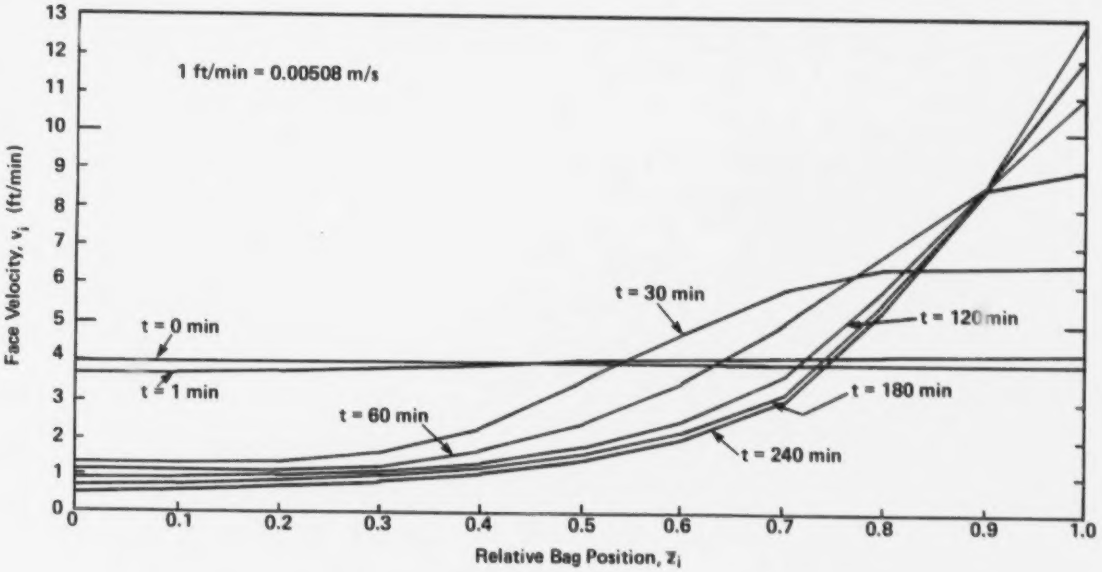

Figure 7. Face velocity distribution as a function of time.

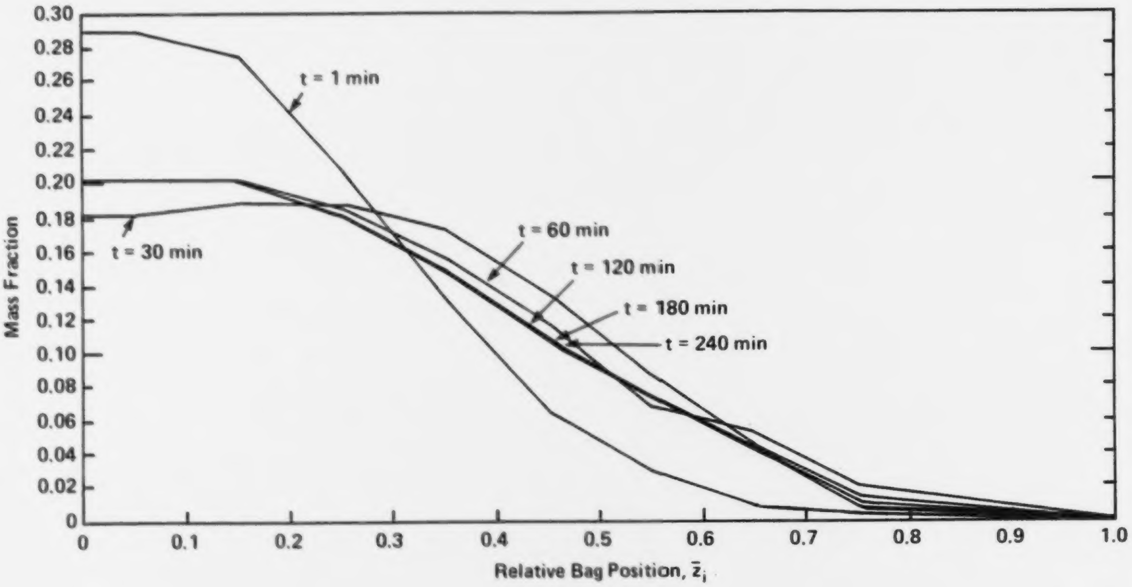

Figure 8. Normalized mass distribution as a function of time.

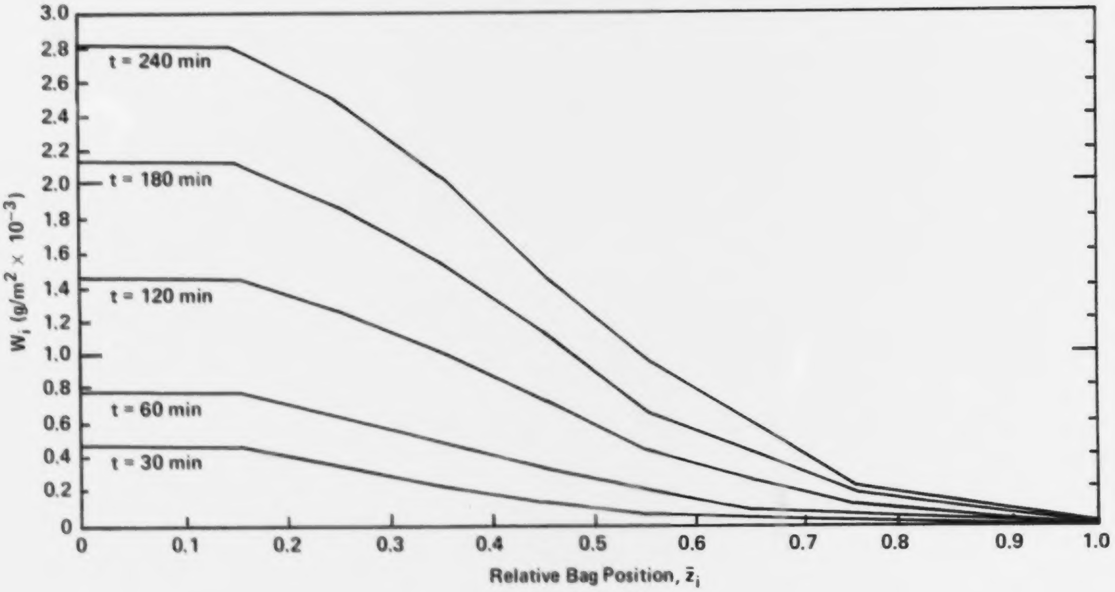

Figure 9. Cumulative areal mass density distribution as a function of time.

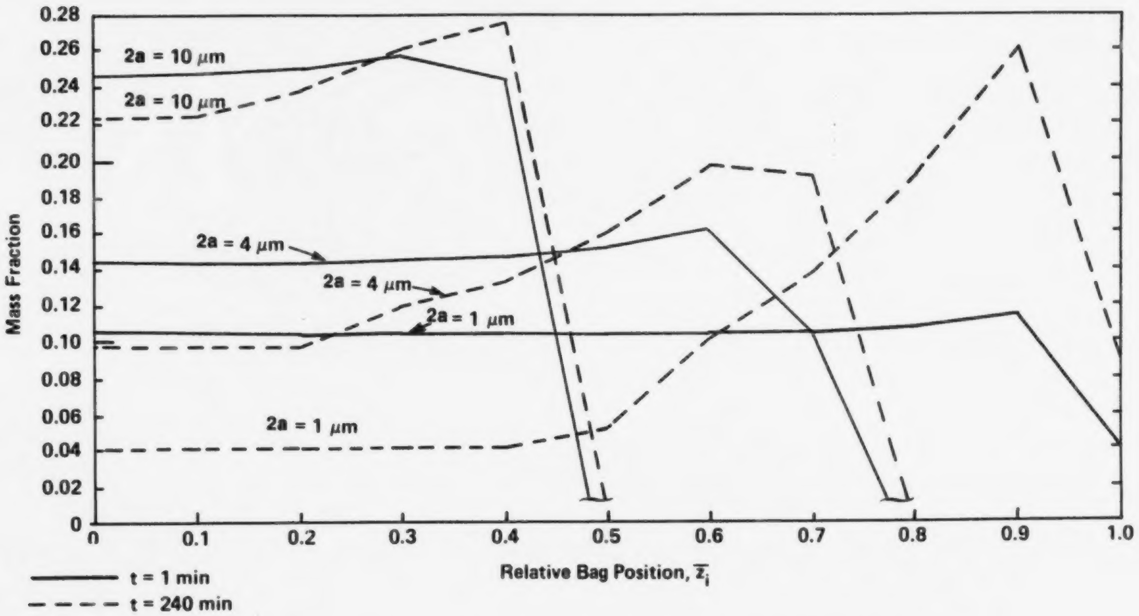

Figure 10. Normalized mass fraction distribution for various particle sizes.

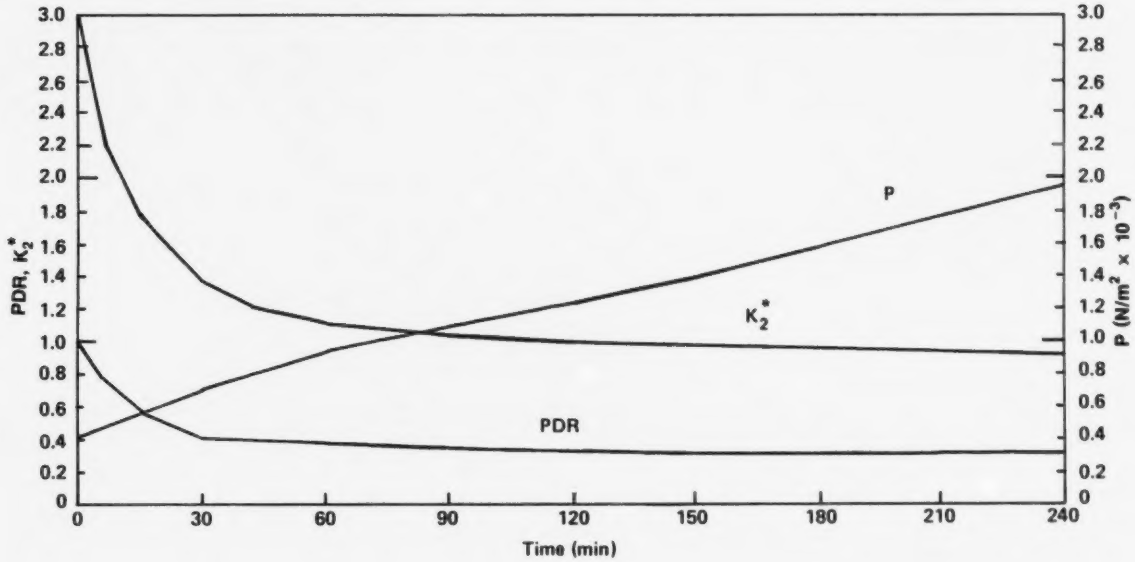

Figure 11. Time dependent P, K_2^*, and PDR.

important in understanding the microscopic structure, morphology, and theory of K_2 of the filter cake.

Figure 11 shows calculations for the time-dependent pressure drop (P), K_2^*, and PDR. The pressure reduction is nonlinear for the first 30 min but approaches linearity as time elapses. This behavior is due to the variations of the flow field that indirectly reflect the K_2^* value. Correspondingly, the value of PDR drops sharply in the first 30 min and gradually decreases, finally approaching a value of 0.31 after t = 240 min.

This model is flexible enough to incorporate most geometric and fundamental parameters that influence the ESFF process. Filtration performance generally is enhanced by reducing the A/C and increasing K_p (or the ES number). It is clear also from the results obtained from this model that the PDR can be lowered by increasing the MMD (or the ES number) and decreasing the standard deviation for given geometric and operating conditions. Direct enhancement of the PDR is achieved also by decreasing S_r. Laboratory and pilot studies support these conclusions through a variety of parametric studies.

CONCLUSIONS

A comprehensive mathematical model for describing the advanced ESFF process was developed to include flow modification. Time-dependent face velocity, mass fraction, areal mass density distributions, pressure drop, and PDR were calculated for a log-normal particle size distribution. The model allows us to gain insight into the detailed deposition process.

A significant reduction of overall pressure drop was demonstrated for advanced ESFF, and direct enhancement of the PDR can be achieved by increasing the ES number and decreasing S_r. The mass distribution of small particles is significantly altered by the flow field, but the distribution of large particles is far less sensitive. Parametric studies at both the laboratory and pilot scales lend substantial support to the conclusions offered by this mathematical model.

REFERENCES

1. Mosley, R.B., Hovis, L.S., and Daniel, B.E. Advanced ESFF laboratory test results. To be presented at the Sixth Symposium on the Transfer and Utilization of Particulate Control Technology, New Orleans, Louisiana, February 1986.

2. Greiner, G.P., Viner, A.S., Hovis, L.S., and Gibbs, R. Operation of electrically enhanced pilot plant on a stoker fired boiler. To be presented at the Sixth Symposium on the Transfer and Utilization of Particulate Control Technology, New Orleans, Louisiana, February 1986.

3. Mosley, R.B., Hovis, L.S., Plaks, N., Yamamoto, T., Viner, A.S., and Ensor, D.S. Advanced electrostatic enhancement of fabric filtration. Presented at Third EPRI Conference on Fabric Filter Technology for Coal-Fired Power Plants, Scottsdale, Arizona, November 1985.

ADVANCED ESFF LABORATORY TEST RESULTS

by: Ronald B. Mosley, Louis S. Hovis, and Bobby E. Daniel
Particulate Technology Branch
Gas Cleaning Division
Air and Energy Engineering Research Laboratory
U. S. Environmental Protection Agency
Research Triangle Park, North Carolina 27711

ABSTRACT

Advanced electrical stimulation of fabric filtration (AESFF) consists of combining electrical precipitation with the usual process of electrically stimulated fabric filtration (ESFF). Through both laboratory and pilot studies EPA has demonstrated a significant improvement in performance when AESFF is applied. In particular, significant pressure drop reductions occur as a result of the reduced dust loading on the upper portions of the bags. This reduced pressure drop allows for the potential either to operate at a lower pressure drop or to operate at a higher gas flow rate.

Areal mass density, cake thickness, and bulk mass density were measured for both resuspended spray dryer material and fly ash. Gas flow redistribution due to non-uniform dust cakes was observed to occur for pressure drops greater than 4 inches of water (996 Pa). Significant reductions in bulk mass density were observed due to deposition under the action of applied electric fields.

This paper has been reviewed in accordance with the U.S. Environmental Protection Agency's peer and administrative review polices and approved for presentation and publication.

ADVANCED ESFF LABORATORY TEST RESULTS

INTRODUCTION

For a number of years, EPA has sponsored studies (1-5) of the effects of electrical stimulation of fabric filtration. Other investigators have also studied this phenomenon (6-8). Some of the early experiments (1,3,8) involved precharging the dust particles. Precharging has been observed to increase collection efficiency, especially in the fine particle size range, and to decrease the pressure drop across the dust cake.

EPA next studied the effects of imposing an electric field parallel to the surface of the dust cake. The application of a field also led to increased collection efficiency and decreased pressure drop (2-5). It was generally observed that either precharging or an applied electric field led to a pressure drop reduction of about 50%.

In an effort to combine these two effects, EPA introduced the center wire arrangement which is used to produce a corona discharge in the reverse-gas-cleaned configuration. A similar arrangement, using a corona discharge wire located symmetrically between the bags, has also been used with the pulse-jet configuration. The high voltage is applied to the discharge wire with the bag (the cages for pulse-jet units) grounded. In some applications, it is necessary to make the bag more electrically conductive by using attached or woven-in electrodes. In these arrangements, the applied electric field is perpendicular to the dust cake. These designs which use corona wires and perpendicular electric fields have become known as Advanced Electrically Stimulated Fabric Filtration (AESFF).

In the laboratory, this new design often reduces the pressure drop by as much as an order of magnitude. This large reduction in pressure drop is envisioned as having the greatest impact on fabric filter applications. In lieu of operating at reduced pressure drops, much higher flow rates can be sustained in a fabric filter. Consequently, the required filtering surface can be reduced, resulting in reduced capital costs for new installations; or, in some applications, the productive capacity of the process can be increased. By retrofitting existing units to operate with lower pressure drops, reduced operating costs can be realized through the reduction of the energy required to operate the draft fans.

PROCEDURES

A description of EPA's laboratory baghouses has been presented elsewhere (9) and will not be repeated here. In the case of AESFF, it has been routinely observed that the bulk of the dust preferentially deposits near the bottom of the bag. It has been speculated that increased flow through the relatively clean area near the top of the bag accounts for the marked reduction in pressure drop that results when an electric field is applied. However, charging the particles has also been observed to reduce the pressure drop by increasing the permeability of the dust cake. To the present time, it has not been possible to distinguish the relative contributions of these two effects; however, it is usually assumed that the former plays the more important role with AESFF.

Several efforts have been made to demonstrate the shift in flow by directly measuring the local velocities at the fabric surface. All such efforts have failed for lack of sensitivity in measuring very low velocities. In the present work the shifts in flow were demonstrated in a qualitative manner by using dusts with contrasting colors. The rationale assumes that, after a non-uniform dust cake has been formed under the action of an applied electric field, very fine dust particles will follow the gas streamlines when there is no applied electric field. If this fine dust has a contrasting color, then the color pattern resulting in the dust cake will be indicative of the gas flow field. A cyclone with an estimated cut point of about 6 micrometers was used to ensure that the second dust would follow the flow lines.

A typical sample was formed by depositing the first dust for 1 to 3 hours at the high injection rate of 7 grains per cubic foot (0.0160 kg/m^3), followed by depositing the second dust for 5 minutes at a low injection rate. The bag was 4 feet (1.2 m) long and 5 inches (12.7 cm) in diameter. It was made of J. P. Stevens 648 fiberglass fabric with Teflon B coating. No electrodes were attached to the bag. The bag had a zipper sewn along its full length so that it could be opened on a flat surface for observations and measurements. The primary measurements to be discussed here are areal mass density and cake thickness. Mass samples were collected by vacuuming the dust from 1 square inch (6.5 cm^2) onto a filter for weighing. Samples were collected every 3 inches (7.6 cm) along the length of the bag, while the cake thickness was measured adjacent to each sampling point. The thickness measurements were made with two different depth gages which agreed remarkably well with each other. The reported thicknesses are the averages of the two measurements.

RESULTS

Figure 1 shows a plot of the areal mass density as a function of the relative position along the bag for four different dust cakes. The upper curve, denoted by squares, corresponds to a dust cake formed by injection of spray dryer material for 3 hours at a rate of about 7 grains per cubic foot (0.0160 kg/m^3). The pressure drop across this dust cake reached 2.25 inches of water (560 Pa) under the action of an applied voltage of 25 kV. The curve denoted by triangles represents a dust cake formed after 70 minutes operation with 30 kV applied, developing a pressure drop of 1.15 inches of water (286 Pa). The dust cake represented by the curve with the circles was formed in 45 minutes under the action of 29 kV. The pressure drop reached 0.4 inches of water (100 Pa). The lower curve, denoted by the rotated squares, corresponds to a dust cake formed after 3 hours under the action of 50 kV. The pressure drop reached 0.62 inches of water (154 Pa). No significant redistribution of the gas flow field was observed for these samples.

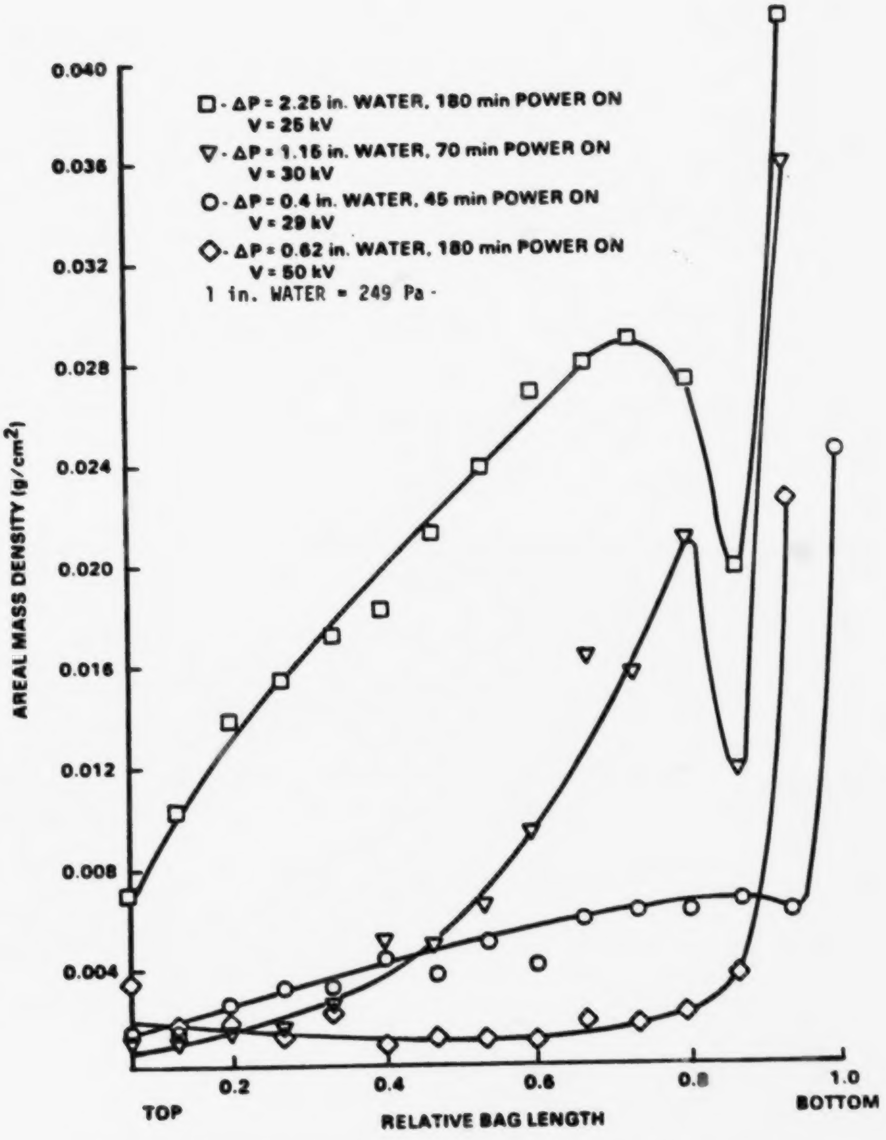

Figure 1. Areal mass density versus relative position in the bag for four different collection times.

The last curve has a shape somewhat different from the first three. s is a result of the higher applied voltage. The peculiar dips in the st three curves are believed to result from the configuration of the charge electrode. The dip corresponds to the point where the 1/8-inch 3 cm) discharge wire is connected to a weight which has a diameter of nches (5 cm). Starting at the bottom of the bag, the areal mass sity decreases rapidly as the particles with natural charge are collected. sudden increase in areal density is believed to be due to the sudden rease in particle charge resulting from the corona current. However, is possible that the enhanced collection is partially due to a corona d produced by the current. Corona wind could be a significant effect ause the face velocity is quite low, and the flow produced by the ona wind could readily pass through the fabric surface without generating normal recirculation flow. In the bottom curve, the dip is masked by low value of areal density.

Figure 2 shows dust cake thickness as a function of position within bag for the same four dust cakes as in Figure 1. The shapes of these ves are very similar to those in Figure 1, and the effects of the ona current are once again apparent in the dips. For the 50 kV case, cake was not thick enough in the upper one-third of the bag to be ably measured with the present technique.

Surprisingly, no apparent change in the flow pattern was observed a number of dust cakes formed under the action of an applied electric d. Although dramatic variations in cake thickness occurred from the tom to the top of the bag, the second (dark colored) dust appeared to lay essentially uniformly along the bag when no electric field was ied. Since the first dust was deposited under the action of an ied field, relatively low pressure drops resulted across the dust s. It was rationalized that perhaps under a larger pressure drop the distribution would be more pronounced. In order to increase the l pressure drop in a reasonable length of time, a uniform dust cake then overlayed by a non-uniform cake which was precipitated under the on of an applied electric field. A very thin layer of a different r dust was then deposited without an applied field. For total pres- drops greater than about 4 inches of water (996 Pa), flow redistribu- s were indicated by a greater fraction of the dark colored dust being sited at the top of the bag where the total deposited mass was least.

Figure 3 shows the areal mass density of the dust as a function of tion within the bag for three dust cakes. The cake represented in upper curve was formed by collecting dust for 2 hours with the power followed by 1 hour of collection with an applied voltage of 45 kV. total pressure drop reached 5.0 inches of water (1.3 kPa). The curve he middle was formed after 80 minutes with the power off followed by inutes with 50 kV applied. The pressure drop reached 5.0 inches of r (1.3 kPa). The lower curve was formed after 77 minutes with the r off. The pressure drop reached 4.0 inches of water (996 Pa). The upper curves illustrate that, under the action of an applied electric d, most of the dust is collected near the bottom of the bag. Figure 4

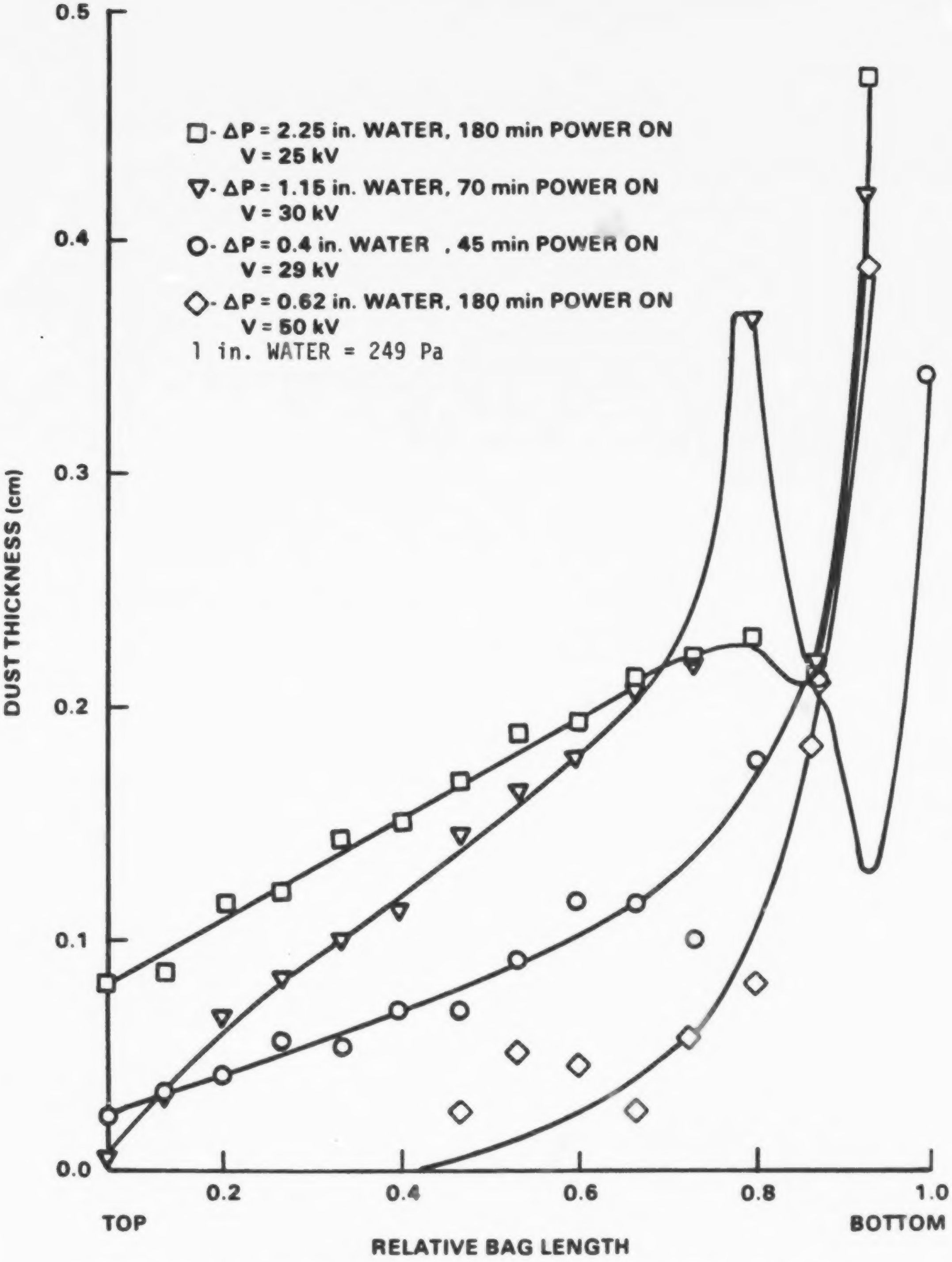

Figure 2. Dust thickness versus relative position in the bag for four different collection times.

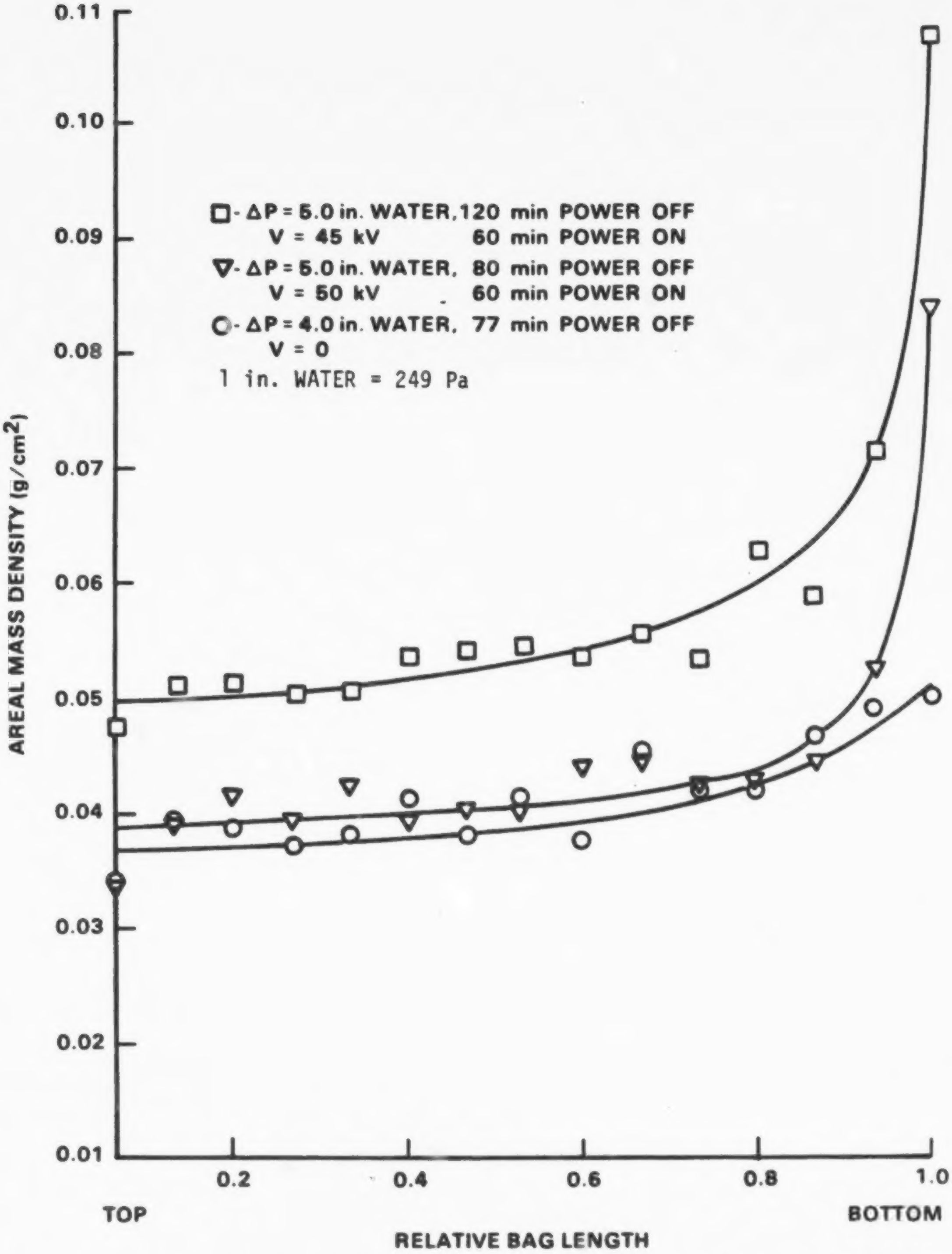

Figure 3. Areal mass density versus relative position in the bag for three different operating conditions.

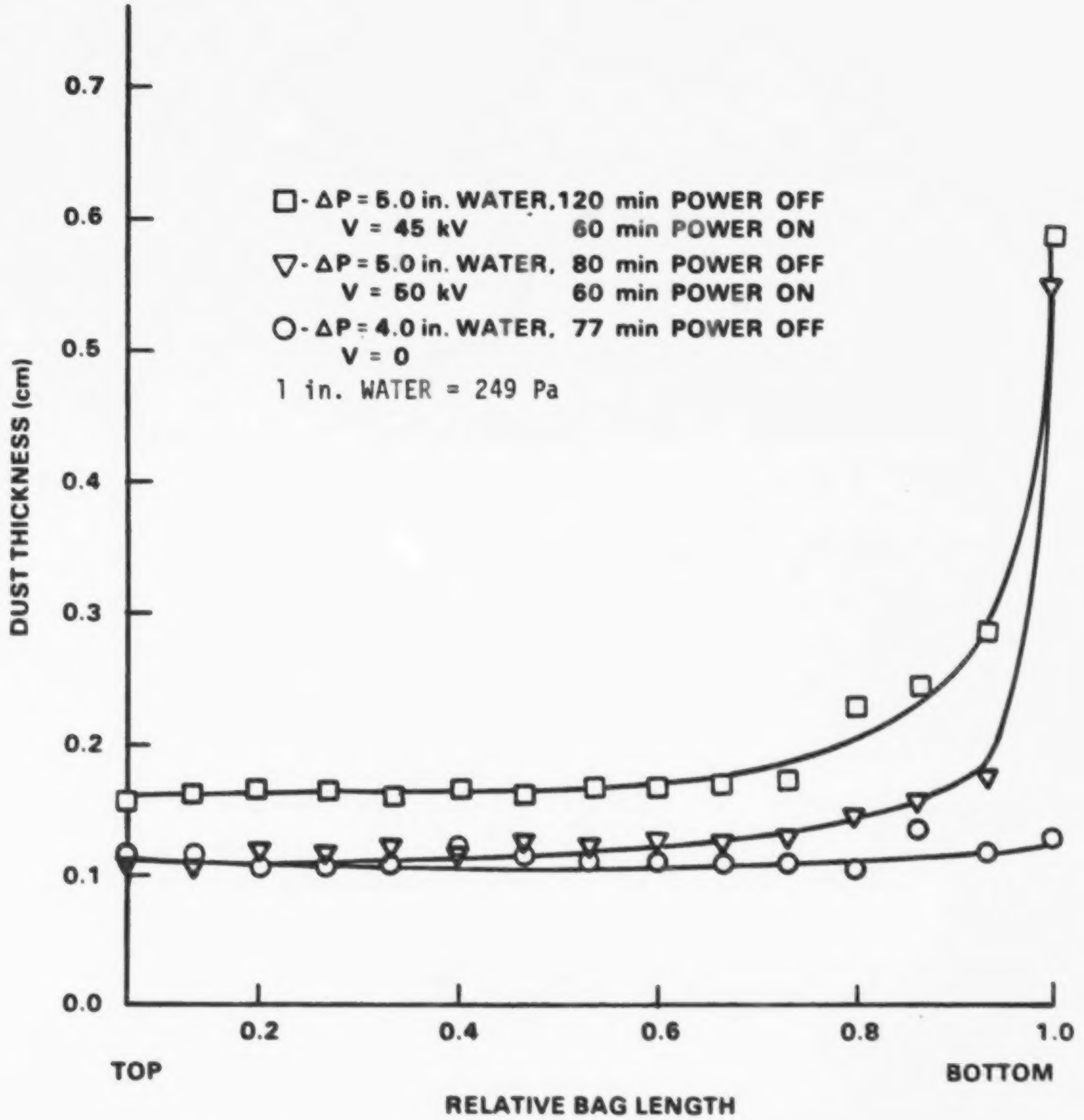

Figure 4. Dust thickness versus relative position in the bag for three different operating conditions.

shows the dust thickness as a function of position for the same three dust cakes represented in Figure 3. Note that the curves have shapes which are very similar to those in Figure 3.

Since the areal mass density and the thickness were measured independently, their ratio can be used to compute the bulk mass density of the dust cake. Figure 5 shows this bulk density as a function of position within the bag for the three cases shown in Figures 3 and 4. Note that the bulk density decreases dramatically when the dust cake is formed under the action of a strong electric field. This bulk-density/electric-field interaction occurs near the bottom of the bag where most of the dust is deposited when the electric field is applied. A reduced mass density implies an increased porosity and, consequently, an increased permeability of the dust cake. This effect offers a potential explanation for why there was little redistribution of the gas flow field at the lower pressures. The increased permeability would partially compensate for the tendency to redistribute the flow. The slight increase in density near the bottom of the bag when no voltage is applied is believed to be associated with the larger particles settling due to gravity. Note that in Figures 3, 4, and 5 the peculiar dips in the curves which were attributed to the onset of particle charging due to the corona current are missing. These dips are not present because the short (4 inch or 10.2 cm) weight was replaced by a longer (14 inch or 35.6 cm) one. Any dip which might occur at the greater distance from the inlet to the bag is apparently masked by the low value of areal mass density in this region. The remainder of the measurements to be discussed in this paper were made with the longer weight on the wire.

Figure 6 shows variations in bulk density for two curves exposed to different pressures and applied electric fields. The dust cake experiencing the higher pressure drop shows the larger value of bulk density. Figure 7 shows a systemmatic variation in bulk density with the maximum pressure to which the cake was exposed. Although the applied voltages were not all the same, it is clear that the pressure is a dominant effect in the regions (top of the bag) where most of the dust was deposited without an applied field. These effects tend to be partially compensated in the regions (bottom of the bag) where a greater fraction of the dust was collected under the action of an applied field.

Figure 8 shows two curves for which the pressure drop was the same but the sample represented by the lower curve was overlayed with dust collected under the action of a relatively high electric field. We see that the bulk density was appreciably decreased by the applied field. The data shown in the first eight figures were obtained using resuspended spray dryer material. The next three figures represent data for fly ash from a low sulfur western coal.

Figure 9 shows two curves illustrating the areal mass density as a function of relative position within the bag for two different exposure times. Figure 10 shows the corresponding thicknesses for the curves in Figure 9. It is peculiar that the thicknesses differ little near the top of the bag. This is explained, at least partially, by the fact that the

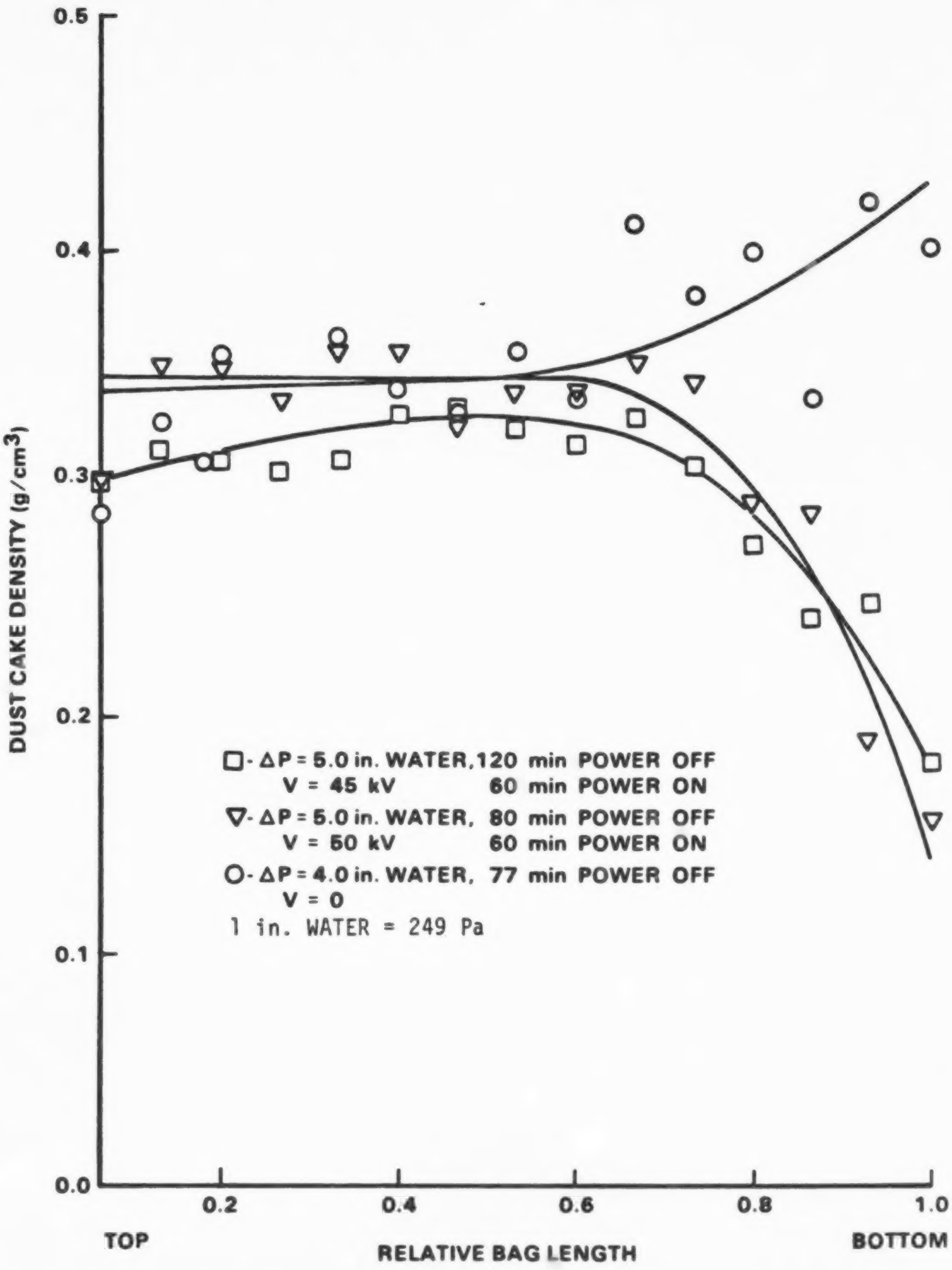

Figure 5. Bulk mass density versus relative position in the bag for three different operating conditions.

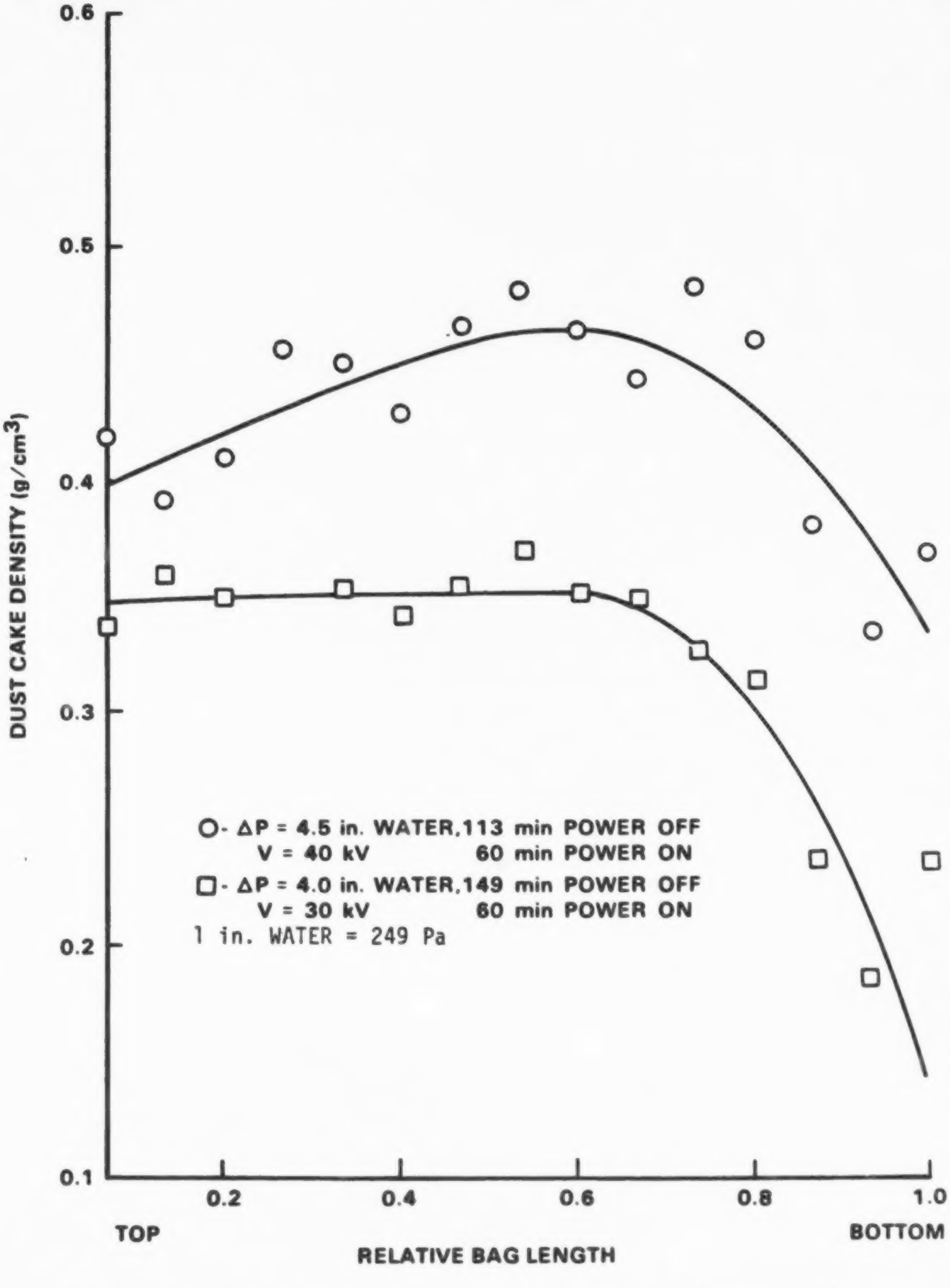

Figure 6. Bulk mass density versus relative position in the bag for two conditions of pressure and applied voltage.

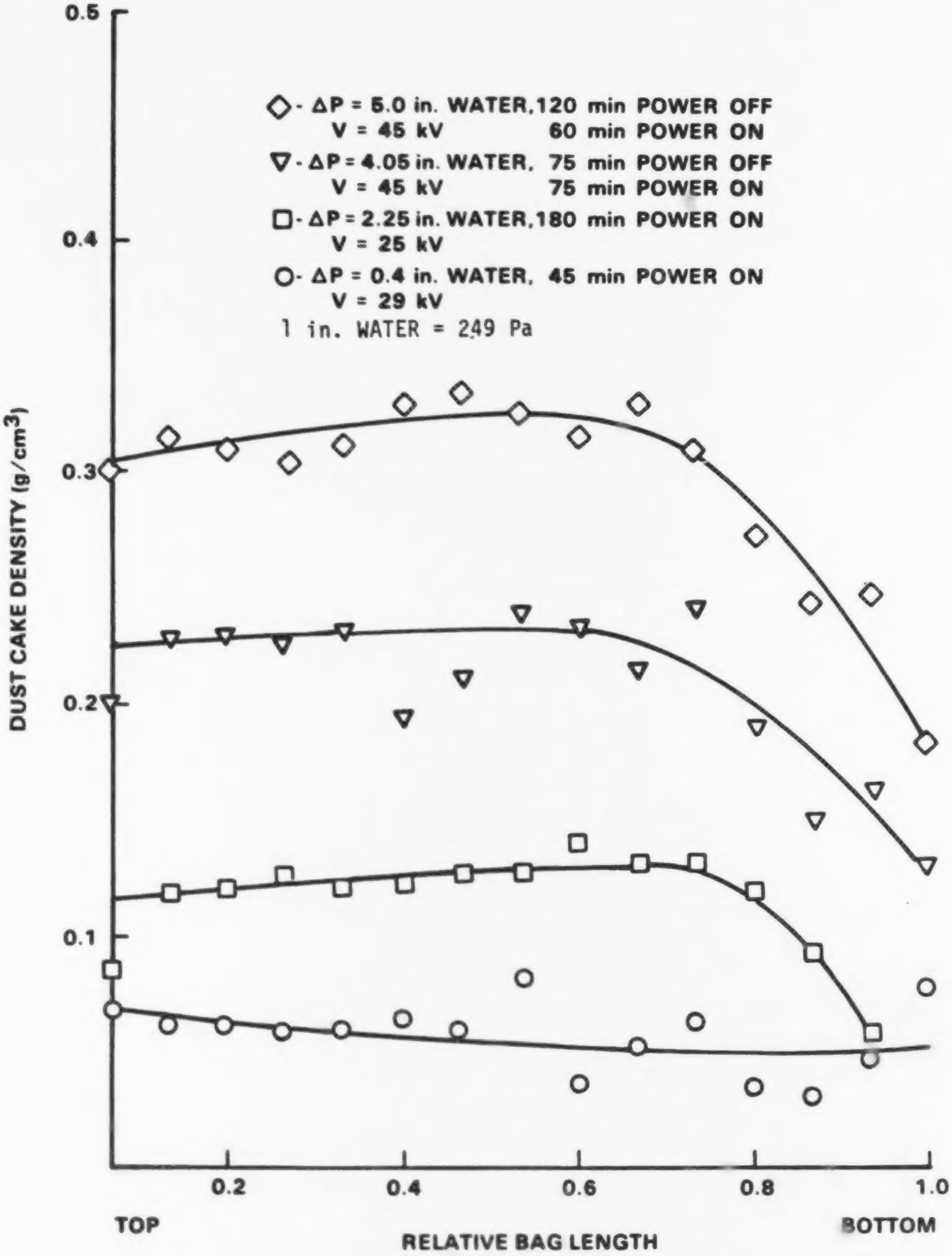

Figure 7. Bulk mass density versus relative position for four different pressure drops.

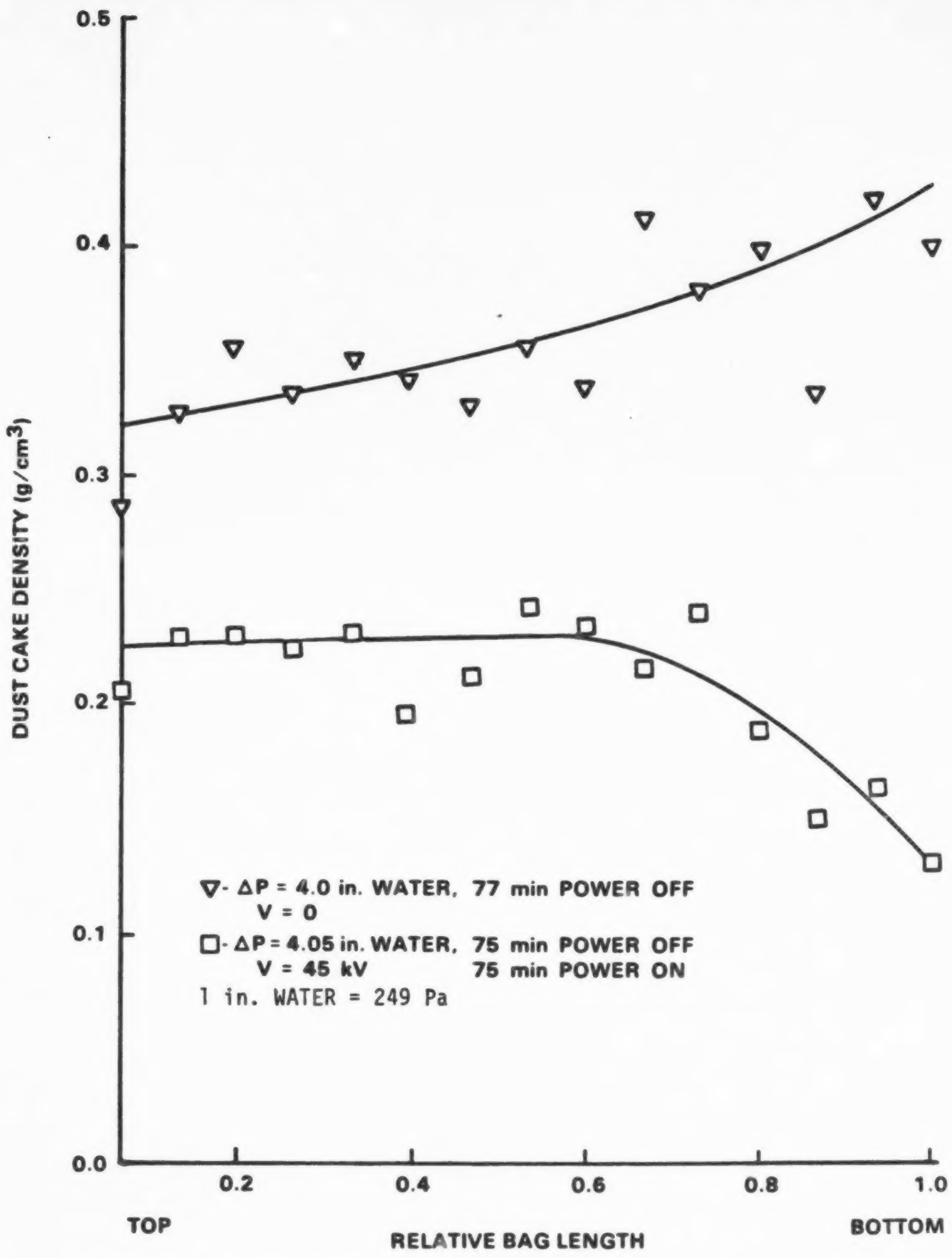

Figure 8. Bulk mass density versus relative position in the bag for two values of applied voltage.

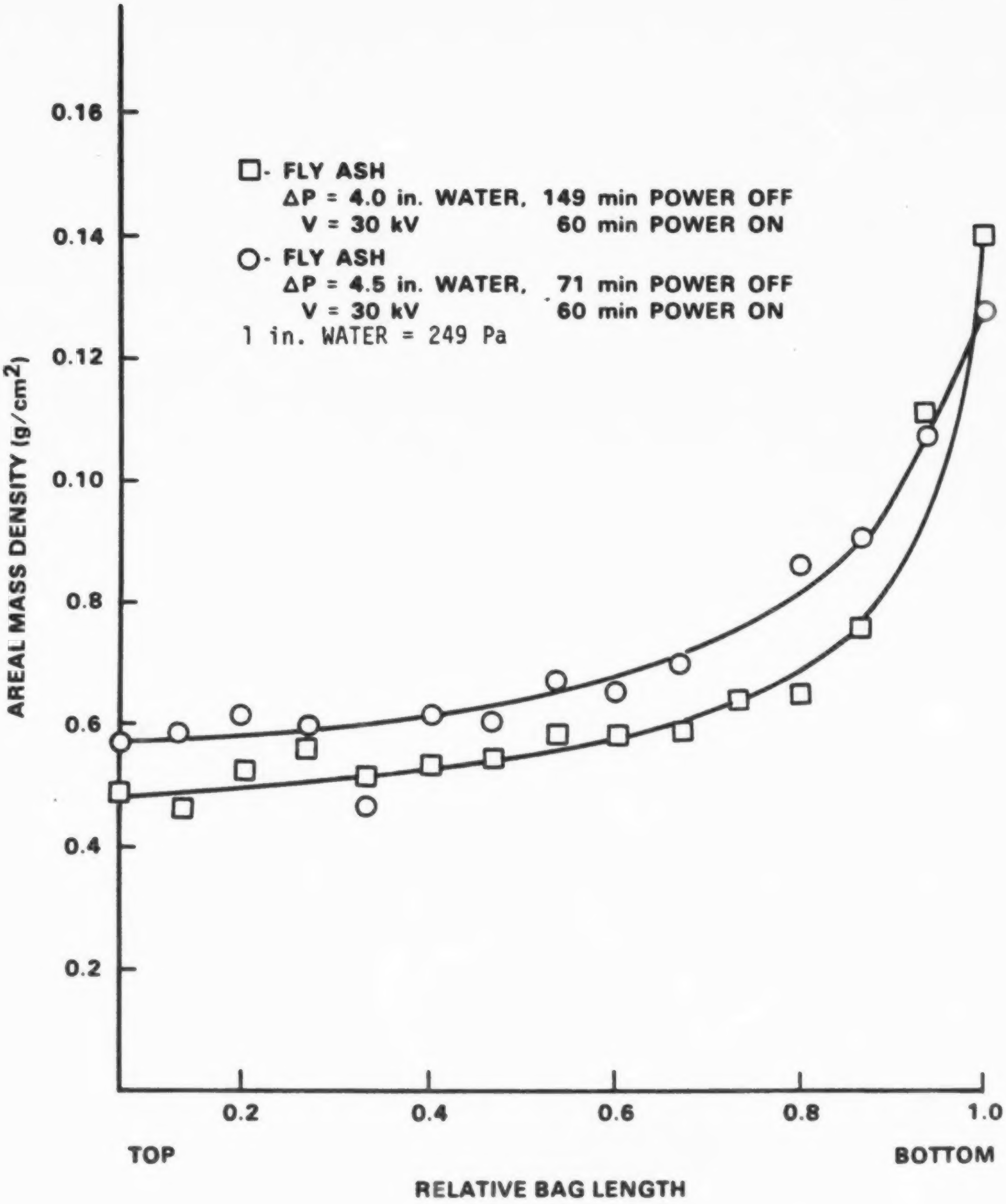

Figure 9. Areal mass density versus relative position in the bag for two fly ash cakes.

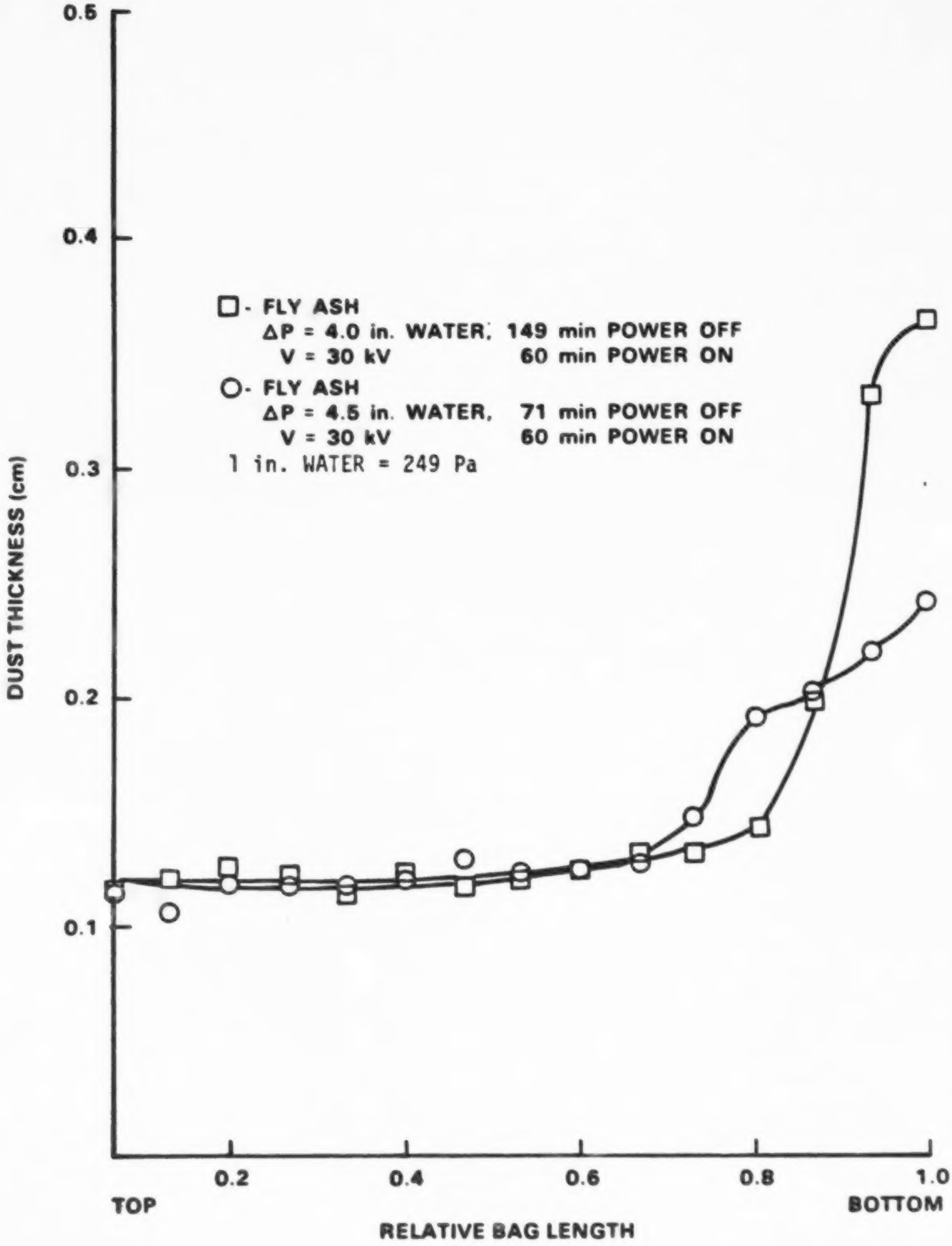

Figure 10. Dust thickness versus relative position in the bag for two fly ash cakes.

bag was discovered to have developed a significant leak when some tape came loose during the long run.

Figure 11 shows the bulk mass density for these same two curves. Note that the layer exposed to the higher pressure has the higher bulk density. This is true in spite of the fact that the lower pressure case was exposed to the flow for a longer time. However, as was pointed out previously, the dust cake did not appear to get much thicker. These latter curves were shown only to illustrate that fly ash behaves in much the same way as spray dryer material insofar as the structure of the dust cake is concerned. The data are believed to be valid for this purpose.

Figure 12 shows a comparison of the measured cake thickness within the bag to that predicted by a theoretical model. The mathematical model used to obtain the calculation has been described elsewhere (10, 11). Although the mathematical mode is somewhat preliminary, the predicted shape of the curve is in excellent agreement with the measurements. One uncertainty which affects the absolute value of the predicted thickness is the total mass which was collected in the bag. In this particular case the total mass collected was not measured. It was simply estimated from the fraction of mass that was collected in a previous run. The problem of knowing the total mass arises because a significant fraction of the dust is precipitated in the hopper and thimble when the applied voltage is large; consequently, the thickness cannot be computed from the inlet mass loading alone.

DISCUSSION AND CONCLUSIONS

AESFF, which uses a corona discharge wire, gives rise to a significant reduction in pressure drop due both to the non-uniformly precipitated dust cake and to the increased permeability of the dust cake resulting from the applied electric field. Data reported here include areal mass density, dust cake thickness, and bulk mass density measured for both resuspended spray dryer material and fly ash. Dusts with contrasting colors were used to investigate the gas flow patterns. It was observed that gas flow redistribution due to non-uniform dust cakes occurred for pressure drops greater than 4 inches of water (996 Pa). However, flow redistributions were probably less pronounced than would be expected from the variation in mass on the filter because increased porosity and, consequently, increased permeability occurred in the regions of the cake that were thickest. The increased permeability partially compensates for the tendency for the gas flow to shift toward the thinner regions of the cake. This helps to explain why little redistribution of the gas flow occurred when the entire cake was deposited under the action of an electric field. It was also observed that the bulk density of the cake increased with increasing pressure and decreased with increasing applied electric field.

Future work will further explore the dependence of permeability on the maximum pressure drop. Attempts will be made to obtain higher pressure drops for cakes deposited under the action of applied electric fields. Interpretation of results would be simplified if the complicating effects

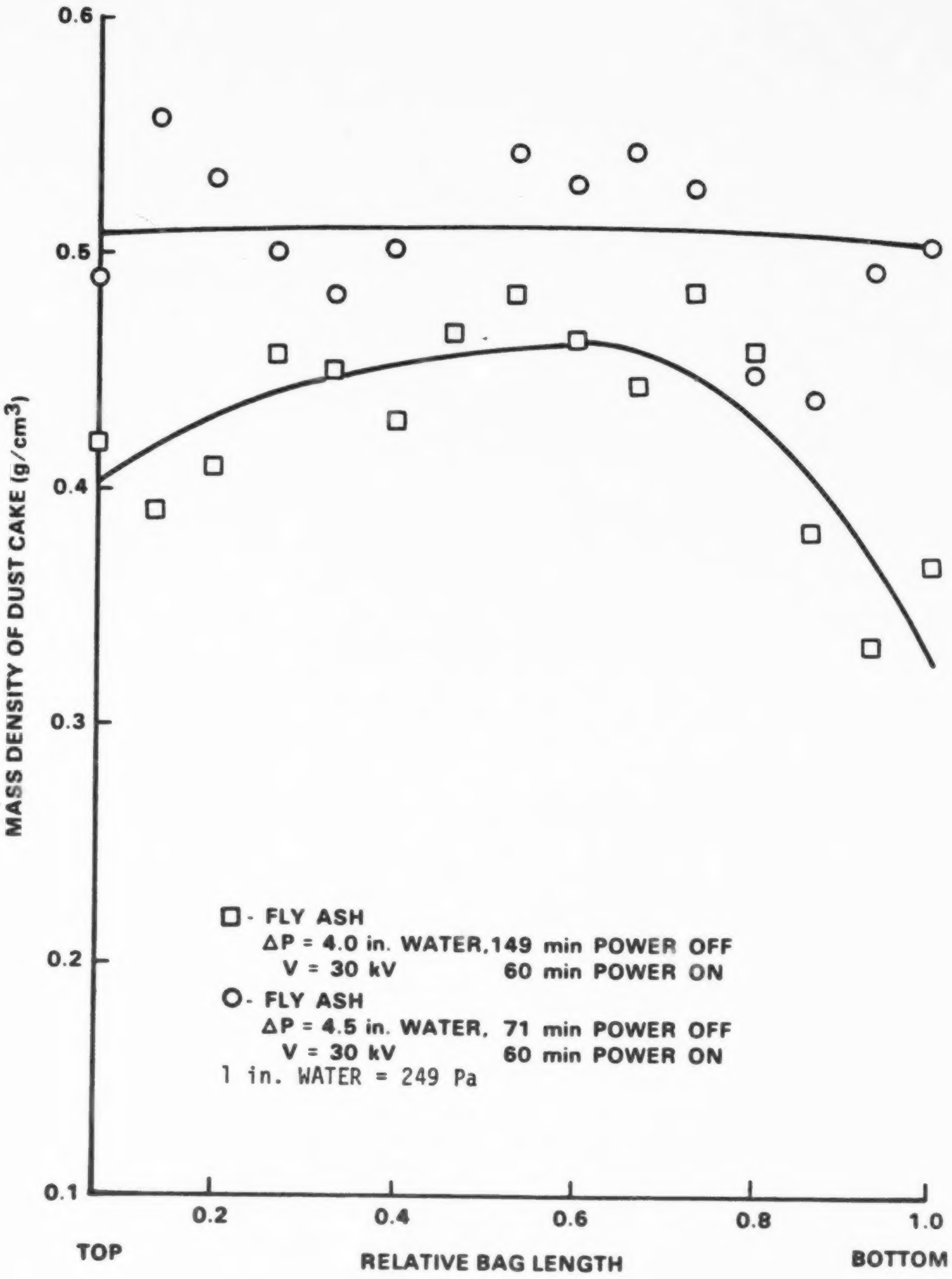

Figure 11. Bulk mass density versus relative position in the bag for two fly ash cakes.

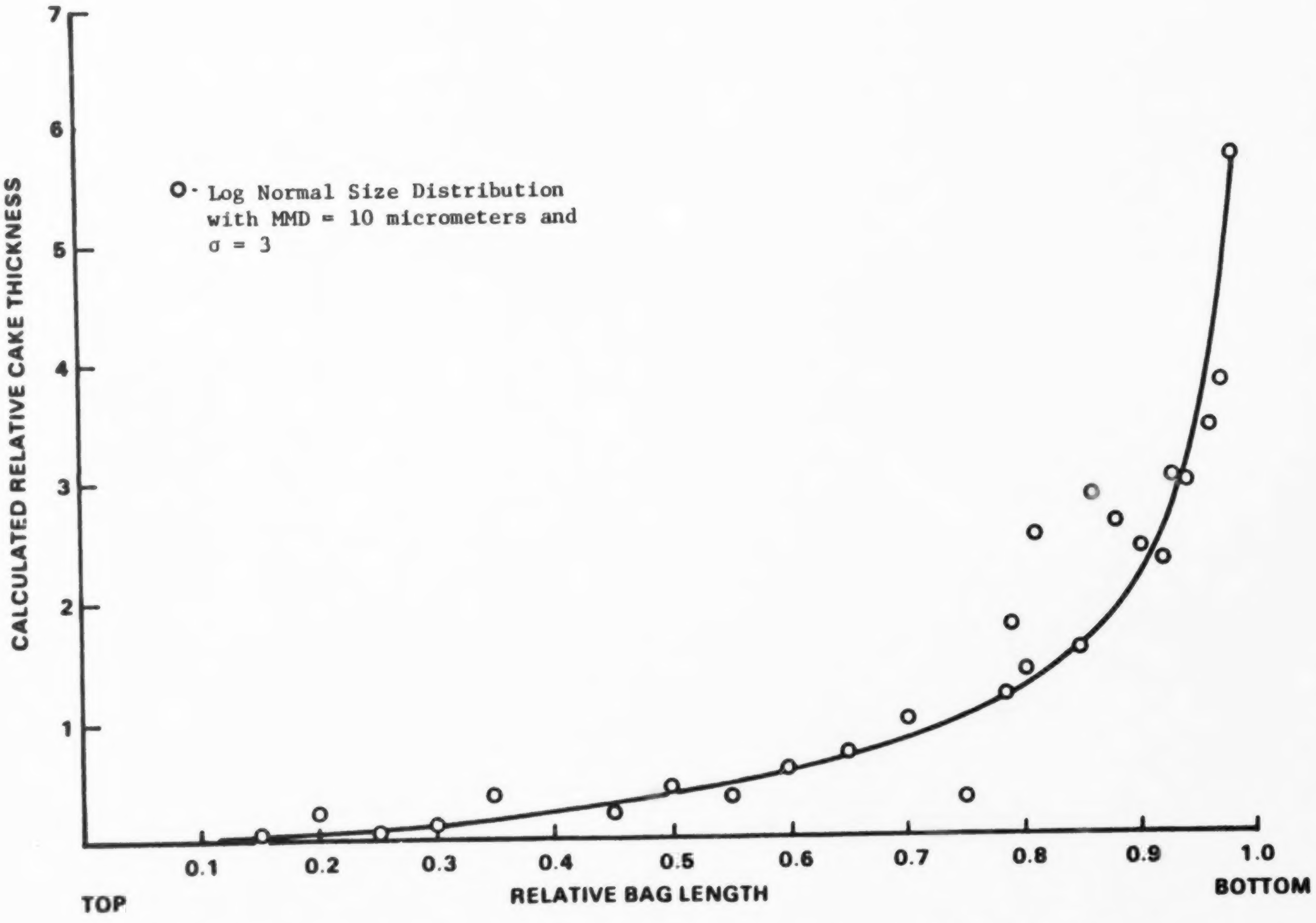

Figure 12. Calculated relative thickness versus relative position in the bag for an industrial sized bag.

the uniformly deposited dust cake could be eliminated. In addition, a e quantitative measurement of the redistribution of the gas flow is ded. A chemical tracer technique is planned for this purpose. It ld also be very useful to measure the local permeability of the dust e as a function of position to be correlated with mass density and parle size distribution. It would be very interesting to attempt to relate measured values of permeability with predictions of existing els.

REFERENCES

Penney, G.W., "Electrostatic effects in fabric filtration: Volume I. fields, fabrics, and particles (annotated data)." EPA-600/7-78-142a (NTIS No. PB 288576), U.S. Environmental Protection Agency, September 1978.

Donovan, R.P., et al., "Electrostatic augmentation for particulate removal with fabric filters." In: Fifth International Fabric Alternatives Forum Proceedings. American Air Filter Company, Inc., 215 Central Avenue, Louisville, Kentucky, January 1981, pp. 12-1 to 12-24.

Lamb, G.E.R. and Costanza, P.A., "A low-energy electrified filter system." Filtration and Separation. 17(July/August): 319-322, 1980.

VanOsdell, D.W., et al., "Electrostatic augmentation of fabric filtration: pulse-jet pilot unit experience." EPA-600/7-82-062 (NTIS No. PB83-168625), U.S. Environmental Protection Agency, Research Triangle Park, North Carolina, November 1982.

Greiner, G.S., et al., "Electrostatic stimulation of fabric filtration." JAPCA 31(10): 1125-1130, (October) 1981.

Bergman, W., et al., "Electrostatic filters generated by electric fields." UCRL-81926, Lawrence Livermore National Laboratory, P. O. Box 808, Livermore, California, 94550, July 23, 1979. (Presented at the Second World Filtration Congress, London, England, September 18-20, 1979).

Chudleigh, P.W. and Bainbridge, N.W., "Electrostatic effects in fabric filters during build-up of the dust cake." Filtration and Separation. 17(July/August): 309-311, 1980.

Chiang, T.K., Samuel, E.A., and Wolpert, K.E., "Theoretical aspects of pressure drop reduction in a fabric filter with charged particles. In: Third Symposium on the Transfer and Utilization of Particulate Control Technology, Volume III. EPA-600/9-82-005c (NTIS No. PB83-149609), U. S. Environmental Protection Agency, July 1982. pp. 250-260.

9. Hovis, L. S., Daniel, B.E., Chen, Y., and Donovan, R.P., "Laboratory studies of electrically enhanced fabric filtration." In: Proceedings: Fifth Symposium on the Transfer and Utilization of Particulate Control Technology, Volume 3, EPA-600/9-86-008c (NTIS No. PB86-167178), U. S. Environmental Protection Agency, February 1986. pp. 19-1.

10. Mosley, R.B., Hovis, L. S., Plaks, N., Yamamoto, T., Viner, A.S., and Ensor, D.S., "Advanced electrostatic enhancement of fabric filtration." In: Third EPRI Conference on Fabric Filter Technology for Coal-Fired Power Plants. Scottsdale, Arizona, November 1985.

11. Yamamoto, T., Ensor, D.S., Mosley, R.B., Hovis, L.S., and Plaks, N., "Mathematical model for advanced electrically stimulated fabric filtration." Presented at Sixth Symposium on the Transfer and Utilization of Particulate Control Technology, New Orleans, Louisiana, February 1986.

ADVANCED ESFF
APPLIED TO A STOKER COAL-FIRED BOILER

Gary P. Greiner
ETS, Inc., Roanoke, VA

Andrew S. Viner
Research Triangle Institute
Research Triangle Park, NC

Louis S. Hovis
U.S. Environmental Protection Agency
Air and Energy Engineering Research Laboratory
Research Triangle Park, NC

Roger Gibbs
Naval Surface Weapons
Dahlgren, VA

ABSTRACT

ADVANCED ESFF APPLIED TO A STOKER COAL-FIRED BOILER

BY:
Gary P. Greiner - ETS, Inc.
Andrew Viner - Research Triangle Institute
Lou S. Hovis - Environmental Protection Agency
Roger Gibbs - U. S. Navy

The ability of an electrostatically stimulated fabric filter (ESFF) to operate at a lower average pressure drop or a higher gas-to-cloth (G/C) ratio than a conventional fabric filter has been successfully demonstrated in the laboratory and in studies at two pilot plants with pulverized coal ashes. Those investigations involved the use of an electric field oriented parallel and in close proximity to the surface of the bag fabric. Recent laboratory investigations have shown that a center wire electrode, producing an electric field perpendicular (rather than parallel) to the surface of the fabric, produced as good or better results. This configuration has the potential advantages of operating on conductive dusts, with standard fabrics, and with less complicated electrode design when applied to reverse air or shaker baghouses.

In order to evaluate the center wire configuration in the field, a pilot baghouse was installed on a slipstream of an industrial coal-fired stoker boiler. The pilot plant contains 8 in.* diameter by 24 ft woven glass bags, employs reverse air cleaning, and can process 700 acfm of flue gas.

Within the standard reverse air baghouse, individual bag flow monitors (IBFMs) are used to evaluate the fabric drag characteristics of each bag, allowing comparison of variables within the common module. Bags with and without electrical enhancement are compared.

The pilot plant includes a data collection system that continuously monitors all key operating parameters, including individual bag flow, locally stores this data for several days, and transmits via telephone lines to both ETS and RTI offices for analysis.

This paper will discuss the program objectives, system design, test plan, and results obtained during 1985.

---

*Readers more familiar with metric units may use the conversion table at the end of this paper.

INTRODUCTION

A pilot plant program applying the Advanced Electrostatic Fabric Filter (ESFF) concept and hardware to a slipstream from a stoker coal-fired boiler was conducted during 1985. The program was funded by the U.S. Navy, and conducted at a government installation by ETS, Inc. and Research Triangle Institute personnel, with support from EPA's Air and Energy Engineering Research Laboratory.

Previous ESFF programs had employed the parallel field electrode configuration, using electrified cages for pulse jet collectors and electrodes woven into the fabric for reverse air or shaker collectors. The parallel field electrode configuration brings the electrodes and field path in intimate contact with the fabric and dust cake and, unless the fabric and dust cake resistivity is high ($>10^8$ ohm-cm), excessive current flow, electric field collapse, and arcing can occur.

This program was the first application of ESFF to a low resistivity ash process and required the Advanced ESFF center electrode configuration.

PROGRAM OBJECTIVES

1) Design and test Advanced ESFF components for a reverse air baghouse.
2) Perform a short-term proof-of-principle test to examine the impact on performance of the Advanced ESFF concept on a reverse air baghouse applied to a stoker coal-fired boiler.
3) Define the potential economic advantages of an Advanced ESFF baghouse over a conventional reverse air baghouse.

PROGRAM TASKS PERFORMED

1) Redesign and modification of an existing 300 acfm pilot plant previously used on the Waynesboro ESFF project, to accommodate full length (24 ft long) x 8 in. diameter bags and flue gas flow of 700 acfm.
2) Installation, start-up, and debugging of the system at the new site.

3) Operation of the pilot plant during the 4 month test period.
4) Data analysis.
5) Economic analysis specific to Advanced ESFF and this application.

PILOT PLANT DESCRIPTION

The pilot plant was installed on the slipstream of flue gas from either of two Keeler spreader stoker boilers, each rated at 77,500 lb/hr steam and producing 36,000 scfm at full load with an outlet emission of approximately 0.8 gr/scf. The coal burned is Eastern Kentucky, 1% sulfur, 13,500 Btu/lb. The boiler gases flow through a multi-cyclone collector operating at about 75% efficiency, before the extraction of the slipstream resulting in a typical inlet loading to the pilot plant of 0.2 gr/scf.

The reverse air baghouse contained six full scale bags, 8 in. diameter x 24 ft long. Each bag location contained an Individual Bag Flow Monitor (IBFM^{TM}), and the Advanced ESFF center electrode components. The IBFM system allowed evaluation of ESFF and control bags simultaneously within the same baghouse. The Advanced ESFF electrode configuration utilized is shown in Figure 1. The baghouse had its own I.D. and reverse air fans with flow control dampers for cleaning and control of the gas flow. The system was fully instrumented to allow monitoring of inlet and outlet flows and temperatures, individual bag flows, ESFF voltages and currents, and tubesheet pressure drop.

DATA COLLECTION AND ANALYSIS

The output from the instrumentation sensors was input to a local data logger and stored on a PC computer located in the pilot plant test trailer. Data could be locally retrieved or accessed via a modem from either the RTI or ETS offices.

Each filtration cycle was analyzed. Instantaneous gas-to-cloth (G/C) ratio and fabric drag vs. time from cleaning could be examined for each bag for any filtration cycle. (See Figures 2 and 3.) Trend analysis was performed of average G/C (Figure 4), extrapolated drag (S_E), average drag (S_{AVG}), and specific resistance coefficent (K_2) for each bag. Normally half of the active bags were powered and ESFF vs. non-ESFF bags compared. This shows the potential impact of ESFF on operating performance if all bag locations in a collector are converted. Further information on analysis procedures utilizing the IBFM^{TM} system is provided.(1)

OPERATING HISTORY

The pilot plant was operated intermittently from 4/10/85 through 6/27/85 and on an almost continuous basis from 6/28/85 through 9/30/85. Because of the low inlet loading, 12 hr filtration cycles were utilized. Gas-to-cloth levels were initially restricted to 2/1 with sequential test periods of 2.6, 3, and 4/1. Field strength levels in ESFF bags were maintained at approximately 2.5 kV/cm or 25 kV with electrode currents 0.5-1 mA per bag. Initially, bags 2, 4, and 6 were powered. Because the drag values were so low (approximately 0.02-0.03 in. W.G./fpm) and to verify that the difference was really due to ESFF, the bag sets were reversed. From 7/19/85 on, bags 1, 3, and 5 were electrified. Intermittent problems with the boilers and conventional pilot plant components created some discontinuity in pilot plant operation and data collection. The Advanced ESFF hardware and IBFM system worked effectively throughout the program.

RESULTS

The powered bags immediately exhibited a lower drag and resultant G/C levels as can be seen in Figure 4, Cycles 16-30. When the bag sets were reversed, the impact can be seen in Figure 4, Cycles 34-46. By Cycle 58, Figure 2, approximately 30 days of operation, a substantially higher G/C level in the ESFF bags is demonstrated. The unpowered bags all look identical. There was spread in the ESFF bags. Bag 3 had woven-in electrodes to provide an independent ground plane and exhibited superior performance characteristics in the early cycles. Once the bag fabric established a permanent, residual, low resistivity, dust cake, this advantage went away.

The ESFF bags showed a performance advantage throughout the test period. The rate of fabric drag rise during a filtration cycle of the ESFF bags was typically 20 to 30% of the control bags and the ESFF bags operated at a higher G/C ratio. The residual drag was always lower for the ESFF bags but the magnitude of the S_E advantage was clouded by the switching of bag sets and the periods of cleaning system malfunctions.

By Cycle 149, the ESFF effect is described by Figure 5. The actual individual bag flows and tubesheet pressure drops were used to calculate the residual drag, K_2, and drag vs. mass loading for each bag. This information then allowed calculation of pressure drop vs. time from cleaning at various gas-to-cloth ratios as shown in Figure 6.

COST ESTIMATES FOR ESFF ON A FULL-SCALE BAGHOUSE

An economic analysis of the potential impact of Advanced ESFF on a full-scale reverse air baghouse of the size typically applied to stoker boilers follows.

Capital Cost Assumptions:

For baghouses in the 50,000 acfm size range, total installed costs consist of the sum of the following:

1) Flange-to-flange hardware = \$16/ft^2 of fabric
2) Installation = \$160,000 + \$9.60/ft^2 of fabric
3) All other costs = \$400,000 (engineering, duct, foundations, debugging, testing, etc.). Since ESFF does not impact on these "other" costs, they are excluded from this analysis.

To equip a baghouse with Advanced ESFF involves the following flange-to-flange cost additions:

1) Electrode cost = \$2/ft^2 of fabric
2) Power supplies = \$1.50/ft^2 of fabric
3) Additional controls = \$25,000

Table 1 presents a capital cost comparison for 50,000 acfm. The percent cost savings shown in Table 1 are presented graphically in Figure 7.

Operating Cost Assumptions:

Operating cost is assumed to include three components: 1) bag replacement, 2) fan electrical power cost, and 3) equipment maintenance.

$$\text{Bag Replacement} = \frac{i\,(1 + i)^L}{(1 + i)^L - 1} \times B$$

where:

i = interest rate = 0.14

L = bag life, years

B = bag cost, \$/ft^2

Fan Power Cost = 1.25 (E) (ΔP) (Q), \$

where:

E = electrical power cost, \$/kWh

$\Delta P = K_1(G/C)$, in. H_2O

Q = total gas flow, acfm

Equipment Maintenance = 0.03C

where:

C = flange-to-flange capital cost, \$

Combining these components and solving for:

Q = 50,000 acfm

E = 0.05 \$/kWh

B = \$1.00 \$/ft^2

Total Annual Operating Cost = bag replacement + fan power cost + maintenance

$$= 50{,}000 \frac{F}{G/C} + 3{,}125\ K_1\ (G/C) + 0.03C$$

where:

F = bag replacement factor = 0.61 for L=2, 0.34 for L=4

G/C = gas-to-cloth ratio, ft/min

C = capital cost, \$

K_1 = average fabric drag, in. H_2O/fpm

K_1 for the conventional bags is defined as:

$$K_1 = \frac{\Delta P_e}{G/C} + \frac{\Delta P_f - \Delta P_e}{2\ G/C}$$

where:

ΔP_e = 3 in. H_2O

ΔP_f = 7 in. H_2O

G/C = 2

K_1 = 2.5

Two cases are to be considered for ESFF bags based on preliminary test results: Case I, where the only impact is a reduction of K_2 to 30% of normal; and Case II, where an additional reduction of S_E by 50% is present:

Case I:

$$K_1 = \frac{\Delta P_e}{G/C} + 0.3 \frac{\Delta P_f - \Delta P_e}{2\ G/C} = 1.8$$

Case II:

$$K_1 = 0.5 \frac{\Delta P_e}{G/C} + 0.3 \frac{\Delta P_f - \Delta P_e}{2\ G/C} = 1.05$$

In addition to these two assumptions for ESFF effect, the following cases were considered:

G/C for ESFF = 2, 3, and 4

Bag Life (both) = 2 and 4 years

Table 2 presents the annual operating costs for these various combinations. Cost savings are presented graphically in Figure 8.

TABLE 1
ADVANCED-ESFF BAGHOUSE CAPITAL COST COMPARISON
50,000 ACFM

	CONVENTIONAL	ESFF		
	G/C = 2	G/C=2	G/C=3	G/C=4
Flange-to-Flange	$400,000	512,500	350,000	268,750
Installation	$400,000	400,000	378,373	323,750
Total Installed Cost	$800,000	912,500	728,333	592,500
Percent Savings	0	-14%	+ 9%	+26%

TABLE 2
ANNUAL OPERATING COST COMPARISON

CASE	BAG LIFE (YEARS)	CONVENTIONAL	ESFF		
			G/C=2	G/C=3	G/C=4
I	2	$42,875	41,875	37,542	38,188
	4	$36,125	35,125	33,042	34,813
II	2	$42,875	37,188	30,510	28,813
	4	$36,125	30,438	26,010	25,438

PERCENT ANNUAL OPERATING COST SAVINGS:

I	2	0	2	12	11
	4	0	3	9	4
II	2	0	13	29	33
	4	0	16	28	30

Case I: PDR = 0.3, $(\text{Drag}_e)_{ESFF} = (\text{Drag}_e)_{CONV}$

Case II: PDR = 0.3, $(\text{Drag}_e)_{ESFF} = 0.5\ (\text{Drag}_e)_{CONV}$

CONCLUSIONS

1) The ESFF effect utilizing Advanced ESFF components was clearly demonstrated.

2) The 70 to 80% reduction in K_2 observed on ESFF bags confirmed results obtained in the EPA Laboratory.

3) Some modest reduction of residual drag was observed, but the magnitude remains in question due to the shortness of the test period and the intermittent system cleaning problems.

4) The potential economics of an ESFF baghouse appear attractive.

THE FUTURE

Present plans call for a follow-on study of Advanced ESFF in a full compartment of a reverse air baghouse applied to a stoker-fired boiler at another government installation.

METRIC CONVERSION TABLE

acfm x 0.0004719 = m^3/s

scfm x 0.0004719 = Nm^3/s

scf x 0.028317 = Nm^3

Btu = 1055.07 abs. joules
 = 0.00029302 Int. kWh

Btu/lb x 0.00225 = MJ/kg

ft^2 x 0.0929 = m^2

in. H_2O x 249 = Pa

in. x 2.54 = cm

ft x 0.3048 = m

lb/h x 0.454 = kg/h

gr/scf x 2.29 = g/Nm^3

ft/min x 0.00508 = m/s

REFERENCE

1 Viner, A. S., L. M. Fickel, and L. S. Hovis, "Computer Monitoring of Pilot Plant Baghouse Performance," presented at Sixth EPA Symposium on the Transfer and Utilization of Particulate Control Technology, New Orleans, LA, February 1986.

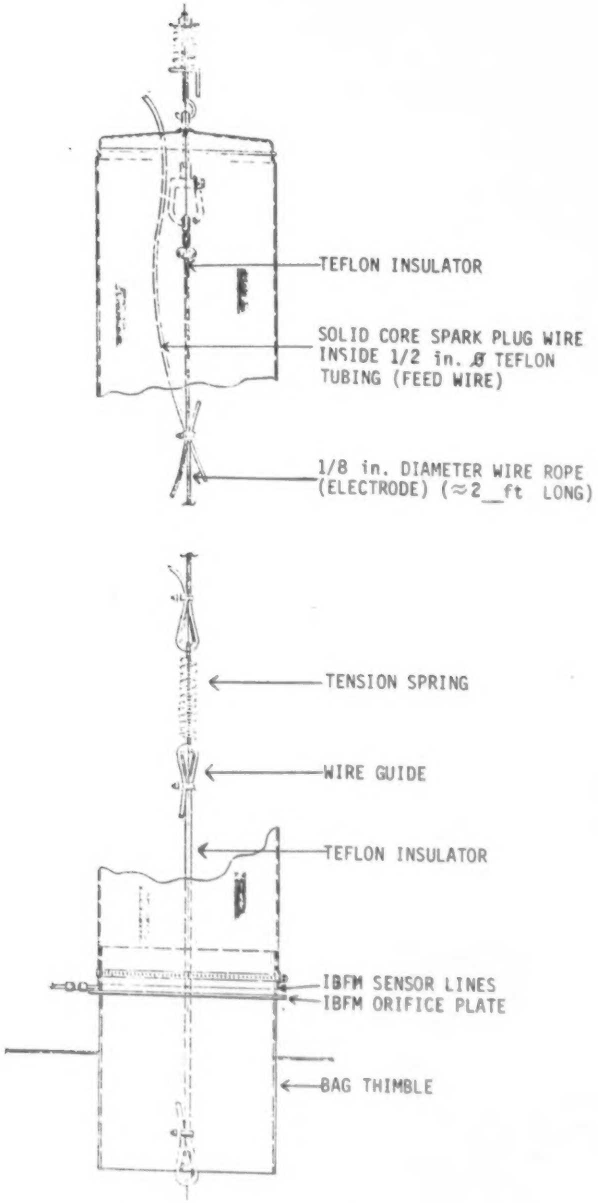
TEFLON INSULATOR
SOLID CORE SPARK PLUG WIRE INSIDE 1/2 in. Ø TEFLON TUBING (FEED WIRE)
1/8 in. DIAMETER WIRE ROPE (ELECTRODE) (≈2 ft LONG)
TENSION SPRING
WIRE GUIDE
TEFLON INSULATOR
IBFM SENSOR LINES
IBFM ORIFICE PLATE
BAG THIMBLE

Figure 1. ESFF Electrode Configuration.

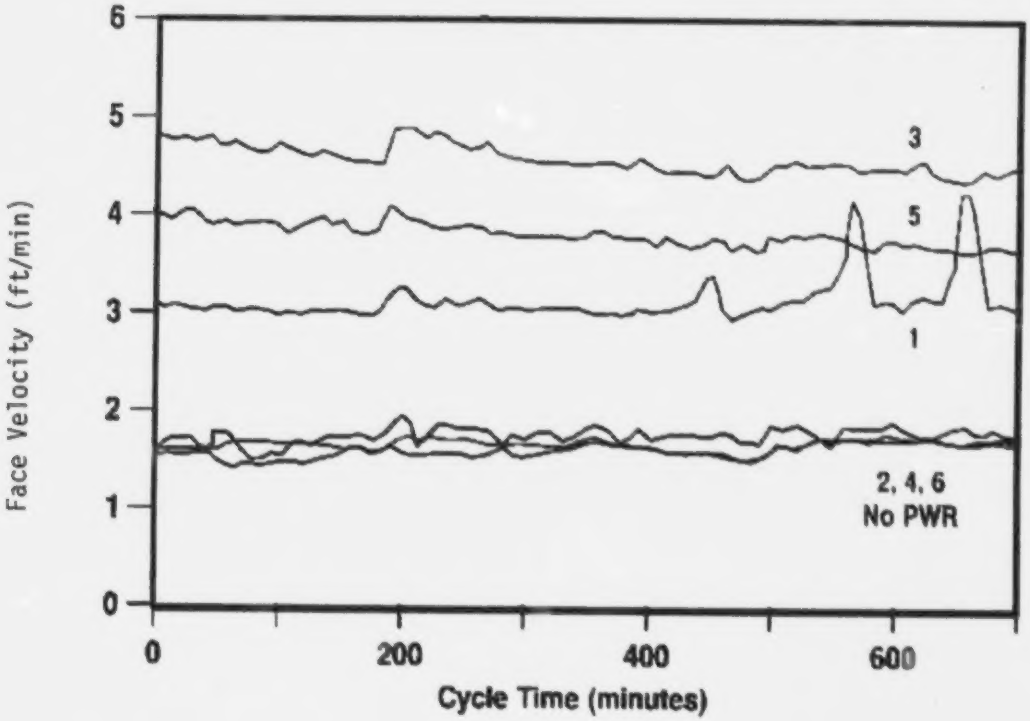

Figure 2. Bag Face Velocities (Cycle 58).

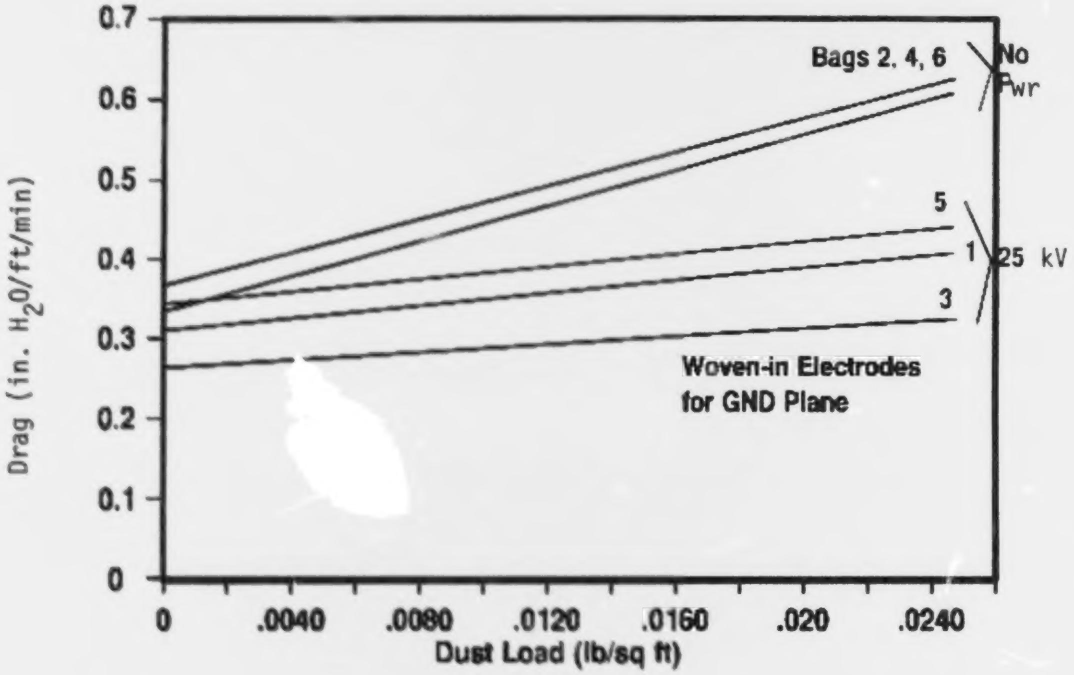

Figure 3. Drag Versus Dust Load (Cycle 58).

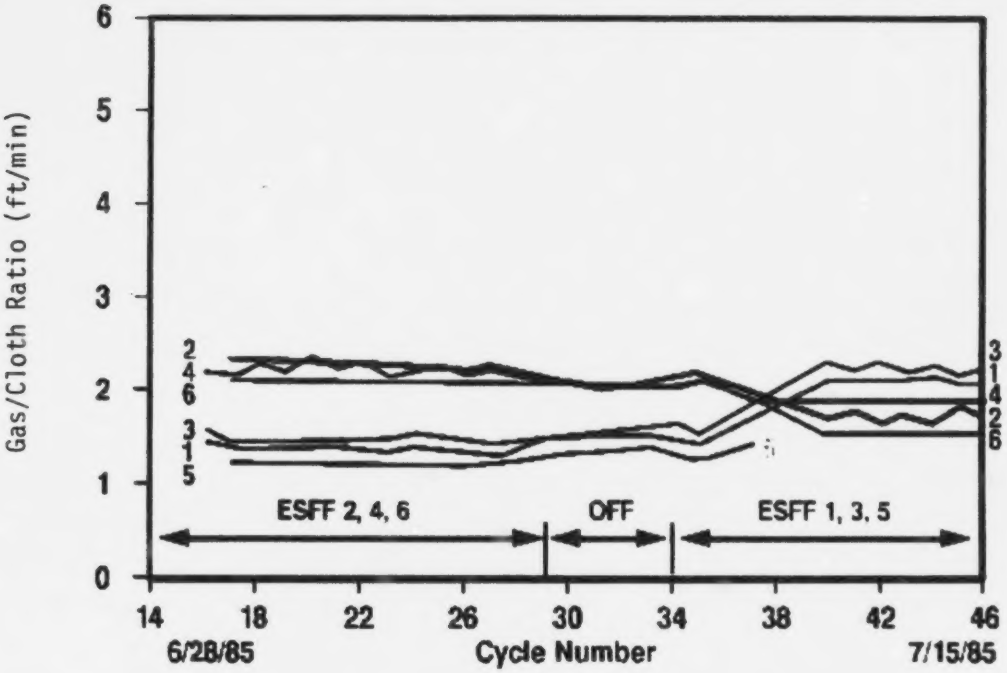

Figure 4. Cycle Average Gas/Cloth Ratio.

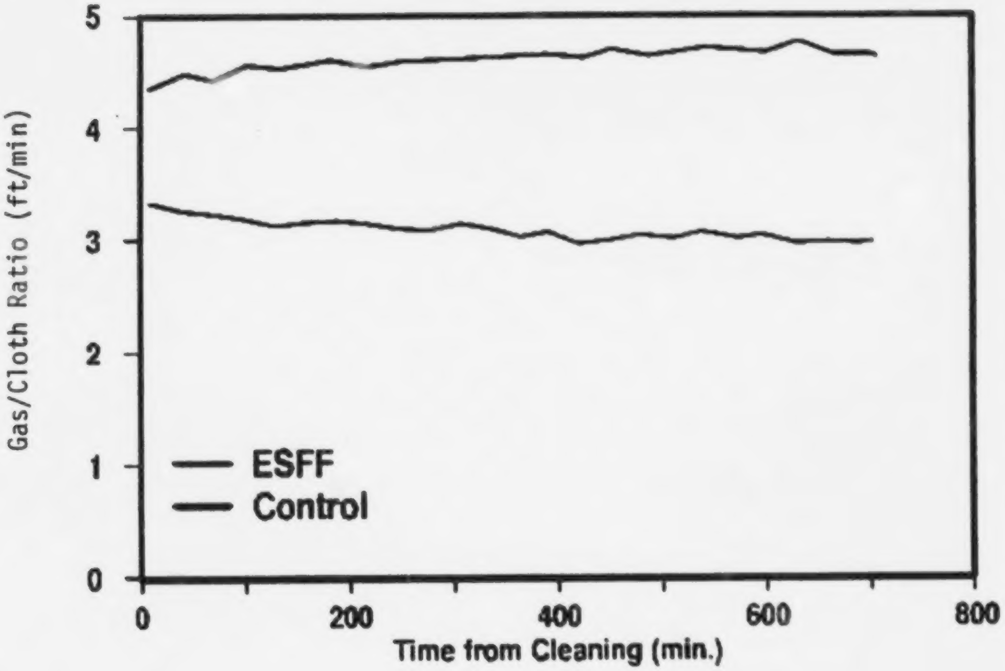

Figure 5. Cherry Point Actual Performances (Data Date 9/22/85, Cycle 149, C_1 = 0.2 gr/acf).

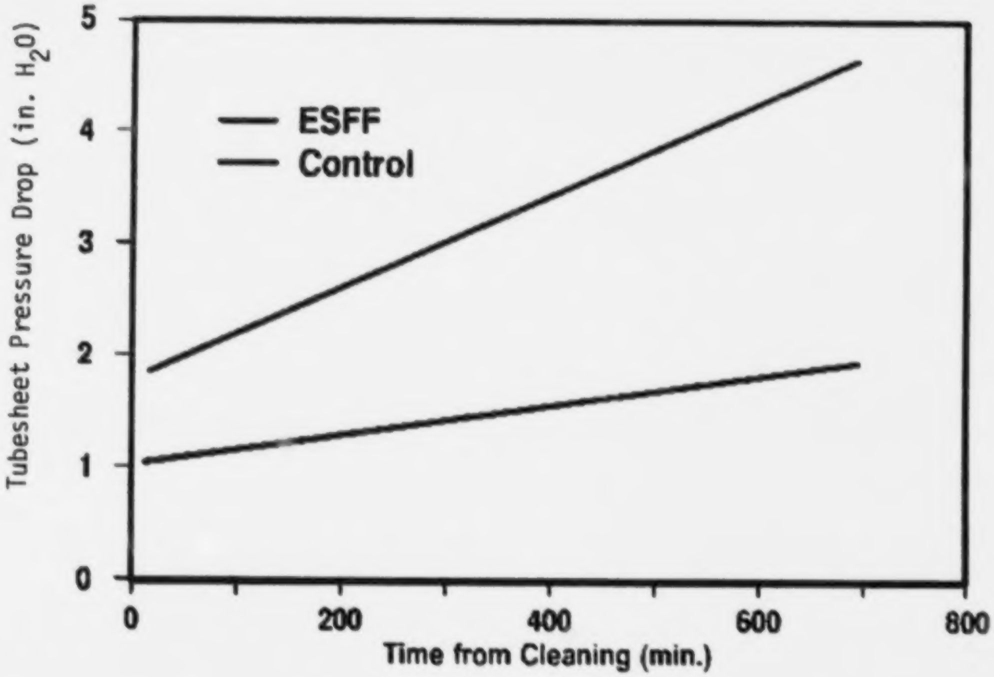

Figure 6. Cherry Point Projected Performance (Data Date 9/22/85, Cycle 149, C_1 = 0.2 gr/acf).

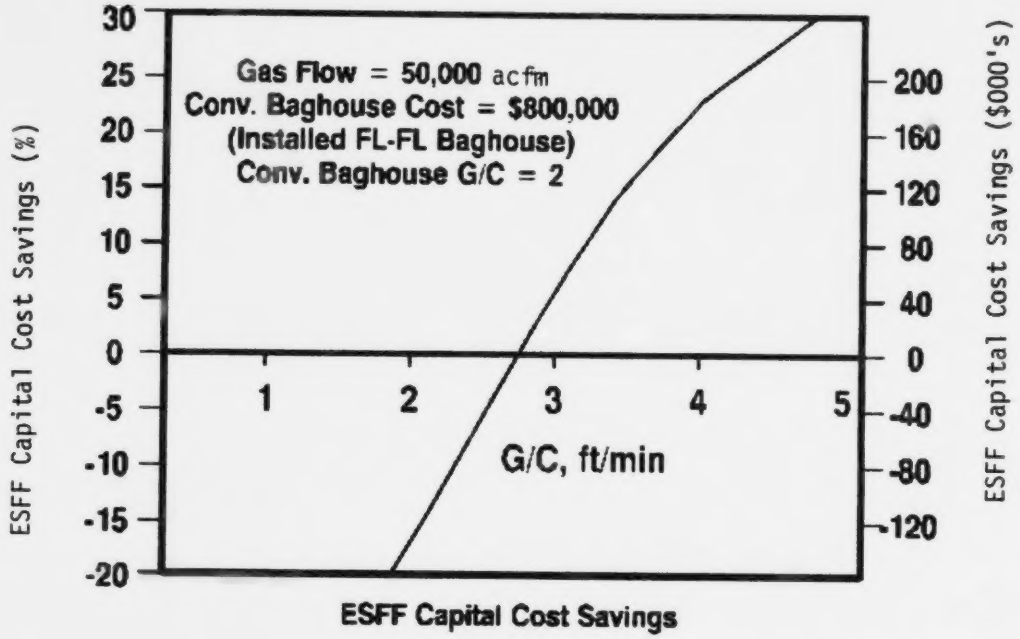

Figure 7. ESFF Capital Cost Savings.

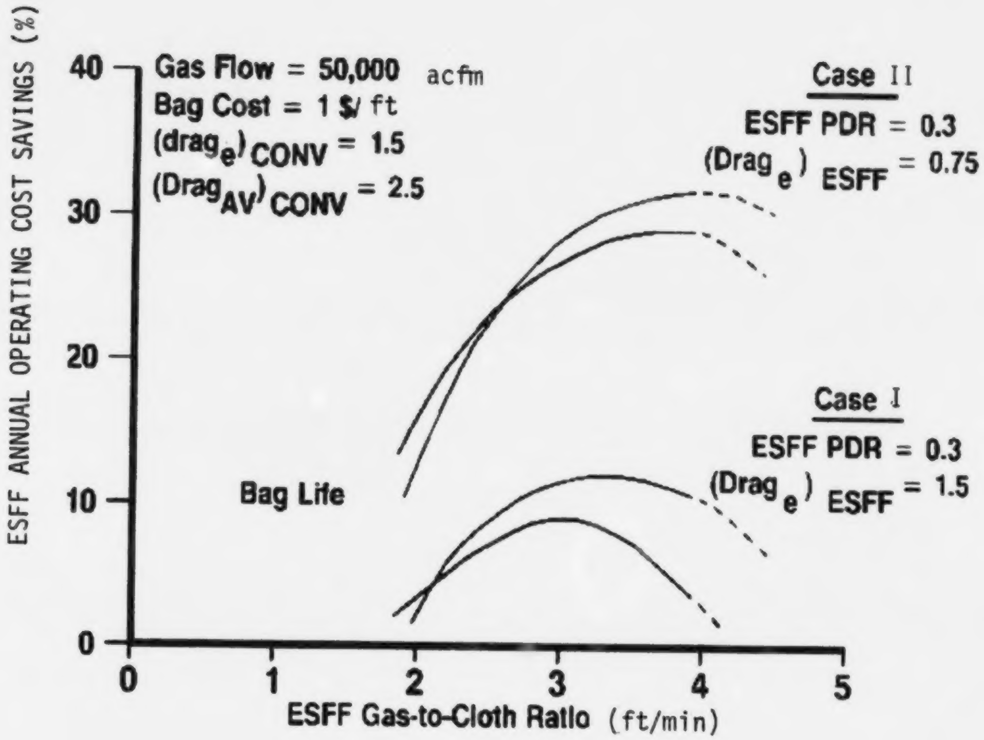

Figure 8. Annual ESFF Operating Cost Savings.

ADVANCED ELECTROSTATIC

FABRIC FILTRATION EXPERIENCE

AT

SOUTHWESTERN PUBLIC SERVICE COMPANY

by

Richard Serrurier

ABSTRACT

In October 1985, the advanced electrostatic fabric filtration (A-ESFF) configuration conversion of the pilot baghouse facility at Southwestern Public Service Company's Harrington Station was completed. Since initial start-up, evolutionary changes in both the operation and configuration have occurred. These changes are discussed herein.

Results to date confirm the existence of a favorable A-ESFF effect. However, it has not been possible to sustain the effect in a steady-state manner. Reasons to explain this behavior have been proposed but remain to be confirmed by future experimental work. Experimental results to date are presented.

This paper has been reviewed in accordance with the U.S. Environmental Protection Agency's peer and administrative review policies and approved for presentation and publication.

The work described in this paper was performed by Southwestern Public Service Company under contract to the U. S. Environmental Protection Agency, Contract 68-02-2659. EPA project officer was Dale L. Harmon.

BACKGROUND

The pilot baghouse unit at Southwestern Public Service Company's (SPS) Harrington Station was installed as an extension of the fabric filter testing program on the main baghouse. SPS's Harrington Station is located northeast of Amarillo, Texas, in the Texas Panhandle.

The pilot baghouse has been operated in a variety of fabric filtration testing programs since being declared operational on May 5, 1980. Most recently, testing of electrostatic fabric filtration (ESFF) using integrally woven electrode bags was conducted from early 1983 through September 1984 (1,2). In this project, it was demonstrated that ESFF would perform with 60% of the pressure drop of conventional bags. The encouraging results of this project suggested that a different electrostatic charging method utilizing higher electrostatic potential might produce even more favorable results. This combination of high voltage field precharging and fabric filter collection has become known as advanced electrostatic fabric filtration or A-ESFF.

The EPA Air and Energy Engineering Research Laboratory at Research Triangle Park, North Carolina, has successfully tested the concept of using a central electrode suspended axially inside a fabric filter bag to which a grounding plane had been attached (3). In these experiments some rather impressive improvements in flowing pressure drop were observed. The Harrington pilot baghouse facility was selected to demonstrate the A-ESFF concept with full scale utility type fabric filter bags.

EQUIPMENT DESCRIPTION

BAGHOUSE

The pilot baghouse at Harrington is a Wheelabrator-Frye, Inc., Model 366, Series 11.5 RS Dustube Dust Collector. It has two 6-bag compartments and uses bags that are 11.5* inches in diameter and 366 inches in length, untensioned. Cloth area per compartment is 549 ft^2 with a full complement of bags.

The unit is operated by a 480 volt control panel and an instrumentation panel. The 480 volt control panel houses the damper controls, hopper heater controls, cleaning cycle timers, fan start/stop controls, and bypass automatic controls. The instrumentation panel houses differential pressure (ΔP), flow, and temperature monitoring devices for each compartment. Pressure drop for the respective bag compartments is measured from the inlet tube sheet to the clean gas side of the filter bags; it is both measured and reported in inches of water (68°F).

---

*Readers more familiar with metric units are asked to use the conversion factors at the end of this paper.

The pilot unit is installed at the southeast corner of the east baghouse on Harrington's Unit 2; Unit 2 is a 360 MWe unit. The inlet flue gas to the pilot unit is pulled from the east inlet duct of the main baghouse and mixed with the hot preheater flue gas through a mixing valve to maintain temperature. Volumetric flows are measured by venturi elements. A simplified flow schematic is shown in Figure I.

The pilot unit is set up for both shaker and reverse air cleaning modes. A variable speed shaker is used on the east compartment and constant speed on the west. During A-ESFF testing, reverse air cleaning was used during test measurement periods.

HIGH VOLTAGE SUPPLY

The required high voltage is developed by a panel mounted Hipotronics Model 850-20 system. This system is capable of operating at 50 kilovolts (kV) and 20 milliamps (mA) for a power level of one kilowatt (kW). Operating polarity can be either positive or negative. The Hipotronics unit output power level is manually controlled by a Variac mounted on the package control panel. Output potential and current flow are indicated by separate meters on the Hipotronics panel. SPS added instrumentation necessary to record the output potential and current flow on strip charts and to provide input to a micro-computer based data logging system.

COAL AND FLUE GAS CHARACTERISTICS

The coal burned at Harrington is a low-sulfur Western coal from the Powder River Basin in the Gillette, Wyoming, area. The coal heating value ranges from 8600 to 8900 Btu/pound and is typically about 8800 Btu/pound. Ash content is usually between 4.9 and 5.0 percent. Sulfur content is typically 0.28 percent (wt.) yielding a release value of 0.637 pounds sulfur dioxide/10^6 Btu. A typical coal analysis is summarized in Table I following.

Flue gas is supplied to the pilot baghouse via a slipstream from the east inlet duct of the main baghouse and enters the pilot baghouse at a pressure of -10 to -15 inches of water (12.56 to 12.38 psia). Flyash content of Harrington flue gas is in the range of 1 to 1.5 grains per actual cubic foot. An analysis typical of flyash collected in the main baghouse is summarized in Table II attached.

FABRIC FILTER BAGS

A-ESFF COMPARTMENT

J. P. Stevens 648 fiberglass fabric with integrally woven Bekaert VN22/1x90 electrodes was used to make the reverse air fabric filter bags for the electrostatic compartment. The bags being used are actually spare

FIGURE I

A-ESFF PILOT PLANT FLOW SCHEMATIC

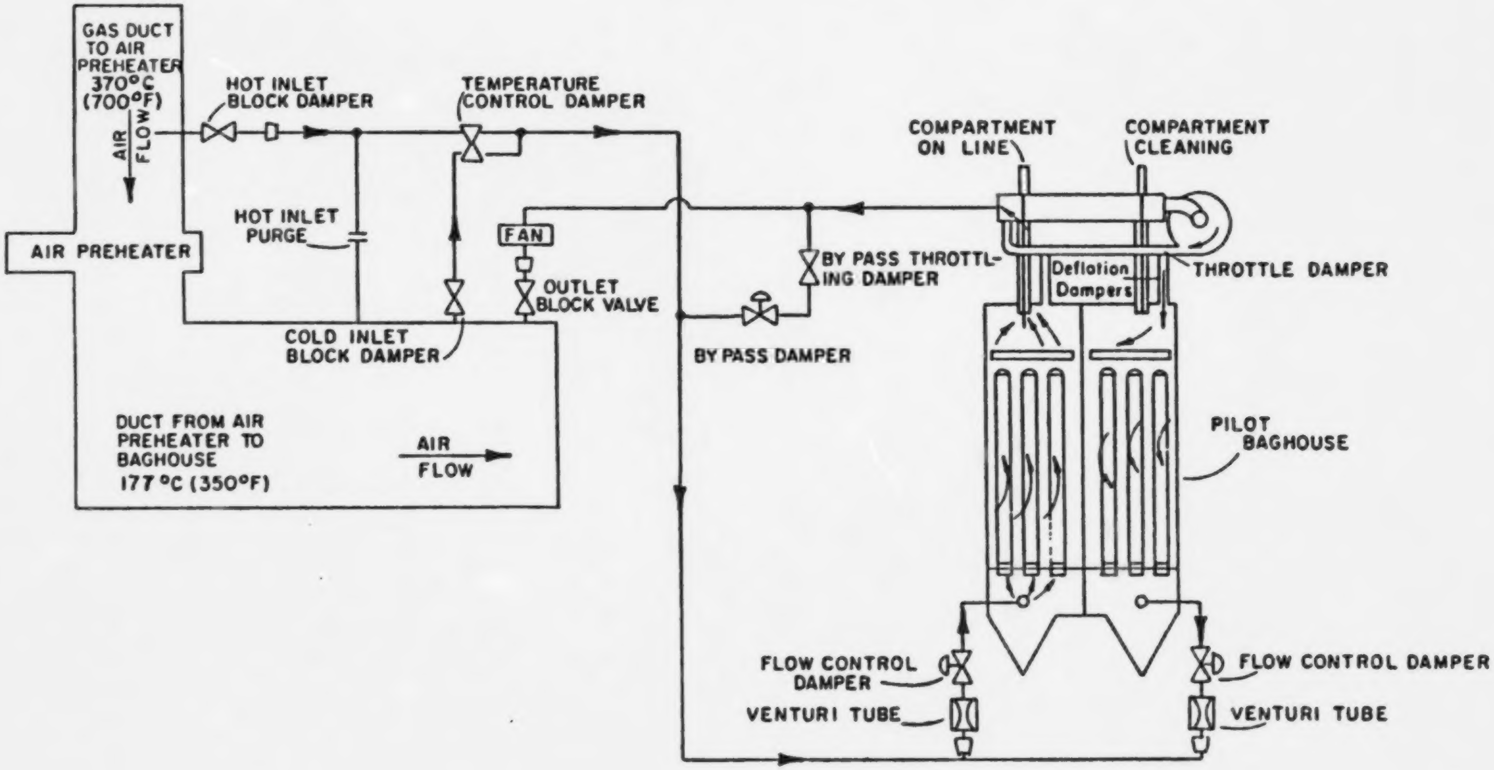
GAS DUCT TO AIR PREHEATER 370°C (700°F)
AIR FLOW
AIR PREHEATER
HOT INLET BLOCK DAMPER
HOT INLET PURGE
TEMPERATURE CONTROL DAMPER
COLD INLET BLOCK DAMPER
FAN
OUTLET BLOCK VALVE
DUCT FROM AIR PREHEATER TO BAGHOUSE 177°C (350°F)
AIR FLOW
BY PASS THROTTLING DAMPER
BY PASS DAMPER
COMPARTMENT ON LINE
COMPARTMENT CLEANING
Deflation Dampers
THROTTLE DAMPER
PILOT BAGHOUSE
FLOW CONTROL DAMPER
VENTURI TUBE
FLOW CONTROL DAMPER
VENTURI TUBE

TABLE I

SOUTHWESTERN PUBLIC SERVICE COMPANY

HARRINGTON STATION: COAL ANALYSIS

Proximate Analysis

	as Received	Dry Basis
% Moisture	26.98	XXXXX
% Ash	4.94	6.77
% Volatile	31.15	42.66
% Fixed Carbon	36.93	50.57
	100.00	100.00
Btu/lb.	8,802	12,054
% Sulfur	0.28	0.39

Ultimate Analysis

	as Received	Dry Basis
% Moisture	26.98	XXXXX
% Carbon	50.81	69.58
% Hydrogen	3.62	4.96
% Nitrogen	0.69	0.94
% Chlorine	0.04	0.05
% Sulfur	0.28	0.39
% Ash	4.94	6.77
% Oxygen	12.64	17.31
	100.00	100.00

MAF Btu/lb.	12,929
% MAF Volatile	45.76
% MAF Fixed Carbon	54.24
Lbs Sulfur Dioxide/10^6 Btu	0.64
% Air Dry Loss	10.79

Moist MM Free Btu/lb	9,298*
% Dry MM Free Volatile	45.38
% Dry MM Free Fixed Carbon	54.62
Lbs Sulfur/10^6 Btu	0.33

*Based on as received moisture: MM = mineral matter

TABLE II

SOUTHWESTERN PUBLIC SERVICE COMPANY

HARRINGTON STATION: ASH ANALYSIS

Chemical Analysis	Results	Spec * Class F/C
Silicon Dioxide (SiO_2) %	30.10	
Aluminum Oxide (Al_2O_3) %	19.90	
Iron Oxide (Fe_2O_3) %	7.60	
Sum of SiO_2, Al_2O_3, Fe_2O_3 % Min.	57.60	70/50
Calcium Oxide (CaO) %	30.80	
Magnesium Oxide (MgO) %	4.30	5.00 Max.
Sodium Oxide (Na_2O) %	0.80	
Potassium Oxide (K_2O) %	0.63	
Sulfur Trioxide (SO_3) %	1.50	5.00 Max.
Moisture Content %	0.13	3.00 Max.
Loss on Ignition %	0.42	12/6 Max.
Available Alkalies (As Na_2O) %	1.20	1.50 Max.
Available Sodium (As Na_2O) %	0.96	
Available Potassium (As K_2O) %	0.34	

* ANSI/ASTM C618-80

bags left over from the previous ESFF experiment and no new cloth was woven for the A-ESFF experiments. Reasons for the choice of fabric, electrode, and construction pattern have been described in previous work (2).

CONTROL (CONVENTIONAL) COMPARTMENT

The control bags from the ESFF project had been used in interim bag test work. Consequently, they were replaced with new Menardi-Southern #996-1 bags. These bags are constructed of the same material and weave pattern (JPS-648) as that used in the woven electrode bags; however, they do not have the separately sewn 6 inch cuff feature of the original control bags. They use a like number of plain steel anti-collapse rings on the same spacing pattern as that used for the electrostatic bags.

MODIFICATIONS FOR A-ESFF OPERATION

In A-ESFF, the electrostatic potential is created between a suspended center electrode operating at either positive or negative polarity and the ground plane formed by the integrally woven electrodes. The suspension system must keep the high voltage electrode centered in the bag cross-section and at the same time allow for vertical dimension changes as the bag expands and contracts with temperature and cleaning forces. Also, the high voltage source must be brought into contact with the center lead through either the bag thimble or cap.

The initial suspension design incorporated a spring at the lower end of the electrode assembly to maintain tension. A sketch of the assembly is shown in Figure II. The electrode assembly consisted of two flat ceramic insulators like those used in Harrington #1's ESP, two J-hooks formed from stainless steel tubing and the necessary length of 1/8" stranded common hardware wire. A simplified schematic of the electrostatic system is shown in Figure III.

The hollow J-hooks allowed the electrode wire to be inserted into the straight part of the "J" and to be secured with hex head set screws; a 4" sleeve of Teflon tubing was slipped down and centered on the wire and J-hook interface to provide both mechanical support and electrical insulation. The high voltage lead was brought through the thimble wall and was secured by set screws to the free end of the lower J-hook to provide the high voltage connection. This connection was sealed with RTV sealant. There was trial and error involved in the initial installation to get the correct center electrode wire length which would provide both proper wire tension and bag tension.

The performance of the high voltage lead wire was critical to the success of the project. The wire had to work at temperatures exceeding 400°F with electrostatic potentials as high as 50 kV. The wire used is Daburn CRT-16-10 and is quite expensive. The thimble routing for the HV lead was chosen primarily to facilitate access for installation and maintenance.

FIGURE II
ORIGINAL CENTER ELECTRODE ASSEMBLY

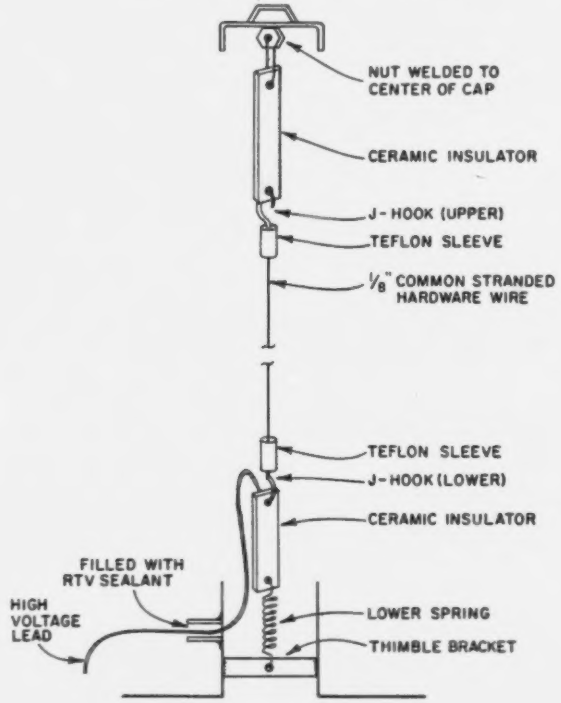
NUT WELDED TO CENTER OF CAP
CERAMIC INSULATOR
J-HOOK (UPPER)
TEFLON SLEEVE
1/8" COMMON STRANDED HARDWARE WIRE
TEFLON SLEEVE
J-HOOK (LOWER)
CERAMIC INSULATOR
FILLED WITH RTV SEALANT
HIGH VOLTAGE LEAD
LOWER SPRING
THIMBLE BRACKET

FIGURE III
SIMPLIFIED ELECTROSTATIC SCHEMATIC

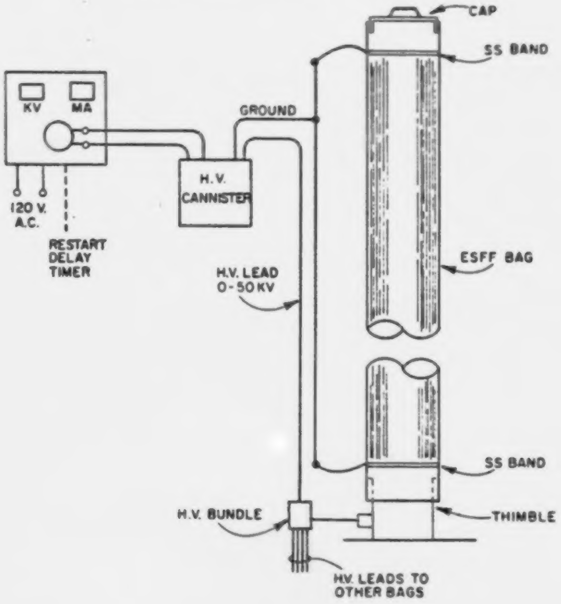
KV
MA
120 V. A.C.
RESTART DELAY TIMER
GROUND
H.V. CANNISTER
H.V. LEAD 0-50 KV
CAP
SS BAND
ESFF BAG
SS BAND
THIMBLE
H.V. BUNDLE
H.V. LEADS TO OTHER BAGS

As previously described, the Hipotronics high voltage control panel was mounted in the #2 baghouse control room replacing the supply used in the ESFF work. The high voltage transformer was mounted externally on the pilot baghouse lower access platform in a weather-proof canister to minimize the length of high voltage wiring runs. A single high voltage lead was brought through the baghouse wall to minimize the number of external connections. Inside the baghouse, individual bag leads were connected to the high voltage supply lead in a common bundle.

START-UP AND OPERATION

SHAKEDOWN AND LEARNING PERIOD

The A-ESFF conversion work was done from September 24 through October 4, 1985. The computer and electrostatic recording instrument interfaces were not installed at this time, but essentially everything else required to operate the electrostatic equipment was in place. From this point on, project events will be discussed on a project day basis referenced to project day 1, October 1, 1985.

Operating conditions for the pilot baghouse were held constant to "simplify" matters. These conditions are summarized as follows:

OPERATING CONDITIONS

Inlet Gas Flow:	915 ACFM/compartment
Filtration Area:	457.5 ft^2/compartment*
Equivalent Air-to-Cloth Ratio:	2.0
Inlet Temperature:	400^oF
Inlet Pressure:	12.4-12.6 psia
Grain Loading:	1-1.5 grain/ACF
Reverse Air Flow:	1.5 air-to-cloth

* 5 of the 6 available bag positions were used.

On day 7, start-up was attempted. Aside from the usual instrument problems, A-ESFF went to ground. This pattern of instrument and electrostatic problems continued for the next several days with the electrostatic problems centering around grounding of the HV lead.

During start-up, the cleaning cycle was being initiated manually until the filtration interval came into the range of the interval timer system. An additional manual operation was introduced because the Hipotronics (HIPO) power supply could not be started automatically after being de-energized for the cleaning cycle. The off-zero interlock prevented a restart of the HIPO with the Variac in a non-zero setting. To restart, the Variac had to be manually returned to the zero output position. Once the Variac was reset to zero, a manual reset was required to restore primary power to the Variac/high voltage canister. The Variac could then be manually returned to its operating position.

The HIPO also had an adjustable current interrupt device (thyratron) which interrupted primary power to the HV transformer when current excursions occurred. It was quite sensitive and required a manual reset whenever a trip occurred.

On day 13, cleaning cycle problems (low reverse air flow) developed in addition to those of the electrostatic system. The cleaning cycle problems (stuck reverse air dampers) were resolved and cleaning was initiated in automatic mode beginning on day 15. The HIPO still had to be manually reset after each cleaning cycle. Finally on day 18 the off-zero interlock circuit was by-passed. This action allowed the HIPO control circuits to be logically tied into the cleaning cycle timer circuitry. The result was that the HV supply could now be started and stopped by the cleaning cycle timer logic.

The thyratron circuit continued to interrupt the HV supply despite sensitivity adjustments. Because the recording equipment was not yet installed, it couldn't be determined how much time A-ESFF was activated. It was suspected, however, that it was not a significant percentage of the filtration time.

Positive polarity had been used during the first phase of start-up. On day 21, polarity was switched to negative to see if A-ESFF performance would be affected. No particular effect, either positive or negative, was observed.

On day 24, the cleaning cycle parameters were modified in an effort to improve electrostatic reliability and filtration characteristics for both compartments. The first step was to increase the reverse air flow time from 45 to 60 seconds. Some improvement was noted and on day 25 the cleaning cycle reverse air period was revised to two 30 second flows separated by a settle period. Both compartments were manually shaker-cleaned on line to return the bags to their clean operating point, a procedure referred to as "base-lining." Significantly, during the remainder of day 25 and through day 26, there were no HV supply tripouts. As the bags began to accumulate dust, HV trips increased to one on day 27 followed by two on day 28 and two on day 29.

On day 29, an oxygen balance was run on the pilot baghouse to check for inleakage. Total inleakage was estimated at 7% of inlet gas flow by volume and was judged to be marginal, but acceptable. The largest leak was above the cell plate in the A-ESFF compartment. This leak was in the wiring conduit for the HV lead and was fixed during the next maintenance outage.

No meaningful data were generated during the first 31 days of operation, but mechanically at least, progress had been made. Electrostatically, operation had been attempted at 30 to 34 kV with resultant current flow in the range of 1 to 4 mA. Electrostatic performance from an operating time standpoint was clearly unacceptable and, although the amount of filtration time which was effectively exposed to A-ESFF was uncertain, it clearly was not enough.

The following were observed as of day 31:

- High voltage supply would be lost primarily on restart because of current surges (thyratron interrupt).
- Dependence on manual coverage to reactivate A-ESFF was unreliable.
- The cleaning cycle energy input requirements appeared to be higher than we had experienced in past work (ESFF).
- As the bags got dirtier, the tendency to lose A-ESFF from current spiking (arcing) would increase (thyratron interrupt).
- After cleaning, 4 to 5 mA was maximum current which could be tolerated by the process without creating disruptive current spikes.
- Both sets of bags could be cleaned down to a repeatable level by shaking; the A-ESFF side always cleaned down farther than the conventional side.

During the next thirty project days, inroads were made concerning electrostatic reliability. Instrumentation was installed to allow recording of the electrostatic data. The earlier observation that the dirtier the bags, the more difficult it was to keep high voltage supplied to the bags was confirmed. The thyratron protective circuit imposed operating difficulties as it would interrupt A-ESFF high voltage at the slightest current excursion.

On day 31, the filtration interval had been reduced to thirty minutes to increase cleaning opportunities. This move seemed to have no particular effect on either the A-ESFF or control performance. Finally, on day 45, the reverse air flow instrumentation was checked and was found to be seriously in error. This was recalibrated and the reverse air dampers were reset to give a nominal reverse air flow of 1.5 air-to-cloth ratio. Both sets of bags responded with a reduction in operating pressure drop. The bags were base-lined to restore them to their respective clean operating points and data taking resumed.

On day 46, the thyratron protection circuit on the HIPO was bypassed. No more losses of high voltage due to this type of protective interrupt were experienced until day 49 when bag (2,2) electrode suspension assembly failed and grounded against its thimble.

Upon examination, it was found that the soft iron wire used to make the top assembly connection had failed. Fortunately, no bag damage occurred as the upper insulator and wire fell into the thimble. It was also found that the bottom tension springs in other bags had become unattached leaving the center wires freely suspended. At this time, the suspension system was modified to a dead-weight assembly and the top-mount was changed to a substantial S-hook as shown in Figure IV. During this downtime, a delay start timer was installed so that the restart of A-ESFF after cleaning could be varied as needed.

Restart was attempted with a return to a 60-minute filtration cycle on day 56, but a ground fault developed in bag (1,1). The insulation on the high voltage lead to bag (1,1) had failed inside the thimble nipple and was the second failure of this type experienced. Start-up was successful on day 57 only to encounter grounding problems on the following day. This time the high voltage bundle (see Figure III) had fallen on the cell plate and had grounded against the bag (1,1) thimble. Repair was made and the bundle was suspended more securely. Restart was accomplished the same day and operation continued for six days until Unit 2 developed a boiler tube leak and had to be shut down for repair.

While efforts to achieve steady state bag conditions had been thwarted once more by a process interruption, definite progress had been made. Reasonable operational integrity had been achieved marking the end of the shakedown period. Although little meaningful pressure drop data were generated in this start-up period, the effect of process changes as reflected by the daily average pressure drop data for each compartment is documented in Figure V (A-ESFF) and Figure VI (Control).

OPERATION AND DATA GENERATION

On day 73, the pilot baghouse was restarted and operated for eleven days. During this period, neither the control nor A-ESFF bags reached equilibrium as shown in Figure VII. A-ESFF current density averaged nearly 10 microamps per square foot at an average input power of 31.3 watts per bag. Electrostatic potential averaged 35.4 kV. This particular run was interrupted on day 83 by mechanical failure of the high voltage connection at the lower electrode J-hook on bag (2,3). The response to loss of A-ESFF was immediate as the last two data points in Figure VII illustrate. Variation of K_2C for each of the bags during this time period is depicted in Figure VIII.

Repair was made on day 84 by employing a screw clamp to mechanically attach the bare primary HV wire to the J-hook. An additional clamp was used to hold the insulated lead in place and to absorb gas flow turbulence forces.

Restart was achieved later the same day and operation continued for eleven consecutive days when Unit 2 developed another boiler tube leak and had to be shut down. Electrostatic conditions were nearly the same as the previous run with the electrostatic potential down slightly at 34.9 kV. During this period of operation, the control (East) bags appeared to

FIGURE IV
MODIFIED CENTER ELECTRODE ASSEMBLY

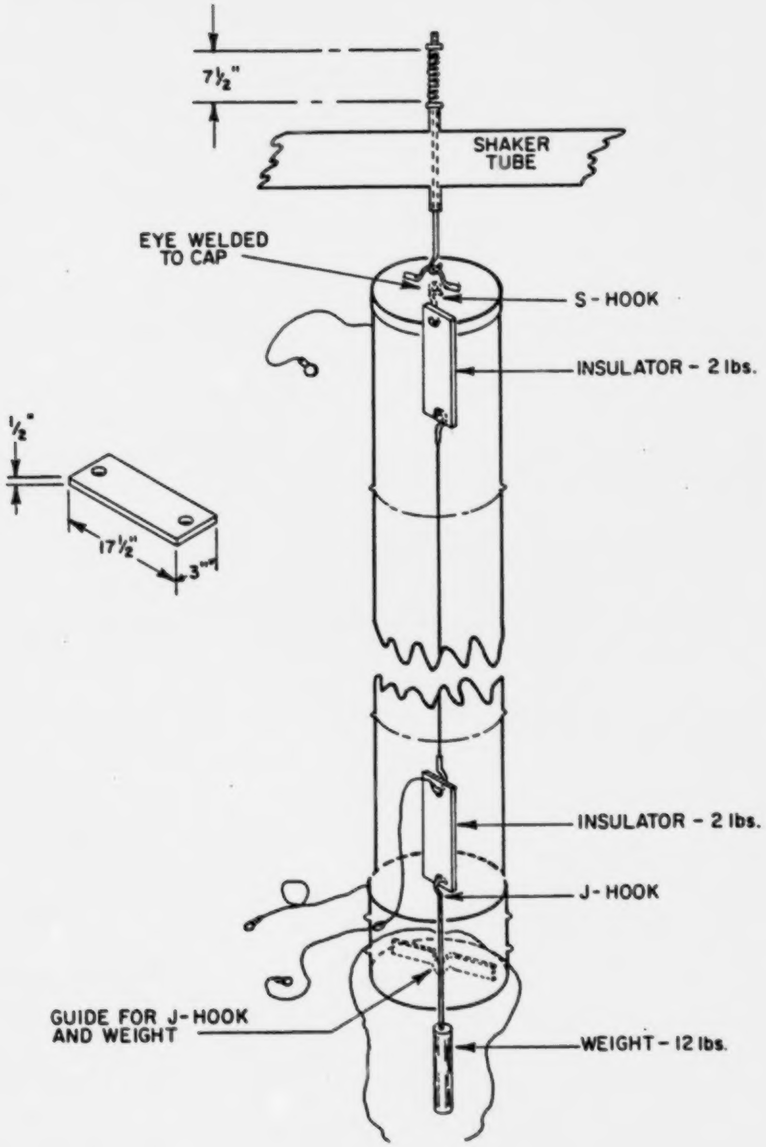
7½"
SHAKER TUBE
EYE WELDED TO CAP
S-HOOK
INSULATOR - 2 lbs.
½"
17½"
3"
INSULATOR - 2 lbs.
J-HOOK
GUIDE FOR J-HOOK AND WEIGHT
WEIGHT - 12 lbs.

FIGURE V

WEST PILOT BAGHOUSE DAILY AVERAGE ΔP's
10-07-85 THRU 12-02-85

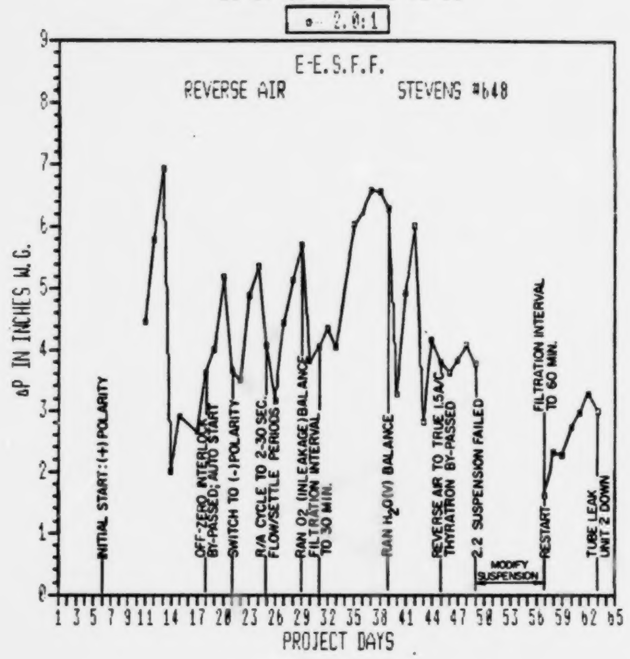

FIGURE VI

EAST PILOT BAGHOUSE DAILY AVERAGE ΔP's
10-07-85 THRU 12-02-85

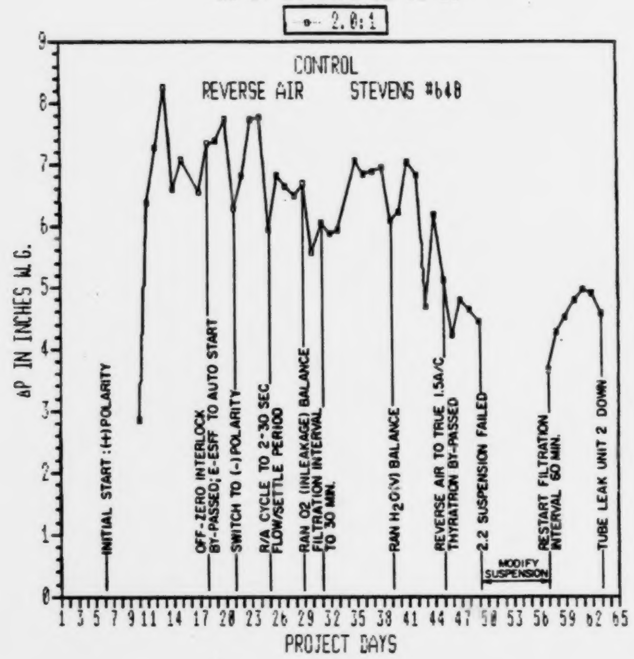

Reproduced from best available copy.

FIGURE VII

AVERAGE DAILY PRESSURE DROP PERFORMANCE: DAY 73-84

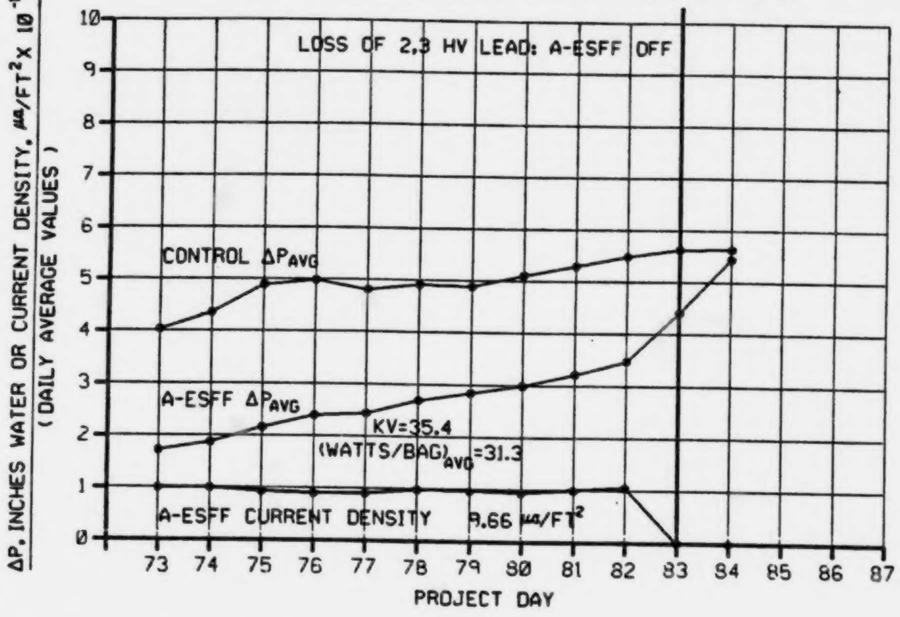

FIGURE VIII

VARIATION IN K_2C WITH TIME: DAY 73-84

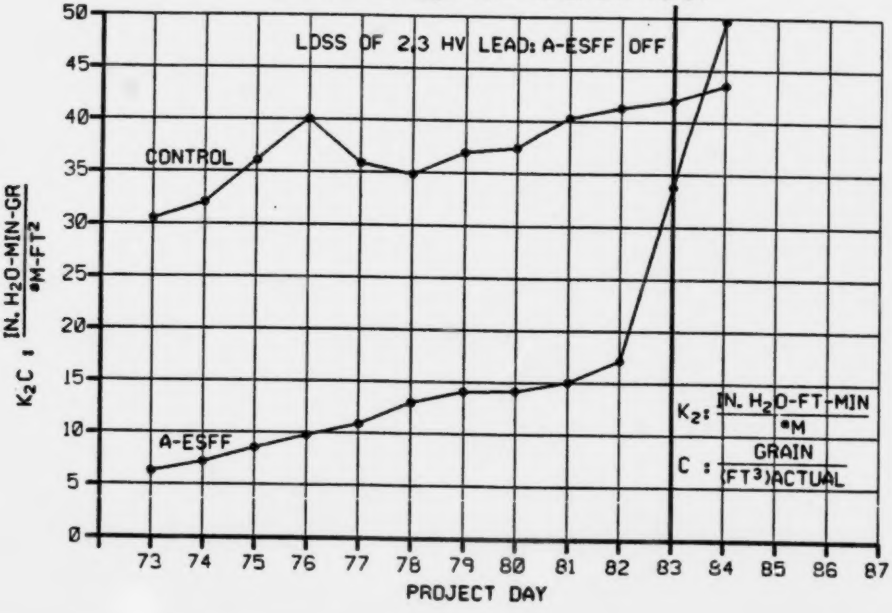

equilibrate at an average daily pressure drop of about 5.4 inches of water. The A-ESFF bags (West) did not equilibrate but appeared to approach equilibrium when the run was ended. The results are depicted in Figure IX. Also of interest in Figure IX is the effect of shutdown and restart on the control bags; the control compartment was not entered during maintenance, but the pressure drop characteristics were nonetheless temporarily altered by the action. Variation in K_2C with time is shown in Figure X.

In the downtime between day 94 and day 112, four attempts were made to restart the pilot baghouse. Problems related to Unit 2 caused two cancellations. The other two were related to A-ESFF problems, including another HV lead insulation blow-out and loss of ground wire integrity. The insulation failure had no obvious, direct cause except possible abrasion failure caused by excessive wire movement within the HV nipple. The RTV seal used in the HV nipples was not holding the HV leads in place and was not forming a secure gas seal between the dirty and clean gas sides of the compartment as evidenced by dust accumulation. A mechanical seal utilizing a ¼" tubing x ½" pipe fitting was installed on each lead. To make the seal, the fitting was drilled out to allow the HV lead (with the nut and ferrule already on the wire) to pass through for connection to the bag. The ferrule and nut were then installed just as if the wire were tubing; the ferrule gripped the HV lead wire to physically secure it and effect a gas seal at the same time. As a precaution, all ground lead connections were redone and all grounding wire was physically rerouted within the baghouse to isolate it from all high voltage leads.

With the above changes, the baghouse was restarted on day 112. The objective was to push current density into the range of 30 microamps per square foot and operate for at least fifteen days. This was accomplished, but electrostatic instability developed in the A-ESFF system over the last three run days.

The average daily pressure drop data for this run are depicted in Figure XI. The control (East) bags equilibrated quickly at a daily average pressure drop of 5.3 inches of water. These data checked well with data from the previous run. Unexpectedly, the A-ESFF (West) bags never reached equilibrium despite an average current density of 29.3 microamps per square foot and an electrostatic potential of 36.7 kV. The average power input per bag was 98.5 watts or over three times the power input of the previous runs. The operating pressure drop ratio (A-ESFF/control) at the beginning of the run was 0.3 while at the end of the run it was approximately 0.79.

Over this test period, the slope (K_2C) of the A-ESFF filtration curve continued to increase as did the extrapolated or filtration time zero pressure drop (ΔP_E). The respective K_2C values for the control and A-ESFF bags are plotted in Figure XII and show that the K_2C value for the control was reasonably constant at near 42.

FIGURE IX

AVERAGE DAILY PRESSURE DROP PERFORMANCE: DAY 84-94

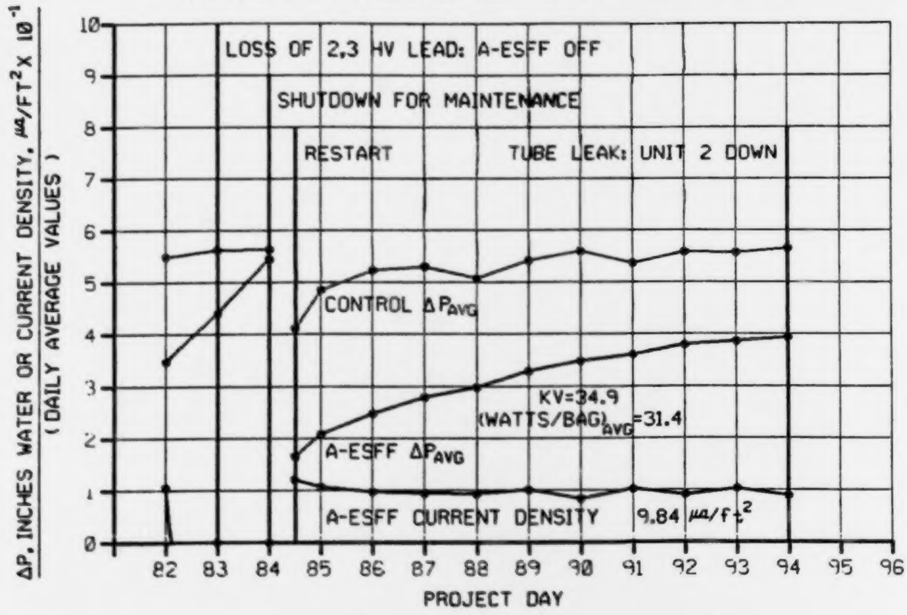

FIGURE X

VARIATION IN K_2C WITH TIME: DAY 84-94

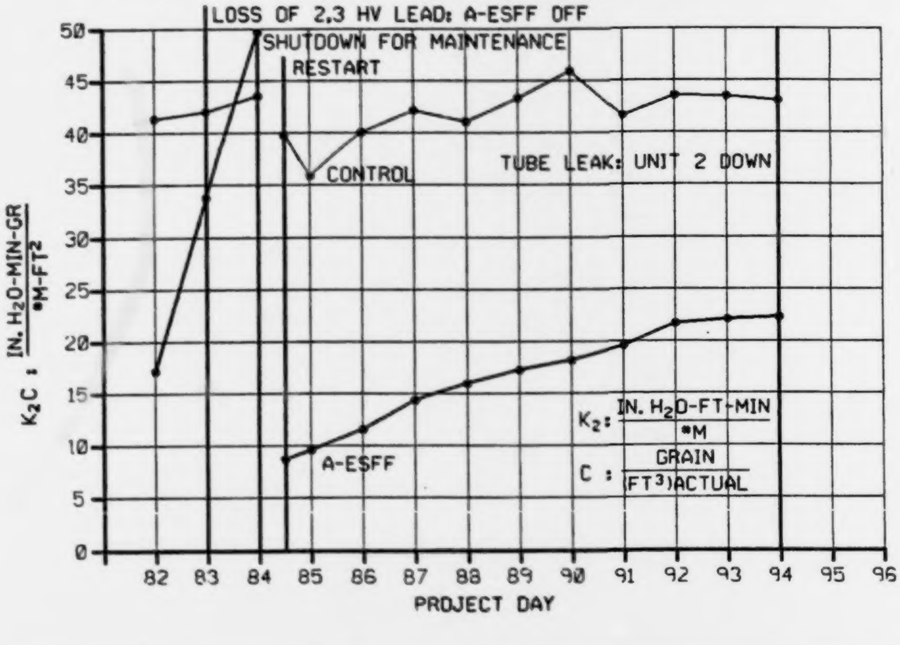

FIGURE XI

AVERAGE DAILY PRESSURE DROP PERFORMANCE: DAY 112-126

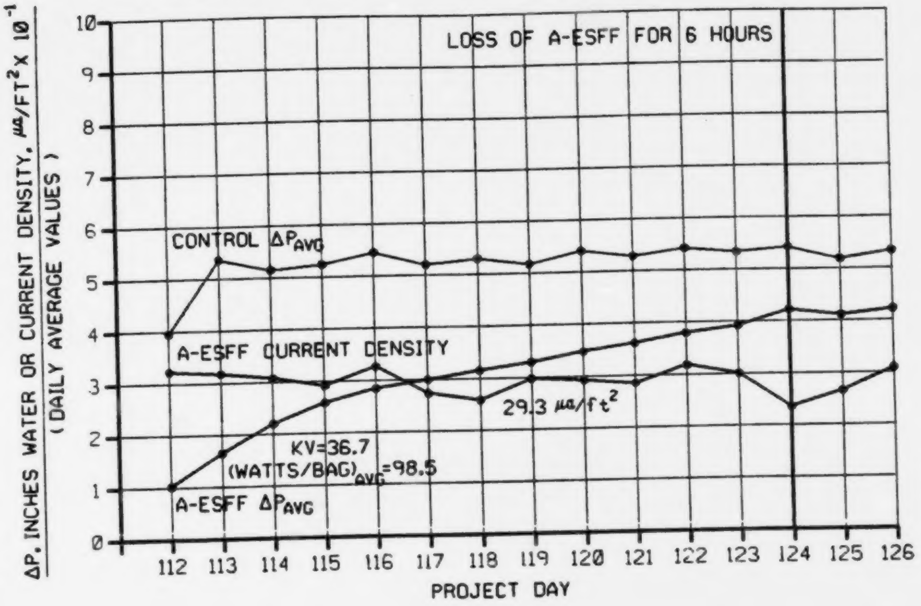

FIGURE XII

VARIATION IN K_2C WITH TIME: DAY 112-126

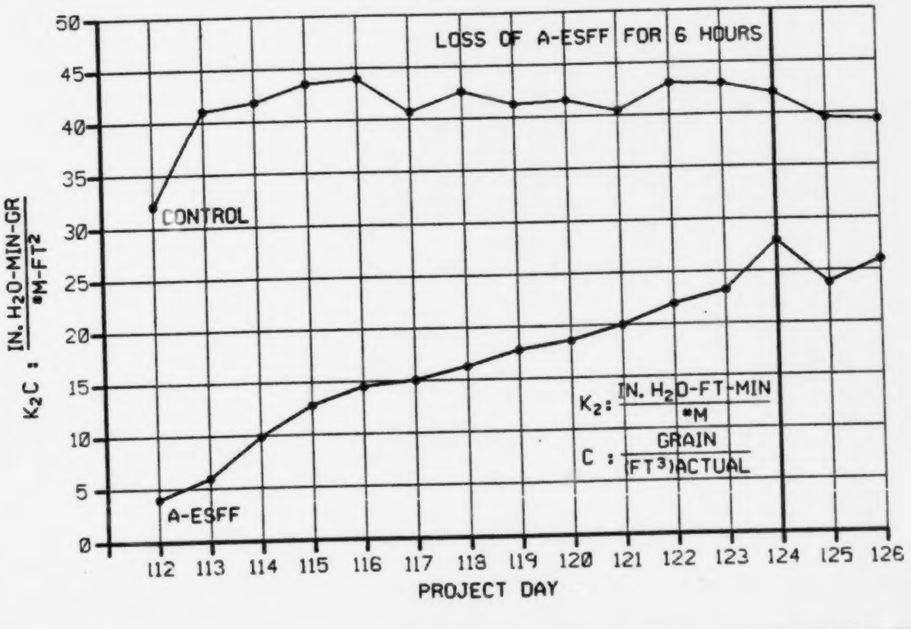

DISCUSSION OF RESULTS TO DATE

What looks to be a rather significant change in K_2C value actually translates into a rather small effect on the average daily pressure drop. Most of the movement of the daily average pressure drop for the A-ESFF compartment is caused by increase of the residual or time-zero pressure drop (ΔP_E). About 87 percent of the change in average daily pressure drop for the A-ESFF bags is attributed to this effect.

It would appear, given the performance of the control bags, that A-ESFF is superimposing an effect on the filtration process. Apparently, the A-ESFF process requires a more vigorous cleaning force than is being provided with the reverse air technique. When each compartment was cleaned by shaking, the A-ESFF bags always cleaned down to a lower residual pressure drop than did the control. This suggests that some residual holding force must be overcome before the filtrate will release from the bag surface. Alternatively, A-ESFF could be preferentially collecting small particles causing blinding of the bags.

In conclusion, to date the following have been observed:

- Extremely low pressure drops can be demonstrated with A-ESFF; however, the initial effect disappears with time for suspected, but unconfirmed reasons.
- Cleaning force requirements for A-ESFF appear to be greater than those for conventional bags. If this is the case, the cleaning force generated by the reverse air cleaning cycle being used is inadequate.
- Shake cleaning will restore both control and A-ESFF bags to repeatable clean performance points with A-ESFF displaying lower values than the control. This supports the idea that some sort of assist to the reverse air cleaning will allow A-ESFF to equilibrate.
- The increase in power in the day 112-126 run was primarily current related. Electrostatic potential increased from about 35 kV in previous runs to 36.7 kV, or about 5 percent. Thus current saturation was most likely achieved in the previous runs with a current density of 10 microamps per square foot.
- Electrostatic reliability has improved, but long term operating solutions have not been developed for all the problems associated with this demanding service.

This somewhat limited data collection indicates that there is a real A-ESFF effect which potentially could reduce fabric filtration operating pressure drop by 60 to 80 percent. However, this effect has not been successfully sustained. Major efforts in the next operational phase will be directed as follows:

- Implement changes which will increase electrostatic potential while providing adequate current density.
- Explore operational changes such as significantly delaying A-ESFF start after cleaning to minimize the early collection of small particles.
- Explore the benefits of increased cleaning force by some as yet undetermined process.

METRIC EQUIVALENTS

Readers more familiar with metric units may use the following to convert to that system.

Nonmetric	Times	Yields Metric
acfm	4.719×10^{-4}	am^3/s
Btu/lb	2.32×10^3	J/Kg
ft	0.3048	m
°F	(°F-32)/(1.8)	°C
gr/acf	2.29	g/m^3
in.	2.54	cm
in. H_2O	249	Pa
$\frac{\text{in. } H_2O\text{-ft-min}}{\text{lb}}$	1.00×10^4	$\frac{P_a\text{-m-s}}{\text{Kg}}$
$\frac{\text{in. } H_2O\text{-min}}{\text{ft}^2}$	1.61×10^5	$\frac{P_a\text{-s}}{\text{m}^2}$
lb	0.454	Kg
lb/MMBtu	430	ng/J
psia	6.89×10^3	Pa
a/ft^2	10.76	a/m^2

REFERENCES

1. Chambers, R., Spivey, J. and Harmon, D. ESFF Pilot Plant Operation at Harrington Station. In Vol. 3, Proceedings: Fifth Symposium on the Transfer and Utilization of Particulate Control Technology, EPA/600/9-86/008c (NTIS No. PB 86 167178). February 1986. pp. 25-1 to 25-17.

2. Spivey, J., Chambers, R. and Harmon, D. Development of Woven-Electrode Fabric and Preliminary Economics for Full-Scale Operation of Electrostatic Fabric Filtration. In Vol. 3, Proceedings: Fifth Symposium on the Transfer and Utilization of Particulate Control Technology, EPA/600/9-86-008c (NTIS No. PB 86 167178). February 1986. pp. 24-1 to 24-19.

3. Hovis, L., Daniel, B. and Donovan, R. Electrostatic Enhancement of Fabric Filtration of Fly Ash and Spray Dryer By-Product. Presented at the 3rd EPRI Conference on Fabric Filter Technology for Coal-Fired Power Plants. Scottsdale, Arizona, 1985.

ECONOMICS OF ADVANCED ELECTROSTATIC STIMULATION OF FABRIC FILTRATION

L.S. Hovis
Air and Energy Engineering Research Laboratory
U.S. Environmental Protection Agency
Research Triangle Park, NC 27711

and

A.S. Viner
Research Triangle Institute
Research Triangle Park, NC 27709

ABSTRACT

Advanced Electrostatic Stimulation of Fabric Filtration (Advanced ESFF), with its center-wire configuration which produces corona charging in particles to augment an external electrical field, has a performance edge over other electrostatic enhancement methods. Laboratory and pilot plant results show a consistently lower pressure drop and a rate of pressure drop rise that is 70 percent less than those of conventional filtration.

A study of the economics of Advanced ESFF was undertaken to determine if the improved performance would more than compensate for the increased cost of electrical hardware and additional maintenance. The cost model that had been developed for conventional ESFF (parallel external field and no particle charging) was modified to account for the center-wire concept and used to compare Advanced ESFF capital and operating costs with those of conventional filters. The economic advantage of Advanced ESFF is based on its ability to operate at a higher air-to-cloth ratio while maintaining the same pressure drop as a conventional filter. The ability to operate with higher air-to-cloth ratios translates to capital cost savings due to smaller baghouse size.

This paper has been reviewed in accordance with the U.S. Environmental Protection Agency's peer review and administrative review policies and approved for presentation and publication.

INTRODUCTION

The strong interest in the development of Electrostatic Stimulation of Fabric Filtration (ESFF) by the Environmental Protection Agency has been based on a potential economic advantage over conventional fabric filtration. While stressing a simple and practical electrical system and the technical advantages over conventional filtration, the idea of a clear and unmistakable economic advantage has been the primary goal. The Advanced ESFF system most closely meets the objective of a simple and effective application of electrostatics to fabric filtration. There are still some unanswered questions before full commercialization can be realized, but Advanced ESFF does appear to meet the desired standards as shown by laboratory and limited pilot results.

The performance of the new center-wire concept of ESFF has been described elsewhere (1), and modeling of the concept has advanced to the point of explaining the ESFF phenomena (2,3). Promising results were obtained at a pilot installation on a stoker-fired boiler producing low resistivity fly ash (4). The results from that study will be used here as a basis for calculating the cost effectiveness of ESFF.

ADVANCED ESFF PROTOTYPE DESIGN

The hardware requirements for implementing advanced ESFF in a conventional baghouse are quite simple: a power supply and controls; an electrode for each bag; and wiring to connect the two. The power supply technology has been available for decades as a result of work on electrostatic precipitators. For a typical filter bag (9.1 m long, 0.3 m diameter), the voltage required to maintain a field strength of 3 kV/cm from the center of the bag to the fabric wall is 45 kV. Pilot plant results indicate that the required current is approximately 0.21 mA/m^2 for a total of 1.86 mA/bag. Assuming that a compartment were designed to contain 400 bags, then a 45 kV, 1 A power supply could provide ESFF power for one compartment (with a 23 percent overcapacity). Control circuitry similar to that used with ESPs would be needed to minimize sparking from the center electrode to the grounded bag surface. Sparks may produce holes in the bags, thereby producing high penetration. Excessive sparking would eventually destroy the bags.

A prototype design for an ESFF electrode is shown in Figure 1. A hook suspended from the cap at the top of the bag supports a nonconductive cable 0.5 m long that isolates the high voltage electrode from the grounded bag cap. The well-insulated wire from the power supply penetrates the bag cap and connects to the high voltage cable where it is attached to the insulating cable. The electrode is a flexible cable 8 m long made of small diameter steel wires. The electrode terminates 0.5 m above the tubesheet where a steel spring (15 cm

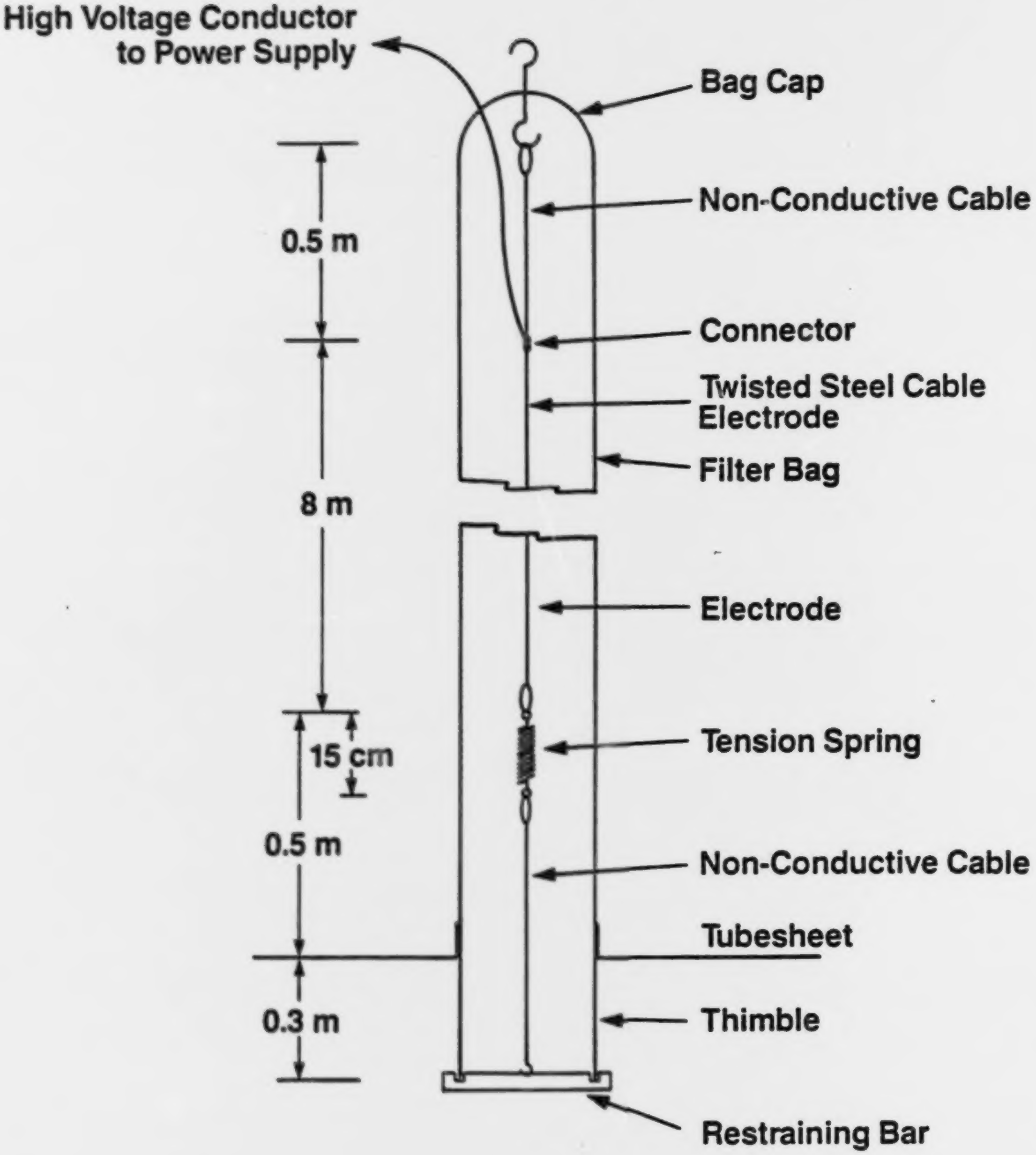
High Voltage Conductor
to Power Supply
Bag Cap
Non-Conductive Cable
Connector
Twisted Steel Cable
Electrode
Filter Bag
Electrode
Tension Spring
Non-Conductive Cable
Tubesheet
Thimble
Restraining Bar
0.5 m
8 m
15 cm
0.5 m
0.3 m

Figure 1. A prototype electrode design for implementation of advanced ESFF.

long) is attached. The lower end of the spring is attached to a nonconductive cable. This cable extends below the tubesheet and is attached to a restraining bar at the inlet of the bag thimble. The restraining bar anchors the electrode and centers it along the bag axis. The spring at the bottom of the electrode permits the electrode to be tensioned simultaneously with the bag.

This design is based on the electrode that was successfully demonstrated in a pilot plant, and it includes improvements based on that experience. The construction materials are readily available, and the construction itself is simple. Installing the electrodes in the bags at the pilot plant proved cumbersome, but the improvements included in the prototype design should simplify the task.

There is one last requirement for successful implementation of advanced ESFF: an electrical ground plane. In the pilot plant study, the ash that was collected had a high unburned carbon content and consequently a low electrical resistivity. The dust collected on the bag was sufficiently conductive to serve as the ground plane for the field. This case provided a good opportunity for demonstrating advanced ESFF. However, in general, the resistivity of ash from a pulverized coal boiler will be much higher. Therefore, to provide a suitable electric field, a method must be found to make the bag conductive. Spivey (5) reported on a successful technique for weaving small diameter wires into the fabric. Alternatively, it may be possible to identify a conductive coating that can be applied to the bag surface. Another possibility would be to sew wire strips to the outside of bag. Many possibilities exist; however, each will result in a higher bag cost that must be taken into account in the evaluation of economic feasibility.

ESTIMATION OF CAPITAL AND OPERATING COSTS

A rigorous evaluation of the economic feasibility of ESFF entails comparing the capital and operating costs of ESFF with those of conventional baghouses. This comparison must include all of those items whose costs would be affected by a change in the collector (i.e., not only the baghouse, but also the ductwork, insulation, and ash handling system). Also, the installation charges must be included along with engineering costs. The cost of the ESFF hardware and installation must also be calculated and added where applicable.

Operating costs include fixed and variable costs (including bag replacement) and the cost of electricity for running the equipment. Of course, there will be an additional expense for electricity in an ESFF baghouse.

The easiest way to estimate the cost of equipment is to scale it according to the size and cost of a similar piece of equipment. Viner and Ensor (6) used this method to develop empirical equations for the cost of conventional baghouses. The most important parameters in determining the cost of equipment are the gas flowrate, air-to-cloth ratio, and the number of individual compartments in the baghouse. Once these design parameters are established, the cost of a piece of equipment can be estimated from the equation:

$$C_b = C_a \times \left(\frac{Q_b}{Q_a}\right)^f \left(\frac{V_b}{V_a}\right)^a \left(\frac{M_b}{M_a}\right)^m \qquad (1)$$

where

C_b is the unknown cost of the item

C_a is the known cost of equipment (base case)

Q_b is the gas flow

Q_a is the gas flow (base case)

V_b is the air-to-cloth ratio

V_a is the air-to-cloth ratio (base case)

M_b is the number of modules

M_a is the number of modules (base case)

The base case size (i.e., Q_a, V_a, and M_a) and cost (C_a) used in this equation were taken from the report by Campbell et al. (7). The exponents f, a, and m were determined by comparing vendors' estimates of equipment and installation costs for various sizes of baghouses. This method of cost estimation provides greater accuracy than simpler methods because of the greater level of detail involved.

The technique described above works well for those cases where there is an existing data base of equipment costs for various sizes. However, for items such as ESFF electrodes, the costs must be developed based on the prototype design. Since every bag in an ESFF baghouse requires an electrode, the simplest way to calculate the capital cost is on a cost-per-bag basis. In this way, the costs of the power supply and controls, wiring from the power supply, and the electrode are lumped together. When costs are allocated in this manner, the highest single cost-per-bag arises from the high voltage power supply and controls. The next highest cost is for the insulated wire that must pass through the bag cap to connect the high voltage bus to the center-wire electrode. Other expensive items include the electrode cable and the insulating cable at both ends of the electrode cable. The total cost for electrode hardware, assembly, and installation of the power supplies and electrodes was estimated as \$128.50 per bag.

Operating costs for baghouses include fixed costs (such as labor and overhead), variable operating costs (such as bag replacement materials and labor), and electricity. Fixed costs can be estimated from historical values, while variable operating costs (which consist largely of bag replacement costs) can be computed from bag failure rates and cost-per-bag. As mentioned above, the bags used in an ESFF baghouse will have to be electrically conductive. By whatever means this is accomplished, the net result will be an increase in the cost of the bags. For this economic evaluation, we have specified that ESFF bags cost 50 percent more than conventional filter bags.

Another additional maintenance cost for an ESFF baghouse would be the replacement of the electrodes. Experience with wire electrodes in electrostatic precipitators (ESPs) indicates that electrodes will need to be replaced periodically. An important difference between an ESP and an ESFF electrode is that, in an ESFF bag, the gas flow is parallel rather than perpendicular to the electrode. This stress on an ESP electrode does not apply to an ESFF electrode. Nevertheless, the other mechanical and thermal stresses will probably cause the electrodes to fail. It is assumed that the mean electrode life in an ESFF baghouse will be 5 years.

Electrical requirements will also be different in an ESFF baghouse. The tubesheet pressure drop in an ESFF baghouse will depend on the design filtration velocity, which will likely be different than that of a conventional baghouse. An ESFF baghouse will have the additional cost of electrode power. Based on pilot plant data, the current per ESFF bag will be 1.88 mA at a field strength of 3 kV/cm. This amounts to 84.5 W/bag additional power requirement for a bag 9.1 m long and 0.3 m in diameter.

Although there may be applications where ESFF technology is used to lower the pressure drop of a filtration process, it is expected that the primary benefit of ESFF will be its use in building smaller baghouses with lower capital costs. This requires that the ESFF baghouses operate at higher air-to-cloth ratios. In general, as the average filtration velocity through a bag increases, the mechanical stresses on the bag increase, thereby shortening bag life. It is not known how the electric field will affect bag life, although some evidence indicates that bags used in an ESFF application will last longer. On the other hand, the possibility of bag damage due to sparking is unknown. Experience may prove otherwise but, until more is known, it is assumed that ESFF bags will have the same life as bags in conventional baghouses.

Chapman et al. (8) report an empirical formula relating bag life to face velocity:

$$L_b = L_a \times \left(\frac{V_a}{V_b}\right)^{0.6} \qquad (2)$$

where

L_b is the life of bag b

L_a is the life of bag a

V_a is the face velocity through bag a

V_b is the face velocity through bag b.

Smith and Carr (9) reported recently that bag life typically ranges from 3 to 7 years in conventional reverse-air-cleaned baghouses. For the purposes of this study, bag life will be assumed as 4 years when the face velocity is 0.61 m/min (2 ft/min). The bag life at other face velocities can then be predicted from the equation:

$$L_b = 4.0 \times \left(\frac{0.61}{V_b}\right)^{0.6} \qquad (3)$$

This value for bag life will be used in determining the contribution of bag replacement cost in the annual maintenance costs. As mentioned earlier, the ESFF bag cost is assumed to be 50 percent higher than the cost of a conventional bag.

RESULTS

Three different utility plant sizes (200, 500, and 1000 MW) were studied in order to determine the relative savings of installing an ESFF baghouse. As described earlier, ESFF affects pressure drop in two ways: it slows the rate at which pressure drop increases, and it lowers the pressure drop of a newly cleaned bag. The available data on the extent of reduction of residual pressure drop are not conclusive, so two different cases of ESFF design were studied. In the first case, it was assumed that the pressure drop after cleaning is the same for both a conventional and an ESFF baghouse. That is, the effect of the electric field does not alter the residual pressure drop of an ESFF bag. In the second case, it was assumed that the residual drag of an ESFF bag is half of the residual drag for a conventional bag. Experience with another type of electrical enhancement (10) indicates that the residual pressure drop is lowered by the presence of the electric field. In some cases, this reduction was as much as 70 percent. Thus, by computing both cases for ESFF, it is possible to identify both a least- and a most-favorable case for ESFF economics.

The size and cost of fans depend on the gas flow rate and the pressure drop across the baghouse. The electrical cost also depends on the flow and pressure drop. Hence, these parameters must be specified before costs can be estimated. The baghouse drag (S) is a convenient parameter for expressing energy requirements in a manner independent of the face velocity through the baghouse. Specifically:

$$S = \frac{\Delta P}{V} = S_r + K_2 W \qquad (4)$$

where

ΔP is the pressure drop after cleaning

V is the face velocity

S_r is the residual drag

K_2 is the specific resistance of the ash layer

W is the dust load per unit area.

A typical residual drag for a conventional reverse-air-cleaned baghouse is 1,230 N•min/m^3 (1.5 in. H_2O/ft/min). A typical K_2 value is 1 N•min/g•m (6 in. H_2O/ft/min•lb/ft^2). Pilot plant data show that an ESFF baghouse has a K_2 value approximately 25 percent that of a conventional baghouse. Thus, for the simulation of case 1, a K_2 value of 0.25 N•min/g•m will be used with the value of the residual drag remaining the same as that of the conventional house. The K_2 value for case 2 will be the same as that of case 1, but the residual drag will be 50 percent of the former value (615 N•min/m^3). Having specified these values, it is then possible to predict the average and maximum pressure drops for the baghouse at various face velocities.

The results of these predictions for a conventional baghouse and ESFF cases 1 and 2 with face velocities from 0.61 to 1.83 m/min (2 to 6 ft/min) appear in Table 1, along with estimated bag life. Average tubesheet pressure

TABLE 1. PREDICTED PRESSURE DROPS BASED ON PILOT PLANT RESULTS

	Face velocity (m/min)	ΔP_{ave} (kPa)	ΔP_{max} (kPa)	Bag life (years)
Conventional Baghouse				
	0.61	1.5	2.25	4
	0.91	2.25	3.375	3.1
	1.22	3	4.5	2.6
	1.52	3.75	5.625	2.3
	1.83	4.5	6.75	2
Advanced ESFF Case 1				
	0.61	0.9375	1.125	4
	0.91	1.40625	1.6875	3.1
	1.22	1.875	2.25	2.6
	1.52	2.34375	2.8125	2.3
	1.83	2.8125	3.375	2
Advanced ESFF Case 2				
	0.61	0.5625	0.75	4
	0.91	0.84375	1.125	3.1
	1.22	1.125	1.5	2.6
	1.52	1.40625	1.875	2.3
	1.83	1.6875	2.25	2

drops are plotted in Figure 2. At a face velocity of 0.61 m/min, the conventional baghouse is predicted to have reasonable average and maximum pressure drops. These values (1.5 and 2.25 kPa, respectively) translate into typical costs for fan capital and operating costs. In ESFF case 1, where it is assumed that the rate of pressure loss is 25 percent that of a conventional baghouse, it is predicted that a face velocity of 1.22 m/min will produce roughly the same operating conditions. In ESFF case 2, where it is assumed that the ESFF baghouse would also have a lower residual drag than a conventional baghouse, a face velocity of 1.83 m/min would approximate the operating conditions of a conventional baghouse at 0.61 m/min. By defining these values of pressure drop as the desirable operating range (i.e., 1.5 - 2.0 kPa average and 2.25 kPa maximum), these three cases can be used as the basis for a consistent economic comparison.

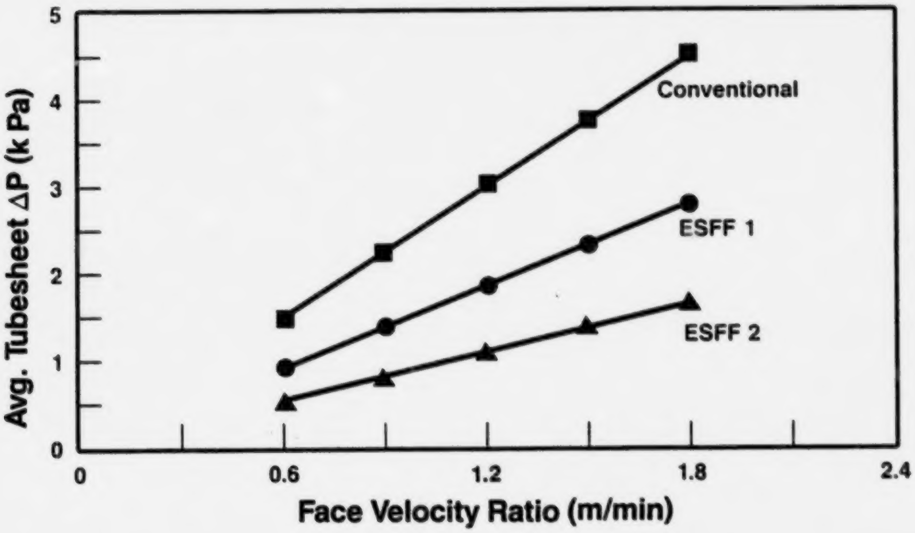

Figure 2. Comparison of tubesheet pressure drops.

The results of the capital cost calculations are shown in Figure 3. For a small plant (200 MW), the turnkey cost of a conventional baghouse was estimated to be $9.8 million. An ESFF baghouse with the pressure drop characteristics of case 1 would be 50 percent of the size of a conventional baghouse and have a turnkey cost of $6.5 million. An ESFF baghouse conforming to the case 2 criteria would be 35 percent of the size of a conventional baghouse and have a turnkey cost of $4.6 million. A detailed list of costs for a 500 MW plant is shown in Table 2. For both cases 1 and 2, the cost of ESFF hardware (including installation) amounts to less than 10 percent of the total turnkey cost.

The cost savings of ESFF can be seen more easily in Figure 4. For all three plant sizes, ESFF case 1 has a turnkey cost at least 35 percent less than that of a conventional baghouse. ESFF case 2 has a turnkey cost 52 percent less than that of a conventional baghouse. The lowest cost savings that can be expected is $15/kW installed. These savings are a direct result of the smaller size of the ESFF baghouses. Clearly, the reduced capital costs easily offset the additional cost of the ESFF hardware.

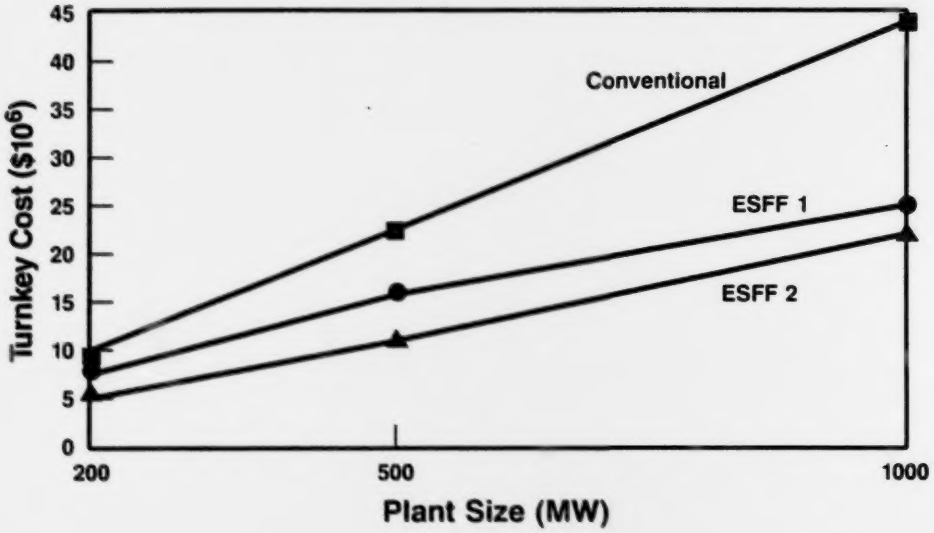

Figure 3. Baghouse turnkey costs.

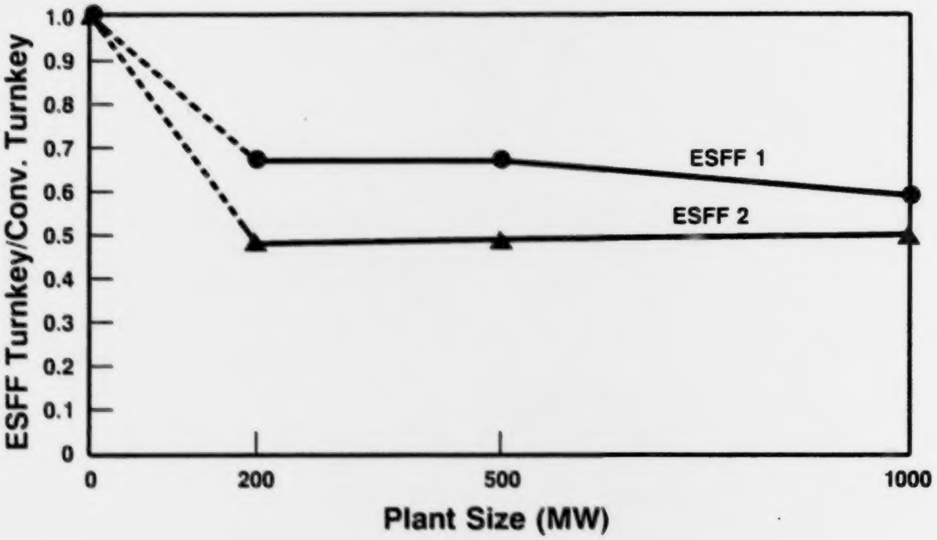

Figure 4. Comparison of turnkey costs.

TABLE 2. A DETAILED BREAKDOWN OF CAPITAL COSTS FOR A 500 MW UNIT

	Conv.	ESFF 1	ESFF 2
Standard Hardware			
Collector and supports	$7,250,000	$3,870,000	$2,610,000
Ducting and supports	$1,040,000	$1,030,000	$1,010,000
Ash removal system	$ 845,000	$ 546,000	$ 395,000
Insulation	$2,030,000	$1,120,000	$ 766,000
ID fan	$ 378,000	$ 376,000	$ 377,000
Miscellaneous	$4,930,000	$2,960,000	$2,140,000
Total baghouse cost	$16,473,000	$ 9,902,000	$ 7,298,000
Engineering	$ 3,294,600	$ 1,980,400	$ 1,459,600
Contingency	$ 3,294,600	$ 1,980,400	$ 1,459,600
Installed cost	$23,062,200	$13,862,800	$10,217,200
ESFF Hardware			
ESFF hardware	$0	$ 1,097,900	$ 731,900
Engineering	$0	$ 219,600	$ 146,400
Contingency	$0	$ 219,600	$ 146,400
Installed cost	$0	$ 1,537,100	$ 1,024,700
Turnkey cost	$23,062,200	$15,399,900	$11,241,900
ESFF percentage of total		9.98%	9.12%

The operation and maintenance (O&M) costs for the different systems (Figure 5) provide an interesting comparison of the tradeoff between the smaller

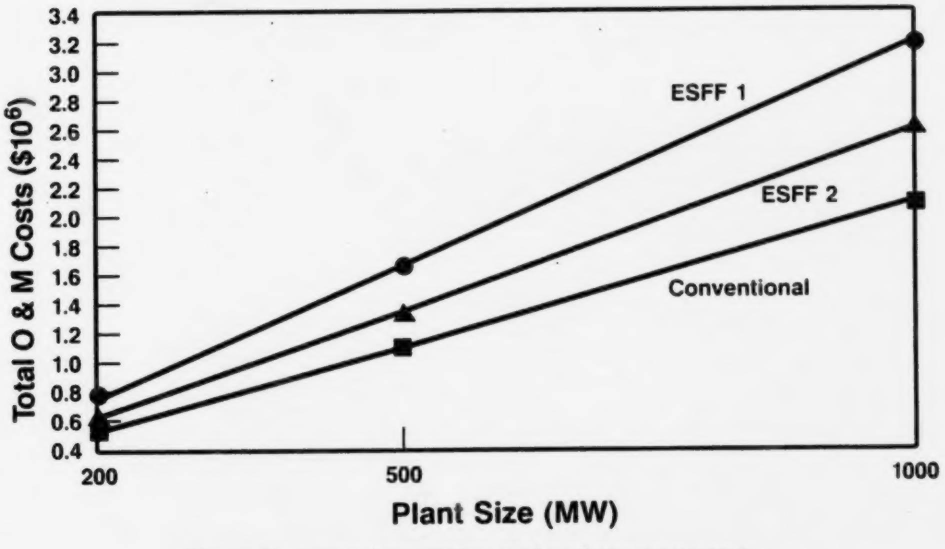

Figure 5. Annual operation and maintenance costs.

size of the ESFF baghouse and the need for more electricity and more expensive bags. In ESFF case 1, the operating costs are 40 to 50 percent higher than those of the conventional baghouse. The costs for ESFF case 2 are 20 to 23 percent higher than conventional costs. Recall that the baghouses were designed to maintain roughly equal average pressure drops, although not exactly the same. Thus, ESFF O&M costs would be expected to be higher because they have the additional cost of electricity for the ESFF electrodes.

Another difference between the ESFF and conventional baghouses is that the life of the ESFF bags is assumed to be shorter (due to the higher face velocities), and the cost of the ESFF bags is 50 percent greater than the cost of the conventional bags. In all cases (200, 500, and 1000 MW), the operating costs of the conventional baghouse are the lowest. Although the ESFF baghouses have fewer bags, the higher face velocity means that the bags must be replaced more often with more expensive bags. The net result is that the ESFF baghouses have higher overall operation and maintenance costs.

The complete picture of ESFF economics is based on the capital and O&M costs. The standard analysis procedure is the life cycle analysis. One type of life cycle analysis is based on Net Present Value (NPV). This is the sum of all present and future costs expressed in terms of current dollar value (June 1985). The current value of operating costs for future years can be computed with a knowledge of the lifetime of the baghouse (n) and the discount rate (R). The cumulative uniform series factor is:

$$b_n = \frac{(1+R)^n - 1}{(1+R)^n \bullet \ln(1+R)} \tag{5}$$

The total amount of money spent on operation and maintanence over the life of the baghouse, expressed in terms of current dollars, is:

Lifetime O&M = b_n • Annual O&M

The NPV can then be calculated as the sum of the turnkey cost and the lifetime O&M cost.

The calculated values of NPV appear in Table 3 and are plotted in Figure 6. The costs are based on an assumed interest rate of 12.5 percent and a 20-year baghouse life. Lifetime cost savings range from $1.5 million for ESFF

TABLE 3. NET PRESENT VALUE (JUNE 1985) FOR CONVENTIONAL AND ADVANCED ESFF BAGHOUSES

Size (MW)	Conventional	ESFF 1	ESFF 2
200	$13,918,300	$12,453,800	$ 9,635,200
500	$31,896,700	$28,645,100	$22,123,200
1000	$61,089,200	$51,093,000	$42,865,200

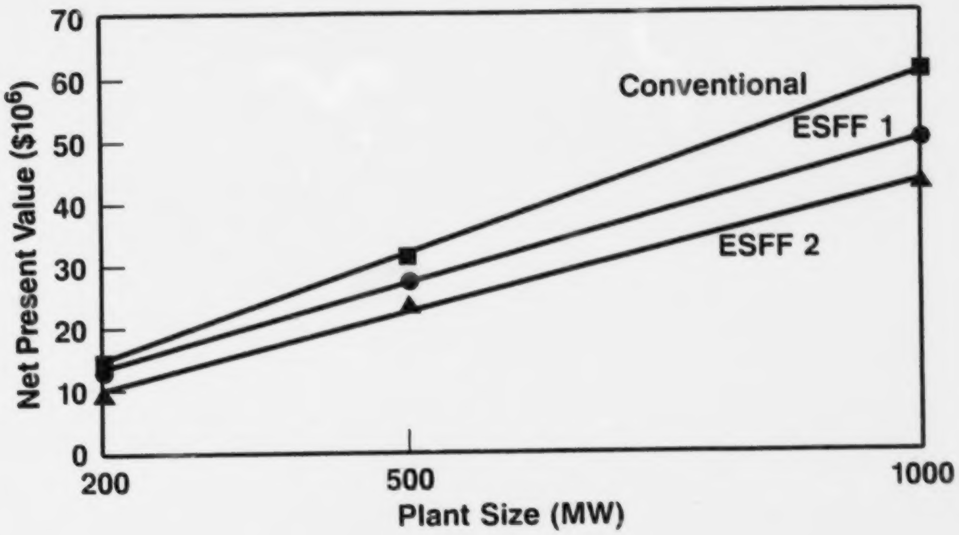

Figure 6. Cost savings for advanced ESFF.

case 1 (200 MW) to as much as $18 million for ESFF case 2 (1000 MW). Figure 7 shows that ESFF offers a lifetime savings of at least 10 percent over the cost of a conventional baghouse. In the event that ESFF has a residual drag of 50 percent of that of a conventional baghouse, the lifetime cost savings may be as great as 30 percent. Unfortunately, there is no conclusive evidence to indicate to what degree ESFF will affect the residual drag of a bag. All data collected to date support the notion that there will be either a reduction in drag or, at worst, no change from the conventional baghouse performance. There is no evidence to suggest that ESFF will have a deleterious effect on bag drag.

In short, the construction of a small ESFF baghouse, as opposed to a conventional baghouse, can be expected to reduce the turnkey capital cost by 33 to 51 percent. The operation and maintenance costs, however, may increase 30 to 50 percent. The net effect over the life of the baghouse will be a 10 to 30 percent decrease in lifetime costs. For a typical 500 MW power plant, this amounts to a savings of $3.25 to 9.77 million in 1985 dollars.

Advanced ESFF offers many advantages over conventional filtration and previously tested methods of electrostatic enhancement. First, Advanced ESFF produces the largest reduction in pressure rise of any electrostatic enhancement technique, thereby making it possible to use smaller baghouses. Second, the hardware required for Advanced ESFF is simple and can be assembled from readily available materials. Third, unlike precharger methods, Advanced ESFF does not require any modification in the baghouse ductwork. Finally, Advanced ESFF is the most economically attractive of all of the various methods proposed for electrostatic enhancement of baghouse performance.

The largest uncertainty to advanced ESFF is that it has not been demonstrated on a large scale for sufficient time to gather data over the complete

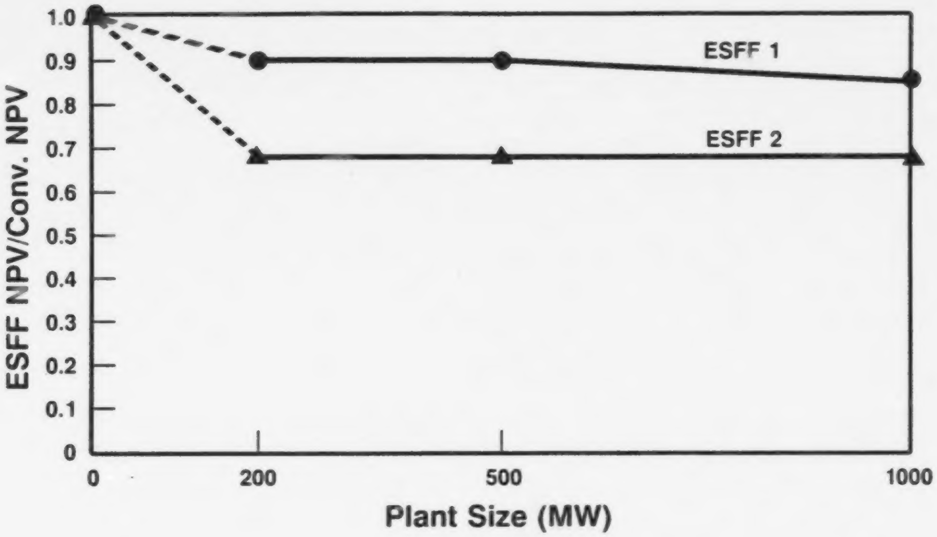

Figure 7. Comparison of lifetime costs for conventional and advanced ESFF baghouses.

life of a bag set. However, a pilot project (11) is currently collecting some of these data. Hopefully, the question of what impact ESFF has on residual drag will be answered in the near future. Acceptance of advanced ESFF in the electric utility community will require that the mechanism of pressure drop reduction be understood. Although no conclusive proof exists, it is believed that the presence of the electric field affects the way dust is distributed in the bag and produces a more porous dust cake. These two effects produce the reduction in pressure drop. A computer model is being developed to explore these and other potential mechanisms for pressure drop reduction (2).

As with any new technology, there is room for improvement in Advanced ESFF. Undoubtedly, the design will evolve as more is learned about electrode performance and maintenance requirements. However, both the promising results obtained in laboratory and field work and the very favorable economic analysis presented here provide a strong incentive to continue developing this technology. The potential savings are too great to ignore.

References

1. Hovis, L. S., B. E. Daniel, and R. P. Donovan. Electrostatic Enhancement of Fabric Filtration of Fly Ash and Spray Dryer By-Product. In: Proceedings of the Third EPRI Fabric Filter Conference, Scottsdale, Arizona. November 1985.

2. Mosley, R. B., et al. Advanced Electrostatic Enhancement of Fabric Filtration. In: Proceedings of the Third EPRI Fabric Filter Conference, Scottsdale, Arizona. November 1985.

3. Yamamoto, T., D. S. Ensor, R. B. Mosley, L. S. Hovis, and N. Plaks. Mathematical Model for Advanced Electrically Stimulated Fabric Filtration. Presented at the Sixth Symposium on the Transfer and Utilization of Particulate Control Technology, New Orleans, Louisiana. February 1986.

4. Greiner, G. P., A. S. Viner, L. S. Hovis, and R. Gibbs. Advanced ESFF Applied to a Stoker Coal-Fired Boiler. Presented at the Sixth Symposium on the Transfer and Utilization of Particulate Control Technology, New Orleans, Louisiana. February 1986.

5. Spivey, J. J., R. L. Chambers, and D. L. Harmon. Development of Woven-Electrode Fabric and Preliminary Economics for Full-Scale Operation of Electrostatic Fabric Filtration. In: Proceedings: Fifth Symposium on the Transfer and Utilization of Particulate Control Technology, Volume 3. EPA-600/9-86-008c (NTIS No. PB 86-167178), February 1986.

6. Viner, A. S., and D. S. Ensor. Computer Programs for Estimating the Cost of Particulate Control Equipment, EPA-600/7-84-054 (NTIS PB84-183573), April 1984.

7. Campbell, K. S., et al. Economic Evaluation of Fabric Filtration Versus Electrostatic Precipitation for Ultrahigh Particulate Collection Efficiency. Electric Power Research Institute Report No. EPRI FP-775, June 1978.

8. Chapman, R. A., D. P. Clements, L. E. Sparks, and J. H. Abbott. Cost and Performance of Particulate Control Devices for Low-Sulfur Western Coals. In: Second Symposium on the Transfer and Utilization of Particulate Control Technology, Volume I, EPA-600/9-80-039a (NTIS No. PB 81-122202), September 1980.

9. Smith, W. B., and R. C. Carr. Reverse Gas Baghouses for the Collection of Fly Ash. In: Proceedings of the Third EPRI Fabric Filter Conference, Scottsdale, Arizona. November 1985.

10. VanOsdell, D. W., and D. A. Furlong. Electrostatic Augmentation of Fabric Filtration: Reverse-Air Pilot Unit Experience. EPA-600/7-84-085 (NTIS No. PB 84-23002), August 1984.

11. Serrurier, R. Advanced Electrostatic Fabric Filtration Experience at Southwestern Public Service Company. Presented at the Sixth Symposium on the Transfer and Utilization of Particulate Control Technology. New Orleans, Louisiana. February 1986.

Session B-3: FF: PRACTICAL CONSIDERATIONS

John D. McKenna, Chairman
ETS, Inc.
Roanoke, VA

EVALUATION OF ACID-RESISTANT SYNTHETIC NEEDLED FELT FILTER MEDIA IN COAL-FIRED BOILER PULSE-JET BAGHOUSES

by: W. Theron Grubb
W. W. Criswell Company
Riverton, NJ 08077

ABSTRACT

Glass fabrics, both woven and needled, have been the most widely utilized filter media for coal-fired boiler pulse-jet baghouses in the U.S. Although glass fabrics, aided by conservative design considerations, have performed adequately in many of these installations, their performance in many other units has been limited by their instrinsically poor abrasion resistance and inadequate resistance to acid conditions in cyclic boiler operations.

Synthetic filter media possess abrasion resistance which is inherently superior to glass, but the use of synthetics has been limited by their lower temperature capabilities, acid resistance inferior to that of glass, or high initial cost. Recent developments such as Ryton (polyphenylene sulfide) fiber, acid resistant treatments for aramid (Nomex) felt, Rastex PTFE scrims, and modified aramid fiber are being evaluated in many boiler baghouses where glass fabric performance was inadequate. The results of several of these on-going trial installations are presented in this paper.

BACKGROUND

When pulse-jet fabric filters were initially being designed for use in applications such as coal-fired boilers, which combined high temperature (>275°F) and acidic gas conditions, no fabric filter media existed which was entirely suitable. Synthetic needled felts had been, and continue to be used to provide adequate dust collection efficiency during the high ratio and high cleaning energy operation of typical pulse-jet units. The only synthetic fibers capable of continuous service above 275°F were Nomex® aramid and Teflon® fluorocarbon. Nomex was unsuitable because of its susceptibility to hydrolysis under hot, moist, acidic flue gas conditions. Teflon felt usage was limited by its extremely high initial cost and to some extent by its lack of dimensional stability at temperatures >400°F.

GLASS PULSE-JET FABRICS

To meet the need for an economical high-temperature fabric which would perform adequately in a pulse-jet collector, woven and felted glass fabrics were developed. The woven fabrics utilized special weaves, either double warp face or double filling face constructions, which enabled the addition of more texturized yarns to achieve some degree of "depth filtration" and resulted in fabric weights of 16-22 oz/yd^2. A glass felt filter media, Huyglas®, was also developed, incorporating a heavy (16 oz/yd^2) open-weave glass support fabric with a resin bonded glass batt needled to one side, for a total fabric wieght of 27 oz/yd^2. Special design considerations were necessary to minimize abrasive wear of these glass fabrics, which are considerably more fragile than synthetic fabrics, and to achieve the desired filtration performance characteristics. Some of these design considerations are as follows:

Cages with closer wire spacing for increased fabric support
Tighter bag/cage fit to minimize flex abrasion
Reinforcement of bag top and bottom to minimize wear
Reduced pulse pressure
Reduced air-to-cloth ratio (woven glass)
Off-line cleaning (16 oz/yd^2 woven glass)
Special bag installation procedures
Special bag shipping procedures (glass felt)

Utilizing these conservative design criteria, glass fabrics, both woven and felted, achieved widespread use in coal-fired boiler baghouses, especially in the U.S. Glass fabrics have performed exceptionally well in some installations, meeting the existing particulate emission standards, operating at a reasonable pressure drop (ΔP) and achieving baglives of three to four years or more in some instances. However, in many other units the performance of glass fabrics has been limited by their instrinsically poor abrasion resistance and inadequate resistance to acidic conditions in cyclic boiler operations.

Glass felt is an exceptionally efficient filter medium due to the very fine (3.5 μm) fibers in the batt, however, it has in many cases achieved relatively short service life, in the 9-18 month range. In these cases, the short baglife, coupled with the relatively high cost of the glass felt, has prompted the user to seek a more durable fabric or a less costly one, if not both.

When poor performance does occur with woven glass pulse-jet bags, it is frequently related to one of the following conditions:

(1) Inadequate acid resistance resulting in overall fabric degradation

(2) Mechanical damage caused by inadequate bag construction design, poor bag/cage fit, inadequate cage support, reuse of damaged or corroded cages, or improper installation procedures

(3) Accelerated pulse cleaning frequency or increased pulse pressure, often necessitated by high ΔP conditions resulting from high A/C ratio, boiler upset conditions, switch to lower grade coal, etc. This increased pulsing frequency or pulse pressure accelerates the normal abrasive action on the glass bags.

Because of the relatively low cost of woven glass pulse-jet bags, users will frequently not be as critical of moderately short bag life and will either resign themselves to periodic bag replacement or attempt to increase life by trying a different woven glass fabric or finish or by buying new cages, following better installation procedures or modifying bag construction. These steps may prove successful to some extent, however if the collector is undersized or poorly designed for the particular ash which is being collected, or if the chemistry of the gas stream combined with cyclic operation is too severe, no glass fabric may perform adequately in that particular unit.

SYNTHETIC FELTS: HISTORICAL USAGE IN CFB PULSE-JETS

Some success has been achieved with Dralon T® homopolymer acrylic needled felts in Australia (1) and Canada (2) on low sulfur coal-fired boiler baghouses by using dilution air to reduce the flue gas temperature below 275°F. At least one boiler/spray dryer FGD system in the U.S. has also used Dralon T successfully. It is not usually feasible to use dilution cooling in the U.S. to reduce flue gas temperatures below 275°F because of the higher acid dewpoints resulting from higher sulfur content. Although normal operating temperatures of spray dryer FGD/boiler baghouses is <200°F, they are usually required to be capable of operation at the spray dryer inlet temperature, typically 325-400°F, so that the flue gas can be passed though the fabric filter when the spray dryer is inoperative. This may also be required to enable the burning of lower sulfur coal or operation at low-load conditions where SO_2 emission standards may be achieved without utilizing the FGD system.

Teflon needled felt has also been successfully used in coal-fired boiler baghouses, but in some instances excessively high operating ΔP has been experienced due to the penetration of fine particulate into the depth of the fabric which is probably related to the relatively coarse diameter (20 μm) of the Teflon fiber compared to other synthetic fibers or glass (3). The largest usage of Teflon felt bags in CFB baghouses has been by the Queensland Electricity Commission, and a recent paper by Barranger and Stranger (1) discusses the excellent performance of Teflon felt on spreader stoker units at Tennyson and Bulimba Power Stations, but high ΔP operation at Callide Station. The difference in performance in these baghouses of similar design was related to the particle size, particle shape, and cohesivity of the fly ash.

RECENT DEVELOPMENTS IN SYNTHETIC FELT FILTER MEDIA

There have been several promising new developments in high-temperature, acid-resistant filter media in recent years: Ryton® polyphenylene sulfide fibers, improved acid-resistant finishes for Nomex felts, Tefaire® felt, and the incorporation of Rastex® expanded PTFE scrims into needled felts.

RYTON® FIBER

Ryton polyphenylene sulfide (PPS) fibers were developed by Phillips Fibers Corporation, a subsidiary of Phillips Petroleum Company, in the mid-1970's. PPS fiber exhibits outstanding retention of its physical properties under extremely adverse conditions. Its resistance to a moist, acidic environment at elevated temperatures is second only to PTFE fluorocarbon fibers (4,5). Pilot-plant fiber was produced in the late-1970's, but due to inadequate PPS polymer capacity and to difficulty encountered in producing a fiber-grade purity resin, Ryton fiber was not available in developmental quantities until late 1982, and was not fully commercialized until 1984.

The pilot plant fiber was produced in sufficient quantity to enable Ryton felt bags to be produced and utilized in several Carter-Day baghouses on coal-fired boilers beginning in 1979. The most notable of these installations was at Adolph Coors Company, where excellent performance was achieved at 300-370°F operating temperatures at ratios up to 5-to-1 with on-line cleaning and 6-to-1 with off-line cleaning, with the low pressure/moderate volume cleaning system (6). Many of the original bags are now in their seventh year of service!

The original "Daytex" fabric used at Coors was a 22-28 oz/yd^2 felt with a 4 oz/yd^2 Rastex® (Gore-Tex PTFE fiber) scrim. It is thought that the heavyweight felt was utilized to compensate for the inconsistent denier of the pilot plant fiber, which averaged 4d to 5d. Based on laboratory testing and recent field experience, it is probable that equivalent performance can be attained with felt weights of 16-22 oz/yd^2 utilizing the uniform 3.0d commercial Ryton fiber.

The maximum continuous operating temperature for Ryton felt filter media has not been determined at this time. Originally this temperature was tentatively established at 375°F with "brief surges" to 450°F, however this recommendation was based on data obtained on fiber produced prior to 1985. Since early-1985, Ryton fiber has been produced with a higher purity resin, which results in a lighter colored fiber. Long-term thermal exposure testing by Phillips (7) has yielded the results shown in Table 1.

TABLE 1. THERMAL STABILITY OF RYTON IN AIR

Exposure Time	Temperature (°F)	% Breaking Strength Retained 1985 Yarn	 1983 Yarn
1000 hours	400	105	85
2000	400	92	76
5000	400	70	-
100 hours	500	76	63
600	500	62	20
1000	500	58	-

This data suggests that current Ryton fiber may be capable of withstanding higher temperatures, both continuous operation and surges, than had previously been recommended with the lower purity fiber. This data also suggests that the concern which Phillips expressed regarding the use of Ryton in gas streams containing >5% O_2 may not be a serious concern with the current higher purity fiber. Additional field evaluation will be required to determine actual temperature and O_2 exposure limitations.

Another factor which has yet to be determined is the relative merits of 100% Ryton felt (using woven Ryton scrim) compared to Ryton felt with Rastex PTFE scrim. A recent study at a municipal waste incineration installation in Sweden by Olofsson and Barranger (8) indicated a relative baglife (relative to untreated Nomex) of 1.5 for 100% Ryton felt compared to greater than 2.2 for Ryton/PTFE felt. This data may not be applicable to coal-fired boiler baghouses, however.

ACID-RESISTANT FINISHES FOR NOMEX FELT

Chemical treatments or finishes which will impart some degree of acid and hydrolysis resistance to Nomex aramid fabrics have been sought for many years by filtration fabric manufacturers and users. It has never been satisfactorily demonstrated that any "acid-resistant" Nomex finish produced in the U.S. has yielded a significant improvement in baglife. Several European needled felt manufacturers have developed acid resistant finishes for Nomex felt. These proprietary treatments have been used successfully in Europe for several years in low sulfur applications, but until recently had been unavailable and thus untried in the U.S. Two European manufacturers, Heimbach and BWF, now market their complete line of needled filtration felts, including their acid-resistant finishes, through U.S. filter bag manufacturers.

Alberta Power has gained much operating experience with acid-resistant Nomex fabrics at their H. R. Milner Generating Station, as recently reported by Cerantola (2). A full scale test with two Canadian finished Nomex felts resulted in the complete degradation of one set within ten months, and while the other set lasted twelve months, its life was also inadequate. The unit was rebagged with a number of different bag types, including three different acid-resistant Nomex finishes, Nomex/Rastex, 100% Ryton and Ryton/Rastex, and is now in the eighteenth month of operation. After fourteen months, no bag failures had been observed with any of the synthetic felt bags. It is interesting to note that a module of experimental 19 oz/yd^2 woven glass bags failed catastrophically in less than one month!

In the Olafsson and Barranger study previously cited (8), 100% Nomex felts with six different acid-resistant finishes were tested to failure in a single test compartment of the municipal waste incinerator/dry $Ca(OH)_2$ injection baghouse system. None of the finishes resulted in a significant improvement either in baglife or inherent viscosity compared to untreated Nomex. Apparently this application is too severe for 100% Nomex fabric regardless of finish.

RASTEX PTFE SCRIM

Several references have already been made to the use of Rastex expanded PTFE as a woven scrim support fabric in high temperature synthetic felts. The concept of using Rastex scrim is based on its temperature capability (500°F) and its inherent chemical resistance, both of which are far superior to either Ryton or Nomex. The theory is that the PTFE scrim functions as the strength member of the needled felt, remaining essentially unchanged in strength during the life of the bags, and as a support for the batt fibers which can continue to function as the filter medium in spite of any drastic loss of their strength caused by chemical or thermal degradation.

Since woven Ryton scrim has only been available for about two years, all of the long-term experience with Ryton felt has been with the Rastex scrim support. To this author's knowledge, there has been no controlled comparison of 100% Ryton to Ryton/Rastex in a coal-fired boiler baghouse for any significant period of time.

Nomex/Rastex felt has been primarily a European development, and has reportedly demonstrated its superiority to 100% Nomex in some coal-fired boiler baghouses. The Olafsson study concluded that PTFE extended the baglife of various acid-resistant Nomex felts by a factor of 2 to 2.5.

Another variable concerning the use of Rastex is the weight and construction of the scrim, which has yet to be optimized. Intuitively, it would seem that a heavier, more tightly woven PTFE scrim which would provide both additional strength and a denser base to which batt fibers would be more firmly attached, would result in longer baglife. However, this result has yet to be demonstrated conclusively. At least four different Rastex scrim constructions have been utilized in Ryton felts in the U.S., as shown in Table 2.

TABLE 2. RASTEX SCRIM CONSTRUCTIONS

Code	Nominal Weight (oz/yd^2)	Thread Count (Warp x Fill)	Weave
A	2.2	20x20	Plain
B	3.0	27x21	3-end Mock Leno
C	4.0	26x40	2-end Leno
D	4.0	36x36	Plain

Some European felt manufacturers utilize heavier PTFE scrims, in the 5.5 - 8.0 oz/yd^2 range.

TEFAIRE® - TEFLON/GLASS FIBER BLEND

Tefaire, a recent development by DuPont, is a needled felt consisting of a batt fiber blend of 80% Teflon PTFE and 20% glass needled into a woven Teflon scrim. This fabric is designed to take advantage of the superior chemical and thermal resistance of Teflon felt, which has resulted in excellent wear resistance and baglife, and to improve it by the addition of fine glass fibers which both reduces dust penetration into the felt and decreases the high initial cost. Excellent performance in trial installations has been reported by Shah (3). Very low outlet emissions and filter drags ($\Delta P \div A/C$) have been reported for Tefaire when compared to 100% Teflon felt.

EVALUATION OF VARIOUS RYTON AND NOMEX FELTS IN STANDARD PULSE-JET COLLECTORS

All full-scale and test installations, which have been cited in this paper, were conducted in collectors equipped with cleaning systems which are atypical of most boiler pulse-jet baghouses in the U.S. The Carter-Day cleaning system is a low-pressure (7.5 psig), moderate volume, direct pulse type, and the Flakt cleaning system is a moderate pressure (30 psig), high volume, semi-direct pulse type. The majority of boiler pulse-jet units in the U.S. are of the traditional high pressure (80-120 psig), low volume, ejector pulse type. In order to evaluate some of the various acid-resistant synthetic felts, two bag test programs were initiated by Criswell; one in a high sulfur coal-fired boiler/spray dryer FGD baghouse and one in a low-sulfur coal-fired boiler with cyclic operation. Both of these installations had experienced problems with glass bags and had opted for synthetic bags of some type. The results to-date of these test programs are presented below.

AUSTELL BOX BOARD TEST PROGRAM

Austell Box Board Corporation, Austell, Georgia, operates a Babcock and Wilcox pulverized coal-fired boiler, rated at 250,000 lb/hr of steam. The plant fires bituminous coal with an average content of 2.2% sulfur, 12% ash and 3% moisture, and a heating value of 12,300 Btu/lb. The boiler's flue gas desulfurization (FGD) and particulate control system, consisting of a two-fluid nozzle spray dryer/absorber utilizing lime slurry for SO_2 removal and a pulse-jet fabric filter for particulate removal, was supplied by Wheelabrator-Frye Inc. The fabric filter is a six-compartment unit with 255 bags per compartment. The bags are nominally six-inch diameter by ten feet long and are supported by cages with twenty (20) vertical wires on 7/8" centers.

Flue gas exiting the spray dryer is reheated with a hot gas bypass to 170-180°F before entering the baghouse, and the unit is equipped with 100% bypass capability to protect the bags in the event of excessively low or high flue gas temperature. The design air-to-cloth ratio was approximately 4-to-1 at full load, but at normal boiler load of 160,000 lb/hr, the estimated actual ratio is approximately 3.3-to-1. Complete boiler and FGD system design information and system performance for the first two years of operation were reported by Bradley (9).

AUSTELL GLASS BAG EXPERIENCE

The Austell baghouse was originally equipped with Huyglas felt bags, which performed very well for ten months with only a few bag replacements. In the eleventh month, however, the bag failure rate accelerated rapidly resulting in high opacity. Bag failures were primarily due to delamination of the fibrous glass batt from the scrim, occurring mainly along the vertical flex creases which typically form 180° apart in pulse-jet bags due to the excess circumference of the bag relative to the cage.

Four of the six compartments were rebagged with 22 oz/yd^2 woven glass fabric, but no improvement in opacity was noted and high pressure drop across the fabric filter was experienced on several occasions. Some failures were observed on the woven glass bags within two weeks after installation. The unit was completely rebagged with the woven glass fabric, replacing two modules of Huyglas bags after sixteen months and the four modules of woven glass bags after 1½-4 months service.

The second set of woven glass bags, with some cleaning cycle adjustments, operated at acceptable opacity and pressure drop levels for about three months. During the fourth and fifth months increasing pressure drop necessitated continuous cleaning at increased pulse pressures to maintain system operation. Bag failures began to occur at a rapid rate after about 5½ months service. A decision was reached by Austell to completely rebag the fabric filter with non-glass fabric media in January 1985.

AUSTELL SYNTHETIC BAG EVALUATION

Since no synthetic bags had ever been tested at Austell, and Ryton and acid-resistant Nomex fabrics were not readily available in the quantity needed on such short notice, Austell was forced to utilize the fabrics available in the industry at that time. Fabrics used are described in Table 3 with complete fabric specifications given in Table 4.

TABLE 3. AUSTELL SYNTHETIC BAG TYPES

Fiber Type Batt/Scrim	Finish Type	Nominal Weight (oz/yd^2)	No. of Modules
Nomex/Nomex	Acid Resistant (Heimbach Zw 184)	15	1
Nomex-Glass/ Nomex	Acid-Resistant (Domestic)	14	1
Ryton/Ryton	None	18	1½
Ryton/Rastex (PTFE)	None	15	2½

A program was proposed to Austell which involved the removal of one bag of each type at periodic intervals for laboratory evaluation.

In addition it was suggested that Austell should monitor the relative flow through each module by measuring the pressure drop across the outlet damper. The unit had been fitted for that capability shortly before the installation of the synthetic bags.

Austell agreed to participate in the test program and insisted that the first test should be conducted after only one month to ease their concern over the uncertainty of using the untested synethetic bags. The bags were installed between January 23-February 2, 1985. Complete sets of bags were tested after one, four, and eight months, and single bags were tested after one week and after three months. The tests performed on all bags are listed in Table 5.

TABLE 4. AUSTELL BOX BOARD: SYNTHETIC FELT BAGS - ORIGINAL FABRIC PHYSICAL PROPERTIES

Felt Type: Bag Supplier:	A. R. Nomex (Heimbach) Criswell*	A. R. Nomex/Glass Other†	Ryton/Rastex Criswell*	Ryton/Rastex Other†	Ryton/Rastex Other†
Batt Fiber Type:	Nomex	Nomex (80%)/glass (20%)	Ryton	Ryton	Ryton
Fabric Wt. (oz/yd^2)	15.0	13.4	15.0	13.6	18.0
Perm (ft^3/min/ft^2)	35.9	25.1	49.6	57.5	37.7
Thickness (in):	0.095	0.061	0.064	0.064	0.078
Mullen Burst (lb/in^2):	613	305	442	425	360
Finish-Chemical:	Acid Resistant (Zw 184)	"Acid Resistant"	NONE	NONE	NONE
Finish-Surface:	Singed (moderate)	Singed (light)	NONE	NONE	NONE
Water Repellancy:	2 hours +	0	0	0	0
Oil Repellancy Rating:	#6	0	0	0	0
Scrim Properties:					
Fiber Type:	Nomex	Nomex	Rastex PTFE	Rastex PTFE	Ryton
Yarn Type:	Spun/Plied	Woolen Spun	Ribbon	Ribbon	Spun
Weave:	Plain	Plain	Plain	Plain	Plain
Count (Warp x Fill)	35 x 35	19 x 10	24 x 24	24 x 20	19 x 14
Weight (oz/yd^2)	4.2	3.6	2.0	2.0	3.1
Thread Type	Rastex	Nomex	Rastex	Rastex	Rastex

*Original properties of Criswell felts are taken from average fabric QC data.

†Original properties of other felts are the results of testing performed on only one bag supplied by Austell.

TABLE 5. TESTING PERFORMED ON AUSTELL BAGS

Test	Condition	Location
Permeability	As Received	Top-Middle-Bottom (3 each)
Permeability	Vacuumed	Top-Middle-Bottom (3 each)
Permeability	Washed	Middle
Fabric Weight	As Received	Middle
Fabric Weight	Washed	Middle
Mullen Burst	Vacuumed	Top-Middle-Bottom (3 each)
Bag Weight	As Received	Entire
Bag Measurement	As Received	Length, Flat Width & Circumference
ph	As Received	Middle
Inherent Viscosity	Vacuumed	Middle (Nomex only)
Bag Inspection	As Received & Vacuumed	Inside & Outside

AUSTELL TEST DATA

No significant fabric wear has been detected on any test bag to date.

Permeability

Permeability tested on "as received" (dirty) fabric indicates very little difference among the various fabrics as shown in Figure 1. It should be noted that the dirty permeability of 2.75 - 3.25 cfm on all synthetic bags after eight months is dramatically higher than permeabilities of the woven glass bags previously tested which were 1.15 cfm, 1.02 cfm, and 0.75 cfm after three, five, and seven weeks service respectively. Permeabilities on vacuumed fabric reflect the wide variation in the Ryton/Rastex felt as was evident in the new fabric, which was not of the most uniform quality. The vacuumed permeability tests on the Nomex/glass fabric appear to indicate increasing dust penetration into the depth of the felt, although this is not reflected in the permeability of the "as received" fabric. Washed permeabilities on all fabrics indicate only that the initial fabric permeability remains unchanged and again reflects the variability of the Ryton/Rastex permeability.

Residual Dust Loading

The differential between dirty and washed fabric weight indicates that the areal density of ash (dust loading) was 5-7 oz/yd^2 after one month, 6-8 oz/yd^2 after four months, and 7-13 oz/yd^2 after eight months. The significant increase in residual dust loading between four and eight months service was not reflected by the fabric permeabilities. Washed fabric weights were virtually equal to those of new fabric.

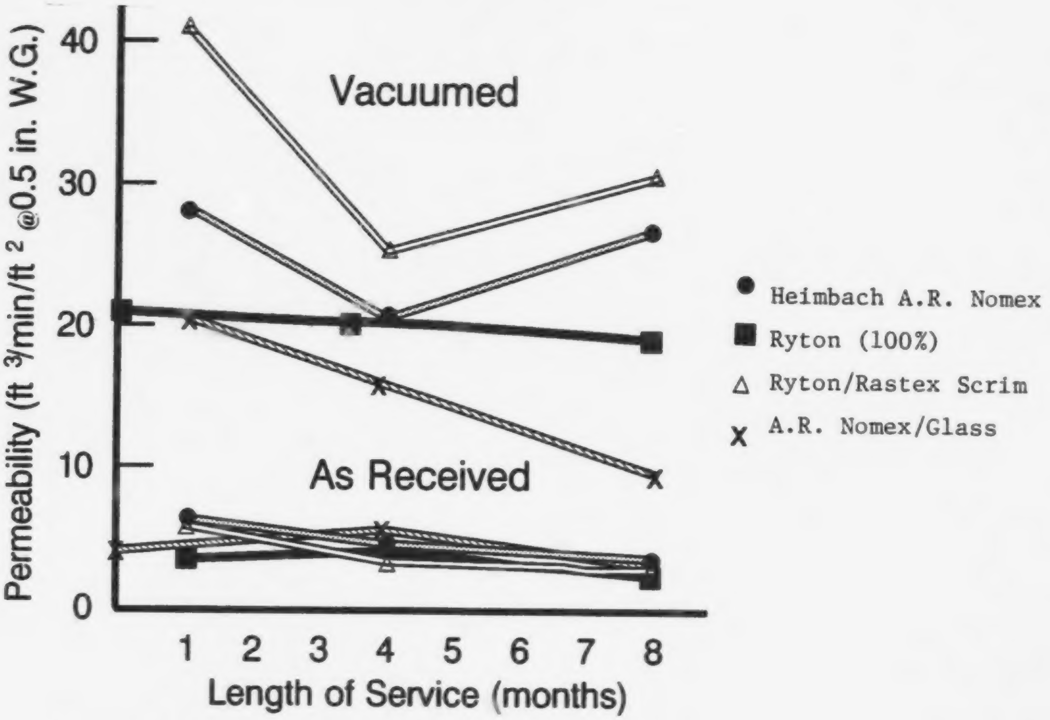

Figure 1. Austell Box Board: Permeability vs. Length of Service.

Mullen Burst Strength

The Mullen Burst strength, as shown in Figure 2, indicates no definite loss in strength of the Ryton/Ryton or the Ryton/Rastex, although this is difficult to determine since the burst strength varied greatly on the Ryton/Rastex. The low initial value of the Ryton/Ryton felt can be attributed to inadequate sampling, being based on testing fabric from one bag only.

The burst strength of both Nomex fabrics appears to be declining at a gradual but steady rate, and after eight months both have lost approximately 20-30% of their original strength. These conclusions are drawn based on the fact that Nomex felts generally have quite uniform burst strength. The low initial strength of the Nomex/glass fabric is rather anomalous and can again be attributed to inadequate sampling. Note that the Heimbach Nomex felt possesses much higher absolute strength than the domestic Nomex/glass felt both initially and after eight months service. The Heimbach felt has also retained its water repellancy after eight months of service.

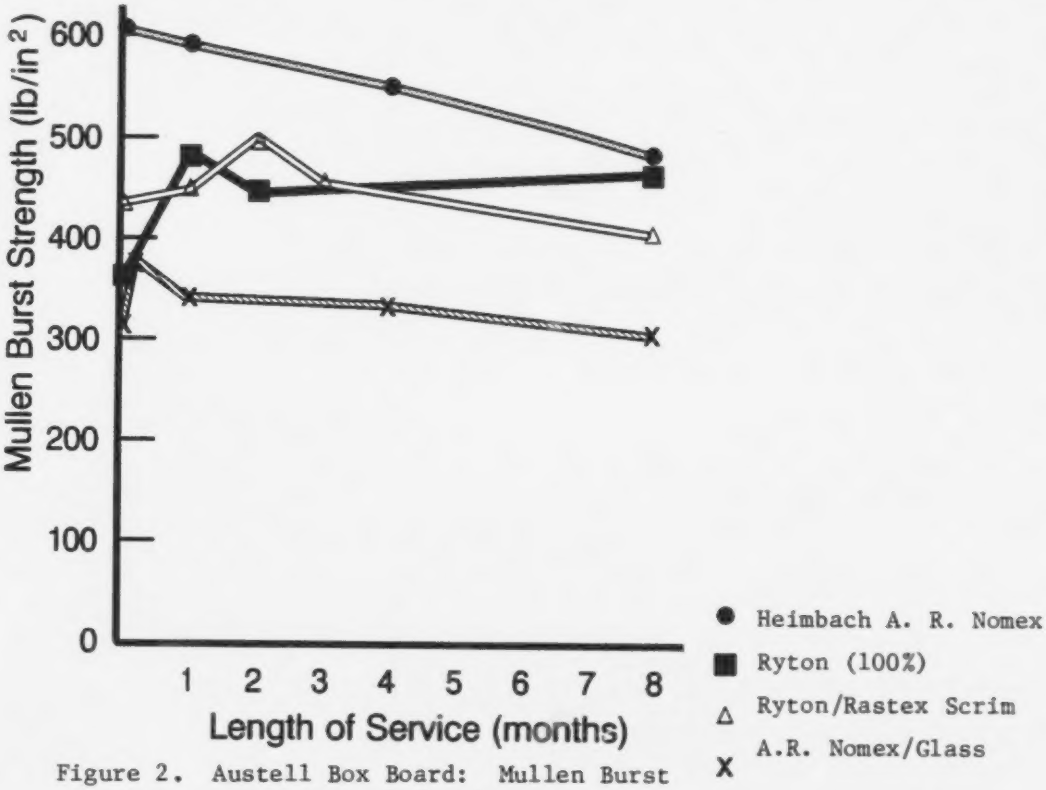

Figure 2. Austell Box Board: Mullen Burst vs. Length of Service

Fabric Shrinkage

Due to reports of "minor shrinkage" of both Ryton/Ryton and Ryton/Rastex at Alberta Power (2), accurate measurements were made on all bags to determine dimensional changes in service. The length of the seam side and opposite seam side, flat widths, and circumferences of bisected bags were all carefully measured. The determination of relatively small dimensional changes was possible on Criswell bags which were manufactured to glass bag tolerances of ± 3/16" in circumference (based on flat width) and ± 1/4" in length. This determination was not as easy, however, on bags from the other supplier, which exhibited much greater variations, especially in length.

Observations of bags on cages can frequently lead to the conclusion that bags have "shrunk", when in actuality the fabric has only "taken a set" in conformation to the cage wires. The same conclusion can be drawn from measuring the flat width of used pulse-jet bags. It is, therefore, necessary to bisect pulse-jet bags and measure the flattened circumference in order to accurately measure dimensional change. Circumference measurements of the Austell used bags indicated no detectable change in any of the bags.

There was no detectable length change in either Criswell bag type, acid-resistant Nomex or Ryton/Rastex, and no determination of length change could be made on the other supplier's bags due to length variation.

Inherent Viscosity

The inherent viscosity of a polymer solution is the ratio of the natural logarithm of the relative viscosity to the concentration of the polymer solution expressed in grams per 100 ml solution, where relative viscosity is the ratio of the flow time of a specific polymer solution to the flow time of the pure solvent, or

$$\eta_{inh} = \ln \eta_r / c$$

Where η_{inh} = inherent viscosity
c = polymer concentration in g/100 ml

and η_r = relative viscosity
= t_s / t_o

where t_s = flow time of polymer solution
t_o = flow time of pure solvent

Inherent viscosity is related to the molecular weight of a polymer and has been used to measure the degradation of Nomex in filtration applications. Olaffson (8) concluded that the "measurement of viscosity of Nomex is a good indicator of bag failure (potential) and better than tensile and tear strength."

Inherent viscosity measurements of the used Austell Nomex bags indicate that, although the viscosity of the Heimbach Zw 184 finished Nomex declined at a slower rate, both types of acid resistant Nomex felts exhibit equal viscosities after eight months, as shown in Figure 3. The viscosity appears to have stabilized at approximately 0.80, much higher than the value of 0.50 observed in the Swedish waste incinerator baghouse where only 11-15 months life was experienced with various 100% Nomex fabrics/finishes. The viscosity of the Austell Nomex bags is lower, however, than the value of 0.89 obtained on the same Heimbach fabric at Alberta Power after ten months service (2).

Inherent viscosity measurement on Ryton fiber has never been used, to this author's knowledge, to measure degradation of Ryton filtration fabrics. This determination must be made in 1-chloronaphthalene at 210°C, according to Phillips Petroleum Test Method 6936-BH-2. There was some question as to whether the high temperature would alter the molecular weight of the Ryton during the 45-60 minute test time, however, the inherent viscosity of Ryton was shown by Stacey (10) to be in excellent agreement with its molecular weight as determined by gel permeation chromatography (GPC). Future inherent viscosity measurements of used Ryton felt bags may prove valuable in predicting bag life.

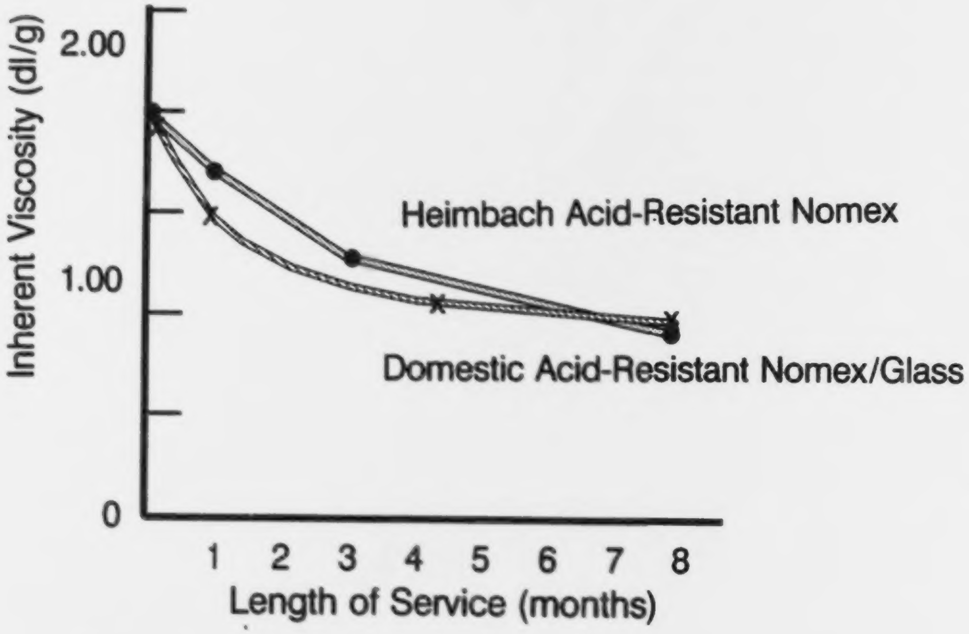

Figure 3. Austell Box Board: Inherent Viscosity vs. Length of Service

Bag Performance and Life

More important than any laboratory data which has been presented is the actual performance of the Austell bags to date. There have been no fabric related failures in over one year of service. Stack opacity has remained unchanged at <5% with no visible emissions, and pressure drop has been maintained at or below the 5" W.G. set point with no appreciable increase in cleaning frequency. In summary, the synthetic felt bags have proved very successful to date, and continued evaluation will hopefully determine the best or most economical fabric choice for Austell and perhaps for other boiler FGD fabric filters.

SYNTHETIC FELT EVALUATION IN A CYCLIC COAL-FIRED BOILER BAGHOUSE

The second test program was conducted in a boiler baghouse at a western U.S. food processing plant. This plant operates a Holman pulverized coal-fired A-style water tube boiler with Koen burners, rated at 70,000 lb/hr of steam. They normally fire a Central Utah sub-bituminous coal with a 0.5 - 0.7% sulfur, 6-7% ash and 8% moisture content, and a heating value of 12,500 Btu/lb. They occasionally fire a Kemmerer, Wyoming coal which is 1% sulfur, 5% ash, 20-21% moisture and has a heating value of 9000-9800 Btu/lb. The ash fushion temperature of this coal is only 2200°F compared to 2400°F for the Central Utah coal.

The boiler is equipped with a Mikropul pulse-jet fabric filter containing 600 bags, 4½" diameter by 10 feet long, in one housing; i.e. uncompartmented. The baghouse handles a flue gas volume of 34,000 scfm at a 6-to-1 air-to-cloth ratio. The inlet gas temperature is typically 280°F with a maximum of 320°F. The boiler is operated six days a week, shutting down cold every Sunday.

Glass felt bags were supplied as original equipment, and were replaced after 1½ years service due to a high moisture condition resulting from a problem with their steam soot blower, which has since been replaced. Prior to the upset condition, however, bag failures due to "fatigue" had already begun to occur. Due to economic considerations and to bag installation difficulties previously encountered, the user decided to seek alternatives to the glass felt bags. They had installed forty (40) Ryton/Rastex bags approximately seven months prior to the occurance of the upset condition, and these bags were apparently in excellent condition, however, based on price and recommendation, they decided to use 100% Ryton felt bags. When they attempted to obtain these bags within a very short time period, a sufficient quantity of 100% Ryton was unavailable, and they had to accept a variety of Ryton, Ryton/Rastex, and acid-resistant Nomex bags.

This appeared to be a perfect opportunity to implement a test program to evaluate these various synthetic felts in a pulse-jet fabric filter on a cyclic boiler operation. The fabrics used are listed in Table 6.

TABLE 6. SYNTHETIC FELTS USED IN CYCLIC BOILER TEST PROGRAM

Fiber Type Batt/Scrim	Scrim Weight* (oz/yd^2)	Nominal Felt Wt. (oz/yd^2)	No. Of Bags
Ryton/Ryton	3	17	142
Ryton/Rastex	2	14-15	152
Ryton/Rastex	3	17	122
Ryton/Rastex	4	16	56
Nomex/Nomex†	4.2	15	130

*See Tables 2 and 4 for scrim constructions
†Heimbach Zw 184 acid-resistant finish

Unfortunately, due to the user's urgent need for these bags in order to install them during a scheduled outage, the Ryton/Ryton and two of the Ryton/Rastex fabrics were grouped together in a single shipment. An unsuccessful attempt was made to mark the bags with a code to identify their type, and these bags were installed as a single group. The Nomex bags and Ryton/Rastex (3 oz/yd^2 scrim) bags were successfully segregated. The forty Ryton/Rastex bags which had already been in service for seven months were supposed to be left in the collector, but were either removed or their location unknown.

The test program was to be conducted similarly to the Austell evaluation. Bags were removed after five months of operation, however, no Ryton/Ryton or twelve-month old Ryton/Rastex bags were obtained due to the loss of identity previously discussed. The test was concluded unexpectedly after eight months when the bags were "ruined", according to the user, during the firing of the high-moisture Kemmerer, Wyoming coal previously described. Samples of only two bag types, Ryton/Rastex (2 oz/yd^2) and acid-resistant Nomex, were salvaged for testing during the rebagging. The collector was rebagged in late-December 1985 with 100% Ryton due to cost considerations although no testing had ever been performed on that type of used bag.

TEST RESULTS

Permeability

The dirty permeabilities of all bag types after five months were very high compared to that of typical pulse-jet felt bags (typically 2-5 cfm) as shown in Table 7. Even after eight months, when the bags had a much higher residual ash loading, the permeabilities remained quite high. Vacuumed permeabilities showed no significant difference among the fabrics, as all were in the 15-25 cfm range. Washed peremabilities were equal to that of new fabric.

TABLE 7. USED BAG PERMEABILITY (CFM): CYCLIC BOILER TEST PROGRAM

Fabric Type	New	Length of Service 5 Months	 8 Months
Ryton/Rastex (2 oz/yd^2)	49.8	8.9	7.3
Ryton/Rastex (3 oz/yd^2)	41.8	9.6	-
Ryton/Rastex (4 oz/yd^2)	34.4	7.0	-
Nomex (acid-resistant)	35.9	8.8	8.1

Residual Dust Loading

The residual dust loading was 1.8 - 3.5 oz/yd^2 after five months and from 3.1 - 16.4 oz/yd^2 after the upset condition occurred at eight months, as shown in Table 8. The weights of washed samples were virtually equal to that of new fabric.

TABLE 8. RESIDUAL DUST LOADING (OZ/YD^2): CYCLIC BOILER TEST PROGRAM

Fabric Type	Length of Service 5 Months	8 Months
Ryton/Rastex (2 oz/yd^2)	2.5	3.1 and 9.2*
Ryton/Rastex (3 oz/yd^2)	3.5	-
Ryton/Rastex (4 oz/yd^2)	1.8	-
Nomex (acid-resistant)	3.0	9.3 and 16.4*

---

*The two bags of each type exhibited significant differences in dust loading. After five months all bags of each type had comparable loadings.

Mullen Burst Strength

An interesting comparison of strength loss was obtained on Ryton felts with various Rastex scrim weights. It is apparent, although inconclusive because of limited data and some variation in the burst strength of the new Ryton/Rastex fabrics, that the strength loss is directly related to the scrim weight, as shown in Table 9. The burst strength of the acid-resistant Nomex appears to be steadily declining, as seen at Austell, however, its absolute strength remains higher than the Ryton/Rastex fabrics.

TABLE 9. MULLEN BURST STRENGTH (LB/IN^2): CYCLIC BOILER TEST PROGRAM

		Length of Service			
Fabric Type	New	5 Months	(% Loss)	8 Months	(% Loss)
Ryton/Rastex (2 oz/yd^2)	430	233	(46%)	242	(44%)
Ryton/Rastex (3 oz/yd^2)	473	313	(34%)	-	-
Ryton/Rastex (4 oz/yd^2)	435	342	(21%)	-	-
Nomex (acid resistant)	613	436	(29%)	390	(36%)

Fabric Shrinkage

In typical Mikropul collectors, the cage is fully inserted into the bag; the raw edge top is tucked into the top of the cage, and the bag is clamped to the cage. The bag is then held at a fixed length, and for this reason, lengthwise shrinkage cannot occur. The circumference of all bags, which had been bisected for easy removal of the cages, was carefully measured. All Ryton/Rastex fabrics were 14-3/16" ± 1/16" in circumference, exhibiting approximately 3% shrinkage from the initial 14-5/8". The acid-resistant Nomex bags were 14-9/16" in circumference, exhibiting no significant shrinkage.

Inherent Viscosity

The inherent viscosity of the acid-resistant Nomex after five months' service was 0.97 on the filtration surface batt fibers and 0.90 on the scrim fibers, compared to 1.65 on new Nomex fiber. These values are approximately equal to the viscosity at Austell after four months. No data has been obtained after eight months.

Nomex Sewing Thread

All Ryton bags were sewn with Rastex PTFE thread, but due to the extreme rush delivery required, the acid-resistant Nomex bags were inadvertantly sewn with standard Nomex thread. This was discovered while examining the five-month test bags. Thread was carefully removed from the vertical chain stitching, both the needle thread (exposed to dust) and looper thread (inside the bag), as well as from the disc stitching. The thread was tested for breaking strength and compared to new Nomex thread in Table 10. No testing has been performed on thread after eight months. The untreated Nomex thread exhibited strength loss comparable to the acid-resistant Nomex felt.

TABLE 10. NOMEX THREAD BREAKING STRENGTH (LB/END)

		Vertical Seam		
	New	Needle	Looper	Disc
Average	8.78	6.64	7.14	6.59
(% Loss)	-	(24.4%)	(18.7%)	(24.9%)

ph Data

The ph of dirty fabric (5g/100ml distilled water) was 9.5 - 10.3 after five months, and 10.9 - 11.2 after eight months. This alkaline ash ph may very well result in a more gradual deterioration of fabric strengths, especially Nomex, than if it were acidic. Southwestern Public Service Company achieved over two years life with Nomex fabric in a shake/deflate boiler baghouse at Harrington Station Unit #2 where ash ph was 11.5 - 12.0 and fabric ph was 10.5 - 11.0.

Water Repellancy

The acid-resistant Nomex fabric had lost all water repellancy after five months' service, unlike the Austell bags. This may be related to the higher exposure temperature or to higher flue gas acidity.

Performance and Life

The synthetic bags provided suitable particulate emission control (no data available) and enabled the user to maintain a 5" tubesheet pressure drop with moderate cleaning, both of which had also been achieved with glass felt bags. The life test was terminated due to the upset condition, although no physical failures occurred, and it is unclear, based on the fabric permeability and appearance, why the bags were replaced. The user greatly prefers the synthetic bags to the glass felt bags due to ease of handling during installation and economic considerations.

SUMMARY AND CONCLUSIONS

Based on the lengthy experience to date with Ryton/Rastex felt in the U.S. and in Europe, the efficacy of this filter medium has been demonstrated in a number of coal-fired boiler pulse-jet fabric filters. The optimum weight and construction of the Rastex scrim has yet to be determined, nor has the optimum composite felt weight been determined for commercial Ryton fiber. 100% Ryton felt remains unproven with regard to its life potential in different boiler types and coal compositions, however, it is showing promise in spray dryer FGD baghouses and in low sulfur coal-fired units with alkaline fly ash.

Acid-resistant treated Nomex felt is essentially an untested filter media in the U.S., although successful operations have been reported in Europe and Canada. There are contradictory data concerning the range of effectiveness of the many proprietary finishes available. Further evaluation is necessary to determine the conditions under which acid-resistant Nomex, both 100% and with Rastex scrim, can be effectively utilized.

In general, acid-resistant synthetic needled felt filter media have been proved effective in many coal-fired boiler pulse-jet fabric filters, some of which were unable to attain adequate performance with woven or felted glass media. In choosing the optimum fabric for a particular application, a long list of alternatives must be considered based on the design parameters, available data from full-scale and test installations, and economic factors. This list of fabrics includes woven glass (16 oz/yd^2 and 22 oz/yd^2), Huyglas felt, Ryton (100%), Ryton/Rastex; Nomex (100%) and Nomex/Rastex, both of which are available with various acid-resistant finishes; Tefaire, and PTFE (100%).

REFERENCES

1. Barranger, C. and Strangert, S. Experience with Pulse Jet Cleaned Fabric Filters on Australian Coal Fired Utility Boilers. Paper presented at the Third Conference on Fabric Filter Technology for Coal-fired Power Plants, Scottsdale, Arizona. November 19-21, 1985.

2. Cerantola, G. Testing and Operating Experience Update H. R. Milner Generating Station Pulse-Jet Fabric Filter. Paper presented at the Third Conference on Fabric Filter Technology for Coal-fired Power Plants, Scottsdale, Arizona. November 19-21, 1985.

3. Shah, J. N. New High Performance Fabric for Hot Gas Filtration. In: Proceedings: Fifth Symposium on the Transfer and Utilization of Particulate Control Technology. EPRI CS-4404, Vol. 1. 1986. p. 21-1.

4. Scruggs, J. G. and Reed, J. O. Polyphenylene Sulfide Fiber - A New Generic Type. Paper presented at the Textile Research Institute 52nd Annual Research and Technology Conference, Charlotte, North Carolina, April 6-7, 1982.

5. Scruggs, J. G. and Reed, J. O. Polyphenylene Sulfide Fibers. In: M. Lewin and J. Preston (ed.), Handbook of Fiber Science and Technology: High Technology Fibers. Vol. 3, Part A. Marcel Dekker, New York, 1985. p. 335.

6. Pearson, G. L. and Capps, D. D. Pulse-Jet Fabric Filter Experience Using Non-Glass Media at Air to Cloth Ratios of 5 to 1 on a Pulverized Coal Fired Boiler. EPA-600/9-84-025a. U.S. Environmental Protection Agency, Research Triangle Park, NC, 1984. p. 121.

7. Phillips Fibers Corporation. Here's to Ryton, the 21st Century Fiber. 1986.

8. Olofsson, H. and Barranger, C. B. Bag Fabric and Fabric Finish Evaluation at a Municipal Waste Incineration Plant. Paper presented at the Third Conference on Fabric Filter Technology for Coal-fired Power Plants, Scottsdale, Arizona. November 19-21, 1985.

9. Bradley, W. H. Operation of a Dry FGD System at Austell Box Board Corporation. In: TAPPI Proceedings 1985 Environmental Conference. Mobile, Alabama, April, 22-24, 1985. p. 31.

10. Stacy, C. J. Molecular Weight Distribution of Polyphenylene Sulfide by High Temperature Gel Permeation Chromatography. Paper to be published in Journal of Applied Polymer Science. 1985.

The work described in this paper was not funded by the U.S. Environmental Protection Agency and therefore the contents do not necessarily reflect the views of the Agency and no official endorsement should be inferred.

"LABORATORY STUDIES OF THE FILTRATION PERFORMANCE OF VARIOUS FILTER MEDIA UNDER SIMULATED FIELD CONDITIONS."

by: P. E. Frankenburg
Research Associate
Industrial Applications Research
E. I. du Pont de Nemours & Co.
Chestnut Run, 701 Building
Wilmington, DE 19898

ABSTRACT

Using laboratory equipment which simulates use conditions in the field, a number of filtration media for coal-fired boilers were studied. The filters were operated in the pulse-jet mode. Variables studied included: dust source, including various fly ashes and other dusts, air/cloth ratio, and cleaning frequency. Dust leakage, filtration efficiencies, and pressure drops were determined. The study led to the conclusion that the behavior of the various filter media investigated was predictable, but the ability to comply with emission requirements was greatly dependent on operating parameters. Limited correlation with full scale field results indicates the laboratory results to be valid and to have predictive value for field operations.

INTRODUCTION

With the current emphasis on achieving measurable improvements in the quality of our atmosphere, filtration of fine particulates from flue gases sourced by coal-fired boilers has become an increasingly important component of efforts to achieve this goal. Among the large number of commercially available textile fibers is Teflon* poly-tetrafluoroethylene multifil fiber, which because of its excellent thermal and chemical resistance appeared to be exceptionally well suited for use in fabric filters. As a result, such filters, made into a needlefelt by carding and needling Teflon® staple fibers into a woven scrim of Teflon® multifil, have been commercially available since the early 70's. They have demonstrated excellent durability exposing them to a dust load of about 2 grains/cu.ft. (5g/cu.m.) at an air velocity of 7 fpm. (2.1 m./min.) for about 16 hours. The apparatus was cleaned, and a test was conducted. Generally a single test lasted 2 hours. The weights of dust rejected, dust allowed to pass, air velocity, and pressure drop across the sample were recorded. From these data, efficiencies, leakage rates, and drag coefficients were calculated.

---

* DuPont Registered Trademark.

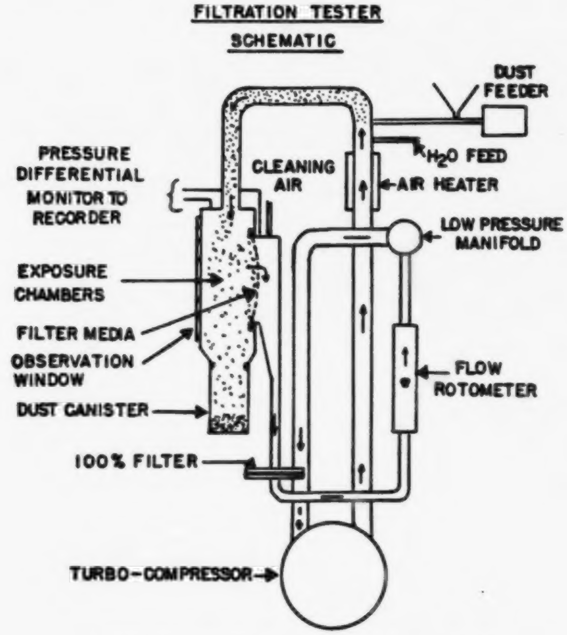
FILTRATION TESTER
SCHEMATIC
DUST FEEDER
H_2O FEED
PRESSURE DIFFERENTIAL MONITOR TO RECORDER
CLEANING AIR
AIR HEATER
LOW PRESSURE MANIFOLD
EXPOSURE CHAMBERS
FILTER MEDIA
OBSERVATION WINDOW
FLOW ROTOMETER
DUST CANISTER
100% FILTER
TURBO-COMPRESSOR

FIGURE 1. FILTRATION TESTER SCHEMATIC

To determine the reproducibility of the data obtained with this apparatus, we evaluated two samples twice at three different air/cloth ratios, and at two different locations in the test apparatus. Data (Figure 2) indicate that the standard deviation of the values observed was about equal to the value itself. The reproducibility of observed pressure drops was of a similar magnitude.

SELECTION OF TEFAIRE® FIBER BLEND RATIO[1]

To establish an optimum blend level of Teflon® and glass fibers, blend levels were evaluated by hand-mixing the components and feeding them through a laboratory garnet card to form a web. The webs were then affixed to both sides of a woven mock-leno scrim of Teflon® multifil fiber with a basis weight of 3.7 oz./sq.yd. (125 g./sq.m.) by needling. The felts were heat-set at 550°F (288°C) for 5 minutes, allowing 20% area shrinkage. Blend in the field, with a record of 10 years currently established at one of our plants.[1]

---

[1] H. H. Forsten, P. E. Frankenburg, J. N. Shah; U. S. Patent #4,361,619

A drawback of this product has been its high cost. In order to minimize this effect, we attempted to operate needlefelt bags of Teflon® at higher air-to-cloth ratios, i.e., in excess of 5.0-5.5 fpm (1.7-1.8 m./min.) so as to increase the through-put per unit area of bag, and thus to reduce the overall investment, not only in bags but also in the baghouse. These attempts have been generally unsucessful, with either bag blinding, and/or excessive leakage being the result.

As a result we set out to improve the product. Early attempts were in the classical direction as described by G. E. R. Lamb and others[2], that is to increase the fiber surface area by using finer fibers, crimped fibers, or by changing their cross-section from oval to cruciform. Although we were able to demonstrate all of these changes, we were not able to achieve the desired improvements in filtration performance. Only when we resorted to the replacement of some of the Teflon® fibers with glass fibers, were we able to attain the desired effect. In fact the effect was appreciably greater than one would anticipate if one considers the increase in fiber surface area alone. These efforts resulted in the commercialization of Tefaire* felt.

TEST METHOD

To quantify the effect of altering filtration media and operating conditions, we had to develop a laboratory apparatus and operating methodology to simulate field conditions. The result of these efforts was a four position filtration tester described schematically in Figure 1.

REPRODUCIBILITY

Air was recirculated through the unit by a turbine, with conditions adjusted to approximate field conditions. The cleaning mode was pulse-jet and the circulating gas temperature was ambient. A known amount of dust was redispersed in the gas stream by feeding it incrementally and at a controlled rate. Dispersion was aided by locally applied compressed air.

During a test run, the dusty air was filtered by a 11.4 x 16.5 cm. test piece. Any dust wich penetrated was captured on an "absolute" filter. Dust rejected by the filter was captured in the collection canister. Filtration efficiencies were obtained with 11.4 cm x 16.5 cm. samples. Air velocities ranged from 7.0 to 15 fpm. (2.1-4.7 m./min.). Cleaning intervals ranged from 1 - 15 minutes. The cleaning air was at 40 psi with a duration of 0.05 seconds, simulating pulse-jet cleaning. Samples were conditioned by

* DuPont Registered Trademark.

---

[1] J. E. Smith; Am. Soc. M.E.; Ind. Power Conf.; Cleveland, OH, 10/23/77

[2] G. E. R. Lamb and P. A. Costanza, Text. Res. J.; Vol. 49, No. 2, Feb., 1979

ratios from 10 - 100% Teflon® fiber were thus produced, and their relative surface area calculated. (Figure 3)

Test:	Panel Test
Test Material:	Tefaire* felt-21 oz.
Test Duration:	2 hours
Pulse Frequency:	15 minute interval
Dust Source:	Penna. Electric, Stoker

Sample #		31		61	
Item #		A	B	A	B
Air / Cloth Ratio (f.p.m.)		Leakage (grns/cu.ft.)			
7.0		0.00030	0.00077	0.00055	0.00037
		0.00059	0.00152	0.00056	0.00054
	Avg.	0.00045	0.00115	0.00055	0.00046
11.0		0.00030	0.00073	0.00047	0.00028
		0.00072	0.00346	0.00085	0.00107
	Avg.	0.00051	0.00210	0.00066	0.00068
15.0		0.00022	0.00128	0.00033	0.00017
		0.00033	0.00228	0.00022	0.00128
	Avg.	0.00028	0.00178	0.00028	0.00073

Average leakages :	Sample A	Sample B
7.0	0.00070 ± 0.00036	0.00051 ± 0.00009
11.0	0.00130 ± 0.00145	0.00059 ± 0.00079
12.0	0.00102 ± 0.00096	0.00050 ± 0.00052

Conclusions :
- o Standard deviation is 50 - 100 % of value
- o Differences between samples potentially greater
- o No variation traceable to position noted

FIGURE 2. REPRODUCIBILITY OF DATA

Substitution of as little as 30% by glass fibers resulted in doubling of the fiber surface area. However, a substitution level of as little as 10% resulted in almost one order of magnitude improvement in performance (Figure 4). Commercialy available Tefaire® felt contains about 25% glass fibers on its surface.

* DuPont Registered Trademark.

Blend Ratio (weight percent) Teflon* and glass	Calculated Surface Area (sq. cm./gram)
100/0	887
99/1	919
98/2	951
97/3	984
95/5	1049
90/10	1212
80/20	1537
70/30	1863
60/40	2189
40/60	2840
10/90	3817

FIGURE 3. EFFECT OF BLEND RATIO OF TEFLON® TETRAFLUORAETHYLENE MULTIFIL AND GLASS ON FIBER SURFACE AREA

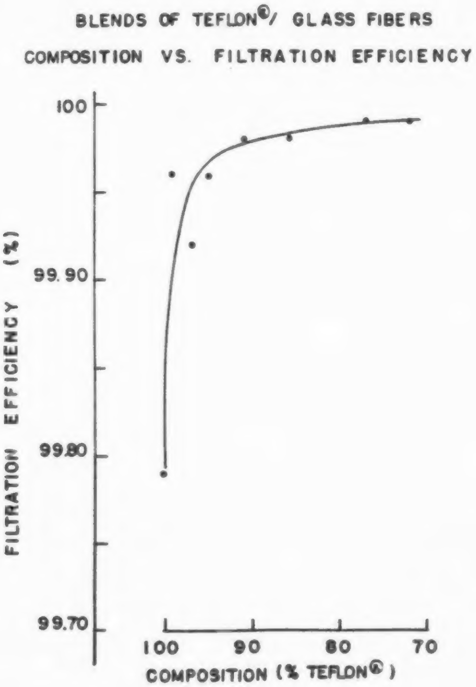

FIGURE 4. BLENDS OF TEFLON AND GLASS FIBERS

* DuPont Registered Trademark.

The reason for this greater than expected efficiency appears to be due to the unique triboelectric behavior of the blend. Recently obtained photomicrographs show the almost exclusive deposition of dust particles on the Teflon® component of the blend, lending support to this hypothesis (Figure 5). This, in spite of the fact that about 40 percent of the filter surface area was Teflon® fiber.

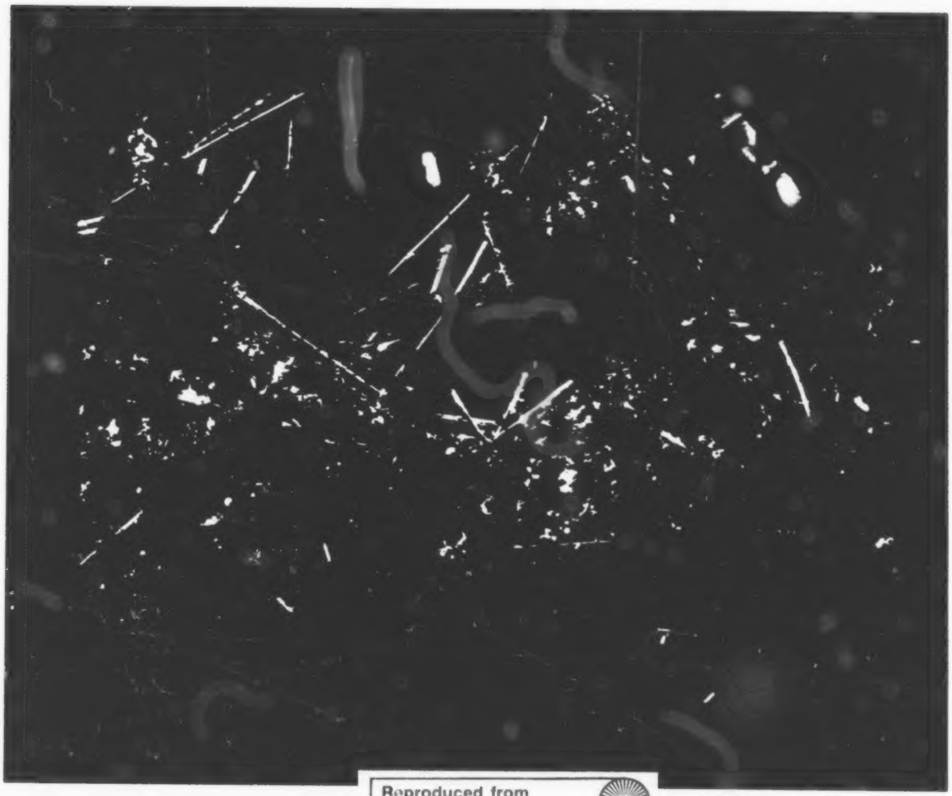

Reproduced from
best available copy.

FIGURE 5. PHOTOMICROPHAPH - FLY ASH ON TEFAIRE® FELT

EFFECT OF OPERATING CONDITIONS - STOKER FLY ASH

Initial trials were made with Teflon® and Tefaire® felts, to see if field experience (which suggested problems with felts of Teflon® at/or above a 6/1 air/cloth ratio) could be reproduced in the laboratory. The Stoker fly ash used in these studies had a particle size distribution as shown in Figure 6.

Tests were conducted at 7.0, 11.0, and 15.0 cu.ft./sq.ft./min air/cloth ratios (2.1, 3.4, and 4.7 sq.m./cu.m./min.) and with cleaning cycles of 15, 5, and 1 minutes. Results are given in Figs 7-9.

Mean Particle Size = 8 - 12 um

Aerodynamic Diameter (um)	Average Mass Fraction			
	Stoker Fly Ash	PC Fly Ash	Alumina	Recirculated PC Fly Ash
0.25 - 0.50	0.005	0.008	0.017	0.0015
0.50 - 1.05	0.021	0.023	0.031	0.008
1.05 - 1.90	0.033	0.093	0.051	0.033
1.90 - 3.40	0.044	0.205	0.063	0.075
3.40 - 5.70	0.097	0.259	0.103	0.136
5.70 - 9.70	0.184	0.202	0.169	0.212
9.70 - 17.2	0.217	0.103	0.180	0.229
17.2 - 50	0.399	0.107	0.386	0.305
Mean Particle Size (um)	8 - 12	4 - 5	0.5 - 1 3 - 5	6 - 8

FIGURE 6. PARTICLE SIZE DISTRIBUTION OF VARIOUS PARTICULATES

Felt	Cycle Interval (mins.)		
A/C Ratio (cu.ft./sq. ft./min.)	15	5	1
	Leakage (grns/cu.ft.)/dP (in. H2O)		
Teflon®			
7/1	0.00507 / 0.5	0.02564 / 0.1	0.01959 /0.1
11/1	0.01644 / 0.8	0.01420 / 0.3	0.02678 /0.1
15/1	0.07184 / 2.1	0.02071 / 0.6	0.01764 /0.4
Tefaire®			
7/1	0.00081 / 0.7	0.00127 / 0.1	0.00220 /0.25
11/1	0.00065 / 2.1	0.00069 / 0.9	-------
15/1	0.00058 / 4.1	0.00069 / 0.9	-------
Nomex* Aramid			
7/1	0.00089 / 0.3	0.00096 / 0.1	0.00116 / 0.1
11/1	0.00087 / 0.7	0.00083 / 0.1	0.00780 / 0.2
15/1	0.00075 / 1.6	0.00146 / 0.7	0.00430 / 0.4
"Ryton"			
7/1	0.00397 / 0.8	0.00291 / 0.7	0.01024 / 0.5
11/1	0.00132 / 1.6	0.00462 / 2.5	0.02169 / 0.5
15/1	0.00173 / 3.1	0.00515 / 4.9	0.01760 / 3.1
Woven Glass (Crowfoot)			
7/1	0.24599 / 4.9	-------	-------
11/1	0.22889 / > 10	-------	-------
15/1	0.23649 / > 10	-------	-------

* DuPont Registered Trademark.

FIGURE 7. FILTRATION PERFORMANCE OF VARIOUS FILTER MEDIA - STOKER FLY ASH

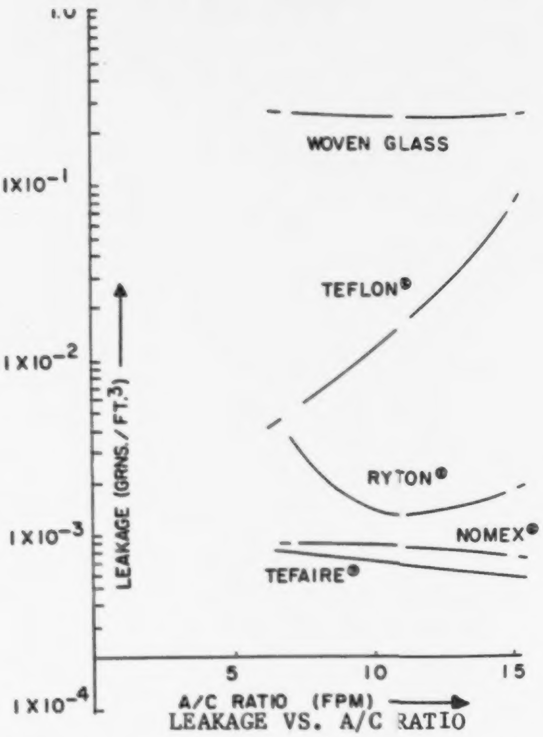

FIGURE 8. LEAKAGE VS. A/C RATIO

In general, the data indicated that increasing the air-to-cloth ratio could either increase or decrease leakage, but that increasing the cleaning frequency generally increased leakage by a mechanism known as "sifting". Specifically, these data show that the excessive leakage of felt of Teflon® observed in field installations at air-cloth ratios in excess of 6 f.p.m., was also observed on our laboratory equipment, though at a somewhat higher air velocity. Furthermore, the data indicates that reasonable performance can be expected from Nomex* aramid felt, provided it is used in a compatible, low acid environment. "Ryton" polyphenylene sulfide fiber felt, provided that thermal and chemical limitations are taken into consideration, was not quite as efficient at high pulsing rates aimed at reducing pressure drop. The data also mirror the incapability of woven glass fabrics to operate at these high air velocities, even though no fabric damage was observed during the test.

EFFECT OF OPERATING CONDITIONS-PULVERIZED COAL FLY ASH

We next expanded the studies to include the effect of altering the morphology of the fly ash. Since it represents a major segment of coal burning technology, we investigated the behavior of fly ash from pulverized coal (PC). The particle size distribution of this fly ash was given in Figure 6. Data obtained for various filter media are presented in Figure's 10 -12.

---

* DuPont Registered Trademark.

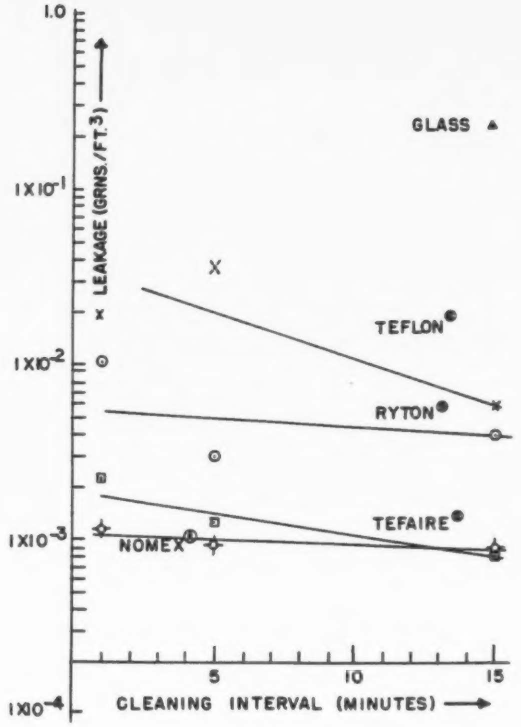

FIGURE 9. LEAKAGE VS. CLEANING FREQUENCY, VARIOUS FILTER MEDIA, 7/1 A/C RATIO, STOKER FLY ASH

A/C Ratio (cu.ft./sq.ft./min.)	15	5	1
	Leakage (grns/cu.ft..)/dP (in.H2O)		
Teflon®			
7/1	0.01763 / 4.2	0.00609 / 2.7	0.00277 / 0.87
11/1	0.07242 / >10	0.01823 / 4.1	0.04098 / 1.5
15/1	0.16026 / >10	0.07132 / 4.7	0.05663 / 2.1
Tefaire®			
7/1	0.00062 / 3.1	0.00156 / 2.0	0.00226 / 1.5
11/1	0.00117 >10	0.00040 / 4.1	0.00172 / 2.6
15/1	0.00619 >10	0.00036 / 8.1	0.00151 / 5.3
Nomex®			
7/1	0.00028 / 4.0	0.00059 / 4.5	0.00095 / 4.7
11/1	0.00126 / 8.7	0.00030 / 5.3	0.00033 / 7.3
15/1	0.00555 / 7.0	0.00015 / 7.0	0.00023 / 7.0
'Ryton'			
7/1	0.00063 / 4.0	0.00334 / 2.1	0.04989 / 2.3
11/1	0.00126 / 8.7	0.00397 / 5.7	0.04642 / 4.4
15/1	0.00172 / 7.0	0.00066 / 9.1	0.13006 / 4.5

FIGURE 10. FILTRATION PERFORMANCE OF VARIOUS FILTER MEDIA-PULVERIZED COAL FLY ASH

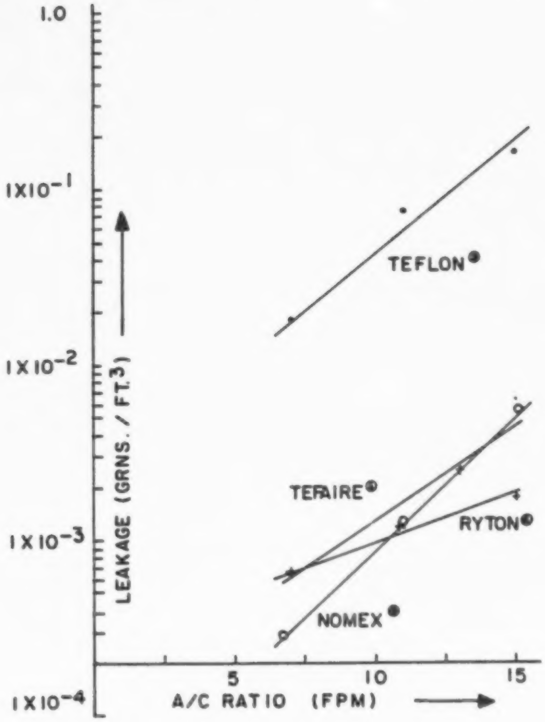

FIGURE 11. LEAKEAGE VS. AIR/CLOTH RATIO, VARIOUS FILTER MEDIA, 15 MINUTE CLEANING INTERVAL, PULVERIZED COAL FLY ASH

Review of the data show that the effect of the decreased mean particle size of the redispersed PC fly ash (2-3 um vs. 5-8 um for Stoker coal) was to increase leakage values appreciably for the filter media studied at 15 minute cleaning cycles. This increase was especially noticable at the higher air-cloth ratios. Comparisons of the graphs detailing the effect of cleaning frequencies show two divergent response patterns for the filters: the leakage increased by a factor of about 3 for Nomex® and Tefaire®, by about 10 for "Ryton", and decreased for Teflon® by a factor of 6. Thus it appeared that there were counteracting effects. On the one hand increased pulsing increased sifting, while at the other hand, high air velocities through remaining air passages in restricted filters caused excessive leakage. If the dust cake resulted in high pressure drops, most of the air passages must have been plugged, and the actual air velocity was much greater through the few remaining passages than the average velocity when the filter was relatively clean. Chances for particles to be captured at high velocities are undoubtedly reduced. When more frequent pulsing is applied, the dP drops, the structure becomes more open, and the chances for particulate capture were substantially improved.

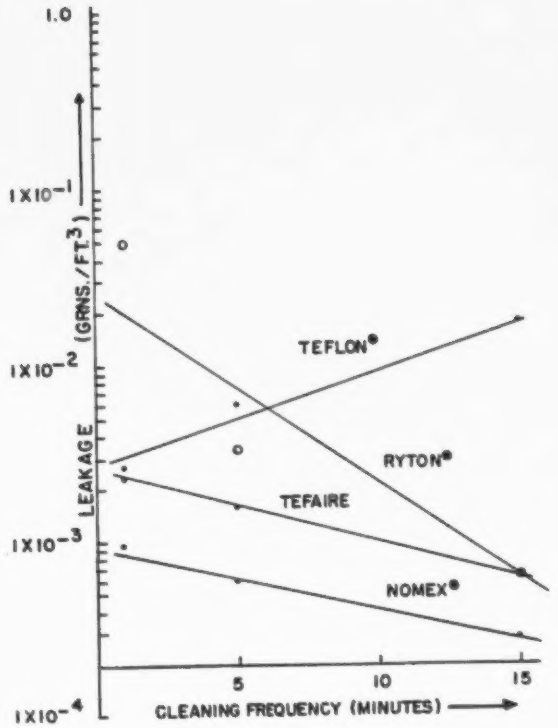

FIGURE 12. LEAKAGE VS. CLEANING FREQUENCY, VARIOUS FILTER MIDIA, 7/1 A/C RATIO, PULVERIZED COAL FLY ASH

EFFECT OF OPERATING CONDITIONS - ALUMINA

To test the effect of particle size further, we evaluated the effect of alumina dust on Tefaire® and Nomex® felts. The alumina used had a bimodal particle size distribution, with high concentrations of particle sizes in the 0.5 - 1.0 and the 3 - 5 um ranges. Data obtained with 15 minute cleaning cycles are listed in Figure 13 which also contains the results obtained with PC fly ash under the same conditions.

Felt	Alumina	PC Fly Ash
	Leakage (grns./cu.ft.)	
Tefaire®		
7/1	0.00454	0.00062
11/1	0.00150	0.00117
15/5	0.00156	0.00619
Nomex®		
7/1	0.00167	0.00028
11/1	0.00159	0.00126
15/1	0.00237	0.00555

FIGURE 13. FILTRATION PERFORMANCE OF VARIOUS FILTER MEDIA ALUMINA VS. PULVERIZED COAL

As can be seen (Figure 14), there was no predictable pattern for leakage. At the lower A/C ratio, the PC fly ash leaked less, while at the higher A/C ratios the alumina was held back more effectively.

These trials were very limited and dP data, which would have been useful in elucidating the leakage mode, were not obtained.

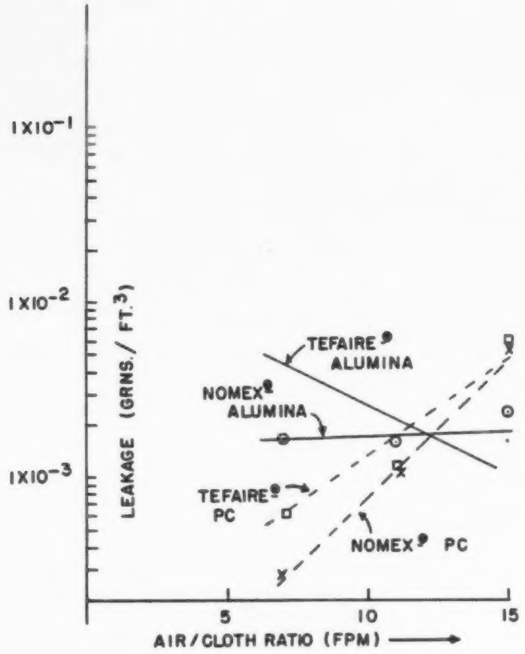

FIGURE 14. LEAKAGE VS. AIR/CLOTH RATIO, TEFAIRE® AND NOMEX®, EFFECT OF ALUMINA AND PC FLY ASH, 15 MINUTE CLEANING INTERVAL

EFFECT OF OPERATING CONDITIONS - RECIRCULATED PC FLY ASH

Finally, data were obtained using a fly ash from a utility installation in which a major portion of the fly was recirculated from the baghouse back to the boiler, melted, and extracted from the system as slag. The particle size distribution analysis of this fly ash was given in Figure 6. It can be seen from the particle size distribution data that this fly ash appeared to be very similar to the PC fly ash investigated earlier. If anything, the PC fly ash was finer. Hence the recirculated fly ash would be expected to filter better. This was, however, not the case. (Figure 15)

The filtration performance of Tefaire® was poorer than anticipated, and the pressure drops did not appear to be as dependent on operating conditions as observed earlier.

Felt	Cycle Interval (min.)		
A/C Ratio (cu.ft./ sq.ft./min.)	15	5	1
	Leakage (grns./cu.ft.)/dP (in.H2O)		
Teflon®			
7/1	0.05156 / 2.5	---	0.05422 / 0.3
Glass Felt			
7/1	0.00462 / 6.8	---	0.00934 / 3.3
Tefaire®			
7/1	0.00941 / 5.4	---	0.01268 / 3.1
15/1	0.00952 / 6.5	---	0.00580 / 2.0

FIGURE 15. FILTRATION PERFORMANCE OF VARIOUS FILTER MEDIA-RECIRCULATED PULVERIZED COAL FLY ASH

SUMMARY OF LABORATORY DATA

A summary of laboratory results with felt of Tefaire® Teflon® and glass exposed to the various dusts indicates the magnitude of the change in filtration performance (Figure 16) that can be encountered with a single filtration medium due entirely to dust morphology. Furthermore, we demonstrated that determination of the particle size distribution was insufficient to categorize particulates. Other differences, such as cohesiveness, appeared to play a substantial role in filtration. To obtain evidence for the cause of the noted differences, we obtained SEM photomicrographs of the various dust samples for a comparison. (Figure 17-19)

Fly Ash Type	Mean Particle Size (um)	Leakage (grns./cu./ft.)//dP (in.H2O 15	5	1
Stoker	5 - 8	0.00081/0.7	0.00127/0.1	0.00220/0.25
Pulverized	2 - 3	0.00062/3.1	0.00156/2.0	0.00226/1.5
Pulverized-Recirculated	3 - 5	0.00462/2.5	---	0.00934/0.3
Alumina	0.5 - 1.0 + 3 - 5	0.00454/--	---	---

FIGURE 16. COMPARISON OF THE EFFECT OF FLY ASH ON TEFAIRE® FELT-7/1 FPM. A/C RATIO , VARIOUS CLEANING INTERVALS

Reproduced from
best available copy.

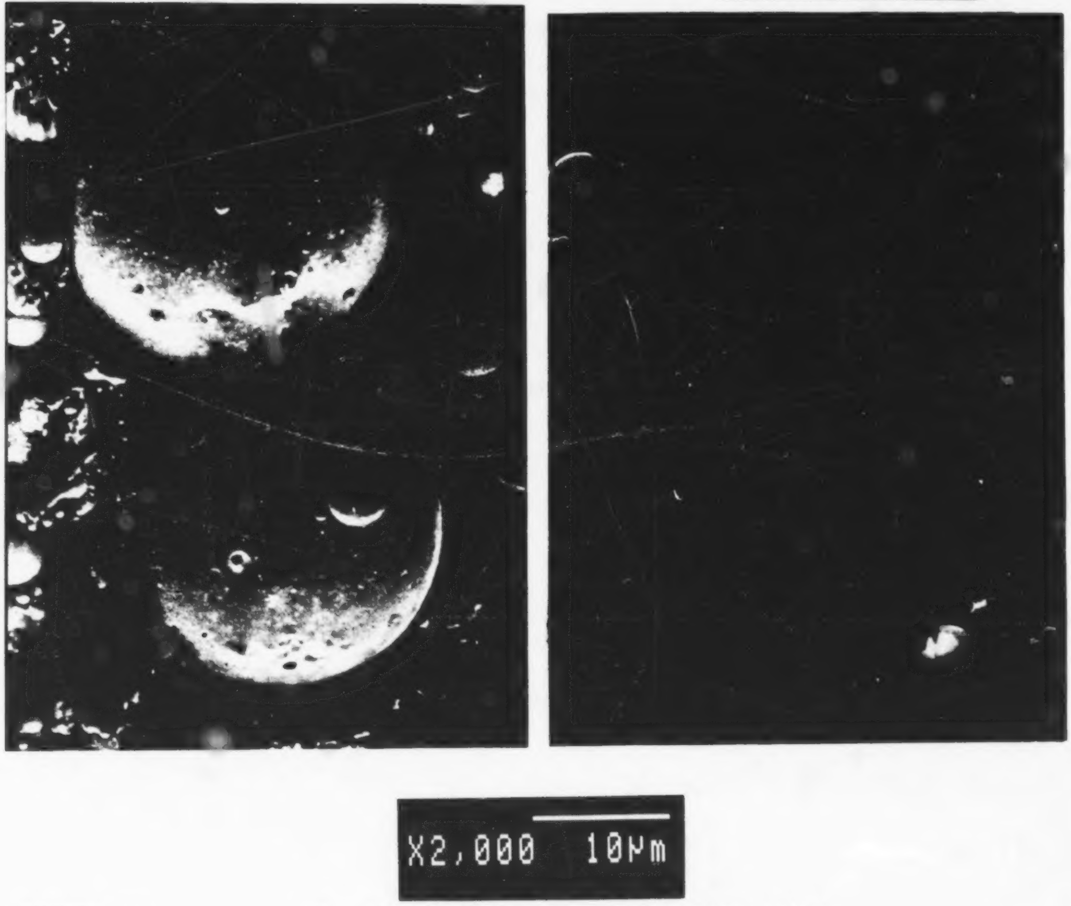

FIGURE 17. FLY ASH MORPHOLOGY, STOKER-FIRED COAL

They confirmed the measured particle sizes, but also suggested that there are differences, such as agglomeration tendencies between samples. Inspection of the photos leads to the conclusion that the smoothness of the surface of the ash particles, may be a very important parameter, in that it may influence agglomeration to a large degree. In fact, the recirculating fly ash distinguished itself from the other coal dusts studied, in that it was easy to feed into the test apparatus, i.e., it was non-agglomerating. The same dust also appeared to have the smoothest surfaces of those investigated. Notation of such tendencies, and their effect on filtration performance are not new. Recent literature[1] describing the performance of fabric filters in Australia, concludes that there is strong evidence for the correlation of the physical characteristics, including morphology, of ash particles and filter operating performance.

---

[1] Stig Strangert et al.; Proceedings Third Conference on Fabric Filter Technology For Coal Fired Power Plants. Scottsdale, Arizona, Nov. 1985

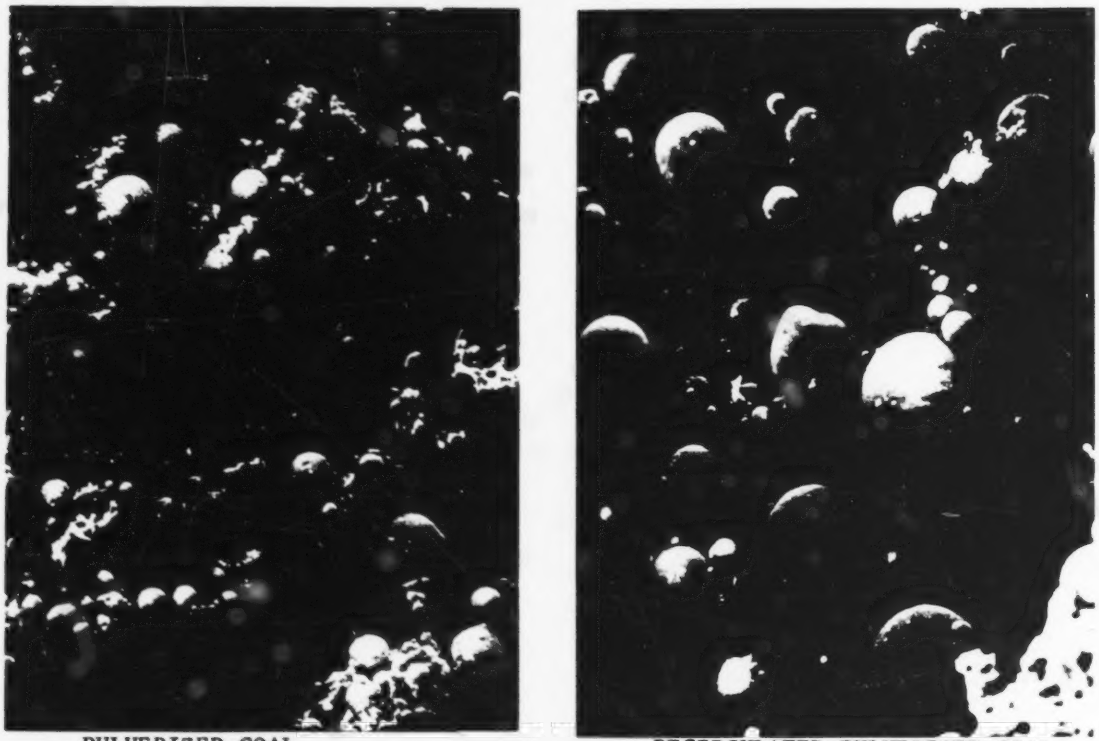

PULVERIZED COAL RECIRCULATED PULVERIZED COAL

FIGURE 18. FLY ASH MORPHOLOGY (CONT.)

FIGURE 19. ALUMINA MORPHOLOGY

APPLICATION

The type of information described in this presentation was used to specify filtration media for a coal-fired utility application involving a recirculating fly ash system. Five months after start-up, the system is operating satisfactorily with Tefaire® felt bags. Highlights of the operating conditions are given in Figure 20.

Note that the results were somewhat better than those obtained in the laboratory. We attribute this to two causes. One, the operating air/cloth ratio was slightly lower than the laboratory data, and the cleaning energy expended on the test sample is probably greater in the laboratory apparatus than in the field installation.

Number of bags: 2688

Filter medium: Tefaire®
Air/Cloth Ratio: 5.9 fpm
Cleaning Mode: On - line
Leakage: > 0.0066 grns./cu.ft.
dP: 3.9 - 7.8 in. H_2O
Temperature: Up to 450°F

In same unit:

- Felted glass failed due to acid attack
- Teflon® felt failed due to excessive leakage

FIGURE 20. OPERATING RESULTS...PUBLIC UTILITY - NON AGGLOMERATING FLY ASH

CONCLUSION

We have described laboratory equipment, and data obtained from it, for the design of fabric filters. Most of the results obtained were predictable by a rationalization process, but the morphological quality of the dust to be filtered was not quantified, leading to unexpected results. This emphasizes the need to investigate filter media under test conditions as close to operating conditions as possible. As long as we are not able to thoroughly classify dusts, such experimentation will have to include the use of the dusts expected to be encountered to avoid unpleasant surprises.

EVALUATION OF A SPECIFIC TYPE OF FILTER BAG SUPPLIED BY VARIOUS VENDORS

by: Yang-Jen Chen, Ph.D.
Philip N. Roberts
Tom D. Tarnok
Western Precipitation Division
Joy Manufacturing Company
4565 Colorado Boulevard
Los Angeles, California 90039

ABSTRACT

A detailed test program was conducted for fabric filter bags procured under the same specification from various bag fabricators, weavers, and finishers of fabric material. The filter bags were inspected for the integrity of the fabric, quality of fabrication and then installed in the same compartment of the N.S.P. Riverside baghouse for field testing. This paper describes the test procedures and presents the results of bag fabrication inspection and field evaluation for this specific type of fabric filter bag. Based on the test results of this test program, specific procedures of bag procurement are recommended.

INTRODUCTION

Fabric filters have become a primary pollution control technology for fly ash and dry FGD applications. At the present time there are more than 100 utility installations in the United States. To date, Joy Manufacturing Company has contracted for twenty-four (24) utility baghouses, over 5700 MW and almost fifty (50) industrial units. In 1986 alone, JOY expects to procure 70,000 filter bags for fly ash and dry FGD applications.

In search of fabric bags with longer life, lower cost, and lower pressure drop characteristics, a test program has been conducted since 1980 to evaluate a variety of fabric materials at the JOY-NIRO N.S.P. Riverside 100 MW dry FGD demonstration unit in Minneapolis, Minnesota. Based on results of the test program, a lightweight type A teflon-coated woven fiberglass material (Table 1) has been identified as the primary candidate filter material for dry FGD and coal-fired boiler applications.

As a major procurer of fiberglass filter bags, JOY has developed extensive procedures to evaluate specific types of filter bags. The purpose of this type A teflon-coated woven fiberglass bag evaluation program is to ensure that JOY and JOY's customers will not only receive quality bags conforming to our specifications, but not be constrained to a single source of supply.

TEST PROGRAM

Through the procurement process, 10 to 30 bags were obtained from each of four bag suppliers (Table 2) based on JOY's specification and drawings. One supplier provided two sets of bags from separate weavers. Materials are from the four major weaving companies. S1 supplier put their own finish on W1 materials; the other fabrics were finished by the weavers. The fabric bags from various sources were inspected and installed in the field for evaluation.

TABLE 2

TEST BAGS FROM VARIOUS SOURCES

SUPPLIER	WEAVER	FINISHER
S1	W1	S1
S2-1	W2	W2
S3	W2	W2
S4	W3	W3
S2-2	W4	W4

A. BAG FABRICATION INSPECTION

Two sample bags from each bag supplier were randomly selected for fabrication inspection. One sample bag from each supplier was inspected by the Engineering Department at Western Precipitation. The other sample bag was sent to an independent testing company for fabrication inspection and material evaluation.

B. FIELD EVALUATION

The test bags were evaluated in the Riverside baghouse, located downstream from the spray dryer absorber (Figure 1). The baghouse compartment, as shown in Figure 2, are arranged in two rows, six compartments to a row. Each compartment consists of 250 twelve-inch diameter, thirty-five foot long bags. Total gross filter area for each compartment is 26,775 square feet. Woven fiberglass materials of various specifications were installed in different compartments for testing. The original lightweight Type A teflon-coated bags have been installed and evaluated in the even compartments since early 1981. A total of 87 Type A test bags were installed in Compartment 3 with Type D material for field testing. The distribution of those Type A test bags inside Compartment 3 is illustrated in Figure 3, and the operation data is summarized in Table 3.

Since the Riverside power plant is a peaking unit and the dry FGD system is a demonstration facility, the baghouse has been through various operating conditions: e.g., with or without spray dryer in service, high and low baghouse inlet temperature, boiler banking and various coal types with sulfur contents ranging from 0.8 to 3.5%.

The gross air-to-cloth ratio varied from 0.7 to 2.5 ft/min., depending on boiler load conditions and number of compartments in service. When the spray dryer is in operation, the baghouse runs at a considerably lower temperature than a non-FGD installation. The operating temperature with the SDA in service has been as low as $18^{\circ}F$ above the adiabatic saturation temperature. The dust loadings with the SDA in operation (4.27 - 12.1 gr./ACF) are much higher than without the SDA (1.2 - 2.9 gr./ACF).

Test bags from S1 supplier were installed on 7/21/83, and the bags from other bag suppliers were installed on 6/15/83. All the sample bags were removed on 12/10/83 for evaluation. The number of operating hours for S1 bags was 1511 hours and 1937 hours for the other bags.

TABLE 3

BAG SAMPLES	NO. OF BAGS	COLUMN IN COMP. 3	INSTALLATION DATE	REMOVAL DATE	TOTAL OPER. HOURS
S1	9	C	7/21/83	12/10/83	1511
S2-1	22	D	6/15/83	12/10/83	1937
S2-2	12	E	6/15/83	12/10/83	1937
S3	22	H	6/15/83	12/10/83	1937
S4	22	J	6/15/83	12/10/83	1937

TEST RESULTS

A. BAG FABRICATION INSPECTION

The results of bag fabrication inspections from our Engineering Department and from the independent testing company are summarized in Tables 4 and 5 respectively. The inspection compared the physical characteristics of the bags to specifications and drawings and examined the quality of the fabrication and materials. Cuff bands, rings, ring-covers, seams and stitches were examined. The findings are as follows:

1. The most common problems were:
    - a. The cuff size and the distance to the first row of the stitching were not in compliance with the specified dimensions of the drawing.
    - b. Loose, wrinkled cuffs around the band (except supplier S1).
    - c. The developed length of the band was 1/32" to 1/8" short, compared to specified dimensions.
    - d. Burrs (Supplier S2) and loose rivets (Supplier S3) in the cuff bands.
2. Bags from S2 supplier had altered ring cover identification marks; apparently incorrectly marked on the first layout. Some marks were done by needles.
3. Seam registration was excellent on S1 bags, good on S2 and S4 bags, and poor on S3 bags.
4. S1 bag had rubber roll marks caused during seaming. Rubber particulate was found embedded in the texturized yarns.
5. Seam yarn strength, cuff yarn strength, and stitch interlocking were all rated good.

B. FIELD EVALUATION

The intention of the field evaluation was to install the test bags from various bag sources in the same compartment and evaluate the materials in service for a period of time under the same condition. The sample bags were removed on 12/10/83 and evaluation tests performed, which included the cloth weight, permeability, breaking strength, Mullen burst, MIT flex cycle, loss of ignition, and water repellancy tests.

The material evaluation results for the virgin bags and the sample bags removed on 12/10/83 are summarized in Table 6. During the testing period, Compartment 3 was on and off-line frequently because of the broken Type D bags and other operation problems. No test bags failed during this period.

Cloth weight and permeability were performed on as-received, vacuumed and washed fabric samples. The results showed that washing returned the original permeability and weight of the material. The as-received samples have considerably less permeability and vacuuming only partially restored the permeability. The permeability of S1 and S2-1 bags have higher values for the as-received and vacuumed condition when compared to S3, S4, and S2-2 bags.

As shown in Figures 4 and 5, no significant losses were found in Mullen burst strengths and breaking strengths in all materials. Loss of ignitions were performed at 500°F and 1200°F. Thermal gravimetric analyses were also performed on all material to evaluate the continuous weight loss vs. temperature variation. The data is summarized in Tables 6 and 7. The measured Teflon finish ranged from 8.9% to 16.10% compared to 10% specified. The in-situ bag weight measurements were performed before the sample bags were removed. The results are tabulated in Table 8. The bag weights (residual dust + material weight) ranged from 23.0 lbs. to 31 lbs.

DISCUSSION OF THE TEST RESULTS

A. BAG FABRICATION

Based on the results of the bag inspection, all the bags had some items which were not in conformance with the specifications. Most causes for rejection were mislocation of the first row of stitching, wrong size of the cuff and band, and burrs and loose rivets on the band; all of which can be corrected with a good quality control program. However, the two major subjects which need special attention in bag fabrication are cuff fit and seam registration. Loose and wrinkled cuffs with excessive folding around the bands will cause problems in bag installation or leakage past the thimble during operation. Too much difference in seam registration will cause problems in bag tensioning. Uneven tension on the bag will result in premature failure of the bag and lower performance of the bag. For a 35-foot bag, seam registration within 1 inch is considered acceptable.

Based on inspection results, S1 bag supplier has demonstrated their ability to make good bags. Other bag suppliers have not been consistent in making good cuffs or keeping the seam registration within tolerances. To fabricate the cuff with no folding and stitch the seam registration within 1 inch requires proven skill in the fabrication process. These abilities should be demonstrated by these bag fabricators before being qualified as a bag supplier.

B. MATERIAL EVALUATION

All the test bags submitted by various suppliers were of similar basic yarn and fabric construction; thread count 53 x 30, weave 3x1 twill, yarn 150-1/2 and 150-1/4 texturized. After being in service for approximately five (5) months, all of the test bags retained very good levels of tensile and Mullen burst strengths. The MIT flex endurance test on all of the bags were also at very good levels below the nominal 50% equilibrium loss, indicating that no chemical or physical fatigue had occurred on the fabrics.

The as-received permeability indicated that the as-received air flow acceptance levels were different. S2-1 bags and S1 bags achieved higher flow levels (3.1 and 2.86) in comparison to the balance of the remaining bags 2.24, 2.2, and 2.46). The vacuumed permeability of the S2-1 bags (13.67) and S1 bags (13.01) also appear to have higher nodular release characteristics than the others (9.8, 9.87, and 10.97).

Under microscopic examination, evenness of the finish treatment, fiber breakage and texturized loft are rated normal for all materials. The test results for loss of ignition (LOI) at 1200°F by an independent testing company indicated that S1, W2, and W4 are rated below 10% as specified. However, S1 and W2 finish bag can be considered within the tolerance.

The thermal gravimetric analysis indicated that all of the materials are rated above 10% for LOI at 1112°F except W4 material, which was only 8.9%. W3 material had the highest LOI 16.10%.

The LOI data from the independent testing company and thermal gravimetric analysis showed that the finish on the W4 material were all consistently below 10% as specified. The finish on the material from W3 ranged from 10% to 16% which indicates that the finish on the material was not uniform. The material from S1 bag supplier and W2 weaver have a consistent finish of approximately 10%.

The S1 fabric yielded very low repellancy time (2 minutes) on the water repellancy testing, as compared to the other material (30 min. plus) and S1 material purchased in 1981. This may indicate that the S1 test bag is not fully cleaned of starches prior to finishing. However, significance on bag performance between 2 minutes and 30+ minutes repellancy time is not fully understood at this time.

S2-2 and S3 bags had lower in-situ bag weights (23.0 lbs. and 25.5 lbs.) compared to other bags (29.5 lbs., 31 lbs., and 28.5 lbs.). This means that the S2-2 and S3 bags had less residual dust. The low texturized yarn content found in the S2-2 material is a possible explanation for the lowest residual dust layer found. Another explanation for low residual dust might be the location of the S2-2 bags (Column E) and S3 bags (Column H). Column E and Column H of the bag location are symmetrical in Compartment 3.

The test results of test bags installed in 1983 are also compared with the results of the same type of bags installed in 1981 after they had been in service for about 1500 hours of operation. The material strengths of both types of bags are rated at good levels after the same period of operating hours. The S1-1981 bag had a 11% teflon finish with a 30-minute water drop repellancy time, while S1-1983 bags had a 10% finish with a 2-minute water repellancy time. The permeabilities under the "as-received," vacuumed and washed conditions on S1-1981 bag are lower than the S1-1983 bag. The difference in Teflon finish and operation conditions between Compartment 2 (S1-1981 bag) might explain the differences in permeabilities.

CONCLUSIONS AND RECOMMENDATIONS

In this test program, all of the test bags had some causes for rejection from a fabrication standpoint. The S1 bag supplier had the fewest. However, all suppliers should be considered as qualified bag fabricators as long as they can demonstrate their ability to correct the nonconformances.

In addition to the S1 material, which has been in service for four and a half years, the W2 material is also recommended (woven and finished by W2) for the following reasons:

1. The material retained very good level of strength.

2. The performance data of S2-1 bag is as good as the S1 bag, although S3 bag, which is also made from W2 material, had a lower performance as indicated in as-received and vacuum permeability. The lower performance might be due to uneven tension because of the excessive misalignment in seam registration.

3. The finish on W2 material is uniform and consistent in the range of 10%.

From the test results, the performance data of W3 and W4 material are at lower levels than the data from S1 and W2 materials. The Teflon finish on W4 material was in the range of 9%, which is considerably less than the 10% specified. Although the Teflon finish on W3 is higher than 10%, the data has shown that finish is inconsistent ranging from 10% to 16%. Low levels of texturizing in yarn content was also found in W3 material. Based on these observations, the application of W3 and W4 materials are not recommended, but not disqualified, at the present time. However, evaluation of W3 and W4 material should be continued.

Based on the test results and experience from this test program, the following procedures are recommended for filter bag procurement to ensure high quality of the bag fabrication and fabric material:

1. A detailed specification and drawing should be prepared for bag procurement. Materials, physical dimensions, fabrication methods, and allowable tolerances should be clearly specified.

2. Sample bags from the various suppliers need be evaluated, not only from the standpoint of fabrication but also from the standpoint of material quality.

3. The definition of Teflon finish percentage measurement should be clearly specified. Thermal gravimetric analysis is recommended to check the impurity level of the finish to assure it is not over maximum allowance.

4. A meeting with all potential bag suppliers should be arranged to allow explanation of any nonconformances in the bag they submit for inspection and discussion of their technical ability to correct these nonconformances.

5. After a bag supplier is identified, it is recommended that the bag supplier submit additional sample bags to demonstrate their ability to correct nonconformances with the specification before bag fabrication proceeds.

6. A good quality control program should be established in both material evaluation and bag fabrication. Material should be examined for strength, percentage of finish and cure of the finish. Unqualified material should be rejected before the material is processed for bag fabrication. During the fabrication process, bags should be inspected from time-to-time to ensure quality.

The work described in this paper was not funded by the U.S. Environmental Protection Agency and therefore the contents do not necessarily reflect the views of the Agency and no official endorsement should be inferred.

Figure 1. JOY/NIRO DRY FGD SYSTEM AT RIVERSIDE

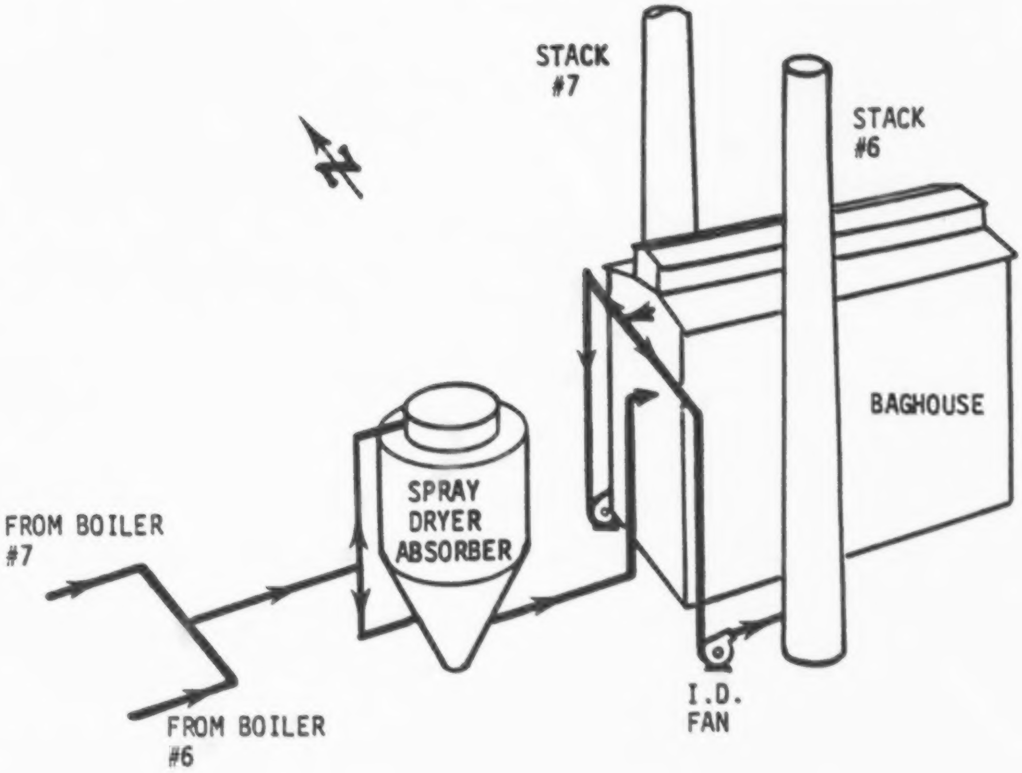
STACK #7
STACK #6
N
BAGHOUSE
SPRAY DRYER ABSORBER
FROM BOILER #7
FROM BOILER #6
I.D. FAN

Figure 2. LOCATION OF THE TEST BAGS IN THE BAGHOUSE

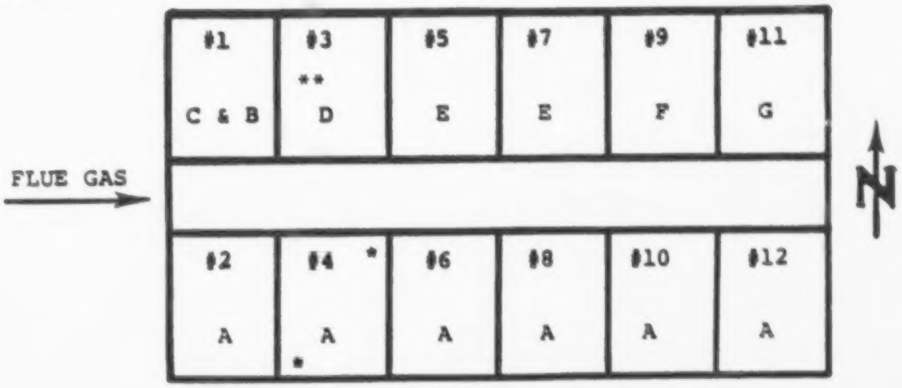

#1 C & B	#3 ** D	#5 E	#7 E	#9 F	#11 G
#2 A	#4 * A *	#6 A	#8 A	#10 A	#12 A

* SONIC HORNS ** Test Bag Compartment

A to G : Woven Fiber Glass Materials with Various Specifications

FIGURE 3 TEST BAGS DISTRIBUTION

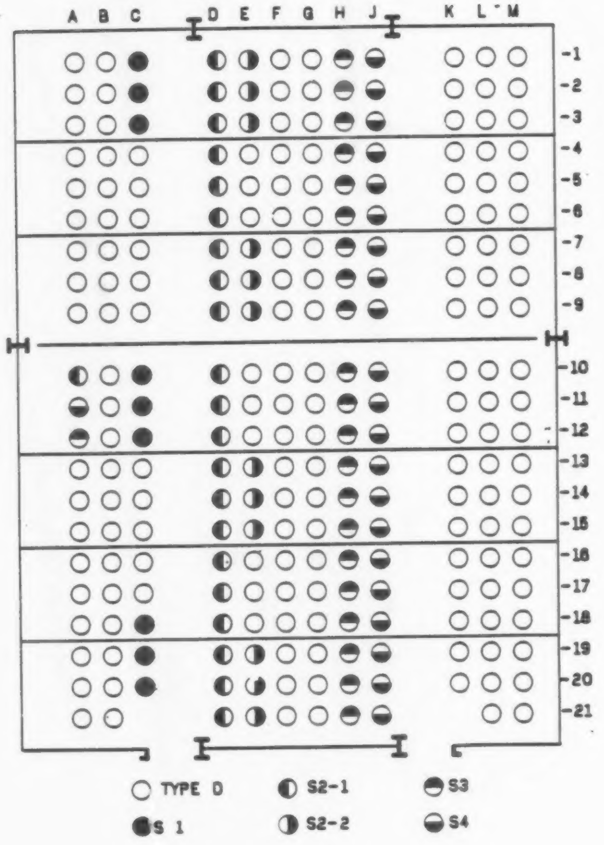
A B C
D E F G H J
K L M
-1
-2
-3
-4
-5
-6
-7
-8
-9
-10
-11
-12
-13
-14
-15
-16
-17
-18
-19
-20
-21
○ TYPE D
● S 1
◐ S2-1
◑ S2-2
S3
S4

FIGURE 4 MULLEN BURST

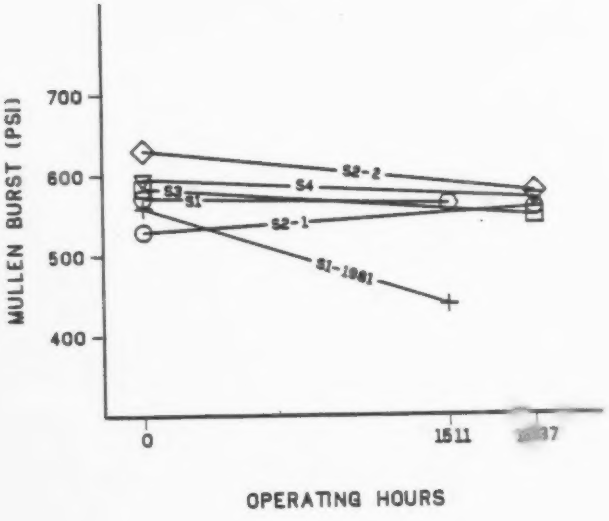

FIGURE 5-1 BREAKING STRENGTH. WARP

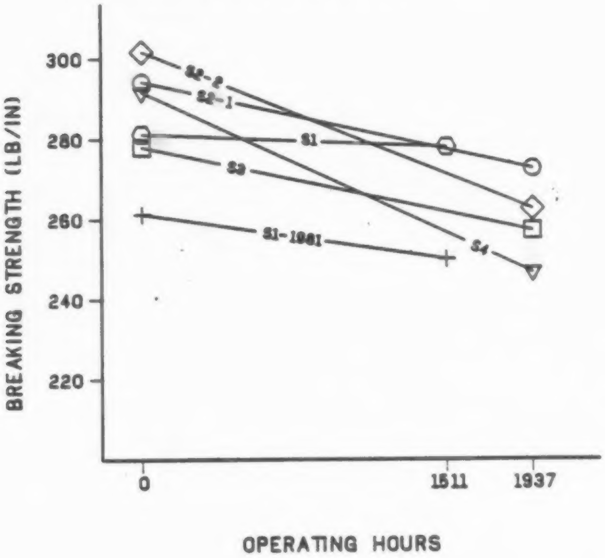

FIGURE 5-2 BREAKING STRENGTH. FILL

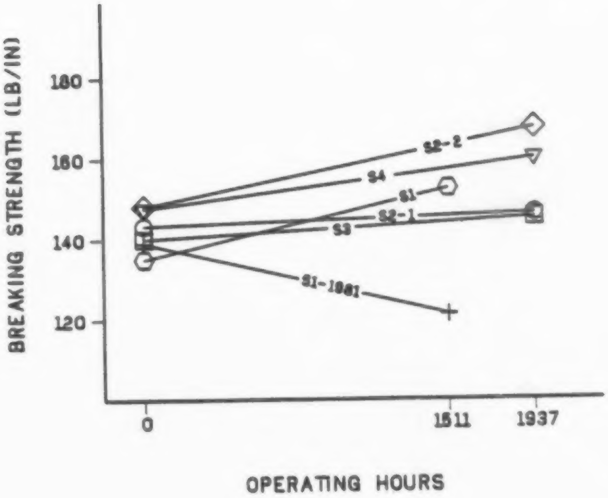

TABLE 1 TYPE A MATERIAL SPECIFICATIONS

THREAD COUNT	53 x 30
WARP YARN	150-1/2
FILL YARN	150-1/4 TEXTURIZED
WEAVE	3x1 TWILL
AVG. WT., OZ./YD ^{2}	9.3
PERMEABILITY, CFM/FT^2	65-80
MULLEN BURST, PSI	595 (450 MINIMUM)
FINISH	TEFLON, 10%
MATERIAL	GLASS

TABLE 4 RESULTS OF BAG FABRICATION INSPECTION

SUPPLIER	S1	S2	S3	S4
CUFFS				
CUFFS A: SIZE	X	X	X	0
DISTANCE TO 1st RING	0	X	0	0
CUFFS B: SIZE	X	X	0	X
DISTANCE TO 1st RING	0	0	0	X
REMARKS	Well made No fold	Loose Much Folding	Very loose Folding	A Well Made B Folding
BAND				
DEVELOPED LENGTH A	X	X	X	X
DEVELOPED LENGTH B	X	X	X	X
THICKNESS A	0	0	0	0
THICKNESS B	0	0	0	0
REMARKS	Well made	A: Burrs B: OK	Loose Rivets	Well made
RING AND RING COVERS	0	X	0	0
COATING	0	Bare Spot	0	0
WELDING	0	0	Burr	0
TOTAL NONCONFORMANCE	4	9	6	5

X = Nonconformance
0 = OK

TABLE 5 BAG FABRICATION INSPECTION RESULTS

BAG SUPPLIER	S1	S2	S3	S4
SEAM TYPE	CHAIN	CHAIN	CHAIN	CHAIN
SEAM YARN	4 PLY	4 PLY	4 PLY	4 PLY
SEAM YARN LOI	12.87%	13.14%	12.63%	12.71%
SEAM YARN STRENGTH (LBS/END)	9.7	9.6	9.8	9.4
STITCHES/INCH	4.5	6.5	7.5	8.0
STITCHES/ROW	2	3	2	2
CUFF TYPE	LOCK	LOCK	LOCK	LOCK
CUFF YARN	4 PLY	4 PLY	4 PLY	4 PLY
CUFF YARN LOI	12.83%	12.71%	12.69%	12.75%
CUFF YARN STRENGTH (LBS/END)	9.9	9.7	9.8	9.5
BAG SUPPLIER	S1	S2	S3	S4
STITCHES/ROW	1	2	2	2
STITCHES/INCH	8	6	6.5	6
SEAM REGISTRATION (INCHES)	0	0.70	1.29	0.53
STITCH INTERLOCKING	GOOD	GOOD*	GOOD	GOOD

*One end on a ring cover stitch broken

TABLE 6

BAG TEST RESULT SUMMARY

(Average Values of Top, Center, and Bottom of the Bags)

BAG SOURCE		S1		S1		S2-1		S3		S4		S2-2	
Operating Time (Hours)		1981		1983		1983		1983		1983		1983	
		0	1580	0	1511	0	1937	0	1937	0	1937	0	1937
CLOTH WEIGHT Oz./Yd.^{2}	As Rec'd	10.68	17.37	9.98	14.64	9.75	14.62	9.92	17.34	10.88	15.27	9.95	15.12
	Vac.		15.44		13.01		12.99		14.74		13.72		13.44
	Washed		10.71		10.10		9.67		10.28		10.68		10.04
PERMEABILITY CFM/Ft.^{2} @ 0.5" H_2O	As Rec'd	48.2	0.98	71.6	2.86	62.4	3.1	70.3	2.24	70.1	2.22	68.9	2.46
	Vac.		5.43		13.37		13.67		9.80		9.87		10.97
	Washed		50.07		65.53		62.23		59.90		67.67		71.20
Breaking Strength Lb/In.	Warp	261	250	281	278	294	271	278	255	291	246	307	266
	Fill	139	122	136	154.3	143	147.3	140	147.7	147	161.7	148	170
Mullen Burst (Psi)		564	422	571	558	528	551	538	541.7	594	561.7	631	571.3
MIT Flex Cycles	Warp	5206	4938	4897	4637	24708	18065	21031	15884	21009	13590	20861	12590
	Fill	512	219	496	388	2004	1203	983	505	2018	1114	2043	1249
L.O.I. %	1200 F	10.99	10.87	9.98	9.89	9.56	9.76	10.04	10.91	10.80	13.31	9.21	9.18
	500 F	0.22		0.41		0.87		0.59		0.63		0.46	
Water Absorption Minutes		30+		2		30+		30+		30+		30+	

Reproduced from
best available copy.

TABLE 7 THERMAL GRAVIMETRIC ANALYSIS

TEMPERATURE °F	WEIGHT LOSS, %				
	SI	W2	W2	W3	W4
500	.45	.12	.15	.30	.28
662	.75	.30	.30	.90	.60
1112	10.50	10.8	10.65	16.10	8.9
1652	10.70	11.42	10.92	16.8	9.55

TABLE 8 IN-SITU BAG WEIGHT TEST

BAG TYPE	LOCATION	BAG WEIGHT	NEW BAG + CAP	DUST CAKE
S1	12-C	29.5	14.3	15.2
S2-1	13-D	31.0	14.0	17
S2-2	13-E	23.0	14.0	9
S3	13-H	25.5	14.5	11
S4	13-J	28.5	14.5	14

Weight in pounds

Date: 12/10/83

CATENARY ANALYSIS OF A FABRIC FILTER BAG DURING REVERSE-GAS CLEANING

By:

Eric A. Samuel
General Electric Environmental Services, Inc.
Lebanon, Pennsylvania 17042

and

John G. Musgrove
Bechtel Power Corporation
Houston, Texas 77252

ABSTRACT

The catenary-like shapes and the corresponding tensions along a utility-size fabric filter bag during reverse-gas cleaning have been calculated by an iterative technique which ensures consistency between the bag tensions and deflections, including the effect of bag stretch under tension. In this analysis, the maximum bag deflections occurring midway in each bag segment between successive anti-collapse rings are first calculated. The axial gas velocity during reverse-gas in each bag segment are then deduced from these deflections assuming a constant reverse gas-to-cloth ratio across the entire bag. Characteristics of a given ring spacing, including curves of calculated deflection and axial gas velocity vs. height are used to compare the effects of reverse-gas pressure drop, dust weight on bag, and springs of variable length and spring constant. This catenary model is useful for optimizing spring design for specialized baghouse operating conditions, such that critical bag parameters such as the bag tension at the thimble, and the maximum axial gas velocity during reverse gas cleaning are within design limits. The analysis shows that the spring tension during reverse-gas cleaning is independent of spring constant provided the spring is fully compressed during the reverse flow. The spring tension during reverse-gas is shown to be much larger than its pre-tension value. This fact appears to obviate precise bag pre-tensioning. Fully compressed operation of the bag spring during reverse-gas flow is shown to be advantageous for baghouse operation. A simple model for explaining the observed time-variation of the bag tension due to the fall of the plug-like dust released within the bags, is also presented. The predictions of this model may be used to factor into the catenary analysis of a bag suspension system, the effects of the time-varying spring tension during reverse-gas flow.

INTRODUCTION

A new bag is installed in a baghouse with a pre-tension. This pre-tension, which is applied to compensate for weight gain on the bag and to prevent loss of tension, will change when the bag is put into service for three reasons: (1) thermal expansion of the baghouse casing resulting in an increase of the height between the points of suspension of the bag; (2) bag elasticity, which results in a decrease in the bag tension; and (3) the extra weight of dust on the bag, which will increase tension at the top of the bag and decrease tension at the bottom of the bag. In the present analysis the thermal expansion effect is neglected since the coefficient of thermal expansion of the structural steel is approximately the same as that of the glass material of the bag.

The force of the reverse-gas on the bag surface during cleaning causes the bag segments between rings to take catenary-like shapes (1). As a result of this deformation, the effective height of the bag is reduced, which in turn causes the bag to pull at its point of suspension with a force greater than during gas flow in the normal filtering mode. This pull causes the bag spring to be compressed even to the point of complete compression. When the spring is fully compressed, there is no upper limit to the bag tension.

This paper describes an analysis of a typical utility reverse-gas bag. First, the effective length of a new bag during pre-tensioning including bag elasticity is calculated by representing the bag as a series of springs, each representing the bag segment between successive anti-collapse rings. Then, the change in bag tension during reverse-gas flow is calculated using Musgrove's Catenary Model (1). Two main features of the present formulation are:

(1) Coupling of the effective bag height with the bag suspension spring to yield a unique bag tension consistent with the catenary equations, the spring compression, and the bag elasticity.

(2) Elastic stretch of the bag under tension, based on measurements performed at the G.E. Turbine Technology Laboratory (2).

The purpose of the analysis is to provide a basis for understanding the relationships of the reverse-gas pressure drop and the suspension spring characteristics (such as the spring constant, spring free-length, and pre-tensioning force) to bag characteristics during reverse-gas (such as the mid-segment bag deflections and axial gas velocities within the bag).

THEORY

BAG SUSPENSION SPRING CHARACTERIZATION

Figure 1 represents a bag suspension spring in three characteristic states of compression: (1) in its uncompressed state with y_{so} representing the free length of the spring, (2) in its pre-tensioned state with y_{sp} representing its pre-tensioned length, and (3) in its fully compressed state with

y_{sm} representing its fully compressed length and y_{sra} representing the additional available compression from its pre-tensioned position. The free length of the spring, y_{so}, is the sum of the two spring compressions, y_{sp} and y_{sra}, and the spring's fully compressed length, y_{sm}:

$$y_{so} = y_{sm} + y_{sp} + y_{sra}$$

The first term on the right hand side of Equation (1) is fixed by the choice of the spring constant, and the wire material for the spring. The second term is fixed by the choice of the pre-tension force. The third factor is fixed by the maximum spring compression to be allowed during reverse-gas. In this study, the effect of varying each of these three spring variables will be discussed.

CHANGE IN BAG TENSION DUE TO DUST LOADING AND BAG STRETCHING

Pre-tension

Figure 2(a) is a schematic of a typical reverse-gas bag suspension system. The bag is p[illegible]-tensioned by applying the required pre-tension on the spring with the ai[illegible]n external force, and moving the pin, P, which holds the spring to the [illegible]ing rod, C, so as to maintain this tension when the applied force [illegible]ed. Figure 2(b) is a representation of this suspension system in term[illegible] equivalent springs. The top spring represents the suspension spring. The other springs represent the elasticity of bag segments between successive rings. If T_p is the suspension spring pretension, and if T_i is the mean tension in the i th bag segment, then the elastic modulus for each spring in Figure 3 may be written as:

$$k_i = [(Y_i - Y_{io})/Y_{io}] / [T_i/(\pi D)] \tag{1}$$

where k_i, Y_i, and Y_{io} are respectively the effective spring constant, the current length, and the length under zero tension of the i th segment. If W_i is the weight of the i th segment, then the mean tensions in each bag segment may be written in general as (1):

$$T_1 = T_p - (W_1)/2 \tag{2}$$

and,

$$T_i = T_1 - \sum_{r=1}^{i} (W_{r-1} + W_r)/2 \tag{3}$$

Equation (1) may be rewritten to give the effective length of each segment as:

$$Y_i = Y_{io}[1 + k_i \, T_i/(\pi D)] \tag{4}$$

Equation (4) when summed for each of the N bag segments, yields for the bag length, Y_p, under pre-tension;

$$Y_p = \sum_{r=1}^{N} Y_i \tag{5}$$

It is possible to calculate the effective length of the connecting rod, Y_o, as:

$$Y_o = H_o + y_{sp} - Y_p \tag{6}$$

where H_o is the height between the tube-sheet and the I-beam supporting the bag suspension springs, and y_{sp} the spring length at pre-tension given by:

$$y_{sp} = y_{so} - T_o/k_s \tag{7}$$

The length of the connecting rod, is fixed at pre-tension and assumed constant during the ensuing routine operation of the baghouse.

Analysis With Reverse-Gas Flow

If T_o is the spring tension in the presence of reverse-gas flow, the average tension in the first bag segment can be evaluated as:

$$T_1 = T_o - \Delta P\ (\pi D^2/4) - (W'_1)/2 - W_c \tag{8}$$

where P is the reverse-gas pressure drop, D the bag diameter, and W_c the weight of the bag cap. In general, the mean tension in the i th bag segment is evaluated from that in the immediately preceding section by subtracting a weight difference, as:

$$T_i = T_{i-1} - (W'_{i-1} + W'_i)/2 \tag{9}$$

In Equations (8) and (9), the weights, W_i and W'_i, of the bag segments of lengths S_i, with and without dust are related to the weights per unit area of the bag cloth and dust, w_b and w_d, through:

$$W_i = (\pi\ D\ S_i)\ w_b \quad \text{and} \quad W'_i = (\pi\ D\ S_i)\ (w_b + w_d) \tag{10}$$

The total vertical distance, Y_i, of a deformed segment, i, in terms of the total arc length, S_i, of that segment, may be obtained from Musgrove's analysis (1) as:

$$Y_i = 2c\ \ell n\ \{\ S_i/(2c) + \sqrt{[\ 1 + (S_i/(2c))^2]}\ \} \tag{11}$$

where c is a constant given in terms of the average tension in the bag segment, T_{avg}, as:

$$c = [T_{avg}/(\pi D)]/\Delta P \tag{12}$$

The maximum deflection, d_i, in a bag segment occurring at its center, is also obtainable from catenary theory (1) as:

$$d_i = c\ \{1 - \cosh\ [S_i/(2c)]\} \tag{13}$$

The arc length, S_i, is subject to elastic stretching at the average tension, T_i, in that segment, and can be evaluated from Equation (1) as:

$$S_i = S_{io} [1 + k_b T_i/(\pi D)] \qquad (14)$$

where S_{io} is the unstretched length of the bag segment, i, assuming all bag segments to have the same elastic modulus, k_b. Equations (11) to (14) are the catenary equations which yield an effective bag height (sum of all Y_i) for a given spring tension, T_o, at the spring. It must be determined whether the effective bag height, and the corresponding spring compression are consistent with the tension, T_o. In order to check for this consistency, the spring length, y_s, corresponding to catenary formation at the assumed initial spring tension, T_o, is evaluated as:

$$y_s = \sum_{r=1}^{N} Y_r + Y_o - H_o \quad \text{for } T = T_o \qquad (15)$$

where Y_o is the connecting rod length from pre-tension (see Equation (6)). If $y_s > y_{sm}$, the bag suspension spring length at maximum compression, then the tension T_o is compared with that predicted by Hooke's law for the spring length, y_s:

$$T'_o = k_s (y_{so} - y_s) \qquad (16)$$

If T'_o is different from T_o, then a new value of T_o is chosen until the two tensions are the same. If the value calculated by Equation (15) is smaller than y_{sm}, then Equation (16) is not used, since the spring is now fully compressed, and the bag tension at the spring can be higher than T_{max}, the tension required to just compress the spring fully. In this case, the assumed tension, T_o, is adjusted to achieve $y_s = y_{sm}$.

The axial velocity of reverse-gas midway in the i th bag segment corresponding to the deflections calculated as described above may be derived assuming a constant gas-to-cloth ratio, v_{ra}, across the entire bag, as:

$$V_i = [4 v_{ra}/D] \sum_{r=1}^{i} (S_{(r-1)o} + S_{ro})/2 \qquad (17)$$

where S_{ro} are the unstretched lengths of the bag segments, and $S_{oo} = 0$.

Time Variation of Reverse-Air Pressure Drop Due to The Falling Dust Plug - Walsh Effect

The spring tension is not constant with time (4). The bag deflections caused at the inception of reverse-gas will lead to release of the collected dust from the bags. As this dust falls within the bag, the pressure inside the bag will vary due to the pressure drop across the falling porous plug. A simple model, based on D'arcy's law (3) may be used to obtain the time dependence of the reverse-gas pressure drop during the time of fall of dust within the bag. The following are the assumptions of the model:

1. At time $t=0$, the entire volume within the bag is filled with dust of uniform porosity. This plug falls within the bag with zero initial velocity and effective acceleration due to gravity, g'.

2. Reverse-gas flow does not begin until after the dust plug has entirely cleared the bottom of the bag.

3. The reverse-gas pressure drop is equal to the pressure drop across the falling plug. The pressure drop across the plug itself is proportional to the instantaneous length, velocity, and weight per unit cross-sectional area of the plug, according to D'arcy's law.

Figure 3 is a representation of the plug at time, t. The weight per unit cross-sectional area (areal density) of the plug, m, is given by:

$$m = (\pi D w_d)\,[1/(\pi D^2)]\,(S_o - y) \qquad (18)$$

where w_d is the areal density of the dust cake prior to being released into the bag at time $t=0$, S_o the bag length, D the bag diameter. The height, h, through which the plug has fallen in time t and the velocity of the plug at time t are given by:

$$h = (1/2)\,g'\,t^2 \quad \text{and} \quad v = g't \qquad (19)$$

The time-dependent reverse-gas pressure drop can now be written using D'arcy's law and Equations (18) and (19) as:

$$\Delta P(t) = K_2\, m\, v \qquad (20)$$

or $$\Delta P(t) = K_2\,[w_d\, g'/D]\,[S_o - (1/2)g'\,t^2]\,t \qquad (21)$$

where K_2 is the coefficient of specific resistance for the plug. This pressure drop shows a maximum due to two competing effects: the effect of the decreasing length of the plug, which leads to a time-decreasing pressure drop, and the effect of the increasing velocity which leads to a timeincreasing pressure drop. The model prediction for the time location of the maximum pressure drop may be obtained by setting the derivative of the pressure drop in Equation (21) to zero. This procedure leads to:

$$t_{max} = \sqrt{[2S_o/(3g')]} \qquad (22)$$

Equation (22) provides a convenient means of ascertaining the effective acceleration, g', of the dust plug from experimental traces of the spring tension during bag cleaning.

RESULTS AND DISCUSSION

INTRODUCTION

Three required attributes of a utility baghouse are: (1) low average tube-sheet pressure drop, (2) low particulate penetration, and (3) high bag life. Good cake release leads to lower residual bag weights and consequently to lower mean tube-sheet pressure drops. One of the factors determining cake release is the bag deflection during reverse air. High deflections, however, will impact bag life. The axial velocity of reverse-gas within the bag increases with increasing deflection. Consequently, bag life can decrease with increasing deflection since the high deflections and the accompanying high velocities may degrade the bag material through abrasion. Thus ring placement must be optimized to maximize cake release and minimize bag abrasion.

BAG SUSPENSION SYSTEM VARIABLES STUDIED

An 'equal' ring spacing was chosen arbitrarily to only exemplify the analytical models presented in this paper. The suspension system variables were spanned in the following ranges in this study:

Ring Placement (fixed) = First ring 2.5 ft. above thimble; all other 7 rings equally spaced above it.

Dust weight, w_d = 50, and 100 lb_f

Reverse-air steady state pressure drop, ΔP = 1, and 2 in. water

Spring Constant, k_s = 40, 75, and 100 lb_f/in.

Spring pre-tension, T_p (Dust weight = 50 lb_f) = 75, 100, and 125 lb_f

Spring pre-tension, T_p (Dust weight = 100 lb_f) = 100, 125, and 150 lb_f

Maximum allowed spring compssion on reverse-air, y_{sra} = 1, 2, and 3 in.

Encompassing all possible combinations of the above variable ranges involved 108 runs of the program.

BAG DEFLECTION AND AXIAL VELOCITY PROFILES

Figure 4 illustrates the variation of the bag deflection and axial velocity along the bag for the case of a 50 lb_f dust weight and 1 in. water reverse-gas pressure drop. The abscissa corresponding to each anti-collapse ring in Figure 4 is the height of that ring measured from the top of the thimble. The deflection profile shows that the largest deflection occurs at that segment whose length is abruptly larger than the segment immediately below it. The maximum axial velocity also occurs at the same location. Profiles such as shown in Figure 4 may be used to characterize a given ring placement scheme and bag suspension system under a given set of assumed reverse-gas operating conditions.

SPRING TENSION AND MAXIMUM AXIAL VELOCITY DURING REVERSE-GAS FLOW

Figures 5, 6, 7, and 8 summarizes the results from the calculations for the following values of the dust weight, w_D (in lb_f), and reverse-gas pressure drop, ΔP (in in. water): Case 1 - $w_D=50$, $\Delta P=1$ (Figure 5); Case 2 - $w_D=50$, $\Delta P=2$ (Figure 6); Case 3 - $w_D=100$, $\Delta P=2$ (Figure 7); and Case 4 - $w_D=100$, $\Delta P=2$ (Figure 8). The spring tensions and the maximum axial velocities within the bag are plotted as a function of the maximum allowance for spring compression during reverse-air, y_{sra}. It should be noted that the length of a spring is varied according to the allowed y_{sra} and pre-tension. All springs in this study were assumed constructed from the same wire material. Two generalizations regarding these characteristic curves are noteworthy:

(1) For a given dust weight, reverse-air pressure drop, and pre-tension, the spring tension vs. y_{sra} curve is independent of spring constant for the case when the spring is in its fully compressed state during reverse-gas flow. However, for each spring constant, there is a minimum tension below which the spring cannot be maintained at full compression. Naturally, this minimum tension corresponds to a maximum allowed y_{sra} above which the spring will not compress fully.

(2) For a given dust weight, reverse-air pressure drop, spring constant, and pre-tension, the spring tension is independent of y_{sra} (or spring length) for the case when the spring is always not fully compressed. When the spring is not fully compressed, the spring tension is constant with respect to y_{sra} (or total spring length).

The sets of curves given in Figures 5 to 8 indicate the variation of the maximum allowed y_{sra} for a given set of bag and spring parameters. The companion curves of axial velocity vs. y_{sra} also follow similar trends as the spring tensions. The velocity curves are useful to assess the potential for abrasion during reverse air. A GEESI maximum axial velocity standard of 1000 ft/sec guide spring and ring placements designs. Tests have shown increased susceptibility to abrasion at axial velocities exceeding 1000 ft/min. The 1000 ft/min limit is easily satisfied at low bag weights and reverse air pressure drops, but become progressively more difficult to achieve with increasing bag weight and reverse-air pressure drops, when the spring is not in its fully compressed state. This is the reason for GEESI spring design which allows fully compressed spring operation during reverse-gas. Increasing reverse-gas pressure drop and dust weight increase the bag tension required to maintain the 1000 ft/min maximum axial velocity. Fully compressed operation of the spring during reverse-air allow these high tensions to be reached.

The increase in spring tension from increasing the reverse-gas pressure drop by 1 in. water at constant dust weight is roughly 3 times the increase obtained by increasing the dust weight by 50 lb_f at constant pressure drop. Increasing both the dust weight by 50 lb_f and reverse-air pressure drop by

1 in. water results in a four-fold increase in spring tension as compared with the increase obtained by changing only the dust weight by 50 lb_f. The axial velocities also show proportionate increases.

TIME VARIATION OF SPRING TENSION DURING REVERSE-GAS (R/A) FLOW

Figure 9 shows the measured time-variation of the spring tension in a utility reverse-air baghouse (4). For this baghouse, the tension during R/A is observed to peak at about 2 seconds following the opening of the R/A damper. Figure 10 shows the predicted time-variation of the spring tension during the fall of a 50 lb_f dust plug for an assumed coefficient of specific resistance, K_2, of 1.34E-4 in.water/[ft/min]/[lb_f/ft^2]. Figure 10 was generated by first calculating the reverse-gas pressure drop for each instant of time using Equation (21). The catenary analysis discussed earlier was then used to translate this pressure drop to a spring tension (see Figure 11). The assumed K_2 value is of the same order of magnitude as calculated on the basis of the Carman-Kozeny model (3), assuming uniform distribution of dust within the plug. In contrast, filter cake K_2 values are in the range 20-50 in the same units. The higher gas velocities, and longer plug length are seen to manifest the small K_2 value for the plug as a measurable pressure--drop. The predicted time dependence of the spring tension during reverse-gas flow also shows the maximum observed from measurements (see Figure 9). The value of the effective acceleration due to gravity, g', was adjusted (6 ft/sec^2) to yield a theoretical maximum occurring at about the same time instant as that measured. The model despite its simple assumptions appears to indicate the physical origin of the maximum in the reverse-air pressure drop, and hence of the spring tension. The predictions of this model may be used to allow for the effects of the time-varying spring tension occurring during reverse-gas flow, in the catenary analysis of a bag suspension system.

CONCLUSION

The method of calculating the bag deflections and axial velocities during reverse-gas presented here is useful in designing springs and anti-collapse ring placements for a given set of expected reverse-gas conditions. The need for designing the spring for complete collapse during reverse-gas flow is explained. The spring constant is not a primary variable which determines bag tension during reverse-air for fully compressed operation of the spring, but enters indirectly through the spring length. The predictions of the model presented here coupled with spring cost analysis will provide narrower choices for spring selection. Also highly accurate pre-tensioning of the bag does not appear necessary since the spring tension during reverse-gas flow is far larger than the pre-tension. A simple model is presented which explains the influence of the falling dust at reverse-gas inception, on the reverse-gas pressure drop, and consequently on the spring tension. This model may be used in conjunction with the catenary model to factor into spring and ring-placement designs, the time-varying spring-tension increase occurring during reverse-gas flow.

REFERENCES

1. J. G. Musgrove, "Optimizing the Location of Anti-Collapse Rings in Fabric Filter." In Proceedings: Fourth Symposium on the Transfer and Utilization of Particulate Transfer Technology, Volume I, EPA-600/9-84-025a, November 1984.

2. R. Sholvey, "Measurement of the Elastic Modulus of Fabric Filter Bag Material", General Electric Turbine Technology Laboratory Report, (1985).

3. E. A. Samuel, "The Temporal Variation of Pressure Drop Across A Fabric Filter During Cake Initiation". In Proceedings: Fourth Symposium on the Transfer and Utilization of Particulate Transfer Technology, Volume I, EPA-600/9-84-025a, November 1984.

4. M. Walsh, "Spring /Bag Tension Testing at Public Service of Colorado Cherokee Station Units #2 and #3". General Electric Environmental Services, Inc. Report, (1981).

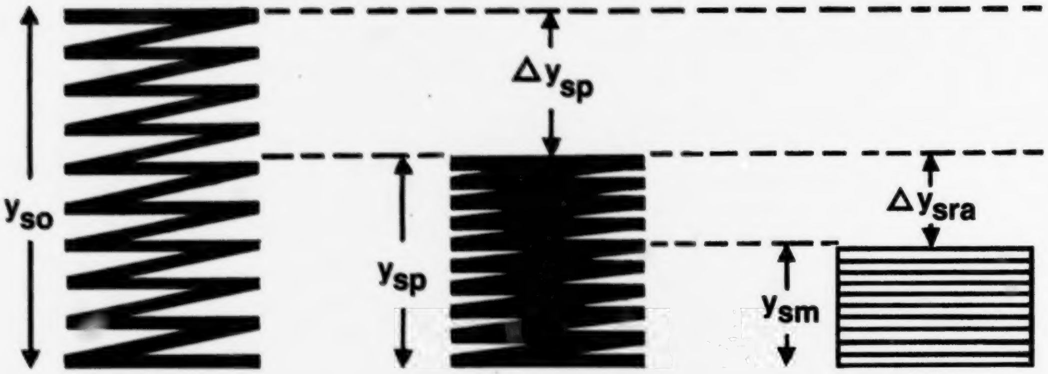

Figure 1. States of compression of a bag suspension spring.

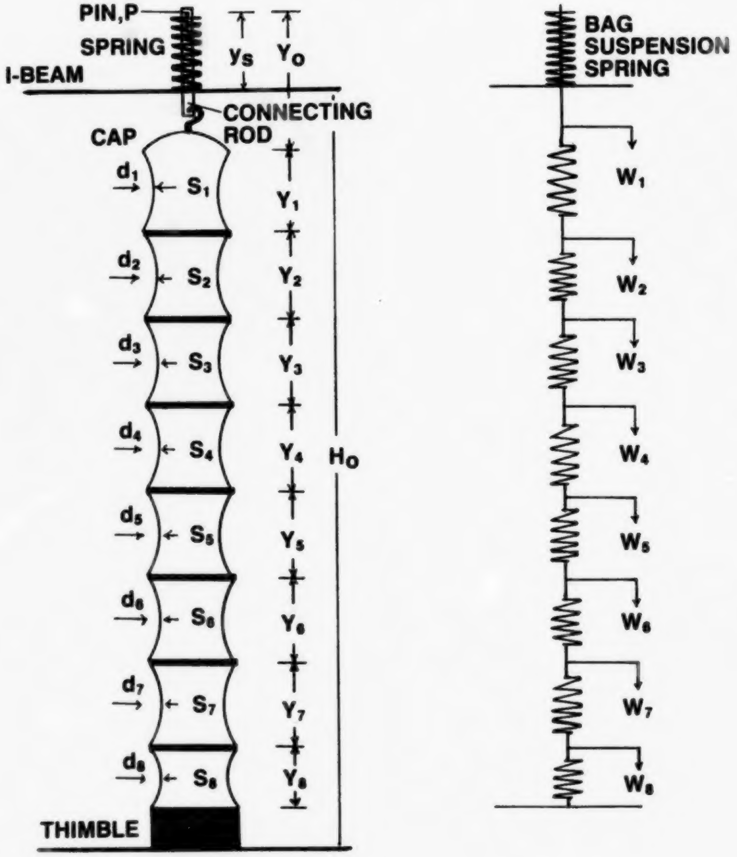
PIN,P
SPRING
I-BEAM
y_s
Y_o
CONNECTING ROD
CAP
d_1
S_1
d_2
S_2
d_3
S_3
d_4
S_4
d_5
S_5
d_6
S_6
d_7
S_7
d_8
S_8
Y_1
Y_2
Y_3
Y_4
Y_5
Y_6
Y_7
Y_8
H_o
THIMBLE
BAG SUSPENSION SPRING
W_1
W_2
W_3
W_4
W_5
W_6
W_7
W_8

Figure 2. (a) Schematic of a typical bag suspension system for a utility reverse-gas baghouse, and (b) representation of this suspension system in terms of equivalent springs.

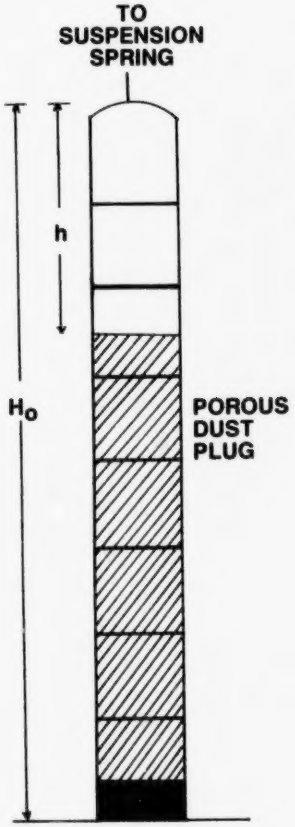
TO SUSPENSION SPRING
h
H_o
POROUS DUST PLUG

Figure 3. Schematic of porous dust plug, which leads to the the time-dependent spring tension during reverse-gas flow.

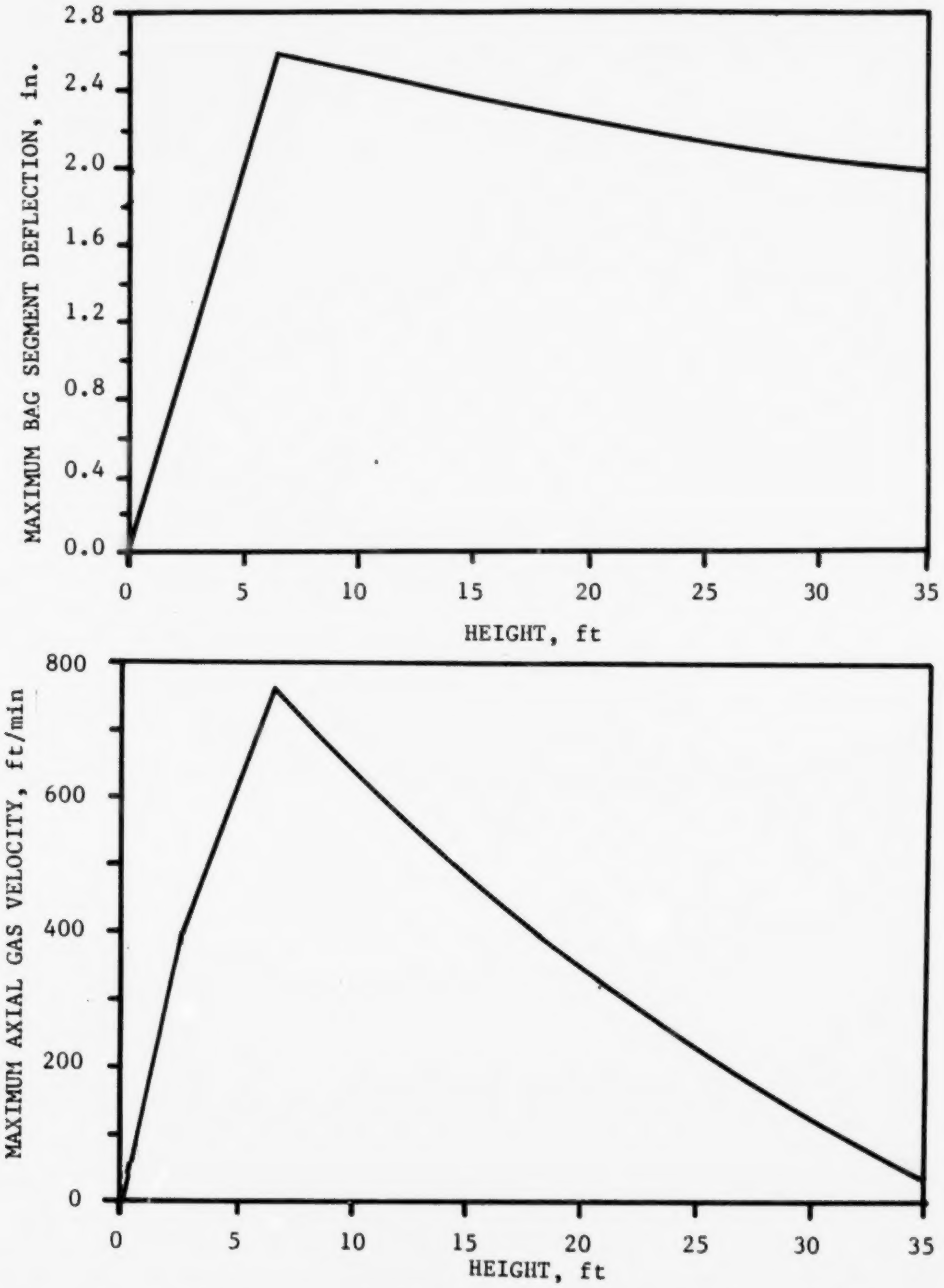

Figure 4. (a) Maximum deflection, and (b) maximum axial velocity profiles across reverse-gas bag predicted by catenary model for a 50 lb_f dust weight, 1 in. water reverse-gas pressure drop, and 'equal' ring spacing.

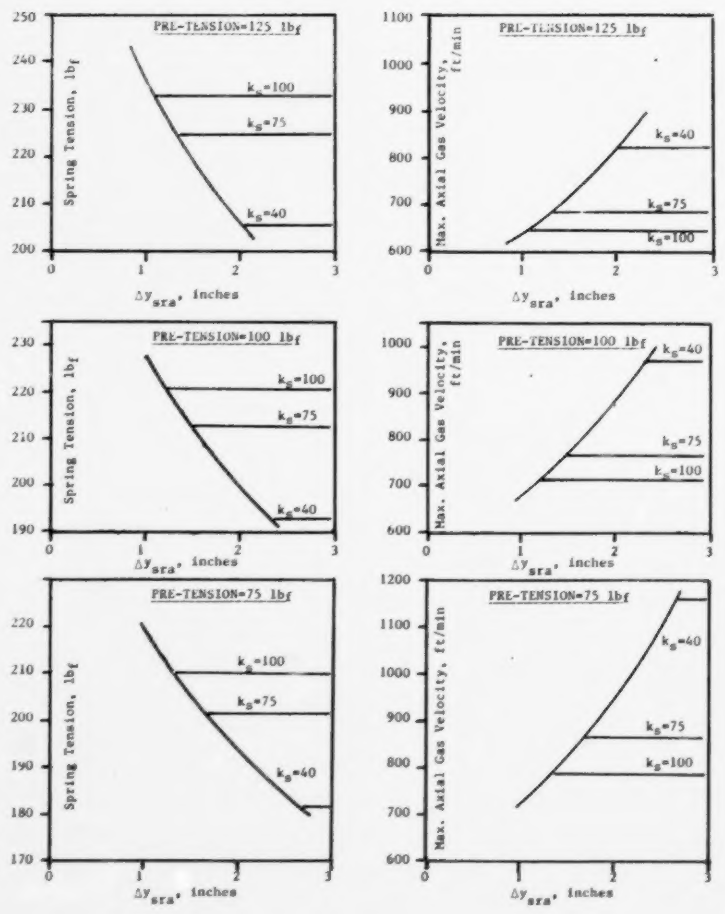

Figure 5. Catenary model prediction for spring tension and maximum axial velocity for 50 lb_f dust weight and 1 in. water reverse-gas pressure drop.

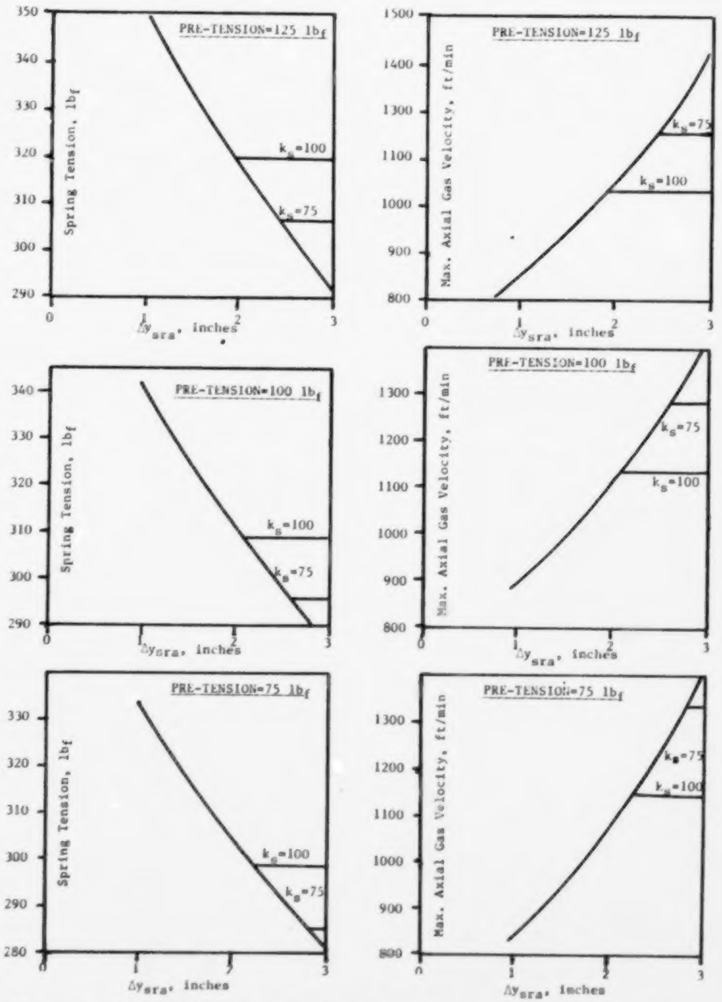

Figure 6. Catenary model prediction for spring tension and maximum axial velocity for 50 lb_f dust weight and 2 in. water reverse-gas pressure drop.

Reproduced from
best available copy.

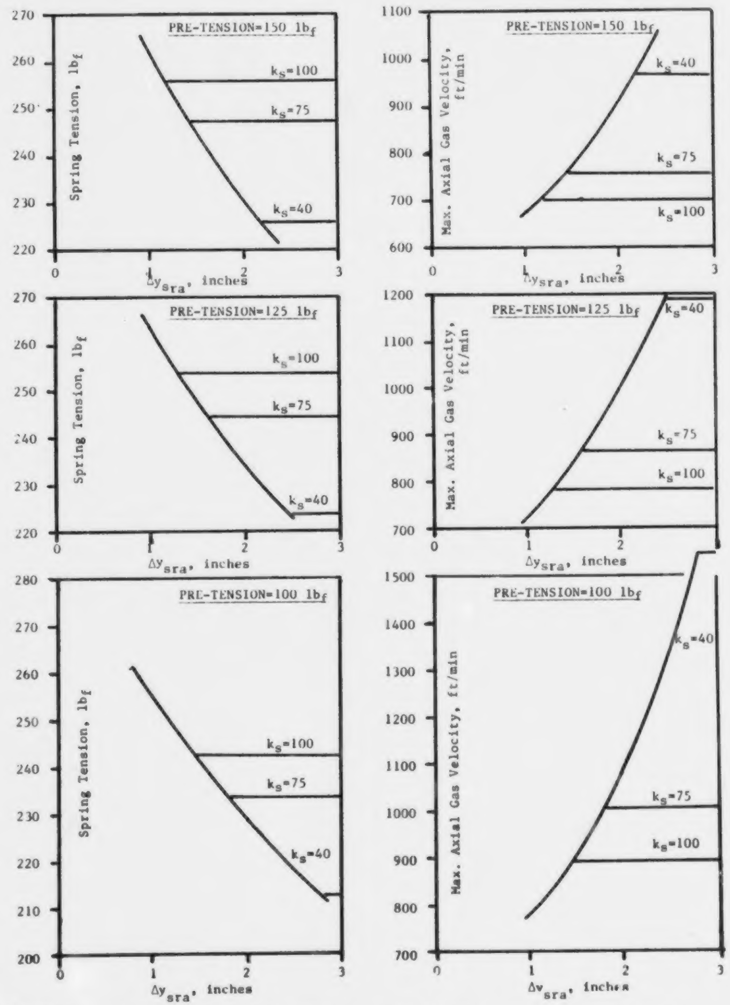

Figure 7. Catenary model prediction for spring tension and maximum axial velocity for 100 lb_f dust weight and 1 in. water reverse-gas pressure drop.

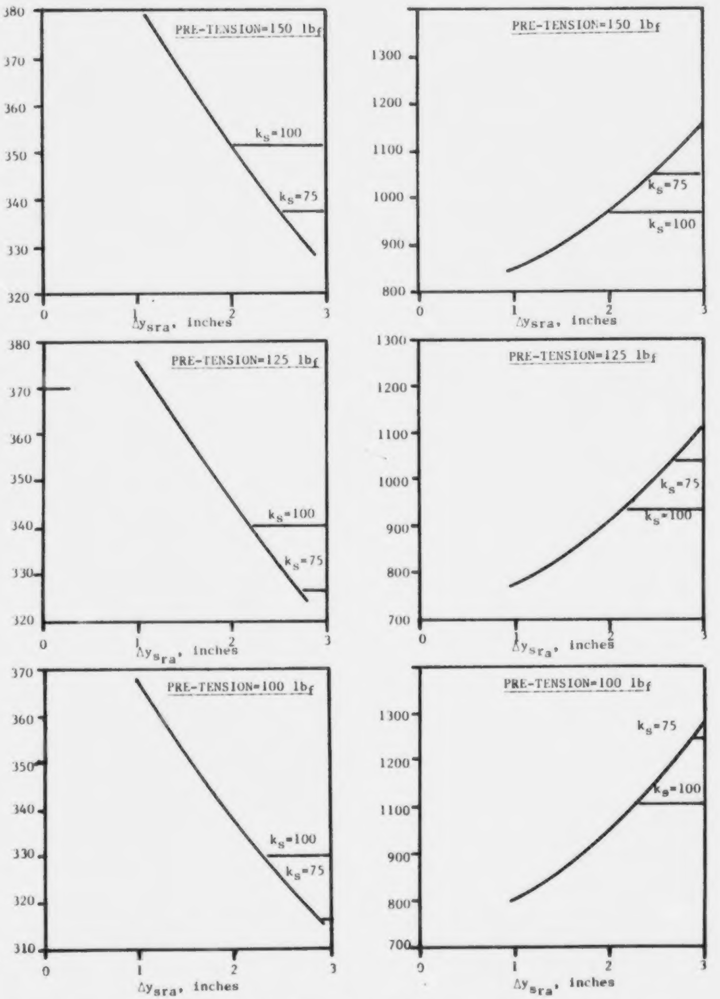

Figure 8. Catenary model prediction for spring tension and maximum axial velocity for 100 lb_f dust weight and 2 in. water reverse-gas pressure drop.

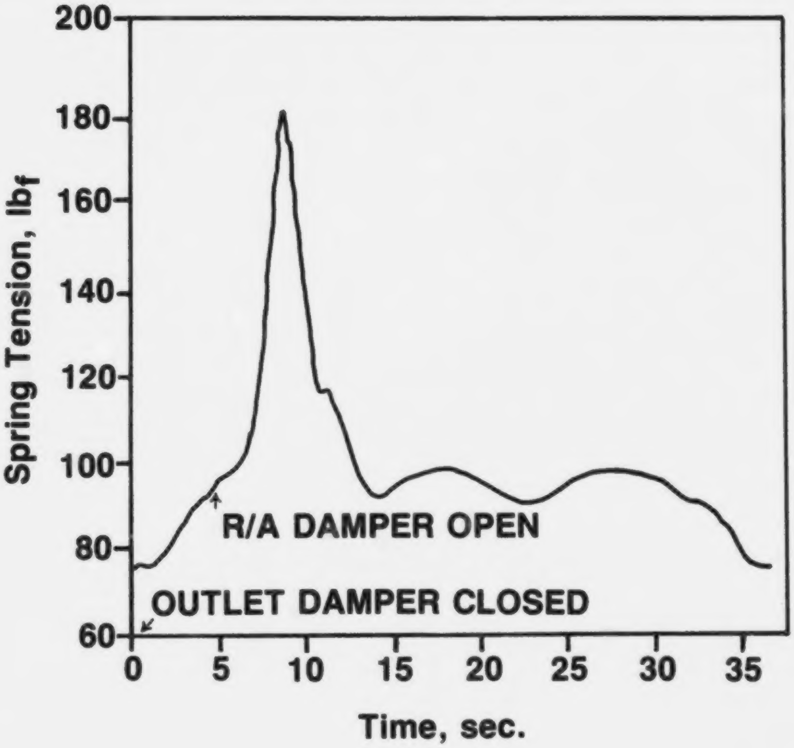

Figure 9. Time variation of the spring tension measured in a utility baghouse (taken from Reference 4).

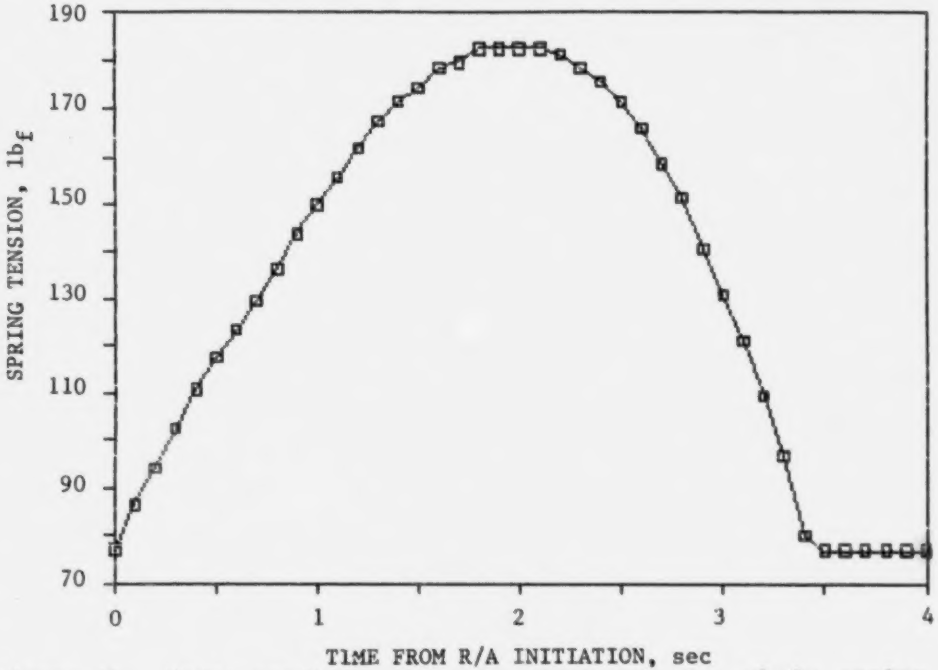

Figure 10. Model prediction for the time-variation of the spring tension during the fall of a 50 lb_f porous plug.

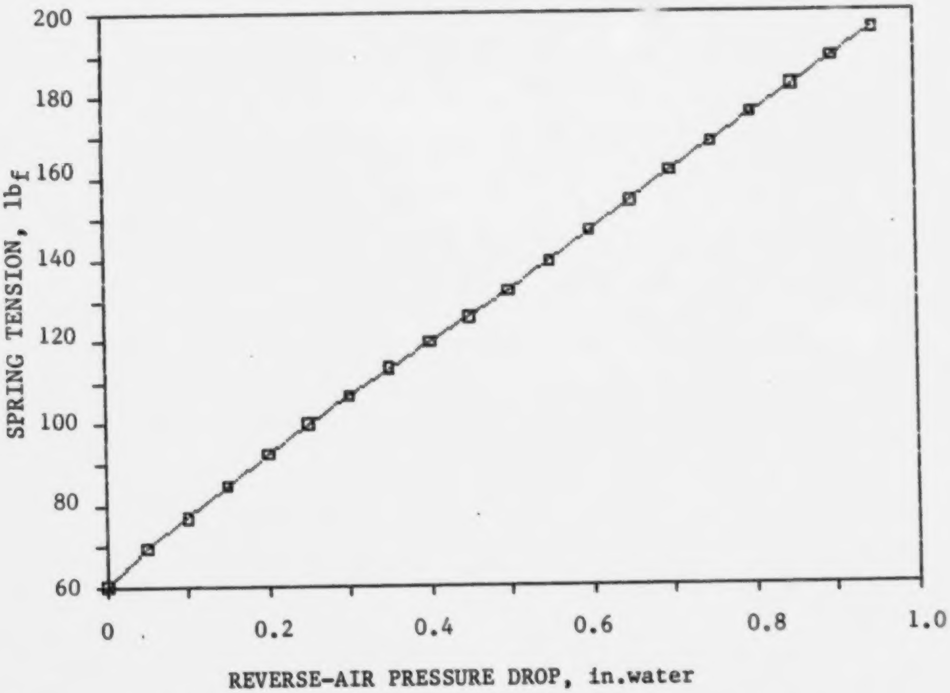

Figure 11. Catenary relationship between spring tension and reverse-gas pressure drop.

AEROSOL DEPOSITION IN FABRIC FILTERS

by: D. S. Ensor, T. Yamamoto, and A. S. Viner
Research Triangle Institute
Research Triangle Park, NC

ABSTRACT

The deposition of particles on fabric filters will determine the pressure drop and collection efficiency of the filter cake and supporting fabric. The morphology of the deposit has been difficult to characterize because of its irregularity. Deposition mechanisms and the resulting theoretical structures have been analyzed using fractal geometry. Potential applications to filtration technology will be discussed.

I. Introduction

The performance of a fabric filter depends greatly on the morphology of the filter cake on the surface of the bags. The complexity of the particle deposits' morphologies was shown in cross-sectional photographs reported by Carr and Smith (1984). They reported that the configuration of the deposit was determined by the adhesion and cohesion of the material. In Carr's research, the particle deposits also were shown to have fissures or cracks. This, in effect, complicates the behavior of the filtration process.

The research reported in this paper is related to the development of a filtration model. Properties such as adhesion of the particles and electrostatic effects must be quantified in order to understand the phenomena and then incorporate them into the design of a baghouse. An additional purpose of a theoretical approach is to evaluate the fundamental mechanisms which, in turn, should lead to ideas for appropriate measurements of the ash and fabric.

II. Baghouse Model

The modern approach to fabric filtration was originated by Stephan et al. (1960) with their hypothesis of parallel resistance. An electrical analogy, Ohm's Law, was invoked to explain the pressure drop through the fabric and the layer of ash. The pressure drop is described by:

$$\Delta P / V = K_2 W + K_1 \qquad (1)$$

where

ΔP is the pressure drop through the filter
V is the face velocity
K_2 is the specific resistance
W is the aeral mass density
K_1 is the residual drag

The first comprehensive effort sponsored by the EPA to develop a baghouse design model was reported by Dennis et al. (1977). During laboratory filtration experiments, they discovered patchy filter deposits after cleaning. With a data base developed largely from laboratory testing, an empirical approach was developed to predict both the pressure drop and the particle penetration. In evaluating this EPA model, Viner et al. (1984) concluded that more detailed information on the properties of the filter cake was required. Recently, Viner et al. (1985) reported a new mathematical model which used simultaneous differential equations to solve the gas flow through the filter cake (assuming a constant specific resistance with a spatial mass frequency distribution oscillating between pre-clean and post-clean conditions).

One important element in the operation of baghouses and, hence, in the modeling of baghouses is electrostatic effects. Electrostatic effects can influence the deposition of particles in two ways: by changing either the spatial mass distribution or the morphology of the deposit. (It is possible for both changes to occur.) Modifications in the spatial mass distribution are described by Yamamoto et al. (1986) and VanOsdell et al. (1986). Both groups performed research to explain the performance of axial high-voltage discharge wires in the center of bags (advanced electrostatic stimulated filtration). Changes in morphology prove more subtle as described by VanOsdell et al. (1986), Mori et al. (1982), and Petroll et al. (1985).

Felix et al. (1983) suggested that adhesion affected pressure drop and particle penetration (in a full-scale baghouse controlling flyash from lignitic coal).

Ensor et al. (1986) reported on research with Monte Carlo deposition models which simulate the formation of particle deposits. This research implied the importance of both adhesion and electrostatic effects. This approach will be developed and elaborated upon in this paper.

III. Pressure Drop Through Porous Media

The pressure drop across flyash particle deposits has eluded satisfactory description for a variety of reasons:

1. The particle deposits do not form a simple packed bed. They rest instead on a fabric.

2. Usually the particle size distribution is not known with sufficient accuracy.

3. The deposit may exhibit structure or organized features, thereby contradicting the assumption of a random medium. This assumption is inherent in most theories concerning porous media.

4. A limitation in measurements develops when small areas of the filter are characterized. Measuring properties such as porosity, permeability, particle size distribution, and mass in small areas is difficult. Also, the question of how to organize the data and then incorporate it into a design model has not been answered.

The underlying issue in the microphysics is the ordering of the particles. It is not known if the particles are deposited randomly. In order to discover some way of incorporating the notion of structure into the model's treatment of porous media, one should begin with a review of current approaches to determining pressure drop through a porous medium. A description of K_2 in Equation (1) also should be given.

The fundamental relationship for pressure drop through a porous medium was determined empirically by Darcy in the 19th century (see Scheidegger, 1974). This was expressed as:

$$dP/dx = \beta/\mu \; Q \qquad (2)$$

where

dP/dx is the pressure gradient through the medium
β is the Darcy permeability
μ is the viscosity
Q is the volumetric flow per unit area

In the past, much of the research on porous media has focused on developing methods for predicting beta. Two distinctly different models (applicable over different ranges of bed porosity) have been developed. Although the equations for these models will not be derived in detail here, the assumptions and results will be reviewed.

The Kozeny Theory

Kozeny first reported this equation where the porous media are assumed to consist of parallel capillarity channels. These channels consist of various cross sections of definite length. The Navier-Stokes equations are solved simultaneously for all channels which pass through a cross section of the flow. The hydraulic radius concept describes the characteristic dimension of the channels. The hydraulic radius is the result of dividing the void volume in the media by the surface area in contact with the fluid. After solving the Navier-Stokes equation in cylindrical coordinates, empirical arguments are made about the dimensionality of the solution to achieve a closed solution.

The resulting equation is:

$$\Delta P/Q = \frac{L \mu C}{H^2 \epsilon} \tag{3}$$

where

L is the thickness of the deposit
C is the Kozeny constant, dependent on the geometry of the pores
H is the hydraulic radius (pore volume/pore area)
ϵ is the void fraction

The assumptions in the application of the Kozeny equation suggest the following restrictions: no blind pores, no tangential component of fluid velocity from expansions and contractions, and the presence of a laminar flow. Carman's (1956) contribution consisted of describing the void volume in terms of the volume of the bed. In typical applications, the hydraulic radius is simplified by assuming that the particles are spherical. Although very irregular particle shapes occur occasionally, in these cases it is recommended that the hydraulic radius be used directly.

The Free Surface Model

The free surface, or cell, model is described in detail by Happel and Brenner (1973). This model assumes that a sphere resides in the center of a spherical cell. By applying this approach, Darcy's Law can be derived from the fundamentals without empirically determined coefficients. The pressure drop across the unit cell is given by:

$$\Delta P/L = \frac{4 \Pi \mu d}{4/3 \Pi b^3} \qquad (4)$$

(force on the particle/volume of the particle)

where

d is the diameter of a spherical particle
b is the cell diameter

The assumptions include Stokes' or creeping flow, the disappearance of normal and tangential stress at the boundary, and independent cells. The Navier-Stokes equations are solved with appropriate boundary conditions for the cell.

Filtration Equations

The thickness of the deposit on the filter is computed from the mass per unit area of filter and is given by:

$$L = \frac{W}{\rho_p (1 - \epsilon)} \qquad (5)$$

where

W is the areal mass
ρ_p is the particle density

Equation (6) is combined with Equations (3) and (5) with an assumption of spherical particles for hydraulic radius (for details, see Donovan, 1985) to derive the familiar relationship:

$$K_2 = \frac{18 \mu R}{\rho_p d^2} \qquad (6)$$

The parameter R from the Kozeny-Carman theory is given by:

$$R = 2 C (1-\epsilon)/\epsilon^3 \qquad (7)$$

where

C is the Kozeny-Carman constant dependent on the shape of the pores

d is the characteristic length or particle diameter

The parameter R from the free surface theory is given by:

$$R = \frac{3 + 2\,(1-\epsilon)^{5/3}}{3 - 4.5(1-\epsilon)^{1/3} + 4.5(1-\epsilon)^{5/3} - 3(1-\epsilon)^{2}} \qquad (8)$$

The only difference between Equations (7) and (8) is the correction factor R. Also, the free surface equation has no empirical coefficients. Rudnick (1978) compared the two expressions with experimental data and recommended using the free surface expression instead of the Kozeny-Carman equation. Since the Kozeny-Carman equation, which has a limit of 1 for porosity, goes to 0 (instead of the expected limit of 1), it is limited to porosities with values of less than 0.7.

Application to Filtration

A basic assumption of both derivations is the lack of structure in the media. The Kozeny expression addresses the question of structure with a variety of approaches. One of these approaches consists of determining and then applying the hydraulic radius directly. Another approach centers on the use of the tortuosity to correct the results. Tortuosity is the ratio of the physical length of the pores to an apparent length and is used widely in the study of porous media. Another approach, proposed by Happel and Brenner (1973) entails modifying the exponent in the terms in R to match experimental data.

Electrostatic augmentation of fabric filtration can be explained by introducing the concepts of structure and modification of porosity of the particle deposit. Both photographs and observations of charged particles which were collected on filters present a visible roughening of the surface of the deposit (Mori et al., 1982).

IV. Fractal Geometry

As discussed earlier, visual evidence suggests a need for introducing the concept of structure of the filter cake into the filtration equations to obtain a realistic description of flyash filtration. Fractal geometry, developed by Mandelbrot (1982) to study irregular structures, may provide a way of introducing this concept. Mandelbrot coined the term "fractal" from the Latin past participle "fractus" which means "broken." A detailed description of fractal geometry is beyond the scope of this brief report, and interested readers should read Mandelbrot's book. As mentioned earlier, the focus of this paper is the possible application of fractal geometry to solving certain problems in fabric filtration.

An important property of fractal geometry is self-similarity. As the image of a structure is magnified, its features appear to be the same. Related to this is an important concept -- the fractal dimension. The fractal dimension is the measurement of the space-filling properties of structure. For example, a straight line has a dimension of 1, and a square has a dimension of 2. An object with an irregular shape can have a fractal dimension of some value between 1 and 2 (depending on how the space is filled). One can determine the fractal dimension of an object's perimeter or boundary with the Richardson plot. In this plot, the logarithm of the length of measurement, the stride length, is plotted against the measured perimeter. An easy way of visualizing this is to use a pair of dividers to "step around" the photographed image of an object. The absolute value of the slope added to 1 is the fractal dimension of the object's perimeter. This approach has been used extensively for particles. It is only one of several different ways, however, of measuring an object's fractal dimension. Rules for improving the reliability of these measurements were reported by Kaye (1984).

These concepts in fractal geometry have been applied to particle systems by several investigators. Kaye (1984) has demonstrated that the shape of a particle can be characterized by calculating its fractal dimension. Pfeifer and Avnir (1983) have shown that the specific surface area of particles, as determined by adsorption isotherms, is fractal. In an application to porous media, Pape et al. (1984) used the fractal properties of the specific surface area and tortuosity to develop equations relating permeability to the fundamental properties of sandstone.

The Richardson plot also provides information on an object's fractal dimension and scale length. This sort of information can provide a useful insight into its morphology. Kaye (1984) observed that aggregates of particles had a fractal dimension at long stride lengths which were characteristic of the structure. He also observed another value at small stride lengths which were characteristic of the texture of the particles. Ensor and Mullins (1985) reported that particle dendrites captured on a fiber had different fractal dimensions for long stride lengths (fiber), moderate stride lengths (structure), and short stride lengths (particle surface). Computer simulations by Meakin (1983) and Houi and Lenormand (1984) indicated that the fractal dimension of a deposit may depend on both the sticking probability and the mechanism of deposition. For example, a deposit resulting from diffusional trajectories will have a different morphology than that resulting from ballistic impaction.

One method of applying fractal geometry would consist of invoking the relationships between the volume, area, and perimeter. The equations, as suggested by Mandelbrot (1982; pages 106 through 130), are:

$$V^{1/3} = K' \; A^{1/D} \tag{9}$$

$$P^{1/D} = K'' \; A^{1/2} \tag{10}$$

where

V is the volume
K', K" are arbitrary constants
A is the area
D is the fractal dimension
P is the perimeter

According to Equation (9), a Euclidian structure in three dimensions with a smooth surface would yield a value of 2 for the fractal dimension (D). However, if the surface were extremely rough, the fractal dimension would have a value of greater than 2 (with a limit of 3). A similar statement can be made about Equation (10). A Euclidian surface would yield a fractal dimension of 1. Irregular surfaces, however, would have fractal dimensions greater than 1 (with a limit of 2).

If we use Equations (9,10) in the filtration Equation (6), the following equations can be developed:

$$K_2 = \frac{18\,\mu\,R}{\rho_p\, d^{4/D}} \qquad \text{(3 dimensional)} \tag{11}$$

$$K_2 = \frac{18\,\mu\,R}{\rho_p\, d^{2/D}} \qquad \text{(2 dimensional)} \tag{12}$$

Any geometric factors would be included in the R. A strong argument can be made for substituting non-Euclidian geometry in these equations because the fractal property is compatible with the assumptions found in the pressure drop models. The Karman equation uses the hydraulic radius concept which is very consistent with fractal geometry and was used with good success in porous media research with sandstone by Pape et al. (1984). Also, Mandelbrot et al. (1984) observed that fissures and cracks in material are fractal.

In the case of the free surface model, it has been shown that agglomerated particles are fractal (Weitz et al., 1985, Kaye, 1984). In this case, one can think of the particle in the cell as an irregular lump with fluid flowing around the obstruction. If the cell were sufficiently larger than the particle, including the drag/mass ratio with a fractal exponent would seem to be a minor modification of the equation. The assumptions of creeping flow and zero velocity (at the surface of the fractal) appear reasonable.

V. Modeling Cases

Model Implementation

The application of Monte Carlo packing models to fabric filtration was first described by Ensor et al. (1986). The boundary conditions in the simulation assumed that the bottom boundary is porous to the gas flow yet traps the particles. Another assumption is that the top boundary is the source of randomly started particles. The dropping particles are carried to the bottom of the screen where they interact with previously deposited particles (in a manner consistent with a set of rules). These rules are summarized in Table 1. The resulting deposit morphologies appear in Figures 1 through 4.

Analysis

The simulated deposits were evaluated with two techniques: perimeter-area plots and Richardson plots. The fractal dimension of the array of particles was computed with the perimeter-area relationship for an array of squares:

$$D = \log(P/4)/\log(\sqrt{A}) \tag{13}$$

where

D is the fractal dimension
P is the perimeter
A is the area

TABLE 1. SIMULATION RULES

Figure	Physical situation	Sticking	Attraction	Logic guiding dropping particle
1	Nonsticky particles	0	0	· If a stationary particle is not present at next lower position, advance dropping particle. · If a stationary particle is present at both sides of next lower position, stop dropping particle.
2	Sticky particles	1	0	· If a stationary particle is not present at next lower position, advance dropping particle. · If a stationary particle is present at either or both sides of next lower position, stop dropping particle.
3	Nonsticky particles with attraction	0	1	· If a stationary particle is not present at next lower position, advance dropping particle. · If a stationary particle is present two units at either side of next lower position, move dropping particle one unit toward stationary particle. · If a stationary particle is present at both sides of next lower position, stop dropping particle.
4	Sticky particles with attraction	1	1	· If a stationary particle is not present at next lower position, advance dropping particle. · If a stationary particle is present two units at either side of next lower position, move dropping particle one unit toward stationary particle. · If a stationary particle is present at either or both sides of next lower position, stop dropping particle.

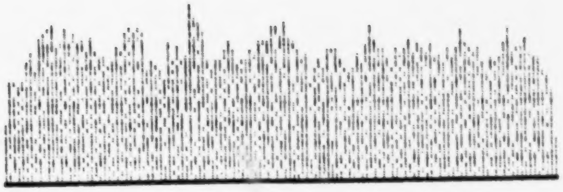

Figure 1. Computer simulation of non-sticking particles with no electrostatic attraction.

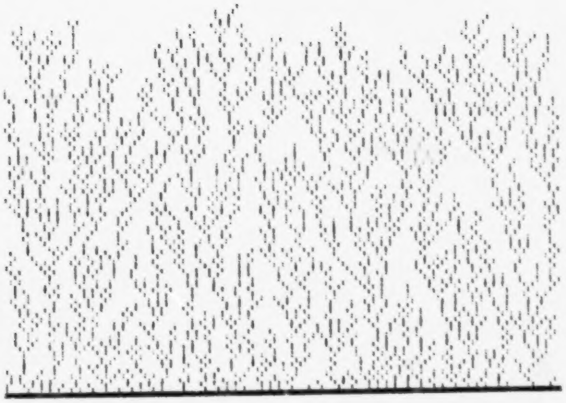

Figure 2. Computer simulation of sticky particles with no electrostatic attraction.

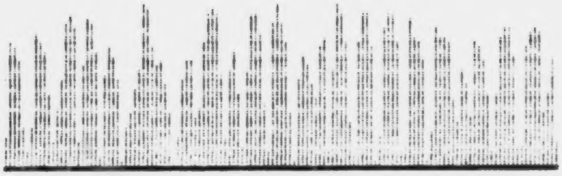

Figure 3. Computer simulation of non-sticky particles with electrostatic attraction.

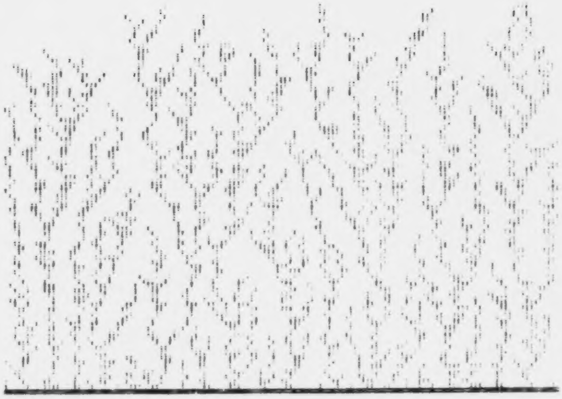

Figure 4. Computer simulation of sticky particles with electrostatic attraction.

The results for the perimeter-area plots for both the structures and voids appear in Figures 5 and 6. The fractal dimension computed from equation (13) is also reported. The packing rules strongly influenced the morphology of both the deposit and its associated fractal dimensions. Of particular interest are the similarities of the perimeter-area plots of the void structure.

A Richardson plot of the modeled cases (Figure 7) contains the long stride/length results. These results illustrate the distribution of the variation in the thickness of the deposit. As the length is reduced, the pores or void structure become significant and have a much larger fractal dimension than the surface. The absence of change in the slope (for the non-sticky case) indicated that the stride length was not short enough to probe the pores.

"Pseudo" K_2 Calculation

As an example, Equation (12) was used to compute a value of K_2 to demonstrate the relative effects of void reaction and fractal dimension. Table 2 illustrates that the void fraction is often more significant than the fractal dimension over the wide range observed in the simulation. For comparison's sake, flyash deposits typically have a porosity of 0.6. In real situations, the morphology of the deposit as characterized by the fractal dimension may be significant because the void fraction may have little variability. Also the surface structure of the filter will be exposed immediately following the cleaning processes.

Comparisons of Fractal Dimensions

It is possible that the fractal dimensions of different real systems tend to be nearly the same. The deposit cross section reported by Carr and Smith (1984) was analyzed with a Richardson plot (Figure 8). The fractal dimension was 1.23, a value very close to the simulation values for long stride lengths. This result increases both the credibility of the simulation and the enthusiasm for applying fractal geometry to fabric filtration.

Another useful comparison is found in Table 3 where typical fractal dimensions for two dimensional cases are compared. The most striking characteristic of this comparison lies in the similarity of the values for the dust cake, particle deposits, and fissures. One simplified conclusion drawn from this application would be that the deposition of particles has constant fractal dimensions under limiting conditions.

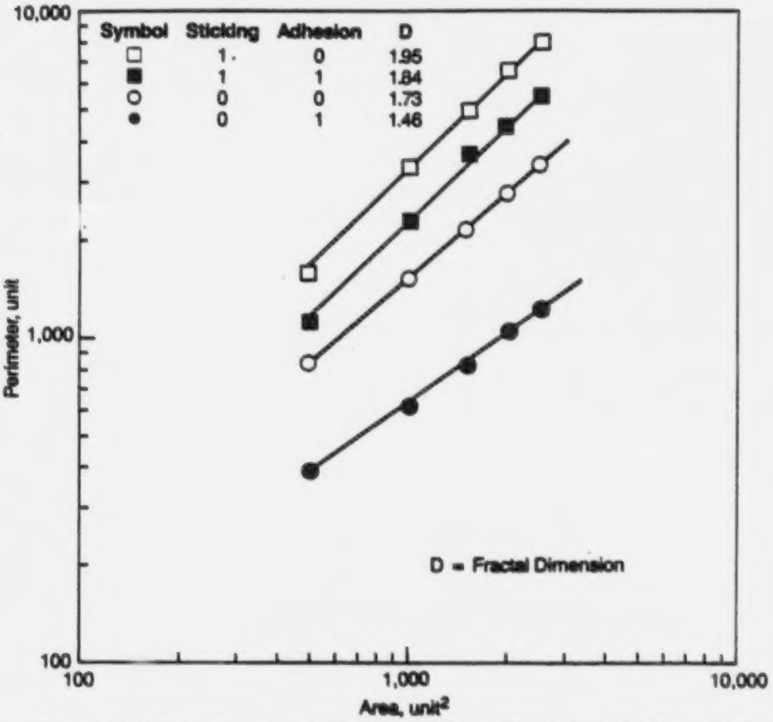

Figure 5. Area-perimeter relationship for simulated cake structure.

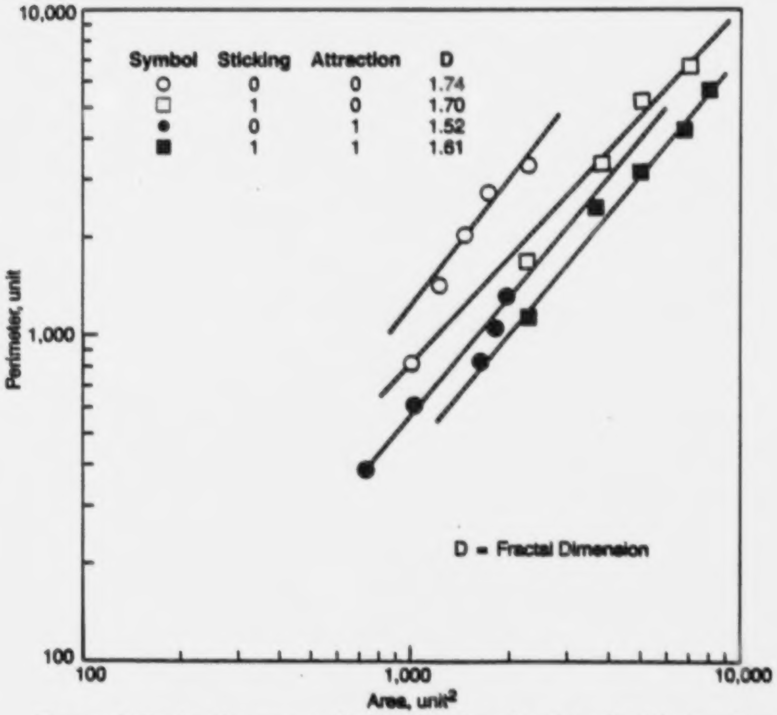

Figure 6. Perimeter-area relationship for simulated void structure.

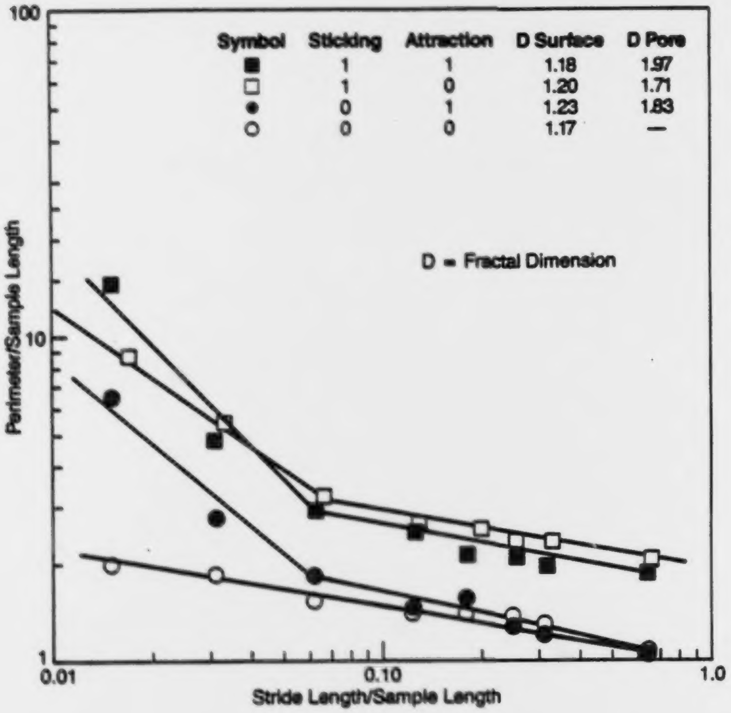

Figure 7. Richardson plot of filter packing simulations.

TABLE 2. SIMULATION CASES[a]

Attraction	Sticking probability	D structures	D voids	ϵ	Pseudo K_2 (D voids)	Pseudo K_2 (D=1)
0	1	1.95	1.70	0.75	3.6	0.53
0	0	1.73	1.78	0.35	102.6	13.6
1	1	1.85	1.61	0.75	3.1	0.5
1	0	1.46	1.52	0.50	17.4	3.6

[a] Equation (12) was used to compute a "pseudo K_2" using the fractal dimension computed from the voids in the structure (D voids) and with the fractal dimension set equal to 1 (D = 1, Euclidian geometry). The R from Kozeny theory was used, Equation (7), and particle density, ϱ_p, was assumed to be 2 g/cm^3, the gas viscosity, μ, was assumed to be 1 unit, and the particle diameter, d, was assumed to be 10 μm.

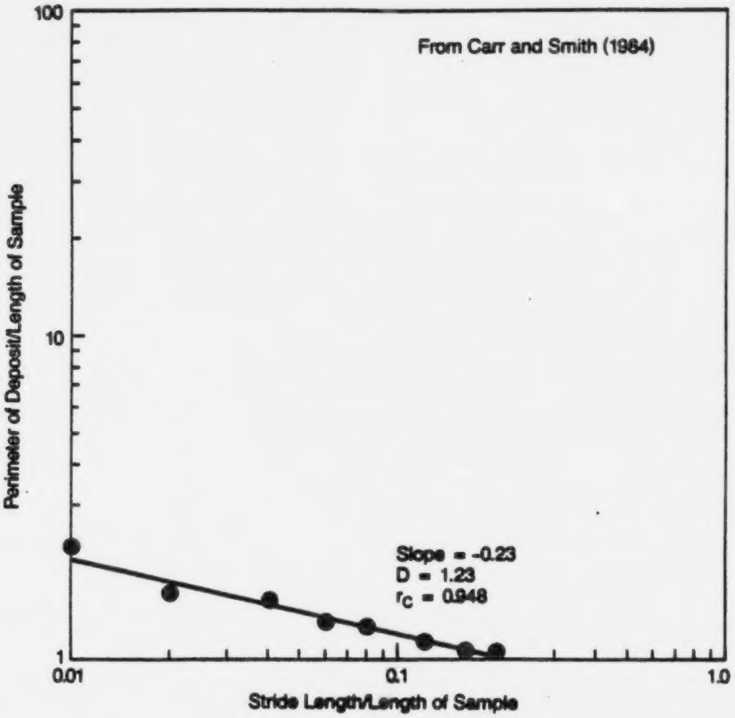

Figure 8. Richardson plot of dust cake.

TABLE 3. TYPICAL FRACTAL DIMENSIONS

System	Fractal dimension 2D	Measurement method	Investigator
Fractures in metals	1.1-1.4	Perimeter/area	Mandelbrot et al. (1984)
Dust cake surface	1.2	Richardson plot	This paper
Dendrites in fibrous filters	1.3	Richardson plot	Ensor and Mullins (1985)
Cracks in coatings	1.27	Computer simulation	Termonia and Meakin (1985)
Sputter deposited metal aggregates	1.88	Moment of inertia	Wolf et al. (1984)
Gold colloidal aggregates	1.75-2.0	Moment of inertia	Weitz et al. (1985)
Particle shape	1.02-1.1	Richardson plot	Kaye et al. (1985)
Particle deposition modeling			
Inertial deposition	1.23	Richardson plot	Houi and Lenormand (1984)
Diffusive deposition	1.68	Computer simulation	

VI. Summary and Conclusions

Fabric filtration design is limited by our fundamental understanding of the morphology of the filter cake. Equations which describe filtration depend on the distribution of mass on the filter (thickness) and the variation in K_2 (specific resistance). An initial attempt has been made to apply some of the concepts from fractal geometry in order to characterize the filter cake's morphology. Using relationships between the volume, area, and perimeter, modifications to the classical pressure drop equations were hypothesized.

With Monto Carlo simulations, several different rules have been applied to develop examples of both sticking and electrostatic effects. These cases were modeled with perimeter/area plots and Richardson plots. The fractal dimension was shown (with hypothetical calculations) to have an effect on pressure. The fractal dimensions of the model systems proved to be similar to the measured values of real systems.

The conclusions from this study are:

1. Baghouse performance depends on both macro- and micro-scale effects.
2. Fractal geometry may allow structure to be introduced into the process of predicting pressure drop and efficiency.
3. Particle deposition is a random process and may have constant fractal dimensions (as found in other fields).
4. New experimental techniques need to be developed to characterize the small-scale properties of dust cakes.

Acknowledgments

This research was conducted in part under United States Protection Agency Cooperative Agreements CR-810152 and CR-812281 with the Research Triangle Institute.

References

Carman, P. C. 1956. Flow of Gases Through Porous Media. New York: Academic Press.

Carr, R. C., and W. B. Smith. 1984. Fabric Filter Technology for Utility Coal-fired Power Plants. Part IV: Pilot-scale and Laboratory Studies of Fabric Filter Technology for Utility Applications. JAPCA 34:399-413.

Dennis, R. et al. 1977. Filtration Model for Coal Fly Ash with Glass Fabrics. EPA-600/7-77-084 (NTIS PB 276489), August.

Donovan, R. P. 1985. Fabric Filtration on Combustion Sources. New York: Marcel Dekker.

Ensor, D. S., and M. E. Mullins. 1985. The Fractal Nature of Dendrites Formed by the Collection of Particles on Fibers. Particle Characterization 2:77-78.

Ensor, D. S., D. W. VanOsdell, A. S. Viner, R. P. Donovan, and L. S. Hovis. 1986. "Modeling Baghouse Performance." In: Proceedings: Fifth Symposium on the Transfer and Utilization of Particulate Control Technology, Volume 3, EPA-600/9-86-008c (NTIS PB86-167178, February.

Felix, L. G., R. L. Merrit, and R. C. Carr. 1983. "Performance Evaluation of Several Full-scale Utility Baghouses." In the Proceedings of the Second Conference on Fabric Filtration Technology for Coal-fired Power Plants, November.

Happel, J., and H. Brenner. 1973. Low Reynolds Number Hydrodynamics. The Netherlands: Noordhoff Leyden Publishers.

Houi, D., and R. Lenormand. 1984. Particle Deposition on a Filter Medium. In Kinetics of Aggregation and Gelation. Edited by F. Family and D. P. Landau, 173-176. New York: Elsevier Science Publishers.

Kaye, B. H. 1984. Multifractal Description of a Rugged Fine Particle Profile. Particle Characterization 1:14-21.

Kaye, B. H., J. E. Leblanc, and P. Abbot. 1985. Fractal Description of the Structure of Fresh and Eroded Aluminum Shot Fine Particles. Particle Characterization 2:56-61.

Mandelbrot, B. B. 1982. The Fractal Geometry of Nature. New York: Freeman Press.

Mandelbrot, B. B., D. E. Passoja, and A. J. Paullay. Fractal character of fracture surfaces of metals. In the Proceedings of the Symposium of the Materials Research Society, November 26-27, 1984, Boston, MA.

Meakin, P. 1983. Diffusion Controlled Deposition on Fibers and Surfaces. Physical Review A27:2616-2623.

Mori, Y., T. Shiomi, N. Katada, H. Minamide, and K. Iinoya. 1982. Effects of Corona Precharger on Performance of Fabric Filter. J. Chem. Eng. of Japan 15:211-216.

Pape, H., L. Riepe, and J. R. Schopper. 1984. The Role of Fractal Quantities as Specific Surface and Tortuosities for Physical Properties of Porous Media. Particle Characterization 1:66-73.

Petroll, J., B. Rabel, and B. Schneider. 1985. Pre-charging and Electrostatic Agglomeration in Fabric Filtration. Filtration and Separation. September/October:298-300.

Pfeifer, P., and D. Avnir. 1983. Chemistry in noninteger dimensions between two and three: I. Fractal theory of heterogeneous surfaces. J. Chem. Phys. 79:3558-3565.

Rudnick, S. N. 1978. Fundamental Factors Governing Specific Resistance of Filter Dust Cakes. ScD Dissertation: Harvard School of Public Health, Boston, MA.

Scheidegger, A. E. 1974. The Physics of Flow Through Porous Media. Toronto: University of Toronto Press.

Stephan, D. G., G. W. Walsh, and R. A. Herrick. 1960. Concepts in Fabric Air Filtration. Amer. Ind. Hyg. Assn. J. 21:1-14.

Termonia, Y., and P. Meakin. The Formation of Fractal Cracks in a Kinetic Fracture Model. In the Proceedings of the Symposium of the Materials Research Society, December 2-4, 1985, Boston, MA.

VanOsdell, D. W., A. S. Viner, K. D. Carter, and L. S. Hovis. 1986. "Study of Electrostatically Stimulated Filtration Fundementals." To appear in the Sixth Symposium on the Transfer and Utilization of Particulate Control Technology. New Orleans, LA, February.

Viner, A. S., R. P. Donovan, D. S. Ensor, and L. S. Hovis. 1984. Comparison of Baghouse Test Results with the GCA/EPA Design Model. JAPCA 34:872-880.

Viner, A. S., R. P. Donovan, and D. S. Ensor, "A Mathematical Model of Baghouse Operation." In the Proceedings of the American Association for Aerosol Research Annual Meeting, Albuquerque, NM, November 1985.

Weitz, D. A., M. Y. Lin, J. S. Huang, S. K. Sinha, and P. Dimon. Fractals in Colloid Aggregration. In the Proceedings of the Symposium of the Materials Research Society, December 2-4, 1985, Boston, MA.

Wolf S. A., W. T. Elam, J. Sprague, D. V. Gubser, D. Van Vechten, and P. Meakin. Sputter Deposited Fractal Aggregates. In the Proceedings of the Symposium of the Materials Research Society, November 26-27, 1984, Boston, MA.

Yamamoto, T., D. S. Ensor, R. B. Mosley, L. S. Hovis, and N. Plaks. 1986. "Mathematical Model for Advanced Electrically Stimulated Fabric Filtration." To appear in the Proceedings of the Sixth Symposium on the Transfer and Utilization of Particulate Control Technology. New Orleans, LA, February 25-28.

Session B-4: FF: PILOT SCALE STUDIES

John S. Maulbetsch, Chairman
Electric Power Research Institute
Palo Alto, CA

PERFORMANCE OF A HIGH-SULFUR-COAL, PILOT-SCALE FABRIC FILTER

by: Robert F. Heaphy and Rufus R. Wilson
Southern Research Institute
2000 Ninth Avenue South
P.O. Box 55305
Birmingham, AL 35255-5305

Walter V. Piulle
Electric Power Research Institute
3412 Hillview Avenue
P.O. Box 10412
Palo Alto, CA 94304

ABSTRACT

To study the effects of flue gas from burning eastern, high-sulfur coal on the performance of fabric filters, the Electric Power Research Institute is evaluating the performance of a 10-MW pilot-scale baghouse. Operation over the past 40 months included cleaning by reverse-gas, reverse-gas with sonic assist and shake/deflate. Outlet emissions were below 0.004 lb/million Btu, and collection efficiencies were greater than 99.9%. The pressure drop across the bags was 5.5 in. H_2O or less for filtering times of three hours. For reverse-gas cleaning, residual dustcake weights were about 1.0 lb/ft^2 versus less than 0.5 lb/ft^2 for sonic-assisted and shake/deflate cleaning. Dustcake weight was also sensitive to startup and shutdown procedures, and it increased rapidly with more frequent shutdowns. High bag failure rates occurring during the shake/deflate operation may be attributable to excessive deflation flows or shaking accelerations.

INTRODUCTION

The need for effective control of particulate emissions from coal-fired electric utility boilers has prompted extensive research on fabric filters (baghouses). Part of this research consists of pilot-scale programs funded by the Electric Power Research Institute. Reflecting current industry installations, most pilot-scale facilities filter flue gas from the combustion of pulverized, western, low-sulfur, subbituminous coal, while one filters flue gas from the combustion of pulverized, eastern, high-sulfur, bituminous coal. The EPRI high-sulfur-coal pilot unit has been in operation for 3-1/2 years, through four test phases covering three different types of cleaning: reverse-gas, reverse-gas with sonic assist, and shake/deflate. Figure 1 shows a summary of major parameters for all testing periods at the EPRI High-Sulfur-Coal Fabric Filter Pilot Plant (HSFP). This paper presents the results of research conducted during these periods.

The HSFP is located at the Gulf Power Company's Scholz Electric Generating Plant near Sneads, Florida. A slipstream is taken from the Unit 2 boiler upstream of the precipitator and is passed through the baghouse. The Babcock and Wilcox boiler is rated at 40 MW but commonly operates at up to 50 MW. Three coals, ranging from 2.4% to 3.9% sulfur (dry basis), have been burned in the Unit 2 boiler during testing. (See Table 1.) With the exception of lime and sulfur trioxide contents in the Peabody ash, the three coals produce similar fly ash. (See Figure 2.)

The 10-MW pilot plant consists of 5 compartments with a total of 210 bags; each bag is 12 in. in diameter and 35 ft long. The baghouse is designed to operate at a constant flow of 35,000 acfm for the designed air-to-cloth ratio (A/C) of 1.6 acfm/ft^2. However, A/C can be varied by adjusting flow rate or by removing bags. The compartments are cleaned one at a time, in sequence, with a set interval between each cleaning. For a 3-h filtering time, one of the five compartments is cleaned every 36 minutes. Cleaning is achieved by reverse-gas flow at an A/C variable up to 4.0 acfm/ft^2 with, or without, sonic assist from two Fuller 200-Hz horns or by shaking at amplitudes up to 1.5 in. (bag-cap deflection from rest) and frequencies up to 4 Hz.

Operation of the fabric filter began in July 1982, following completion of air-load tests. Midwesco 14-oz. glass fiber bags with a Burlington I-625 acid-resistant coating were used during testing of reverse-gas cleaning. The Unit 2 boiler burned Hallmark and Peabody coals, which had typical sulfur contents of 2.8% to 3.4%. This testing interval was characterized by low pressure drop and high dustcake weight.

Sonic-assisted, reverse-gas cleaning began in November 1983 and lasted 17 weeks. Menardi-Southern 10-oz. glass fiber bags with 10% Teflon B finish filtered fly ash from Hallmark coal. At sound pressures of 114 Pa, this method showed potential for stabilizing dustcake weight and pressure drop.

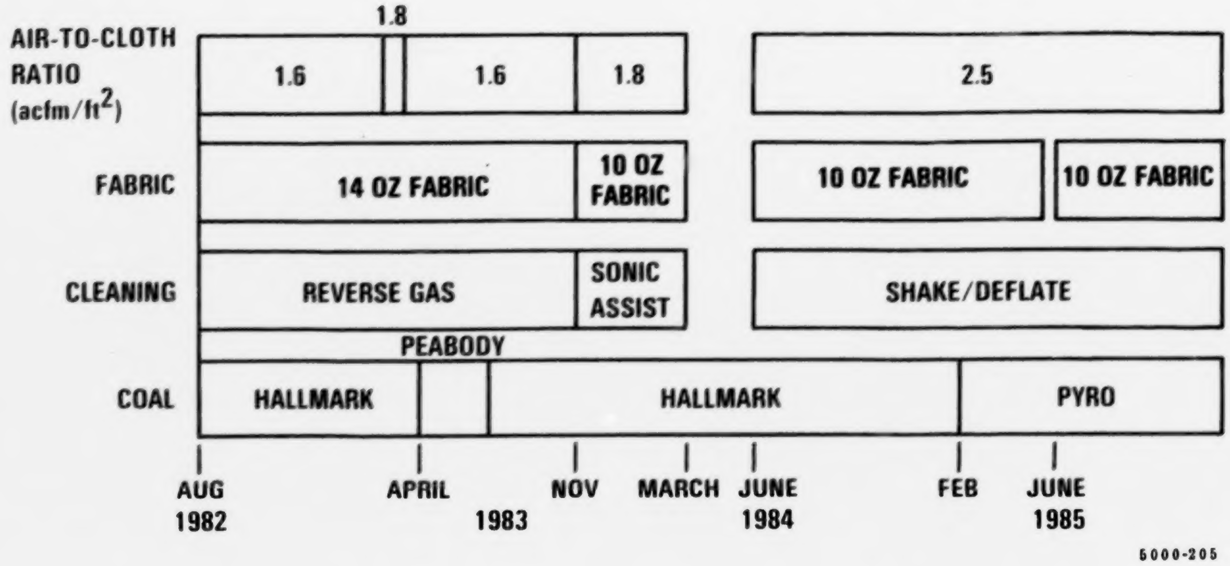

Figure 1. Summary of major testing parameters at the EPRI High-Sulfur-Coal, Fabric Filter Pilot Plant.

TABLE 1. COMPARATIVE COAL ANALYSIS

	Hallmark	Peabody	Pyro
Heat Content Btu/lb	13144	13097	12193
% Carbon	72.31	71.96	71.96
% Hydrogen	4.93	4.99	4.87
% Nitrogen	1.37	1.43	1.40
% Chlorine	0.12	0.14	0.31
% Sulfur	2.77	3.35	3.42
% Ash	10.66	11.06	11.93
% Oxygen	7.84	7.07	6.11

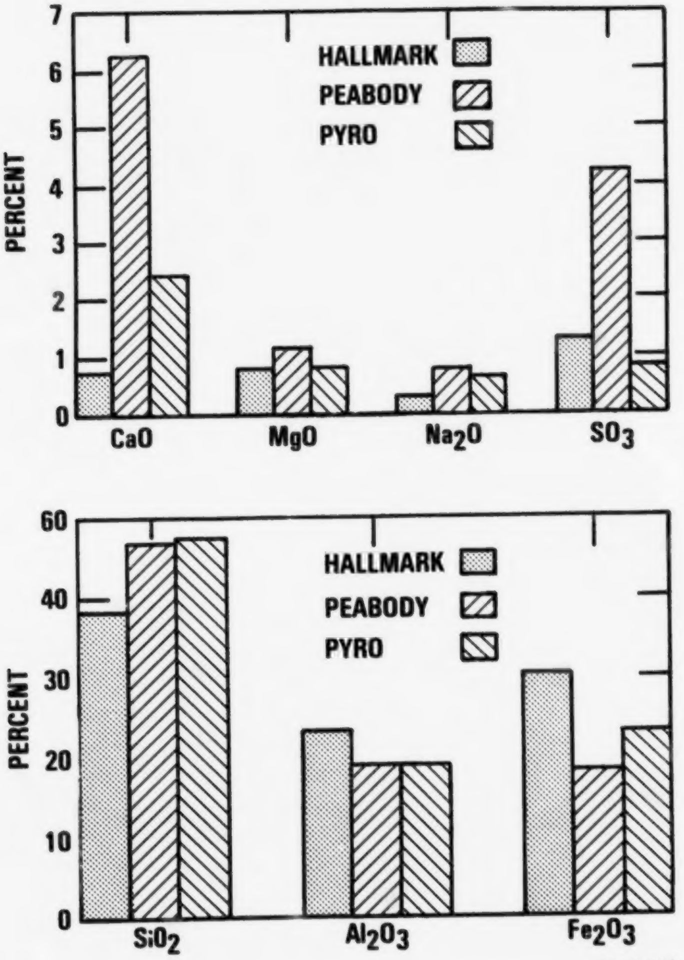

Figure 2. Comparison of mineral analyses of HSFP hopper ash from each of the three coals burned at Scholz Unit 2.

Since June 1984, shake/deflate cleaning has been evaluated at the HSFP. Menardi-Southern 10-oz. glass fabric non-ringed bags have been used throughout the shake/deflate testing. Hallmark and Pyro coals have been burned during this period. Shake/deflate cleaning has allowed operation without significant dustcake weight and pressure drop problems, but both have continued to increase slowly throughout these tests. The study of shake/deflate cleaning will continue through mid-1986.

Emissions have been well-controlled by the baghouse, maintaining levels well below the requirements of federal and state regulations.

This paper will discuss the effectiveness of these three methods of cleaning and the performance of the HSFP with each cleaning method. Several worst-case operations were performed, which have provided more information on effectiveness of the cleaning method and more performance data for the baghouse.

RESULTS OF THE THREE MAJOR TESTING PERIODS

Reverse-Gas Cleaning

The evaluation of the first cleaning method, reverse-gas cleaning, began in August 1982, at an A/C of 1.6 acfm/ft^2 and a filtering time of 6 h. After 183 days tube sheet pressure drop increased from less than 1.0 in. H_2O at startup to 2.5 in. H_2O. A strong dependence of pressure drop on boiler load was observed and has been seen throughout all subsequent testing. Since the baghouse was operated at a constant flow rate, this load dependence of pressure drop has been attributed solely to measured changes in inlet mass concentration and particle size distribution. Overall, pressure drop with reverse-gas cleaning was very low.

A significant problem was encountered when residual dustcake weights exceeded 0.71 lb/ft^2* after 6 months of operation. The added load from the weight of the dustcake raised concerns that, if the weight continued to increase, bag life might be adversely affected, although, over the balance of the test period (10 months), bag failures were not a problem.

The baghouse was operated at an A/C of 1.8 acfm/ft^2 for four weeks. A 40% increase (to 3.5 in. H_2O) in tube sheet pressure drop resulted from the 12.5% increase in A/C. The average residual dustcake weight increased 0.1 lb/ft^2 over this period.

Alternate Coal Evaluation--

Following the period of operation at a higher A/C, a 10-week supply of Peabody Eagle II Composite coal was burned. The Peabody coal was very similar to Hallmark coal except that the sulfur content of the Peabody coal was higher, as shown in Table 1. Tube sheet pressure drop slowly increased from 2 to 3 in. H_2O during the 74 days of operation at the design A/C of 1.6 acfm/ft^2. Based on previous operation, a similar increase in tube sheet pressure drop would have been expected had Hallmark coal been in use during that period. Little difference in baghouse operation with each of the two coals could be discerned other than an increase in corrosion rates from 0.18 mils/10,000 h, while burning Hallmark coal to 0.70 mils/10,000 h, while Peabody coal was burned. These corrosion rates were based on weight loss of mild steel samples.

---

*75 lb/bag for a 12 in. diameter by 35 ft long bag.

Adverse Operating Conditions Test--

Beginning August 16, 1983, a special test was conducted to evaluate baghouse performance under worst-case operating conditions. To simulate operation of a "peaking unit", an electric generating unit that is operated only during peak load demand periods, the baghouse was operated 8 h each day and then shut down without purging the compartments of hot flue gas. The baghouse remained off line for 16 h and was allowed to cool. The daily schedule for the adverse operations test is shown in Figure 3. This operating schedule was followed for 25 days within a 30-day test period. Corrosion rates measured during this test were 4.0 mils/10,000 h of operation, over four times greater than the corrosion rate of the preceding reverse-gas operating period. The period of adverse operations had no discernible effect on tube sheet pressure drop. Residual dustcake weights, however, increased at a rate of 2.1 lb/bag/day, a rate of increase five times greater than during routine operation with the same cleaning method. The adverse operations test resulted in a very tenacious dustcake, which continued to increase throughout the test. Subsequent to this test, it was observed that normal shutdowns, where compartments were purged of hot flue gas and allowed to cool, also resulted in increased dustcakes. Since heavy dustcakes lead to bag failures and structural damage to the bag suspension system, the need for further study of the mechanisms producing these increases is evident. Development of better startup and shutdown procedures is planned. Figure 3 shows a summary of operating conditions and conclusions drawn from the adverse operations test.

Reverse-Gas Cleaning with Sonic Assist

Preliminary testing of sonic-assisted, reverse-gas cleaning was conducted for 17 weeks following rebagging with 10-oz. fabric. The test was conducted at an A/C of 1.8 acfm/ft^2 at a filtering time of 3 h with two commercially available 200-Hz (nominal) horns in each compartment. Operation during the first ten weeks was conducted with sound pressure levels from 50 to 70 Pa. During this period, pressure drop increased to 2 in. H_2O and average residual dustcake weight increased to 0.34 lb/ft^2. Insulation installed inside the compartments to protect personnel was found to absorb sonic energy in significant quantities during this period. After removal of this insulation, sound pressure levels increased to 114 Pa. The pressure drop then stabilized at 2.5 in. H_2O and the average residual dustcake weight stabilized at 0.4 lb/ft^2. The subsequent three weeks of operation was considered too brief an interval, however, to accurately evaluate the higher energy, sonic-assisted cleaning.

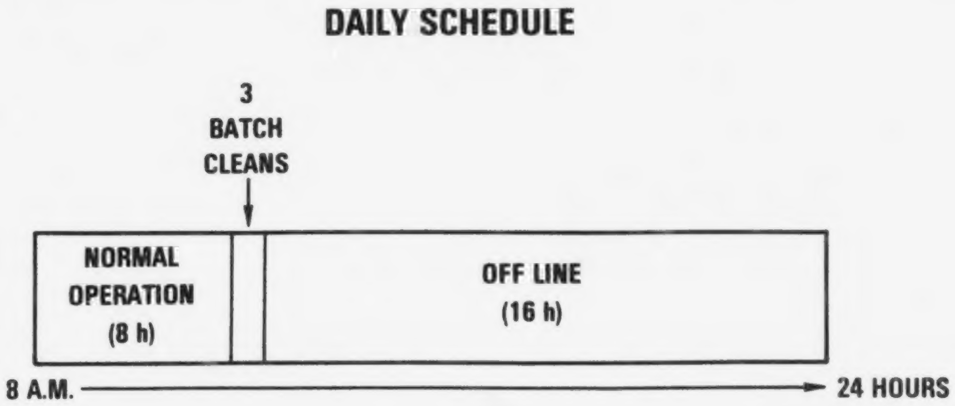
DAILY SCHEDULE
3
BATCH
CLEANS
NORMAL
OPERATION
(8 h)
OFF LINE
(16 h)
8 A.M.
24 HOURS

CONCLUSIONS

- COMPARTMENTS WERE NOT PURGED OF FLUE GAS UPON SHUTDOWN
- FILTERING TIME = 3 h DURING NORMAL OPERATION
- 25 SHUTDOWNS (INCLUDING 3 EXTENDED SHUTDOWNS)
- NO CHANGE IN PRESSURE DROP
- CORROSION RATES INCREASED FROM 0.9 TO 4.0 mils/10,000 h
- DUSTCAKE WEIGHTS INCREASED 62% (FROM 89 TO 144 lb/bag)
- SUBSEQUENT NORMAL OPERATION FOR 2 WEEKS LOWERED DUSTCAKE WEIGHT BY 13 lb/bag
- FREQUENT SHUTDOWNS WITH PURGING ALSO SHOW LARGE DUSTCAKE INCREASES

5000-206

Figure 3. Daily schedule during adverse operations test.

Even though the results are not conclusive, reverse-gas cleaning with sonic assist has shown promise of controlling bag weights and achieving acceptable pressure drop levels in high-sulfur-coal baghouses. This method of cleaning may also be a means of eliminating bag life concerns associated with more energetic cleaning methods. These very promising preliminary results, as well as possible retrofit applications for this cleaning method in reverse-gas baghouses having pressure drop and bag weight problems, have led to the scheduling of further testing of reverse-gas cleaning with sonic-assist, beginning in mid-1986.

Shake/Deflate Cleaning

First Period--

On June 4, 1984, after rebagging with Menardi-Southern 10-oz, non-ringed bags, operation began with a shake/deflate cleaning cycle at an air-to-cloth ratio of 2.5 acfm/ft^2 at a filtering time of 3 h. Shake/deflate is an attractive alternative cleaning method for baghouses filtering highly cohesive and tenacious high-sulfur-coal ash because of the higher cleaning energy associated with it. Initially, the cleaning cycle consisted of a deflation flow of 3200 acfm for 20 s followed by a 20-s shake, with a bag cap amplitude of 0.75 in. (1.5 in. peak-to-peak) at a frequency of 4 Hz. These shaking parameters yield a nominal bag-cap acceleration of 0.92 g (g = 382 in./sec^2).

By the end of January 1985, the steadily increasing average tube sheet pressure drop was 5.5 in. H_2O and the average residual dustcake weight was 0.32 lb/ft^2. On January 24, 1985, the shaking amplitude was increased to 1.5 in. (3.0 in. peak-to-peak), yielding a nominal bag-cap acceleration of 1.8 g. Following the increase in shaking energy, average tube sheet pressure drop did not decrease as expected, but continued to increase slowly. Residual dustcake weight, however, was controlled by the increase in shaking energy, increasing by only 0.04 lb/ft^2 of residual dustcake by May 1 (11 months). Outlet emissions increased from 0.0009 to 0.0028 lb/10^6 Btu as a result of the more energetic cleaning.

The frequency of bag failures became a serious problem, culminating in a cumulative bag failure rate of 17% by May 21, 1984, when this portion of the shake/deflate testing was terminated, and the baghouse was taken off line for rebagging. The failure of the shaker bags after only 11-1/2 months of service, an unacceptable bag life, was attributed to overly energetic cleaning. The increase in bag-cap acceleration from 0.9 g to 1.8 g was initially believed to have been the primary cause of the abbreviated bag life. However, deflation flows of up to 3600 acfm (deflation A/C = 1.23 acfm/ft^2) used during much of the first shake/deflate testing interval are a more likely cause of the premature bag failure (1), since utility baghouses employing bag-cap accelerations of 2.0 g have reported bag lives of 3 to 5 years.

Second Period--

The baghouse was rebagged with new Menardi-Southern 10-oz bags and returned to service at a gross air-to-cloth ratio of 2.5 acfm/ft^2 and using shake/deflate cleaning with a filtering time of 3 h.

Since overly energetic cleaning (through either deflation or shaking) had apparently caused the bag failures, a series of short tests designed to determine minimum deflation and shaking energy needed to produce adequate reduction of tube sheet pressure drop were conducted during July and August. Initially, a series of 3-day tests were conducted to define the minimum deflation volumetric flow rate and minimum duration needed to control pressure drop. Figure 4A shows the results of a series of tests conducted at a duration of 20 s to determine the minimum volumetric flow rate needed for stable operation. Flows less than 750 acfm resulted in an ever-increasing pressure drop, requiring a manually initiated batch-clean of all five compartments to restore pressure drop to acceptable levels. Figure 4B shows the results of a series of tests conducted at a flow rate of 900 acfm to determine the minimum duration of deflation flow needed for stable operation. Deflation flow durations of less than 25 s were inadequate to control tube sheet pressure drop at this flow rate.

Since the product of flow rate and flow duration yields a total deflation volume, existing data were plotted in terms of total deflation volume. Figure 4C shows that a deflation volume greater than 300 ft^3 was needed to stabilize tube sheet pressure drop.

The results of these tests indicated that a deflation flow rate of 900 acfm for 25 s would be an acceptable minimum for operation. The baghouse was then operated with these deflation parameters, with only slight changes, during the second shake/deflate test phase.

Deflation is a critical component of the shake/deflate cleaning cycle, but most of the energy imparted to the bags during cleaning comes from shaking. Bag-cap acceleration, as a measure of the energy level and the duration of shaking, determine the cumulative amount of energy delivered to the bags. Shaking duration was investigated in a series of short (3 days each) tests following the evaluation of deflation. With a bag-cap acceleration of 0.9 g shaking time was reduced from 20 to 15, 10, 5, 3, 2, and finally 1 s, and pressure drop was maintained at stable levels at each duration. However, due to the small size of the shaker mechanism and the large inertia of the motor, the shakers continued to run for about 13 s after power was turned off, so that the actual shake time in Figure 5 was the time shown, plus 13 s of shaking at a continually decreasing frequency until the shaker came to rest. Because the run-on shaking had an unknown effect on the cleaning efficiency, the shake time was arbitrarily left at 5 s for the remainder of the test phase.

The second period of shake/deflate testing includes characterization of roles of filtering time, air-to-cloth ratio, and shaking force and their effects on tube sheet pressure drop or drag (the ratio of pressure drop to

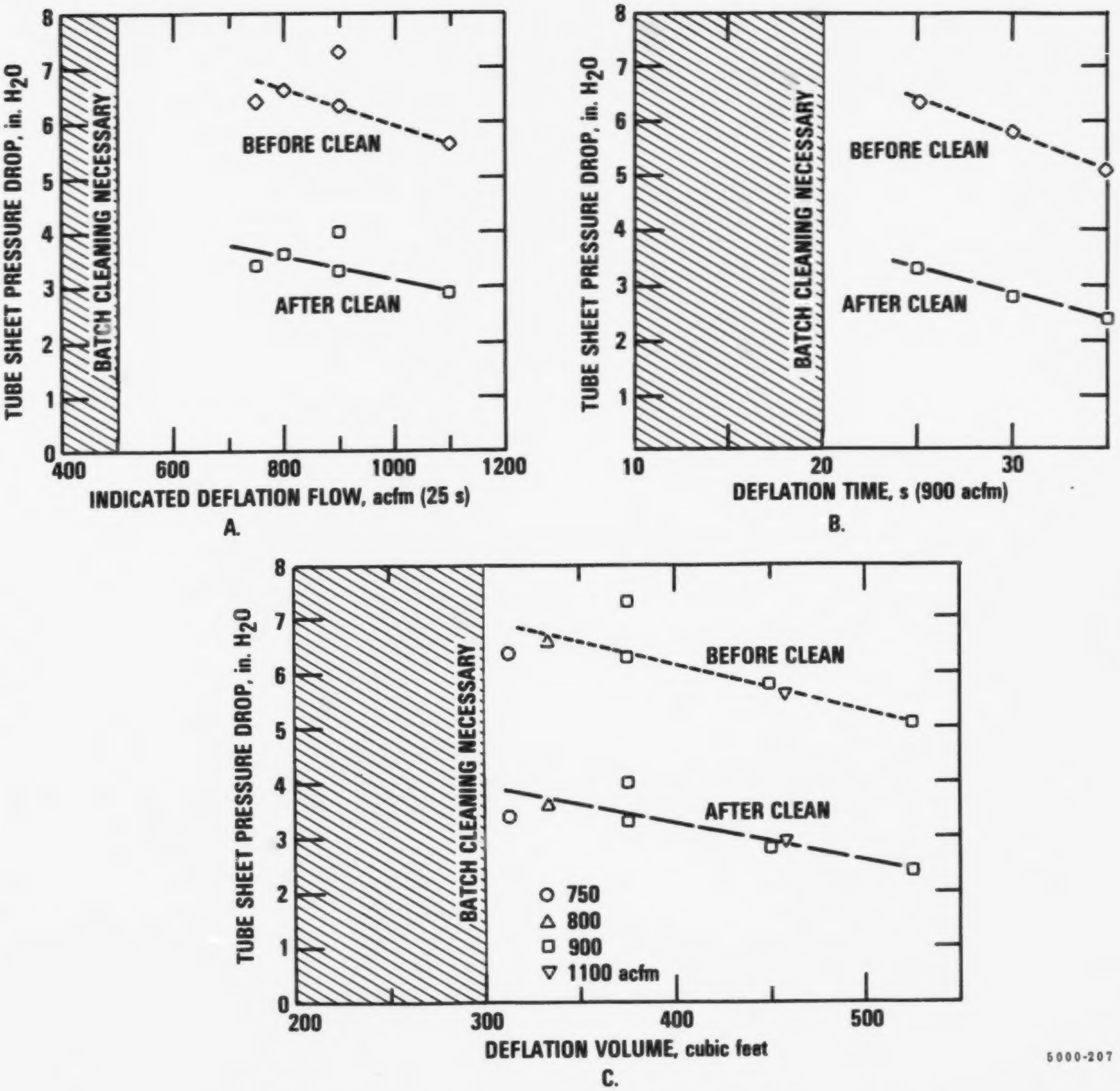

A.

B.

C.

Figure 4. Test results for determinations of minimum deflation volume needed to control tube sheet pressure drop. June-July 1985.

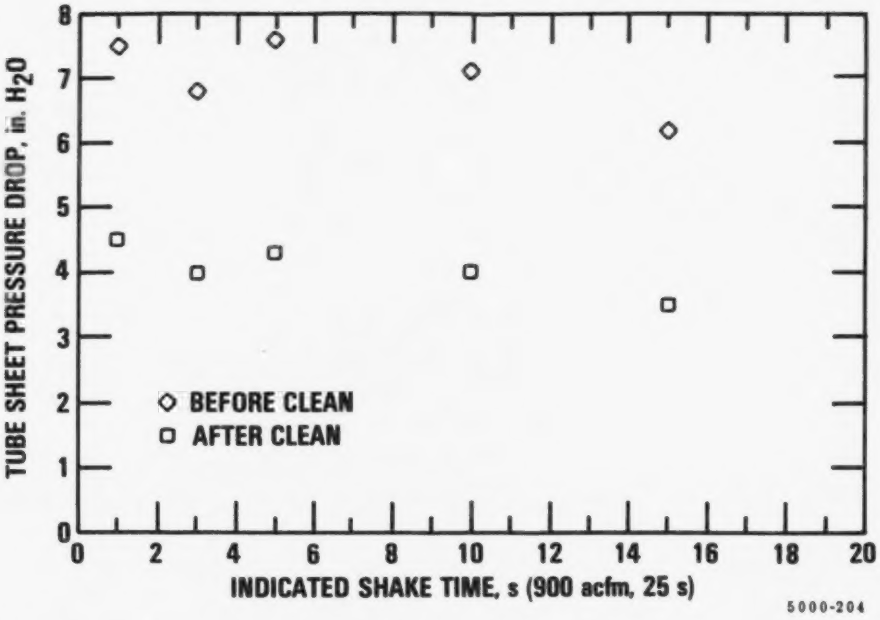

Figure 5. Short-term tests of shake time at the HSFP.

air-to-cloth ratio) and emissions. The analysis of the effects of 1, 2 3-h filtering times has been concluded. Figure 6 compares the 24-h average drag at full Unit 2 load (425,000 lb/h steam flow) for each of the three filtering times tested. Note that average drag increased from 2.06 in. H_2O/(ft/min) at a filtering time of 1 h to 2.50 in. H_2O/(ft/min) at a 3-h filtering time. With shake/deflate cleaning, a 1.0 in. H_2O decrease in average tube sheet pressure drop was obtained by reducing filtering time from 3 h to 1 h.

SUMMARY

The characterization of fabric filters filtering flue gas from utility boilers burning high-sulfur coal has yielded the following preliminary conclusions:

- Reverse-gas cleaning while operating at a gross A/C of 1.6 acfm/ft^2 maintained low pressure drops (3.5 in. H_2O), but residual dustcake weights increased to unacceptably high values (greater than 0.7 lb/ft^2). Based upon these high dustcake weights, it is concluded this method of cleaning is not sufficiently energetic for a high-sulfur-coal application.

- Reverse-gas cleaning with sonic assist at a gross A/C of 1.8 acfm/ft^2 showed potential for controlling residual dustcake weight (0.4 lb/ft^2) and tube sheet pressure drop (2.5 in. H_2O). Because it has potential for wide application to baghouses on utility boilers burning high-sulfur-coal and because it is particularly attractive for retrofitting reverse-gas baghouses, further testing of sonic assisted cleaning is planned.

- Shake/deflate cleaning with the baghouse operating at a gross A/C of 2.5 acfm/ft^2 controlled both dustcake weight (<0.4 lb/ft^2) and tube sheet pressure drop (5.5 in. H_2O), but initially unacceptable bag life resulted from excessive deflation. Subsequent testing is establishing acceptable deflation flow, deflation duration and shake duration and indicating the dependence of drag on filtering time. Bag life is also being re-evaluated. This cleaning method also has the potential for successful application on utility boilers burning high-sulfur coal. Characterization of shake/deflate cleaning is continuing and will be concluded in 1986.

CONCLUSIONS

The three conventional methods of cleaning baghouses filtering flue gas from coal-fired, electric generating facilities—reverse-gas, reverse-gas with sonic assist, and shake/deflate—have been evaluated. Comparing

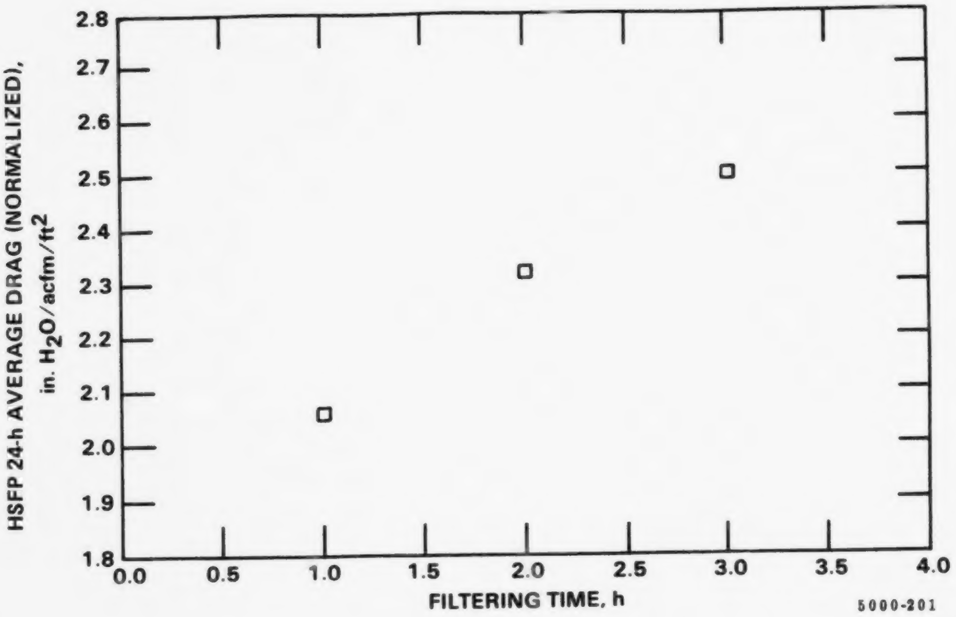

Figure 6. Results of the shake/deflate filtering-time tests.

the three cleaning methods, it is recognized that differing air-to-cloth ratios and thus, variable capital costs (cost analysis is not a topic of this paper), are associated with each method. (The reverse-gas testing phases, including sonic assist, were conducted at gross A/C's of 1.6 to 1.8 acfm/ft^2, and the shake/deflate testing was conducted at a gross A/C of 2.5 acfm/ft^2.)

Beyond air-to-cloth ratios, differences also exist between the three cleaning methods in boiler load and filtering time. It has been shown during studies at the EPRI Fabric Filter Pilot Plant in Denver, Colorado, that the average drag of reverse-gas cleaned baghouses is insensitive to filter time. This allows a direct comparison of the drags for the three cleaning methods, even though the filtering times are different (6 h for reverse-gas cleaning and 3 h for sonic-assisted, reverse-gas and shake/deflate cleaning). Drag was found to be dependent upon boiler load for all three test periods, even though the flow rate through the baghouse was held constant. This dependence is attributed to boiler load changes in particle concentration and size distribution. Since the boiler operated mainly at low load during the reverse-gas test periods and at high load during the shake/deflate test period, the drag for the shake/deflate cleaning period is presented for both low and high load cases. For low boiler loads, the average drag during the shake/deflate test phase was 1.4 in. H_2O/acfm/ft^2, roughly equivalent to the drags obtained during the two reverse-gas test periods. (See Figure 7-A.)

Dustcake weights at the end of each of the three cleaning periods are shown in Figure 7-B. Although they represent different operating durations, the trend of decreasing dustcake with increasing cleaning energy is evident. The dustcake weights for reverse-gas cleaning are above an acceptable amount at 0.7 lb/ft^2 (12 months of operation). Sonic-assisted, reverse-gas cleaning stabilized dustcake weights when higher sonic energy (114 Pa) was applied, after initial dustcake increases at low sonic energies (50-70 Pa) (17 weeks of operation). Shake/deflate cleaning produced the lowest and most stable dustcake weights, over an operating period of 12 months.

Average emissions for the three cleaning methods are shown in Figure 7-C. Reverse-gas cleaning was characterized by emissions one-hundredth of the 1978 New Source Performance Standard of 0.03 lb/million Btu for coal-fired power plants. Emissions increased as the cleaning energy was increased, with wide variations in emissions observed during shake/deflate cleaning due to shaking energy changes. The highest emissions observed, however, were still less than a tenth of the New Source Performance Standard. A clear stack and excellent mass removal efficiency, exceeding 99.9%, are among the most attractive attributes of the fabric filter.

FUTURE PLANS

A testing matrix designed to characterize the roles of filtering time, bag-cap acceleration, and air-to-cloth ratio in shake/deflate cleaning is in progress. These tests are projected to conclude during the summer of 1986. Continuing research will attempt to define an optimum cleaning

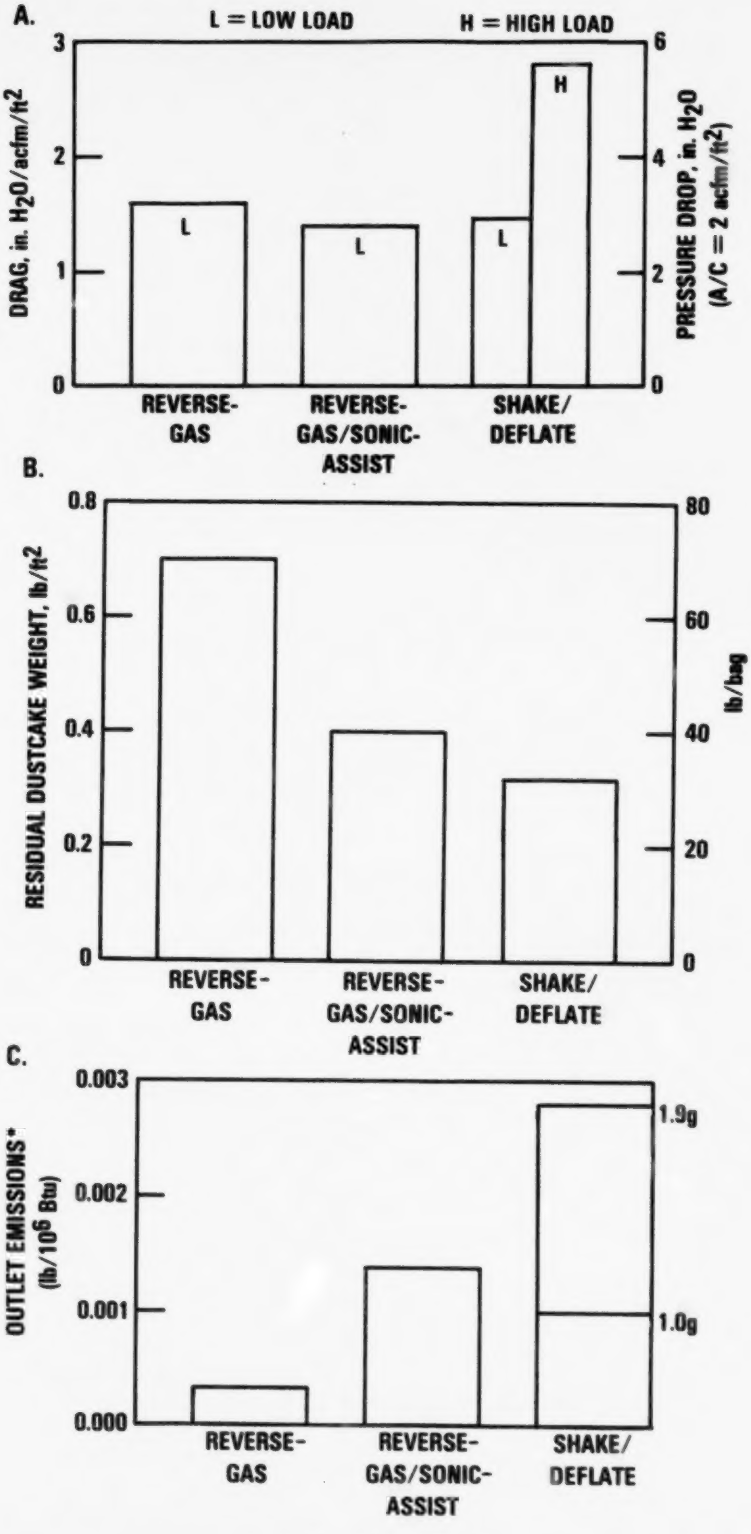

* NSPS LIMIT (SEPT. 1978) = 0.03 lb/10^6 Btu

5000-208 B

Figure 7. Average HSFP drag, residual dustcake weight, and outlet emissions for each of the three major test intervals.

method, filtering time, A/C, and bag fabric to produce acceptable residual dustcake weight, pressure drop, and bag life for the operation of a baghouse filtering flue gas from a boiler burning high-sulfur coal.

REFERENCES

1. Chambers, Richard. Southwestern Public Service, Private Communication, 1985.

FLUE GAS CONDITIONING FOR IMPROVED BAGHOUSE PERFORMANCE

Dennis L. Laudal and Stan J. Miller
University of North Dakota Energy Research Center
Box 8213, University Station
Grand Forks, North Dakota 58202

ABSTRACT

Baghouse performance has been shown to be dependent on both the chemical and physical properties of the ash. Small amounts of ammonia and sulfur trioxide were added to the flue gas as conditioning agents to modify ash characteristics and reduce fine particulate emissions from a pilot-scale coal combustion/baghouse system.

Tests were made with three western low-rank coals which produce difficult to collect fly ash. Total particulate emissions over several cleaning cycles were substantially reduced and fine particulate emissions were reduced up to four orders of magnitude between the cycles. With conditioning baghouse pressure drop increased at a slower rate and reached a lower operating pressure drop after several cleaning cycles.

Ash samples were analyzed to determine physical and chemical changes due to ammonia and sulfur trioxide addition. Several ammonia-sulfur compounds were found indicating a complex chemical mechanism. Changes in the fly ash particle size distribution and bulk ash cohesiveness may help explain the physical mechanism by which both pressure drop and particulate emissions are reduced.

INTRODUCTION

Fabric filters are being applied to utility coal-fired boilers in increasing numbers but major questions exist as to the cause and effect relationships between ash properties and emission levels as well as pressure drop. Although most baghouses are able to meet or exceed current New Sources Performance Standards, high emissions from a utility baghouse have been reported (1). Increased concern over respirable particulate emissions and the possibility of regulation of fine particulate matter also indicate a need for a better understanding of the causes of variation in fabric filter performance.

The particulate characterization project at the University of North Dakota Energy Research Center (UNDERC) has focused on identifying and quantifying those particulate characteristics of low-rank coals that are critical to control device performance and the environment. The long range goal of the work is to develop an increased understanding of coal and collector specific emissions and to investigate economical methods of increasing collection efficiency of fine particulate matter.

Previous tests of 26 low-rank coals with a pilot combustor and baghouse resulted in a penetration range of 0.1% to 24% with woven glass fabric and shaker cleaning (2,3). Since these tests were conducted with the same fabric, cleaning cycle, and face velocity it was concluded that differences in penetration originated with differences in the fuels. Additional tests with several fabrics and three different cleaning modes confirmed that some fly ashes can be more difficult to collect in fabric filters than others. One of the project goals, therefore, was to invesigate methods of altering characteristics of difficult to collect ashes to reduce fine particulate emissions from a fabric filter. After a number of exploratory tests with additives to the coal and flue gas, a combination of ammonia (NH_3) and sulfur trioxide (SO_3) was found to significantly reduce particulate emissions as previously reported (4). This paper presents further data that show ammonia and SO_3 conditioning not only reduces particulate emissions but also lowers pressure drop.

EXPERIMENTAL

Tests were conducted with the UNDERC particulate test combustor (PTC) and pilot baghouse. The PTC is a 550,000 Btu/hr pulverized coal-(pc) fired combustor which was specifically designed to generate fly ash representative of large pc-fired boilers. The pilot baghouse consists of three main chambers which can be operated with different cleaning modes; pulse jet, low pressure expansion, and shaker. For this study, only the shaker and pulse jet chambers were used. A more complete description of the PTC and pilot baghouse is given in a previous paper (2). The fabrics used in the baghouse were 10 oz woven glass with 10% teflon B finish (Filter Media Products fabric 601E) in the shaker chamber and 22 oz felted Ryton fiber with Gortex scrim (Carter-Day Daytex fabric) in the pulse jet chamber. The baghouse temperature for all the tests was 300°F. The air-to-cloth ratios were approximately 3 to 1 for the shaker chamber and 8.5 to 1 for the pulse jet.

Two methods of injecting SO_3 have been used for the conditioning tests. The first, reported previously (4), involved passing dry nitrogen over 30% fuming sulfuric acid and maintaining the acid bath temperature at 105°F to ensure a steady SO_3 injection rate. This injection method has several drawbacks. Fuming sulfuric acid is a very hazardous material to handle and also the quantity of SO_3 obtained is depleted over time, requiring the acid be replaced. Since it was impractical for longer term tests, a generator, shown in Figure 1, that uses vanadium pentaoxide (V_2O_5) to catalytically convert SO_2 to SO_3 was designed and constructed. Sulfur dioxide and air are passed through a V_2O_5 filled reactor that is heated to 800°F oxidizing the SO_2 to SO_3. The conversion of SO_2 to SO_3 was measured using SO_2 analyzers and was found to be greater than 99%. Therefore the quantity of SO_3 injected was determined by using an accurate flow meter to control the SO_2 flow to the generator.

An injection location upstream of the baghouse was chosen to provide enough residence time for adequate mixing of the SO_3 and ammonia with the flue gas. At this injection point the flue gas temperature was 700°F. A calibrated flow meter was used to monitor the added ammonia which was injected just upstream of the SO_3 as shown in Figure 1. Additive concentrations in the flue gas for the conditioning tests were 12 ppm SO_3 and 45 ppm ammonia, with the exception of one short run where the concentrations were increased to 60 ppm SO_3 and 225 ppm ammonia to help evaluate the ammonia - SO_3 reaction products.

Tests with three low-rank coals were conducted to evaluate the effect of flue gas conditioning with SO_3 and ammonia on fine particulate emissions from a fabric filter. Two of the coals, Falkirk, North Dakota lignite and Big Brown, Texas lignite were chosen because earlier tests (2,3) with these coals resulted in high fabric filter emissions. The third coal, South Hallsville, Texas lignite was chosen because a previously reported correlation between ash composition and baghouse emissions indicated that this coal would also produce a difficult to collect ash (2). For each coal a baseline test was conducted without conditioning and then compared to an identical test performed with SO_3 and ammonia injection to determine differences in emissions and pressure drop. Tests with the three coals were completed with the baghouse shaker chamber starting with new or hand vacuumed bags. The first 2-3 hours of each test were performed without bag cleaning to measure particulate emissions and pressure drop as a function of time with dust cake build-up on the fabric. Bag cleaning was then initiated, and over several cleaning cycles emissions as a function of time as well as total dust loading measurements were taken. In addition, two 50 hour tests utilizing South Hallsville lignite, were made to evaluate the longer term effects of conditioning on emissions and pressure drop.

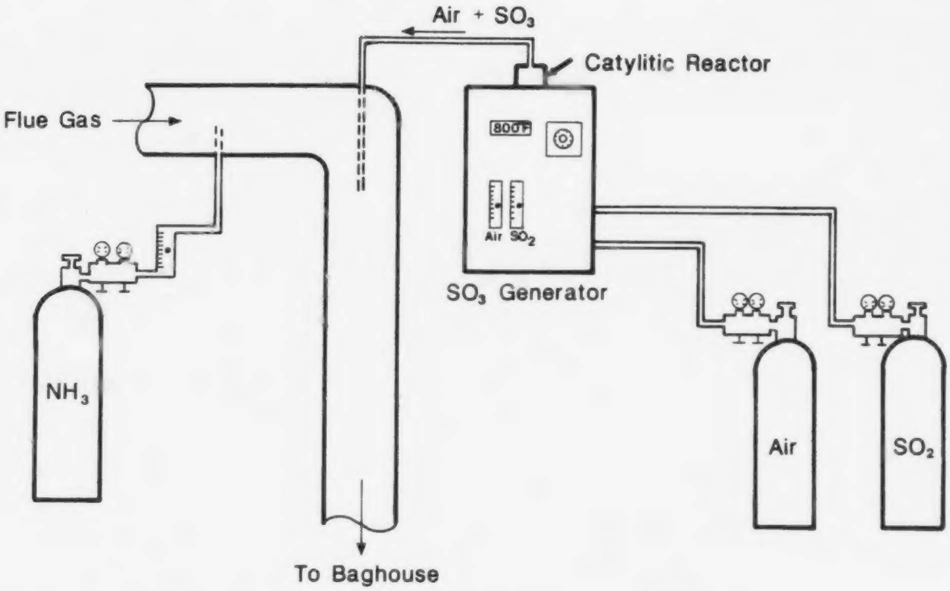

Figure 1. Schematic of SO_2 to SO_3 generator.

A flow sensor six stage multicyclone was used to measure the inlet fly ash particle size distribution as well as to collect size fractionated samples for subsequent analyses. Real-time particulate emissions from the baghouse were measured with a TSI APS 33 laser aerodynamic particle sizer. The use of the APS 33 for particle size measurements of fabric filter emissions was described previously (5). Submicron particles (0.01-1.0 µm) were measured using a TSI Differential Mobility Particle Sizer (DMPS). This instrument separates various size particles using electrical mobility, which is dependent on particle size, and then counts the number of particles in the resultant monodispersed aerosol with a condensation nucleus counter (CNC).

Physical and chemical characterization methods included routine coal and ash analyses, scanning electron microscopy (SEM), x-ray diffraction (XRD), electron spectroscopy for chemical analysis (ESCA), and ash cohesiveness testing. To measure ash cohesiveness a method was developed at UNDERC (6) which involved forming a disk shaped ash pellet (30 mm diameter by 5 mm thickness) in a high pressure press and then applying a force to the center of the pellet while supported on its edge. The force required to break the pellet is a measure of the pellet strength which is dependent on the ash cohesiveness.

RESULTS AND DISCUSSION

BAGHOUSE EMISSIONS

Baghouse removal efficiency results determined by inlet and outlet dust loading measurements, taken over several cleaning cycles using woven glass bags and shaker cleaning, are given in Table 1. A significant improvement in removal efficiency is clearly seen using SO_3 and ammonia conditioning. Baghouse penetration for Big Brown, South Hallsville, and Falkirk coals were reduced by factors of 400, 98, and 15, respectively. Efficiency for a nonconditioned test with Beulah coal is included as a reference since previous Beulah tests resulted in the highest value of all coals tested (3).

The APS 33 measures emissions as a function of time for particle size distribution from 0.5 to 15 μm but to avoid multiple graphs for different particle sizes the respirable mass function of the APS 33 was used. This is a weighted sum of 0.5 to 10 μm emissions including the mass of all particles from 0.5 to 1.5 μm and decreasing percentages of the mass of larger particles up to 10 μm. To convert number concentration to mass concentration spherical particles are assumed and the calculations then made using the particle density. Figure 2 shows respirable mass emissions from the shaker chamber with no cleaning cycle for all three coals starting with clean bags. With conditioning respirable mass emissions quickly drop for the first 40 minutes of dust cake build-up and then appear to remain constant. After 40 minutes respirable mass emissions are reduced by 3 to 4 orders of magnitude by conditioning with SO_3 and ammonia. The baghouse removal efficiency at this point is $\geq$ 99.999%. Emissions with time, including cleaning cycle effects for South Hallsville lignite are shown in Figure 3. As expected, just after bag shaking there is an increase in

TABLE 1. PERCENT BAGHOUSE REMOVAL EFFICIENCY DETERMINED BY DUST LOADINGS OVER SEVERAL CLEANING CYCLES

Coal	Nonconditioned	Conditioned
Beulah	99.93	NA
Falkirk	94.70	99.64*
Big Brown	80.00	99.95
South Hallsville (Dried)	92.17	99.92
South Hallsville (As Received)	91.03	99.90
South Hallsville (Felted Fabric)+	99.03	99.76

* A leak between compartments caused some forward flow through bags while shaking. Removal efficiency would likely be higher if the leak had not occurred.

+ Pulse jet - all other tests performed with woven glass bags and shaker cleaning.

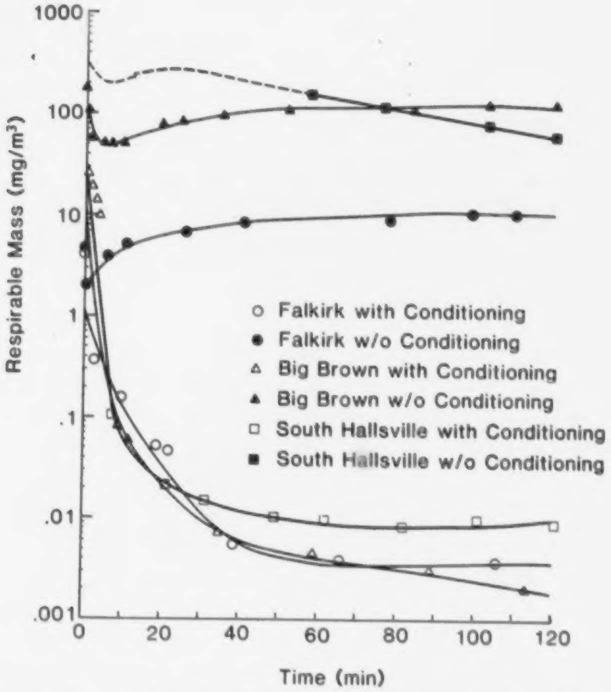

Figure 2. Respirable mass emissions for Falkirk, Big Brown, and South Hallsville coals without bag cleaning.

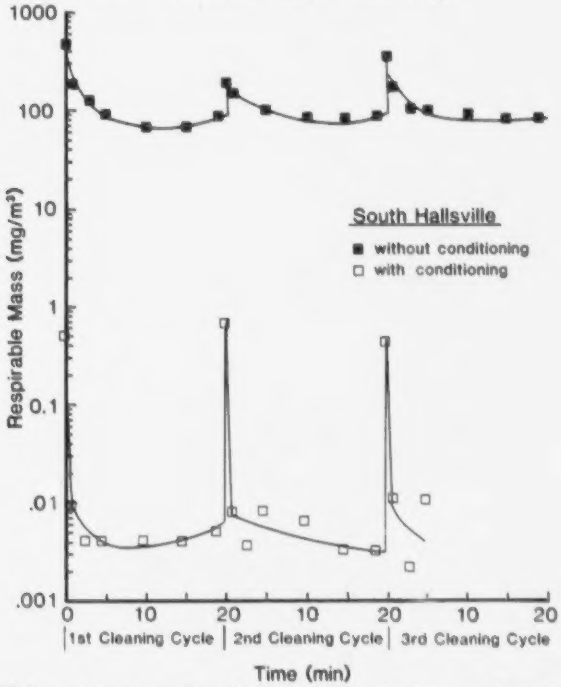

Figure 3. Respirable mass emissions for shaker cleaning cycle with South Hallsvile coal.

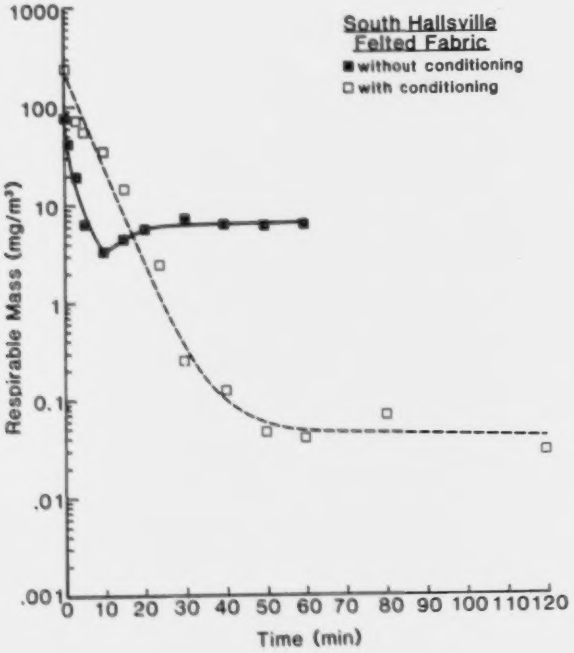

Figure 4. Respirable mass emissions from felted fabric with South Hallsville coal without bag cleaning.

emissions but with conditioning there is rapid recovery. Through several cleaning cycle intervals conditioning results in a significant reduction in fine particle emissions. Results with Falkirk and Big Brown (not shown) also revealed large reductions in emissions over several cleaning cycles. Since there was a concern that conditioning could produce a large number of submicron particles that may penetrate the fabric filter the DMPS and CNC were used to measure these particles. Results for the South Hallsville tests show that submicron particle emissions were also reduced at the baghouse outlet by over 3 orders of magnitude when comparing the conditioned to the nonconditioned test.

Tests were also conducted using a felted fabric and pulse jet cleaning with South Hallsville coal. From Figure 4 it can be seen that conditioning again produced a significant decrease in respirable mass emissions. Starting with a new fabric, emissions were about the same for both tests for the first 20 minutes. After 20 minutes emissions without conditioning remained steady, however, with conditioning emissions continued to drop until they were reduced by two orders of magnitude. This indicates that conditioning will result in reduced particulate emissions with both woven glass and felted fabrics. Results show that for the coals tested, total mass, respirable mass, and submicron particulate emissions are significantly reduced when ammonia and SO_3 are injected upstream of the baghouse.

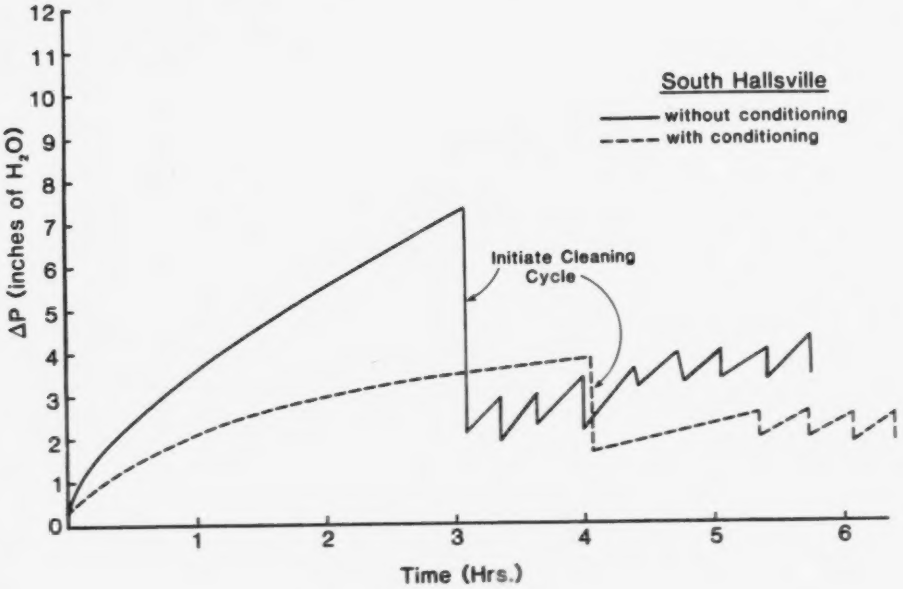

Figure 5. Presure drop vs. time with and without conditioning for South Hallsville using the shaker chamber.

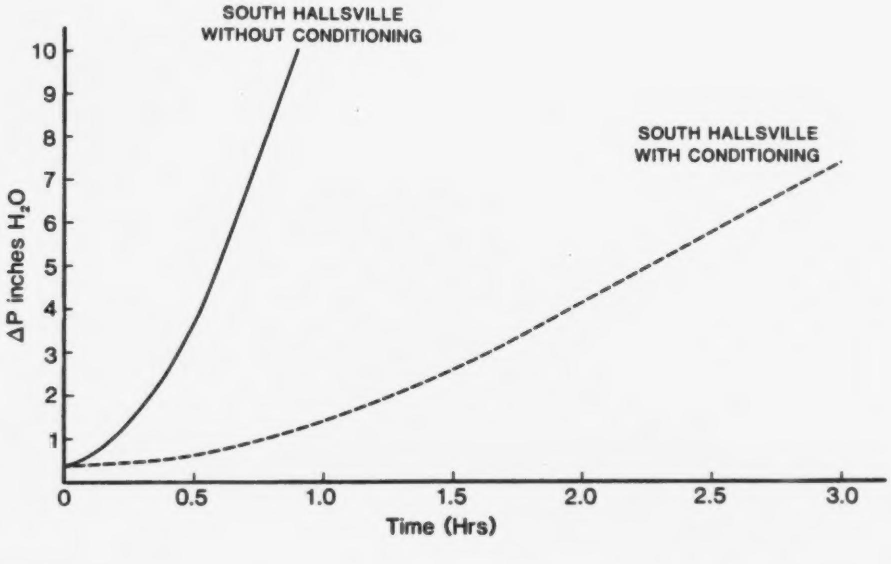

Figure 6. Pressure drop vs. time with and without conditioning for South Hallsville coal using the pulse jet chamber.

PRESSURE DROP

Any evaluation of a process to reduce emissions must also address how the process effects pressure drop. In Figures 5 and 6 pressure drop is plotted for South Hallsville lignite showing a comparison between the conditioned and nonconditioned tests. During the initial dust cake build-up, starting with new fabric, the slope of ΔP vs time was less for the conditioning test, indicating that conditioning reduces the rate of pressure drop increase. After initiating the cleaning cycle (Figure 5) the reduced pressure drop appears to continue. Using felted fabric in the pulse jet chamber the reduction in pressure drop due to conditioning is dramatic as is shown in Figure 6. Without pulsing the bags the pressure drop reached 10 inches of H_2O in less than 1 hour for the baseline test but when flue gas conditioning was used the ΔP was less than 7 inches H_2O after 3 hours of dust cake build up. Previously reported (4) short term results with Big Brown and Falkirk coals also showed significant reductions in pressure drop.

Fifty hour baseline and conditioning tests were completed for South Hallsville lignite to evaluate the longer term effects of conditioning on pressure drop. Figure 7 presents the data, before the cleaning cycle was initiated and the ΔP immediately before each shake, for both the baseline and conditioning tests. From Figure 7 it can be seen that the pressure drop for the test with SO_3 and ammonia conditioning was lower than for the test performed without conditioning and remained lower throughout. Available data appear to be consistent for the three coals indicating that SO_3 and ammonia conditioning facilitates the formation of a more porous dust cake resulting in a lower pressure drop.

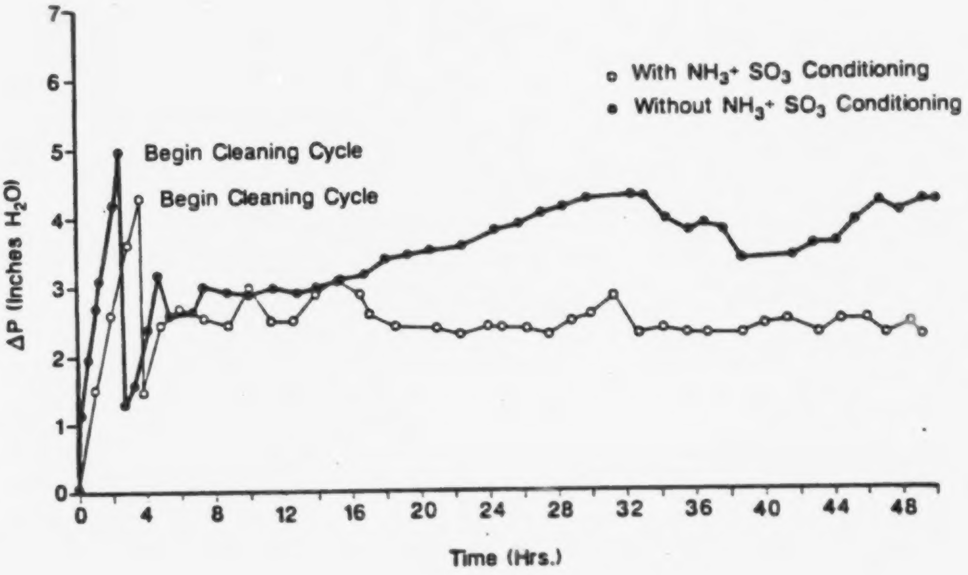

Figure 7. Pressure drop vs. time for 50 hour tests with and without conditioning for South Hallsville using the shaker chamber.

PHYSICAL AND CHEMICAL CHARACTERIZATION

Injection of SO_3 and ammonia into the flue gas must have produced physical and chemical changes in the fly ash and (or) dust cake to account for the observed enhanced particulate removal and lower pressure drop. ESCA analyses for sulfur and nitrogen of the baghouse hopper ash samples for each of the test coals and size fractionated Big Brown ash are given in Tables 2 and 3. The conditioned baghouse hopper ash samples have significantly higher surface concentrations of nitrogen and sulfur than the nonconditioned ashes indicating the SO_3 and ammonia (SO_3-ammonia product) are absorbed on the fly ash surface as would be expected. Surface concentrations of sulfur and nitrogen appear to increase with decreasing particle size but the difference in concentration found by subtracting nonconditioned values is quite uniform for all particle sizes except for nitrogen which is higher in the smallest size cut. Although the ESCA analysis penetrates the surface only 30-100 angstroms the depth of the ammonia-SO_3 layer may be as small as 12 angstroms (4). The presence of aluminum, silicon, and calcium confirms the ESCA analysis did penetrate the surface layer. The ESCA analyses does indicate uniform deposition of the ammonia-SO_3 compound on the surface of all the fly ash particles.

SEM micrographs did not show any clear differences in surface morphology between the conditioned and nonconditioned samples at magnifications up to 30,000 X. Resolution of the SEM is not high enough, at 30,000 X to see the angstrom level changes caused by conditioning which may have occurred in surface morphology.

The exact ammonia-SO_3 species that is deposited on the fly ash surface is not clear. ESCA analysis reveals the measured sulfur to be present as a sulfate rather than a sulfite which is consistent with results reported by others (7). Sulfur trioxide being a strong Lewis acid will react with the ammonia that is present. At the injection temperature of 700°F the likely compound to be formed will be ammonium hydrogen sulfate. Other possible ammonia-SO_3 compounds, such as ammonium sulfate, which would be favored at lower temperatures, dissociate at this temperature. Ammonium hydrogen sulfate has a dissociation temperature of 770°F but dissociation is not complete until 842°F is experienced (8). At 700°F ammonium hydrogen sulfate is above its melting point and therefore it must be in a liquid state and in equilibrium with its dissociation products (9).

TABLE 2. ESCA ANALYSIS FOR NITROGEN AND SULFUR
(PERCENT ELEMENTAL CONCENTRATION OF SURFACE)

Baghouse Hopper Ash	Nonconditioned		Conditioned	
	N	S	N	S
Falkirk	0.2	4.8	2.6	8.2
Big Brown	0.6	5.2	4.6	7.4
South Hallsville	0.4	6.4	3.7	7.6

TABLE 3. ESCA ANALYSIS FOR NITROGEN AND SULFUR OF SIZE FRACTIONATED BIG BROWN ASH
(PERCENT ELEMENTAL CONCENTRATION OF SURFACE)

Nonconditioned			Conditioned			Difference	
D_50 µm	N	S	D_50 µm	N	S	N	S
6.31	0.3	3.8	6.60	3.3	5.9	3.0	2.1
2.73	0.4	4.0	2.89	3.1	6.0	2.7	2.0
1.94	0.4	3.3	2.14	3.5	6.4	3.1	3.1
0.79	0.9	4.8	0.83	4.1	6.8	3.2	2.0
0.43	1.3	5.5	0.43	4.7	6.9	3.4	1.4
<0.43	1.2	5.3	<0.43	6.9	7.7	5.7	2.4

XRD analysis was completed on the size fractionated samples but only the multicyclone backup filters revealed any crystalline ammonia-sulfur species. Since XRD sensitivity is limited to concentrations of 5% or more it would be expected that these species would be detected only in the smallest particle sizes. At injection concentrations of 12 ppm SO_3 and 45 ppm ammonia XRD did not detect either ammonium hydrogen sulfate or ammonium sulfate. Therefore, if ammonium hydrogen sulfate was initially formed, further reactions must have taken place downstream as the flue gas cooled. XRD has tentatively identified triammonium hydrogen sulfate, ammonium iron (III) sulfate, and ammonium calcium sulfate depending on which fly ash was tested. These compounds could be products of ammonia compound reactions at temperatures lower than 400°F (9). When the concentration of ammonia and SO_3 was raised to 5 times the normal level XRD identified only ammonium sulfate. At these higher concentrations there may be enough excess ammonia to complete the reaction of ammonium hydrogen sulfate to ammonium sulfate once the flue gas temperature dropped below the dissociation temperature of ammonium sulfate. The exact chemical mechanisms occurring are complex and more laboratory study of the reactions of ammonia, SO_3, and fly ash at elevated temperatures needs to be completed.

When an ammonia balance was made on the system 33% of the inlet flue gas ammonia concentration of 45 ppm was unaccounted for. Ammonia that was deposited on the baghouse ash was determined by leaching with water the highly soluble ammonia and ammonia salts from the ash. This solution was then filtered and the filtrate analyzed for total ammonia. From the dust loading the concentration of ammonia deposited on the fly ash was found to be 14 ppm. The ammonia slip was determined by dissolving the ammonia in the exit flue gas stream in dilute sulfuric acid and analyzing the solution using a specific ion electrode. The slip measurement was calculated to be 16 ppm. This leaves 15 ppm ammonia not accounted for. It is possible that some catalytic reduction of the ammonia and NO_x to N_2 and water may have occurred. South Hallsville coal tested at UNDERC produced fly ash containing 15-25% iron (measured as Fe_2O_3) and it is known certain phases of Fe_2O_3 catalyze ammonia and NO_x at temperatures between 600° and 900°F (10).

A change in fly ash cohesiveness due to conditioning was observed. Data presented in Table 4 show the ash from all three coals increased in cohesiveness when SO_3 and ammonia was added to the flue gas. Cohesiveness of Falkirk ash increased by a factor of 5, Big Brown by 4 and South Hallsville by 1.5. To help verify this data samples of the nonconditioned and conditioned Big Brown ashes were sent to Southern Research Institute (SoRI) to determine cohesiveness using a shear cell method. This method also indicated a substantial increase in cohessiveness due to conditioning. Other nonconditioned ash samples sent to SoRI showed the same relative cohesiveness as that obtained at UNDERC, confirming the validity of the UNDERC test method.

Ash cohesiveness would be expected to affect the residual dust cake weight on the bags. If the ash is too "sticky" it may not be easily removed. On the other hand if the cohessiveness of the ash is increased while the adhesion to the fabric remains unchanged, bag cleaning may be easier since the dust would be removed in large agglomerates. At the end of the 50-hour tests, bag weights were measured just after shaking 3 of the 9 bags. The residual dust cake weights for the cleaned bags were reduced by about 50% for the conditioned test compared to the baseline. Although this reduced bag weight was observed for only one test result, the data indicates that the conditioned ash is more easily removed from the bags, which is consistent with the lower observed pressure drop. The reduced pressure drop at the end of the test may be the result of a lighter residual dust cake as well as increased permeability.

TABLE 4. COHESIVE STRENGTH OF FLY ASHES AS MEASURED BY UNDERC'S COHESIVE TEST METER

Coal Fly Ash	Breaking Force (lbs) x 10^{-2}	
	Nonconditioned	Conditioned
Beulah	52	NA*
Falkirk	4.4	23
Big Brown	5.5	21
South Hallsville	12	18

*Conditioning tests were not completed for Beulah lignite.

MECHANISMS

Pressure drop in a granular bed filter is related to bed parameters as given in Darcy's Law:

$$\Delta P = \frac{\mu V L}{K}$$

where: μ = gas viscosity
V = superficial gas velocity
L = bed depth
K = permeability

Since velocity and gas viscosity are constant, only a change in bed depth or permeability could account for the reduced pressure drop observed with flue gas conditioning. The inlet dust loading should not change substantially due to conditioning; therefore the bed depth would also not change significantly over similar time periods. Although a change in permeability may also cause a small increase in bed depth (e.g. a more porous dust cake would be thicker) the change in bed depth would be much less than the change in permeability.

The permeability term depends on properties such as particle size, bed porosity, and bed structure. Several researchers have attempted to relate permeability to these properties. Among these relationships, the Kozeny-Carman equation appears to be widely accepted at least for porosity values less than 0.7 (11, 12). The Kozeny-Carman equation is given as:

$$K = \frac{\epsilon^3}{k\ S_0\ (1-\epsilon)^2}$$

where: K = permeability
ϵ = dust cake porosity (void volume fraction)
k = constant depending on bed structure, $k \approx 2$ to 5
S_0 = specific surface

A small change in porosity, ϵ, can cause a significant change in permeability. For example, an increase in porosity from 0.45 to 0.55 would cause the permeability to increase by a factor of 2.73. Other properties remaining constant, the bed depth would also increase by a factor of 1.22 which would partially cancel the effect of increased permeability on pressure drop. However, the net effect from Darcy's Law would be a reduction in pressure drop of 55%. Therefore, a small change in dust cake porosity would be a likely explanation for the reduced pressure drop seen with flue gas conditioning.

The specific surface term in the Kozeny-Carman equation is primarily dependent on the particle size and to a lesser extent on arrangement structure. At the 700°F injection point of ammonia and SO_3 the fly ash particle size distribution has already been determined since the fusion temperature of all the major fly ash constituents is much higher than 700°F. Conditioning could affect the particle size distribution in two ways. An increase in submicron mass could result from formation of ammonium sulfate particles, and loose agglomerates could be formed in the duct upstream of the baghouse due to increased cohesiveness. An increase in submicron particles would, however, increase the specific surface lowering permeability which contradicts the observed effect. Also loose agglomerates may increase the measured mean particle size but likely would not reduce the specific surface since the loose agglomerates would be porous. Based on the above discussion it does not appear that the increase in permeability can be explained by a change in particle size distribution.

The other term in the Kozeny-Carman equation, k, which is dependent on bed structure, may be somewhat changed due to conditioning but the change, if any, would be related to porosity. A likely explanation for the observed reduction in pressure drop is that the conditioned ash forms a more porous dust cake which would increase the overall dust cake permeability. A more porous dust cake would result from an increase in ash cohesiveness since it would be less susceptible to packing and pore collapse.

There are two penetration mechanisms which could account for high emission levels for difficult to collect ashes. One possible mechanism which may be present with woven glass fabrics is pinhole penetration (13). Large pore openings in the weave are not bridged over as the dust cake builds up on the fabric resulting in pinholes in the dust cake through which gas velocity is high compared to the superficial face velocity. Particles that penetrate the fabric through pinholes are never collected since the pinhole size is much larger than the average particle size.

A second possible mechanism is penetration by seepage which refers to particles that were initially collected but eventually penetrate the fabric (14). For example, some seepage through a woven fabric is expected when a fabric strikes the cage after a cleaning pulse in pulse jet cleaning. This same effect may occur with shaker cleaning or even with reverse gas cleaning if the fabric snaps from the collapsed position to the expanded position when flow is reintroduced to a compartment. Seepage may also occur during normal filtration if pinhole plugs break loose or if ash is reentrained off the rear face of the dust cake.

The basic difference between direct penetration (such as through pinholes) and seepage is that in direct penetration particles are never collected while in seepage particles are initially collected but are reentrained in the exiting flue gas. With direct penetration it is expected that significant concentrations of submicron particles would be found at the baghouse outlet. With penetration strictly by seepage a proportionately lower concentration of nuclei-sized particles would be expected since the submicron particles would be attached to larger ones and would not easily be reentrained as separate particles (13).

Results for the nonconditioned tests show that high concentrations of submicron particles are present indicating that at least some of the emissions are by direct penetration. This is not surprising since the tests were started with new fabric and the ashes were low in cohesiveness making bridging of pinholes more difficult. A possible explanation for the reduced particulate emissions for the conditioned tests is that the increase in ash cohesiveness facilitates bridging large pores and thus minimizes pinhole penetration. It would also appear that an increase in ash cohesiveness would minimize penetration by seepage since particles collected would be held more firmly in place. A reduction in emissions was noted with a felted fabric with flue gas conditioning indicating that penetration by seepage was also reduced.

CONCLUSIONS

Although this study was exploratory in nature and presents relatively new data several conclusions can be made:

- Results clearly show enhanced particulate removal with SO_3 and ammonia conditioning. For the given coals, fabric, and cleaning cycle, conditioning is an effective means of reducing fine particulate emissions from a baghouse.

- For the given coals and test conditions, conditioning reduces pressure drop both during initial dust cake deposition and after initiating the cleaning cycle.

- Although the physical and chemical mechanisms are complex, surface deposition of an ammonia-SO_3 product and a resulting increase in fly ash cohesiveness partially explain the higher collection efficiency and lower pressure drop.

The work described in this paper was not funded by the U.S. Environmental Protection Agency and therefore the contents do not necessarily reflect the views of the Agency and no official endorsement should be inferred.

REFERENCES

1. Carr, R.C. and Smith, W.B. Fabric Filter Technology for Coal-Fired Power Plants, Part III: Performance of Full Scale Utility Baghouse. Journal of the Air Pollution Control Association. 34:3, 1984. pp. 281-293.

2. Sear, D.R. and Miller, S.J. Impact of Fly Ash Composition Upon Shaker Baghouse Efficiency. Paper 84-56.6 presented at the 77th Annual Meeting of the Air Pollution Control Association, San Francisco, California, June 24-29, 1984.

3. Miller, S.J. and Sears, D.R. The Influence of Coal-Specific Fly Ash Properties Upon Baghouse Performance: A Comparison of Two Extreme Examples. In: Proceedings of the 5th EPA/EPRI Symposium on the Transfer and Utilization of Particulate Control Technology Vol. 3. Kansas City, Missouri, 1984. p 22-1.

4. Miller, S.J. and Laudal, D.L. Particulate Removal Enhancement of a Fabric Filter using Flue Gas Conditioning. Paper presented at the Third EPRI Conference of Fabric Filter Technology for Coal-Fired Power Plants, Scottsdale, Arizona, Nov. 1985.

5. Miller, S.J. and Laudal, D.L. Real-Time Measurement of Respirable Particulate Emissions from a Fabric Filter. Paper presented at the International Symposium Workshop on Particulate and Multi-Phase Processes and 16th Annual Meeting of the Fine Particle Society with 1985 Particulate and Powder Technology Exhibition, Miami Beach, Florida, April 1985.

6. Miller, S.J. Particulate Characterization. Low-Rank Coal Research Under the UND/DOE Cooperative Agreement. Quarterly Technical Progress Report, DOE/FE/60181-1682. University of North Dakota Energy Research Center, Grand Forks, November 1984. p 7-1.

7. Spafford, R.B., Dismukes, E.G., and Dillon, H.K. Analysis of Thermal Decomposition Products of Flue Gas Conditioning Agents. EPA-600/7-79-1, U.S. Environmental Protection Agency, Cincinnati, Ohio, 1979.

8. Kiyoura, R. and Kale, U. Mechanisms, Kinetics and Equilibrium of Thermal Decomposition of Ammonium Sulfate. Ind. Eng. Chem. Process Des. Development 9:4, 1970. pp. 489-494.

9. Tu, K.W. and Kanapilly, G.M. Generation and Characterization of Submicron Ammonium Sulfate and Ammonium Hydrogen Sulfate Aerosols. Annual Report, Inhalation Toxicology Research Institute. 1977. pp. 273-279.

10. Weber, G.F. SO_x/NO_x Control. Low-Rank Coal Research Under the UND/DOE Cooperative Agreement. Quarterly Technical Progress Report, DOE/FE/60181-1531. University of North Dakota Energy Research Center, Grand Forks, January 1984. p 6-1.

11. Donovan, R.P. Fabric Filtration for Combustion Sources. Marcel Dekker, Inc. New York, 1985. pp. 150-193.

12. Billings, C.E. and Wilder, J. Handbook of Fabric Filter Technology, Vol. 1 Fabric Filter Systems Study. GCA-TR-70-17-6. GCA Corporation, Bedford, Massachusetts, December 1970. p 2-115.

13. Dennis, R., Cass, R.W., Cooper, D.W., Hall, R.R., Hampl, V., Klemm, H.A., Langley, J.E., and Stern, R.W. Filtration Model for Coal Fly Ash with Glass Fabrics. EPA-600/7-77-084. U.S. Environmental Protection Agency, Cincinnati, Ohio, 1977.

14. Leith, D. and Ellenbecker, M.S. Theory for Penetration in Pulse Jet Cleaned Filter Fabric. Journal of Air Pollution Control Association, 30:8 1980. pp. 877-891.

Session B-5: OPERATION AND MAINTENANCE

Robert P. Gehri, Chairman
Southern Company Services
Birmingham, AL

OPERATION AND MAINTENANCE EXPERIENCE AT HARRINGTON STATION

By: Wanda Hooks
Olon Plunk
Southwestern Public Service Company
Amarillo, Texas 79170

Dale L. Harmon
Environmental Protection Agency
Air and Energy Engineering Research Laboratory
Research Triangle Park, NC 27711

ABSTRACT

Operation and maintenance of a shake/deflate baghouse controlling flyash emissions in a 360 MW coal-fired plant are discussed. Cost data on the various systems are provided. Discussion of bag life is also presented.

This paper has been reviewed in accordance with the U.S. Environmental Protection Agency's peer and administrative review policies and approved for presentation and publication.

I. INTRODUCTION

In 1977, SPS, under contract to the Environmental Protection Agency, began preparations to test a shake/deflate baghouse on a western subbituminous coal-fired plant. A part of the contract was to determine the operating and maintenance cost associated with the operation of the baghouse.

SPS is an electric utility based in Amarillo, Texas. The Company provides electricity to a 52,000 mi^2* service area. Traditionally a gas-fired utility, SPS began its switch to coal-fired generation in 1976 when Harrington Station Unit 1 was placed into service. Harrington Station is located 5 miles north of Amarillo. The facility consists of three units each with an electrical output of approximately 360 MW. Unit 2, in 1978 was the first new large electric utility boiler to be equipped with a fabric filter system for emission control. The boiler utilizes pulverized, low sulfur western coal to produce 2.688×10^6 lb of steam per hour (see Table 1 for fuel analysis). Flue gas from the boiler flows through the preheater directly through the fabric filter system and then to the stack (see Figure 1).

II. BAGHOUSE DESCRIPTION

The fabric filter system (or baghouse) actually consists of two Wheelabrator-Frye Inc. (WFI) structural baghouses with shake/deflate cleaning. Each baghouse consists of 14 compartments with 204 bags per compartment for a total of 5,712 bags; each bag is 11.5 in. in diameter and 30.5 ft long before tensioning. The baghouse was specified at 1.65×10^6 acfm of flue gas at 313°F, thus yielding a design air/to/cloth ratio of 3.17 to 1 (gross) or 3.4 to 1 (net) (see Table 2). Located adjacent to Harrington Unit 2 is Harrington Unit 3. Harrington Unit 3 is also equipped with a WFI fabric filter which also employs shake/deflate cleaning. The Unit 3 baghouse, however, has four additional compartments which yield air/to/cloth ratios of 2.78 to 1 (gross) and 2.98 to 1 (net). These baghouses allow these two units to operate with subbituminous western coal with no visible emissions at the stack.

III. DESCRIPTION OF SYSTEMS

For purposes of describing the installation, the baghouse is divided into the following operating systems: damper, deflation air, shaker, and bag.

---

* Readers more familiar with metric units are asked to use the conversion factors at the end of this paper.

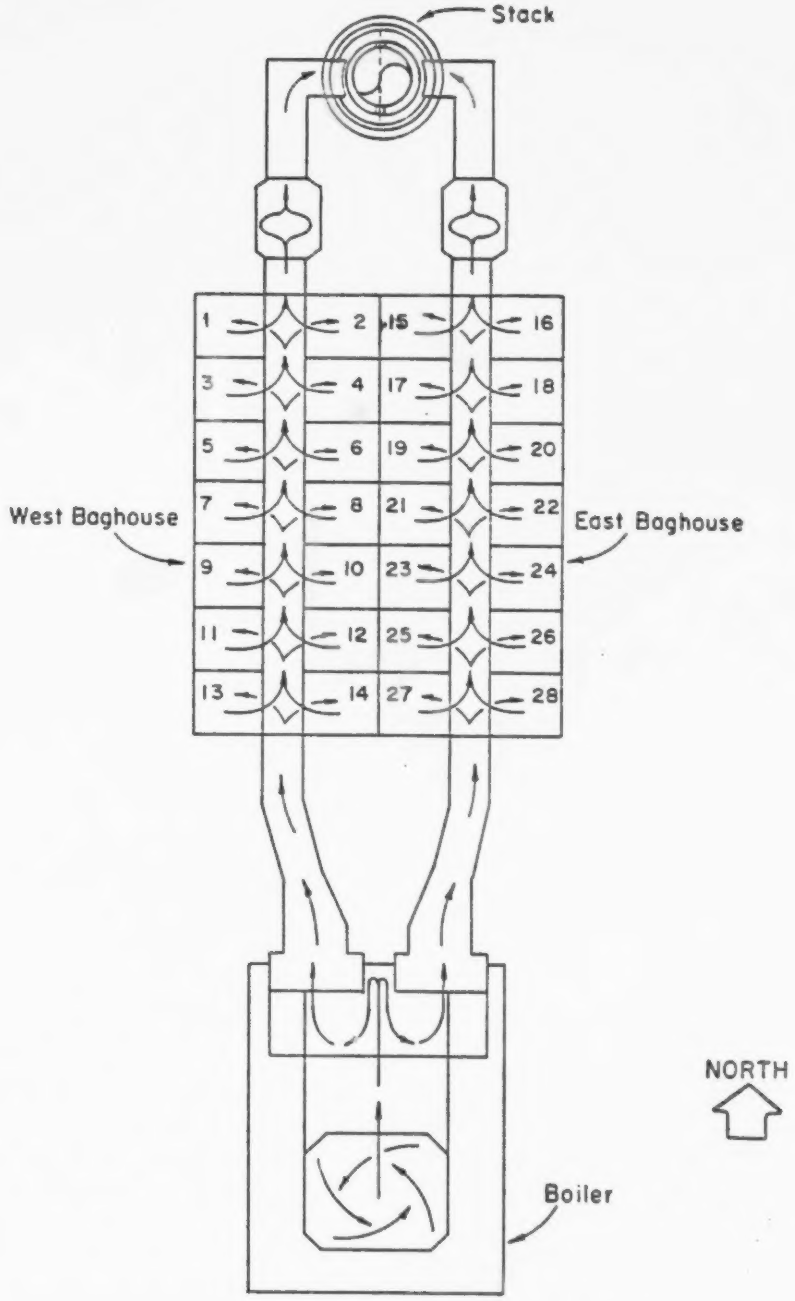
Stack
1
2
15
16
3
4
17
18
5
6
19
20
7
8
21
22
West Baghouse
East Baghouse
9
10
23
24
11
12
25
26
13
14
27
28
NORTH
Boiler

Figure 1. Harrington Unit 2 flue gas flow diagram.

A. Damper System

Six varieties of dampers are involved in the baghouse system. All dampers are poppet except the inlet. The inlet is a manual chain-driven butterfly. The various dampers with descriptions are presented in Table 3.

a. Bypass Damper

Each baghouse is equipped with a bypass damper to allow flue gases to be bypassed when burning natural gas during system start-ups, shutdowns, or other system requirements.

b. Deflation Damper

Each compartment is equipped with a 30-in. deflation poppet. The deflation cycle allows the compartment pressure to be slightly negative to prevent dirty gas flow during cleaning. Care must be taken during deflation to ensure that reverse gas does not flow sufficiently to pressurize or pancake the bag.

c. Outlet Damper

Each compartment is equipped with a 70-in. poppet outlet damper. The purpose of the outlet damper is twofold: it stops gas flow by closing during the cleaning mode, and it prevents gas flow during compartment isolation to allow personnel inside the compartment for maintenance.

d. Recirculation Damper

Each baghouse is equipped with a 12-in. recirculation poppet damper on the south end of the deflation duct. The recirculation damper allows deflation air to return to the outlet duct when compartmental deflation is complete. Closing during compartmental deflation allows deflation air to go into the compartment to the clean side of the bags for proper deflation.

e. Reinflation Damper

Each compartment of the baghouse contains a 12-in. reinflation poppet damper. The reinflation damper is a mini-outlet damper which allows the compartment to re-establish flow after the cleaning cycle without popping the bags when the main outlet damper opens. Reinflation prevents excessive wear on the bags when a compartment is returned to service.

f. Inlet Damper

Each compartment contains a 60-in. manually (chain) operated inlet butterfly damper. When open, the inlet damper allows dirty flue gas to enter through the ash hoppers just below the cell plate. This damper is closed when the compartment is isolated from service for maintenance. This compartment isolation is essential for safe access of personnel into the compartment.

B. Deflation Air System

Each baghouse contains a deflation air system. Even though its purpose is quite different, the deflation system on a shaker baghouse is similar to the design of a reverse air system on a reverse air baghouse. Gas is withdrawn from the clean gas outlet duct in front of the I.D. fan and discharged into a manifold with dampers to each compartment. Each system consists of a deflation fan and fan drive. This provides a clean hot source to deflate each bag before cleaning.

Bags can be cleaned only with careful control of the deflation system. To get proper control, it has been necessary to make changes in the transmitter ranges. Originally the transmitter range was set up for -5 in. water to 0 in. water. The control is presently set with a range of -1 in. water to +1 in. water. Additionally, the transmitter taps have been placed on a monthly preventive maintenance schedule. Originally the transmitter taps had problems with condensation and some ash pluggage. The transmitter system supply lines were black iron. Due to problems with corrosion and scaling, the black iron has been changed to PVC. This change and monthly inspection have minimized problems with the taps.

Another operational change that has improved the deflation system has been simply the cleaning cycle pattern. Originally the baghouse cleaned in an X pattern. This has been changed to a circular pattern, which allows the controller to adjust as the cleaning cycle moves closer to or away from the deflation air source. This change has made deflation much more consistent by giving better control.

C. Shaker System

The shaker system consists of a 5 hp 900 rpm motor attached to a drive to shake the 12 shaker tubes inside each compartment. Each shaker tube supports 17 bags with a J hook assembly. The philosophy of operating the cleaning cycle has changed several times since June 1978. The changes have been from one extreme to the other. At one time, in an effort to reduce pressure drop, the cleaning cycle was operated continuously. The philosophy was to clean as many times as possible during a 24 hour period. During this time, in an effort to clean the next compartment, the second outlet damper was closing before the previous compartment was back in service.
The cleaning cycle is now set so that the cleaning of a compart-

ment takes about 2.5 minutes. This allows one compartment to be back in service about 5 seconds before the next outlet damper closes. The first settle allows ample time to ensure that flow has stopped before deflation begins. The second settle allows time for the deflation damper to close before the shaker starts.

The philosophy regarding the rest (time between cleanings for a compartment) timers has also changed. The rest timers originally supplied with each baghouse only allowed 2.5 hours of rest between cleaning cycles. This was inadequate at low loads. Timers that allow rest up to 30 hours have been installed. The rest timers have been set at a 6 hour interval, but now are set at a 3 hour interval. The present philosophy is not to clean if the pressure drop is less than 5 in. or if it's been less than 3 hours since cleaning.

Shake time has also changed. Since 1978 the shake time has decreased from 20 to 5 seconds, in 5 second increments. Last summer, when operating at very high unit loads, the shake times were increased to 10 seconds. See Table 4 for the cleaning cycle setup.

D. Bag System

The Harrington Unit 2 bag system consists of 5,712 bags each of which is 30 ft. 8-3/4 in. long by 11.5 in. in diameter at 60 lb tension. The bags are arranged with a two bag reach. Each of the 28 compartments contains 204 bags. The preferred bag at this time is 10 oz 10 percent Teflon-coated fiberglass. In a shaker baghouse, the proper tension on the bags is of paramount importance. The tension as originally specified was 45 lb. This has been changed to 60 lb. This tension is checked at least annually during the unit outage for preventive maintenance. If a bag does not have proper tension, its bottom tends to blouse over the thimble causing excessive wear and premature failure. This also is detrimental to cleaning the bag.

When setting up a new compartment, the bags are installed and left overnight with the hopper heaters on to let the wrinkles fall out. The next day the bags are deliberately over-tensioned at 72 lb. After several weeks of operation, the tension is checked (normally it is found to be right on the 60 lb specification). Specific bag tensioning methods may vary with different fabrics.

a. Bag Life

The Harrington Unit 2 baghouse now contains bags that have been in service from 5 to 59 months. The bags with 59 months life are expected to give considerable additional life. It is of interest to note that the bags in Harrington Unit 3 were 68 months old on February 15, 1986. At Harrington, bag failure rate is counted in two ways:

total failure rate and actual failure rate. Of the 6,528 bags in Unit 3, a total of 198 have been replaced. This represents only 3 percent of the total bags. Total failure rate includes bags which have fallen, as well as mated failures, which were the result of a single blown bag which went undetected for a prolonged period of time. Actual failure rate does not include bags which were damaged as a result of mechanical failure or as the result of human error. There have been 111 actual bag failures on Unit 3, for a failure rate of 1.7 percent. These bags are expected to last at least another year. Similar bag life is expected on Unit 2. Individual compartment bags generally are replaced when the compartment reaches 10 percent actual failure.

b. Bag Failure Detection

A single blown bag can be detected in a compartment by using the stack opacity monitor. To detect a blown bag the opacity is observed as the compartment is removed from service. If the opacity drops by as little as 2 percent when the outlet damper closes and increases when the compartment comes back into service, there is a strong possibility of a bag failure. As soon as a blown bag is isolated to an individual compartment, it is removed from service and inspected for bag failures. The entire compartment is inspected from both the top and the bottom. The bag failure is recorded on a dustube failure log (see Figure 2). These logs are filed by compartment so that a complete record of all failures is available at all times.

c. Bag Specification

Harrington has a written bag specification. All bags ordered are within this specification. All vendor exceptions to the specification must be submitted in writing with the written quote.

IV. OPERATIONS

A. Manpower Requirements

At Harrington, one "B" operator is assigned to the baghouse 4 hours during each 8 hour shift. Various pieces of equipment are checked at 1, 4, 8, and 24 hour intervals. Table 5 lists the equipment inspected and their schedules. In addition to the "B" operator, a foreman allocates 2 hours of each 8 hour shift to the baghouse facility.

Page ________ of ________

HARRINGTON STATION
FABRIC FILTER SYSTEM
DUSTUBE FAILURE LOG

Unit No. ______

Compartment No. ______

No. Faulty Dustubes ________

Date of Inspection ________________

Inspector ____________________

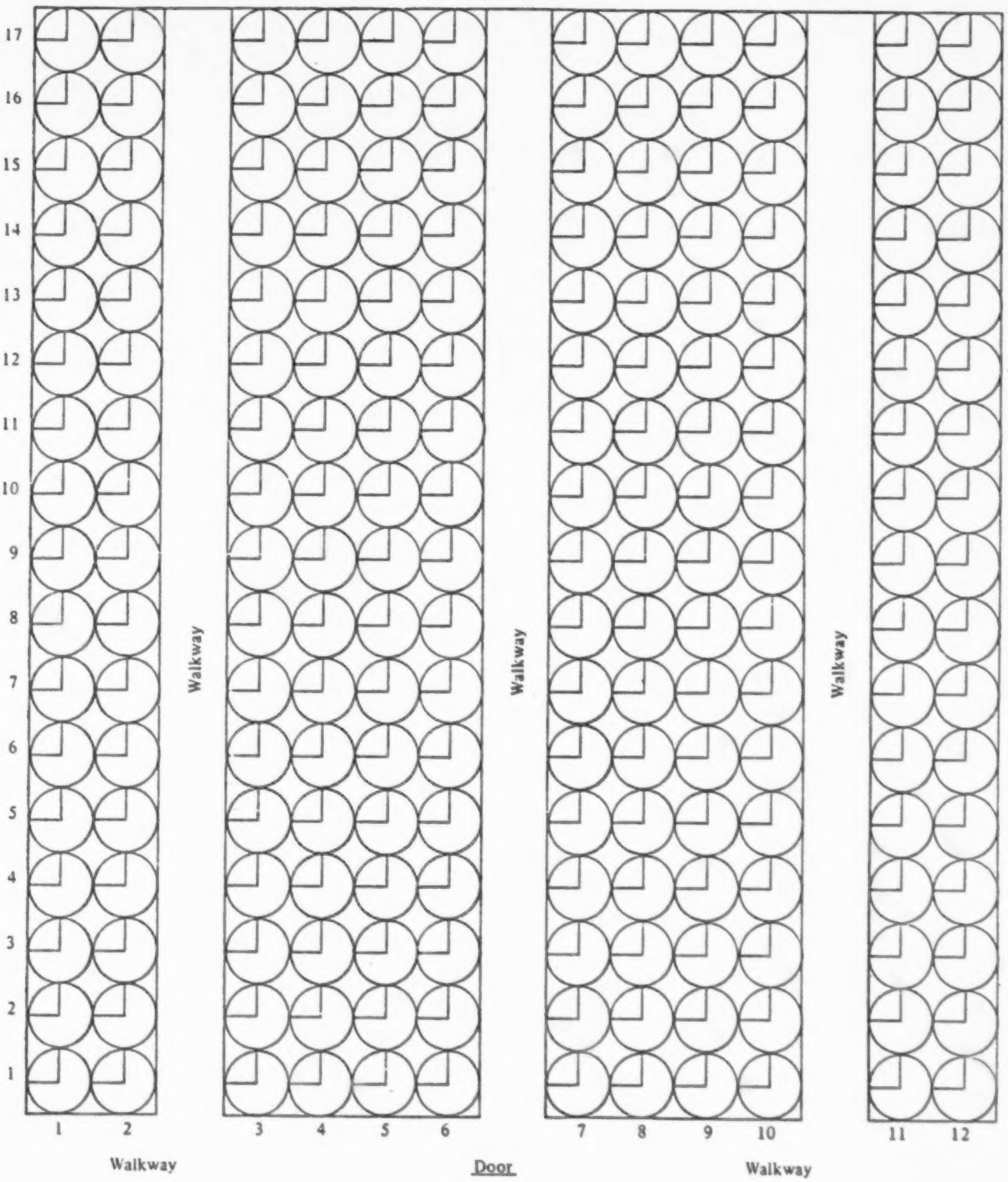
17
16
15
14
13
12
11
10
9
8
7
6
5
4
3
2
1
Walkway
Walkway
Walkway
1
2
3
4
5
6
7
8
9
10
11
12
Walkway
Door
Walkway

Figure 2. Dustube failure log.

CODE FOR LOCATION OF DUSTUBE FAILURE

Compartment No. ________________

1. Lower cuff
2. Seam
3. Upper cuff
4. Lower 1/3 fabric
5. Middle 1/3 fabric
6. Upper 1/3 fabric

Shaded Red – bag has been tied off

ADDITIONAL INFORMATION

DATE	BAG NO.	REMARKS

Figure 3. Code for location of Dustube failure.

B. Training

Prior to operating the baghouse, each operator attends a formal 8 hour baghouse training session followed by 5 to 6 weeks of hands-on training under the supervision of a qualified operator. Operators trained in troubleshooting are valuable assets.

C. Safety

Safety is an essential part of the baghouse training program. Prior to removing shakers, damper drives, deflation fans, or compartments out of service for maintenance, a hold card procedure must be complied with. This procedure includes a vital device hold card with a lock and a group of related hold cards. Additionally mechanical safeguards have been installed on all compartment doors to prevent trapping personnel in a compartment.

V. MECHANICAL MODIFICATIONS

A. Damper Drives

All of the outlet damper drive jackscrews have been replaced due to a factory machining problem. The new jackscrews were replaced by the original vendor at no cost. Since the jackscrews were replaced, problems have been minimal with the damper drives.

B. Shakers

During the first few months of operation, numerous failures occurred with the shaker system. Modifications by Harrington personnel have corrected the cause of these failures. During the past several years the baghouse has experienced only an occasional shaker failure.

a. Eccentric Bearings

The eccentric bearing system has been modified since original installation. The original design allowed the bearing to move until the bolts pulled out during the shake cycle. Some chocks and a pillow bearing were installed to eliminate this problem.

b. Flangette Bearings

The original shaker tube shaft flangette bearings began to fail after 1 year. The bearing was not capable of withstanding the high temperatures. The bearing was installed inside the compartment wall. The high negative pressure of the compartment pulled the grease from the bearing. These bearings were replaced with pillow block bearings spaced off the compartment wall to allow for cooling. These were secured with fine threaded double nuts to prevent failures.

c. During the first couple of years the shaker tube support steel began to sag. Turnbuckles were installed to pull the I-beam back into place to support the shaker tubes.

d. Catcher Bars

During the third year of operation, Harrington Unit 2 experienced a shaker tube fall in a compartment. To prevent a recurrence, angle iron shake tube catchers were installed just beneath each shaker tube. These catchers help to hold the shaker tubes in place if the shaker tube shafts fail.

VI. MAINTENANCE

A. Preventive Maintenance

A regular program of preventive maintenance can reduce the possibility of catastrophic failures.

a. Monthly Shaker Inspections

In addition to the routine inspections conducted by operating personnel, maintenance personnel inspect each of the 28 shaking mechanisms in operation monthly. This inspection helps detect problems that are not obvious while the shakers are idle. Maintenance requests are prepared for any problems found, and the defects are repaired.

b. Quarterly Damper Drive Inspections

Quarterly, maintenance personnel inspect each of the dampers in operation. They also check for packing leaks; defects are repaired.

c. Presently on these shaker baghouses at Harrington, we cannot identify any particular area of high maintenance. This is reflected in the operations and maintenance cost shown in Table 6.

VII. OPERATION AND MAINTENANCE COSTS

The maintenance procedures implemented at Harrington Station by SPS have resulted in a process that allows accurate accounting of the maintenance costs associated with various pieces of equipment. Prior to any maintenance being performed, a written maintenance request is prepared and is ultimately entered into a data base with the equipment and manhours required for repairs. As a result, the maintenance cost at Harrington Unit 2 has been captured. These costs have been defined for the major components of the fabric filter system. The material cost has been totaled for the shakers, dampers, bags, and miscellaneous items. The maintenance labor has been accounted for as actually charged to each maintenance job. This is because some of the replacement parts are machined at the plant rather than purchased from a supplier, and because the regularly scheduled monthly and quarterly inspections are conducted by maintenance personnel. This cost is charged as labor rather than material. The operator time is not captured direct but is allocated due to the various tasks associated with different pieces of equipment. These costs are presented in Table 6. All salary and maintenance material costs have been increased by the appropriate percentage to account for overhead. Because there has not been a complete bag replacement during the last 4 years, the bag costs have been annualized assuming a 6 year bag life. Based on experience at Harrington Units 2 and 3, this is not unreasonable; in fact, 6 years may be too short a life.

Table 6 shows that the highest cost component of operating and maintaining the fabric filter is the energy cost to pull the flue gas through the filter system. The energy costs have been calculated based on average load, pressure drop, and fan characteristics. The cost for energy to operate the system is based upon SPS's average system fuel cost.

VIII. SUMMARY

Operating and maintenance costs at Harrington Unit 2 during the past 4 years have not been excessive. Preventive maintenance helps alleviate massive failures. No particular item at this time stands out as being a maintenance problem. Bag life appears to be well under control and is expected to exceed 6 years.

Future programs to minimize operating and maintenance costs should be directed at minimizing pressure drop. This is the highest operation and maintenance component, and reducing its cost should be challenging.

METRIC EQUIVALENTS

Readers more familiar with metric units may use the following to convert to that system.

Non-metric	Times	Yields Metric
acfm	4.719×10^{-4}	am^3/s
Btu/lb	2.32×10^{3}	J/kg
^oF	$(^oF-32)(1.8)$	^oC
ft	0.3048	m
hp	7.46×10^{2}	W
in.	2.54	cm
lb	0.454	kg
lb/hr	1.21×10^{-4}	kg/s
mi	1.61×10^{3}	m
mi^2	2.59×10^{6}	m^2
oz	28.3	g
psi	6.89×10^{3}	Pa

TABLE 1

SOUTHWESTERN PUBLIC SERVICE
HARRINGTON STATION
COAL ANALYSIS

PROXIMATE ANALYSIS

	As Received	Dry Basis
Moisture,%	26.98	XXXXX
Ash,%	4.94	6.77
Volatile,%	31.15	42.66
Fixed Carbon,%	36.93	50.57
	100.00	100.00
Btu/lb	8,802	12,054
Sulfur,%	0.31	0.39

TABLE 2

SOUTHWESTERN PUBLIC SERVICE
HARRINGTON STATION
BAGHOUSE SPECIFICATIONS

UNIT 2

Wheelabrator Frye-Inc.

Shake/Deflate

28 Compartments

204 Bags per Compartment

5,712 Bags

11.5 in. Dia. x 30 ft 8 3/4 in. Long
@ 60 lb Tension

1.65 x 10^6 acfm

313 ^{o}F Design

3.17 to 1 Gross A/C

3.40 to 1 Net A/C

TABLE 3
BAGHOUSE DAMPERS

Damper	Size, in.	Number	Drive	HP	RPM	Type
Bypass dampers	68	4/baghouse	Motor	3	180	Poppet
Deflation dampers	30	1/compartment	Motor	2	1200	Poppet
Outlet dampers	70	1/compartment	Motor	3	1800	Poppet
Recirculation dampers	12	1/baghouse	Motor	1	1200	Poppet
Reinflation dampers	12	1/compartment	Motor	1	1200	Poppet
Inlet dampers	60	1/compartment	Manual	-	-	Butterfly

TABLE 4

HARRINGTON UNIT 2
CLEANING CYCLE[a]

Mode	Time, Seconds	Description
Interval Between Compartments	45	Allows compartment previously cleaned time to get back into service.
Outlet Damper Full Travel	20	Travel time for outlet and reinflation dampers which start to drive closed at the same time.
1st Settle	20	Null
Deflation	40	Time for deflation damper to open and deflate bags before cleaning.
2nd Settle	20	Null to allow time for deflation damper to close before the shake.
Shake	10	Bags shake to dislodge dust.

---

[a] Total compartment cleaning time: 2 minutes, 35 seconds.

36 minutes, 10 seconds to clean half a baghouse.

TABLE 5

BAGHOUSE EQUIPMENT INSPECTION

HOURLY

1. Annunciator panel.
2. Temperature (Inlet Unit 2) (Inlet & Outlet Unit 3)
3. Δ P's (recorder)
4. Flyash recorder and system.
5. Opacity.
6. Gas Flow (Unit 2 only)
7. Check all recorders for paper and ink.
8. Deflation ------ Range 0.1 to 0.3 in.

TWICE PER SHIFT

1. Shakers
   a. Eccentrics
   b. Eccentric clevis pins, along with clips or keys.
   c. Clevis pins, along with clips or keys.
   d. Limit switches.
   e. Shaker tube or pillow bearings.
2. Deflation fans.
3. Deflation fan outlet damper control arms.
4. Hopper heaters.

ONCE PER SHIFT OR AS OFTEN AS NEEDED

1. Flyash silo.
2. Flyash hoppers.

MIDNIGHT

1. Check all recorders for correct time and stamp with the proper date.

TABLE 6
HARRINGTON UNIT 2
MAINTAINENCE COSTS[a]

Item	1985	1984	1983	1982
Shakers	0.002	0.002	0.008	0.002
Dampers	0.001	0.001	0.002	0.003
Bags	0.023	0.022	0.026	0.029
Miscellaneous Material	0.003	0.003	0.004	0.001
Maintenance Labor	0.027	0.020	0.018	0.043
Operating Labor	0.046	0.042	0.048	0.050
Energy	0.054	0.071	0.074	0.069
Subtotal (Excludes Energy)	0.102	0.090	0.106	0.128
TOTAL	0.156	0.161	0.180	0.197

a. NOTES

1. All costs are in mill/kWh.
2. All salary and material costs are adjusted for overheads.
3. Energy is based on average pressure drop, load, and system fuel costs.
4. Bag costs are annualized based on 6 year bag life.

Computer Monitoring of Pilot Plant Baghouse Performance

by

A.S. Viner and L.M. Fickel
Research Triangle Institute
Research Triangle Park, NC

and

L.S. Hovis
Air and Energy Engineering Research Laboratory
U.S. Environmental Protection Agency
Research Triangle Park, NC

Abstract

A computerized monitoring system was installed on a pilot plant baghouse to permit unattended operation of the unit. Sensors were installed to measure inlet and outlet gas temperatures, pressure drops across flow orifices, tubesheet pressure drops, and electrical conditions in an electrostatically augmented compartment. The signal lines from these sensors were connected to a programmable datalogger which also served as the interface to a microcomputer. Data were recorded on the data logger and stored on a fixed disk in the microcomputer. A modem coupled with computer software allowed researchers to call the microcomputer from long distance and collect data daily. Once retrieved, the data were quickly analyzed to evaluate performance and to identify any problems in operation. In addition, the datalogger could be reprogrammed through the phone link. The strip chart from the datalogger served as a backup of the data recorded on the microcomputer disk.

The system worked very well for the duration of the project with the exception of a few minor problems. Daily analysis of the data permitted timely evaluation of the progress of the experiments and the status of equipment. The goal of unattended operation was achieved and would not have been possible without this system. A possible enhancement would be the addition of a relay board to the datalogger, thereby permitting a limited amount of remote control over process variables.

This paper has been reviewed in accordance with the U.S. Environmental Protection Agency's peer and administrative review policies and approved for presentation and publication.

INTRODUCTION

Baghouses have been widely accepted in the electric utility industry ever since the first was installed on a coal-fired boiler over a decade ago. Compared with electrostatic precipitators, which have been in use in utilities for decades, baghouses are still in their infancy. There is great potential for the improvement of baghouse design and operation to reduce both capital and operating costs. Two ideas that have been proposed for improved baghouse operation are Advanced Electrostatic Fabric Filtration (Advanced ESFF), and the top-inlet design. Both of these designs have been tested on a small scale and found to lower the pressure drop associated with dust cake buildup on fabric filters (1). Based on those promising results, the U.S. Environmental Protection Agency, in conjunction with the U.S. Navy, established a pilot program to evaluate these new designs on a pilot scale baghouse.

There were two constraints that affected the design of this pilot program: time and money. The amount of time available for the project was fixed by the 1 year availability of the site. The funding available for the project precluded the possibility of maintaining an operator on-site every day. A unique combination of baghouse monitoring hardware was assembled to meet the goals of the program within these constraints. This paper describes how a system of Individual Bag Flow Monitors (IBFMs), in conjunction with a microcomputer-based data acquisition system, helped meet the goals of this program.

DESIGN OF THE PILOT PLANT

The fabric filter pilot plant at the Cherry Point Marine Corps Air Station in Havelock, North Carolina, was designed to filter flyash from a slipstream from two spreader-stoker-fired boilers. The boilers were rated at a maximum of 9.77 kg steam/s (77,500 lb/hr) with only one boiler operating at any given time during the test. The fuel was an eastern coal with 1 percent sulfur, 5 percent water, and a heat content of 31,600 kJ/kg (13,600 Btu/lb). Since the flyash had a high unburned content of carbon, its electrical conductivity was relatively high for a coal ash.

The pilot plant had identical baghouse compartments located side by side with a test trailer nearby. Each compartment was fitted with woven glass bags that were 7.3 m long and 0.2 m in diameter. Each compartment was serviced by a separate fan with a capacity of 19.82 m^3/min (700 ft^3/min) of gas drawn from a common duct. The duct pulled gas from the inlet of the electrostatic precipitators which were downstream of each boiler. In the event of one of the boilers being taken off line, it was possible to close the inlet ducts. One reverse-air fan provided the ambient air necessary for cleaning the two compartments, and the dust was deposited in large barrels below each hopper. Plant personnel emptied the ash barrels three times each week.

In designing the pilot plant, the central problem was how to test three types of filtration--advanced ESFF, top-inlet, and conventional bottom-inlet--in only two compartments. This had to be accomplished while maximizing the amount of run time for each condition. The decision was made to use a set of individual bag-flow monitors (IBFMs) to permit the simultaneous operation of the advanced ESFF and conventional filtration (which are both bottom-inlet designs) in the same compartment. This meant that the second compartment could be devoted to testing the top-inlet design. Therefore, the top-inlet compartment did not require the use of an IBFM system.

An IBFM consists of a calibrated orifice plate at the inlet of the bag (on top of the compartment tubesheet). The pressure drop across the orifice is measured with pressure taps on the upstream and downstream sides of each plate. The flow into each bag can be calculated from the data on the pressure drop, temperature of the gas, and the orifice calibration. Once the data on the tubesheet pressure drop and inlet dust concentration are obtained, the dust cake's specific resistance and residual drag can be calculated. In this way, it was possible to monitor the performance of individual bags and compare the performance of the conventional (non-electrified) bags with that of the electrostatically enhanced bags. In addition, the performance of the top-inlet compartment could be compared with that of the conventional bags.

DATA ACQUISITION AND ANALYSIS

Data Acquisition System

The pilot program was designed with a simple test plan that did not require frequent adjustment of the hardware. This eliminated the necessity of having an operator on-site at all times. The absence of on-site personnel had important implications for data collection and analysis. Most importantly, it was essential to have ready access to the data so as to monitor the baghouse operation. In addition, it was desirable to analyze the data as quickly as possible to get experimental results. Given these considerations, the most logical approach to gathering the data was to create an automatic data acquisition and retrieval system. The system had to be easy to assemble, easy to service, and inexpensive. The best way to meet these needs was with an off-the-shelf system of hardware and software. Fortunately, these require- ments were easily met by combining a microcomputer and software with a programmable datalogger. A system was designed to automatically measure, record, and store on a computer the pressure, temperature, and electrical conditions. The flexibility of the microcomputer software made it possible to include the features necessary for long-distance retrieval of the recorded data. This data acquisition system offered a number of advantages, the most important being the elimination of labor costs associated with collecting and entering the data on a computer (and the associated potential transcription errors), and the long-distance retrieval of data. The ability to retrieve the data by telephone enabled off-site engineers to monitor the operation of the plant and analyze the data on a daily basis.

Data requirements included the gas inlet and outlet temperatures, tubesheet and orifice pressure drops, electrical conditions, and dust inlet loading. All of these conditions were measured electronically except the dust inlet loadings (which were measured with standard EPA Method 5 procedures). Temperatures were measured with Type K thermocouples fitted with electronic icepoints; tubesheet and orifice pressure drops with pressure transducers rated at 0 to 2.5 kPa; and the IBFM pressure drops with smaller transducers rated at -1.25 to 1.25 kPa. The voltage output from the electrode power supply was scaled from a range of 60 kV to a range of 6 V, and the electrode current to ground was measured directly. Electronically shielded cable was used to connect all of the signal lines to a Molytek Model 2702 programmable datalogger which had an RS-232 port. The Molytek fed data through this port to a Tandy 1200 microcomputer which contained two RS-232 ports, 640 Kbytes of memory, and a 10 Mbyte hard disk. An Anchor Automation Mark XII modem was used for outside communications. All of these devices were located inside the test trailer next to the baghouses. The microcomputer was protected from power failures by a SOLA Model SPS 800-A standby power supply. This system is illustrated in Figure 1.

At 10-minute intervals, the datalogger transmitted instantaneous readings to the microcomputer. The data transmission included the scaled output from all of the datalogger's 32 channels, as well as the date and time of the reading. The data was read into the microcomputer by custom-developed software and stored in a file according to the date. The multi-tasking feature of the Concurrent PC-DOS operating system made it possible to execute the data collection/storage program and a remote communications system simultaneously. The multi-user capability of the Concurrent system, in conjunction with the high-speed modem, enabled the off-site engineers to call the on-site computer and read data files from previous days. Once they had retrieved the information, the engineers read the data into a worksheet developed with the Lotus 1-2-3 program for analysis and plotting graphs.

Data Analysis

The one disadvantage of testing two different kinds of filtration (conventional and advanced ESFF) in the same compartment was that it ruled out the possibility of making an "on-the-spot" evaluation of peformance based on tube-sheet pressure drop. Thus, the data had to be analyzed before the results were known. This disadvantage, however, was far outweighed by the numerous advantages of the design.

The process of analyzing the data began with the widely accepted model of pressure drop behavior in fabric filters where it is assumed that the drag across the filter increases linearly with increasing dust load. This is expressed as:

$$S(t) = \frac{\Delta P}{V(t)} = S_e + K_2 W(t - t_{clean}) \tag{1}$$

where

$S(t)$ is the drag across the filter at time t

ΔP is the pressure loss across the dust on the filter

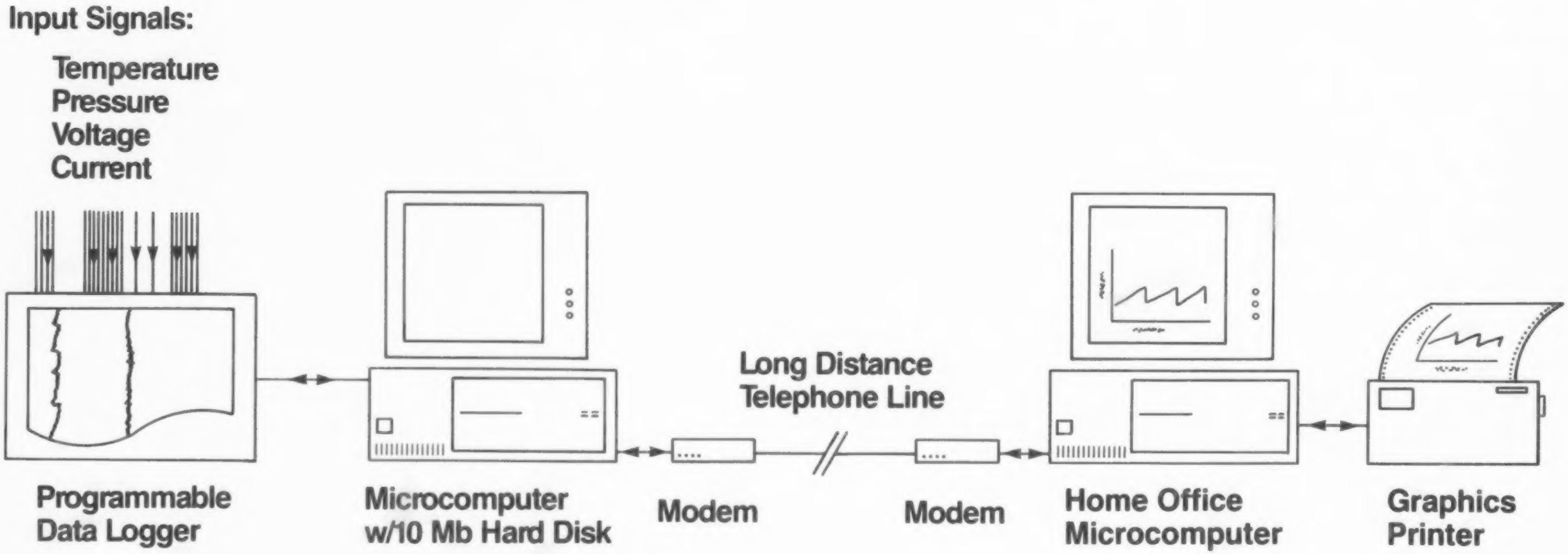
Input Signals:
Temperature
Pressure
Voltage
Current
Programmable
Data Logger
Microcomputer
w/10 Mb Hard Disk
Modem
Long Distance
Telephone Line
Modem
Home Office
Microcomputer
Graphics
Printer

Figure 1. Data acquisition system.

$V(t)$ is the filtration velocity at time t

S_e is the effective residual drag

K_2 is the specific resistance of the dust

$W(t-t_{clean})$ is the mass of dust deposited per filter area (since the most recent bag cleaning at time t_{clean}).

The areal dust load is a function of the rate at which the dust is deposited on the filter:

$$W(t-t_{clean}) = C_i \int_{t_{clean}}^{t} V(t)dt \tag{2}$$

where

C_i is the dust concentration at the inlet of the filter.

By measuring tubesheet pressure drop and individual bag face velocities as a function of time (with a given dust concentration), it was possible to calculate individual bag drags [S(t)] and dust loads [W(t)] and then use linear regression to estimate the specific resistance (K_2) and residual drag (S_e) for each of the conventional and ESFF bags. A similar analysis was performed on the data for the top-inlet compartment except that the total compartment flow was measured and used to calculate the face velocity through the bags. This calculation assumed that all of the bags in the top-inlet compartment performed in an identical fashion.

RESULTS

The pilot plant was installed over a period of 2 months in 1985 (February and March) and then was brought on-line in April. During April and May, the hardware was debugged. Data collection began in early June. Only minor problems were encountered during the installation of the data collection system, the most significant being a question of how to provide adequate ground protection for the transducer signals. This problem was solved with some experimentation. Once debugged, the system worked quite well, although there was one disturbing problem that occurred randomly (about once a month): on random occasions, the pilot plant microcomputer would not respond to commands from the home office computer. That is, the modem would answer an incoming phone call (an engineer calling for data). However, the microcomputer would not respond to commands. Although this problem hampered the data retrieval efforts, it did not seem to affect the collection and storage of data. Thus, while the data were being recorded on the computer, it was inaccessible at times. The only remedy for this problem was to physically reset the computer. This required someone to be on-site. The source of this problem was not clearly identified, but it is probable that it resulted from a bug in the communications system of the Concurrent PC-DOS software.

For the most part, the data acquisition system worked very well. Likewise, the IBFM system was an important part of the experimental design. An example of the data from the IBFM system is shown in Figure 2. The orifice pressure drops for four bags in the bottom-inlet compartment are shown as a function of time. The upper two curves correspond to the advanced ESFF bags, and the lower two curves correspond to the conventional filter bags. The compartment was operated with a 12-hour (720 minute) cleaning interval. This is reflected in the figure, which begins at time t=0 (just after cleaning). As the dust layer on the bags built up, the flow began to differentiate between the conventional bags and the ESFF bags. Gradually, the ESFF bags carried a higher and higher percentage of the overall flow (and therefore dust), due to the lower flow resistance of the dust cake on those bags. At the end of the filtration cycle, the forward flow was stopped, and the cleaning air was introduced into the compartment. This reverse flow of air is indicated by the sharp negative spike in the orifice pressure drop curves. When the compartment is returned to service, the orifice pressure drops reflect the flows indicative of "just-cleaned" filters.

When the data from Figure 2 are reduced to terms of drag and dust load (as indicated in equations (1) and (2)), the results in Figures 3 and 4 are obtained. These results show that the assumption of a linear relationship between drag and dust load (equation 1) is valid for these data. The straight line through the data is a regression fit, which can be used to obtain realistic estimates of the specific resistance (K_2) and residual drag (S_e) for the conventional and ESFF bags. These results indicate that the electrostatically enhanced filter bags had a much lower drag than the conventional bags and that the rate of increase was also much lower. These results are typical of the results obtained for the advanced ESFF filter. The economic implications are quite significant and are discussed elsewhere (2).

The other purpose of this pilot program was to evaluate the feasibility of top-inlet filtration. Unfortunately, the results from the top-inlet compartment were affected by two problems. First, there was a breakdown of the fan that supplied cleaning air to the compartment during part of the test program. Another problem developed when a loose wire on a solenoid valve caused one of the flow-control valves to act erratically. The former problem was easily detected from the data. The latter problem proved difficult to diagnose because it occurred only intermittently. In addition, the information received over the modem from the Tandy 1200 provided conflicting pictures of the status of the compartment. Data collected during the cleaning cycle seemed to indicate that there was a flow of cleaning air, but the tubesheet pressure drop continued to rise over a period of many cleaning cycles. Eventually it became clear that no cleaning was occurring. The problem was identified after a prolonged on-site observation of the cleaning sequence. The latter problem with the solenoid valve occurred over a significant portion of the test program and severely limited the amount of useful data available for the top-inlet compartment.

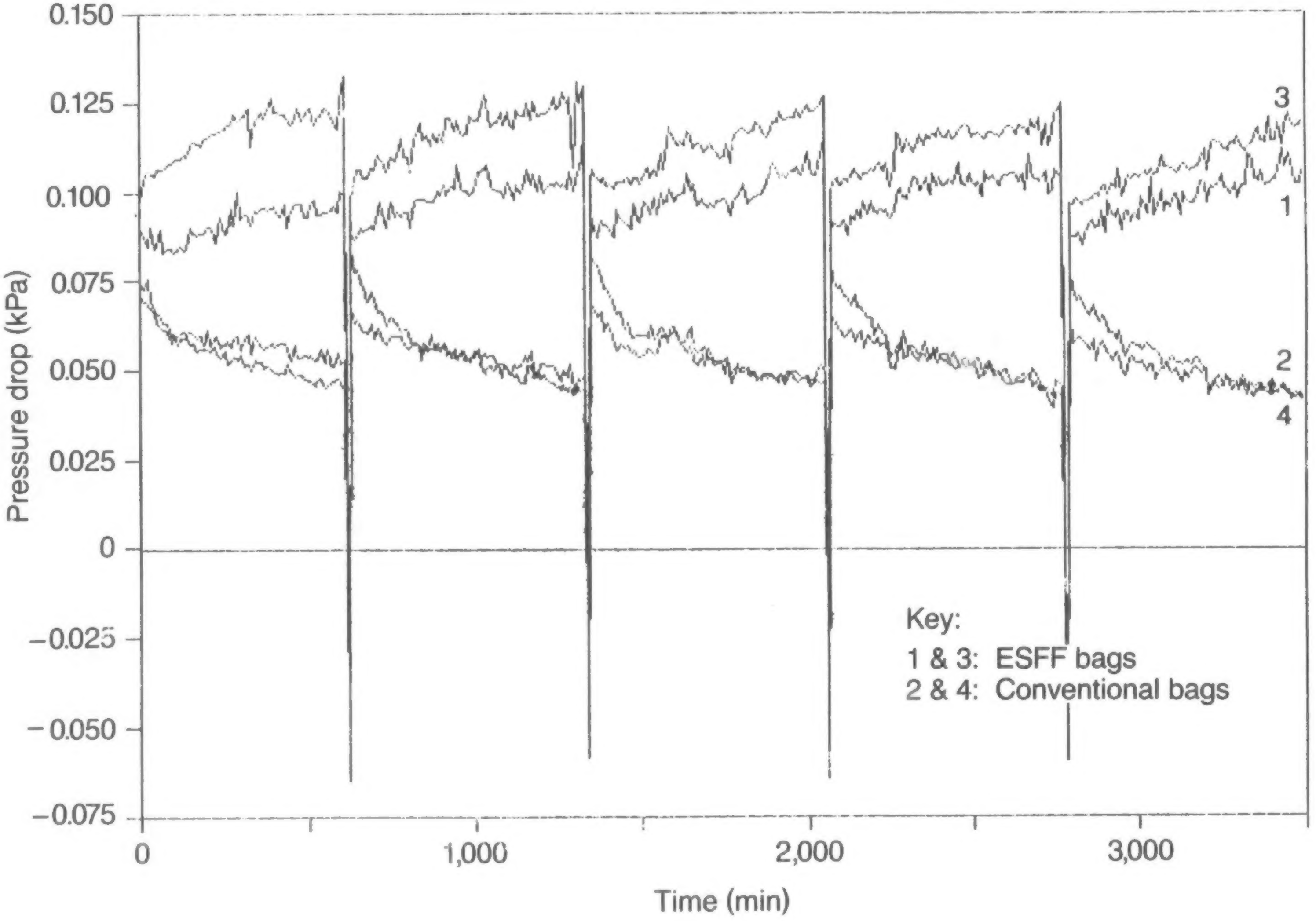

Figure 2. IBFM pressure drop curves: August 29 through August 31 (No. 126-130).

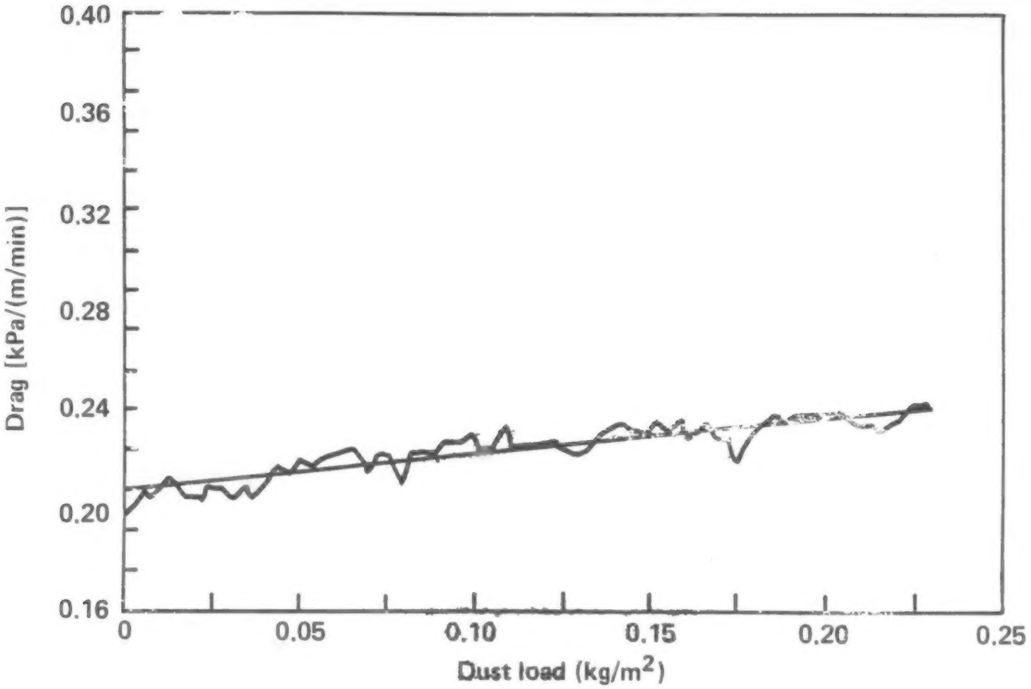

Figure 3. Drag correlation for bag No. 1 (ESFF).

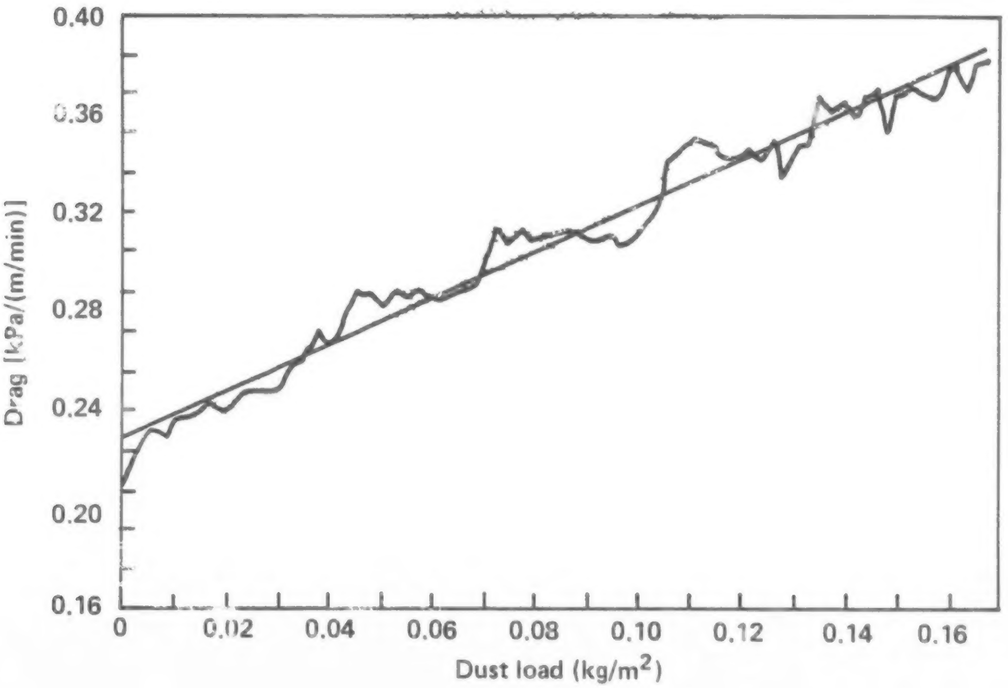

Figure 4. Drag correlation for bag No. 2 (conventional).

CONCLUSIONS AND RECOMMENDATIONS

The IBFM system worked very well. This system made it possible to use both the ESFF and conventional bags in the single compartment while providing more detailed information than would have been obtained from dual compartments without IBFMs. Also, by combining advanced ESFF and conventional bags in a single compartment, the second compartment was available to test the top-inlet design. The data analysis required for the IBFM data was simple and easily accomplished on a microcomputer. The linear drag-dust load model was a proper description of the data.

The automated data acquisition and analysis system also worked well, permitting the plant to run for days at a time without an on-site operator. However, the need for on-site inspection was never entirely eliminated. Random events, such as boiler outages and power failures, required that an operator visit the plant on a regular basis. Another important conclusion drawn from this project was that assembling a data acquisition and analysis system of this sort is a simple task. It is simply a matter of buying equipment that is commercially available and then assembling it with a minimum amount of programming.

Two recommendations can be made. First, more sensors should be used to provide information on the status of the system. Problems such as that which arose with the cleaning fan on the top-inlet compartment would have been more easily diagnosed if there had been sensors indicating the positions of important valves. In essence, the computer served as the "eyes and ears" of the project officer for a large part of the project. Therefore, a larger number of sensors will increase the reliability of the system.

A second recommendation is to expand the capability of the system to permit some degree of remote control over experimental conditions. It is possible, for example, to incorporate a relay board into the Molytek data logger that can be programmed to trigger up to 16 different switches. It was demonstrated during the current work that the datalogger itself could be reprogrammed over long distance telephone lines. In the same way, it should be possible to modify experimental conditions over the phone. Of course, it would be necessary to verify the proper functioning of the relays (as indicated above). With this improvement, a sophisticated data acquisition and control system could be assembled to serve as the eyes, ears, and hands of an engineer back in the office.

References

1. Mosley, R.B., et al. Advanced Electrostatic Enhancement of Fabric Filtration. In: Proceedings of the Third EPRI Conference on Fabric Filter Technology for Coal-Fired Power Plants, Scottsdale, AZ, November 1985.

2. Hovis, L.S. and A.S. Viner. Economics of Advanced Electrostatic Stimulation of Fabric Filtration. In: Proceedings of the Sixth Symposium on the Transfer and Utilization of Particulate Control Technology, New Orleans, LA, February 1986.

THE DESIGN OF REPAIRS TO UPGRADE 10-YEAR-OLD INDUSTRIAL PRECIPITATORS

by: Vincent L. Kunzweiler, P.E.
Joseph B. Landwehr, P.E.
Burns & McDonnell Engineering Co.
P.O. Box 173
Kansas City, MO 64141

ABSTRACT

This paper will discuss the design of precipitator repairs and upgrade for two 1976 model industrial size precipitators on two 236,000 lb/hr, 450 psig pulverized coal boilers.

Prior to our inspection and design of repairs, both units were seriously derated due to noncompliance with emission regulations.

Problems encountered as well as specific parts failures will be discussed. Some of the specific problems that will be examined include the failure of rapper rods, rapper assemblies, wires and wire weights, insulators, and insulator housings.

INTRODUCTION

This project resulted from a contract to do an emissions test on No. 2 boiler stack (Powerhouse No. 1). at the Army Sunflower Ammunition plant located in Desoto, Kansas. The test was commissioned by Hercules Aerospace Division, the operating contractor. Powerhouse No. 1 has two units, both of which are designed for dual fuel utilization, being capable of operation on either oil or coal. Both units had been run for the most part on oil. It was the Army's desire to go to all coal firing that necessitated the need for testing. The operation on coal firing was so poor that the stack test had to be abandoned. Opacity was running higher than the 50 percent level.

The boilers were designed to burn pulverized coal, and were fabricated by Combustion Engineering. Installation took place in 1941. The boilers were refurbished in the 1970s, and retrofitted with precipitators in 1976 and 1977. The precipitators were manufactured by Precipitair Pollution Control Company of Longview, Texas, and are the weighted wire type, with 3-9 ft fields designed for the following conditions:

1. Flue Gas Volume	125,450 ACFM
2. Temperature	750 degrees F
3. Inlet Dust Loading	3.32 gr/ACF max.
4. Excess Air	0-25 percent

5. Coal Range:	
a. Moisture	5-15 percent
b. Volatiles	35-55 percent
c. Ash	15 percent
d. Sulfur	0.5 to 3.6 percent
e. Btu (dry)	10,500 to 13,500 per lb
6. Removal Efficiency	99.85 percent
7. Outlet Grain Loading	0.005 gr/ACFM
8. Gas Velocity	3.22 ft/sec
9. SCA	433 sq ft/1,000 ACFM

PRECIPITATOR INSPECTION

Following the aborted stack test, Burns & McDonnell was selected to investigate the problem or problems and come up with a solution.

The initial step in the investigation was to perform a detailed internal inspection of each of the two precipitators. This inspection identified some structural failures involving the collecting plate support system as well as other mechanical failures. In the Unit No. 1 precipitator only the first field had any chance of working. The plate suspension system had failed, allowing the plate carrier system to fall down upon its safety stops. Only the safety stops prevented the plates from falling into the hoppers. In this position, the plates were rigid and could not be rapped, as the rapping system is part of the plate suspension system (Figure 1).

Unit No. 2 precipitator [illegible] also damaged, with approximately 50 percent of the second field being nonfunctional. The welds were cracked, but not completely failed to where it would drop the plate system. The third field in this unit was in fair shape in that there was no failure of the suspension system.

The following deficiencies were found during the internal inspection of the precipitators:

PRECIPITATOR NO. 1

Each of the three fields in the precipitator was given a thorough inspection, including checking high voltage, wires, collecting plates, insulators, rapper rods, and plate hanger assemblies. The internal deficiencies are shown in Exhibits 1, 2 and 3.

The major failures had occurred in the rapper rod assemblies and collecting plate support system. In each case, damage was attributable to failure of the field weld on the top of the coupling joining the rapper rod top extension to the rod on the plate hanger assembly (Figure 2). Where this occurred, the plate assembly had fallen about an inch, coming to rest on the safety stops welded to the side of the precipitator frame. In several cases, this had happened at both ends of the plate assembly. These plates then were supported rigidly, making the rappers completely ineffective. Continued rapping of these plates with failed supports could have caused further structural damage.

The high-voltage insulators had a substantial dust buildup inside, and required cleaning. As found with Precipitator No. 1, tops of the insulators were black and charred from sparking and voltage leakage through the dust. It was recommended that the insides of the insulators be cleaned at least once a year during the annual overhaul.

Alignment problems were found in the second field of this precipitator. The north wire frame was out of alignment and would have to be moved 3/4-inch to the south in order to get the proper clearance of 4-1/2 inches on each side of the wires. There was also a bent plate in this section. The 14th plate from the north was bent about one-third of the way down. This plate would require straightening, or replacement. The wires which had been removed in the area of the bent plate would then be replaced.

There were a number of kinked wires in the second field of Precipitator No. 2. It was found that many of the wires were stretched out and the wire weights were bottomed out on the weight guide frame just above the hoppers. These wires all required replacement in order to put the required tension on the wires.

A screen door spring was wrapped around one expanded sway brace insulator guide ring in the Unit 2 hopper area. It was our understanding that this screen door spring system had prevented any further breakage of the insulators and had been operating satisfactorily. Since screen door springs are not the best spring steel, and considering the intense heat to which they were subjected, we recommended that the spring be removed and the insulator guide be readjusted for proper alignment. Again, it was recommended that all insulators be thoroughly cleaned to prevent voltage tracking in the dust buildup.

Several high-tension vibrator support plates had cracked welds in the penthouse area. Cracked welds were found in first field-north side, and the second field-north side. The vibrator rubber insulating boot was cracked open on both high-tension vibrators on the third field.

The high-voltage vibrator insulator above the barrel insulator on the north side of the second field was cracked and needed to be replaced.

GENERAL - BOTH PRECIPITATORS

The precipitator external support and expansion systems were throughly inspected and found to be in good repair. Nothing unusual was found in the slide plates or guides.

The perforated plates in the inlet transition duct to the precipitators appeared to be in good order with no unusual dust buildup.

Some rapper housings were removed on each precipitator to inspect the Belleville spring washers and rapper assembly (Figure 3). Some rappers had the Belleville washers installed in the wrong sequence. In some cases, spacer washers and/or spring washers were missing. In one case, the retaining nut at the top of the rapper rod was broken in two. It was recommended that all rapper housing assemblies be removed and the washer assembly checked to see that they were assembled according to the detail drawing. Cracked or broken washers and nuts were to be replaced.

As expected, dust buildup was heaviest in the first field, and diminished slightly in each succeeding field. High-voltage insulators were found to have a heavy dust buildup on the inside. Nearly all of the insulators showed a circular spiral pattern of dust caused by the purge air system to the insulators. The purge air system was working, but it was not efficient enough to keep the insulators clean over a long period of time. In all cases, a dark charring was found on the tops of the insulators, which indicated sparking and voltage tracking in the dust buildup. It was recommended that these insulators be thoroughly cleaned during the annual unit overhaul. This would help prevent voltage tracking, thus putting more power into the wire system.

Some alignment problems were found during the inspection. Proper alignment and clearances are important in maintaining power input to the precipitator. In the third field, the alignment checked out within proper allowances. In the second field, the north wire frame had a bent wire carrier next to the farthest south carrier. The wire carrier was bent 3/4-inch out of alignment and required straightening or replacement. In the first field, the south wire frame was out of alignment and needed to be realigned 1/2-inch to the south. Maintaining the 4-1/2-inch plate to wire and wire to plate measurement was necessary for proper power input.

In the hopper area, the lower higher-voltage frames in the second field were out of alignment by 1/2-inch. The two frames needed realigning and the sway brace insulators required readjusting to hold the frames in place.

It was recommended that the sway brace insulators be thoroughly cleaned in order to prevent voltage tracking through the dust. Insulators should be cleaned at least once a year during the unit's annual overhaul.

Broken rubber boot covers on the vibrator rod on the first field-south side, and on the third field north side were found during the inspection of the penthouse. It was recommended they be replaced.

PRECIPITATOR NO. 2

Each of the three fields in Precipitator No. 2 was given a thorough inspection, checking wires, collecting plates, high-voltage insulators, rapper rods and plate hanger assemblies. The internal deficiencies are shown in Exhibits 4, 5 and 6.

The major problem in Precipitator No. 2 was identical to that found on Precipitator No. 1; failure of the rapper rod assemblies and plate support system (Figure 1). Again, in each case, failure occurred at the field weld on the top of the coupling joining the top rapper rod extension to the rod on the plate assembly (Figure 2). As in Precipitator No. 1, the plate assembly had fallen about one inch onto the safety stops welded to the side of the precipitator frame. Consequently, the rapping was ineffective and virtually useless.

Precipitator No. 2 did not have as much dust buildup as No. 1. Dust was heavier in the first field and somewhat less in each succeeding field. There was a black soot buildup on the internals resulting from the effects of oil firing in the boiler.

Reproduced from
best available copy.

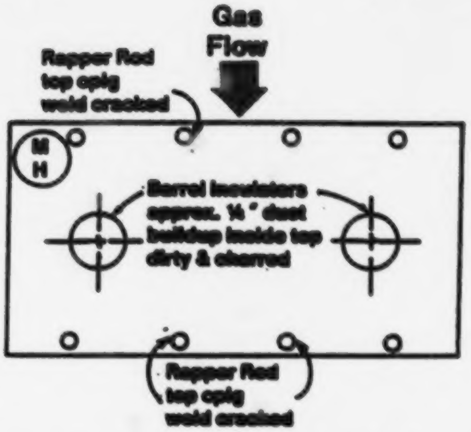
Gas Flow
Rapper Rod top cplg weld cracked
M H
Barrel insulators approx. ¼" dust buildup inside top dirty & charred
Rapper Rod top cplg weld cracked

Wire Deficiencies

1. South wire frame out of adjustment by 1/2-inch, needed to move south.
2. Two wires missing, row 6 and 7 from south.
3. Six wires kinked, various places.
4. One pair of wires crossed to opposite weights, third row from north.

Exhibit 1. Precipitator No. 1
First Field

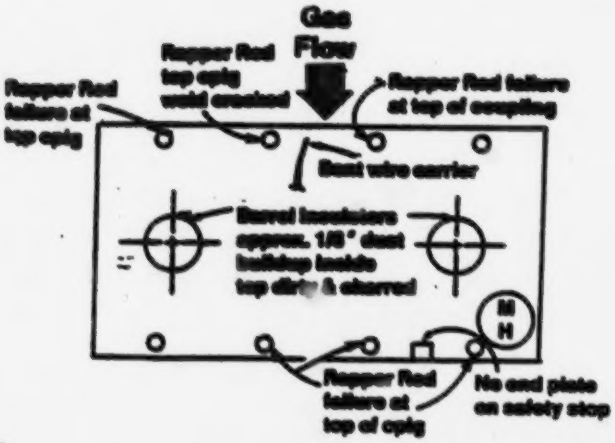
Gas Flow
Rapper Rod failure at top cplg
Rapper Rod top cplg weld cracked
Rapper Rod failure at top of coupling
Bent wire carrier
Barrel insulators approx. 1/8" dust buildup inside top dirty & charred
M H
Rapper Rod failure at top of cplg
No end plate on safety stop

Wire Deficiencies

1. North wire frame, wire carrier next to south carrier bent 3/4-inch on east end, bent to the south.
2. Two wires kinked, need replacing.
3. One pair wires crossed to opposite weights, sixth row from north.

Exhibit 2. Precipitator No. 1
Second Field

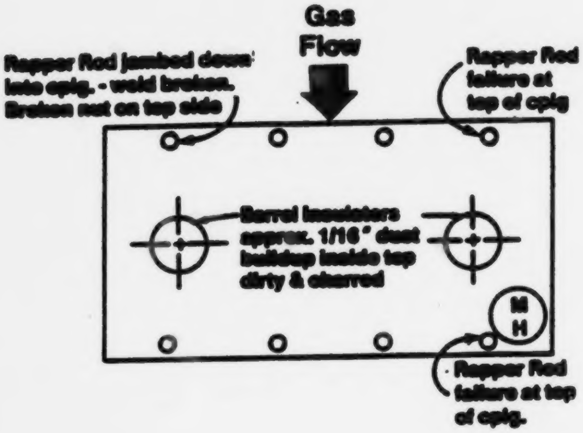
Gas
Flow
Rapper Rod jambed down
into cplg. - weld broken.
Broken nut on top side
Rapper Rod
failure at
top of cplg
Barrel insulators
approx. 1/16" dust
buildup inside top
dirty & charred
M
H
Rapper Rod
failure at top
of cplg.

Wire Deficiencies
1. One set of safety stops for plate system missing end plates.
2. No wire problems.

Exhibit 3. Precipitator No. 1
Third Field

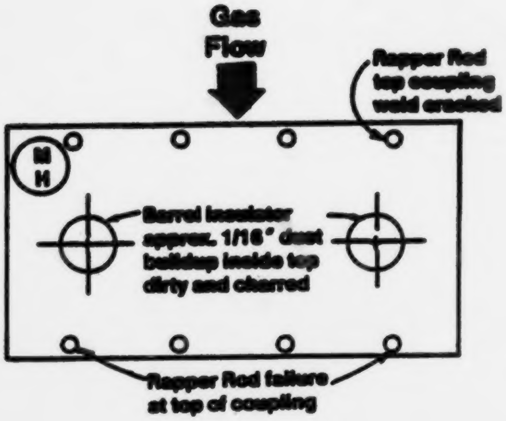
Gas
Flow
Rapper Rod
top coupling
weld cracked
M
H
Barrel insulator
approx. 1/16" dust
buildup inside top
dirty and charred
Rapper Rod failure
at top of coupling

Wire Deficiencies
1. Some soot buildup from oil operation.
2. No wire problems.

Exhibit 4. Precipitator No. 2
First Field

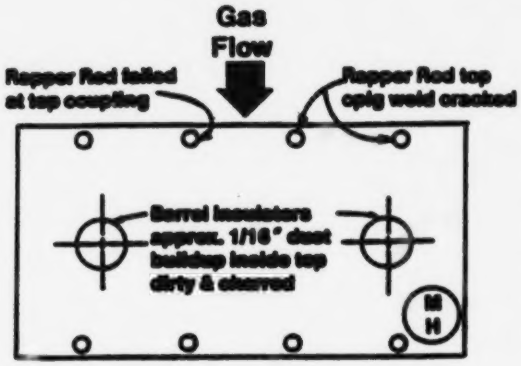
Gas
Flow
Rapper Rod failed
at top coupling
Rapper Rod top
cplg weld cracked
Barrel insulators
approx. 1/16" dust
buildup inside top
dirty & charred
M
H

Wire Deficiencies

1. North wire frame out of adjustment needs to move 3/4-inch to south.
2. Wires 1, 2, 6, 7 and 8 from west missing, 14th row from north.
3. Fourteenth plate from north, plate bent one-third way down.
4. Fourteen wires kinked various places in field.

Exhibit 5. Precipitator No. 2
Second Field

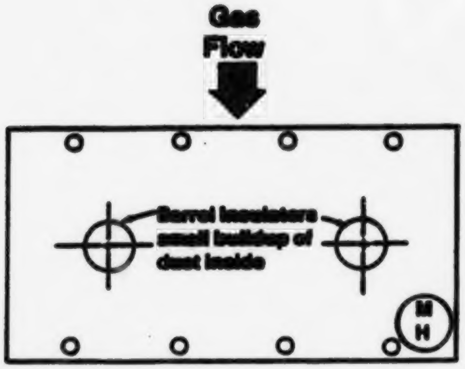
Gas
Flow
Barrel insulators
small buildup of
dust inside
M
H

Wire Deficiencies

1. Fourteenth row wires from north second pair from east twisted together.
2. Tenth row wires from south third wire from west kinked.

NOTE: There were no rapper rod failures in this field and no signs of cracked or failing welds.

Exhibit 6. Precipitator No. 2
Third Field

DESIGN OF REPAIRS

Before design started, we conducted an investigation to determine if the precipitators could perform as they were intended to. We have in-house a computer modeling program that will accurately predict the operations of a precipitator. We have validated this data by inputting from previous precipitator stack tests. The program was run on the two precipitators at design conditions. Following is a summary of the results:

"As-is Condition" with Boiler at 100% Capacity

Precipitator Efficiency = 93.9%
ACFM = 125,450
ACA = 433 sq ft/1,000 ACFM
Average Applied Voltage = 24.3 kV per TR
Fly Ash Resistivity = 1.0 x 10^{10} ohm/cm
Inlet Grain Loading = 3.320 gr/ACFM
Gas Sneakage Through Hoppers = 0.10
Gas Temperature = 750 degrees F
Outlet Loading = 0.21169 gr/cu ft
Opacity = 56.7%

"Design Conditions" with Boiler at 100% Capacity

Precipitator Efficiency = 99.5%
ACFM = 125,450
ACA = 433 sq ft/1,000 ACFM
Average Applied Voltage = 44.1 kV per TR
Fly Ash Resistivity = 1.0x10^{10} ohm/cm
Inlet Grain Loading = 3.320 gr/ACFM
Gas Sneakage Through Hoppers = 0.10
Gas Temperature = 750 degrees F
Outlet Loading = 0.01489 gr/cu ft
Opacity = 3.1%

After evaluating this information, we could safely predict that we would be able to bring these units into compliance with state regulations. Kansas State emission regulations for these units is 0.17 lb/mmBtu. This equates to approximately .05 gr/cu ft. Our modeling program predicted that design conditions would exceed State Regulations by a considerable margin.

The next phase of work concerned the design of the repairs necessary to bring the precipitators back to, or as close as possible, to the original design conditions.

The principal failure had been the rapper rods which also served as the suspension system for the plates. Gusset plates of 1/2-inch plate were designed to be welded to each side of the rapper rods (Figure 4). Where the rod had failed, it was replaced. The fix was applied to all rapper rods. The collecting plates and header plate assembly were raised and adjusted to provide the necessary clearances.

Each rapper was to be disassembled, and the Belleville spring washers and adjusting nut inspected by the repair contractor (Figure 3). During our field inspection, we had found one broken castellated nut and one or two rappers where the Belleville spring washers were in the wrong sequence. When this rapper disassembly was undertaken during repairs, it was found that 25 percent of the rapper nuts had failed. Only a couple were broken, but the others had cracked nuts, sheared cotter pins and damaged threads. Each of these rapper rods was replaced. On all rappers, a double nut, one adjusting and one jamb nut, was installed and spot welded together. Broken or damaged Belleville springs were replaced.

All rapper coils were inspected and a slug lift test was performed on each. Only one coil had to be replaced.

The top wire frames were realigned for proper clearances and the bent wire carrier straightened. Wires were replaced where they had stretched or kinked. The crossed or twisted wires were also straighted out. Altogether, about 50 wires were replaced. The bottom wire frames were realigned and the sway brace insulators cleaned, repaired, and readjusted. The make-do screen door spring arrangement used to maintain stability and clearances was removed, and the bracket readjusted for proper clearance (Figure 1).

The high-voltage barrel insulators were cleaned. It was evident from the dust on the inside of the insulators that not enough air was getting into the insulator from the purge air system. The insulator top plate was designed to introduce purge air through 6-3/8-inch-diameter holes drilled at a 45-degree angle in order to swirl the air, since the dust buildup pattern inside the insulator was in a swirl configuration (Figure 5). We added six more 3/8-inch-diameter holes on a smaller diameter than the originals, but had them drilled straight in order to break up the swirl and do a better job of keeping the insulators clean. A 1/4-inch-diameter pipe nipple with cap was installed in the wall of each high-voltage housing to take pressure readings to facilitate the balancing of the amount of purge entering each housing (Figure 6).

The one broken vibrator rod insulator was replaced, and all other insulators cleaned of dust buildup. Broken vibrator support brackets were rewelded where cracked, and broken vibrator flexible sleeves were replaced.

During our inspection, we had confirmed that the wire weights were only 15-pound weights. Even though the good wires were stretched tightly, they did not have the proper amount of tension. They were straight, but not as taught as required. We included an alternate in the specifications to change out all of the 15-pound weights to 25-pound weights. The cost proved to be prohibitive and this was not done.

FIELD WORK AND START-UP

This portion of the work was accomplished by Hercules Aerospace Division, the operating contractor at the plant.

It was during this portion of the project that additional broken and damaged rapper rod nuts were discovered. Burns & McDonnell's structural engineers suggested that rods with damaged threads be replaced. Also, a double nut system should be used in place of the castle nut and cotter pin configuration of the original design.

Another problem which showed up during start-up and testing regarded the suspension system for the bottom wire frame and weight guides. The bottom frame is supported from the top frame by four 1/2-inch-diameter solid steel rods one in each corner (Figure 1). During start-up, differential expansion of these rods was twisting the bottom frame out of alignment and shorting out the entire system.

Various manufacturers use steel cables or chains to support the lower frame, which prevents this differential expansion, and resulting short-circuiting from happening. It was suggested that Hercules consider replacing these rods with chains. Hercules came up with their own unique fix for this problem. They chose to thread a 75-pound weight onto the bottom of each rod. The added weight was enough to overcome the differential expansion of the rods during start-up and low-load conditions, and served to maintain proper alignment.

SUMMARY

The final results of the evaluation, design, and implementation of repairs is that both units are now operating with a clear stack. The stack test has not been rerun as yet to verify emission rates, but with a clear stack, there should be no problems.

This project is a prime example of cooperation and team work between the Engineer and the operating contractor bringing older units up to operating standards to meet present day emission rates.

The work described in this paper was not funded by the U.S. Environmental Protection Agency and therefore the contents do not necessarily reflect the views of the Agency and no official endorsement should be inferred.

Figure 1. Precipitator cross section

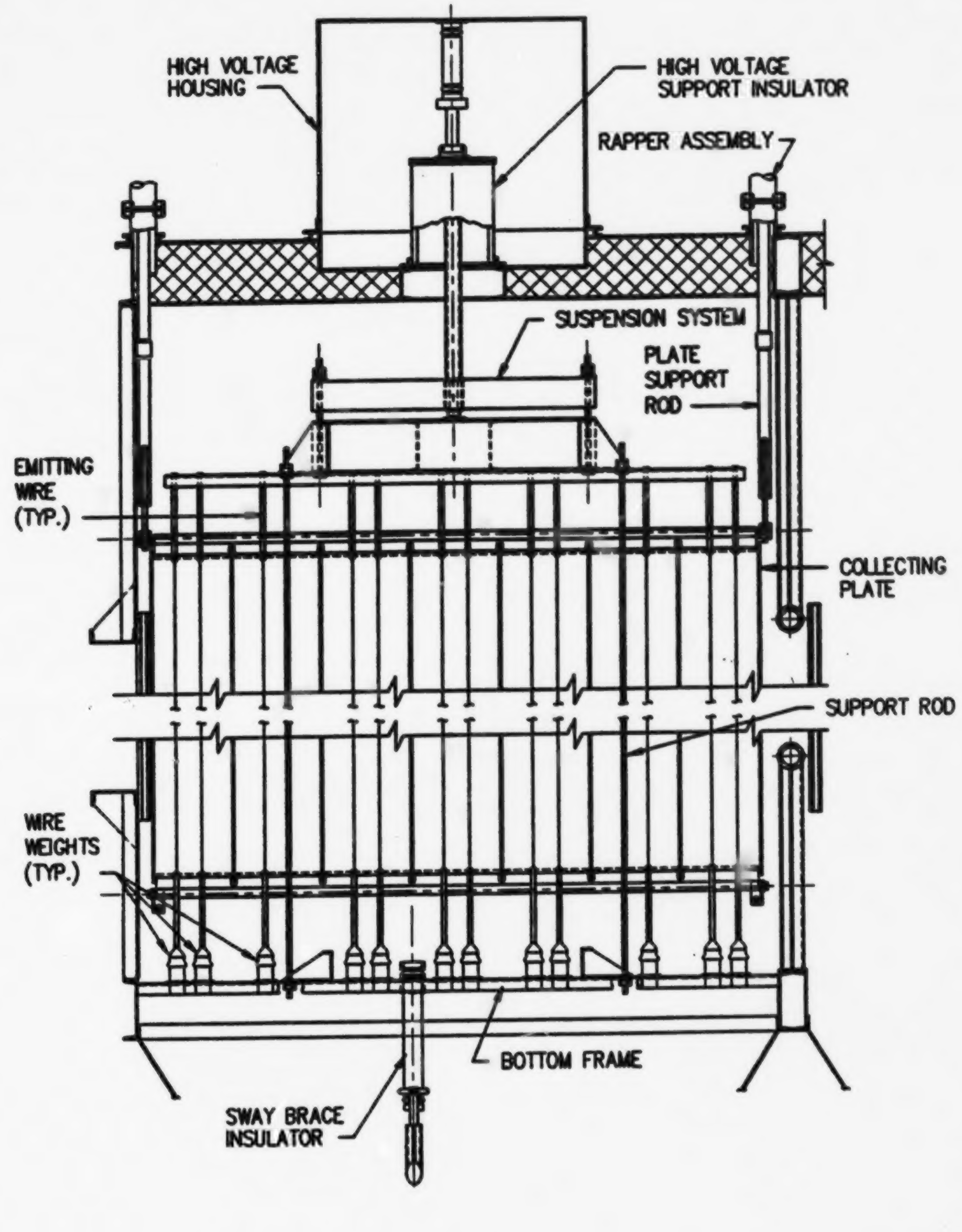
HIGH VOLTAGE HOUSING
HIGH VOLTAGE SUPPORT INSULATOR
RAPPER ASSEMBLY
SUSPENSION SYSTEM
PLATE SUPPORT ROD
EMITTING WIRE (TYP.)
COLLECTING PLATE
SUPPORT ROD
WIRE WEIGHTS (TYP.)
BOTTOM FRAME
SWAY BRACE INSULATOR

Figure 2. Collecting plate support system

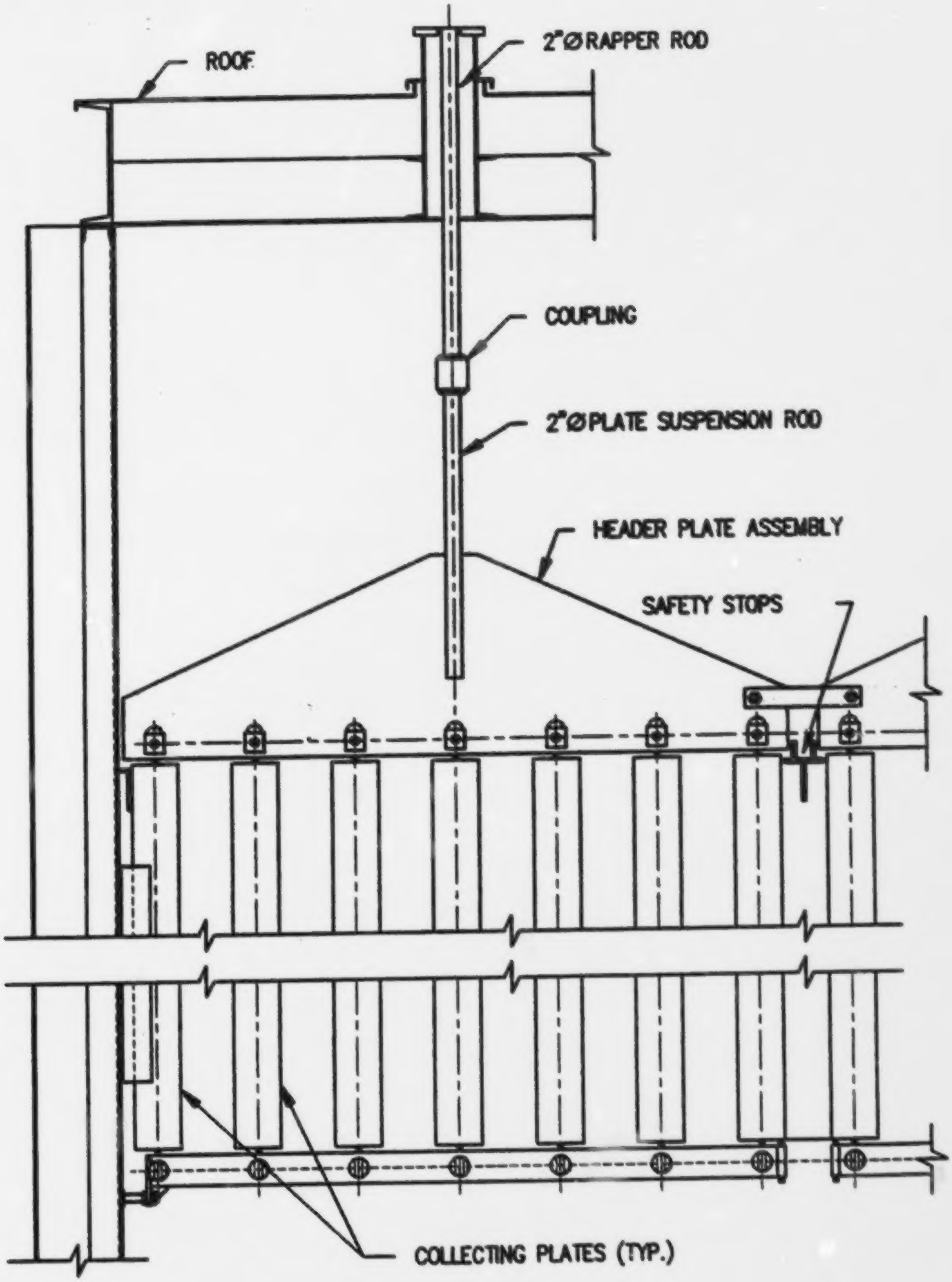
2"Ø RAPPER ROD
ROOF
COUPLING
2"Ø PLATE SUSPENSION ROD
HEADER PLATE ASSEMBLY
SAFETY STOPS
COLLECTING PLATES (TYP.)

Figure 3. Detail, rapper rod

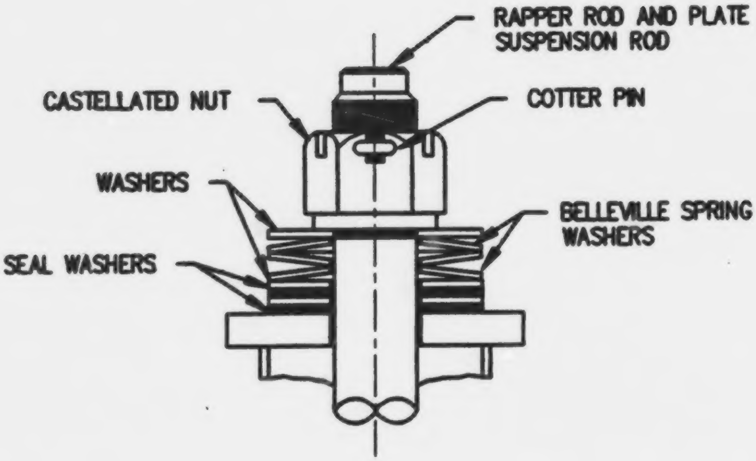
RAPPER ROD AND PLATE SUSPENSION ROD
CASTELLATED NUT
COTTER PIN
WASHERS
BELLEVILLE SPRING WASHERS
SEAL WASHERS

Figure 4. Support rod repair

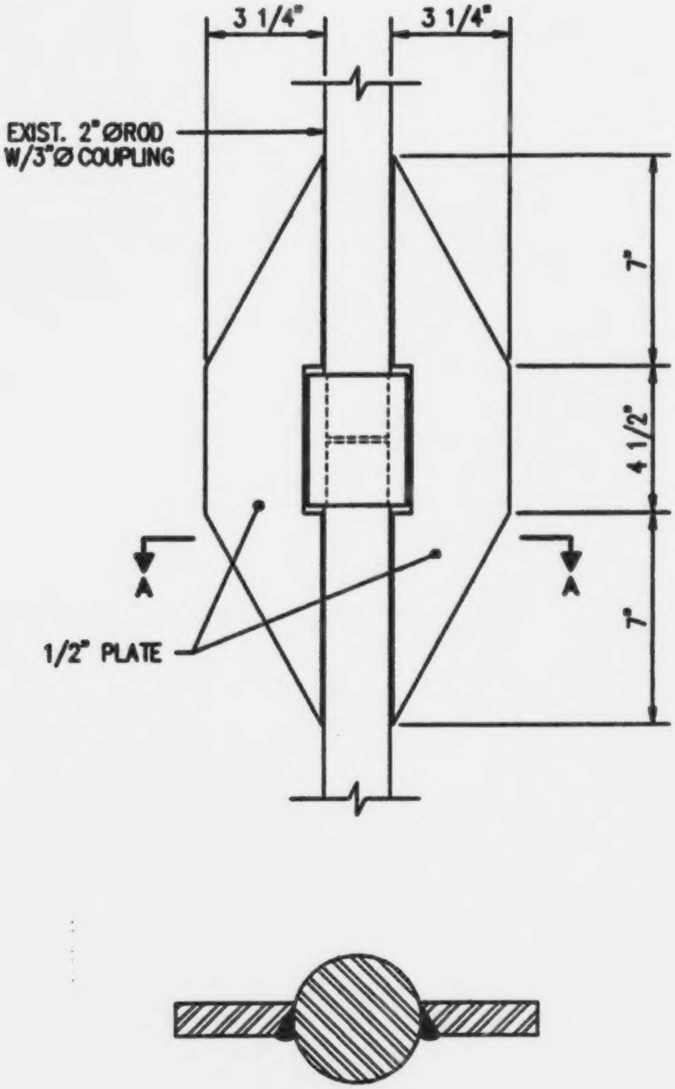
3 1/4"
3 1/4"
EXIST. 2"ØROD
W/3"Ø COUPLING
7"
4 1/2"
7"
A
A
1/2" PLATE

SECTION A-A

Figure 5. Insulator top plate

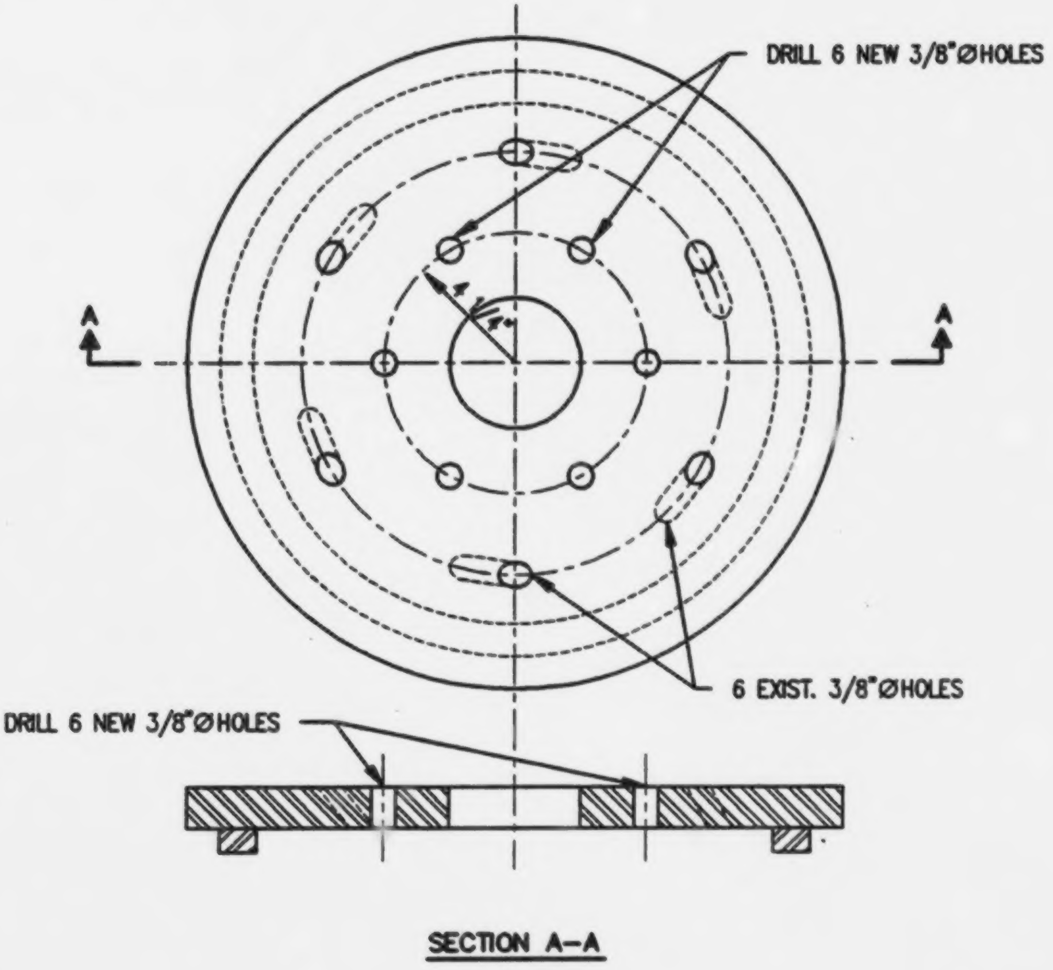
DRILL 6 NEW 3/8"Ø HOLES
A
A
6 EXIST. 3/8"Ø HOLES
DRILL 6 NEW 3/8"Ø HOLES
SECTION A-A

Figure 6. High voltage housing

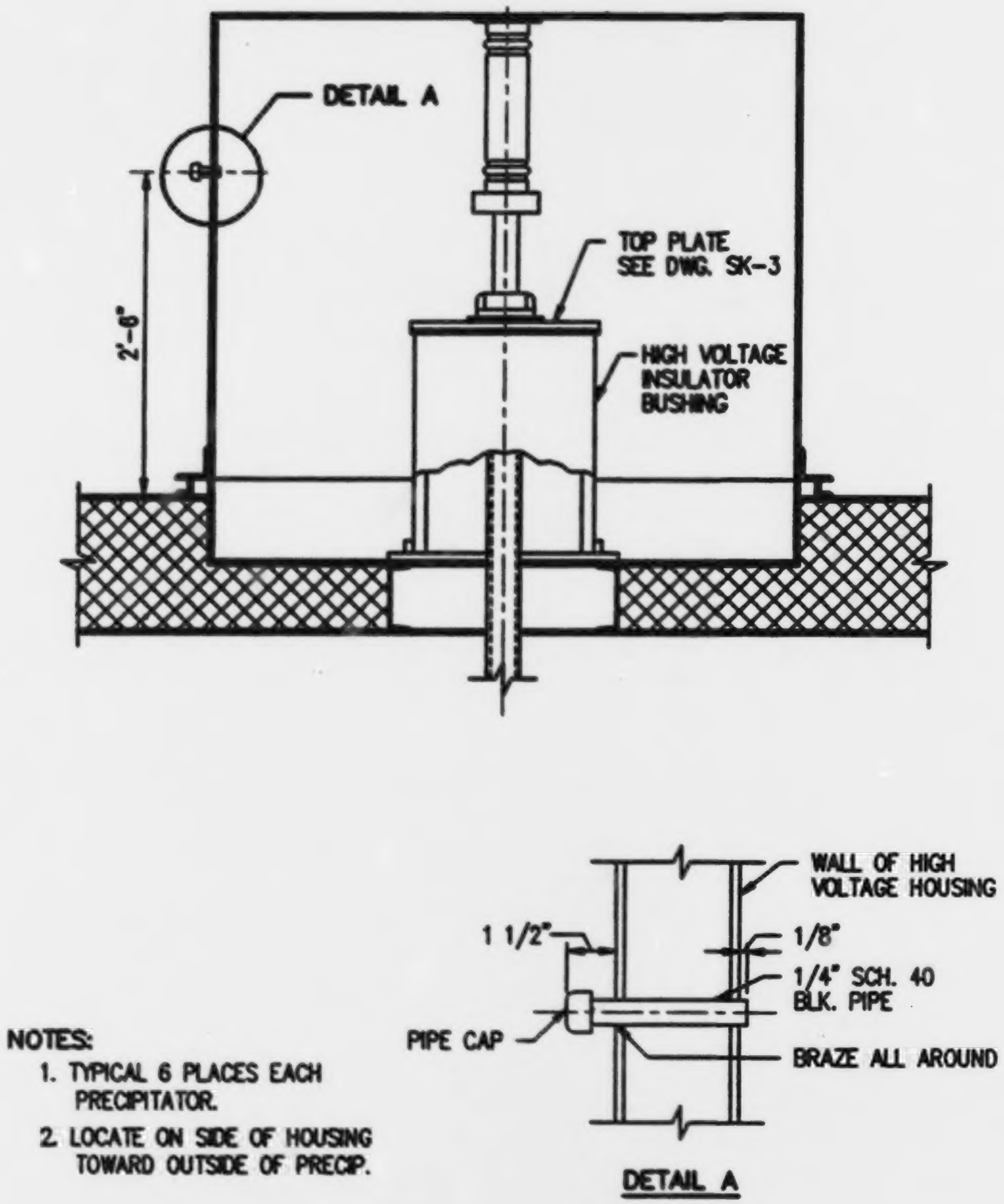
DETAIL A
TOP PLATE
SEE DWG. SK-3
HIGH VOLTAGE
INSULATOR
BUSHING
2'-6"
WALL OF HIGH
VOLTAGE HOUSING
1 1/2"
1/8"
1/4" SCH. 40
BLK. PIPE
PIPE CAP
BRAZE ALL AROUND
DETAIL A

NOTES:

1. TYPICAL 6 PLACES EACH PRECIPITATOR.
2. LOCATE ON SIDE OF HOUSING TOWARD OUTSIDE OF PRECIP.

PERFORMANCE IMPROVEMENT HISTORY OF INADEQUATELY PERFORMING PRECIPITATORS

John G. Musgrove, Bechtel Power Corporation
William R. Lane, Bechtel Power Corporation
Maurice W. Wei, Aluminum Company of America

ABSTRACT

This paper describes a successful effort to improve performance of three electrostatic precipitators at the Sandow Generating Station, Rockdale, Texas. Their installation in 1973 required an efficiency of 98 percent. Recent operation has not been satisfactory, allowing emissions in excess of their design value. As part of the Sandow Betterment Program, Bechtel Power Corporation was asked to study the performance of the precipitators and to make recommendations to improve their performance.

The study included evaluation of operating data, performance testing, rapping acceleration tests, gas flow distribution tests, and precipitator modeling. Following evaluation of the tests, Bechtel made several recommendations; these included changes to the rapping system and the automatic voltage control system. The modifications, installed by Bechtel, have resulted in the following improvements: emission reductions of greater than 45 percent and opacity excursion reductions of over 75 percent. The tests conducted and details of improvements are presented in this paper.

INTRODUCTION

The Sandow Generating Station Units 1, 2, and 3, located near Rockdale, Texas, produce electric power for an adjacent aluminum plant. Sandow Units 1, 2, and 3 each have a generating capacity of 120 MW and utilize electrostatic precipitators for particulate collection. The recent performance of these precipitators has not been satisfactory, and as part of the Alcoa/Sandow Plant Betterment Program begun in the fall of 1983, Bechtel Power Corporation was asked to study the performance and to make recommendations to improve their efficiency and reliability. Several of the recommendations were implemented, resulting in substantial improvements in emissions and reductions in opacity violations.

The purpose of this paper is to present information regarding the recommendations and resulting improvements made to the existing precipitators. Future studies, if necessary, could include flue gas conditioning, lignite mine plan alterations, and additional precipitator capacity.

STUDY

COAL EVALUATION

Approximately 1,100 core analyses from the mine were evaluated, and with precipitator test data, used to determine precipitator adequacy. No study of specific mining plans was conducted in this phase of the precipitator improvement study.

The Sandow Station burns dried local lignite. As is typical of Texas lignite, the properties are highly variable. For example, the average sulfur content is 1.82 percent on a dry basis; however, the standard deviation is 0.64 percent, or 35 percent of the average. Sulfur content varies from under 1 to over 3 percent.

The 1984 performance tests were conducted during a period when relatively high sulfur (2.0 dry basis) lignite was burned. Precipitator performance is expected to deteriorate when lower sulfur content lignite is burned. An estimated 11 percent of the Sandow lignite (based on analyses of 1,100 core samples) has too little sulfur for adequate precipitator performance. Approximately 5 percent of the lignite has too much ash for adequate performance. A total of 16 percent of the lignite would not be suitable for the existing precipitators in their original operating condition.

ELECTROSTATIC PRECIPITATOR ORIGINAL DESIGN SPECIFICATIONS

Operating Conditions (per boiler)

Volume, acfm	460,000
Inlet dust loading, grains/scfd	1.0 (0.60 grains/acf)
Outlet dust loading, grains/scfd	0.02 (0.012 grains/acf)
Collection Efficiency, %	98.00
Moisture in flue gas, % by volume	7.0 to 10.0
Gas temperature, F	300
Gas pressure, inches WC	-18

Physical Data (per precipitator, two per boiler)

Gas passages	46 on 9-inch centers
Mechanical fields	3 @ 10.625' x 23'
Electrical fields	3 @ 10.625' x 23'
Collecting area, ft^2	67,447.5
SCA, ft^2/acfm	293.25
Velocity, fps	4.83
Aspect ratio	1.39
Treatment time, seconds	6.6
Collection plate rappers	24
Plate area per rapper, ft^2	2,810
Plate height, feet	23
Plate length, feet	10.5
Spacing, inches	9.0
Discharge electrode rappers	16

PRECIPITATOR EVALUATION

Performance Tests

This section discusses the performance of the Unit 1 precipitator, prior to precipitator upgrading, as determined during performance tests. These tests, conducted in the spring of 1984 by Mullins Environmental Testing, Inc. (Metco), have allowed conclusions to be determined regarding the adequacy of the precipitators.

- Gas Flow Rate

  The gas flow rate was measured at the inlet and outlet of the two precipitators serving Unit 1. The average of six measured gas flow rates was 476,200 acfm (actual cubic feet per minute) proportioned to an assumed full load condition of 120 MW. The measured gas flow rate is within 3.5 percent of the originally specified gas flow rate of 460,000 acfm.

  An imbalance of gas flow between the two precipitators serving Unit 1 was observed. Calculations indicated that an unequal flow though the two precipitators of the magnitude observed could increase emission opacity by 2 percent. For example, if operating at the limit of 30 percent opacity, a balancing of the flow would reduce opacity to 28 percent.

o Inleakage and Excess Air

The level of excess air at which the boiler is operated and the amount of inleakages in the air preheater, ducting, and precipitator greatly influence precipitator performance as they affect the gas velocity and the specific collection area (SCA).

During Unit 1 precipitator performance testing, Metco used an Orsat to determine the level of excess air at the precipitator. The tests indicated an average of 56.2 percent excess air at the precipitator inlet and 60 percent at the precipitator outlet. Separate tests by Combustion Engineering measured similarly high values. This indicated a severe inleakage problem between the boiler and precipitator.

During the precipitator tests, boiler control panel data indicated operation at approximately 4.5 percent oxygen which corresponds to 26 percent excess air at an assumed 15 percent CO_2 level. This is a typical boiler excess air level. Unfortunately, the independently confirmed test data proved that boiler control panel readings were in error.

o Precipitator Collection Efficiency

The precipitators were designed for a particulate collection efficiency of 98.0 percent at a gas flow rate of 460,000 acfm per boiler. Figure 1 shows collection efficiency versus precipitator specific collection area. The gas flow rate is reflected in the SCA values shown.

The measured gas flow rate was close to the specified value; however, the precipitator collection efficiency was lower than that specified. Figure 1 indicates that the precipitator did not achieve its design collection efficiency except during one test at reduced gas flow (increased SCA). The average measured collection efficiency was 97.4 percent compared to a design of 98.0 percent. This produces emission rates 30 percent higher than design levels.

o Percent Fly Ash

To determine the precipitator adequacy for the range of Sandow fuel properties, an estimate of the amount of fly ash was necessary. From the lignite flow rate and the lignite sample analyses, the ash production rate was determined. The precipitator performance tests determined how much ash was entering the precipitator. A comparison of the two values indicated fly ash percentages of 24, 23, and 31 for the three tests with an average of 26 percent of the ash becoming fly ash, with the remaining 74 percent going to bottom ash.

- Ash Combustibles

Six ash samples were collected at the precipitator inlet. These were tested for combustible content. The combustible content ranged from 5.0 to 10.2 percent with an average of 8.4 percent.

This compares to other plants for which we have data as follows:

Plant A, lignite	7.4%
Plant B, bituminous	11.8% full load
	3.0% half load
Plant C, subbituminous	1.0%
Plant D, subbituminous	4.7%
Plant E, subbituminous	0.5%
Average	4.7%

This combustible content, while not as high as at some plants, is higher than the average of five other plants surveyed.

- Particle Size Distribution

The size distribution of particulate exert a strong influence on electrostatic precipitator performance and on emission opacity. Tests were conducted on all three units to determine inlet and outlet particle size distribution.

The precipitator inlet particle size distribution was similar to that of pulverized coal plants burning subbituminous coals, as shown in Figure 2.

	Other Plants	Sandow
Precipitator Inlet Particle Size		
Percent Under -		
1.0 micron	4.9	5.5
2.0 microns	10.4	11.0
5.0 microns	23.0	24.0
10.0 microns	31.0	45.0

The precipitator outlet particle size distribution, Figure 3, was highly variable. The variation among test results was random with no consistency between boilers and is probably due to several factors including variable coal properties, operating conditions, and precipitator collection efficiency. The Sandow emission particle sizes are larger than observed for subbituminous coals at other plants because the precipitator collection efficiency is lower. With higher collection efficiency, the large particles would be preferentially removed, leaving the smaller particles.

Opacity Correlation

To determine the level of adequacy of the existing precipitator for the range of lignite properties in the mine, a correlation of emission particulate concentration to emission opacity was determined.

Average opacity as calculated by the plant computer was compared to chimney emissions measured during the performance tests. This correlation is shown on Figure 4. The slope of the average line shown is based on the opacity being proportional to ash concentration. Figure 4 also shows opacity correlations for approximately seven other plants (adjusted to the same chimney diameter). The Sandow data are representative of the other plants.

The opacity correlation indicates that the plant's 30 percent opacity limit is achieved when emissions are under 0.052 grain/acf. The correlation depends heavily upon particle size distribution. Therefore, considerable scatter is noted. Plants with finer particle sizes or larger chimney diameters would be limited to a lower emission rate to achieve the same level of opacity.

Emission Limit

In addition to the 30 percent opacity criteria, the Sandow Units 1, 2, and 3 must comply with an emission limit of 0.3 lb particulate/million Btu. The Metco tests indicated an average emission rate 0.188 lb/million Btu using the EPA "F" factor method of calculation. The average measured emission concentration was 0.0385 grain/acf. The emission rate limit of 0.3 lb/million Btu would therefore correspond to 0.06 grain/acf. This is more lenient than the 30 percent opacity criteria corresponding to 0.052 grain/acf. Therefore, a limit of 0.052 grain/acf, corresponding to 0.26 lb/million Btu, was assumed for further analysis.

Velocity Distribution

Nels Consulting Services, Inc., conducted a velocity distribution test in one of the Unit 1 precipitators. The tests were conducted with hot wire and vane annemometers inside the precipitator with the unit off-line and the induced draft fans operating and indicated that gas velocity distribution was not up to current standards.

If the velocity through the precipitator is not uniform, some areas of the precipitator are "underworked" while other areas are "overworked". The net result is a decrease of particulate collection efficiency and an increase of emissions.

A flow model study by Nels indicated that collection efficiency could be improved significantly by improving the velocity uniformity with modifications at the inlets and outlets. Bechtel calculations indicated a potential 5 to 10 percent emission reduction. The model study recommendations included: modifications to the inlet and outlet perforated plates to assure uniform gas distribution, modifications to the inlet turning vanes, and trimming of the antileakage baffles.

Rappers

The precipitator vibrating rappers were inadequate, being incapable of rapping hard enough to dislodge high resistivity ash produced from low sulfur lignite. The timing system was inadequate for proper rapper control. Excessive-rapping-induced opacity spikes caused emission violations.

Rapping system tests on the precipitator conducted by Neundorfer, Inc., consisted of plate rapping force (acceleration) measurement on Unit 1. Observations of rapping system operation were also conducted by Bechtel on Unit 3. The test program provided data for analysis of the adequacy of the rapping system.

Rapping force was measured on the Unit 1 precipitator collecting plates by using an ultralight weight transducer attached to the plates with beeswax. Several plates from two suspension frames were tested, with measurements taken at the four corners of each plate. Four different rapping configurations were tested:

- The existing Syntron electric vibrators were tested to establish a baseline.
- Four plates were welded firmly to the anvil beam saddles to determine if significant dissipation of rapping force is occurring in the saddles.
- Neundorfer's NAVCO pneumatic repetitive-impact rappers were tested for possible rapping force improvement over the existing rappers.
- A magnetically induced, gravity-impact (MIGI) rapper was tested for comparison with the existing Syntron and NAVCO rappers.

The Syntron rappers were operated at 100 percent intensity to achieve their maximum rapping force. The NAVCO pneumatic rappers were operated at 45 psi to achieve maximum rapping force; NAVCO literature recommends an operating air pressure of 25 to 35 psi. The impact energy of the NAVCO rapper at 45 psi is approximately 11 ft/lbs. The MIGI rapper was tested with a 20-pound slug at 6- and 12-inch drop heights, yielding impact energies of 10 and 20 ft/lbs, respectively. The impact energy of the existing Syntron vibrators is unknown.

The results of the tests are shown below:

Rapper Type/Configuration	Rapping Force Range, G's	Rapping Force at Impact Corner, G's	Rapping Force at Far Corner, G's	Average Rapping Force, G's
Existing Syntron	7-41	26	9	13
Syntron with welded saddles	6-27	11	15	13
NAVCO at 45 psi	21-127	87	31	48
MIGI at 6-inch drop	11-259	153	33	63
MIGI at 12-inch drop	27-396	242	44	96

Current design practice would specify rappers with a minimum rapping force of at least 50 G's for this application. Welding the plates in the saddles did not improve the rapping force transmission of the existing rappers. The MIGI rapper generated the highest average rapping force and the highest average rapping force at the plate locations farthest from the rapping location. The NAVCO and existing Syntron rappers showed less rapping force loss across the plate than the MIGI rapper; 65 versus 78 to 82 percent. The NAVCO rapper has the potential of doing an excellent cleaning due to its multiple cycles per second of high acceleration during its "on time".

Rapper Controls

The original rapper controls could only be adjusted for rapper "on time" and rapper "off time". The maximum off time was approximately 50 seconds before the next rapper was activated. Each timer controls eight sets of two rappers. Therefore, the maximum time before reactivating a given rapper was approximately seven minutes. The maximum on time was 25 seconds, but this adjustment is usually of little value outside a range of 0.5 to 1 second. Rapping the plates for more than one second is usually not beneficial for dust collection.

Current precipitator design practice commonly includes rapper controls which allow variation in rapper cycle times for each rapper from a few minutes to at least one hour between raps. The original system rapped all of the outlet field rappers (16) of one boiler's precipitator in approximately seven minutes. A better method is to stagger this rapping over a one-hour period to minimize the magnitude of emission opacity spikes and reduce the frequency of six-minute emission opacity violations.

Automatic Voltage Control

Bechtel monitored the performance of the original voltage controls for all three units during the various test programs conducted as part of this study. Several deficiencies in the voltage control system operation were noted. These were:

- Most of the controls did not recover from sparking correctly.

- The majority of controllers failed to maintain maximum power input under low sparking conditions.

- The controls did not respond to load swings.

The precipitator voltage control system installed in 1973 could not respond to changes in operating conditions, and as a result, emissions were needlessly high.

The power input to most precipitator fields was much lower than could be achieved because the voltage was limited to a manually preset value. Emissions will decrease as more power is utilized by the precipitators. Manual voltage adjustment of the Unit 1 precipitators demonstrated that it was often possible to increase the power to the precipitators by over 55 percent.

The voltage controls were also monitored during boiler load decrease. They did not respond to the change in boiler and precipitator operating conditions as would a properly designed system. For instance, during a load decrease on Unit 3, the opacity increased from 20 to 30 percent (probably due to decreased ash resistivity with lower temperature and resulting high rapping reentrainment losses). The voltage controls did not increase power input as could have been expected due to lower gas temperature and ash resistivity, which would have reduced emissions. Manual adjustment of the controllers reduced emissions from 30 percent opacity to approximately 10 percent. The power level increase which could have been achieved (demonstrated by manual adjustment) by proper automatic voltage control averaged about 99 percent during this load reduction.

New automatic voltage controllers were estimated to be able to reduce emissions by up to 40 percent during a significant portion of the plant operation. The exact amount of reduction was not possible to calculate due to the large number of variable operating conditions.

Increased Power

Figure 5 shows a correlation of power to precipitator collection efficiency for several plants. The Sandow operating data indicate a power density before the modifications of 85 to 120 watts/1,000 acfm. This is consistent with the measured 97.4 percent collection efficiency (in comparison with the other plant data shown on Figure 6).

Figure 5 indicates that an increase in power corresponds to an increase in collection efficiency as high as 99.0 to 99.5 percent. Therefore, the installation of automatic voltage control systems which constantly seek the highest possible power input were anticipated to cause significantly improved performance.

Plate Alignment

Representatives of the precipitator supplier performed an inspection of the precipitator internals, particularly for plate alignment. Those plates found to be out of alignment by more than 1/4 inch were adjusted to bring them into proper alignment.

Discharge Electrodes

Discharge electrode failures were reported to be a problem with the Sandow precipitators. The breakage rate at Sandow was also reported to be increasing with time. Past periods of excessive sparking had deteriorated the electrodes.

The most common reason for electrode failure is electrical erosion. Failure due to corrosion or mechanical stress is less common. The observed poor performance of the automatic voltage control system may have been responsible for most of the electrode failures at Sandow, especially considering the age of the electrodes (9 to 10 years).

MODIFICATIONS

RAPPERS

The original rappers were replaced with repetitive impact electromagnetic rappers capable of higher impact energy. Repetitive impact electromagnetic rappers capable of up to 25 ft/lbs maximum impact energy with frequency and impact intensity adjustments were the best choice for this application since lignite quality variation may result in the need for high impact intensity (for highly resistive ash) or low impact intensity (to help solve the current rapper reentrainment problem).

Installation of the new rappers was done on-line by deactivating one field of rappers per day. The existing rapping shafts which penetrate the precipitator roof were retained and used with the new rappers. The rapping shafts were manually rapped throughout the day as the new rappers were being installed. Brief transformer/rectifier outages were necessary to replace the discharge electrode rappers.

RAPPER CONTROLS

The new rapping control system was easy to install. The controllers were provided in a new control cabinet which was installed in the existing precipitator control room. Existing wiring from the control room to the rappers was utilized.

The new system is a microprocessor based system with digital controls. The rapper program is independent for each field, permitting fine tuning for individual fields. The control program among fields is easily modified from the field sequence matrix board. All controls settings are made with slide and thumbwheel switches so that there is no need for rapper system reprogramming following a power outage.

Error detection and recording for open or short-circuits to rapper sections is also provided with rapper operation continuing during the fault readout mode.

AUTOMATIC VOLTAGE CONTROLLERS

The new automatic voltage controllers are of the analog, thristor type. They were easily located in the existing control cabinets after removal of the replaced equipment. The first controller replacement took approximately six hours. With practice, subsequent controllers were changed in just a few hours each. The work was done with the boiler operating by taking one precipitator transformer/rectifier out of service at a time.

New controllers respond much faster to changes in operating conditions. This allows a higher average power input to the precipitator without experiencing excessive sparking.

DISCHARGE ELECTRODES

It was decided to replace the electrodes with barbed electrodes in the inlet fields and unbarbed electrodes in the outlet field. It is expected that with new electrodes and automatic voltage controllers, the electrode failure rate would decrease.

RESULTS OR PERFORMANCE IMPROVEMENTS

Four areas were identified as having significant potential for improving precipitator performance. The extent of improvement appears to be as follows:

- The newly installed rapping system has greatly increased the flexibility in system operation. Control of individual rappers is permitted and sequencing of the rappers in field 3 has greater freedom for variations in operation. Also, the field 3 rappers in Units 1 and 2, which share a common chimney and opacity monitor, are intertied to assure that they are not operated simultaneously, which might cause concurrent opacity spikes higher in value than that for a single unit. A new rapper system and rapper control system were estimated to be able to reduce short-term emission opacity spikes by up to 50 percent. Based on operating data since the new voltage control equipment was installed and new rappers installed, opacity excursions have been reduced by over 75 percent.

- Installation of new automatic voltage controllers has significantly increased power input to the precipitator. Direct comparison of power levels before and after modifications indicated an actual increase of

103 percent, which exceeds the 55 percent potential increase originally observed. Adjustment of the controllers with rapper program optimization could possibly increase further the levels of power input. The increased power results in an increase in power density to approximately 250 watts/1,000 acfm. Based on operating data since the new equipment was installed, emission reductions have been greater than 45 percent and substantially higher power levels are being attained (Figures 6 and 7). The data of Figure 7 represent the average of 323, 110, and 134 daily average opacity values, respectively.

- o Replacement of the discharge electrodes will improve precipitator reliability and performance by reducing the frequency of wire breakage by replacement of those which had a long operating life and could be expected to fail in the immediate future.

CONCLUSIONS

Installation of new voltage controllers, rapper controllers, rappers, and discharge electrodes has produced an actual power increase to 250 watts/1,000 acfm. This has resulted in improved precipitator performance, reduced daily opacity values, and fewer daily opacity excursions from Sandow Units 1, 2, and 3. If further emission reductions are necessary, incorporation of the recommendations made as a result of the model tests will be considered. Flue gas conditioning also would be beneficial for the periods when low sulfur lignite is burned.

The work described in this paper was not funded by the U. S. Environmental Protection Agency and therefore the contents do not necessarily reflect the views of the Agency and no official endorsement should be inferred.

FIGURE 1
COLLECTION EFFICIENCY vs SCA
GUARANTEE vs UNIT 1 TEST DATA

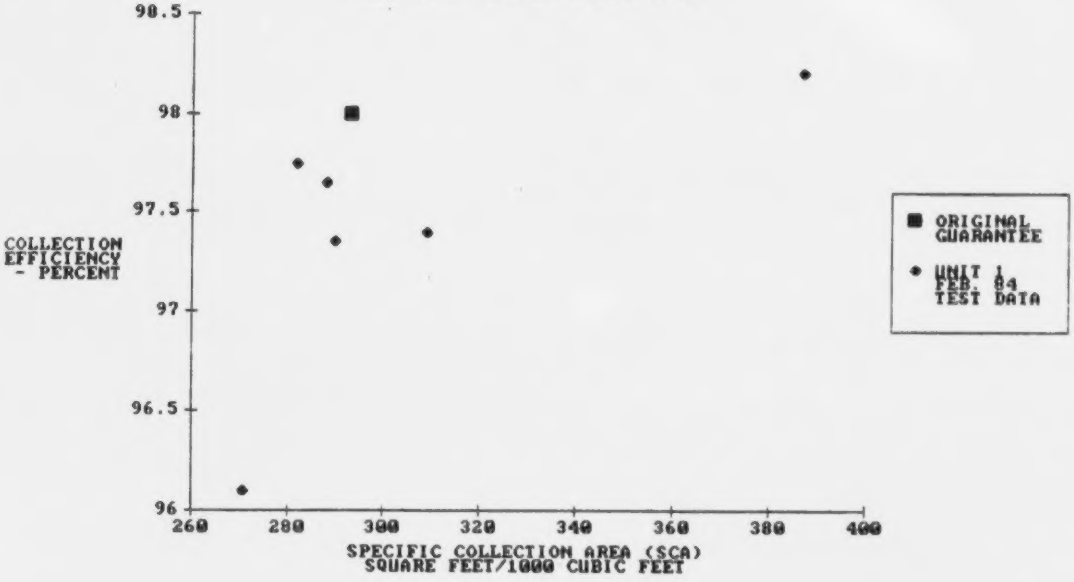

FIGURE 2
PARTICLE SIZE DISTRIBUTION
PRECIPITATOR INLET

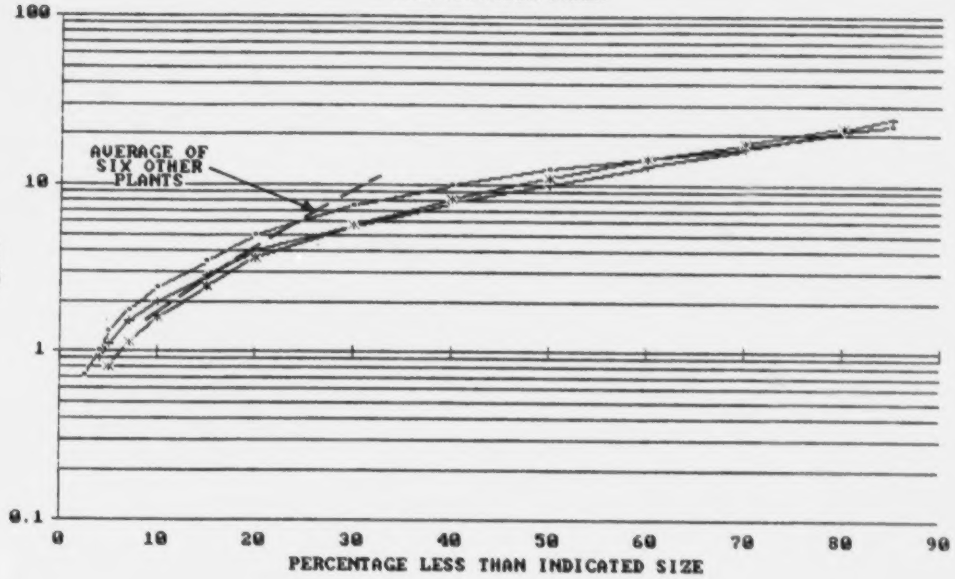

FIGURE 3
PARTICLE SIZE DISTRIBUTION
PRECIPITATOR OUTLET

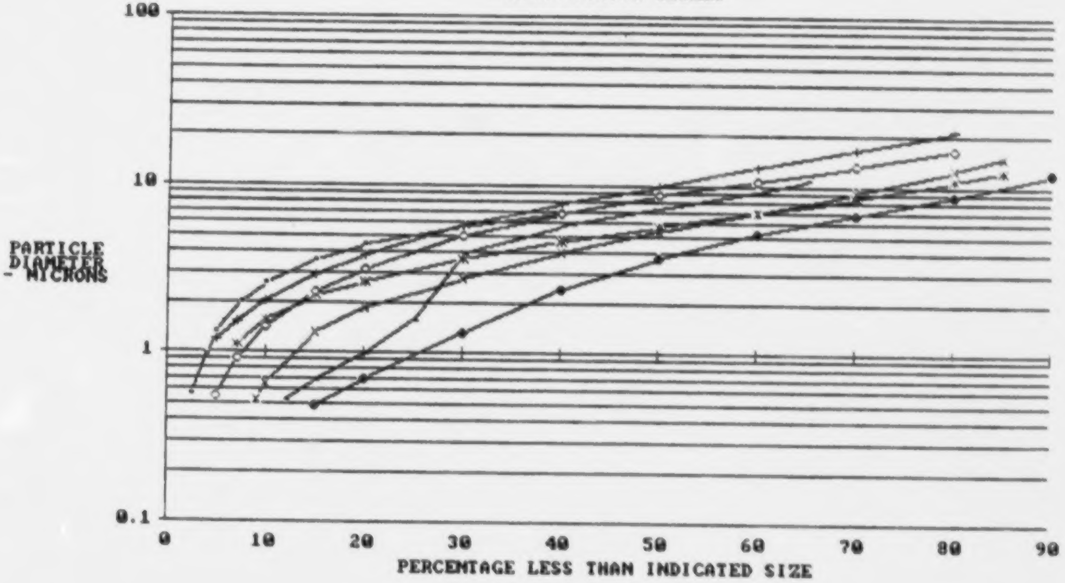

FIGURE 4
OPACITY vs GRAIN LOADING

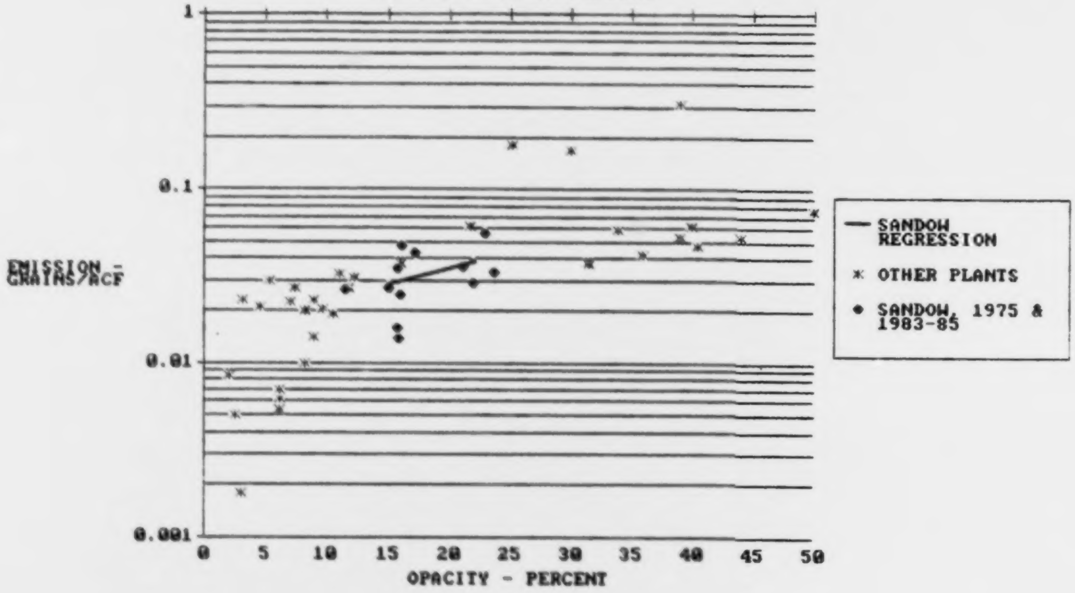

FIGURE 5
POWER vs COLLECTION EFFICIENCY
SANDOW AND OTHER PLANTS

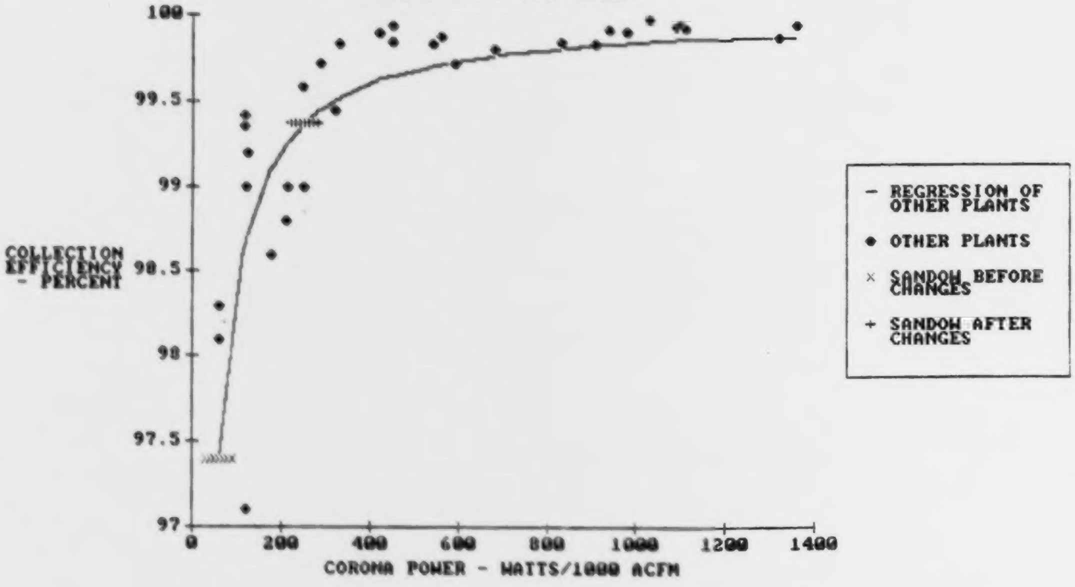

FIGURE 6
PERFORMANCE IMPROVEMENT

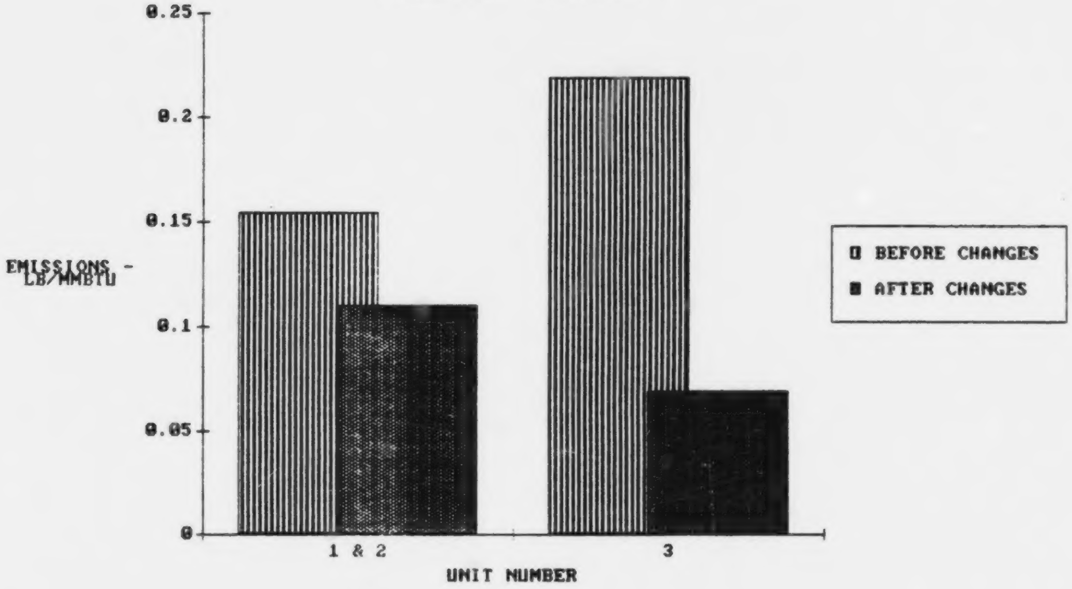

FIGURE 7
AVERAGE DAILY OPACITY
(OPACITY LIMIT = 30%)
APRIL 83 - NOVEMBER 85

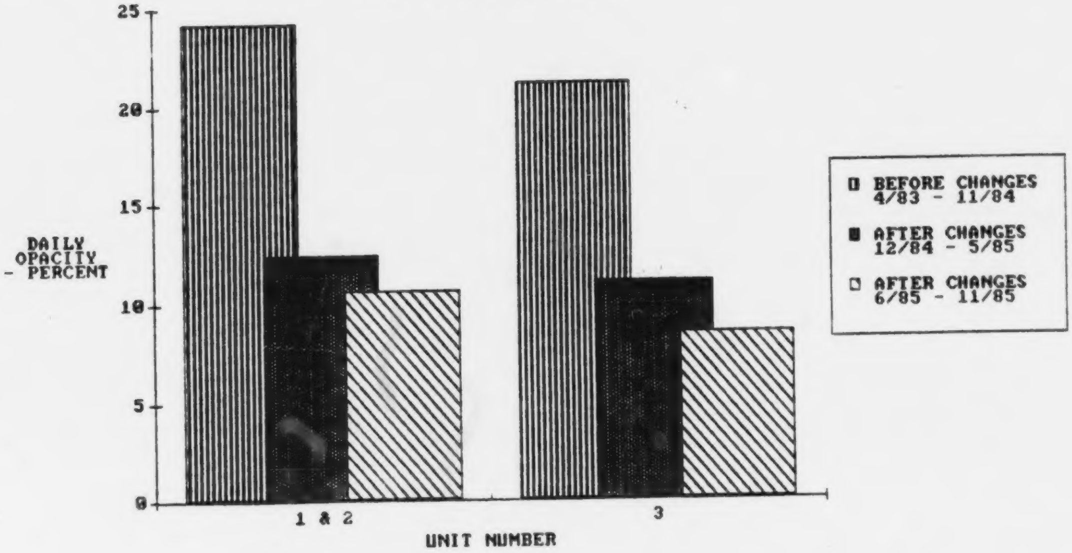

PERFORMANCE IMPROVEMENT AND FIRE PREVENTION IN FLY ASH COLLECTION SYSTEM AT A 50MW WOOD FIRED POWER PLANT

by: E. Gal and M. Murphy
General Electric Environmental Services, Inc.
Lebanon, PA 17042

ABSTRACT

Burlington Electric, J. C. McNeil Generating Station is the largest (50MW) wood fired power plant in the U.S. Mechanical cyclones and an electrostatic precipitator (ESP) are used in series to meet the stringent emission limit of 0.003 grains/acf. During initial operation, the particulate collection system experienced internal fires as well as plugging of cyclone and ESP hoppers. The cause of this problem was determined to be a combination of high combustible content of the fly ash, low cyclone efficiency resulting from lower than design gas flow rate, and improper operation of the fly ash removal system. A detailed system analysis was performed to identify operational modifications which were implemented with minimal disruption to plant operation. The corrective measures improved cyclone collection efficiencies, eliminated the fires and significantly improved performance and reliability of the fly ash removal system. Since the modifications were completed in October 1984, the particulate collection system has been operating smoothly, and has consistently exceeded particulate emission reduction requirements.

INTRODUCTION

Burlington Electric's J.C. McNeil Station is a wood fired 50MW power plant. The boiler is designed to produce 480,000 lb/hr steam at a temperature of 950°F and pressure of 1275 psi. Ash content and high heating value of the wood chips fed to the boiler are 0.9% and 8170 Btu/lb respectively based on bone dry wood while the moisture content is as high as 55%. The fly ash produced during the combustion of the wood is rich in combustible material with a low overall mass/volume ratio. This results in light particulates which are easily entrained. Fly ash emissions are controlled by mechanical cyclone collectors and an electrostatic precipitator installed in series between the air heater outlet and the ID fan inlet. The outlet particulate emission is guaranteed not to exceed 0.003 grain/acf which at design inlet conditions, represents 99.9% particulate collection efficiency.

The particulate collection system consists of four Buell (now GEESI) model No. 6B56CG37 cyclone collector banks, and one GEESI model BA1.2x52K4443-6.4P electrostatic precipitator. A plan view schematic of the particulate collection system is shown in Figure 1 and equipment details are given in Table 1. The need for refractory lined cyclones arises from the presence of a high percentage of combustible-rich burning particulates. These particles are collected in the hoppers and reinjected to the boiler. During the first six months of operation, the fly ash collecting system experienced hopper plugging and fires in hoppers and on ESP collecting plates.

TABLE 1. PARTICULATE COLLECTION SYSTEM EQUIPMENT DETAILS

Four Cyclone Collector Banks:

- Buell (GEESI) Model No. 6B56CG37
- Six Individual Cyclones per Bank
- Common Top Outlet Box per Bank
- Common Hopper with one Level Indicator per Bank
- Hexmesh Refractory Linings
- One Inlet Damper per Bank
- Dry Chain Conveyor Ash Removal System

One Electrostatic Precipitator:

- GEESI Model No. BA1.2x52K4443-6.4P
- Two Cells Wide, 52 Gas Passages per Cell
- Thirty Feet High Collecting Plates
- Fifteen Bus Sections, 3 Feet deep each
- Electromagnetic Impact Electrode Cleaning System
- Inlet/Outlet Nozzles
- Interconnecting Ductwork
- Structural Support Steel
- Dry Chain Conveyor Ash Removal System

BACKGROUND

REASONS FOR FLY ASH FIRES

Fires in the fly ash collecting system occurred due to the following simultaneous conditions:

1. Particulates rich in combustible material.
2. Environment rich in oxygen.
3. Burning particulates and/or a source of ignition.

In electrostatic precipitators, particularly those installed on bark and wood boiler applications where combustible content of the fly ash is high and sparking is a common phenomena, accumulation of fly ash on the collecting plates should be avoided. Based on the design conditions for the J.C. McNeil Station, it is estimated that it would take only 1 to 2 hours for a potentially combustible layer of fly ash to accumulate on the ESP collecting plates. The collecting plate cleaning system set up to operate frequently is enough to prevent dangerous accumulation of fly ash, but problems may arise in case of system malfunction. Because of this, the ESP electrode cleaning system must be reliable and flexible enough to allow at least several cleaning sequences to be performed without causing reentrainment problems. Accumulation of fly ash should also be minimized in the hoppers and ducts where highly combustible particulates can burn for long periods. Fly ash in a plugged cyclone hopper was reported to be hot and glowing three days after a boiler shutdown. Continuous evacuation of the fly ash from the system eliminates the fuel which is required to sustain a fire.

Fly ash accumulation becomes potentially dangerous in the presence of oxygen rich flue gas since the rate of oxidation (fire) of combustible material is determined by the rate of oxygen supply. It is recommended that the free oxygen level in the boiler outlet be kept below 4% to ensure safe operating conditions. Unfortunately the oxygen level may be much higher through leakages, open access doors or an increase in combustion excess air, especially at low load operation. Once the combustible-rich, hot fly ash is exposed to oxygen-rich flue gas in either hoppers, ducts or on collecting plates, the potential for a fire significantly increases.

HISTORY OF OPERATIONAL PROBLEMS

The J.C. McNeil Station went on line in early 1984 and was operating within opacity and emission limits. However, operation related problems with the particulate collection system did develop and included the following:

1. Cyclone and electrostatic precipitator hopper fires and plugging.
2. Electrostatic precipitator internal fires.

Fires within the precipitator or in its hoppers caused serious collecting plate damage. During inspection in May 1984, 220 collecting plates were bowed and out of tolerance. The collecting plate damage was caused by a fire that started in one of the hoppers and spread to the plates above. During another inspection in August 1984, a total of 75 collecting plates were bowed about 2 to 3 inches. This time there were no signs of a hopper fire and it was assumed that the fire started on the plates themselves.

Major hopper plugging occurred at least four times during a six month period. In one case a hopper containing fly ash was not evacuated until a few days after a boiler shutdown. The fly ash in the hopper had bridged and burst into flames when an access door was opened.

PROBLEM DEFINITION

The design conditions for the J.C. McNeil Station are summarized in Table 2, along with the actual conditions measured by GEESI's field service personnel on November, 7-9, 1984.

TABLE 2. DESIGN AND ACTUAL MEASURED CONDITIONS

		DESIGN	ACTUAL
1. Steam generation,	Lbs/hr	480,000	489,000**
2. Wood feed to burner,	Lbs/hr	208,700	150,000*
3. Excess air,	%	50	20-25**
4. Free Oxygen,	%	5.2	3.2*
5. Moisture in wood,	%	55	43**
6. Moisture in flue gas	%	24	23.8*
7. Overall boiler efficiency,	%	66.5	75**
8. Flue gas volume,	acfm	418,000	270,000*
9. Flue gas flow rate, max.	Lbs/hr	1,080,000	790,000**
10. Flue gas temperature,	°F	335	290*
11. Fly ash inlet load,	grains/acf	2.95	0.56*

* Measured ** Calculated

The impact of excess air and moisture content of the wood on moisture content of the flue gas, the wood feed rate to the boiler, the boiler overall thermal efficiency, the free oxygen level in the flue gas and the volumetric flow rate of the flue gas over the 290-335°F normal operating range are illustrated in Figures 2-6 respectively. The design and actual values are also shown. At full steam generation, the flue gas volume is 35% lower than design due to a combination of low excess air, reduced fuel moisture content and low air preheater outlet flue gas temperature.

Efficiency of cyclones decreases with a decrease in gas flow rate and with a decrease in particulate specific gravity as shown in Figure 7. Since combustible-rich particulates are lighter than particulates with low combustible fraction (see Table 3), their collection efficiency decreases faster with the decrease in flue gas volumetric flow rate. The average specific gravity of the fly ash in the J.C. McNeil Station is 1.3 with a range of 0.5 to 2.0. Thus the decreased gas flow rate not only reduced cyclone collection efficiency and increased total grain load to the electrostatic precipitator, but also increased the load of the light combustible-rich particulates to the electrostatic precipitator. Mass and composition balance on a cyclone (see Figure 8) shows that at 70% collection efficiency, 35% of the cyclone gas outlet grain loading (electrostatic precipitator inlet) is combustible material compared to almost 50% in the collected ash. When cyclone efficiency decreases, additional material normally collected in the cyclone, exits at the gas outlet, increasing the combustible load to the electrostatic precipitator. As was mentioned, combustible rich particulates in the electrostatic precipitator increase the potential of fire and must be avoided.

TABLE 3. SPECIFIC GRAVITY OF FLY ASH AS A FUNCTION OF COMBUSTIBLE CONTENT

Combustibles %	Specific Gravity
100	0.5
86	0.68
77	0.85
66	1.00
54	1.23
45	1.32
35	1.47
0	2.0

Specific gravity of char - 0.5
Specific gravity of inorganic ash - 2.0

As boiler load is decreased below 100%, flow rate of flue gases further decreases. During low load operation, cyclone collection efficiency is very low as long as all cyclones remain operating. Allowing low flow rates through the cyclones increases the potential of fire in the electrostatic precipitator due to the high ash carry-over. While there is a consistent temperature drop of about 20°F at full load through the precipitator, it was observed that ESP temperature gradient at low load was irregular, ranging from a loss of 5°F to a gain of 5°F. In one case the recorded outlet temperature was as high as 12°F above the recorded inlet temperature indicating the presence of burning particles and possibly a fire in the electrostatic precipitator.

CORRECTION MEASURES

The low flue gas flow rates through the cyclones resulted in lower than 50% collection efficiency. To improve efficiency, one cyclone out of six was closed in each bank increasing the flow rate per cyclone by 20% and the total pressure drop by about one inch W.G. which was offset by opening the ID fan damper. The cyclones were closed permanently by blind flanges in the gas and solid outlets.

By reducing the number of operating cyclones from 24 to 20 and assuming that the measured conditions (see Table 2) represent an average, the flow rate per cyclone increased from 11,250 acfm/cyclone to 13,500 acfm/cyclone. Collection efficiency of the cyclones increased to an average of 70% and combustibles percentage in cyclone top outlet was reduced from 35-45% to 25-35%.

Even with this modification, the 70% collection efficiency at the full boiler load is less than the design efficiency of 83% because the flow rate per cyclone is still lower than the design rate of 17,500 acfm/cyclone. Collection efficiency may be increased by shutting down more cyclones. Shutting down of four more cyclones (one in each bank) will increase the average flow rate to 17,000 acfm/cyclone, which is close to the original design flow rate. Due to potential flow distribution problems, only an even number of cyclones can be closed. Individual cyclone closing is permanent since inlet dampers were not installed in each cyclone. As a result, a permanent shut down of more cyclones would limit the plant if changes in flue gas flow rates due to variation in wood moisture content, combustion excess air, and increased load occur.

At lower than 50% boiler load operation, typically occurring at night, the two outer banks are shutdown and the plant operates with ten cyclones. The flow rate per cyclone through the ten operating cyclones increases to maintain high collection efficiency.

The hopper plugging problem results from fly ash accumulation which causes sintering and bridging of the material at the bottom of the hoppers. This problem was addressed by the recommendation to keep hoppers evacuated at all times by continuously operating the fly ash removal systems; i.e., rotary valves, vibrators, hopper heaters, mechanical conveyors and the ESP electrode cleaning system. In case of a shutdown, the removal systems are kept going until all hoppers are empty.

Since the implementation of previous recommendations regarding the shutdown of a total of four cyclones and the operation of the fly ash removal systems (which covers the period of late October 1984 to the end of 1985), the unit has operated smoothly with no reported fires or major hopper plugging.

On November 13, 1984, particulate collection system successfully passed emission tests with a measured outlet grain loading of 0.001-0.0015 grain/acfm as compared to the guarantee of 0.003 grains/acfm.

CONCLUSIONS

The combination of refractory lined mechanical cyclone collectors and an electrostatic precipitator installed on a wood fired boiler can operate with low risk of fires. Burning particles which reach the mechanical collectors are typically large and can be effectively collected. The particles which pass downstream of an efficient mechanical collector are small, with relatively low combustibles. To ensure high cyclone efficiency, flow rate through individual cyclones should be as close to the design conditions as possible. Lower than design flue gas flow rate at low boiler load or due to low excess air or moisture content is addressed by reducing the number of operating cyclones. An on-off flow control to individual cyclones is recommended for efficient mechanical collector system performance.

Accumulation of fly ash in hoppers for long periods of time should be avoided and ash handling systems should be continuously operated to remove the accumulated material. Otherwise the particles which are rich in combustibles may burn inside the hoppers causing internal damage to the collecting plates and plugging of the hoppers and fly ash removal system.

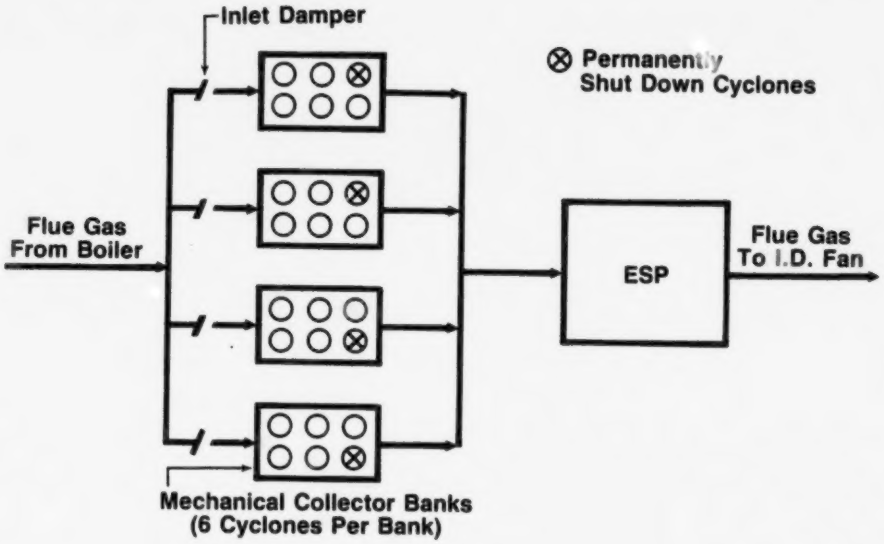
Inlet Damper
⊗ Permanently Shut Down Cyclones
Flue Gas From Boiler
ESP
Flue Gas To I.D. Fan
Mechanical Collector Banks (6 Cyclones Per Bank)

Figure 1. Schematic Plan View of Particulate Collection System

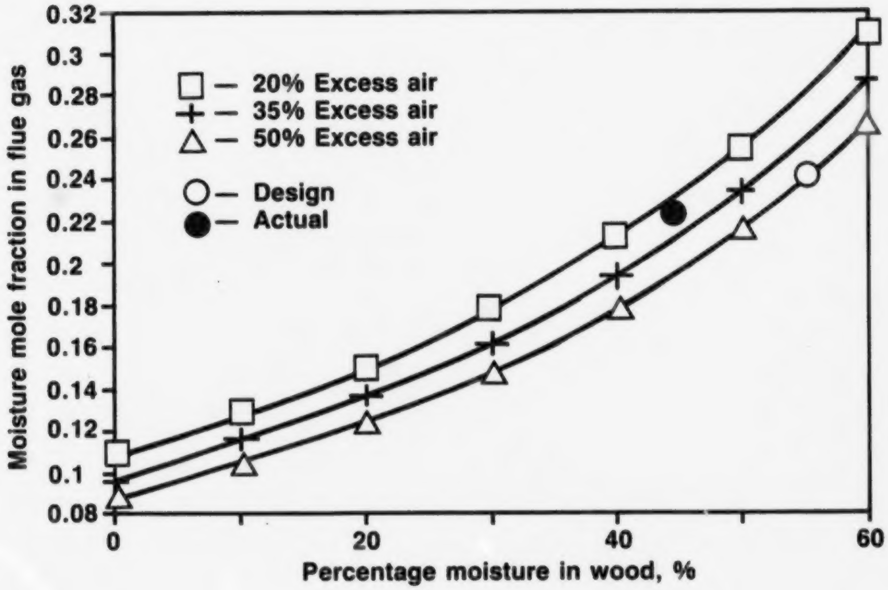

Figure 2. Water Mole Fraction in Flue Gas as a Function of Wood Moisture and Excess Air

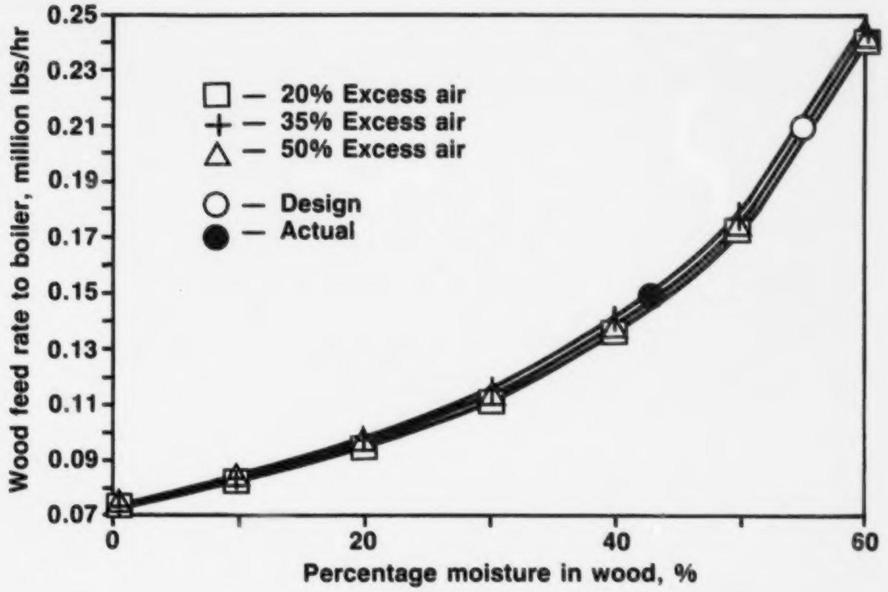

Figure 3. Wood Feed Rate to Boiler as a Function of Wood Moisture and Excess Air

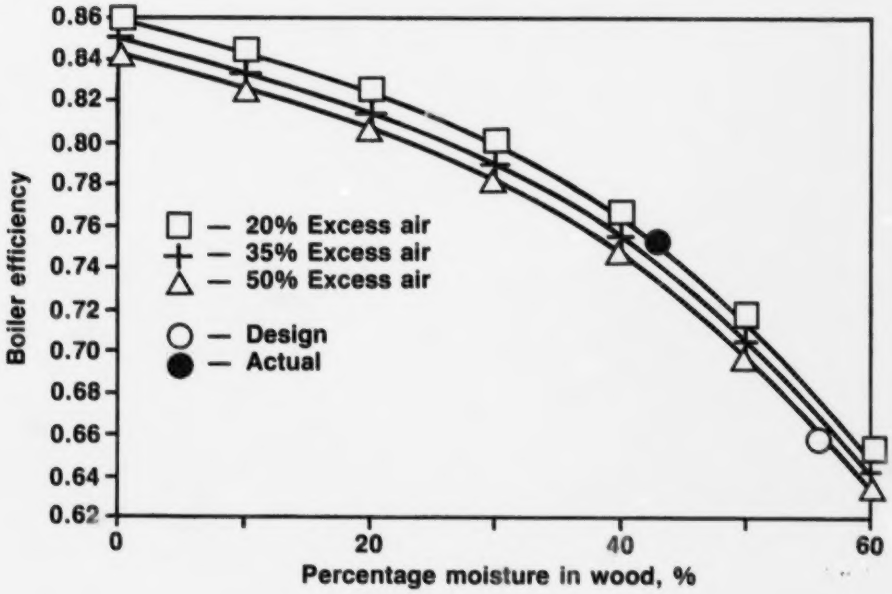

Figure 4. Boiler Thermal Efficiency as a Function of Wood Moisture and Excess Air

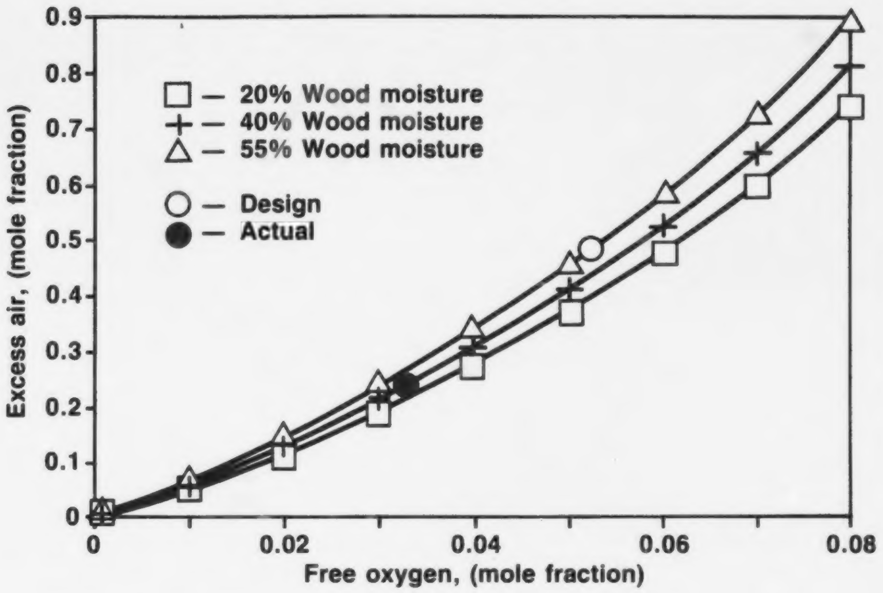

Figure 5. Free Oxygen in Flue Gas as a Function of Wood Moisture and Excess Air

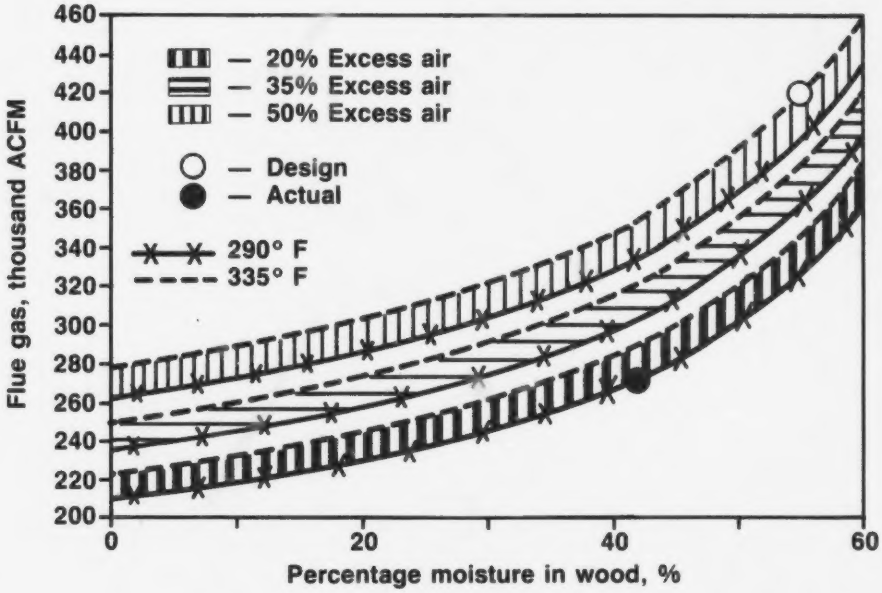

Figure 6. Flue Gas Flow Rate as a Function of Wood Moisture and Excess Air

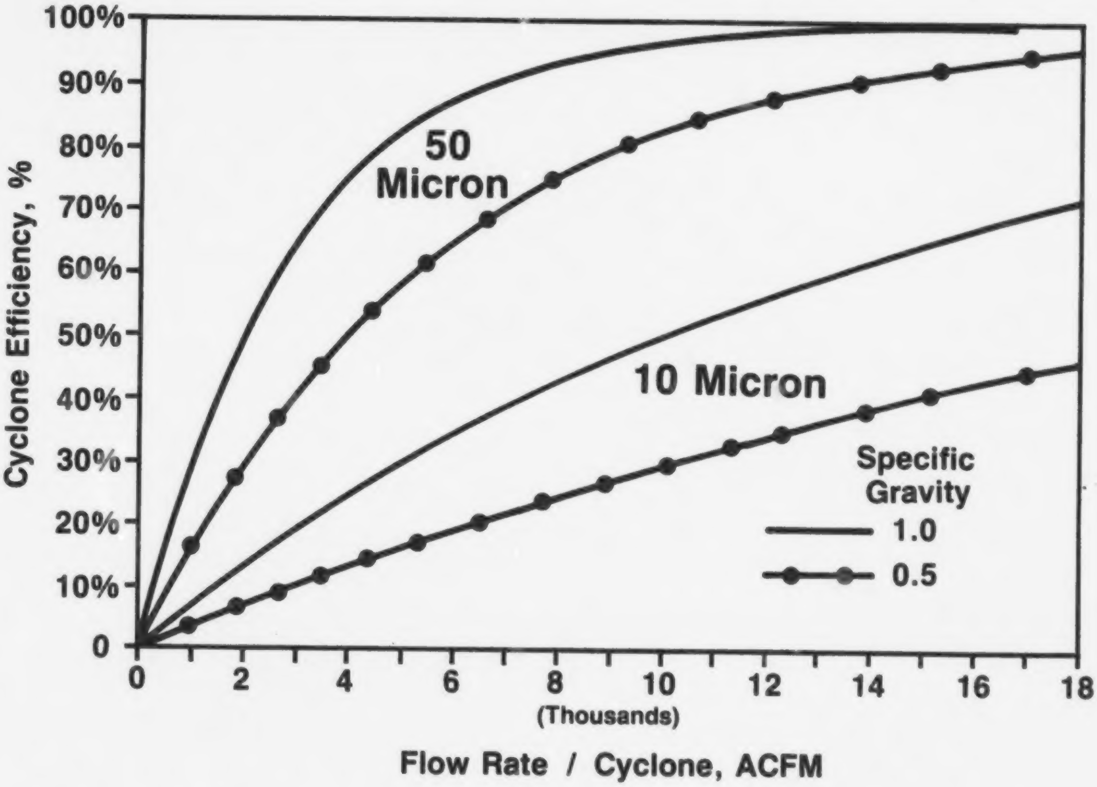

Figure 7. Cyclone Efficiency as a Function of Flue Gas Flow Rate

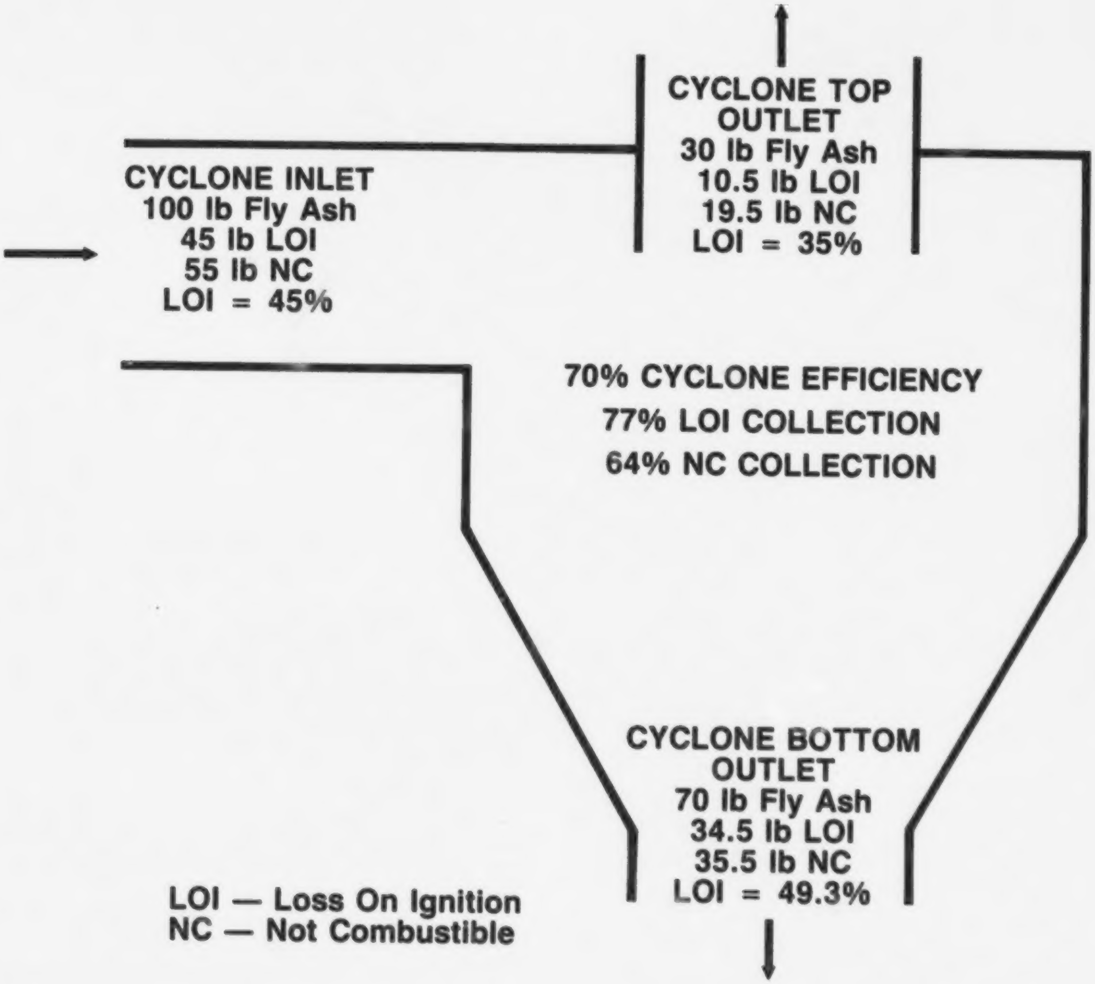
CYCLONE TOP OUTLET
30 lb Fly Ash
10.5 lb LOI
19.5 lb NC
LOI = 35%
CYCLONE INLET
100 lb Fly Ash
45 lb LOI
55 lb NC
LOI = 45%
70% CYCLONE EFFICIENCY
77% LOI COLLECTION
64% NC COLLECTION
CYCLONE BOTTOM OUTLET
70 lb Fly Ash
34.5 lb LOI
35.5 lb NC
LOI = 49.3%
LOI — Loss On Ignition
NC — Not Combustible

Figure 8. Cyclone Mass and Content Balance

Session C-7: FUGITIVE EMISSIONS

Dale L. Harmon, Chairman
U. S. EPA/AEERL
Research Triangle Park, NC

IDENTIFICATION, ASSESSMENT, AND CONTROL OF FUGITIVE PARTICULATE EMISSIONS

by: Chatten Cowherd, Jr.
John S. Kinsey
Midwest Research Institute
Kansas City, Missouri 64110

Dale L. Harmon
Air and Energy Engineering Research Laboratory
U.S. Environmental Protection Agency
Research Triangle Park, North Carolina 27711

ABSTRACT

The U.S. Environmental Protection Agency (EPA) has funded the preparation of a technical guidance document for the identification, assessment, and control of fugitive particulate emissions. The purpose of this document is to assist control agency personnel in evaluating fugitive emissions control plans and to assist industry personnel in the development of cost-effective control strategies. The document describes procedures for developing a cost-effective strategy for the control of fugitive particulate emissions within any specific plant or geographic setting. Also, it provides sources of data or, in some cases, the actual data needed to implement the procedures, along with fully worked examples.

This paper summarizes the content of the above guidance document. Although a variety of control techniques applicable to sources of fugitive particulates are discussed, control efficiency values are specified only for those control options which have been tested for effectiveness. Also, greater emphasis is placed on open dust sources than on process sources. This is consistent with the larger body of available data on the performance of open dust source controls. Finally, procedures for the determination of control costs and cost-effectiveness are summarized, and cost elements are described for the major generic classes of fugitive controls.

This paper has been reviewed in accordance with the U.S. Environmental Protection Agency's peer and administrative review policies and approved for presentation and publication.

INTRODUCTION

Fugitive particulate emissions are discharged by a wide variety of sources both in the industrial and in the nonindustrial sectors. Fugitive emissions refer to those air pollutants that enter the atmosphere without first passing through a stack or duct designed to direct or control their flow.

Fugitive particulate emission sources may be separated into two broad categories: process sources and open dust sources. Process sources of fugitive emissions are those associated with industrial operations that alter the chemical or physical characteristics of a feed material. Examples are emissions from charging and tapping of metallurgical furnaces and emissions from crushing of mineral aggregate. Such emissions normally occur within buildings and, unless captured, are discharged to the atmosphere through forced or natural draft ventilation systems. Open dust sources entail the entrainment of solid particles into the atmosphere by the forces of wind or machinery acting on exposed materials. Open dust sources include industrial sources associated with the open transport, storage, and transfer of raw, intermediate, and waste materials, and nonindustrial sources such as unpaved and paved public roads and construction activities.

To assist regional, state,and local air pollution control agency personnel in evaluating fugitive emissions control plans and to assist industry personnel in the development of cost-effective control strategies, the U.S. Environmental Protection Agency has funded the preparation of a technical guidance document on the identification, assessment, and control of fugitive particulate emissions (1). The document, which is summarized in this paper, describes the procedures for developing a cost-effective strategy for the control of fugitive particulate emissions within any specific plant or area setting. Also, it provides sources of data or in some cases actual data needed to implement the procedures. Cost-effectiveness is defined as the annualized cost of control divided by the reduction in total annual particulate emissions ($/Mg), as a result of the fugitive emissions control system being employed. Control costs include the capital, operating, and maintenance costs associated with the system over its useful life.

Whether the sources of interest are contained within a specific industrial facility or distributed over an air quality control jurisdiction, the general procedure for control strategy development is the same. The steps are:

Step 1: Source identification.

Step 2: Preparation of an emissions inventory.

Step 3: Identification of control alternatives.

Step 4: Estimation of control system performance.

Step 5: Estimation of control costs.

Step 6: Selection of cost-effective controls.

Figure 1 graphically summarizes the procedure. This paper focuses on Steps 3, 4, and 5.

CONTROL ALTERNATIVES

Typically, there are several options for the control of fugitive particulate emissions from any given source. This is clear from the mathematical equation used to calculate the emission rate:

$$R = M\,e\,(1 - c)$$

where:

R = estimated mass emission rate

M = source extent

e = uncontrolled emission factor; i.e., mass of uncontrolled emissions per unit of source extent

c = fractional efficiency of control

To begin with, because the uncontrolled emission rate is the product of the source extent and uncontrolled emission factor, a reduction in either of these two variables produces a proportional reduction in the uncontrolled emission rate.

Although the reduction of source extent results in a highly predictable reduction in the uncontrolled emission rate, such an approach in effect usually requires a change in the process operation. Frequently, reduction in the extent of one source may necessitate the increase in the extent of another, as in the shifting of vehicle traffic from an unpaved road to a paved road. The option of reducing the source extent is beyond the scope of this paper and will not be discussed further.

The reduction in the uncontrolled emission factor may be achieved by process modifications (in the case of process sources) or by adjusted work practices (in the case of open sources). The degree of the possible reduction of the uncontrolled emission factor can be estimated from the known dependence of the factor on source conditions that are subject to alteration. For open dust sources, this information is embodied in the predictive emission factor equations for fugitive dust sources as presented in Section 11.2 of Reference 2.

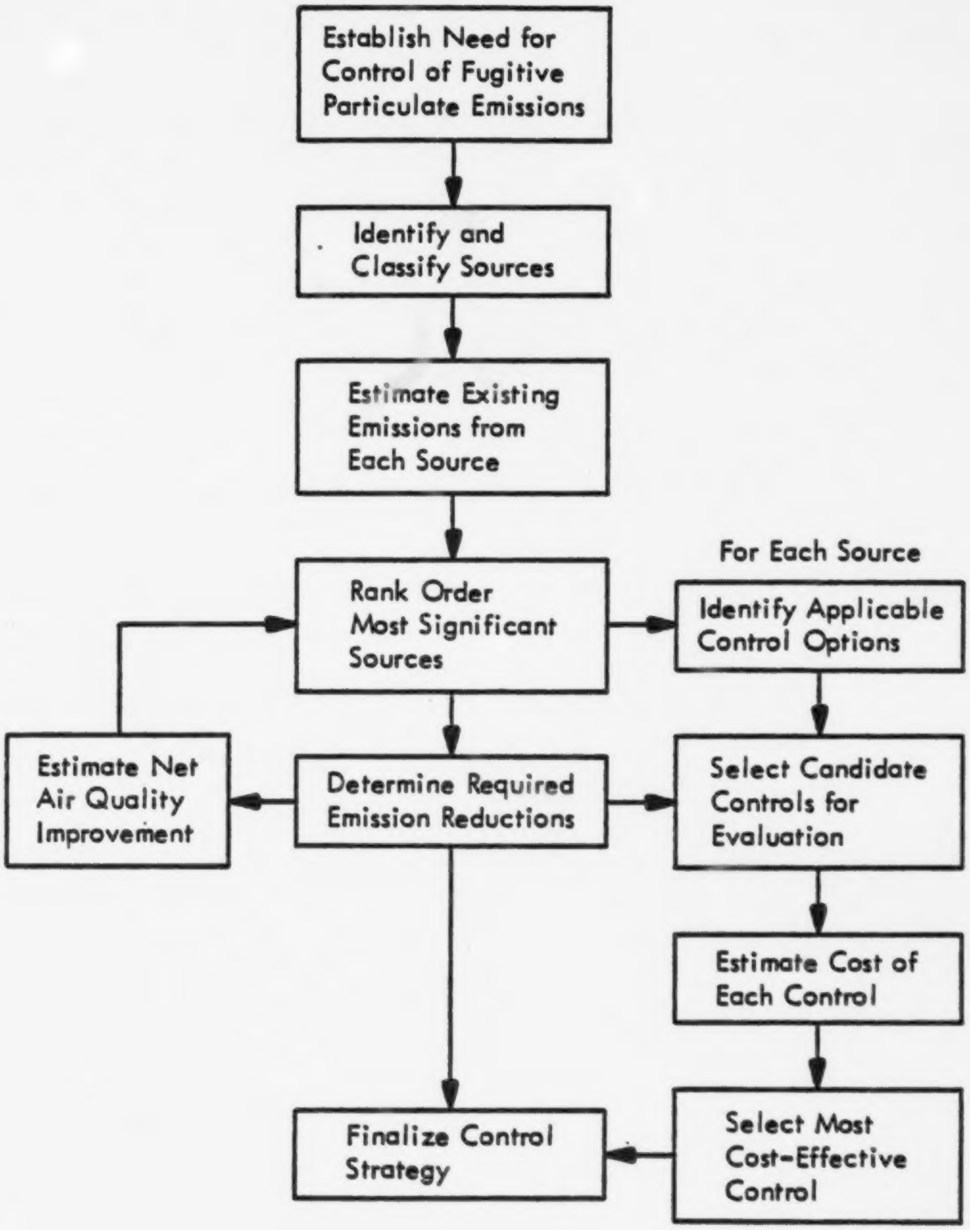
Establish Need for Control of Fugitive Particulate Emissions
Identify and Classify Sources
Estimate Existing Emissions from Each Source
For Each Source
Rank Order Most Significant Sources
Identify Applicable Control Options
Estimate Net Air Quality Improvement
Determine Required Emission Reductions
Select Candidate Controls for Evaluation
Estimate Cost of Each Control
Finalize Control Strategy
Select Most Cost-Effective Control

Figure 1. Flow diagram for the identification, assessment, and control of fugitive particulate emissions.

The reduction of source extent and the incorporation of process modifications or adjusted work practices are preventive techniques for control of fugitive particulate emissions. In addition, there are a variety of add-on measures which can be used for (a) prevention of the creation and/or release of particulate matter into the atmosphere, or (b) capture and removal of the particles after they have become airborne.

The alternative add-on approaches available for the control of open dust sources include:

1. Stabilization of Unpaved Travel Surfaces
    - Wet suppression
    - Chemical stabilization
    - Physical stabilization
    - Paving
2. Improvement of Paved Travel Surfaces
    - Surface cleaning
    - Resurfacing
    - Reduction of mud/dirt track-on
3. Stabilization of Piles/Exposed Areas
    - Wet suppression
    - Chemical stabilization
    - Physical stabilization
4. Enclosure of Piles/Exposed Areas or Materials Handling
    - Passive enclosures (including wind fences)
    - Active enclosures
5. Wet Suppression for Materials Handling
6. Plume Aftertreatment for Materials Handling
    - Fine water sprays
    - Charged fog

All of these techniques are preventive measures except for active enclosures and plume aftertreatment, which are capture/removal methods. Plume aftertreatment refers to any system which injects fine water droplets into a dust plume to capture and agglomerate the suspended particles, thereby enhancing gravitational settling.

Most of the preventive measures involve periodic rather than continuous control application. Familiar examples are the watering of unpaved travel surfaces and the cleaning of paved travel surfaces. The resultant control efficiency follows a cyclic pattern, decaying in time from the highest value immediately after application. Because of the finite durability of these control techniques, ranging from hours to months, it is essential to relate an average efficiency value to a frequency of application. For measures of extended durability such as paving, the application program required to sustain control effectiveness should be indicated. One likely pitfall to be avoided is the use of field data collected soon after control measure application to represent the average control efficiency over the lifetime of the measure.

For a periodically applied control measure, the most representative value of control efficiency is the time average, given by:

$$C(T) = \frac{1}{T} \int_{o}^{T} c(t)\, dt \qquad (1)$$

where:

$C(T)$ = average control efficiency during period of T days between applications (percent)

$c(t)$ = instantaneous control efficiency at t days after application (percent), where $t \leq T$

It must be emphasized that the rate of control efficiency decay is heavily dependent upon the source and control variables discussed in the following section.

The alternative add-on approaches available for the control of process fugitive emissions include:

1. Wet Suppression
    - Water sprays (with and without chemical additives)
    - Foams
2. Enclosures
    - Passive enclosures (without evacuation)
    - Active enclosures (with evacuation to a dust collector)
3. Hooding Systems
    - Receiving hoods
        - Canopy hoods
        - Close capture hoods
        - Hoods for mechanically directed plumes
    - Capture hoods
        - Side draft hoods
        - Push/pull hooding systems
        - High velocity low volume hoods
        - Close capture hoods

4. Plume Aftertreatment
    - Fine water sprays
    - Electrostatic foggers

Wet suppression and passive enclosures are preventive measures; whereas, hooding systems and plume aftertreatment are capture/removal methods. All of these controls are designed to be continuously applied.

CONTROL PERFORMANCE

The performance capability of a fugitive particulate emissions control system depends on the characteristics of the uncontrolled source emissions and on the design of the control system. Therefore, in utilizing published control efficiency data for control performance assessment, care must be taken to document the source and control parameters tied to each control efficiency data set.

One of the important characteristics of the uncontrolled source emissions is the particle size distribution. Published control efficiency data are tabulated in the subject document for the following particle size fractions:

TP	Total airborne particulate matter.
TSP	Total suspended particulate matter, as represented approximately by particles equal to or smaller than 30 µm in aerodynamic diameter, as measured by a standard high-volume sampler.
IP	Inhalable particulate matter consisting of particles equal to or smaller than 15 µm in aerodynamic diameter.
PM_{10}	Particulate matter consisting of particles equal to or smaller than 10 µm in aerodynamic diameter.
RP	Respirable particulate matter consisting of particles equal to or smaller than approximately 3.5 µm in aerodynamic diameter, corresponding to the penetration characteristics of a standard cyclone for industrial hygiene measurements.
FP	Fine particulate matter consisting of particles equal to or smaller than 2.5 µm in aerodynamic diameter.

For purposes of illustration, this paper summarizes the control performance data for the PM_{10} particle size fraction, which comprises a small but representative subset of the total published control performance data.

The control of dust emissions from unpaved roads has received the widest attention in the literature (see Table 1).

TABLE 1. CLASSIFICATION OF TESTED ROAD DUST SUPPRESSANTS

Dust suppressant category	Trade name	Number of valid controlled tests
Petroleum-based	Petro Tac	8
	Coherex	124
	Arcote 220	4[a]
	Arco 2200	20
	Arco 2400	91
Lignosulfonates	Lignosite	73
	Trex	3
	Flambinder	4[a] + 28
Salts	Peladow	1
	Liquidow	34
	Dustgard	11 (17)[b]
	Oil Well Brine	4
Polymer	Soil Sement	24
Surfactant	Biocat	3

[a] Arcote 220/Flambinder mixture.

[b] Numbers without parentheses represent TSP, and numbers in parentheses represent respirable particulate.

The PM_{10} control efficiency decay functions developed from testing of road dust suppressants are shown in Table 2. Table 3 shows average PM_{10} control efficiency data for watering of unpaved roads.

Although no published PM_{10} control efficiency data were found for water sprays or foam suppression systems applied to open dust sources, limited data were compiled for plume aftertreatment systems as shown in Table 4. Also, PM_{10} published control efficiency data were found for water sprays (Table 5) and capture systems (Table 6) applied to process sources of fugitive particulate emissions. Regarding use of the data in Table 6, it is usually appropriate to assume that the effectiveness of a capture/collection system is limited by the efficiency with which the plume is captured for ducting to a typically more efficient collection device.

TABLE 2. INSTANTANEOUS PM_{10} CONTROL EFFICIENCY AS A FUNCTION OF VEHICLE PASSES FOR UNPAVED ROAD DUST CONTROL TECHNIQUES[a]

Control measure	Time after application (days)	Average No. of vehicle passes per day	Mean vehicle parameters			Application intensity (L/m^2)	Dilution ratio ($L/L\ H_2O$)	Least-squares fit of PM_{10} control efficiency[b] (%)
			Weight (Mg)	Weight (tons)	No. of wheels			
Petro Tac - initial application	2-116	414	27	30	9.2	3.2	1:4	102 - 0.00113 V
Coherex® - initial application	7-41	95	34	38	6.2	3.8	1:4	94.9 - 0.0134 V
Coherex® - reapplication[c]	4-35	94	39	43	6.0	4.5	1:7	100 - 0.00430 V

[a] Based on tests at steel plants using the profiling measurement method (Reference 3).

[b] V represents cumulative vehicle passes after application. Complete mitigation is assumed immediately after application (i.e., c(0) = 100%).

[c] Main test section of road was retreated 44 days after initial application.

TABLE 3. FIELD DATA ON AVERAGE CONTROL EFFICIENCY OF UNPAVED ROAD WATERING[a]

Location	No. of tests	Month	Application intensity (L/m^2)	Average time between applications (hr)	Average traffic rate (hr^{-1})	Average potential evaporation (mm/hr)	Average control efficiency[b] (%)
N. Dakota	4	October	0.2	1.8	40	0.084	59
New Mexico	5	July/August	0.2	2.0	23	0.23	69
Ohio	3	November	0.6	4.5	98	0.042	77
Missouri	2	September	1.9	2.8	72	0.26	88

---

[a] Taken from Reference 4.

[b] No significant difference in control efficiency as a function of particle size was observed.

TABLE 4. AVERAGE CONTROL EFFICIENCY DATA FOR PLUME AFTERTREATMENT SYSTEMS (OPEN DUST SOURCES)

Ref.	Type of process	Type of material	Fogger system[a]	Measurement technique	Average control efficiency
5	Belt conveyor (located inside a building)	Quarry stone	2-Ransburg REA foggers at 180 degrees from each other along direction of belt travel; WFR = 94.6 cc/min total AF = 5.7 m^3/hr total	Near belt: 7-stage Andersen cascade impactor	70% (< 9 μmA)
6	Front loader dump into partially enclosed hopper (3-sided enclosure; 10 dumps/25 min; enclosure volume ≅ 40 m^3)	Bentonite ore (8% < 37 μm)	1-AeroVironment CFG mounted at end of enclosure; WFR = 60 L/hr AF = Not specified	Single pt: Hi-Vol w/cyclone and 2-stage impactor[b]	45% (< 7.3 μmA)
7	Open belt-to-belt transfer (drop height = 1.2 m)	Sinter fines	2-Ritten Fogger IVs 2-AeroVironment CFGs located 180 degrees from each transfer point; WFR = 56.8 L/hr/fogger AF = 3.8 m^3/hr/Ritten fogger; 50% max. (AV)	Above and next to source: Hi-vol; Hi-vol w/SSI; Hi-vol w/cyclones and 4-stage impactor[b,c]	31-55% (< ~ 6 μmA)
7	Crusher conveyor (conveyor tunnel = 3 m diameter)	Crushed limestone (< 10 mm)	1-Ritten Fogger IV 2-AeroVironment CFGs spray spray injected into tunnel counter-current to direction of belt movement; WFR = 113.5 L/hr (Ritten); 56.8 L/hr/AV fogger AF = 113.5 L/hr (Ritten); 50% maximum (AV)	Above and next to source: Hi-vol; Hi-vol w/SSI; Hi-vol w/cyclone and 4-stage impactor[c,d]	2-30% (< 6 μmA)

---

[a] The Ransburg and Ritten foggers are based on the original Hoenig design which uses induction charging and commercial spray nozzles. The AeroVironment prototype units use a rotary atomizer and direct charging to produce charged fog. AeroVironment CFG = 200 μm drops; $1.2(10)^{-6}$ C/g @ 4 kV; 16-24 m^3 spray volume. Ritten Fogger IV = 60 m drops @ 75 L/hr; $0.11(10)^{-}$ C/g @ 12.5 kV. WFR = water flow rate; AF = airflow to fogger(s).

[b] Hi-vol = standard high volume sampler; Hi-vol w/SSI = high volume air sampler equipped with Sierra 15 μmA size-selective inlet; Hi-vol w/cyclone and impactor = high volume air sampler equipped with Sierra Model 230CP cyclone precollector and Sierra Model 230 slotted cascade impactor.

[c] No background samples collected during test program.

[d] Samplers located both in tunnel next to conveyor and above tunnel exit.

TABLE 5. AVERAGE PM_{10} CONTROL EFFICIENCY DATA FOR WATER SPRAYS (PROCESS SOURCES)[a]

Type of process	Type of material	Control system parameters	Measurement technique[b]	PM_{10} efficiency (%)
Secondary crusher[c]	Limestone	Water spray - not specified	Downwind tracer; Type 1 test scheme[d]	92
Tertiary crusher[e]	Limestone	Water spray - not specified	Downwind tracer; Type 1 test scheme	83

[a] Taken from Reference 8.

[b] Type 1 tests include measurements of a single source with and without control.

[c] 385 Mg/hr, 8 cm material size.

[d] No calibration or wind data.

[e] 115 Mg/hr, 2 cm nominal material size.

TABLE 6. AVERAGE CONTROL EFFICIENCY DATA FOR CAPTURE/COLLECTION SYSTEMS (PROCESS SOURCES)

Ref.	Type of process	Type of material	Capture mechanism/ air pollution control device	Control system parameters	Measurement technique	Capture efficiency[a] (%)
9	Aluminum reduction cell-anode	Molten aluminum	Close capture hood/NA	Flow = 50 m^3/min	Tracer (H_2) in control system duct	70
				Flow = 80 m^3/min	Tracer (H_2) in control system duct	77
				Flow = 120 m^3/min	Tracer (H_2) in control system duct	91
				Flow = 160 m^3/min	Tracer (H_2) in control system duct	98
9	Aluminum reduction cell tapping	Molten aluminum	Close capture/NA	Flow = 120 m^3/min	Tracer (H_2) in control system duct	96
9	Anode removal	Molten aluminum	Close capture/NA	Flow = 120 m^3/min	Tracer (H_2) in control system duct	86
10	Banbury mixer	NA	Capture hood/NA	Hood 1 m from mixer, cooling fan off	Tracer (oil mist) in control system duct	90
				Hood 1 m from mixer, cooling fan on	Tracer (oil mist) in control system duct	40
				Hood 3 m from mixer, cooling fan off	Tracer (oil mist) in control system duct	70

---

[a] Measured indirectly with a tracer; no measurements of source emissions.

COST EFFECTIVENESS

The most informative method for comparing control measures or control strategies for particulate fugitive emissions sources is on a cost-effective basis. Mathematically, cost-effectiveness is defined as:

$$C^* = \frac{C_a}{\Delta R} \tag{2}$$

where:

C^* = cost-effectiveness (\$/mass of emissions reduced)

C_a = annualized cost of control equipment (\$/year)

ΔR = annual reduction in particulate emissions (mass/year)

The annual reduction in particulate emissions can be calculated from:

$$\Delta R = M\ e\ c \tag{3}$$

where:

M = annual source extent

e = uncontrolled emission factor (i.e., mass of uncontrolled emissions per unit of source extent)

c = average control efficiency expressed as a fraction

The annualized costs of control equipment can be calculated from:

$$C_a = CRF\ (C_p) + C_o + 0.5\ C_o \tag{4}$$

where:

C_a = annualized costs of control equipment (\$/year)

CRF = Capital Recovery Factor (1/year)

C_p = installed capital costs (\$)

C_o = direct operating costs (\$/year)

0.5 = plant overhead factor

The annualized cost of capital equipment is calculated by using a capital recovery factor (CRF). The capital recovery factor combines interest on borrowed funds and depreciation into a single factor. It is a function of the interest rate and the overall life of the capital equipment and can be estimated by:

$$CRF = \frac{i(1 + i)^n}{(1 + i)^n - 1} \qquad (5)$$

where:

i = interest rate (annual % as a fraction)

n = economic life of the control system (year)

The other major components of the annualized cost are operation and maintenance costs (direct operating costs) and associated plant overhead costs. Operation and maintenance costs generally include labor, raw materials, utilities, and by-product costs or credits associated with day-to-day operation of the control system. Another component of the operating cost is overhead, which is a business expense not charged directly to a particular part of the process but allocated to it.

SUMMARY

A variety of alternative control methods are available for fugitive particulate emissions. The efficiency and cost-effectiveness of each method depend to a large extent on the type of source being controlled and how the control is actually applied. Limited test data exist on efficiencies associated with the various control techniques. Of the available control measures, chemical suppression of unpaved road emissions has received the greatest attention.

ACKNOWLEDGEMENT

The work upon which this paper is based was performed pursuant to EPA Contract No. 68-02-3922. Dale L. Harmon served as EPA project officer for this study.

REFERENCES

1. Cowherd, C., and J. S. Kinsey. Identification, Assessment, and Control of Fugitive Particulate Emissions. Draft Final Report prepared by Midwest Research Institute for U.S. Environmental Protection Agency, Office of Research and Development, Washington, D.C. EPA Contract No. 68-02-3922, May 16, 1986.

2. Compilation of Air Pollutant Emission Factors, Fourth Edition, Volume I. EPA Report AP-42, GPO 055-000-00251-7, September 1985.

3. Muleski, G.E., T. Cuscino, Jr., and C. Cowherd, Jr. Extended Evaluation of Unpaved Road Dust Suppressants in the Iron and Steel Industry. EPA-600/2-84-027, NTIS PB84-154350, U.S. Environmental Protection Agency, Research Triangle Park, NC, February 1984.

4. Cuscino, T., Jr., G. E. Muleski, and C. Cowherd, Jr. Iron and Steel Plant Open Source Fugitive Emission Control Evaluation. EPA-600/2-83-110, NTIS PB84-110568, U.S. Environmental Protection Agency, Research Triangle Park, NC, October 1983.

5. Hoenig, S.A. Use of Electrostatically Charged Fog for Control of Fugitive Dust Emissions. EPA-600/7-77-131, NTIS PB276645, U.S. Environmental Protection Agency, Research Triangle Park, NC, November 1977.

6. Mathai, C. V. A New Charged Fog Generator for Inhalable Particle Control. EPA-600/7-84-016, U.S. Environmental Protection Agency, Research Triangle Park, NC, April 1984.

7. Brookman, E.T., and K. J. Kelley. Demonstration of the Use of Charged Fog in Controlling Fugitive Dust from Large-Scale Industrial Sources. EPA-600/2-83-044, NTIS PB83-217828, U.S. Environmental Protection Agency, Research Triangle Park, NC, June 1983.

8. Eimutis, E.C., T. R. Blackwood, and R. Wachter. Particulate Emissions from Stone Crushing Operations. Monsanto Research Corporation, Dayton, OH, November 1979.

9. Johnson, A.R., T. A. Lowe, W. W. Hanneman, and R. J. Schlager. A Study of Reduction Cell Fluoride Emissions. Conference Proceedings, The Metallurgical Society of AIME, Light Metals, 1980.

10. Ellenbecker, M. J., R. F. Gempel, and W. A. Burgess. Capture Efficiency of Local Exhaust Ventilation Systems. American Industrial Hygiene Association Journal, 44(10):752-755, October 1983.

PROCESS FUGITIVE PARTICULATES—DESIGN METHODS FOR ENCLOSURES

by

Howard D. Goodfellow
Tony Cesta
Hatch Associates, Ltd.
21 St. Clair Avenue East
Toronto, Ontario M4T IL9

and

Edward R. Kashdan*
David W. Coy
James J. Spivey
Research Triangle Institute
P.O. Box 12194
Research Triangle Park, NC 27709

and

Dale L. Harmon
Office of Environmental Engineering and Technology
Air and Energy Engineering Research Laboratory
U.S. Environmental Protection Agency
Research Triangle Park, NC 27711

---

*Currently with Environmental Monitoring & Services, Combustion Engineering, Inc., 800 Eastowne Drive, Chapel Hill, NC 27514.

ABSTRACT

Regulatory officials charged with the responsibility of reviewing hood systems for capture of process fugitive emissions face a difficult task. A manual has been prepared to provide these officials with a reference guide on the design and evaluation of hood systems and enclosures. This paper presents design methods for enclosures. In particular, enclosures for inertial process fugitive sources and for buoyant sources are discussed. Equations are given to estimate the required exhaust rate for the enclosures. Mechanical design considerations are listed for enclosures applied to buoyant sources.

This paper has been reviewed in accordance with the U.S. Environmental Protection Agency's peer and administrative review policies and approved for presentation and publication.

1.0 INTRODUCTION

Process fugitive particulate emissions have been defined as "particulate matter which escapes from a defined process flow stream due to leakage, materials charging/handling, inadequate operational control, lack of reasonably available control technology, transfer, or storage" (Jutze et al., 1977). Secondary hood systems consisting of enclosures, local hooding, or remote hooding are the practical means of capturing these emissions. Once captured, the gas stream can be ducted to high-efficiency air pollution control devices. Frequently, the capture efficiency of the hood is far less than the removal efficiency of the control device. Emissions missed by the hood usually escape to the atmosphere.

Considering the diversity of sources classed as process fugitives, it is not surprising that the design of secondary hood systems varies greatly; a large range is found in size, exhaust rate, and arrangement. Regulatory officials responsible for reviewing hood systems for either existing or planned sites face a difficult task. The behavior of process fugitive particulate plumes is complex. Process equipment interference may change plume dimensions and location, and in-building air currents may cause plume drift. As a result, the interaction of the hood and plume is not always predictable. Moreover, most of the traditional industrial ventilation texts do not consider process fugitive sources specifically. These texts have emphasized general design rules rather than a thorough understanding of hood design or the limitations of design methods. The emphasis of the technical manual (from which these highlights have been extracted) is on the design and evaluation of actual hood systems used to control various fugitive particulate emission sources. Engineering analyses of the most important hood types are presented to provide a conceptual understanding of the design process, which consists of identification of source parameters, calculation procedures, and techniques for evaluating hood performance. Some of the design techniques have been introduced in technical papers by Hatch Associates and have been formalized in this manual. Case studies of actual hood systems not only illustrate the application of these design methods but also identify their limitations. Several of the case studies are from the files of Hatch Associates and provide unique insight into the diagnosis of an existing system.

The purpose of the manual is to provide regulatory officials with a reference guide on the design and evaluation of hood systems to capture process fugitive particulate emissions. Much of the hood design information is of necessity analytical, based on a mathematical or engineering approach. However, every effort has been made to explain the physical processes in qualitative terms and to separate the formal equations.

This paper discusses enclosures for inertial process fugitive sources and for buoyant sources. Enclosures represent the preferred method for control of process fugitive emissions because escape of emissions is restricted to gaps or openings in the enclosures. Therefore, consideration always should be given to the use of enclosures in planning a ventilation system, although they may not always be practical where ready access to the process source is necessary.

Design of enclosures for inertial sources is completely different than design for buoyant sources. The dust produced by inertial sources arises from the motion of the particulate matter itself rather than from the thermal head of the air in the case of buoyant sources. In Section 2.0, dust-producing mechanisms of inertial sources are discussed. Emphasis is placed on a common and significant application of enclosures to gravity transfer operations of bulk materials. In Section 3.0, design considerations for enclosing buoyant sources are presented. Design procedures for enclosures are outlined, and practical experiences are summarized.

2.0 ENCLOSURES FOR INERTIAL SOURCES

Enclosures are practically the only hood suitable for large-scale inertial sources such as bulk materials handling operations. Unlike buoyant sources, dust generated by these operations does not travel in predictable paths, and the range of travel is usually limited. These considerations preclude the use of remote hooding. Local hooding (i.e., receiving hoods) are sometimes used for inertial sources that have a single direction of travel, such as particles projected from a grinding wheel. But, for large-scale inertial sources, dust generation takes place in all directions. Exterior hoods are generally found to be unable to alter the motion of coarse particulate matter that is projected away from the hood.

As with any hood system, design methods are used to obtain required exhaust rates and hood dimensions. For enclosing inertial sources, various mechanisms of dust production that arise from the motion of the particulate matter determine the required exhaust rate. The enclosure dimensions are also affected by these mechanisms, although process requirements are factors as well. Positioning the exhaust offtake (connection between hood and branch duct) is of special importance in the design of enclosures for inertial sources. Section 2.1 discusses dust-producing mechanisms applicable to all inertial sources, Section 2.2 presents the design of enclosures for gravity transfer operations, and Section 2.3 offers considerations in the use of nonexhausted enclosures.

2.1 DUST GENERATION IN INERTIAL SOURCES

Dust generation mechanisms for inertial sources have been reviewed by Hemeon (1963). All these mechanisms of dust production arise from the motion of the particulate matter and therefore are dependent on the size distribution of the material, adhesiveness of the material, moisture content, friability of the material, and other factors. The main mechanisms of dust generation are air induction, material splash, air displacement, and air entrainment, as shown in Figure 1.

Air induction is probably the most important consideration in the design of enclosures for inertial sources. During the motion of coarse particulate matter, each particle imparts momentum to the surrounding air stream. The macroscopic effect is an induced air stream. On reaching an enclosure, the air streams outward through openings (e.g., access doors, chutes, and gaps), carrying dust with it. This phenomenon of air induction is familiar, as it is observed around a shower bath. For the quantities of materials handled in industrial applications, the volume of air induced is substantial.

Material splash refers to the violent escape of air and dust when falling materials suddenly impact a hard surface. Obviously the effect is

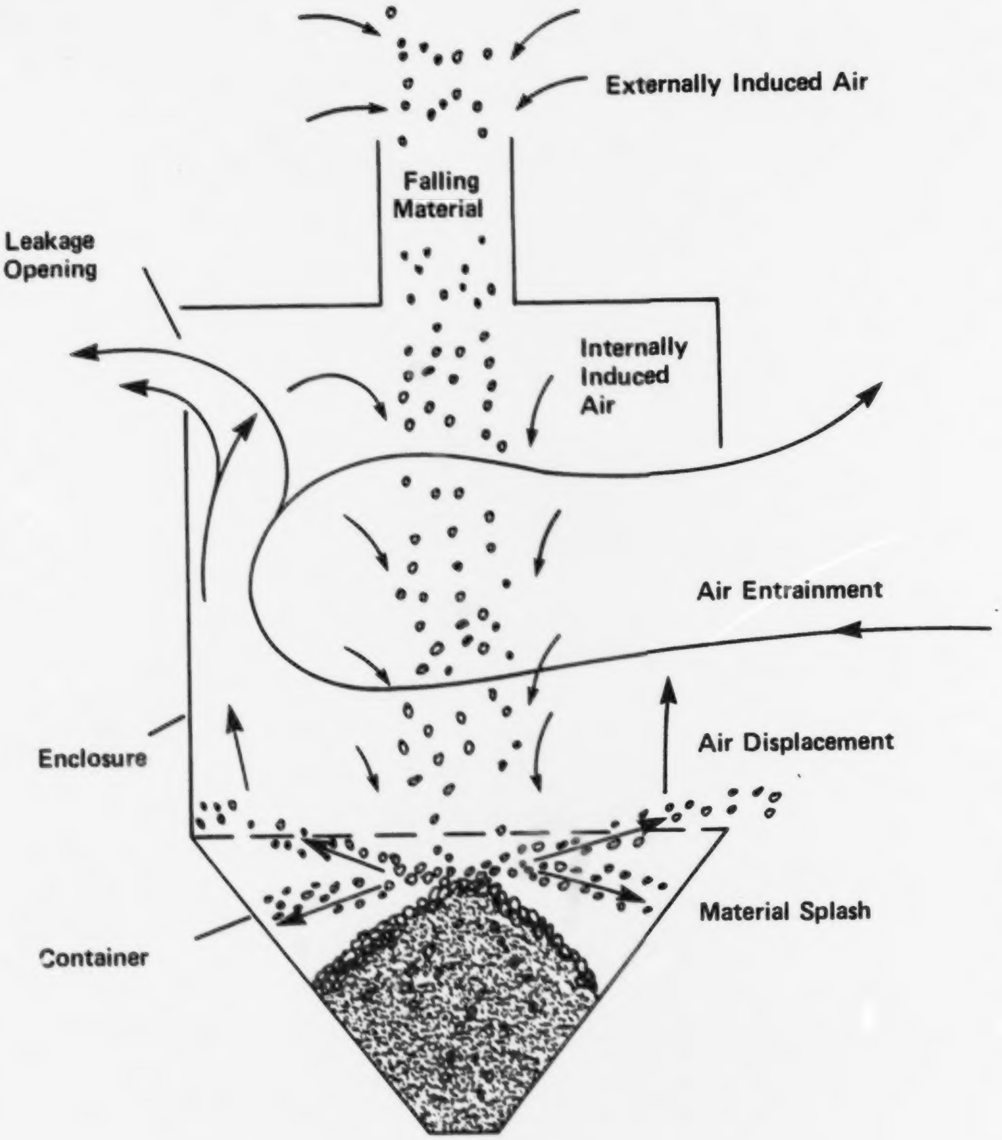
Externally Induced Air
Falling Material
Leakage Opening
Internally Induced Air
Air Entrainment
Enclosure
Air Displacement
Material Splash
Container

Figure 1. Mechanisms for dust generation and dispersion during material fall in an enclosure.

important for gravity transfers of material, although no quantitative measure of the effect has been established. As pointed out by Hemeon (1963), escape of dust by the action of material splash is local to the compacting pile and therefore may be distinguished from escape by air induction, which occurs throughout all openings regardless of location.

Air displacement refers simply to the air displaced by the material as the material is discharged into a container. The velocity and direction of expelled air depend on the geometry of the container and the amount of open area. Generally, the volume of displaced air will be small compared to the volume of induced air, but the quantity is easily calculated.

Air entrainment of dust occurs when any secondary air movements cause further dispersion. The source of such currents may be random air currents or external winds. Entrainment of dust can be an important consideration, especially when the cause of secondary air motion is the primary dust producing machine (e.g., a pneumatic chisel).

Of the dust-producing mechanisms above, air induction and air entrainment are important for determining the exhaust rate for enclosures. Air displacement and material splash are important for determining the size and shape of the enclosure.

2.2 EXHAUSTED ENCLOSURES FOR GRAVITY TRANSFER OPERATIONS

A common and important application of exhausted enclosures is to bulk material transfer points such as at chutes, bins, and dumping sites. Design equations for estimating the required exhaust rate follow. Consideration is also given to sizing the enclosure and positioning the offtake.

The exhaust rate for an enclosure for controlling emissions from a falling materials operation should equal the sum of the following quantities:

1. Flow rate of air induced by the falling material. (This quantity is typically much larger than air displacement; however, air displacement may also be separately estimated.)
2. Flow rate of air entering the enclosure by entrainment.
3. Flow rate sufficient to provide a working indraft velocity of air through all openings (i.e., control velocity).

Hemeon (1963) developed equations for estimating the volumetric flow rate of induced air based on the power generated by the stream of falling particles; that is, the work done by the drag force over the distance fallen per unit time. The recommended equation for estimating the induced air flow rate is the following (Morrison 1971 and Dennis 1983):

$$Q_1 = 0.631\left(\frac{W\ H^2\ A_s{}^2}{\rho_s\ d}\right)^{1/3} \quad (1)$$

where

Q_1 = flow rate of induced air (m^3/s)
W = material flow rate (kg/s)
H = drop height (m)
A_s = cross-sectional area of falling stream (m^2)
ρ_s = bulk solids density (kg/m^3)
d = particle mass median diameter (m).

The flow rate of displaced air is given simply by the materials flow rate divided by the bulk density:

$$Q_2 = \frac{W}{\rho_s} \ . \quad (2)$$

Last, for a recommended control velocity of 0.5 to 1.0 m/s through the total area of the openings, A, the flow rate is given by:

$$Q_3 = A \times V \quad (3)$$

where

V = control velocity (0.5 m/s for well-protected sources; 1.0 m/s for vigorous motion operations).

Sizing the enclosure is more important than might first appear. If the enclosure walls are close to the compacting pile of material, material splash effects will cause losses through openings in these walls. Therefore, the use of a larger enclosure allows the velocity of these air streams to decrease before reaching the walls. Since no quantitative estimates may be made as to the magnitude of the material splash effects, field observations of an existing system and experience are the only guides. Air entrainment becomes a factor when the enclosure has large areas or complete sides that must remain open. Winds or local air currents then can enter and exit the enclosure, thereby removing dust. The flow rate of ingress air can be calculated in a straightforward manner from the wind velocity, open area, and entry loss coefficient of the opening. However, the ingress air is usually found to be quite large so that it may not be practical to attempt to counteract it by enclosure exhaust alone. Positioning the exhaust offtake close to the active zone of dust generation may capture the most concentrated portion of airborne dust before recirculation and mixing with entrained air can occur, thereby reducing needed exhaust to that for air induction and control velocity only.

Selection of the offtake position is important from the standpoint of the amount of material removed. Locating the offtake in the proximity of the material stream or at points of splash will result in greater removal of materials. This positioning may be desirable as a means to control splash effects provided the offtake velocity is kept low.

2.3 NONEXHAUSTED ENCLOSURES

Nonexhausted enclosures may be used to contain dust arising from inertial sources and to protect against entrainment by winds. All the difficulties attendant in the use of exhausted enclosures apply equally to nonexhausted enclosures. Since nonexhausted enclosures do not maintain an inward air flow through openings, tight sealing is the only means for restricting the escape of dust. No design procedures for nonexhausted enclosures can be given, but provisions should be made for removal of settled dust and for access to any equipment inside the enclosure.

2.4 CAPTURE PERFORMANCE

Capture efficiency on an existing enclosure installation can be estimated by measuring the portions of captured and spilled dust. The measurement program can be quite involved depending on enclosure size, intermittance of operation, dust settlement in the enclosure, and the extent of air entrainment. The measurement program would have to be custom designed to best suit the operation.

3.0 ENCLOSURES FOR BUOYANT SOURCES

Enclosures are used in many industries to capture emissions from buoyant sources. The following discussion concerns large enclosures used on metallurgical process vessels. Many of the design equations and procedures developed for buoyant source hoods apply to large enclosure designs. Process vessels successfully using enclosures include electric arc furnaces, top- and bottom-blown oxygen steel conversion furnaces, and nonferrous metals industry converters.

Use of enclosures for capture of fugitive emissions offers the following advantages:

1. Total capture of emissions is possible and is as effective as building evacuation. The enclosure, unaffected by in-plant drafts, offers total containment.
2. As a side benefit with electric arc furnaces, the enclosure offers a great potential for noise control.
3. Working conditions outside the enclosure are drastically improved. The bulk of heat, fume, and dust from the furnace are contained within the enclosure.
4. On small and low-production furnaces, the enclosure can be used as both primary and secondary control, thereby reducing the need for other hardware.

The main disadvantage of using an enclosure is the potential for interference with the normal operation and maintenance of a furnace. A major design effort is required to overcome this disadvantage. All aspects of the furnace operation must be considered. Lines of sight for furnace and crane operators, access for crane-held ladles and buckets, furnace movements, and maintenance access must be accommodated by the enclosure design. This is more easily achieved in a new installation. Enclosure design on existing sites becomes very difficult and may require a compromise between furnace operation and fume capture performance.

Figures 2 and 3 illustrate examples of enclosures on oxygen steel conversion vessels and electric arc furnaces. Many different enclosure shapes for similar furnaces demonstrate that enclosure design is very site-specific. Several patents exist for enclosures. Use of a patented

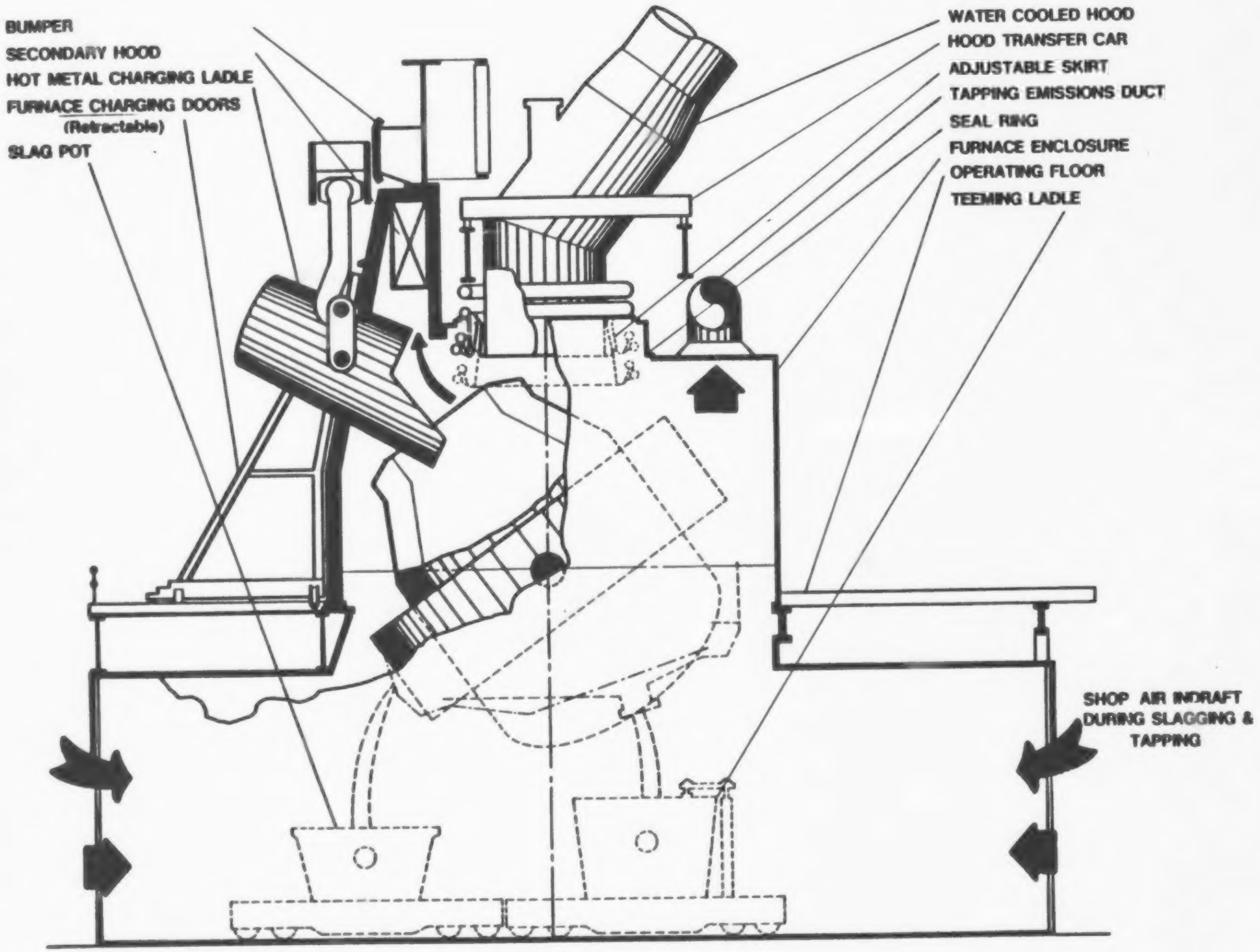
BUMPER
SECONDARY HOOD
HOT METAL CHARGING LADLE
FURNACE CHARGING DOORS (Retractable)
SLAG POT
WATER COOLED HOOD
HOOD TRANSFER CAR
ADJUSTABLE SKIRT
TAPPING EMISSIONS DUCT
SEAL RING
FURNACE ENCLOSURE
OPERATING FLOOR
TEEMING LADLE
SHOP AIR INDRAFT DURING SLAGGING & TAPPING

Source: Nicola 1979.

Figure 2. Schematic arrangement for BOF furnace enclosure.

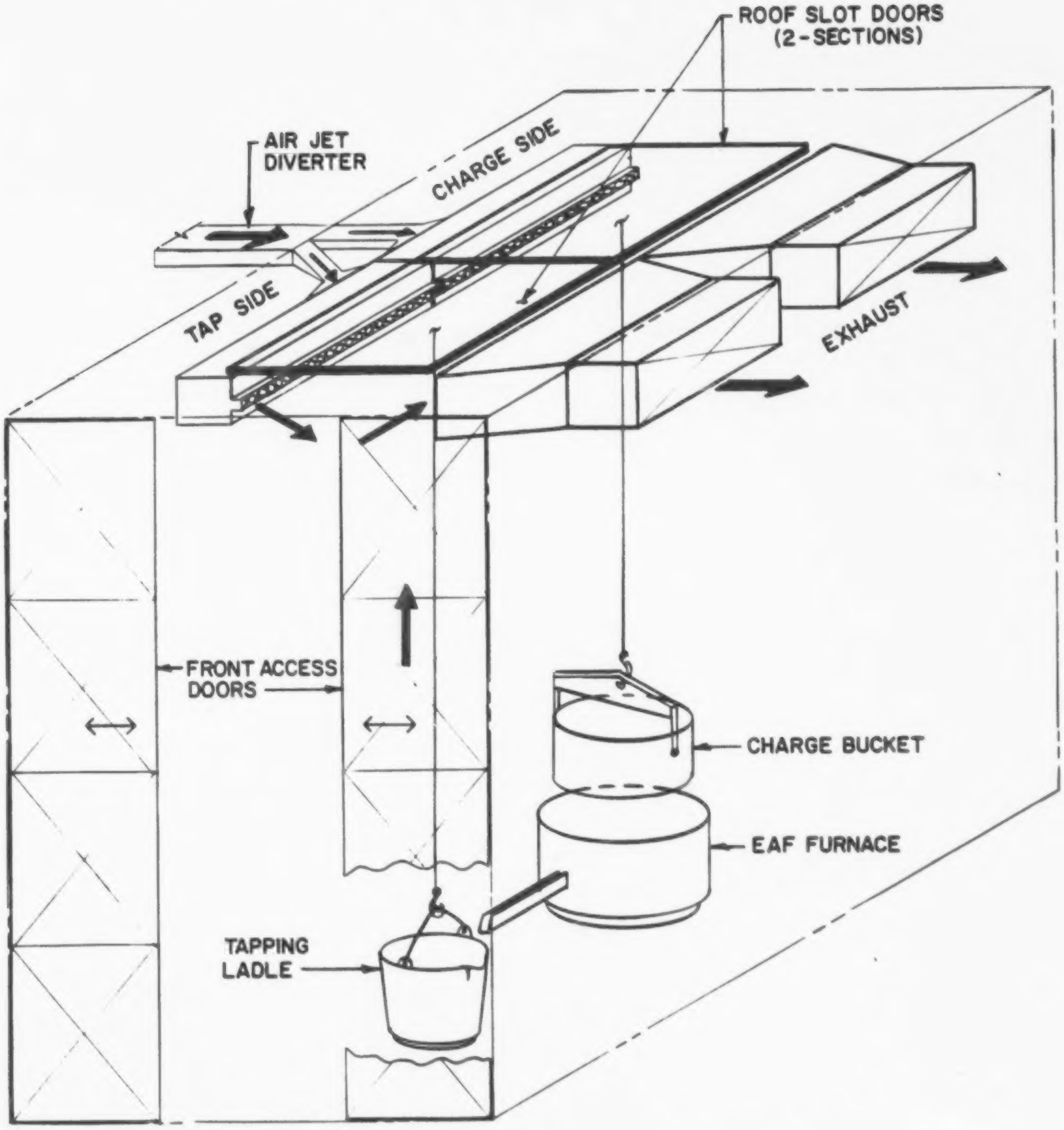
ROOF SLOT DOORS (2-SECTIONS)
AIR JET DIVERTER
CHARGE SIDE
TAP SIDE
EXHAUST
FRONT ACCESS DOORS
CHARGE BUCKET
EAF FURNACE
TAPPING LADLE

Figure 3. Enclosure for an electric arc furnace (EAF).

enclosure does not automatically imply success. Each installation is different and requires that proper design procedures be followed.

Considerations in the design of enclosures for buoyant sources divide into three areas: process and layout requirements, fume capture, and mechanical design. The following discussion emphasizes electric arc furnace enclosures.

3.1 PROCESS AND LAYOUT REQUIREMENTS

When planning an enclosure for a metallurgical furnace the following questions should be asked:

1. Are primary and/or secondary emissions to be controlled by the enclosure?
2. What is the extent of furnace and related equipment movements?
3. How will the enclosure affect the furnace operation process control?
4. Where must enclosure openings be located?

3.1.1 Fume Control System

On oxygen steel conversion furnaces, primary fume control is usually achieved by a separate close capture hood positioned over the vessel mouth. The enclosure then is used for secondary fume control on charging, turndown, tapping, and slagging emissions.

On electric arc furnaces, an enclosure can be used for both primary and secondary fume control; however, for large high-production furnaces, it is more economical to provide separate direct evacuation control for primary melting emissions. Use of separate gas cooling equipment to handle the heat content of primary emission off-gas on high-production furnaces is often less expensive than directly quenching with large amounts of dilution air from an enclosure. The amount of air dilution is dictated by fabric filter temperature limitations. Generally, if the enclosure exhaust rate for secondary fume capture is similar to or greater than that required for primary control, the enclosure system is designed to handle both emissions.

Where primary control is afforded by the enclosure and fume leaves the furnace via electrode openings, the extra wear and tear on electrode holding equipment must be taken into account. This problem is particularly evident on ultra high power (UHP) furnaces where the holding equipment would be constantly exposed to high-temperature flame. As a possible solution, the furnace could be equipped with a roof-mounted water-cooled stub stack which naturally draws fume from the furnace and into the enclosure, thus diverting fume and resulting damage from electrode equipment.

When primary fume capture is performed by the enclosure, furnace off-gas combustion efficiency is lower than that for furnace direct evacuation control. The off-gas (rich in carbon monoxide) rises from furnace roof openings, partially burns, and cools with enclosure air. Significant levels of carbon monoxide (CO) have resulted in enclosures and exhaust ducting from this type of combustion. These levels are not explosive but present a potential hazard to personnel working in the enclosure or in downstream fume cleaning equipment.

Therefore, as a final consideration, environmental regulations that limit the amount of CO discharge from a meltshop may force primary emissions to be handled by a high-combustion-efficiency fume control system.

3.1.2 Furnace and Related Equipment Movements

Various furnace movements must be accommodated by the enclosure. Furnace tilting for tapping and slagging, electrode vertical lift, and direction of furnace roof swing must be accounted for in the design of the enclosure shape and the location of the exhaust offtake.

Movement of related equipment must also be considered. The size and position of doors and openings in the enclosure are determined by the following furnace operations and associated rigging: tapping ladle and slag pot positioning, charge bucket positioning, and routine removal of furnace roof and water-cooled panels. Also, emergency measures must be anticipated throughout the design. For example, a full ladle trapped in the enclosure because of a door jam must be removed before the metal solidifies.

3.1.3 Furnace Operation and Process Control

The following items affecting furnace operation and process control should be addressed as the enclosure shape is considered:

1. Line of sight for crane operators and furnace attendants

2. Furnace control points and attendants' location
3. Method of charging additives
4. Furnace ancillary equipment location
5. Equipment maintenance access requirements.

Furnace control points and ancillary equipment may be located within or outside of the enclosure. If the bulk of furnace ancillary equipment is located in the enclosure, layouts must allow for proper servicing. If attendants must work in the enclosure during furnace operation, emission capture design must provide a relatively fume-free work environment.

3.1.4 Enclosure Openings

In general, enclosure opening requirements should be minimized during the layout stage.

Bucket charging of an electric arc furnace requires a roof slot for crane access. Sliding doors can be used to cover these openings. After the bucket has entered the enclosure, the side doors are closed; however, roof slot doors remain open. An air curtain blowing across the roof slot can be used to prevent charging emissions from escaping through the roof slot. Ample clearance is required to fit doors and air curtain equipment on the enclosure roof. A roof slot is also required during tapping if the ladle is held by the crane.

3.2 FUME CAPTURE

Fumes are captured by a combination of the following enclosure features:

1. Containment and storage of the emission
2. Air extraction from the enclosure
3. Air curtain and exhaust offtake.

If acceptable working conditions must be maintained in the enclosure during the furnace operation, attention must be given to internal air flow patterns; i.e., minimization of fume recirculation in the enclosure.

3.2.1 Containment and Storage of the Emission

The main function of the physical enclosure is to contain secondary furnace emissions from tapping, slagging, charging, and, perhaps, primary emissions from melting. These emissions are thermally entrained against the enclosure roof. If the enclosure is not built tightly, these emissions can overcome the indraft effect of the extraction system. Gaps around roof slot doors can also present a severe leakage problem. When the roof doors are open for crane rope access, an air curtain can be used effectively to contain emissions.

The enclosure is also capable of storing fume surges during bucket charging. With proper design, the top of the enclosure will fill with fume while the lower working level remains clear. The key to producing this effect is to reduce fume recirculation in the enclosure by proper placement of the air curtain with respect to the exhaust offtake.

Tapping, slagging, and melting are prolonged operations; therefore, the enclosure should not be used for fume storage during these periods. The enclosure exhaust capacity must be greater than the emission plume flow rate to avoid fume buildup in the enclosure during these operations.

3.2.2 Required Exhaust Rate

To determine the air exhaust rate from the enclosures the following steps are recommended:

1st Step--Primary Emission Heat Content

The heat content of furnace emissions and the temperature limitation on the fume collector are considered for this step. The off-gas heat content is calculated for furnace reactions during melting and refining periods. (This lengthy calculation procedure is not covered in this paper.) Assuming a fabric filter collector is used with polyester cloth, a 121 °C (250 °F) temperature limit is imposed for continuous operation.

The fume volumetric flow rate after dilution is determined from:

$$Q = q/[(\rho)(C_p)(T_s - T_{amb})] \quad (4)$$

where

Q = actual volume flow rate after dilution (m^3/min)
q = heat transfer rate from furnace off-gas (J/min)
ρ = air density at T_s (kg/m^3)
C_p = specific heat of air at T_s (J/kg·K)
T_s = specified air temperature after dilution (K)
T_{amb} = ambient dilution air temperature (K).

For a high-production furnace, the fume volume flow rate, after air dilution to 121 °C, will be considerably higher than for secondary fume control by the enclosure, and a separate primary fume capture system would be used.

For the remaining steps, a small low-production furnace is under consideration, with both primary and secondary emissions being captured by the enclosure.

2nd Step--Secondary Emission Plume Flow Rate

The fume flow rate for charging and tapping is then predicted by the following method. The enclosure height is taken as the limit of plume rise. The plume rise from the open furnace before charging should also be calculated. This event is a prolonged emission.

Heat release--Assuming a rate of temperature drop of ladle and furnace as 5.6 K/min, the rate of heat release is:

$$q = C\ (500\ \mathrm{J/kg \cdot K})(5.6\ \mathrm{K/min}) \tag{5}$$

where

q = heat release (J/min)
C = furnace or ladle capacity (kg).

Plume flow rate--Plume flow rate is calculated using an equation from Hemeon (1963):

$$Q = 0.122\ (Z)^{1.5}(q)^{1/3} \tag{6}$$

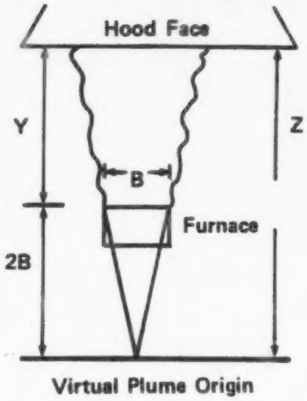

where

Q = fume volume reaching the canopy hood (m^3/min)

Z = height of canopy hood above the virtual plume source (m)

Z = Y + 2B, where Y is the distance from the top of the source to the hood face, and B is the source diameter in meters

q = heat release (J/min).

3rd Step--Enclosure Exhaust Rate

The volume flow rate from prolonged emissions during roof swung open, melting, and tapping sets the minimum exhaust rate required to ensure a relatively fume-free enclosure environment. The fume volume flow rate after dilution (from 1st step) is compared to the highest of the calculated plume flow rates from the prolonged emissions. The greater of these two rates determines the enclosure exhaust rate.

Although the charging plume flow rate can be higher than that for tapping, it does not set the enclosure exhaust rate. Instead, the enclosure is used to store this approximately 30-second surge.

3.2.3 Air Curtain and Exhaust Offtake

Air curtain design and exhaust offtake location are very important considerations.

The air curtain is applied on roof openings that are typically 2.5 to 3.0 m wide and that are used for crane rope access. The opening may extend the length of the enclosure and should therefore be served by two sets of independently working doors--one for tapping and one for charging. This feature minimizes the open area when one of the two events occurs, as shown in Figure 3.

The optimum position for the exhaust offtake is directly opposite the air curtain discharge. Rising fume with the highest concentration is directed straight into the offtake without excessive recirculation in the enclosure.

The main purpose of the air curtain is to contain the vertical updrafts from charging and tapping emissions. Because of the upward momentum of these emissions, the air curtain slot discharge should therefore be pointed downward (15 to 25 degrees from the horizontal) to achieve an approximately horizontal resultant flow.

The air curtain design procedure is outlined in the manual, and a case study is presented. The plume data for furnace charging are used in this step. Note that the plume volume flow impinging on the width of the slot should be used rather than the whole plume flow.

During melting, the air curtain should efficiently direct fume toward the exhaust offtake without allowing recirculation within the enclosure. The air curtain design should therefore also account for this fume trajectory when a lower updraft velocity from melting is experienced.

The air curtain supply air can be taken from either inside or outside the enclosure; however, there is a net flow advantage to taking this air from the inside.

Elevated work area temperatures in the enclosure at operating floor level may be a problem. Limited louver openings or wall fans can be used for cooling if operators must normally spend prolonged periods in the enclosure.

3.3 MECHANICAL DESIGN

The success of an enclosure installation depends heavily on acceptance by operations and maintenance personnel. Mechanical and structural reliability must therefore be designed into the enclosure. Design details to be considered include:

1. After opening locations and proper clearances have been established, the enclosure frame support system should be considered. Major support beams placed at the edge of openings will provide extra strength against the rubbing of crane cables. The overall construction should be light, which allows fast easy repair in the event of collision with crane-held objects. Collision with a sturdy enclosure would still result in damage and probably be more difficult to repair.

2. Enclosure doors should be designed with generous clearances and be easily operated by simple mechanisms. Wheels, guide rollers, and pneumatic cylinders can be used as part of door mechanisms.

3. To minimize leaks, roof doors that are susceptible to fume updrafts should overlap the inside of the enclosure shell. All roof construction must be tightly sealed.

4. Access for easy maintenance must be provided. Removable roof panels for access to furnace subassemblies are desirable. Water-cooled equipment, electrode and roof movement mechanisms, etc., all require overhead access for proper maintenance. Small jib cranes may have to be located in the enclosure.

5. Material selection for the enclosure shell should consider environment corrosiveness. Aluminized sheeting is preferred over zinc-coated materials in a steel production environment.

6. The damaging sound levels produced by an electric arc furnace can be contained within a furnace enclosure if a proper acoustical design is carried out. Any design should be made, or at least checked, by an acoustical engineer. The following points should be considered:
   - The material should be sufficiently heavy. In most cases structural requirements already ensure this.
   - The cladding should be sufficiently stiffened or damped to preclude resonances at the furnace frequency and its first few harmonics.
   - The inside of the enclosure should be lined with sound-absorbing material (e.g., fiberglass) selected for the frequencies involved and suitably protected from damage.
   - Holes, openings, and air leaks should be minimized, treated, or at least located away from people where possible.
   - Operating practices should minimize the amount of time operators have to spend inside the enclosure or near an opening while the furnace is operating.

4.0 REFERENCES

Dennis, R., and Bubenick, D. V. 1983. Fugitive Emissions Control for Solid Materials Handling Operation. J. Air Pollu. Control Assoc. 33(12):1156-1161.

Hemeon, W. C. L. 1963. Plant and Process Ventilation. 2nd ed. Industrial Press, Inc., New York, New York.

Jutze, G. A., Zoller, J. M., Janszen, T. A., Amick, R. S., Zimmer, C. E., and Gerstle, R. W. 1977. Technical Guidance for Control of Industrial Process Fugitive Particulate Emissions, EPA-450/3-77-010 (PB272288), March.

Morrison, J. N. 1971. Controlling Dust Emissions at Belt Conveyor Transfer Points. Trans. AIME. 150:68.

Nicola, A. G. 1979. Best Available Control Technology (BACT) for Fugitive Emissions Control in the Steel Industry. In: Third Symposium on Fugitive Emissions Measurement and Control (October 1978, San Francisco, CA) EPA-600/7-79-182 (PB80130891), August, pp. 281-312.

FIELD EVALUATION OF WINDSCREENS AS A FUGITIVE DUST CONTROL MEASURE FOR MATERIALS STORAGE PILES

by: Robert A. Zimmer
Kenneth Axetell, Jr., PE
Thomas C. Ponder, Jr., PE, CCE

ABSTRACT

The Air and Energy Engineering Research Laboratory (AEERL) has instituted a coordinated program for development of a technology for the control of fugitive particulate sources. The AEERL has identified windscreens as a promising control technique for one of the major sources--storage piles. Before this technology can be effectively applied, however, application criteria need to be developed. These criteria include (1) screen porosity, (2) screen width, (3) screen height, and (4) the distance between the screen and the pile.

AEERL and the Environmental Sciences Research Laboratory (ESRL) have completed an in-house study designed to determine changes in windspeed (not changes in emissions) due to windscreens. The ESRL wind tunnnel was used in experiments conducted to determine the optimal windscreen porosity, size, and location for control of fugitive dust emissions from storage piles. Before this information could be applied to the design of windscreens, it was necessary to conduct a field study to validate the wind tunnel studies with respect to windspeed changes, and to determine the relationship between changes in windspeed and changes in fugitive dust emissions.

This field study was conducted during the summer of 1985. Testing was performed simultaneously on two cone shaped piles of shredded topsoil 8 feet* high and having a base diameter of 25 feet. One pile was exposed and the other was controlled with a 50 percent porosity windscreen. Sensors were located at the surface of each pile to determine windspeed. Exposure profiling towers with samplers at four heights were used to determine total particulate emissions. Windspeed data were collected continuously by an onsite computer. Profiler data were averaged for a complete test and selected filters were subjected to laser diffraction analysis to obtain particle size data.

---

*Readers more familiar with metric units are asked to use the conversion factors at the end of this paper.

The windscreen parameters found to be most effective in the field for reducing windspeed on the pile surface under perpendicular winds were 1.25 pile heights high, 1.5 pile heights wide, and 2.0 pile heights upwind. Both the wind tunnel study and this study recorded negative screen efficiencies in the lee of the pile, but the field study showed this result to a much greater extent.

Regression analyses of data for particulate emission reduction and other variables showed a strong linear relationship between emission reduction and windspeed for the largest particle size ranges evaluated. These analyses also showed that emission rates were directly related to windspeed and inversely related to the moisture content of the pile surface. These relationships held regardless of the particle size fraction considered.

Optimum windscreen design parameters recommended for permanent or semi-permanent installations are porosity = 50 percent; height = 1.0H; width = 5.0D; and distance = 2.0H for a pile of height H and diameter D.

This paper has been reviewed in accordance with the U.S. Environmental Protection Agency's peer and administrative review policies and approved for presentation and publication.

INTRODUCTION

The Air and Energy Engineering Research Laboratory (AEERL) has instituted a coordinated program for the development of a technology for the control of fugitive particulate sources. The AEERL has identified windscreens as a promising control technique for storage piles, a major source of these emissions. Before this technology can be effectively applied, however, application criteria need to be developed.

Together, AEERL and the Environmental Sciences Research Laboratory (ESRL) have completed an in-house study (1), designed to determine changes in windspeed (not changes in emissions) due to windscreens. The ESRL wind tunnel was used in experiments conducted to determine the optimal windscreen porosity, size, and location for control of fugitive dust emissions from storage piles. Before this information could be applied to the design of windscreens, it was necessary to conduct a field study to validate the wind tunnel studies with respect to windspeed changes and to determine the relationship between changes in windspeed and changes in fugitive dust emissions.

More specifically, the three objectives of this study were:

(1) To verify that the data collected in the wind tunnel with respect to changes in windspeed are accurate under field conditions.
(2) To determine the relationship between changes in windspeed and changes in particulate emissions by particle size.
(3) To develop windscreen design parameters.

Previous studies have yielded contradictory results concerning the relationship between particle emissions and windspeed (2-9). Similar contradictions were found in the two studies performed to investigate reductions in dust concentrations due to the use of windscreens (10-11). The Billman study (1) and the study described herein are the first laboratory and field studies that attempt to measure windspeed or particulate reductions at or near a pile surface.

The Billman study simulated, in a wind tunnel, the effect of a windscreen in reducing windspeed on the surface of a storage pile. The scale-model storage pile used was 11 cm high and was covered with gravel having diameters less than 4 mm. A variety of windscreen parameters were evaluated during the study and isotachs of windspeed and windspeed reduction were presented for both unscreened and screened piles.

FIELD SAMPLING

The current study entailed a field exercise to evaluate the results of the Billman study under actual field conditions. The basic sampling protocol used was to measure windspeed and particulate concentrations on two identical storage piles simultaneously. One pile was controlled with a windscreen of 50 percent porosity and one had no windscreen. A critical parameter in such a test protocol is that the piles be identical initially and throughout the test period with respect to dust-emitting characteristics. The piles were constructed out of the same highly erodible material (shredded topsoil) and were shaped exactly the same.

The field site was located on a privately owned farm in the Wichita, Kansas, area. This area had the desirable characteristics of relatively high-speed winds with a persistent direction. The 24-acre field was located in a rural area about 7 miles northwest of the Wichita Mid-Continent Airport. This level area was bounded by a paved road on the western edge and an unpaved road on the northern edge (downwind).

The entire field was covered with grass, which grew to a height of 2 to 6 inches. There were no continually active particulate sources in the upwind direction (south) from the field, just additional pastures and fields with mature crops. Nor were there any tall windbreaks within ½ mile to the south. Trees that grew along the stream at the south end of the field only extended 10 to 15 ft above field level and were at least 500 ft distant from the sampling area.

The identically constructed storage piles consisted of dried, shredded topsoil. The piles were conical in shape, with a height of 8 feet and a base diameter of 25 feet and were located 150 feet apart. A detailed test plot is shown in Figure 1. The instrument trailer was located 75 feet downwind of the piles. Screen widths up to five pile diameters were accommodated with this layout.

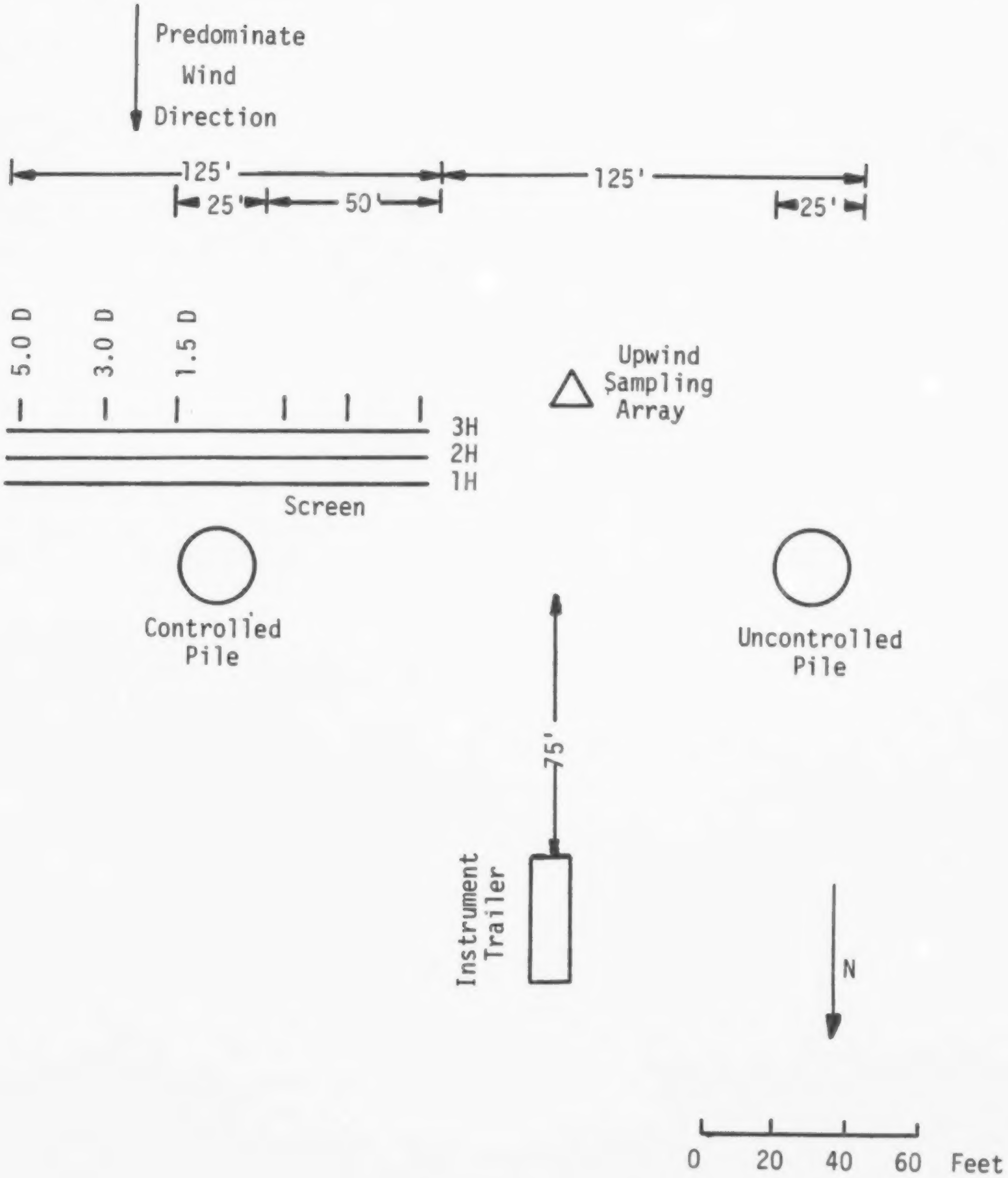
Predominate Wind Direction
125'
125'
25'
50'
25'
5.0 D
3.0 D
1.5 D
3H
2H
1H
Screen
Upwind Sampling Array
Controlled Pile
Uncontrolled Pile
75'
Instrument Trailer
N
0
20
40
60
Feet

Figure 1. Test plot layout.

SAMPLING EQUIPMENT AND DEPLOYMENT

Windspeed was monitored with several windspeed sensors. The sensor was a rotating cup assembly with a pulsed output. The output was directed through a windspeed translator module that converted the signal to a standardized analog voltage. This signal was translated to a digital signal, through the use of an analog-to-digital converter, which was then processed by a personal computer.

Wind direction was monitored upwind with a wind direction sensor. The signal was input to a translator module and an analog-to-digital converter for computer processing.

A total of 10 windspeed sensors were used, one of which was located upwind at a height of 8 feet to correspond with the height of the storage pile. Placement of the sensors was guided by verification of wind tunnel testing, as it was desirable to obtain windspeed measurements at the same locations as in the wind tunnel testing. The wind tunnel testing, however, involved 108 windspeed measurement locations, nine sensors at a time. Pile rotation to 12 positions yielded 108 measurements. Such a protocol was impractical for a field test because of the equipment required and because wind direction in the field is not fixed as it is in a wind tunnel test.

A total of nine windspeed sensors were deployed downwind of the screen, five on the uncontrolled pile and four on the controlled pile. The sensors were set at a fixed position on the pile, about 6 inches above the surface of the pile and perpendicular to the ground. The positions were set relative to the prevailing wind direction, and they remained fixed over the 8-week test period.

So that identical instruments could be positioned at the same relative locations on each pile, a true north point and true south point were determined for the base of each pile. A string was then run across the peak of the pile to connect the two points. Vertical distances were measured along the string, and horizontal dimensions were measured perpendicular to the string.

Particulate was measured with a total particulate exposure profiler head. The exposure profiler head consisted of a high-volume motor with a variable flow rate, a filter holder, and a circular intake nozzle that was oriented directly into the wind during testing. The filter was the standard, glass-fiber high-volume filter. Because the sampler collects all ambient particles indiscriminately, the emission data obtained represented total particulate (TP).

The sampling heads were operated approximately isokinetically so as not to skew the particle size distribution of the collected sample. This design was potentially difficult because the wind currents induced by the pile and windscreen would not follow the standard logarithmic profile, and would change with changing wind direction and windscreen height. This problem was overcome by mounting rotating cup anemometers near each profiler head mounted on the profiler tower. The anemometers sent data to an onsite Apple computer for averaging.

Particle size data were obtained from the exposure profiler filters to permit a determination of windscreen control efficiency by particle size. Alternative methods for obtaining the size distribution from the filter were optical microscopy, scanning electron microscopy, and laser diffraction. All methods share the same two weaknesses: material must be removed from the filter, and physical size data must be converted to aerodynamic size data. Laser diffraction with the Microtrak Particle Size Analyzer is the most reliable and cost-efficient of the methods. This device outputs particle size distributions in up to 13 particle size classes over a range of 1 to 175 micrometers. Project resources were adequate to use laser diffraction on one filter from each tower per test. Each sample was then subjected to the particle-sizing analysis.

Four exposure profilers were mounted on an 11-foot tower. The tower was located 10 feet behind the midline and 2 feet to the side of the top of the conical pile. Profiler head heights were 4, 5, 8, and 11 feet. The following independent variables were monitored:

- Pile surface silt content
- Pile surface moisture

Soil samples were taken from the pile by removing the top ½ inch of soil in a vertical strip of 1 x 48 inches from the middle of the pile.

A detailed quality assurance report (12) was prepared prior to field sampling and adhered to throughout the study. The principal elements of the quality assurance procedures can be found in the project report. (13)

OBJECTIVE 1--VERIFICATION OF WIND TUNNEL WINDSPEED DATA

The first objective of the study was to compare the wind tunnel data with the windspeed data collected in the field. The two major elements of comparison were:

(1) Comparison of the windspeed isotachs on an unscreened pile.

(2) Comparison of the windspeed isotachs on screened piles by screen configuration.

WINDSPEED COMPARISONS BETWEEN WIND TUNNEL AND FIELD TESTING FOR AN UNSCREENED PILE

The wind tunnel windspeed data are presented as a set of contours of normalized windspeed, u/u_r, where u is the windspeed at the pile surface, and u_r is the windspeed at the maximum height of the pile measured in the absence of the pile.

A direct comparison of the field data and the wind tunnel data required the following data manipulations of the unscreened pile data:

(1) Preparation of a data base with 5-minute average data of windspeeds corresponding to incoming wind direction.

(2) Preparation of u/u_r values for each sampler location.

(3) Summarization of u/u_r values derived from the field for comparison with the wind tunnel data.

A computerized data base was prepared. It consisted of 5-minute average windspeed data stratified by incoming wind direction in 10 degree cohorts.

Composite u/u_r values were calculated for the 10 degree wind direction cohorts, as shown in Table 1. As the wind direction moves around the pile, the locations of the sensors are effectively shifted to new positions. This same approach was used by Billman in the original wind tunnel study. In the field study, however, the wind direction was varied rather than the pile orientation. Utilization of the entire data base yields a total of 55 data points. Because only 110 degrees of the compass are shown, a substantial portion of the compass is left unresolved. Some of the data points are plotted in Figure 2. The data are plotted over the isotachs from the wind tunnel study.

TABLE 1. U/U_r VALUES FOR THE UNSCREENED PILE
125- to 234-degree WIND DIRECTIONS

Wind Direction, 10-degree Cohort	Position 1	Position 2	Position 3	Position 4	Position 5
125-134	0.82	1.08	0.72	1.36	1.05
135-144	0.68	1.08	0.71	1.34	1.08
145-154	0.65	1.13	0.83	1.35	1.14
155-164	0.56	1.07	0.81	1.21	1.06
165-174	0.46	1.09	0.82	1.07	1.00
175-184	0.53	1.09	0.84	0.94	0.95
185-194	0.57	1.11	0.88	0.74	0.82
195-204	0.60	1.08	0.86	0.45	0.64
205-214	0.67	1.11	0.88	0.33	0.49
215-224	0.82	1.16	1.02	0.20	0.39
225-234	0.88	1.25	1.07	0.28	0.38

As shown in Figure 2, the data on the front of the pile match reasonably well for $u/u_r < 0.8$; however, the area where the ratio is >1.0 appears to be larger than that found in the wind tunnel. The field data for the back side of the pile yielded significantly higher u/u_r ratios than the wind tunnel study. In fact, the highest ratios measured during the field testing occurred

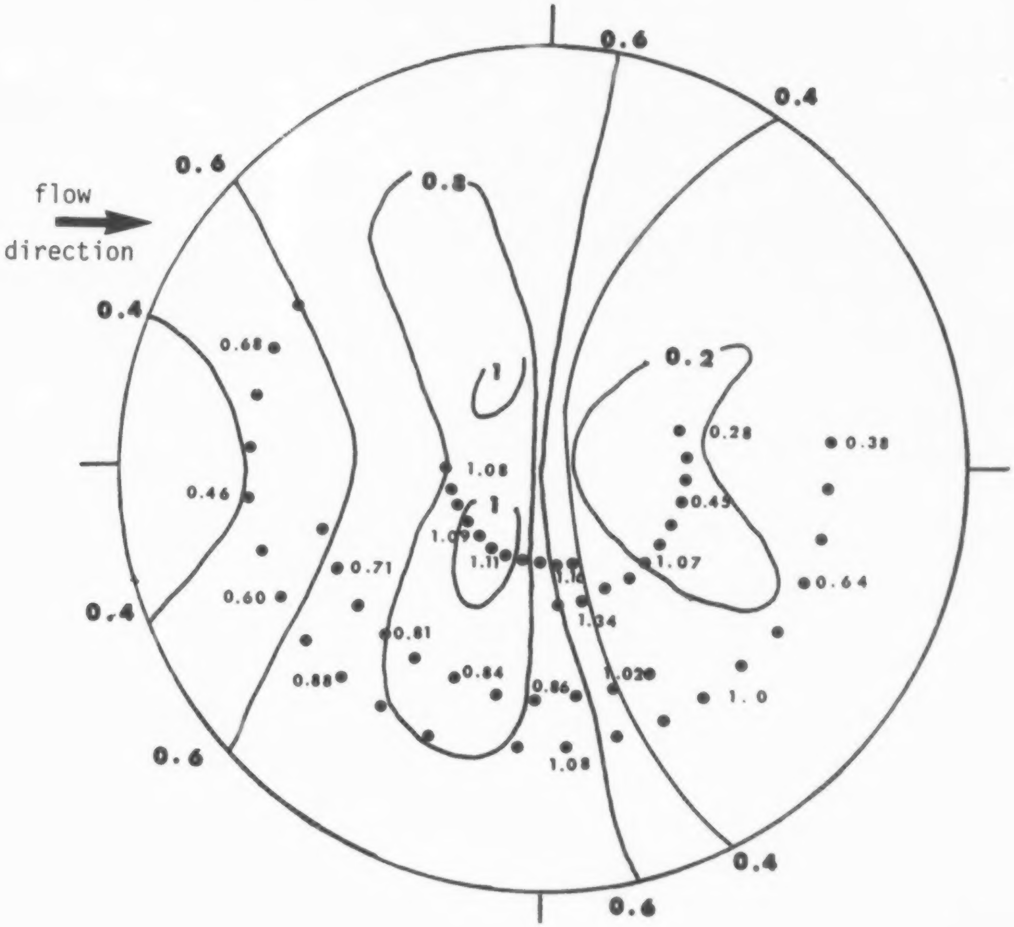

Figure 2. Composite u/u_r values for an unscreened pile--filed testing and wind tunnel data

on the back of the pile. The testing suggests that the high windspeed flow lines not only extend around to the back of the pile, but are reinforced in some fashion.

The differences noted between this study and the Billman study can be attributed to a number of factors:

(1) Ambient windspeeds and wind directions measured in the field are much more variable than those observed in the wind tunnel and resulted in higher turbulence.
(2) Actual pile configuration and composition during the field testing may not have been comparable to the idealized scale model pile used in the wind tunnel, possibly a significant factor.

(3) Experimental equipment used in the two studies may not have been comparable. The extent to which the wind sensors correspond to the laboratory thermistors is unknown.
(4) Experimental errors between the two studies may not have been of comparable magnitude.
(5) The presence of reentrained dust from the pile surface may have some effect on the measurements. For example, it may be that the inherent kinetic energy of the entrained particles from the front of the pile can be transferred to the wind sensors behind the pile and result in higher apparent windspeeds.

WINDSPEED CONTROL EFFECTIVENESS FOR WINDSCREENS

The wind tunnel windspeed data for screened piles are presented as a series of isotach lines. The isotach lines are presented in the form of 1 - (u/u_0), where u and u_0 are windspeeds with and without a windbreak.

The field data were also manipulated into the 1 - (u/u_0) format. Data were also stratified by incoming wind direction and screen configuration. Data could not be presented as a series of isotach lines like the Billman report, because only four data points on the pile were obtained (in contrast to 108 data point in the Billman study).

A portion of the data were reformatted to indicate the maximum windscreen wind reduction by incoming windspeed and screen configuration.

Several conclusions could be drawn from the analyses. Windspeed reduction was greatest for perpendicular screen orientations. A 2.0-pile-height distance, 1.5-pile-diameter width, and a 1.25-pile-height screen were found to be most effective. For nonperpendicular winds, on the other hand, the 3.0-pile-diameter screen width was the most effective. In the lee of the pile, negative control efficiencies were recorded.

Findings of the Billman study were compared with those of the current study. Both studies found the taller windscreens to be most effective. Billman found a 3.0-pile-height distance to be more effective than 1.0-pile-height distance. A 2.0-pile-height distance was not evaluated. The current study found a 2.0-pile-height distance to be more effective than either the 1.0 or a 3.0-pile-height distance. Both studies found a 1.5-pile-diameter screen length to be more effective than a 1.0-pile-diameter screen length. Both studies recorded negative screen efficiencies in the lee of the pile, but the field study showed this result to a much greater extent. In general, the wind tunnel efficiencies were higher than those measured in the field.

OBJECTIVE 2--COMPARISON OF WINDSPEED REDUCTIONS AND PARTICULATE CONTROL EFFICIENCIES

The second objective of the study was to compare average windspeed reductions with particulate emission reductions for entire tests as measured by the exposure profilers. There were 42 valid tests in the data set.

All applicable data for windspeed versus total particulate (TP) emission reductions are shown in Table 2. A linear regression of windspeed (WS) versus total particulate (TP) reductions yielded a correlation of 0.372, R^2 of 0.138, significance level of 0.015, slope of 0.841, and y-intercept of -0.150. These results indicated a significant relationship between the two variables that was nearly one to one.

When the linear regression was forced through 0 (no windspeed reduction results in no TP reduction), the correlation improved to 0.417, R^2 was 0.174, the significance level was 0.005, and the slope was 0.466. This relationship was more significant than the one above and indicated TP reductions slightly less than half of the corresponding windspeed reductions.

There were 15 negative TP reductions in the 42 tests. A negative TP reduction means that a higher emission rate was measured on the screened pile than on the exposed pile. Many of these tests in which the screen appeared to increase emissions could be the result of differences that were less than the measurement error for exposure profiling, but several of the differences in emission rates were large enough to indicate the probability that these measurements reflected actual occurrences of increased emissions. This observation agreed with the findings (discussed previously herein and in the Billman study) that the windscreen actually produced increased windspeeds on the lee side of the pile.

If the negative TP reductions were assumed to be due to measurement errors and set at 0, the correlation was virtually unchanged at 0.404, R^2 was 0.163, the significance level was 0.010, the slope was 0.626, and the y-intercept was 0.175.

It was observed that many of the tests were taken at windspeeds too low to cause wind erosion, and during other tests, the moisture content of the pile was so high that erosion would not occur even with high windspeeds. Twenty of these tests with negligible emissions were eliminated to see whether the windspeed-emission rate relationship was stronger during tests with wind erosion. The results of this regression analysis were: $R = 0.287$, $R^2 = 0.082$, significance level = 0.184, slope = 0.859, and y-intercept = -0.122. According to this analysis, the tests with negligible emissions did not appear to be distorting the first calculated relationship between the two variables.

From the above regression analyses, one can conclude that a highly significant relationship exists between windspeed and particulate emission reductions, and that the relationship is approximately linear with a slope less than one (1 percent reduction in windspeed results in less than 1 percent reduction in particulate emissions). Also, in some instances windspeed on the front face of the pile appears to be reduced by the windscreen, but emissions from the pile actually increase as a result of higher windspeeds on the back side of the pile.

TABLE 2. COMPARISON OF WINDSPEED AND TOTAL PARTICULATE REDUCTIONS

Test	Windspeed, ft/min Piles		Wspd. rdn.	TP, lb/m Piles		TP rdn.
	Screened	Exposed		Screened	Exposed	
1B	1679	1755	0.043	9.82	8.36	-0.175
2	951	1480	0.357	1.45	1.34	-0.082
3	1039	1653	0.371	2.92	2.34	-0.250
4	791	1228	0.356	1.04	0.98	-0.058
5	969	1354	0.284	1.26	2.52	0.499
6	545	1024	0.468	0.54	0.66	0.180
7	598	1026	0.417	0.46	0.49	0.051
9	473	1070	0.558	0.38	0.47	0.197
10	350	524	0.332	0.02	0.04	0.453
11	312	869	0.641	0.02	0.04	0.471
12	257	409	0.372	0.03	0.03	-0.061
13B	198	314	0.369	0.01	0.01	0.371
14	477	1018	0.531	0.04	0.06	0.394
15A	661	1020	0.352	0.03	0.02	-0.188
15B	641	679	0.056	0.03	0.03	0.101
16	493	580	0.150	0.01	0.01	0.029
17	386	508	0.240	0.03	0.08	0.588
19A	256	294	0.129	0.03	0.02	-0.596
19B	350	388	0.098	0.01	0.01	-0.111
20	343	342	-0.003	0.01	0.01	0.180
21A	402	993	0.595	0.04	0.04	0.108
21B	494	985	0.498	0.06	0.34	0.825
22	512	1010	0.493	0.07	0.91	0.928
23A	562	1031	0.455	0.20	2.15	0.908
23B	230	380	0.395	0.02	0.04	0.486
24	426	455	0.064	0.02	0.03	0.192
25A	714	961	0.257	0.29	0.19	-0.509
25B	680	820	0.171	0.15	0.10	-0.555
26	902	986	0.085	0.04	0.03	-0.431
27	577	1009	0.428	0.17	0.12	-0.403
28B	424	721	0.412	0.09	0.13	0.290
29	375	609	0.384	0.01	0.02	0.358
30A	419	680	0.384	0.04	0.03	-0.599
30B	433	620	0.302	0.02	0.03	0.301
31	313	545	0.426	0.01	0.01	0.357
32	305	356	0.143	0.01	0.01	0.063
33	174	289	0.398	0.04	0.03	-0.147
34A	214	275	0.222	0.01	0.01	0.391
34B	198	272	0.272	0.01	0.01	-0.071
35	310	410	0.244	0.01	0.01	0.218
36	256	380	0.326	0	0	0.000
105	408	389	-0.049	0	0	0.000

PARTICLE SIZE DATA

The emission rates of particles within several size ranges were determined by selecting a heavily loaded filter from each profiling test and subjecting it to laser diffraction analysis. The resulting percentages of net sample weight by particle size range were then multiplied by the TP emission rate for the test to obtain emission rate by particle size range. The effectiveness of the windscreen in reducing emissions for each size range was then calculated as $(1 - ER_{scr}/ER_{exp})$ for that range.

The particulate reductions by size range were then compared with corresponding windspeed reduction in the same manner as with the TP reduction data; i.e., by regression analysis.

None of the particle size ranges had as significant a relationship with windspeed as TP did, partially because of the smaller data sets available with the particle size data (19 tests instead of 42). Particle size data could not be obtained on many filters because of their light mass loadings. The particle size emission reductions that had the highest correlations with windspeed reduction were 30 to 62 μm and 62 to 176 μm. The two small particle size ranges (<10 μm and 10 to 30 μm) both had poor correlations. Slopes of regression lines for the two particle sizes that were reasonably significant were higher than the slopes for TP, which indicates an emission reduction (in those size ranges) almost equal to windspeed reduction. No explanation was apparent for differences in variation with windspeed for the different particle sizes.

The same frequent negative emission reductions were observed in all particle size ranges, as was the case for TP. This indicates that increased emissions were actually occurring as a result of the screen, rather than as the anomalous result of sampling or laboratory analysis errors.

FACTORS OTHER THAN WINDSCREEN AFFECTING EMISSION RATES

Multiple linear regression (MLR) analysis was used to identify external variables affecting emission rates. Only test data from the unscreened pile were utilized because these emission rates were not altered by the presence of the windscreen.

The variables included in the analysis were windspeed, moisture content, and silt content of surface material. Particle size was also a variable in that MLR analyses were run with four different sets of emission rates (<10 μm, <30 μm, <62 μm, and TP) as dependent variables to examine the effects of the external variables on different size ranges of particles.

These regression analyses showed a strong linear relationship between TP emission rate and windspeed and a strong inverse relationship between TP emission rate and moisture content of the pile. Approximately the same relationship was observed between the two variables and emission rates regardless of the size fraction considered.

OBJECTIVE 3--DEVELOPMENT OF WINDSCREEN DESIGN PARAMETERS

The final objective of the study was to develop windscreen design parameters. For the three windscreen design parameters that were varied by test, the field test results should provide better information than wind tunnel data for optimizing design values. Conditions such as wind direction variation, surface moisture content, and crusting could be incorporated in field testing, but not in wind tunnel studies.

Stepwise MLR was the statistical test employed. The three windscreen variables--height, length, and distance from pile--were entered along with exogenous variables such as windspeed, surface moisture content, and silt content. None of the exogenous variables had such an overriding effect on relative emission rates with and without the screen that they obscured the impacts of changes in screen parameters. By including these variables in the MLR, the relatively small effects of these variables were taken into account rather than acting as interferences in the direct comparison of test results.

Combining the results of the MLR with graphical analysis led to several design conclusions. Screen lengths of 5.0D appear to be appropriate for permanent or semipermanent installations. Given the wind direction variations that occur in real situations, the 1.0D to 1.5D lengths tested in the wind tunnel are probably too short. The 2.0H screen-to-pile distance was found to be optimum. This distance yielded slightly greater emission reductions than the 1.0H or 3.0H distance. Both the wind tunnel study and this study showed that the 0.5H height windscreen was not as effective as screens of 1.0H. Also, the screen height of 1.0H is nearly as effective as higher screens. In general, the optimum design parameters appear to be: porosity = 50 percent; height = 1.0H; width = 5.0D; and distance = 2.0H.

RECOMMENDATIONS

The field study has helped to identify several important areas for further investigation. Although the wind tunnel study and the field study are in general agreement for the front of the pile, the results are contradictory in one significant area. The field study showed that large portions of the back of the pile had windspeeds higher than the reference windspeed. This observation was reinforced by the particulate emission data. Negative emission reductions were noted for the screened pile in a large number of tests. This basic result is in direct conflict with the bulk of the wind tunnel data. Although Billman did find some negative reductions, the field study showed negative reductions as large as 40 percent.

There must be some ongoing physical process or processes that have not been adequately investigated. The results to date raise questions on the applicability of windscreens for reducing emissions from storage piles. Before windscreens are recommended as a control measure, it is imperative that the observed relationship between the use of windscreens and the emission rate be investigated further.

The work described in this paper was performed by PEI Associates, Inc., under contract to the U.S. Environmental Protection Agency, Contract No. 68-02-3995, Task No. 15. Dale L. Harmon was the EPA Project Officer for this study.

METRIC EQUIVALENTS

Readers more familiar with metric units may use the following to convert to that system.

Nonmetric	Times	Yields metric
acre	4047	m^2
ft.	0.305	m
in.	2.54	cm
lb.	0.454	kg
mi.	1.609	km

REFERENCES

1. Billman, B. J., and Arya, S.P.S. 1985. Windbreak Effectiveness for Storage Pile Fugitive Dust Control--A Wind Tunnel Study. EPA-600/3-85/059 (NTIS PB85-243848). U.S. Environmental Protection Agency, Research Triangle Park, NC.

2. Bagnold, R. A. 1941. The Physics of Blown Sand and Desert Dunes. Methuen, London.

3. Gillette, D. 1978. A Wind Tunnel Simulation of the Erosion of Soil: Effect of Soil Texture, Sandblasting, Wind Speed, and Soil Consolidation on Dust Production. Atmos. Environ. 12:1735.

4. Blackwood, T. R., and R. A. Wachter. 1978. Source Assessment: Coal Storage Piles. EPA-600/2-78-004k (NTIS PB 284297). U.S. Environmental Protection Agency, Cincinnati, OH.

5. Gillette, D. 1978. Tests With a Portable Wind Tunnel for Determining Wind Erosion Threshold Velocities. Atmos. Environ. 12:2309.

6. Gillette, D. A., J. Adams, A. Endo, and D. Smith. 1980. Threshold Velocities for Input of Soil Particles into the Air by Desert Soils. J. Geophys. Res. 85(C10):5621, October 20, 1980.

7. Cowherd, C., Jr., R. Bohn, and T. A. Cuscino. 1979. Iron and Steel Plant Open Source Fugitive Emission Evaluation. EPA-600/2-79-103 (NTIS PB 299385). U.S. Environmental Protection Agency, Research Triangle Park, NC.

8. Cowherd, C., Jr. 1982. Emission Factors for Wind Erosion of Exposed Aggregates at Surface Mines. Proc. 75th APCA Annual Meeting. Paper 82-15.5.

9. Cuscino, T., G. E. Muleski, and C. Cowherd, Jr. 1983. Iron and Steel Plant Open Source Fugitive Emission Control Evaluation. EPA-600/2-83-110 (NTIS PB84-110568). U.S. Environmental Protection Agency, Research Triangle Park, NC.

10. TRC Environmental Consultants. 1982. Evaluation of Preliminary Field Test Results on Windscreen Dust Control Efficiency. Denver, CO.

11. PEDCo Environmental, Inc. 1984. Fugitive Dust Control Techniques at Hazardous Waste Sites, Interim Technical Field Sampling Report No. 3. Control of Storage Pile Emissions With Windscreens and Chemical Dust Suppressants. Prepared for U.S. Environmental Protection Agency, Municipal Environmental Research Laboratory, Cincinnati, OH.

12. PEI Associates, Inc. 1985. Verification of Model for Windscreens Applied to Storage Piles--Quality Assurance Project Plan. Prepared for Air & Energy Engineering Research Laboratory, Research Triangle Park, NC.

REFERENCES (cont.)

13. PEI Associates, Inc. 1985. Field Evaluation of Windscreens as a Fugitive Dust Control Measure for Material Storage Piles. Draft Report. EPA Contract No. 68-02-3995. Prepared for U.S. Environmental Protection Agency, Air & Energy Engineering Research Laboratory, Research Triangle Park, NC.

MEASUREMENT OF FUGITIVE EMISSIONS IN A COAL-FIRED POWER PLANT

by: G. E. Muleski, F. J. Pendleton
Midwest Research Institute
425 Volker Boulevard, Kansas City, MO 64110

W. A. Rugenstein
The Detroit Edison Company
2000 Second Avenue, Detroit, MI 48226

ABSTRACT

Coal-fired power plants contain several potential sources of airborne fugitive emissions, and utilities and regulatory agencies face an increasing need to estimate these emissions. This paper presents the methodology and results of a field testing program designed to characterize size-specific emissions from two sources at a modern power plant--the loading of fly ash into truck/trailer combinations and wind erosion of various surfaces within the plant's coal yard. Test results are used to determine annual emission rates which are compared to estimates using models available in the literature.

INTRODUCTION

Coal-fired power plants contain numerous potential sources of airborne fugitive particulate emissions. The majority of these emissions result from routine plant operations, such as the movement and storage of coal, the handling of ash and sludge, and vehicular traffic.

A recent survey[1] found that, despite the large amount of recent literature on fugitive emissions, much of the information is largely based on conjecture. In addition, available test data often have proven to be highly variable and sometimes contradictory. Furthermore, only very few field characterizations of fugitive emissions have been conducted at power plants. As a result, many estimates of fugitive emission levels in coal-fired power plants are ultimately based on either tests conducted in other industries (such as iron and steel or western surface mining) or upon unsupported conjecture.

This paper summarizes the results of a field testing program conducted by Midwest Research Institute (MRI) at Detroit Edison's River Rouge power plant. Two sources of fugitive emissions were characterized:

a. The loading of fly ash into truck/trailer combinations.

b. Wind erosion of various surfaces within the plant's coal yard.

Four emission tests of the fly ash loading operation and nine tests of wind-generated emissions from coal surfaces were conducted September 22 through 27, 1984. In addition, three other tests of the threshold wind speed for other coal surfaces were performed.

The airborne particle size fractions of interest are:

TP	Total airborne particulate matter.
SP	Suspended particulate matter consisting of particles equal to or smaller than 30 μm in aerodynamic diameter.
IP	Inhalable particulate matter consisting of particles equal to or smaller than 15 μm in aerodynamic diameter.
PM_{10}	Thoracic parti[illegible]ate matter consisting of particles equal to or smaller than 1[illegible]n aerodynamic diameter.
FP	Fine particulat[illegible]r consisting of particles equal to or smaller than 2.5 μm in a[illegible]amic diameter.

The SP size fraction in this study reflects potential air quality impact as measured by the standard high-volume sampler. The 50% cutpoint for this sampler can range between 25 and 50 μm in aerodynamic diameter (μmA) depending on wind speed and direction. An effective cutpoint of 30 μmA is usually assigned to the standard high-volume sampler.[2,3]

EMISSIONS FROM FLY ASH LOADING

Source Description

The River Rouge power plant has three generating units; No. 1 unit is oil-fired and the others (No. 2 and 3) are pulverized-coal-fired. Fly ash from the coal-fired boilers is collected by ESPs. Fly ash from the No. 3 unit at the River Rouge plant is retained in the No. 2 silo until it is loaded into truck/trailer combinations for disposal outside the plant. During the testing period, all fly ash loading in the plant was done at the No. 2 silo because the No. 2 unit (which feeds the No. 1 silo) was temporarily shut down.

The No. 2 silo has a 52-ft long loading bay which is equipped with two chutes used to load the ash. At each end of the east-west bay are flexible plastic curtains and metal garage doors. Because the fly ash is loaded into 55-ft long truck/trailer combinations, the doorway is alternately open and blocked by the truck during loading.

In order to facilitate testing, a slight modification of the loading procedure was employed:

a. As usual, the truck entered the bay, driving into the wind, and loading commenced.

b. After the 25-ft long truck bed was loaded, the truck left the bay and reentered facing the other way.

c. The 30-ft long trailer was then loaded. The loaded truck then left the test site after being washed down with the spray bars at the west end of the bay.

By reversing the truck's orientation in the middle of the loading operation, MRI was able to keep the downwind doorway blocked during the entire time that fly ash was loaded. This, in turn, simplified air sampling equipment deployment and operation.

The only other change from the normal loading procedure during testing was keeping the bottom of the downwind garage door at a 12-ft height. This modification was employed to (a) reduce the necessary height of the downwind sampling array and (b) avoid the difficulty in attempting to isokinetically sample the particulate mass passing through the flexible curtain. Because none of the above changes altered the loading process, the mass emissions were unaffected and were merely rerouted through the open areas of the doorway.

Air Sampling Equipment and Technique

The exposure profiling technique used for the tests in this study was based on the isokinetic profiling concept that is used in conventional source testing. The passage of airborne pollutant immediately downwind of the source was measured directly by means of simultaneous multipoint sampling over the effective cross section of the open dust source plume. This technique used a mass-balance calculation scheme similar to EPA Method 5 stack testing rather than requiring indirect calculation through the application of a generalized atmospheric dispersion model.[4]

The equipment deployment for these tests is shown in Figure 1. All samplers on a side were mounted on an aluminum mast. The mast itself was fixed to a dolly which could be rotated into and out of the doorway, thus allowing the trucks to easily enter the bay. Although the sampling system was designed to be easily relocated, this was not necesary because all tests were conducted with sampling array in the plane of the east doorway.

Each profiler head (Figure 2) was operated as an isokinetic exposure sampler directing passage of the flow stream through a settling chamber and then upward through a standard 8-in. by 10-in. glass fiber filter positioned horizontally.

High-volume, parallel-slot cascade impactors with 20 cfm flow controllers were used to measure the downwind particle size distribution on each side. As shown in Figure 3, the impactor units were equipped with cyclone preseparators to remove coarse particles which otherwise would tend to bounce off the glass fiber impaction substrates, causing fine particle measurement bias. To further reduce particle bounce problems, each stage of the impactor substrates was sprayed with a stopcock grease solution to provide a sticky impaction surface. Provision was also made to measure the upwind particle size distribution and total particulate concentration using a cyclone/impactor combination.

Particulate Sample Handling and Analysis

The sampling and analysis procedures followed in this field testing program were subject to certain quality assurance (QA) guidelines. These guidelines met or exceeded the requirements specified in the reports entitled "Quality Assurance Handbook for Air Pollution Measurement Systems, Volume II - Ambient Air Specific Methods" (EPA 600/4-77-027a) and "Ambient Monitoring Guidelines for Prevention of Significant Deterioration" (EPA 450/2-78-019).

As part of the QA program for this study, routine audits of sampling and analysis procedures were performed. The purpose of the audits was to demonstrate that measurements were made within acceptable control conditions for particulate source sampling and to assess the source testing data for precision and accuracy. Examples of items audited include gravimetric analysis, flow rate calibration, data processing, and emission factor calculation. The mandatory use of specially designed reporting forms for sampling and analysis data obtained in the field and laboratory aided in the auditing procedure. Further detail on specific sampling and analysis procedures is provided in the test report[5] and elsewhere.[4,6]

Aggregate Materials Sampling and Analysis

Samples of the fly ash were taken in the course of this study. Three to four composite fly ash samples were taken for each truck during testing periods from the hopper feed (past the point at which water was introduced). Detroit Edison personnel informed MRI that this was the point at which they generally inspect the wetted fly ash prior to and during loading.

Each bulk field sample was split with a riffle to a sample size amenable to laboratory analysis. The basic procedure for moisture analysis was determination of weight loss on oven drying. Moisture analysis was usually performed in the field laboratory, on the same day as sample collection. In this fashion, the measured value was a more reliable estimate of the field conditions at the time of the test. The basic procedure for silt analysis was mechanical, dry sieving, based on the ASTM-C-136 method discussed in AP-42 Supplement 14.[3] The silt analysis was performed upon return to the main MRI laboratories.

FLY ASH TEST RESULTS

Test site parameters for the four tests of fly ash loading are given in Table 1. Table 2 presents emission factors for each test for the various size fractions. Also shown in this table are parameters that affect emissions from material handling operations in the ambient atmosphere.[3] A few remarks about the representativeness of these parameters are in order. First, as mentioned earlier, the material sample was taken from the hopper feed at the top of the bay. In earlier tests of outdoor materials handling operations, MRI took composite samples from the resulting piles. This was not done here because of greater interference with normal plant operation and because of possible safety problems in taking samples from a 10-ft high truck that moved every 2 to 3 min.

TABLE 1. EXPOSURE PROFILING TEST PARAMETERS

Run	Date	Test start	Duration[a] (min)	Ambient air temperature (°C)		Mean wind speed (mph) On-site[b]	
				(°C)	(°F)	On-site[b]	Delray[c]
AN-1	9-25-84	11:32	60	21	69	6	11.5
AN-2	9-25-84	14:28	20	22	72	6	10.0
AN-3	9-26-84	7:52	19	12	54	4	7.3
AN-4	9-26-84	10:12	16	12	54	4	7.8

[a] Includes only time downwind samplers operated.

[b] Value taken from 2.5 m high instrument located just west of test site.

[c] Developed from meteorologic data furnished by Detroit Edison from its Delray site (10 m height, approximately 2 miles north of River Rouge plant).

In addition, visual observation of dumping prior to emission testing indicated that the material was not homogeneous in terms of moisture content. Water seemed to run down the sides of the chute, and the outside shell of the falling material appeared to be quite wet. However, upon impact, the inner core appeared fairly dry and a "puff" of dust emissions (presumably from this core) was observed. Similar nonuniform mixtures have been reported for Detroit Edison's St. Clair plant.[7] This inhomogeneity would present considerable difficulty in obtaining representative samples directly from the truck load.

TABLE 2. EXPOSURE PROFILING TEST RESULTS

	Fly ash properties			Emission factor (lb/ton)				
Run	Silt[a] (%)	Moisture[b] (%)	Fly ash transferred (tons)[c]	TP	SP	IP	PM_{10}	FP
AN-1	25[d]	30	128	0.10	0.0058	0.0036	0.0026	0.00077
AN-2	35	29	43.0	0.16	0.0065	0.0034	0.0018	0.000065
AN-3	28	26	44.7	0.11	0.0038	0.0021	0.0017	0.00049
AN-4	40	29	46.9	0.058	0.0017	0.00099	0.00058	0.000053

[a] Actual fraction passing a 200-mesh sieve probably higher. See discussion in text.

[b] Moisture content of composite samples taken from hopper feed. See discussion in text.

[c] Data provided by front gate personnel at River Rouge Plant. Value given above is somewhat greater than true amount of ash loaded because the trucks were weighed after the drivers had sprayed water on the load prior to leaving the silo.

[d] Average of two samples.

Finally, the silt contents reported in Table 2 are believed to be lower bounds on the fraction of material that would pass a 200-mesh screen upon dry sieving. MRI's standard procedure calls for sieving no more than 40 min. However, all silt contents were continuing to increase by more than the 3% permitted at the end of this time. Furthermore, Foley[8] indicates that roughly 90% of fly ash from pulverized coal fired boilers passes a 200-mesh screen, although it is believed that this is based on wet sieving. Analysis of an additional sample from Run AN-3 for approximately 60 min showed that at least ~ 60% could be passed through the 200 mesh upon dry sieving.

These measurement-based emission factors are, in general, fairly constant through the four tests. The summary statistics for the tests are given below in Table 3.

TABLE 3. MEAN EMISSION FACTORS FOR FLY ASH LOADING

Size range	Arithmetic mean (lb/ton)	Coefficient of variation (%)
TP	0.10	39
SP	0.0044	48
IP	0.0025	48
PM_{10}	0.0017	50
FP	0.00034	100

The large variation in FP emission factors is due to (a) the difficulty in separating the FP emissions of the source from the FP fraction of the upwind concentration and (b) particle bounce of larger particles through the impactor stages.

CHARACTERIZATION OF COAL YARD WIND EROSION

Air Sampling Equipment and Technique

The portable wind tunnel method employed in this study allowed *in situ* measurement of emissions from wind erosion of storage piles and exposed areas. The MRI portable, pull-through, wind tunnel (Figure 4) consisted of an inlet contraction, a working section, a sampling section, and a power system. The open-floored working section of the tunnel was placed directly on the surface to be tested, and the tunnel air flow was adjusted to values corresponding to the means of the upper NOAA wind speed ranges. Tunnel wind speed was measured by a pitot tube at the downstream end of the working section and was related to wind speed at the standard 10-m height by means of a logarithmic profile.

To minimize the dust levels in the tunnel air intake stream, testing was conducted only when ambient winds were below the threshold velocity for erosion of the exposed material. A portable, high-volume sampler with an open-faced filter was operated on top of the inlet contraction to measure background dust levels.

An emissions sampling section was used with the pull-through wind tunnel in measuring particulate emissions generated by wind erosion. As shown in Figure 4, the sampling section was located between the working section outlet hose and the blower inlet. The sampling train, which was operated at 15 to 25 cfm consisted of a tapered probe, cyclone precollector, parallel-slot cascade impactor, backup filter, and high-volume sampler. Substrates were greased in the same manner as described earlier. Interchangeable probe tips were sized for isokinetic sampling over the desired tunnel wind speed range.

Particulate Sample Handling and Analysis

The quality assurance procedures for sampling and analysis followed in this phase of the testing program were identical to those discussed above.

Once the source testing equipment was in place on the test surface, a threshold velocity test was performed. The purposes of this preliminary test were to determine the minimum velocity at which wind erosion was initiated and to gather other data needed for sampling and analysis. The threshold velocity for a particular surface was determined by observing the onset of surface particle movement as the wind velocity was gradually increased. A subthreshold velocity profile was then measured using the pitot tube in the working section. This subthreshold velocity profile allowed the calculation of the surface roughness height.

After these data were obtained, tunnel air speeds were determined corresponding to the means of the first three upper NOAA wind speed ranges above the threshold velocity of the uncontrolled test surface. A sampling train flow rate and probe tip were selected to ensure isokinetic sampling at the selected wind speed. A test series consisted of runs at these three wind speeds (in ascending order) at the same site. Further detail on specific sampling and analysis procedures is provided in the test report[9] and elsewhere.[6]

Experience has shown that, on surfaces with limited amount of material available for erosion, the mass eroded during 30 min under a steady wind closely approximates the erosion potential of the surface (i.e., the total amount of material per unit area that can be eroded at that wind speed.)[6] Under this assumption, the erosion potential, at a given wind speed U, can be found by adding together the total mass eroded (per unit area) during all tests of the surface with wind speeds less than or equal to U.

Aggregate Materials Sampling and Analysis

Samples of each wind erosion test surface were collected, when possible, before and after each test. When several tests were performed back-to-back, samples could only be obtained before and after the series. Samples were removed from a known area using a dust pan and whisk broom. The depth of the sample was based on the largest piece of raw material in the surface. Each sample was analyzed for silt and moisture contents using the same techniques discussed earlier.

WIND TUNNEL TEST RESULTS

A map of the plant's coal yard is given as Figure 5 and shows the six test sites. The site parameters for the 12 wind tunnel tests are shown in Table 4. Table 5 presents data on the threshold velocities, as well as the surface properties which are believed to have a significant effect on emission rate. Surface moisture tends to decrease, as expected, as wind erosion occurs. The increase in silt contents from Runs AN-10 through AN-15 is believed to be the result of large particle creep, in which large particles, while not entrained in the airflow, nevertheless roll away from their original positions under the action of the wind. As a result less mass of loose material remains on the surface, but with the removal of large particles by creep, a greater fraction of this smaller mass consists of silt-size particles. This was the case for Runs AN-10 through -15.

Tables 6 and 7 summarize the wind erosion test results. Table 6 presents the erosion rates for each run on a per-test basis, while Table 7 shows erosion potentials (i.e., cumulative mass eroded).

The SP and PM_{10} erosion potentials are shown in Figure 6. These are the two size fractions of the most interest in terms of air quality at the present time. As can be seen from the figure, the erosion potentials for Sites A and B tend to increase rapidly with increasing wind speed above the onset of erosion at ~ 26 to 27 mph. In addition, the data from Runs AN-16 through AN-18 indicate that the erosion potential of surface at Site C (between the scraper tracks) tends to level off with increasing wind speed after the initial increase from the threshold. It is conceivable that the other sites would exhibit similar trends at higher wind speeds.

Estimation of Annual Emissions from Wind Erosion

In order to estimate annual emissions from the coal yard, it is necessary to combine erosion characteristics of the different surfaces with the frequency of wind speeds above the threshold velocity. Because the actual rate of emission depends upon the joint frequency of surface disturbance (e.g., vehicular traffic, addition of fresh material, etc.) and wind speed, and because information of this type is not readily available, an attempt was made to obtain conservatively high estimates of emission rates using the data available.

TABLE 4. WIND EROSION TEST SITE PARAMETERS

Run	Surface	Site[a]	Date	Start Time	Sampling duration (min)	Average velocity in test section (m/s)	Average velocity in test section (mph)	Ambient air temperature (°C)	Ambient air temperature (°F)
AN-10	Concrete Pad covered by material dropped from conveyor	A	9/22/84	17:00	30	4.7	10	31	88
AN-11		A	9/22/84	18:20	30	6.0	14	31	88
AN-12		A	9/22/84	19:10	30	7.4	16	31	88
AN-13	Day pile	B	9/24/84	19:18	30	8.9	20	24	75
AN-14		B	9/24/84	20:00	30	11	25	24	75
AN-15		B	9/24/84	20:40	30	13	29	24	75
AN-16	Main Pile - between scraper tracks	C	9/26/84	18:52	30	7.8	17	12	54
AN-17		C	9/26/84	19:29	30	8.8	20	12	54
AN-18		C	9/26/84	20:04	30	10	23	12	54
AN-19A[b]	Main pile - on scraper tracks	D	9/27/84	8:42	NA	NA	NA	8	46
AN-19B[b]	Main pile - crusted area between tracks	E	9/27/84	10:44	NA	NA	NA	10	50
AN-19C[b]	Main pile - top road	F	9/27/84	12:00	NA	NA	NA	10	50

[a] Letters refer to test site locations shown on Figure 5.

[b] These are threshold tests; no emissions sampling was performed.

TABLE 5. PROPERTIES OF SURFACES TESTED

Runs	Site	Roughness height (cm)	Before erosion		After erosion		10-m Equivalent threshold velocity (mph)
			Silt (%)	Moisture (%)	Silt (%)	Moisture (%)	
AN-10-12	A	0.2	8.5	3.0	15	2.5	26
AN-13-15	B	0.003	2.4	3.4	4.6	4.2	27
AN-16-18	C	0.07	1.8	1.9	1.3	1.2	33
AN-19A	D	0.05	1.9	1.9	NA	NA	41
AN-19B	E	0.006	1.8	4.6	NA	NA	43
AN-19C	F	0.0004	2.6	6.3	NA	NA	39

TABLE 6. WIND EROSION RATES

Run	Erosion rate (mg/m²/s)				
	TP	SP	IP	PM_{10}	FP
AN-10	3.24	1.00	0.648	0.486	0.162
AN-11	14.7	3.53	2.65	2.06	0.735
AN-12	25.1	4.52	3.01	2.31	0.778
AN-13	2.12	0.403	0.318	0.276	0.186
AN-14	15.9	2.54	1.75	1.30	0.445
AN-15	12.9	2.19	1.55	1.22	0.452
AN-16	1.11	0.633	0.533	0.466	0.289
AN-17	0.804	0.482	0.402	0.362	0.233
AN-18	0.302	0.187	0.157	0.145	0.0966

TABLE 7. WIND EROSION POTENTIALS

Run	Equivalent 10 m wind speed (mph)	Erosion potential (g/m²)				
		TP	SP	IP	PM_{10}	FP
AN-10	28	5.8	1.8	1.1	0.87	0.29
AN-11	35	32.2	8.2	5.9	4.6	1.6
AN-12	43	77.6	16	11	8.7	3.0
AN-13	35	3.8	0.72	0.57	0.50	0.33
AN-14	44	32	5.3	3.7	2.8	1.1
AN-15	51	56	9.2	6.5	5.0	1.9
AN-16	41	2.0	1.1	0.96	0.84	0.52
AN-17	46	3.4	2.0	1.7	1.5	0.94
AN-18	54	4.0	2.3	2.0	1.8	1.1

The coal yard (as shown in Figure 5) was divided into the 10 areas shown as Figure 7. TP, SP, and PM_{10} emission rates were determined for each of these areas and a total emission rate due to wind erosion was then calculated. Details of this operation (for SP) are shown in Table 8. Note that the dotted area S_{10} in Figure 7 represents level travel areas in the yard.

A few remarks about these estimates are in order. The average number of observations per year of wind speeds above the threshold velocities was assumed equal to the number of occurrences of winds in this speed class per year. It was also assumed that the total mass erodible at the upper wind speed of the class was eroded during each occurrence; that is, the surface had been disturbed (thus regenerating the erosion potential) prior to each high wind event. Finally, no correction for the 12.8-m height of the wind instrument at Detroit City Airport was deemed necessary because the increase in threshold velocity at 12.8 m was less than 3% over the value at 10 m for all surfaces under consideration.

The annual TP, SP, and PM_{10} erosion rates are estimated as 8.4, 2.1, and 1.1 tpy, respectively. These values may be conservatively high because of the following assumptions employed:

a. Each surface was assumed to erode to its full erosion potential each time the wind exceeded the threshold velocity. This would represent the maximum amount of erosion possible for each high wind event.

b. The erosion potential for the upper end of the wind speed class was used in the calculations.

However, it should be noted that the estimates do reflect the conditions under which the tests were performed, and are especially dependent upon the moisture contents of the tested surfaces. These values fluctuate during the year.

A final critical assumption is that of the number of high wind events per year. The estimates are based on the most suitable wind data available during the analysis. Meteorological data of a more complete nature than currently available would be required to improve the estimates.

DISCUSSION

Very little information is available for estimating fugitive emissions resulting from fly ash handling. One recent survey[1] found only two emission factors related to these operations, and only one of these entailed truck loading at a specific rate. It has been estimated that the disposal of material such as fly ash generates uncontrolled handling and windage losses of 20 to 100 lb/ton.[10] Because the test results given above represent only one part of the handling process and because the measured emission levels reflect partially controlled (i.e., enclosed bay, water addition) conditions, no comparison to this estimate was attempted.

TABLE 8. CALCULATION OF ANNUAL SP EROSION

Erosion areas on Figure 7	Total area (1,000 m^2)	Erosion potential (g/m^2)[a] at upper wind speed (mph)			Unit annual erosion ($g/m^2/yr$)	Annual erosion rate (tpy)
		25-31 (23)	32-38 (2)	39-50[b] (1)		
S_1	29	0^c	0.7^c	2.3^c	3.7	0.12
S_2, S_3, S_4, S_8, S_9	19	0^d	0^d	2.3^d	2.3	0.048
S_5	2.8	0.3^e	1.5^e	8.1^e	18	0.056
S_6	3.9	0.2^f	1.1^f	5.2^f	12	0.052
S_7, S_{10}	11	4.7^g	11^g	23^g	150	1.8

[a] Value in parentheses is average number of observations (every 3 hr) per year for wind speed class at Detroit City Airport from 1974 through 1977.

[b] Average annual fastest mile of wind for Detroit.

[c] Based on results of AN-16 through -18.

[d] Based on results of AN-16 through -18, but with a 39 mph threshold velocity.

[e] Based on results of AN-13 through -15.

[f] Based on average of results for AN-13 through -15 and AN-16 through -18.

[g] Based on results of AN-10 through -12.

On the other hand, many authors have suggested emission factors for use in estimating wind erosion. The recent EPRI-sponsored survey[1] discussed 17 references in connection with erosion of coal storage piles, with no less than 10 emission factors presented. Of those factors expressed in terms of an emission rate per unit surface area and having a quality rating of at least C, a range of 4.6 to 290 $\mu g/m^2/sec$ was found. In estimating annual erosion at the River Rouge plant, however, emission rates for a comparable particle size range varied from 0.073 to 4.8 $\mu g/m^2/sec$, with an average value of 0.92 $\mu g/m^2/sec$. Furthermore, these plant estimates are considered conservatively high. Although the two ranges overlap at their extremes, it does not appear that present models provide adequate estimates for annual erosion rates.

This inadequacy presents a great difficulty in developing cost-effective control programs. Wind erosion of coal piles and exposed surfaces has been estimated to account for 30 to 50% of annual controlled emissions at hypothetical power plants.[1] If available wind erosion models overpredict by an order of magnitude, then this contribution would be only 5 to 10% of the total. This lower contribution would in turn allow funds to be redirected to the control of other sources.

CONCLUSIONS

The results of this field testing program conducted at a coal-fired power plant indicate that measurement-based fugitive emission levels for the tested sources may be substantially different from estimates based on available models. This is especially true for wind erosion in the plant's coal yard, because available models can easily overpredict wind erosion by an order of magnitude.

The inadequacy of available models in estimating fugitive emissions at coal-fired plants is not particularly surprising given the fact that many of the estimates are ultimately based on testing in other industries or unsupported conjecture. As noted earlier, better characterization of fugitive emission levels at coal-fired power plants would enable the industry to develop programs that identify major sources and control these sources in a cost-effective manner.

REFERENCES

1. Currier, E. L., and B. D. Neal. Fugitive Emissions from Coal-Fired Power Plants. EPRI CS-3455, Electric Power Research Institute, Palo Alto, California, June 1984.

2. USEPA. Reference Method for the Determination of Suspended Particulate Matter in the Atmosphere (High-Volume Method). Federal Register, December 6, 1982. p. 54899f.

3. USEPA. Compilation of Air Pollution Emission Factors (Supplement No. 14). Office of Air Quality Planning and Standards, Research Triangle Park, North Carolina. AP-42. May 1983.

4. Muleski, G. E., C. Cowherd, Jr., and T. Cuscino, Jr. Current Procedures for Open Source Particulate Emission Measurements. Final Report, MRI Project No. 7993-L, Prepared for Southern Research Institute. December 1983.

5. Muleski, G. E. Fugitive Emission Measurement of Fly Ash Loading at the River Rouge Power Plant. Final Report, MRI Project No. 8162-L, Prepared for Detroit Edison. March 1985.

6. Cuscino, T., Jr., G. E. Muleski, and C. Cowherd, Jr. Iron and Steel Plant Open Source Fugitive Emission Control Evaluation. EPA-600/2-83-110. USEPA, Research Triangle Park, North Carolina. October 1983.

7. Rowsome, R. J., and A. H. Van Sickle. Control of Fugitive Dust During the Loading of Trucks with Western Coal Fly Ash. Coal- and Ash-Handling Systems Reliability Conference and Workshop Proceedings. Electric Power Research Institute, Palo Alto. August 1981.

8. Foley, R. B. Fly Ash Collection in Kent's Mechanical Engineer's Handbook: Power Volume, Edited by K. K. Salisbury. John Wiley and Sons, New York. 1950.

9. Muleski, G. E. Coal Yard Wind Erosion Measurement at the River Rouge Power Plant. Final Report, MRI Project No. 8162-L, Prepared for Detroit Edison. March 1985.

10. PEDCo Environmental, Inc. Technical Guidance for Control of Industrial Process Particulate Emissions. EPA-450/3-77-010, USEPA, Research Triangle Park, North Carolina. March 1977.

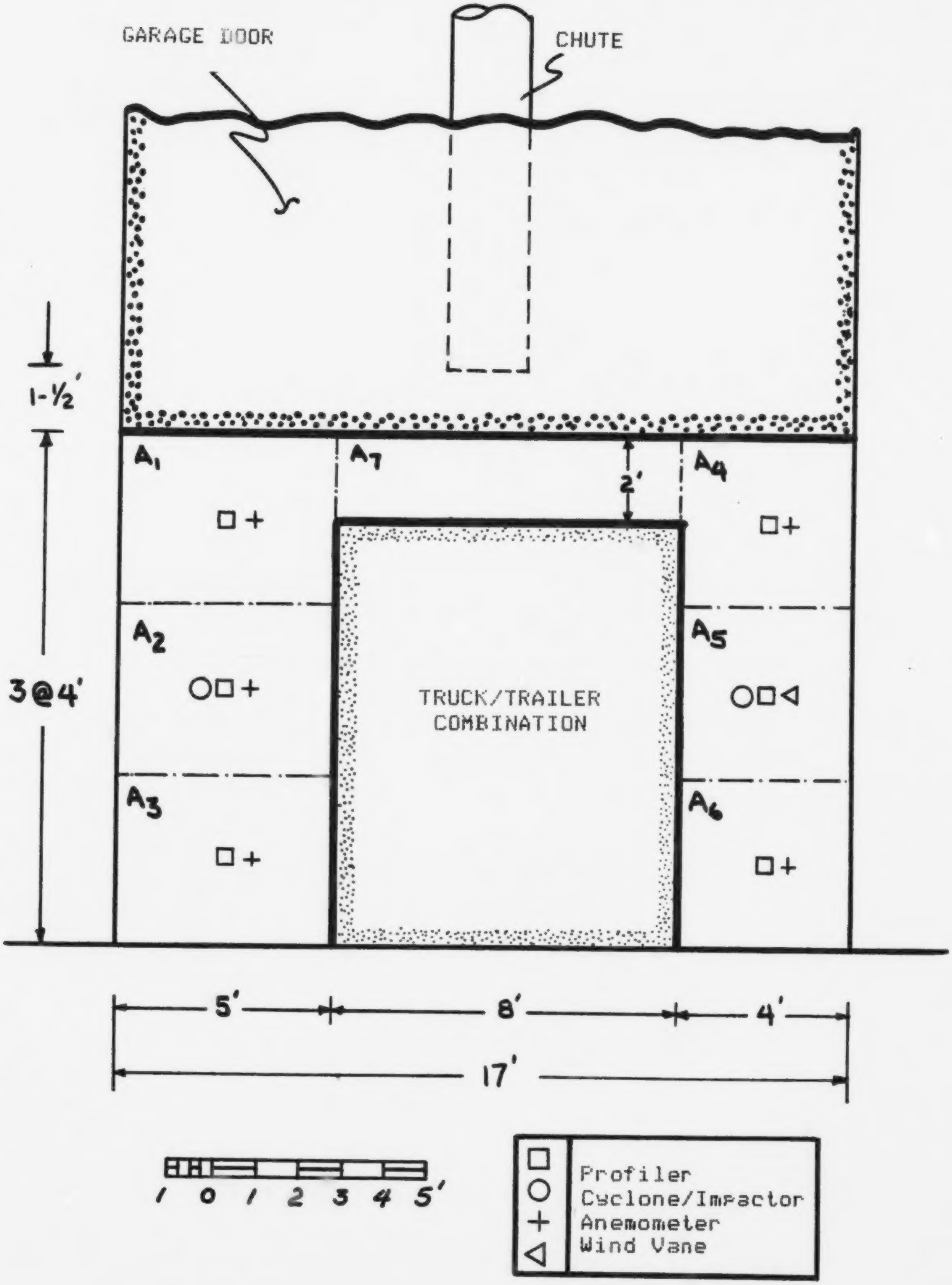
GARAGE DOOR
CHUTE
1-½'
3@4'
A1
A7
2'
A4
A2
A5
A3
A6
TRUCK/TRAILER COMBINATION
5'
8'
4'
17'
1 0 1 2 3 4 5'
□ Profiler
○ Cyclone/Impactor
+ Anemometer
◁ Wind Vane

Figure 1. East elevation of No. 2 silo.

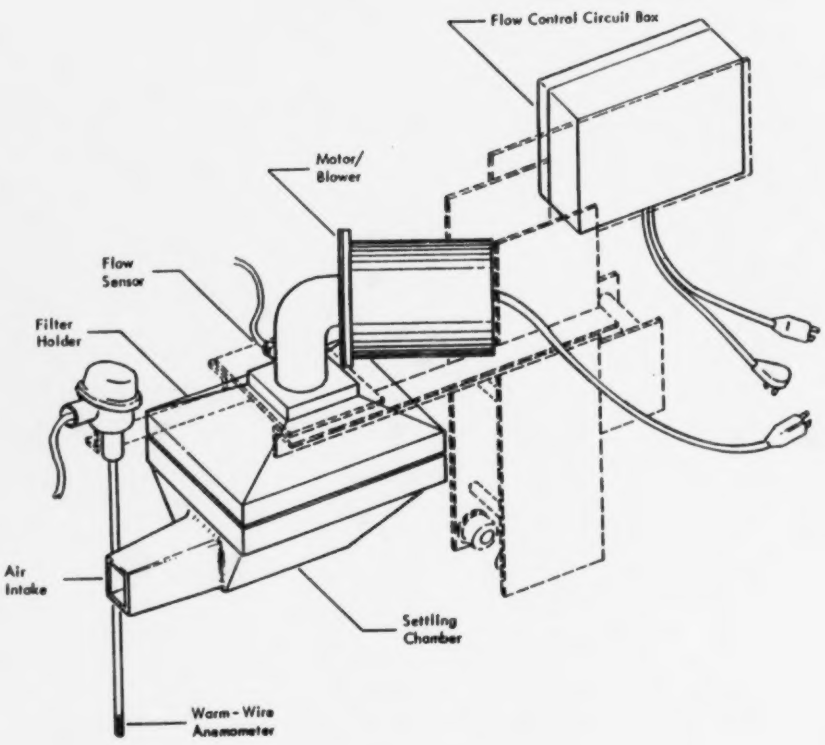
Flow Control Circuit Box
Motor/ Blower
Flow Sensor
Filter Holder
Air Intake
Settling Chamber
Warm-Wire Anemometer

Figure 2. MRI exposure profiler.

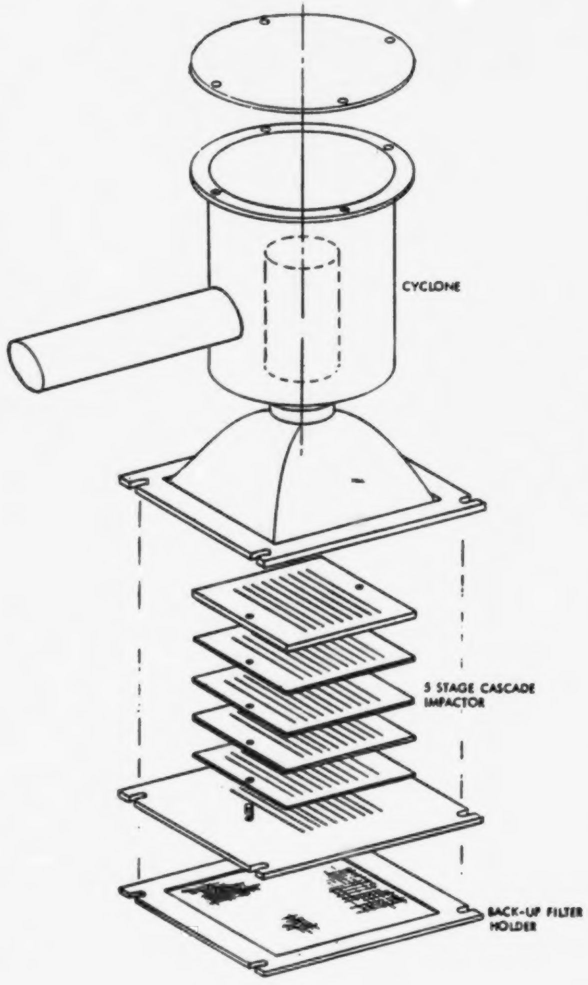
CYCLONE
5 STAGE CASCADE IMPACTOR
BACK-UP FILTER HOLDER

Figure 3. Cyclone/impactor combination.

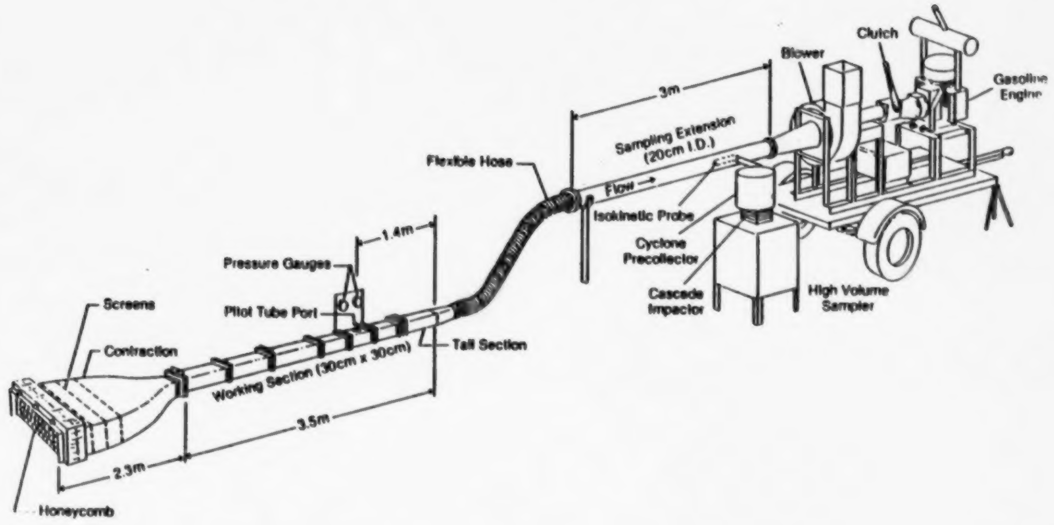
Clutch
Blower
Gasoline Engine
3m
Sampling Extension (20cm I.D.)
Flexible Hose
Flow →
Isokinetic Probe
Cyclone Precollector
Cascade Impactor
High Volume Sampler
1.4m
Pressure Gauges
Screens
Pitot Tube Port
Contraction
Tail Section
Working Section (30cm x 30cm)
3.5m
2.3m
Honeycomb

Figure 4. MRI portable wind tunnel.

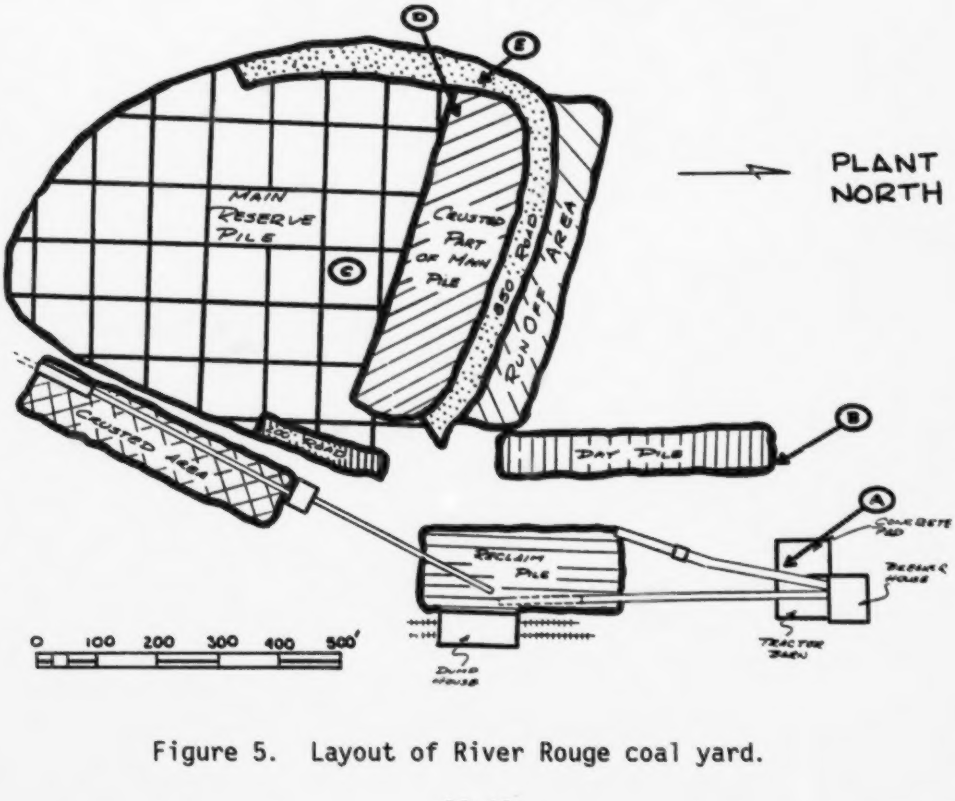
D
E
PLANT NORTH
MAIN RESERVE PILE
C
CRUSTED PART OF MAIN PILE
850' ROAD
RUN OFF AREA
CRUSTED AREA
200' ROAD
DAY PILE
B
A
CONCRETE PAD
RECLAIM PILE
BREAKER HOUSE
TRACTOR BARN
DUMP HOUSE
0
100
200
300
400
500'

Figure 5. Layout of River Rouge coal yard.

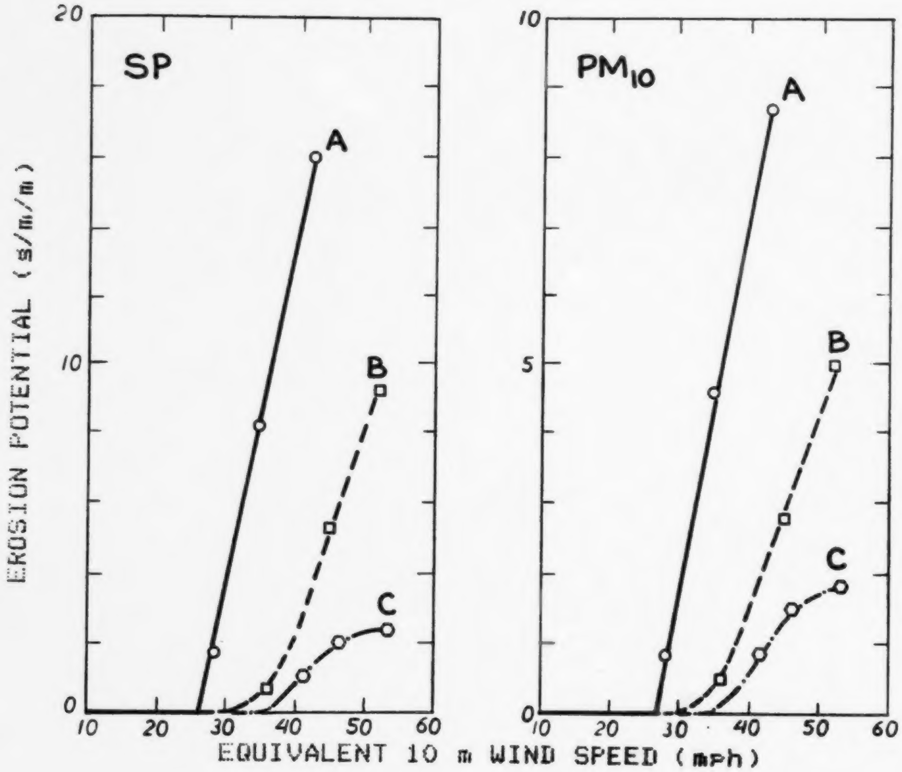

Figure 6. SP and PM_{10} erosion potentials.

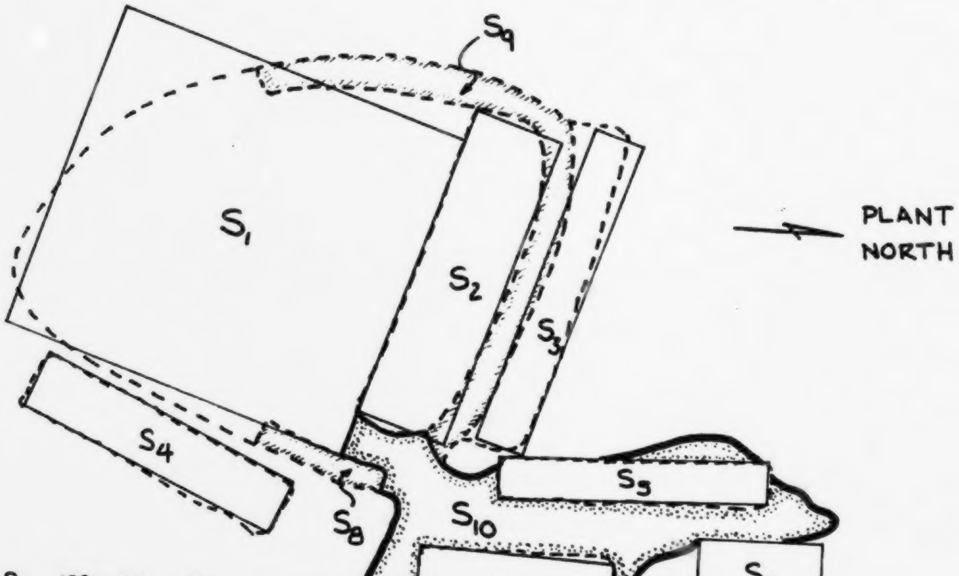

S1
S2
S3
S4
S5
S6
S7
S8
S9
S10
PLANT NORTH
0
100
200
300
400
500'

Figure 7. Areas used to estimate coal yard erosion.